

**FACULTY
OF MATHEMATICS
AND PHYSICS**
Charles University

MASTER THESIS

Veronika Vranková

**Molecular simulations of the effect of
intense subTHz electric field on proteins**

Department of Chemical Physics and Optics

Supervisor of the master thesis: doc. Ing. Pavel Soldán, Dr.

Supervisor's department: Department of Chemical Physics
and Optics

Study programme: Biophysics and Chemical Physics

Study branch: Theoretical Biophysics and
Chemical Physics

Prague 2024

I declare that I carried out this master thesis independently, and only with the cited sources, literature and other professional sources. It has not been used to obtain another or the same degree.

I understand that my work relates to the rights and obligations under the Act No. 121/2000 Sb., the Copyright Act, as amended, in particular the fact that the Charles University has the right to conclude a license agreement on the use of this work as a school work pursuant to Section 60 subsection 1 of the Copyright Act.

In date

Author's signature

I want to thank my supervisor, doc. Ing. Pavel Soldán, Dr. and consultant Michal Cifra, for their guidance and helpful advice during my studies. My thanks also go to my colleague, Dr Saurabh Kumar Pandey, whose assistance was truly appreciated during the initial stages of my molecular dynamics journey. Finally, I am also very grateful for the support and encouragement from my family and boyfriend throughout my studies.

Title: Molecular simulations of the effect of
intense subTHz electric field on proteins

Author: Veronika Vranková

Department: Department of Chemical Physics and Optics

Supervisor: doc. Ing. Pavel Soldán, Dr., Department of Chemical Physics and Optics

Abstract: The aim of this thesis was to probe the effect of the subTHz electric field on a key protein - tubulin dimer, which is crucial for the cell's stability, motility and division. This study was done *in silico*, which means that we studied the system through the simulations. We worked in the framework of classical molecular dynamics with force-fields. We used the GROMACS package together with our own Python and bash scripts. We were dealing with nonequilibrium molecular dynamics simulations since the external electric field (EEF) was applied. To study the effect EEF on the structure and stability of tubulin dimer, root mean square deviations, root mean square fluctuations and dipole moment analysis were performed. Additionally, we also analyzed the rotational motion caused by EEF. We probed 15 different frequencies of EEF - 10, 20, 30, ..., 150 GHz in 6 different directions. For statistics, all calculations were done three times, each time with different initial velocities assigned before equilibrations, to probe different parts of the phase space. For better results, much larger statistics needs to be done in the future. Unfortunately, this was not possible since the simulations had already been very computationally expensive. Still, we were able to learn a lot from our results, such as that the electric field of 10 - 40 GHz had a strong rotational effect on the tubulin dimer, where it rotated in such a way that its longitudinal axis became parallel to the electric field oscillation direction. Regarding the conformational changes, they are evident for all frequencies and directions, but yet again, more statistics is needed. Additionally, we saw some changes in rigidity of the parts of the tubulin that are important for binding the anti-tubulin drugs, such as vinca alkaloids, colchicine and a small effect on paclitaxel binding site. Furthermore, the effect on the β :M-loop and α :H1-B2 loop, which are important in lateral interactions of tubulin in microtubules, was observed. Since our tubulin also has two unstructured C-terminal ends (which are crucial for many tubulin functions, such as binding the microtubule-associated proteins), we were able to study their switching between different conformational ensembles under the effects of EEF. These C-terminal ends are very sensitive to the effect of EEF since they are negatively charged and intrinsically disordered.

Keywords: tubulin subTHz electric fields non-equilibrium molecular dynamics

Contents

Introduction	4
1 Why tubulin?	5
1.1 The role of tubulin	5
1.2 Microtubule dynamics	7
1.3 C-terminal ends	9
1.4 Drugs targeting the tubulin	10
1.5 Microtubules and neurons	11
2 Electric field effects on proteins	13
2.1 Electric field effects on tubulin dimer	13
2.1.1 Experimental studies	14
2.1.2 Computational studies	16
3 Essentials of Molecular Dynamics simulations	18
3.1 Classical Molecular Dynamics	19
3.2 Force fields	19
3.3 Periodic boundary conditions	22
3.4 Minimum Image convention	23
3.5 Long-Range Interactions	24
3.5.1 van der Waals interactions	24
3.5.2 Electrostatic interactions	24
4 Hamiltonian systems	28
4.1 Hamiltonian mechanics	28
4.2 Statistical mechanics	32
5 Non-Hamiltonian systems	35
5.1 Generalized Liouville equation	36
5.2 Nosé equations	38
5.3 Nosé-Hoover equations	40
5.4 Pressure coupling	44
6 Simulation workflow	46
6.1 PDB structure and Solvation	46
6.2 Minimization	46
6.3 Equilibration	47
6.4 Production run	48
6.4.1 Directions of applied Electric Field	49
6.4.2 Rotation of icosahedron program	51
6.5 Trajectory conversion	51
7 Methods	53
7.1 Root Mean Square Deviation (RMSD)	53
7.2 Root Mean Square Fluctuations (RMSF)	53
7.3 Rotational analysis	54

7.4	Analysis of dipole moment dynamics	54
8	Results	56
8.1	Outline	56
8.2	RMSD Analysis	56
8.2.1	RMSD - Batch 1	56
8.2.2	RMSD - Batch 2	68
8.2.3	RMSD - Batch 3	80
8.3	RMSF of residues	91
8.3.1	Tubulin α	93
8.3.2	Tubulin β	94
8.4	RMSF of residue - averaged over whole batches (initial conformations and directions)	95
8.4.1	Tubulin α	96
8.4.2	Tubulin β	96
8.5	RMSF of selected residues that make up a binding site	97
8.5.1	Binding site of colchicine	108
8.5.2	Binding site of Paclitaxel	117
8.6	Rotational analysis	130
8.7	Dipole Moment Analysis	146
8.7.1	Dipole moments of the whole tubulin dimer	146
8.7.2	Dipole moments of the tubulin dimer without C-termini	154
9	Discussion	158
9.1	Conformational changes	158
9.2	Rotational movement	164
9.3	Our decisions throughout this work	165
	Conclusion	166
	Bibliography	168
	List of Figures	176
	List of Tables	196
10	Appendix	197
10.1	Input parameter files	197
10.1.1	Energy Minimization parameter files	197
10.1.2	NVT solvent equilibration parameter file	198
10.1.3	NPT solvent equilibration parameter file	199
10.1.4	NPT - equilibration of unrestrained protein	201
10.1.5	Simulation with electric field	202
10.2	Rotation of icosahedron vertices - program	203
10.3	Trajectory conversion script	210
10.4	Rotational analysis - Python script	211
10.5	Dipole moment analysis - Python script	214
10.6	RMSF of residues - original data	218
10.6.1	Tubulin α - Batch 1	218

10.6.2	Tubulin α - Batch 2	225
10.6.3	Tubulin α - Batch 3	233
10.7	RMSF of residues - original data	240
10.7.1	Tubulin β - Batch 1	240
10.8	RMSF of residues - original data	240
10.8.1	Tubulin β - Batch 1	240
10.8.2	Tubulin β - Batch 2	248
10.8.3	Tubulin β - Batch 3	255
10.9	RMSF _{diff} of residues - individual simulations	263
10.9.1	Tubulin α - Batch 1	263
10.9.2	Tubulin α - Batch 2	270
10.9.3	Tubulin α - Batch 3	278
10.9.4	Tubulin β - Batch 1	285
10.9.5	Tubulin β - Batch 2	293
10.9.6	Tubulin β - Batch 3	300
10.10	Averaged RMSF _{diff} over all batches (initial conditions and direction of EF)	308
10.10.1	Tubulin α	308
10.10.2	Tubulin β	315
10.11	RMSF of residues - averaged only over initial conditions	324
10.11.1	Tubulin α	324
10.11.2	Tubulin β	339
10.12	RMSF - Binding sites of vinca alkaloids	354
10.13	RMSF - Binding sites of colchicine	357
10.14	RMSF - Binding sites of paclitaxel	362
10.15	Rotational dynamics	370
10.16	Dipole moment graphs	377
10.17	What did not make it into the thesis	388

Introduction

A modulation of microtubules' dynamics by the electric field of various characteristics (static, alternating, pulsed) has been of great interest in recent years, due to the possible anti-cancer effects of such fields. Microtubules are tubular structures that have many crucial roles inside the cell, one of which is also a cell division. Hence, why targeting these proteins with electric fields can have anti-tumor properties. These microtubules consist of tubulin dimer subunits, which have been a centre point of this *in silico* study. Already, a vast amount of studies, experimental or computational, have been published that try to elucidate the action of different electric fields on these essential protein structures. In this work, alternating electric fields in subTHz range (10-150 GHz) in 6 different directions were applied, and structural and dynamical properties of the tubulin dimer were consequently investigated by molecular dynamics simulation.

This work is divided into the following Chapters:

1. In the first Chapter, we will briefly mention the most important parts of biochemistry and the importance of the tubulin dimer in living systems.
2. Next, the research that has already been done on electric-field effects on tubulin and microtubules is summarized.
3. An intro to classical molecular dynamics simulations is presented in this chapter.
4. To dive a bit deeper into the theory behind molecular dynamics, we also included Chapters about Hamiltonian,...
5. ... and Non-Hamiltonian mechanics, where we presented the emergence of state propagators in molecular dynamics simulation.
6. Chapter named Simulation workflow is a collection of important information regarding how the simulations were set.
7. The results of those simulations and their descriptions are provided.
8. Interpretation of the results with potential implications are theorized.
9. Concluding remarks are stated, and potential outlooks are discussed.
10. The majority of Figures are depicted in the Appendix. Some of the codes, scripts, and simulation parameter files are also presented.

1. Why tubulin?

1.1 The role of tubulin

In the world of cellular dynamics, tubulin dimer can be considered as one of the fundamental building blocks of eukaryotic cells. Tubulin is a protein of 110 kD. It is also a heterodimeric protein, which means it consists of two monomers named α -tubulin and β -tubulin. These tubulin $\alpha\beta$ subunits polymerize and form polar protofilaments, which connect laterally to form a hollow tube-like structure called a microtubule. Even though the number of protofilaments that make up a microtubule can vary, the most common case of a microtubule consists of 13 protofilaments. The so-called minus end of the microtubule, capped by α -tubulin, is usually attached to microtubule organizing centres, which are located near the nucleus of the cell. The plus end of the microtubule, which is capped by β -tubulin, is the site of growth or shrinkage of the microtubule. These microtubules have a crucial role - they form, together with other filaments, the cytoskeleton of a cell, and thus, they provide its shape and structure and connect the cell to the extracellular environment. [1]

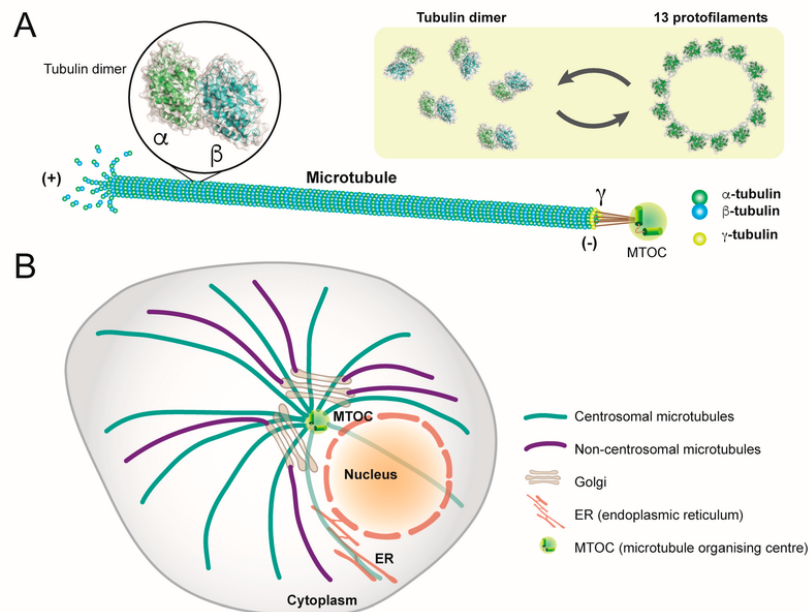


Figure 1.1: A - Tubulin dimer consisting of α and β tubulin subunits can form microtubule - tubular structures made of usually 13 protofilaments. There is another special form of tubulin called γ that is used to anchor the minus ends of microtubules to MTOCs; B - A model of a cell. In the cytoplasm, microtubules create dynamic networks that are stably anchored at MTOCs, such as the centrosome and Golgi apparatus; the illustration taken from [2]

Additionally, microtubules also make up cilia and flagella, which are protruding hair-like structures of the cell, which can convert chemical energy into

mechanical one, therefore acting as a fundamental unit of cellular motion.

Even more importantly, microtubules provide a means of transfer of the cell's "goods" with the help of motor proteins kinesin and dynein, which can move along these microtubules while holding and transporting a cell's cargo. This intracellular transport is involved in a variety of cellular processes and many different macromolecular assemblies, organelles or secretory vesicles are moved by these structures.

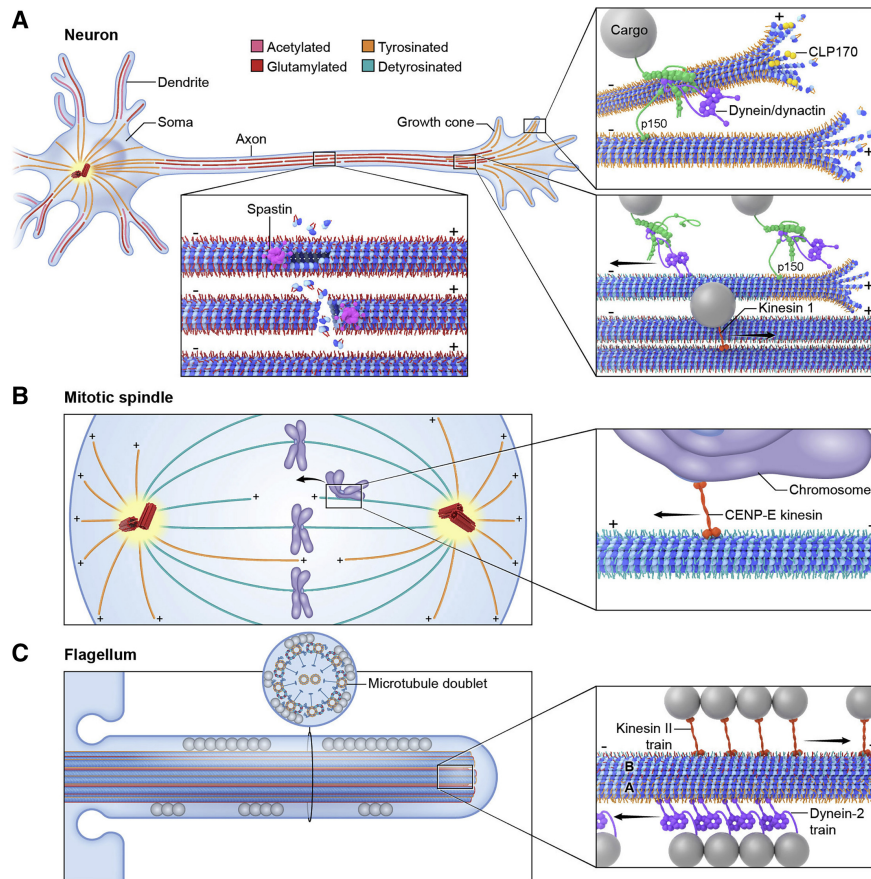


Figure 1.2: A - A depiction of the different post-translational modifications of tubulin in a neuron model; also, kinesin and dynein “walking” on these microtubules are also shown here. B - A depiction of mitosis, where kinesin is connected to the chromosome and walks along the microtubule. C - A flagella is depicted, we can again see the movement of cargo via kinesin and dynein along the microtubule; the illustration is taken from [3]

One of the most important tubulin functions is their role in cell division, whether it is mitosis or meiosis. Microtubules made of tubulin heterodimers form mitotic spindle during the M-phase of eukaryotic cell division. During mitosis, they connect to the kinetochores of the chromosomes and provide the means to take chromosomes apart from each other and hence divide the cell.

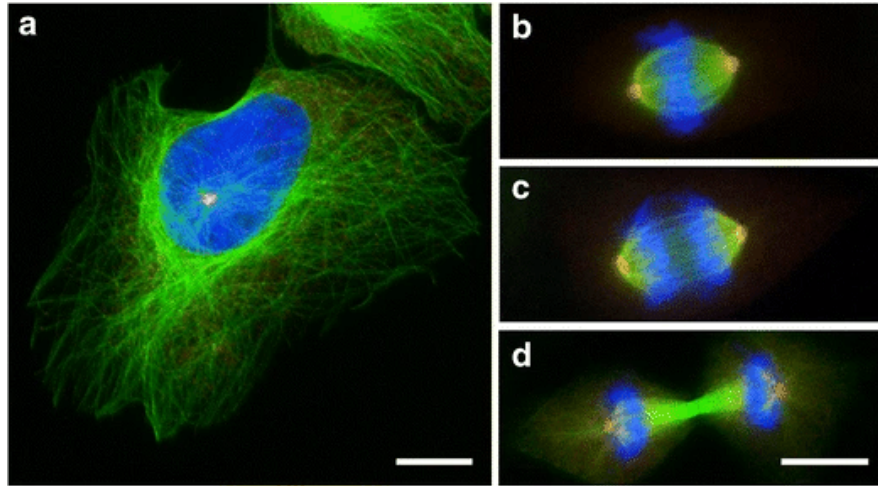


Figure 1.3: Human osteosarcoma cells in different phases of mitosis - **a** interphase, **b** metaphase, **c** anaphase, **d** telophase. α tubulins are stained with polyclonal antibody (green), γ tubulin with monoclonal antibody TU-30 (red) and DNA by DAPI(blue). Bars = 10 μm ; the illustration is taken from [4]

1.2 Microtubule dynamics

The tubulin dimer, comprising α - and β -tubulin subunits, is central to microtubule dynamics. Both tubulin subunits house a guanosine nucleotide binding site. The α tubulin houses a guanosine-triphosphate(GTP) which is non-hydrolyzable and therefore this site is called the "N-site". In the β -tubulin's binding site, both the guanosine-triphosphate (GTP) and guanosine-diphosphate (GDP) can reside. When the tubulin-dimer is not a part of the microtubule and is free in a solution, this binding site on β tubulin allows the exchange of nucleotide that resides there, hence it is known as the "E-site". But when this dimer is bound in a microtubule, the nucleotide is non-exchangeable [5].

GTP-bound tubulin dimers exhibit a higher affinity for neighbouring subunits, promoting polymerization and microtubule growth. GTP-bound tubulin subunits form the growing plus-end, known as GTP-cap, which recruits various microtubule-associated proteins, including end-binding proteins, microtubule polymerases, depolymerases, and kinesins, which collectively regulate microtubule dynamics [5].

Shortly after the GTP-tubulin dimer incorporation into the microtubule lattice, GTP bound to the β -tubulin subunit undergoes hydrolysis, resulting in a phosphate release. What remains bound to the β -tubulin in the microtubule lattice is the GDP. Therefore, tubulin acts as a GTPase, and the GTP hydrolysis is considered to be the pivotal event governing a microtubule behaviour [5].

The state of the nucleotide — GTP or GDP — in the E-site dictates the stability and dynamics of the microtubules. GDP-bound tubulin dimers are inherently less stable and more prone to depolymerization. Therefore, the loss of stabilizing GTP-cap triggers rapid microtubule shrinkage, known as a "catastrophe," while occasional rescue events, where microtubules regain stability and resume their growth, can happen. This stochastic switching between the phases of shrinkage and growth of microtubule demonstrates its dynamic instability and is intricately linked to the GTP/GDP-bound tubulin dimer ratio along the polymer, together

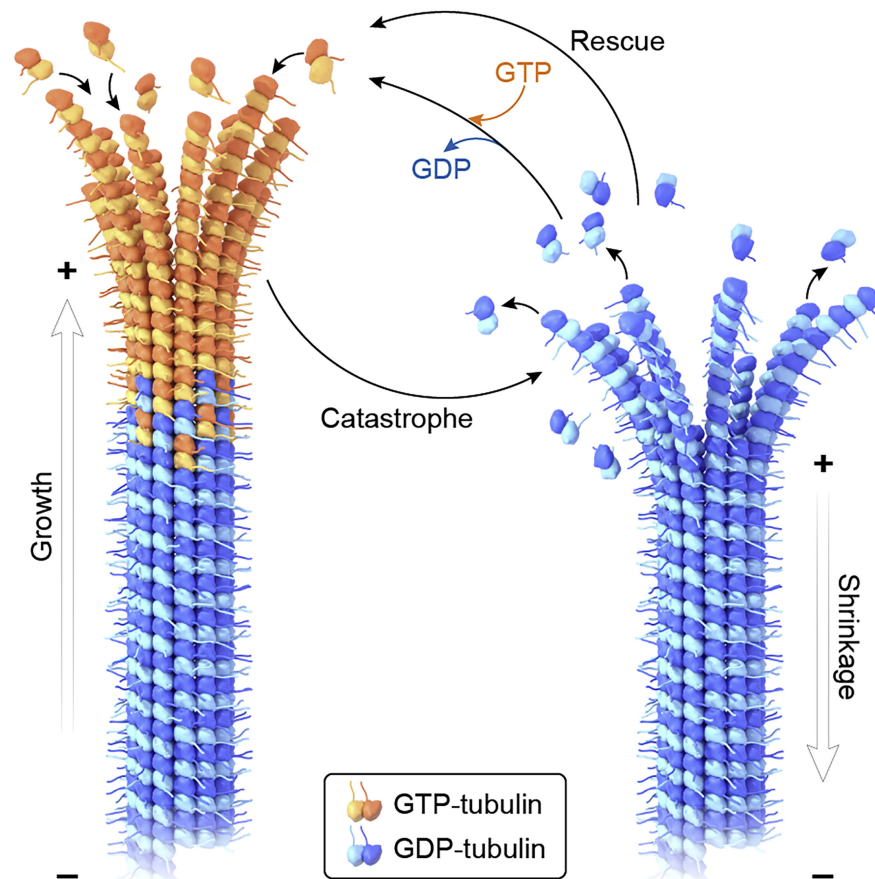


Figure 1.4: Dynamic instability of microtubules, during the catastrophe, the rate of phosphate release from the GTP cap is higher than the addition of new GTP tubulins. During the rescue, it is vice versa; the illustration is taken from [3]

with many different factors that affect the tubulin, such as previously mentioned MAPs or external forces. This kind of regulation of microtubule behaviour ensures precise control over cytoskeletal dynamics [1, 6].

Additionally, the GTP/GDP exchange on tubulin dimers plays an important role in cellular processes such as intracellular transports. Molecular motors such as kinesins and dyneins, which provide a means of transport of various cargo molecules, can be bound to the microtubules, which represent "freeways" in the intracellular world. The nucleotide state of tubulin directly influences motor protein binding and motility, with the GTP hydrolysis often triggering cargo release or motor detachment [1].

Tubulin assemblies exhibit a range of conformations: curved shapes are prevalent in single protofilaments and unpolymerized states, while straight configurations dominate within microtubules, featuring variations in length known as expanded and compacted states. Tubulin goes through these periodically and this cyclic change in conformation reflects a mechanical phenomenon, where the tension-relieved, yet stabilized, straight configurations experience release of stress during depolymerisation, possibly exerting mechanical work [1, 6].

Understanding the intricacies of the tubulin-dimer dynamics has far-reaching implications. Dysregulation of microtubule dynamics is implicated in various diseases, including cancer and neurodegenerative disorders, highlighting the ther-

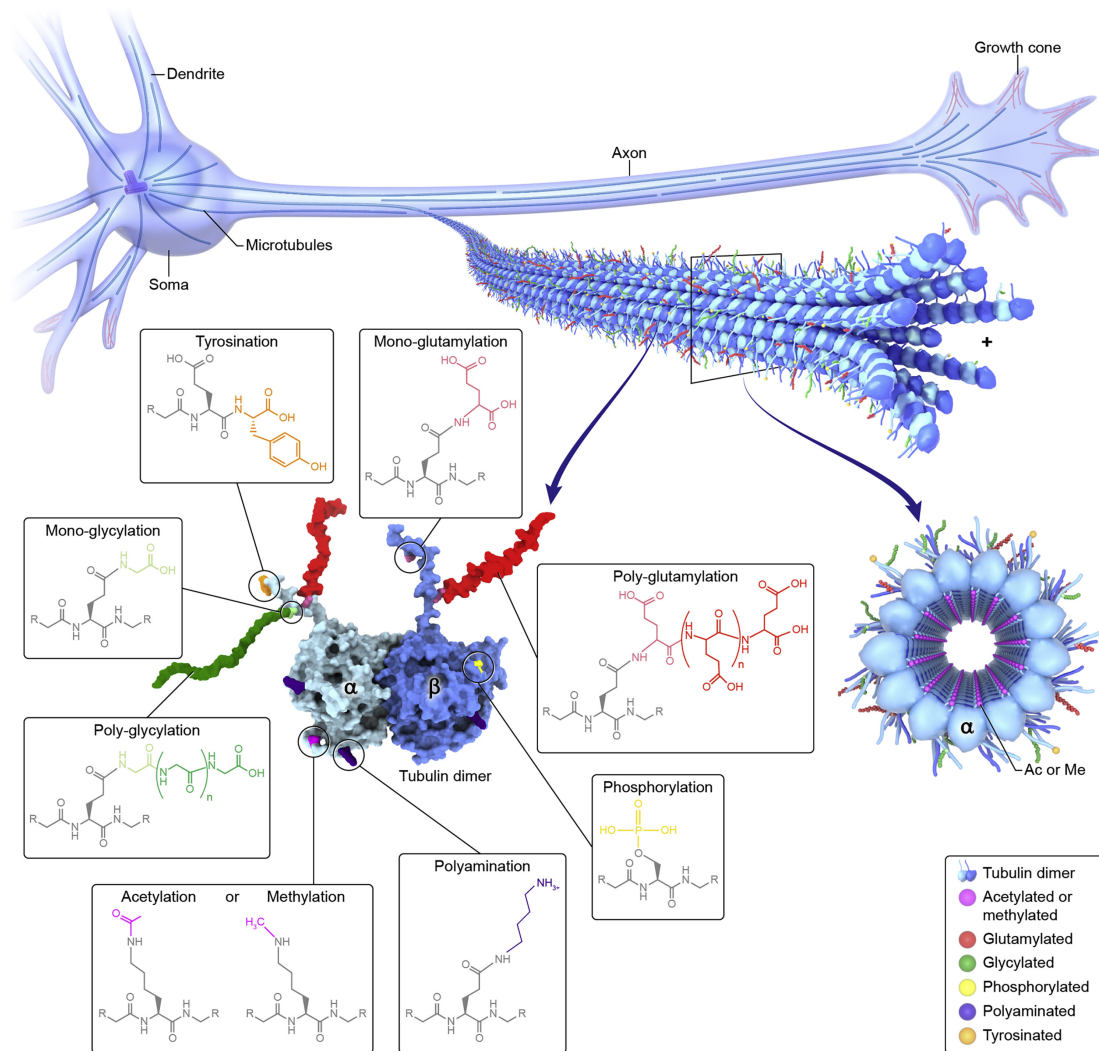


Figure 1.5: Post-translational modifications of tubulins; the illustration is taken from [3]

apeutic potential of targeting tubulins and associated regulatory proteins. The studies that will be mentioned in the next chapter have shown that external electric fields can have profound effects on the protein assembly or disassembly and, thus, on its function.

There exists a vast amount of isotypes of these tubulin subunits. Moreover, the tubulin also undergoes a variety of post-translational modifications, such as acetylation, phosphorylation, and polyamination [7]. These influence the dynamics of the protein and are subjects of studies on their own. The primary sites for post-translational modifications are C-terminal ends. See Figure 1.5.

1.3 C-terminal ends

C-terminal ends, or how we will call them further in this work - C-termini, are intrinsically disordered domains of the tubulin dimer. The intrinsically disordered domains (IDD) do not possess a fixed conformation, but due to their rapid movement keep switching between the collection of states called conforma-

tional ensemble. It seems that the correct conformational ensemble is crucial for a protein to function as intended [8, 9]. The intrinsic flexibility of the IDD has advantages, such as increased speed of interaction and ability to bind to a variety of molecules.

When it comes to C-termini, it was shown in [10] that their genetic deletion makes a microtubule more sensitized to the destabilizing drugs. Additionally, deleting the β tubulin C-terminus causes mitotic defects [10]. C-terminal ends have also been found to be important for the formation and function of cilia [11, 12]. Therefore, it seems that the change of this conformational ensemble of the tubulin's C-termini leads to the change of tubulin's function. Since these C-termini are very flexible, there are not that many studies done on their conformational ensemble. Experimentally, they are very hard to resolve unless they are bound to associated proteins. In this way, the X-ray crystallography and cryo-electron microscopy have revealed the conformation of the bound state, which does not coincide with the conformational ensemble of the free C-termini [13, 14, 15]. When it comes to theoretical (molecular dynamics) studies, people prefer to simulate the tubulin without the C-termini since a bigger simulation box is needed for this, and hence, a lot more water molecules (or other solvent molecules) are needed. This causes the simulation to run longer and requires a lot more storage.

1.4 Drugs targeting the tubulin

Various known drugs can influence the dynamic equilibrium between the polymerization of $\alpha\beta$ dimer into microtubules and their depolymerization. An abundance of studies have already shown the pivotal role of microtubules in cancer biochemistry justifying the tubulin being a target for drug development. We can divide these tubulin-binding drugs into two families: microtubule stabilizers and destabilizers. Together they are also known as anti-tubulin drugs. Interestingly, both of these types of drugs disturb the microtubule dynamics and as a result act as anti-mitotic agents, stopping the cell division. After binding to the specific sites on tubulin, the mitotic spindle dynamics is suppressed resulting in a mitotic arrest, which leads to cell death. [16]

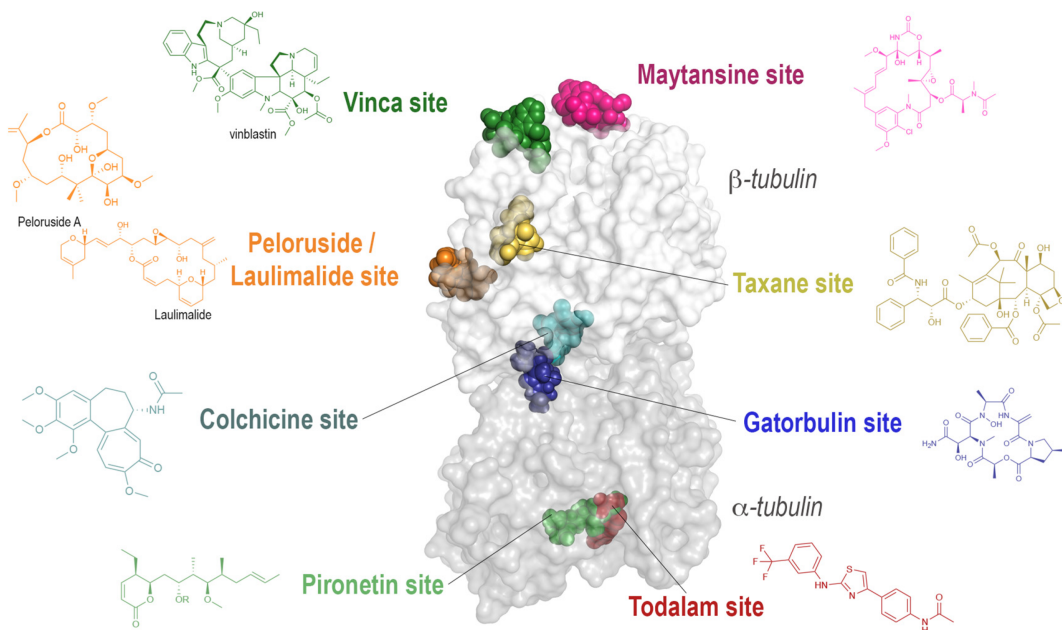


Figure 1.6: Antitubulin agents and their binding sites; the illustration is taken from [16]

Colchicine, taxanes or vinca alkaloids (such as vincristine and vinblastine) are all examples of microtubule destabilizers, which inhibit microtubule polymerization whereas paclitaxel, docetaxel or epothilones are examples of the microtubule stabilizer. These antimetabolic agents bind to various binding sites. 27 distinct binding sites have been identified; of these 11 have been found quite recently [17]. The well-documented binding sites are the laulimalide, taxane/epothilone, vinca alkaloid and colchicine sites. Other ones are pironetin, todalam, gatorbulin or maytansine sites. All of these can be viewed in Figure 1.6.

When the hydrolysis of GTP undergoes in the β -tubulin, the microtubule lattice is destabilized and that causes an increased curvature of the protofilaments. This puts a strain on the lattice [18]. Paclitaxel, a stabilizer of microtubule binds to β -tubulin subunits and stops the disassembly of microtubules [19]. This in turn causes chromosomes to be unable to form a metaphase spindle configuration. Mitosis is therefore blocked and apoptosis of the cell is triggered [20, 21]. What paclitaxel does is that it straightens the GDP tubulin heterodimers inside microtubules. As a consequence, the transition from a straight configuration to a curved configuration is slowed down [18]. These tubulin dynamics-disrupting drugs are widely used in cancer chemotherapy and many novel drugs are being investigated.

1.5 Microtubules and neurons

Microtubules play a crucial role in the structure and function of neurons, and their disruption can lead to problems with transport and organization within a cell causing neurodegenerative diseases. In ‘Microtubules in health and degenerative

disease of the nervous system', Baas *et al* (2016) [22] reported that microtubules in neurons play a crucial role in maintaining specialized morphologies, transporting proteins and organelles, and contributing to early developmental stages.

Microtubules are essential for the development and maintenance of axons and dendrites throughout the life of the neuron and are vulnerable to degradation and disorganization in a variety of neurodegenerative diseases. In the axons, microtubules are for the most part uniformly oriented with the plus ends reaching out, whereas, in dendrites, microtubules have mixed orientations [23, 24, 25]. The minus domain of microtubules in developing neurons is stable, whereas the plus domain is labile [26]. Abnormalities in microtubule systems, such as microtubule mass being diminished are linked to neurodegenerative diseases when polarity patterns of microtubules and consequently also the microtubule-mediated transport are corrupted [22]. Neurons need to maintain the correct polarity of microtubules in their axons to work properly, and that is why they have developed a mechanism, where dynein is transporting misaligned microtubules back to the cell body [27]. Therefore, the disruption of this mechanism can lead to microtubule loss, which is seen in neurodegenerative disorders. Whether the microtubule disorganization is a primary causative factor of neurological diseases or whether it is a secondary effect, does not change the fact that potential correction of these abnormalities in microtubule networks could lead to an improvement of the ill-effects of nervous system diseases.

2. Electric field effects on proteins

Plenty of studies have shown the effects of the EEF on the dynamics or structure of biomolecules in general. It is known that electrostatic interactions are crucial for protein stability and function. Strong intrinsic electric fields mediate protein-ligand interactions, protein-solvent interactions [28, 29] or protein folding [30]. Exposing proteins to external electric fields (EEF) may alter their structural properties, leading to potential consequences to their function. Molecular dynamics simulations have already shown that electric fields affect conformations of many proteins, such as insulin [31, 32, 33], lysozyme [34, 35, 36, 37], β -amyloid [38, 39], myoglobin [40, 41], and many more.

2.1 Electric field effects on tubulin dimer

When it comes to microtubules, their tubular structure and relatively high elasticity [42] have raised questions about whether they can act as waveguides or cylindrical resonators for electromagnetic radiation [43, 44, 45]. Potential coupling with radiation could induce longitudinal vibrations within microtubules [46]. Theoretical studies have proposed microtubules exhibiting vibrations in the MHz-GHz range [46, 47]. Additionally, experimental observations have confirmed that electromagnetic radiation in this range can facilitate microtubule self-assembly [48] and disassembly [49].

Given the potential interactions between electric fields and proteins, along with the widespread use of GHz electric fields in daily life, particularly in communication technologies, it is crucial to consider the effects of such fields on the structure or dynamics of microtubules that can lead to an alteration of the dynamic instability of microtubules, therefore to their improper function and potential cell death.

From the point of view of material science, microtubules are interesting adaptive natural material and have a central position in bioinspired materials research. However, controlling the dynamics of the tubulin system is still a challenge. Electric fields of a particular frequency could be the answer to such control.

In the previous section, we have mentioned the use of different drugs, which could either stabilize or destabilize the microtubules and which are used in cancer chemotherapy. A question is whether a similar behaviour can be reached with an application of the external electric fields instead of drugs such as paclitaxel or vinblastine, which affect the mechanical properties of microtubules.

In the next sections, we will mention just a fraction of the research done on the phenomena of external electric fields on tubulin and microtubules observed either by molecular dynamics or experimentally. It will be shown, that specific electric fields do affect the structural properties of microtubules. Therefore, more research into these effects and in different frequency range, could lead to a potential outside control of microtubule dynamics, which could be useful in the treatment of diseases that are associated with microtubules, such as cancer.

2.1.1 Experimental studies

A study from 2021 [49] showed an inhibition of the microtubule dynamics, in particular, significant disassembly of the microtubules by exposure to the train of intense THz pulses of a picosecond duration. The authors showed that the rate of disassembly is dependent on the intensity and the frequency of the radiation. They used THz bandpass filters to transmit narrow 0.5 THz and 1.5 THz bands and compared them to broadband exposure in order to probe the spectral dependence of the protein disassembly. They found that disassembly after using 0.5 THz radiation is faster even for significantly lower field strength and lower doses than for the 1.5 THz radiation. This means that the microtubule disassembly by THz radiation is significantly frequency dependent. The broadband measurement also supported this explanation since it showed that mainly low-frequency energy caused the microtubules to disassemble, while the high-frequency EF did not lead to a disassembly but instead was probably absorbed by the media or thermalized.

In their study, they took into consideration the thermal effects or field-induced shockwaves that can also influence the effect of THz radiation on the microtubules. To ensure negligible heating of the media, they used only a limited amount of radiation - 1kHz train of picosecond-duration pulses, while the maximum temperature increase per pulse is estimated to be roughly 5 mK. They measured the average steady-state heating due to this pulse trains with a thermal imager to be less than 1 K. They used taxol-stabilized microtubules that are stable at room temperature for several hours and are, therefore, usually used in experiments to control for thermal effects. Additionally, at higher temperatures, the taxol-stabilized microtubules tend to polymerize even faster. Therefore, the opposite effect of disassembly supports the evidence that the THz radiation affects the biological structure non-thermally by coupling to the oscillatory dynamics of microtubular structures.

Regarding the shockwave effects, they assumed that the shockwave amplitude is probably not sufficiently large to produce such a significant effect, but it could not be proved by their study and, therefore, should be explored in the future. Nevertheless, the effects of THz radiation on microtubules suggest a potential therapeutic use for cancer and other microtubule-associated diseases.

The Chafai *et al.* study [50] shed light on the promising potential of modulation of the tubulin self-assembly by the intense nanosecond pulsed electric fields. Electric fields applied were in the form of DC pulses. The applied voltage pulse width was 11 ns and the frequency of the repetition was 1 Hz. The number of pulses was a variable parameter. Their study was done *in vitro* and showed that nanosecond electropulses (nsEPs) induced conformational changes and electrostatic forces disequilibrium in tubulin, affecting its polymerization capability. The effects of nsEPs on tubulin dimer were evaluated by autofluorescence of tryptophan and tyrosine since their fluorescence is dependent on the local environment, and therefore, they can be used to probe conformational changes. Dose-dependent changes, such as peak shift to the blue region and change of peak intensity, were observed.

The authors theorized that changes in the C-termini of tubulin dimer, which are altered by the pulses the most, can allosterically change the structure of the rest of the tubulin, where fluorescent aromatic residues reside. The find-

ing that conformational changes due to nsEPs are initiated at C-termini, which have a high negative charge, was also supported by zeta-potential measurements and dynamic light-scattering measurements, from which hydrodynamic radii of the tubulin were obtained. The authors proposed that the fluorescence quenching implicates changes in the binding sites on the tubulin body and that these conformational changes follow after the C-termini changes, all due to nsEPs. Whether the change is reversible or irreversible depends on the nsEPs dose.

Additionally, atomic force microscopy showed that after the application of nsEPs, the structures formed by tubulins differ from the untreated tubulins. Tubulins that were not treated by nsEPs formed typical microtubule structures - tubular or collapsed structures, whereas tubulin treated with nsEPs produced open-up structures - see Figure 2.1. This work showed that nsEPs can cause reversible or irreversible changes to the tubulin structures and that the dosage of nsEPs determines whether the polymerization-competent conformation can be recovered.

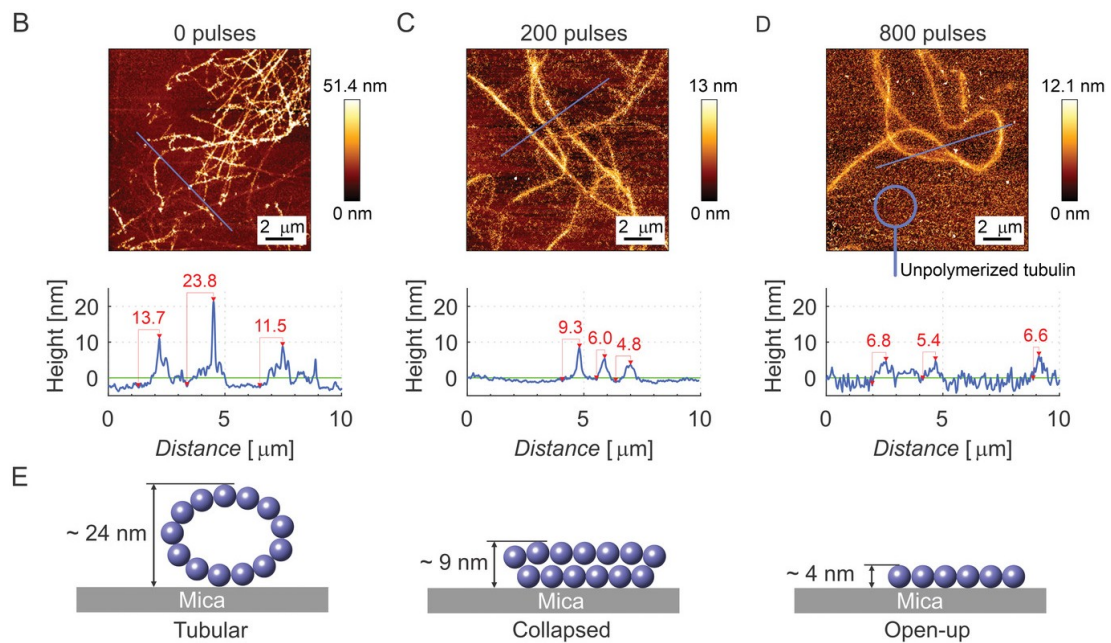


Figure 2.1: Atomic force microscopy images of structures formed from B) untreated tubulin, C) treated tubulin by 200 pulses, D) treated tubulin by 800 pulses. In D) the schematic representations of those structures are depicted; [50]

In the following study from 2020, Djamel *et al.* [51] looked at the changes caused by nanosecond pulsed electric fields (nsPEFs) in microtubule networks in vivo. They probed the effects of different values of nsPEFs and found a minimal nsPEF dosage that is needed to disrupt the microtubules in different types of cells. After the application on nsPEFs, they studied the microtubule recovery or cell apoptosis. They found out that nsPEFs resulted in the modulation of microtubule binding properties to the end-binding protein EB1. It was shown that nsPEFs can trigger the remodelling of microtubule networks instead of complete destruction and that the dose depends on the cell type. Additionally, the environment also played a role in network rearrangements. In the low-conducting buffer, microtubules in cells depolymerized after the administration of nsPEFs, however,

microtubules afterwards recovered in the cell culture medium. Cells that were treated by nsPEFs in a culture medium were only remodelled, not depolymerized. This can have implications for the engineering of self-healing materials and other nano-biotechnological applications.

When it comes to these nsPEFs of 10s and 100s of kV/cm that are of ns duration, many *in vitro* and *in vivo* studies on cancer cells were done and showed remarkable anti-cancer effects.

As an example, in the study done in 2012 by Dong Yin et al. [52], the therapeutic efficacy of nsPEF in treating cancer cells both *in vitro* and *in vivo* was investigated. The authors utilized a prototype medical device - nsPEF generator capable of delivering pulses ranging from 7 to 30 nanoseconds in duration at programmable amplitudes and frequencies. The study demonstrated that nsPEF induced apoptotic pathways in various cancer cell lines, with cell death rates depending on the voltage and number of pulses applied. In an animal model of carcinogen-induced tumours, particularly cutaneous papillomas and squamous cell carcinomas, the nsPEF treatment with 14 nanosecond pulses efficiently eliminated lesions after one treatment session, and in some cases, complete removal was achieved after the next treatment session. The therapeutic effect was associated with reduced expression of anti-apoptotic proteins and increased apoptosis. This research suggests that nsPEF holds promise as a potential therapy for human squamous carcinoma.

When it comes to fields of 100-300 kHz frequency range, also known as TTF - tumor treating fields, as the name suggests, these EFs showed an evident inhibitory effect on the growth of different kinds of human and rodent tumour cells. Moreover, the authors of [53] also showed the inhibition of growth in human brain tumours *in vivo*. Besides the antimetabolic effects of TTF, perturbation of cell migration, permeability and immunological responses have been observed [54]. So even though these fields disrupt the microtubules *in vitro*, no sole mechanistic action has been proven as the culprit. The anti-tumour effect of TTF probably stems from all the effects above.

Administration of these TTF was already implemented by the newly developed device called Optune (R), which is already approved by the FDA to treat glioblastoma [55, 56, 57].

2.1.2 Computational studies

To complement the information regarding nsPEFs from the experimental section of this chapter, we will also mention a theoretical study published in 2018 by Timmons *et al.* [58]. These authors performed molecular dynamics simulations, where external EFs (EEFs) from 50 to 750 kV/cm were applied for 10 ns to a tubulin dimer. Changes in flexible regions, such as C-termini, loops (most importantly α :H1-B2, β :M-loop) were the most evident. Since the mentioned loops are crucial for lateral interactions of microtubules, a change in their native rigidity could cause the microtubule to collapse. Additionally, they observed the tubulin to elongate and slightly bend under the effect of EEF.

Research of H. R. Saedi & A. Lohrasebi [59] in 2014 showed that the me-

chanical properties of the tubulin heterodimer were affected by the application of static or 1 GHz oscillating electric field. The simulations in this work and the next two that followed were done in a way that mimics an AFM experiment and, therefore, probes the elastic constant of the structures. In the case of the constant electric field of 0.03 V/nm, Young's modulus of the heterodimer was decreased. On the other hand, Young modulus was increased when an oscillating 1 GHz electric field was applied to the structure.

In the following work of A. Lohrasebi with S. S. Setayandeh [60] the influence of GHz electric fields on the mechanical properties such as Young's modulus of tubulin heterodimers in microtubules were studied again and the results agreed with the previous study that the Young's modulus of the microtubules, which were under the effect of electric fields, differed from the unperturbed case. Moreover, the exact frequency of the applied electric field was crucial since the protein became more rigid for the frequencies 2, 5 and 7 GHz and more flexible for the 1 or 6 GHz. Since the change of rigidity of microtubules can affect the cell division rate, an external 1-10 GHz electric fields could potentially be used as an alternative to the tubulin-binding drugs for chemotherapy, such as taxol, which also causes the microtubules to become less rigid.

S. S. Setayandeh and A. Lohrasebi [61] continued the research of the electric-field effects on tubulin dimer. In the next work, they investigated the effects of external electric fields of 900 MHz and 2450 MHz and the peak intensity of 0.01 V/nm on tubulin heterodimer alone - denoted as system A and on tubulin heterodimer stabilized by paclitaxel - denoted as system B. Besides Young's modulus determination, root mean square deviations (RMSD) of the atoms of tubulin heterodimers were also calculated. Bigger the value of RMSD of tubulin atoms the more flexible the structure is. The paclitaxel was found to make tubulin heterodimer more rigid. The electric field of 900 MHz induced more fluctuations into the system B (tubulin+paclitaxel), therefore making it less rigid than that of 2450 MHz. Additionally, both electric fields made systems A and B more flexible than in the case of no electric field. Changes in the rigidity of the tubulin heterodimer affected the speed of straight-to-curved conformation transitions of the microtubule protofilaments. Moreover, it was found that the system B was affected by electric fields to such an extent that as a consequence they could negate the therapeutic effect of paclitaxel, whose main function is to stabilize microtubules - making them more rigid. At the same time, for the system A, a change of its normal rigidity can cause the cells to become cancerous, authors theorised. Since 2450 MHz is in the microwave region, whereas 900 MHz is in the range of cell phone frequencies, one should take these effects into consideration when dealing with chemotherapy by paclitaxel.

3. Essentials of Molecular Dynamics simulations

Molecular Dynamics (MD) is a computational methodology which allows us to study molecular systems of various sizes. These *in silico* studies complement experimental ones and usually try to explain the experiments or provide further proof of the outcome of the experiment. We can divide Molecular Dynamics into classical MD, *ab-initio* MD and quantum-mechanical MD. In a classical MD, we are taking into account the motions of atoms, which are explained by the laws of classical molecular mechanics. We do not consider the inner structure of an atom. In the *ab-initio* MD, we do consider the electronic structure, which is, of course, described by quantum mechanics, but the motion of nuclei is still governed by classical mechanics. The holy grail is the quantum mechanical MD, where quantum mechanical laws are applied to a whole system - electrons and also nuclei.

The reason behind using the approximate versions of MD is due to the lack of computational power to simulate large systems or even smaller systems for a long period of time. Classical molecular dynamics is able to describe systems of the order 100 000 atoms for up to several μs , which, unfortunately, the *ab-initio* MD is not capable of doing yet. Due to the progress in quantum computation, this can change in the future. To see the feasible timescales and sizes of the system of interest that can be simulated by different types of MD, see Figure 3.1

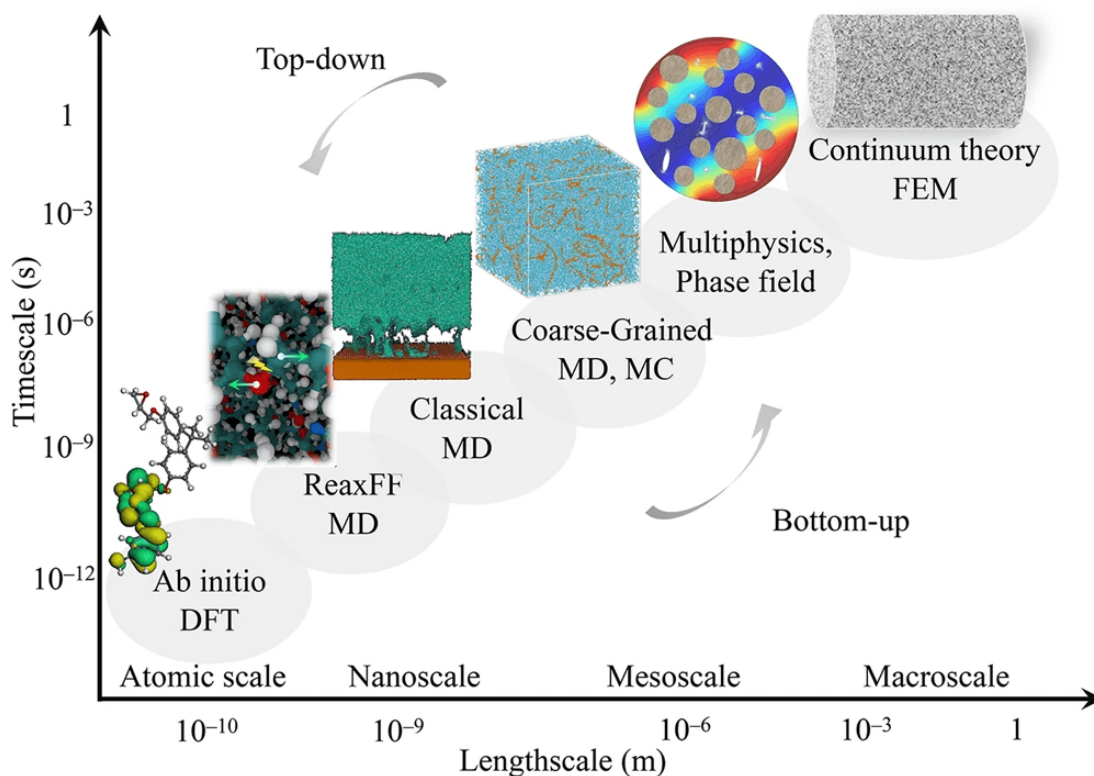


Figure 3.1: Timescales and lengthscales accessible by different types of physical system simulations; the illustration taken from [62]

3.1 Classical Molecular Dynamics

Even though the true behaviour of physical systems in the nanoscale is governed by quantum mechanics, classical molecular dynamics has proven to be a good approximation for a wide variety of systems. Given the initial conditions - coordinates and momenta - one can calculate the forces acting upon the atoms and then numerically solve the equations of motion to get the trajectory of the system of interest. To simulate such systems properly, we need to find the correct forces acting upon the atoms. These are calculated as a gradient of the potential energy surface, which is approximated by some force-field function.

3.2 Force fields

A variety of the so-called force fields (FF) were constructed in the past decades. Each of the force fields is suitable for different kinds of systems. These force-fields have various parameters that are fitted to the outcomes of *ab-initio* calculations or experiments.

The first approximation used is the Born-Oppenheimer approximation, which separates the motions of nuclei and electrons. It assumes that the heavy nuclei move on the so-called effective field, generated by the fast-moving electrons. At first, the time-independent Schrödinger equation for electrons for different nuclei positions needs to be solved for us to get this effective field $U_{\text{electronic}}$. Consequently, nuclei are moving on a potential energy surface U_{total} given by the sum of the effective field and the interaction potential of the nuclei:

$$U_{\text{total}}(\vec{R}_1, \vec{R}_2, \dots, \vec{R}_M) = U_{\text{electronic}}(\vec{R}_1, \vec{R}_2, \dots, \vec{R}_M) + \frac{1}{4\pi\epsilon_0\epsilon} \sum_{A=1}^M \sum_{B>A}^M \frac{Z_A Z_B}{r_{AB}},$$

where M is the number of atoms. This potential energy surface is then approximated by an analytical function called "force field". By doing this we are able to describe the movement of nuclei classically.

In this work we have decided to use a CHARMM36 force field (3.1), which is suitable for simulating biomolecules such as proteins, nucleic acids or lipids [63].

$$U(\vec{R}_1, \vec{R}_2, \dots, \vec{R}_M) = \tag{3.1}$$

$$= \sum_{\text{bonds}} K_b(b - b_0)^2 + \sum_{\text{angles}} K_\theta(\theta - \theta_0)^2 + \sum_{\text{dihedrals}} K_\phi[1 + \cos(n\phi - \delta)] \tag{3.2}$$

$$+ \sum_{\text{Urey-Bradley}} K_{U-B}(S - S_0)^2 + \sum_{\text{impropers}} K_\omega(\omega - \omega_0)^2 \tag{3.3}$$

$$+ \sum_{\text{non-bonded pairs}} \left\{ \epsilon_{AB}^{\min} \left[\left(\frac{R_{AB}^{\min}}{r_{AB}} \right)^{12} - 2 \left(\frac{R_{AB}^{\min}}{r_{AB}} \right)^6 \right] + \frac{q_A q_B}{4\pi\epsilon_0\epsilon r_{AB}} \right\} \tag{3.4}$$

$$+ \sum_{\text{residues}} U_{\text{CMAP}}(\phi, \psi) \tag{3.5}$$

Variables written in blue are the force-field parameters that need to be determined before the simulation itself. The variables in red are the structural input values calculated from the coordinates.

This potential energy function comprises bonded and non-bonded interactions as a function of the atomic coordinates. The six terms (3.2) & (3.3) & (3.5) represent the bonded contributions, where b are the bond lengths, θ are valence angles, ϕ and ψ are dihedral angles and ω are improper angles. Variables with the subscript 0 are the corresponding equilibrium values.

Bonded potentials except the dihedral term are all approximated by harmonic potentials, which makes the CHARMM force-field rather fast for even quite large biomolecular systems.

The dihedral term is a periodic function where n is the periodicity and δ is the phase shift.

Urey-Bradley (U-B) contribution solely exists in CHARMM force-fields and, together with the improper dihedral term, is implemented to optimize the fit to vibrational spectra and out-of-plane motions. U-B is represented by a harmonic potential - a quadratic function of a distance between the atoms A and C when we assume the bonding to be A-B-C.

The CMAP (correction map) term is a correction term for the backbone torsion potential that improves the description of the protein secondary structure leading to more accurate simulations of protein folding and dynamics. The backbone is the name of the main chain of the structure, usually a protein. The inclusion of the CMAP term in CHARMM36 is one of the notable differences compared to the older CHARMM22 FF.

The visualisation of the degrees of freedom of these potentials can be seen in Figure 3.2.

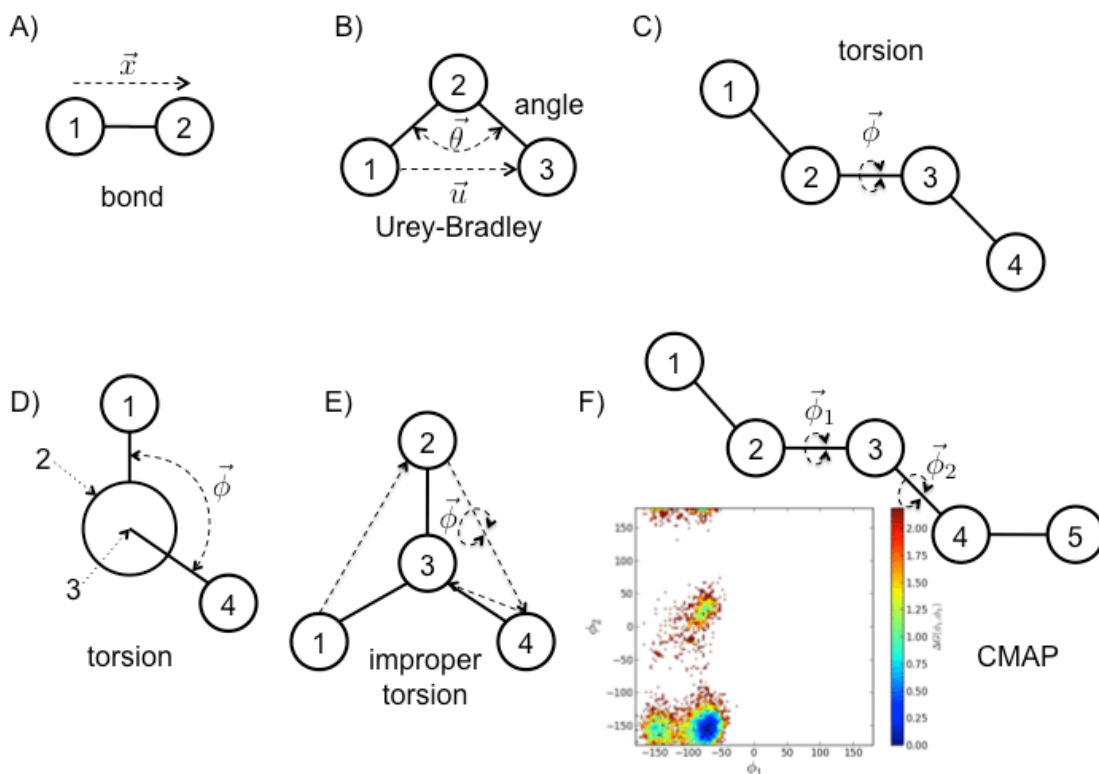


Figure 3.2: Degrees of freedom of the individual force-field potentials; the illustration taken from [64]

Non-bonded terms in (3.4) comprise the Coulombic interaction and Lennard Jones potential, which is an approximation to the core-core repulsion and attractive van der Waals interaction (collective name for dipole-dipole and polarizable interactions such as dipole-induced dipole and induced dipole-induced dipole interactions).

These non-bonded interactions are evaluated for all atom pairs within an already specified interatomic cutoff distance but not for the atoms which are separated by one or two covalent bonds.

In the Coulombic term, when dealing with an explicit solvent in the calculations, the relative dielectric constant ϵ is set to be 1. Therefore, the permittivity $\epsilon\epsilon_0$ corresponds to the vacuum permittivity ϵ_0 .

General Lennard-Jones potential can be seen in Figure 3.3 There are two parameters that need to be assigned to every atom pair within the cutoff distance.

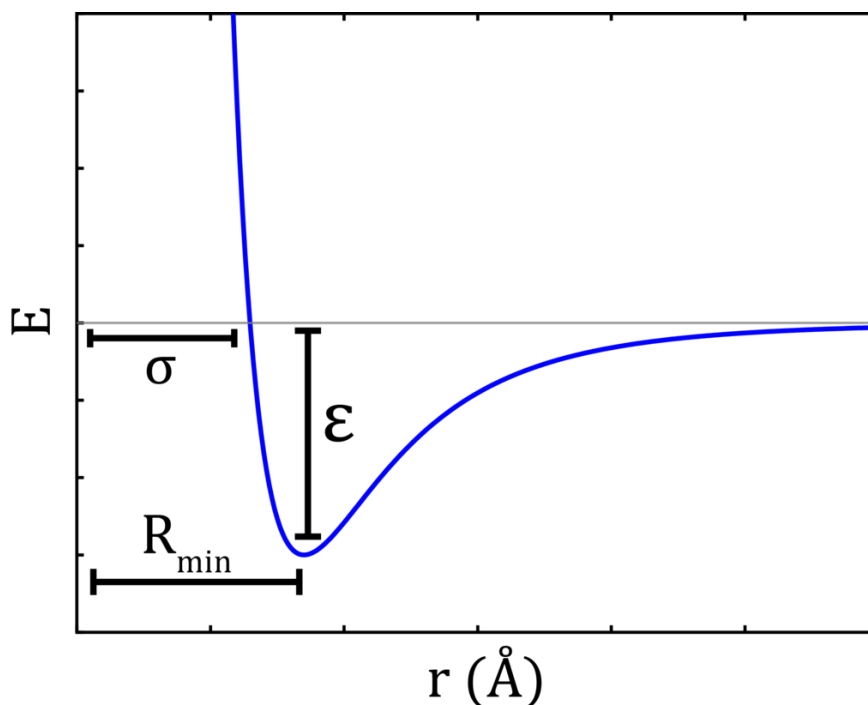


Figure 3.3: Lennard-Jones potential; ϵ is ϵ_{AB} in our notation, R_{\min} is R_{AB}^{\min} in our notation; the illustration taken from [65]

The first parameter, ϵ_{AB}^{\min} , denotes the depth of the potential well for the interacting atoms A and B . The second one, R_{AB}^{\min} , is the interatomic distance where Lennard-Jones potential has its minimum. The usual way of determining these parameters is to calculate the ϵ_{AA}^{\min} and R_A^{\min} for individual atom types first, and then apply combination rules to get ϵ_{AB}^{\min} and R_{AB}^{\min} for the interacting atoms which are of a different type. There are more combination rules used but in the CHARMM36 ϵ_{AB}^{\min} are calculated via the geometric mean and R_{AB}^{\min} via the

arithmetic mean:

$$\varepsilon_{AB}^{\min} = \sqrt{\varepsilon_{AA}^{\min} \varepsilon_{BB}^{\min}}, \quad (3.6)$$

$$R_{AB}^{\min} = (R_A^{\min} + R_B^{\min})/2. \quad (3.7)$$

To summarize, the potential energy function (3.1), whose constituents are mainly harmonic terms, is adequate for the simulation of biomolecules at or near the room temperature, even though the approximation can be perceived as rather severe.

In different force-fields there can be several different parameters and potential terms, where for example polarizability can be included explicitly. These kinds of polarizable force fields are much more computationally demanding. We were considering the use of a polarizable force-field at the beginning of this project, but since our system is already computationally very heavy, we have abandoned this idea.

3.3 Periodic boundary conditions

In molecular dynamics simulation programs the system of interest is being put into a box and usually solvated with water or other kinds of solvents. One can choose from different shapes of boxes of various sizes. However, when dealing with isolated clusters, there is a problem with edge effects, such as the atoms on the outskirts "feeling" the vacuum (= lack of interactions), which does not correspond to the experimental conditions. This is especially troublesome for systems like proteins, which might drift towards the vacuum, which is most certainly not something we want to simulate. Thus, periodic boundary conditions are used to minimize edge effects. This involves surrounding the simulation box with translated copies of itself. As a consequence, our system is devoid of artificial boundaries, ensuring a more faithful representation of the physical reality. However, when simulating non-periodic systems, such as a protein immersed in a solution, we inevitably introduce certain artefacts. Nevertheless, the errors stemming from these artefacts are expected to be less significant compared to those resulting from the presence of artificial boundaries with vacuum.

As was already mentioned, there are several different shapes for the boxes, which we will also call a unit cell. Although GROMACS supports triclinic boxes of any shape, one of the most commonly used unit cells are cubic box, rhombic dodecahedron and truncated octahedron. When dealing with a spherical macromolecule, rhombic dodecahedron and truncated octahedron, considered to be an approximation to the sphere, are more suitable. In this case, there are fewer solvent molecules required to fill the unit cell, hence lowering the computational cost [66].

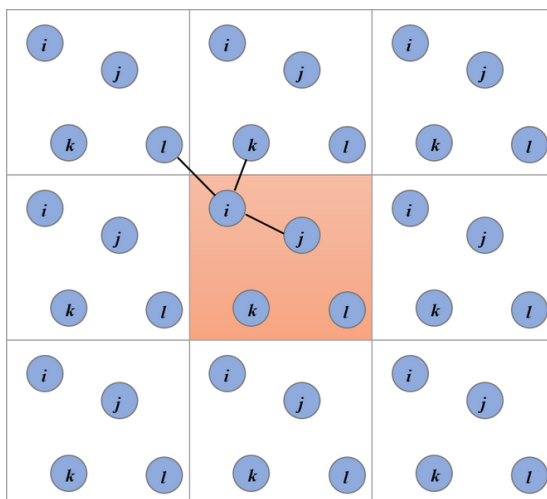


Figure 3.4: Minimum Image Convention; the illustration taken from [67]

3.4 Minimum Image convention

GROMACS implements periodic boundary conditions alongside the so-called minimum image convention. The minimum image convention dictates that the cut-off radius utilized to truncate non-bonded interactions cannot surpass half the length of the shortest box vector. This limitation ensures that only one - closest image of each particle is considered for short-range non-bonded interaction calculations.

However, when examining macromolecules like proteins in solution, this restriction alone is inadequate. Ideally, a single solvent molecule should not have access to both sides of the macromolecule. Therefore, the length of each box vector must exceed the length of the macromolecule along that edge direction, plus twice the cut-off radius.

Our system of interest - tubulin dimer - can be considered to be, for the most part, a prolate ellipsoid. We say "for the most part", since it also has two fast-moving unstructured C-termini, which are not a part of the folded structure of the protein. The C-termini are very mobile and can extend in different directions. This forced us to use a rather large cubic box with the edge length of 18 nm to avoid the violation of the minimal image convention [66].

3.5 Long-Range Interactions

In Molecular Dynamics, there exist a few methods of calculation of the electrostatic and van der Waals interactions. In this section, we will discuss some of them.

3.5.1 van der Waals interactions

van der Waals interactions represented by Lennard-Jones potential are usually truncated at the cut-off distance, since the long-range part $\approx r^{-6}$ approaches zero rather fast. This cut-off value for the van-der Waals interaction is user-specified but there is usually a strong suggestion by the authors of the specific force-field. The simple truncation would cause discontinuity, therefore a switch function is usually used to smooth the transition. Consequently, a switch distance has to be also set. The usual values for the switch distance are 0.9 – 1 nm and 1.2 nm for cut-off distance. The use of the switch function is depicted in Figure below

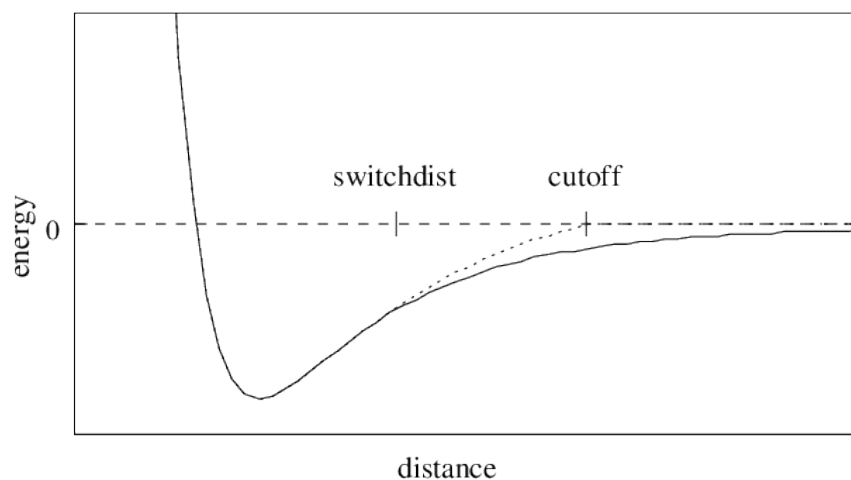


Figure 3.5: Switch function used for the truncation of the van der Waals interactions; [68]

To make the simulation run faster a list of atom pairs, whose distance between each other is less than the cut-off value (the so-called pair-list) is generated at some user-defined interval since there is no need to update this list at every computational step.

3.5.2 Electrostatic interactions

For long-range electrostatic interactions, a simple cut-off approach may lack accuracy. Hence, to address this, lattice sum methods like the Ewald Sum, Particle Mesh Ewald (PME), and Particle-Particle Particle-Mesh (PPPM) have been incorporated in simulations in the past.

The total electrostatic energy of N particles and their periodic images can be

calculated straightforwardly as follows [69]:

$$U_{\text{elstat}} = \frac{1}{8\pi\epsilon_0} \sum_{\vec{n}^*} \sum_i^N \sum_j^N \frac{q_i q_j}{r_{ij,\vec{n}}} \quad (3.8)$$

$$r_{ij,\vec{n}} = |\vec{r}_i - \vec{r}_j + \vec{n}|, \quad (3.9)$$

where \vec{n} denotes the vector connecting the origins of individual boxes. Omission of the terms, corresponding to $i = j$ and $\vec{n} = \vec{0}$, is being denoted by $*$ in the sums.

Electrostatic potential vanishes in a much slower fashion with larger interatomic separations ($\approx \frac{1}{r}$) than the van der Waals potential, for which we have used the cutoff method. Even though this sum under some conditions is convergent, the convergence is rather slow. That is why other methods have been introduced in the past, such as the Ewald summation, which takes advantage of the periodic structure and, therefore, can calculate the interactions not only for the main unit cell but for all the copies of the boxes. Originally developed for crystals, the Ewald summation breaks down the total electrostatic energy into three terms - direct sum in Cartesian space, reciprocal sum in Fourier space and a constant term [69, 70]:

$$U_{\text{elstat}} = U_{\text{direct}} + U_{\text{reciprocal}} + U_{\text{constant}}, \quad (3.10)$$

$$U_{\text{direct}} = \frac{1}{8\pi\epsilon_0} \sum_{i,j}^N \sum_{\vec{n}^*} q_i q_j \frac{\text{erfc}(\beta r_{ij,\vec{n}})}{r_{ij,\vec{n}}}, \quad (3.11)$$

$$U_{\text{reciprocal}} = \frac{1}{8\pi^2\epsilon_0 V} \sum_{k,l}^N q_k q_l \sum_{\vec{m}^*} \frac{\exp(-(\pi\vec{m}/\beta)^2 + 2\pi i\vec{m} \cdot (\vec{r}_k - \vec{r}_l))}{m^2}, \quad (3.12)$$

$$U_{\text{constant}} = -\frac{\beta}{4\pi^{3/2}\epsilon_0} \sum_i^N q_i^2, \quad (3.13)$$

where \vec{m} is a lattice vector in reciprocal space and V is the volume of the unit cell. This separation was done with the use of a general formula:

$$1 = \text{erfc}(\beta r_{ij}) + \text{erf}(\beta r_{ij}), \quad (3.14)$$

which basically means that we add and subtract a screening Gaussian charge distribution to all point charges in the system, as illustrated in Figure 3.6. Parameter β represents the width of the screening densities.

The first term U_{direct} (3.11) denotes part of the Ewald sum, which is evaluated in a direct space.

The second term $U_{\text{reciprocal}}$ (3.12) is the part of the Ewald sum, which is evaluated in the reciprocal space.

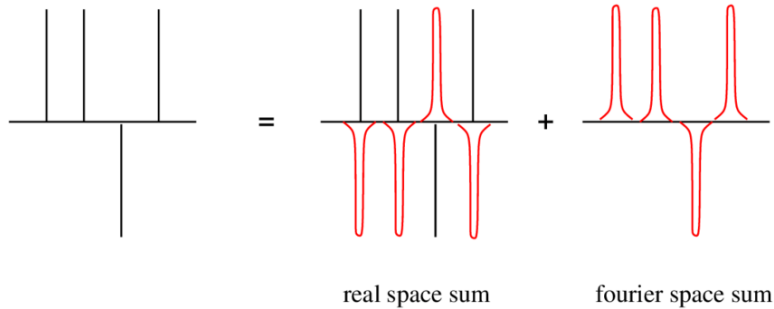


Figure 3.6: Screening in the Ewald summation, [71]

The third term U_{constant} (3.13) is a trivial constant.

To be exact, U_{elstat} contains also the additional fourth term

$$U_{\text{surface}} = \frac{1}{2\varepsilon_0(2\varepsilon_s + 1)V} \left| \sum_i^N q_i \vec{r}_i \right|$$

which is usually disregarded since the dielectric constant of a usual solvent ε_s - water is approximately equal to 80, which makes this term rather small.

The successful implementation of this method requires careful consideration of simulation parameters. Even though the total electrostatic energy is invariant with respect to the parameter β , the choice of this scaling parameter influences the balance between direct and reciprocal space contributions and therefore controls the convergence of each sum. Increasing β will make the direct sum U_{direct} converge faster, while the convergence of the reciprocal term $U_{\text{reciprocal}}$ will be slower.

By a wise choice of β , electrostatic energy is split in such a way that the direct energy term is negligible beyond a certain cut-off distance, while the reciprocal energy term consists of a slowly varying function for all distances, thus is representable by a few vectors in Fourier space. Therefore, for the direct part of the Ewald summation, a cut-off distance can be introduced and that is why we can think of the direct sum as a short-range component of electrostatic interaction and of reciprocal term as the long-range component. Consequently, the computational cost is reduced from $O(N^2)$ to $O(N)$.

Regarding the reciprocal part of the Ewald sum, one cannot just introduce a cut-off here, since we are working in the Fourier space. The practical usefulness of the Ewald summation is thus limited by the high computational cost ($O(N^2)$) of the reciprocal space calculation, which increases quadratically with the system size. That is the reason why Darden et.al. [72] proposed a new method, which makes use of the Fourier transform and interpolation techniques to evaluate the long-range - reciprocal - part of the electrostatic interaction. This method is called Particle-Mesh Ewald (PME) and scales more efficiently, $O(N \log N)$, making it particularly suitable for medium to large systems. However, for very small systems, where the setup and transformation overheads may outweigh the benefits, the Ewald summation may still be preferred. As the name suggests, PME uses a periodic mesh. Charges are then interpolated onto the mesh points with appropriate weights depending on the distance between the mesh point and the charge. This is shown in Figure 3.7. For PME, parameters such as the grid spacing and interpolation order significantly affect computational accuracy and

efficiency.



Figure 3.7: Particle Mesh Ewald interpolation diagram for the evaluation of long-range electrostatics in molecular dynamics simulation; the illustration taken from [73]

4. Hamiltonian systems

4.1 Hamiltonian mechanics

When dealing with a closed system of interacting objects with no external forces acting upon them, very well-known and elegant laws, called Hamiltonian Canonical Equations (HCE) govern their motion:

$$\frac{dq_\alpha}{dt} = \frac{\partial \mathcal{H}}{\partial p_\alpha} \equiv \nabla_{p_\alpha} \mathcal{H} = \{q_\alpha, \mathcal{H}\} \quad (4.1)$$

$$\frac{dp_\alpha}{dt} = -\frac{\partial \mathcal{H}}{\partial q_\alpha} \equiv -\nabla_{q_\alpha} \mathcal{H} = \{p_\alpha, \mathcal{H}\} \quad (4.2)$$

where \mathcal{H} is the Hamilton function that consists of kinetic and potential term

$$\mathcal{H}(\vec{p}, \vec{q}) = \sum_{\alpha=1}^{3N} \frac{p_\alpha^2}{2m_\alpha} + U(\vec{q}_1, \dots, \vec{q}_N), \quad (4.3)$$

which represents the total energy of the system of N particles; $\{X, Y\}$ denotes the so-called Poisson bracket:

$$\{X, Y\} = \frac{\partial X}{\partial q} \frac{\partial Y}{\partial p} - \frac{\partial X}{\partial p} \frac{\partial Y}{\partial q}. \quad (4.4)$$

The total energy of the closed system is being conserved. Substituting (4.3) in the HCE will yield:

$$\frac{dq_\alpha}{dt} = \frac{\partial \mathcal{H}}{\partial p_\alpha} = \frac{p_\alpha}{m_\alpha} \quad (4.5)$$

$$\frac{dp_\alpha}{dt} = -\frac{\partial \mathcal{H}}{\partial q_\alpha} = -\nabla_{q_\alpha} U(\vec{q}_1, \dots, \vec{q}_N) \equiv \vec{F}_\alpha \quad (4.6)$$

since the potential U depends only on the positions q_i . If we introduce a phase space vector \vec{x} defined as

$$\vec{x} \equiv \{\vec{p}_i, \vec{q}_i\}_{i=1}^N, \quad (4.7)$$

we can rewrite the HCE very efficiently:

$$\frac{d\vec{x}}{dt} = \{\vec{x}, \mathcal{H}\} \quad (4.8)$$

Therefore by the specification of a potential we obtain equations of motion of the corresponding system, and by their integration, we obtain the corresponding

trajectories.

We will define a classical Liouville operator

$$iL := \{\cdot, \mathcal{H}\} = \sum_{\alpha=1}^{3N} \left(\frac{\partial \mathcal{H}}{\partial p_\alpha} \frac{\partial}{\partial q_\alpha} - \frac{\partial \mathcal{H}}{\partial q_\alpha} \frac{\partial}{\partial p_\alpha} \right), \quad (4.9)$$

which is a linear self-adjoint operator acting on the space of quadratically integrable functions. Substituting the equations (4.5) and (4.6) into (4.9) we get:

$$iL := \{\cdot, \mathcal{H}\} = \sum_{\alpha=1}^{3N} \left(\frac{p_\alpha}{m_\alpha} \frac{\partial}{\partial q_\alpha} + \nabla_{q_\alpha} U(\vec{q}_1, \dots, \vec{q}_N) \frac{\partial}{\partial p_\alpha} \right), \quad (4.10)$$

Consequently, $\{\vec{x}, \mathcal{H}\}$ in equation (4.8) can be rewritten as iLx . Formal integration of such an equation gives us the solution of the Hamilton equations of motion:

$$\frac{d\vec{x}}{dt} = iLx \quad \Rightarrow \quad x(t) = e^{iL(t-t_0)}x(t_0) = U(t-t_0)x(t_0) \quad (4.11)$$

where we have introduced an evolution operator or the so-called propagator $U(t-t_0)$. This operator is a unitary operator.

Liouville operator (4.9) can be divided into two terms:

$$iL = iL_q + iL_p, \quad (4.12)$$

where

$$iL_q = \sum_{\alpha=1}^{3N} \frac{p_\alpha}{m_\alpha} \frac{\partial}{\partial q_\alpha} \quad (4.13)$$

$$iL_p = \sum_{\alpha=1}^{3N} \nabla_{q_\alpha} U(\vec{q}_1, \dots, \vec{q}_N) \frac{\partial}{\partial p_\alpha} \quad (4.14)$$

and thus the solution for the phase space vector looks as:

$$x(t) = e^{i(L_q+L_p)t}x(t_0) \quad (4.15)$$

This solution is only formal because we cannot evaluate the action of the propagator in this way. To treat this numerically, we need to separate these two parts inside the exponential. Since the (4.13) and (4.14) are noncommuting operators, it does matter in what order they will be applied to a function. For such noncommuting operators, we cannot simply separate $\exp(iL_q + iL_p)$ into a product $\exp(iL_q)\exp(iL_p)$. To separate the propagator from the product of the propagators acting on q and p alone, the Trotter expansion theorem is used. This theorem says that given operators A and B , which do not commute, meaning $[A, B] \neq 0$, we can do the following:

$$e^{A+B} = \lim_{P \rightarrow \infty} [e^{\frac{A}{2P}} e^{\frac{B}{P}} e^{\frac{A}{2P}}]^P, \quad (4.16)$$

where P is an integer. To be exact, this is actually the symmetric Trotter theorem or the Strang splitting formula, where the actual Trotter theorem is used. After introducing the timestep $\Delta t = \frac{t}{P}$, we can write the propagator as:

$$e^{i(L_1+L_2)t} = \lim_{P \rightarrow \infty} [e^{iL_1 \frac{\Delta t}{2}} e^{iL_2 \Delta t} e^{iL_1 \frac{\Delta t}{2}}]^P, \quad (4.17)$$

which means that this formula holds when the timestep $\Delta t \rightarrow 0$ and at the same time the number of steps goes to infinity.

Practically, we cannot have an infinite amount of infinitesimal steps. Therefore, the Trotter expansion cut-off is another approximation that is being used. Luckily, it is a good approximation generating not too large errors. For a finite number of steps P , we can write:

$$e^{iLt} \approx [e^{iL_1 \frac{\Delta t}{2}} e^{iL_2 \Delta t} e^{iL_1 \frac{\Delta t}{2}}]^P + \mathcal{O}(P\Delta t^3) \quad (4.18)$$

Therefore the global error of a trajectory of P steps is approximately

$$P\Delta t^3 = t\Delta t^2 \quad (4.19)$$

For simplicity, the next equations will be written only for one particle.

We have a scheme of propagation for one step:

$$\exp(iL\Delta t) \approx \exp(iL_p \frac{\Delta t}{2}) \exp(iL_q \Delta t) \exp(iL_p \frac{\Delta t}{2}) \quad (4.20)$$

$$= \exp\left(\frac{\Delta t}{2} F(q) \frac{\partial}{\partial p}\right) \exp\left(\Delta t \frac{p}{m} \frac{\partial}{\partial q}\right) \exp\left(\frac{\Delta t}{2} F(q) \frac{\partial}{\partial p}\right) \quad (4.21)$$

Given the initial position and momenta $(q(0), p(0))$, a numerical update of these variables is calculated as:

$$\begin{pmatrix} q(\Delta t) \\ p(\Delta t) \end{pmatrix} \approx \exp\left(\frac{\Delta t}{2} F(q(0)) \frac{\partial}{\partial p(0)}\right) \exp\left(\Delta t \frac{p(0)}{m} \frac{\partial}{\partial q(0)}\right) \times \quad (4.22)$$

$$\times \exp\left(\frac{\Delta t}{2} F(q(0)) \frac{\partial}{\partial p(0)}\right) \begin{pmatrix} q(0) \\ p(0) \end{pmatrix}, \quad (4.23)$$

where $\frac{\partial}{\partial p(0)} \equiv \frac{\partial}{\partial p} |_{t=0}$. The operators in the form of $\exp\left(c \frac{\partial}{\partial x}\right) g(x)$, where c is independent of x , are called displacement operators. Their action on an arbitrary function can be easily derived using the Taylor expansion:

$$\exp\left(c \frac{\partial}{\partial x}\right) g(x) = \sum_{k=0}^{\infty} \frac{1}{k!} \left(c \frac{\partial}{\partial x}\right)^k g(x) = \sum_{k=0}^{\infty} \frac{1}{k!} c^k g^{(k)}(x) = g(x+c) \quad (4.24)$$

Now we can calculate the action of the propagators on the initial condition phase space vector:

$$\exp\left(\frac{\Delta t}{2} F(q) \frac{\partial}{\partial p}\right) \begin{pmatrix} q(0) \\ p(0) \end{pmatrix} = \begin{pmatrix} q(0) \\ p(0) + \frac{\Delta t}{2} F(q(0)) \end{pmatrix}, \quad (4.25)$$

$$\exp\left(\Delta t \frac{p}{m} \frac{\partial}{\partial q}\right) \begin{pmatrix} q(0) \\ p(0) + \frac{\Delta t}{2} F(q(0)) \end{pmatrix} = \begin{pmatrix} q(0) + \Delta t \frac{p(0)}{m} \\ p(0) + \frac{\Delta t}{2} F\left(q(0) + \Delta t \frac{p(0)}{m}\right) \end{pmatrix}, \quad (4.26)$$

$$\exp\left(\frac{\Delta t}{2} F(q) \frac{\partial}{\partial p}\right) \begin{pmatrix} q(0) + \Delta t \frac{p(0)}{m} \\ p(0) + \frac{\Delta t}{2} F\left(q(0) + \Delta t \frac{p(0)}{m}\right) \end{pmatrix} = \quad (4.27)$$

$$= \begin{pmatrix} q(0) + \frac{\Delta t}{m} \left(p(0) + \frac{\Delta t}{2} F(q(0))\right) \\ p(0) + \frac{\Delta t}{2} F(q(0)) + \frac{\Delta t}{2} F\left(q(0) + \frac{\Delta t}{m} \left(p(0) + \frac{\Delta t}{2} F(q(0))\right)\right) \end{pmatrix}. \quad (4.28)$$

Since $q(0) + \frac{\Delta t}{m} \left(p(0) + \frac{\Delta t}{2} F(q(0))\right) = q(\Delta t)$, we can write the final expression as:

$$\exp(iL\Delta t) \begin{pmatrix} q(0) \\ p(0) \end{pmatrix} = \begin{pmatrix} q(0) + \frac{\Delta t}{m} \left(p(0) + \frac{\Delta t}{2} F(q(0))\right) \\ p(0) + \frac{\Delta t}{2} F(q(0)) + \frac{\Delta t}{2} F(q(\Delta t)) \end{pmatrix} \quad (4.29)$$

This algorithm is called Velocity Verlet and the final expressions can be written as:

$$q(\Delta t) = q(0) + \frac{\Delta t}{m} p(0) + \frac{\Delta t^2}{2m} F(q(0)), \quad (4.30)$$

$$v(\Delta t) = v(0) + \frac{\Delta t}{2m} (F(q(0)) + F(q(\Delta t))), \quad (4.31)$$

and can be implemented as a three-step procedure:

$$p(\Delta t/2) = p(0) + \frac{\Delta t}{2} F(q(0)) \quad (4.32)$$

$$q(\Delta t) = q(0) + \frac{\Delta t}{m} p(\Delta t/2) \quad (4.33)$$

$$p(\Delta t) = p(\Delta t/2) + \frac{\Delta t}{2} F(q(\Delta t)) \quad (4.34)$$

This is the algorithm for the integration of the equations of motion which yield the trajectory in a phase space (\vec{q}, \vec{p}) . It can be very easily shown that we are dealing with a symplectic algorithm. Having a symplectic algorithm means that the Jacobian of the transformation of coordinate change $x_t \rightarrow x_0$ is $J = 1$. The first step of the algorithm gives us:

$$J_1 = \begin{vmatrix} 1 & 0 \\ \Delta t/2 F(\cdot) & 1 \end{vmatrix} = 1 \quad (4.35)$$

The second step of the algorithm gives us:

$$J_2 = \begin{vmatrix} 1 & \Delta t/m \\ 0 & 1 \end{vmatrix} = 1 \quad (4.36)$$

Consequently, the phase space volume is conserved, therefore it generates unitary, time-reversible dynamics, hence preserving classical mechanics symmetries.

The extension of these formulae to the system of N particles in 3 dimensions is straightforward, since all the terms in iL_q commute with each other. The same holds for iL_p .

Besides the Velocity-Verlet algorithm, there exist more algorithms, such as Euler, Position-Verlet, Leapfrog, and others. In our simulations, we have used the Leapfrog integrator, which is a modified version of the Velocity-Verlet algorithm. The difference, which is also its disadvantage, is an asynchronous calculation of positions and velocities with respect to the time step. Positions and velocities are calculated at alternating time points, arranged in a manner where they "leapfrog" past one another. The Leapfrog and Velocity-Verlet integrators give equivalent trajectories. The Leapfrog is the most used algorithm since its advantages are only one calculation of energy per step, better use of the memory or possible use of a longer time step. The algorithm looks as follows:

$$\vec{v}(t + \Delta t/2) = \vec{v}(t - \Delta t/2) + \Delta t \frac{\vec{F}(\vec{q}(t))}{m}, \quad (4.37)$$

$$\vec{q}(t + \Delta t) = \vec{q}(t) + \Delta t \vec{v}(t + \Delta t/2). \quad (4.38)$$

[74]

4.2 Statistical mechanics

Classical MD is successful in predicting macroscopic thermodynamic and dynamic observables with the use of classical statistical mechanics, which is based on a Hamiltonian formulation of mechanics. To calculate an experimental observable means to determine an ensemble average on the phase space $\mathcal{D}(\Omega)$.

$$\langle a \rangle = \frac{1}{\Omega} \int_{\mathcal{D}(\Omega)} a(\vec{q}, \vec{p}) f(\vec{q}, \vec{p}) d\vec{q} d\vec{p}, \quad (4.39)$$

where $f(\vec{q}, \vec{p})$ is a phase-space distribution function. Integration of $f(\vec{q}, \vec{p})$ over the available phase-space will give us the partition function - multiplicity Ω - which represents the number of available microstates. Microstates are all the possible combinations of atoms' positions' and momenta, such that macroscopically, the outcome is the same macrostate defined by the variable of that ensemble.

$$\Omega = \int_{\mathcal{D}(\Omega)} f(\vec{q}, \vec{p}) d\vec{q} d\vec{p}, \quad (4.40)$$

The phase space function $f(x, t)$ evolves according to Hamilton's equation of motion and therefore satisfies the Liouville equation

$$\frac{\partial f}{\partial t} + \dot{x} \cdot \nabla f = \frac{df}{dt} = 0, \quad (4.41)$$

which means that for the Hamiltonian systems, the phase space distribution function is conserved. Additionally, the phase space volume $d\vec{q}d\vec{p}$ is also conserved by Hamiltonian dynamics. Given a subset of systems with initial conditions within a phase space volume element $d^n x_0$, the trajectories $x_t(t; x_0)$ obtained by solving Hamilton's equations of motion for each initial condition x_0 will describe a volume element $d^n x_t$ in phase space such that $d^n x_0 = d^n x_t$. This means, that the phase space is incompressible for Hamiltonian systems.

To proceed further, we must first mention the fundamental requirement of a simulated system to be *ergodic*. Ergodicity is a property much needed in practical use since an important consequence of a dynamical system being ergodic is that in $t \rightarrow \infty$ time averages of system properties are equal to the averages of these properties over configurational ensemble,

$$\lim_{t \rightarrow \infty} \frac{1}{t} \int_0^t a(\vec{q}(s), \vec{p}(s)) ds = \langle a \rangle \quad (4.42)$$

Since in practice, we are dealing with time-discretized dynamics, which we get by iterative mapping S , we prefer to write:

$$\lim_{n \rightarrow \infty} \frac{1}{n} \sum_{k=1}^n a(S^k(\vec{q}_0, \vec{p}_0)) = \langle a \rangle \quad (4.43)$$

Therefore, for sufficiently long simulation trajectories, thermodynamic properties such as equilibrium constants, transition rates and many other experimental observables, which are inherently ensemble averages, can be determined from time-averaged quantities. Unfortunately, for many simulation methods, ergodicity does not hold, and therefore, there is still active research being done on this matter. Molecular dynamics simulation which fails to satisfy (4.43) will not reflect the force-field accurately since it will not generate a correct ensemble [75].

Dynamical systems are ergodic if and only if they are both invariant, which means measure-preserving and irreducible. Irreducibility means that the system will eventually (in infinite time) reach all of the accessible phase space points from any accessible starting point. A transformation S on Ω is f -invariant if $f(S^{-1}A) = f(A)$ for every measurable $A \subset \Omega$, or equivalently, if for any $a \in L_1(\Omega)$,

$$\int_{\Omega} a(x) df = \int_{\Omega} a(S(x)) df \quad (4.44)$$

meaning that the dynamics has f as an equilibrium and as such, together with irreducibility, means that the equilibrium is unique and the dynamics will eventually converge to f from any starting point.

This chapter dealt with Hamiltonian dynamics, which describes the closed (isolated) systems where the energy, volume and number of particles are being conserved. A collection of such systems isolated from any surrounding is called a microcanonical ensemble. All members of the ensemble have the same Hamiltonian $\mathcal{H}(x)$, therefore the phase-space distribution function is a uniform distribution on a hypersurface of constant energy and zero elsewhere:

$$f(\vec{x}) \approx \delta(\mathcal{H}(x) - E), \quad (4.45)$$

where \vec{x} is a phase space vector of all positions and momenta. This yields the statistical averages as functions of the total energy E (and of the other parameters of the Hamiltonian). Thus, this ensemble can be generated by the time evolution of a dynamical ergodic system according to the Hamiltonian canonical equations of motion, which we have already dealt with in the previous subchapter. [76]

5. Non-Hamiltonian systems

When trying to simulate real-life conditions, we must take into consideration the openness of our system of interest. In the experiment, a probed system is usually in contact with the surrounding environment (thermal bath) with which the system of interest can exchange energy. This bath is often also called a thermal reservoir. Differently to Hamiltonian mechanics, which describes a system isolated from its surroundings, non-Hamiltonian mechanics can describe systems that are in contact with a thermal bath, and the trajectories generated in this way are a collection of microstates that sample canonical distribution. For this ensemble number of particles, volume and temperature are held constant (NVT ensemble). However, the experiments are generally rather performed under the conditions of constant pressure than constant volume. The ensemble generated under these conditions is called isothermal-isobaric (NPT). Other real-life conditions of experiments can be with a fixed chemical potential, rather than a constant number of particles, which generates a grand canonical ensemble (μVT). Therefore, the interaction with the surroundings does not need to be only thermal. External forces, such as electric fields, can interact with the system of interest. These driven, stressed or constrained systems are also described by non-Hamiltonian equations of motion.

In a canonical ensemble, the energy of the system of interest is no longer conserved, only the energy of the system + bath, which we will call the universe.

$$f(x) = \int_{bath} \delta(\mathcal{H}_{system}(x) + \mathcal{H}_{bath}(x) - E). \quad (5.1)$$

We are only interested in the \mathcal{H}_{system} , therefore we integrate over the bath degrees of freedom, which gives us the phase space distribution function - equilibrium canonical probability distribution function or so-called Boltzmann distribution:

$$f(x) \approx \exp(-\beta\mathcal{H}_{system}(x)), \quad (5.2)$$

Due to the coupling of the system to the thermal bath, the energy of the system fluctuates, thus generating this Boltzmann distribution. Even though in the thermodynamic limit ($N \rightarrow \infty, V \rightarrow \infty$) these fluctuations vanish, the simulations are usually done for small systems and small enough volume far from the thermodynamic limit, so this property cannot be used [77].

To incorporate this kind of fluctuations into the system and generate this statistical ensemble, the so-called thermostats have been developed, which are trying to mimic the effect of the thermal reservoir. Even though the easiest algorithms of temperature control to incorporate are simple periodic rescaling of velocities, they do not always generate a canonical phase-space distribution. To correct that, we can sample the velocities from the Maxwell-Boltzmann distribution, which guarantees to provide canonical distribution. Andersen thermostat improved upon this approach by selecting the velocity according to a collision frequency ν , which is preset. The "collision" of a particle in a time Δt is a re-sampling event with a probability of $\nu\Delta t$. [78, 74]

5.1 Generalized Liouville equation

Generally, non-Hamiltonian microscopic equations can be written as

$$\frac{dx}{dt} = \xi(x, t) \quad (5.3)$$

In non-Hamiltonian systems the phase-space compressibility $\nabla_x \cdot \frac{dx}{dt} = \nabla_x \cdot \xi(x, t)$ can be nonzero. If the phase space compressibility is nonzero, we are dealing with a non-Hamiltonian system, but one can propose non-Hamiltonian equations of motion that would lead to vanishing compressibility. For the Liouville equation to hold, compressibility must be zero. Therefore, for non-Hamiltonian systems, where the dynamics is compressible, we must introduce a new generalized Liouville equation and a phase-space metric. For Hamiltonian systems, the Jacobian of transformation $x_0 \rightarrow x_t$, $J(x_t; x_0)$, which satisfies

$$\frac{d}{dt} J(x_t; x_0) = \nabla_x \cdot \frac{dx}{dt}(x_t; x_0), \quad (5.4)$$

is 1, since the phase-space compressibility

$$\kappa(x_t, t) = \exp \left[\int_0^t ds \kappa(x_s, s) \right] \quad (5.5)$$

is zero. For a non-Hamiltonian system, this cannot be assumed, therefore the Jacobian does not have to be unity which leads to the fact that the Liouville theorem $dx_t = dx_0$ does not hold. It can be shown that a new conservation law exists

$$\exp[-w(x_t, t)] dx_t = \exp[-w(x_0, 0)] dx_0. \quad (5.6)$$

Here a weighted phase space volume is conserved which implies that a conservation law exists on a non-Euclidean or Riemannian phase space or the so-called manifold. Since these spaces are locally curved, the transformation to move from one phase space volume to another introduces a nontrivial metric. Therefore we can denote a corresponding volume element $\sqrt{\det(g(x))}dx$, where $g_{ij}(x)$ is a second-rank tensor called the metric tensor. For a coordinate transformation from x_0 to x_t , the Jacobian looks as

$$J(x_t; x_0) = \frac{\sqrt{g(x_0, 0)}}{\sqrt{g(x_t, t)}}, \quad (5.7)$$

where

$$\sqrt{g(x_t, t)} = e^{-w(x_t, t)}. \quad (5.8)$$

Here the metric has an explicit time dependence. Having this kind of a generalized metric is only natural since the phase space is only a mathematical construction and there is no need to describe the system by Euclidian space. On the other hand, it is only reasonable to allow the properties of a dynamical system dictate the geometry of the phase space in which it resides.

The generalized Liouville equation that also holds for non-Hamiltonian dynamical systems can be written as:

$$\frac{\partial}{\partial t} \left(f(x, t) \sqrt{g(x, t)} \right) + \nabla_x \cdot \left(\frac{dx}{dt} \sqrt{g(x, t)} f(x, t) \right) = 0 \quad (5.9)$$

Since the actual derivation of the generalized Liouville equation is rather cumbersome, we only give here the final result and suggest the reader to check [78, 77] for the derivation itself.

Combining previous equations together, one can show that

$$\frac{\partial}{\partial t} f(x, t) + \xi(x, t) \cdot \nabla_x f(x, t) = \frac{d}{dt} f(x_t, t) = 0, \quad (5.10)$$

which means that when we consider a non-Euclidian form of the phase space, the ensemble distribution $f(x_t, t)$ is conserved even for the non-Hamiltonian systems. We can therefore write the following:

$$f(x_t, t) \sqrt{g(x_t)} dx_t = f(x_0) \sqrt{g(x_0)} dx_0 \quad (5.11)$$

If in equilibrium, time dependence vanishes in $f(x_t, t)$ and $\sqrt{g(x_t, t)}$ and (5.11) reduces to

$$f(x_t) \sqrt{g(x_t)} dx_t = f(x_0) \sqrt{g(x_0)} dx_0. \quad (5.12)$$

Therefore, equilibrium averages can be performed at any time, same as in the case of Hamiltonian systems. When it comes to equilibrium Liouville equation

$$\xi \cdot \nabla_x f(x) = 0, \quad (5.13)$$

it has the same form as in the case of Hamiltonian systems, but it cannot be rewritten in the form of Poisson brackets with the Hamiltonian since there is no Hamiltonian from which the equations of motion $\frac{dx}{dt} = \xi(x)$ are generated. Nonetheless, if we can determine the full metric tensor $g_{ij}(x)$, then we can also define the generalized Poisson bracket for non-Hamiltonian systems. Unfortunately, at least to our knowledge, there is no general theory of this metric tensor yet.

We can still construct a distribution function $f(x)$, for which $\frac{df}{dt}$ holds, with the knowledge of all the conservation laws:

$$\Lambda_k(x_t) - C_k = 0, \quad (5.14)$$

such that

$$\frac{d}{dt} \Lambda_k(x_t) = 0, \quad (5.15)$$

where $k = 1, \dots, N_c$ and N_c is the number of conservation laws. Then a general "microcanonical" distribution function for the whole universe can be constructed and it samples the intersection of hypersurfaces defined by the conservation laws

$$f(x) = \prod_{k=1}^{N_c} \delta(\Lambda_k(x) - C_k). \quad (5.16)$$

From this we can write the "microcanonical" partition function as:

$$\mathcal{Z} = \int dx \sqrt{g(x)} f(x) = \int dx \sqrt{g(x)} \prod_{k=1}^{N_c} \delta(\Lambda_k(x) - C_k), \quad (5.17)$$

which represents the number of microstates that can be reached when the system is determined by $f(x)$. For this, a metric tensor has to be used, since it must be integrated with respect to the conserved volume element, which for non-Hamiltonian systems is $\sqrt{g(x)}dx$.

5.2 Nosé equations

In our work, we have decided to use one of the extended phase space methods in which besides having N coordinate and momentum vectors (describing classical N -particle systems) there is also one or a set of additional control variables that are coupled to other degrees of freedom. These introduce fluctuations in the system of interest and as such are acting as a heat bath.

These extended phase-space methods are either Hamiltonian or non-Hamiltonian. For example, the Nosé Hamiltonian which was originally introduced in 1983-1984 by S. Nosé, introduces a variable s that checks whether the instantaneous kinetic energy is higher or lower than the one prescribed by the preset desired temperature and then accordingly scales the velocities. Thus the Nosé Hamiltonian for a system of coordinates $\vec{r}_1, \dots, \vec{r}_N \equiv \vec{r}$ and momenta $\vec{p}_1, \dots, \vec{p}_N \equiv \vec{p}$ has a form

$$\mathcal{H}_N = \sum_{i=1}^N \frac{\vec{p}_i^2}{2m_i s^2} + U(\vec{r}_1, \dots, \vec{r}_N) + \frac{p_s^2}{2Q} + gk_B T \ln s, \quad (5.18)$$

where T is the goal temperature, k_B is the Boltzmann constant, p_s is a conjugated momentum to s , and Q determines the time scale on which this additional degree of freedom acts. s is present in the kinetic energy term since its purpose is to scale this energy and therefore to control its fluctuation. The term $gk_B T \ln s$ has been derived to ensure that a canonical distribution in the phase space will be obtained. The parameter g is also determined from the condition that the microcanonical distribution of $2dN + 2$ - dimensional phase space will yield a canonical distribution in the $2dN$ -dimensional phase space. Under the assumption of ergodicity, molecular dynamics simulations using the Hamiltonian \mathcal{H}_N will sample the canonical distribution $\exp[-\beta\mathcal{H}(\vec{r}, \vec{p})]$, which we will show in the next few steps. We will see that a microcanonical distribution of the Nosé Hamiltonian \mathcal{H}_N leads to a canonical distribution in the physical Hamiltonian \mathcal{H} . First, we introduce this microcanonical partition on the "universe" which in this case is $2dN + 2$ dimensional phase space:

$$\Omega = \int d^N \vec{r} d^N \vec{p} ds dp_s \delta \left(\sum_{i=1}^N \frac{\vec{p}_i^2}{2m_i s^2} + U(\vec{r}_1, \dots, \vec{r}_N) + \frac{p_s^2}{2Q} + gk_B T \ln s - E \right) \quad (5.19)$$

After the integration over s and p_s in the previously defined microcanonical partition function,

$$\Omega = \int d^N \vec{r} d^N \vec{p} ds dp_s s^{dN} \delta \left(\sum_{i=1}^N \frac{\vec{p}_i^2}{2m_i} + U(\vec{r}_1, \dots, \vec{r}_N) + \frac{p_s^2}{2Q} + gk_B T \ln s - E \right) \quad (5.20)$$

$$= \int d^N \vec{r} d^N \vec{p} ds dp_s s^{dN} \delta \left(\mathcal{H}(\vec{r}, \vec{p}) + \frac{p_s^2}{2Q} + gk_B T \ln s - E \right) \quad (5.21)$$

where first a substitution $\vec{p}_i = \frac{\vec{p}_i}{s}$ and then subsequent renaming back to \vec{p}_i was used, and in which $\mathcal{H}(\vec{r}, \vec{p})$ denotes the physical Hamiltonian, we get a distribution in the phase space of our physical system (without the additional degree of freedom that mimics a bath)

$$\Omega = \frac{e^{E/k_B T} \sqrt{2\pi Q k_B T}}{(dN + 1) kT} \int d^N \vec{r} d^N \vec{p} e^{-\mathcal{H}(\vec{r}, \vec{p})/k_B T} \quad (5.22)$$

in which the g value was chosen to be $dN + 1$. We can see that we have got our desired canonical partition function, apart from the prefactors. By this, we have effectively introduced a heat bath that controls the fluctuations of the kinetic energy of our system and hence we call this mechanism a thermostat. Nosé Hamiltonian leads to the following equations of motion

$$\frac{d\vec{r}_i}{dt} = \frac{\partial \mathcal{H}_N}{\partial \vec{p}_i} = \frac{\vec{p}_i}{m_i s^2} \quad (5.23)$$

$$\frac{d\vec{p}_i}{dt} = -\frac{\partial \mathcal{H}_N}{\partial \vec{r}_i} = \vec{F}_i \quad (5.24)$$

$$\frac{ds}{dt} = \frac{\partial \mathcal{H}_N}{\partial p_s} = \frac{p_s}{Q} \quad (5.25)$$

$$\frac{dp_s}{dt} = -\frac{\partial \mathcal{H}_N}{\partial s} = \sum_{i=1}^N \frac{\vec{p}_i^2}{m_i s^3} - \frac{gkT}{s} = \frac{1}{s} \left[\sum_{i=1}^N \frac{\vec{p}_i^2}{m_i s^2} - gkT \right] \quad (5.26)$$

More intuitive kinetic energy form can be recovered by the introduction of non-canonical variables \vec{p}'_i, p'_s and dt'

$$\vec{p}'_i = \frac{\vec{p}_i}{s} \quad p'_s = \frac{p_s}{s} \quad dt' = \frac{dt}{s}, \quad (5.27)$$

whose substitution to (5.23),(5.24),(5.25),(5.26) yields equations of motion in a

form:

$$\frac{d\vec{r}'_i}{dt'} = \frac{\vec{p}'_i}{m_i} \quad (5.28)$$

$$\frac{d\vec{p}'_i}{dt'} = \vec{F}_i - \frac{sp'_s}{Q}\vec{p}'_i \quad (5.29)$$

$$\frac{ds}{dt'} = \frac{s^2 p'_s}{Q} \quad (5.30)$$

$$\frac{dp'_s}{dt'} = \frac{1}{s} \left[\sum_{i=1}^N \frac{(\vec{p}'_i)^2}{m_i} - gkT \right] - \frac{s(p'_s)^2}{Q} \quad (5.31)$$

Unfortunately, because of the noncanonical transformation, the last form of the Nosé equations is not of a symplectic nature and therefore the phase space volume is no longer incompressible. Additionally, the time is defined rather unconventionally, since it is being rescaled by the variable s , which also makes the implementation of these equations rather tricky.

Even though we do not work within Hamiltonian dynamics anymore, not sticking to Hamiltonian (phase space volume-preserving) dynamics does not mean that it is wrong, since the purpose is to sample an ensemble [74].

In this section, we have introduced a collective system (universe) that is isolated, then have used Hamiltonian mechanics to describe it as a whole and after the integration over the variables that represent the bath, the phase space distribution of the system of interest has been determined. One can also get to a non-Hamiltonian dynamics that works the opposite way, which means to propose a set of non-Hamiltonian equations of motion first, and only then to prove that they result in a wanted ensemble distribution. In this way, we can simulate systems that are in contact with a heat bath and particle reservoir or, are subject to external driving forces such as an external electric field, which is also our case.

In the next section we will talk about the thermostat that we have actually used in this work, which is called a Nosé-Hoover thermostat, which is just a reformulation of the Nosé equations.

5.3 Nosé-Hoover equations

One of the most used thermostating techniques in molecular dynamics simulations are Nosé-Hoover equations introduced in 1985 by W. G. Hoover [79]. He and later Martyna *et al.* [80] proposed a noncanonical change of variables in Nosé equations

$$\vec{p}'_i = \frac{\vec{p}_i}{s}, \quad dt' = \frac{dt}{s}, \quad \frac{1}{s} \frac{ds}{dt'} = \frac{d\eta}{dt}, \quad p_s = p_\eta \quad (5.32)$$

and also a redefined a parameter g to a value dN , which yields the following equations of motion:

$$\frac{d\vec{r}_i}{dt} = \frac{\vec{p}_i}{m_i} \quad (5.33)$$

$$\frac{d\vec{p}_i}{dt} = \vec{F}_i - \frac{\vec{p}_\eta}{Q} \vec{p}_i \quad (5.34)$$

$$\frac{d\eta}{dt} = \frac{\vec{p}_\eta}{Q} \quad (5.35)$$

$$\frac{dp_\eta}{dt} = \sum_{i=1}^N \frac{\vec{p}_i^2}{m_i} - dNkT \quad (5.36)$$

In momentum equation (5.34) the additional term could represent a "friction" term, which cannot be regarded as a proper friction term since it can be either positive or negative. From the equation (5.36) we can see that the evolution of this so-called friction variable is determined by the discrepancy between the instantaneous value of the kinetic energy times 2 and canonical average $dNkT$ determined by the preset goal temperature T . These equations represent one of the trivial non-Hamiltonian systems since they are derived from the Hamiltonian one by the use of noncanonical variables.

Nosé-Hoover equations are derived in the opposite way, first, we write them down and only then we have to prove that they really sample the canonical distribution of a physical system. As we have written in the 5.1, first the conservation laws need to be identified. The Nosé-Hoover equations conserve the following energy:

$$\mathcal{H}'(\vec{r}, \eta, \vec{p}, p_\eta) = \mathcal{H}(\vec{r}, \vec{p}) + \frac{p_\eta^2}{2Q} + dNkT\eta, \quad (5.37)$$

where $\mathcal{H}(\vec{r}, \vec{p})$ denotes the physical system Hamiltonian. In the case of

$$\sum_{i=1}^N \vec{F}_i \neq 0 \quad (5.38)$$

(5.37) is the sole conservation law. This is the case when we have external forces acting upon our physical system, which is also the case in this work, where we probe the effect of an external electric field on a physical system. If this were not the case and external forces would be absent, we know that we have another conservation law

$$\vec{P}e^\eta = \vec{K}, \quad (5.39)$$

as a consequence of the third Newton's law

$$\sum_{i=1}^N \vec{F}_i = 0. \quad (5.40)$$

$\vec{P} = \sum_{i=1}^N \vec{p}_i$ is the center-of-mass momentum of the system, \vec{K} is an arbitrary vector in d dimensions. When dealing with a systems with this additional conservation law, the Nosé-Hoover equations do not yield the correct distribution.

[74]

Next the compressibility need to be computed:

$$\kappa = \sum_{i=1}^N \left[\nabla_{\vec{p}_i} \cdot \frac{d\vec{p}_i}{dt} + \nabla_{\vec{r}_i} \cdot \frac{d\vec{r}_i}{dt} \right] + \frac{\partial \frac{d\eta}{dt}}{\partial \eta} + \frac{\partial \frac{dp_\eta}{dt}}{\partial p_\eta} \quad (5.41)$$

$$= - \sum_{i=1}^N d \frac{p_\eta}{Q} \quad (5.42)$$

$$= - dN \frac{d\eta}{dt}, \quad (5.43)$$

from which we can immediately identify the metric

$$\sqrt{g} = \exp(-w) = \exp(dN\eta). \quad (5.44)$$

Using this metric and the energy conservation law, we can write the microcanonical partition function of this universe as follows,

$$\mathcal{Z}_T(N, V, C_1) = \int d^N \vec{p} \int_{D(V)} d^N \vec{r} \int dp_\eta d\eta e^{dN\eta} \quad (5.45)$$

$$\times \delta \left(\mathcal{H}(\vec{r}, \vec{p}) + \frac{p_\eta^2}{2Q} + dNkT\eta - C_1 \right), \quad (5.46)$$

which parametrically depends on the temperature T . After integration over η we get:

$$\mathcal{Z}_T(N, V, C_1) = \frac{e^{\beta C_1}}{dNkT} \int dp_\eta e^{-\beta p_\eta^2/2Q} \int d^N \vec{p} \int_{D(V)} d^N \vec{r} e^{-\beta \mathcal{H}(\vec{r}, \vec{p})}, \quad (5.47)$$

where we can already see that we got the canonical distribution function for the physical system Hamiltonian only with different prefactors. We proved that the Nosé-Hoover equations generate the correct canonical ensemble in the presence of external forces [74].

Now we will go back to the numerical treatment of equations of motion, in this case for a non-Hamiltonian system that can be derived from the formalism of the Liouville operator. We have already mentioned that for a Hamiltonian system, a symplectic property must be preserved, which implies the conservation of the phase-space volume. Even though there is no symplectic property analogue for non-Hamiltonian systems, the generalized Liouville theorem says that the measure $\sqrt{g(x)}dx$ should be preserved. Numerical solvers for non-Hamiltonian systems need to be therefore measure-preserving and this is the minimal requirement needed to be adhered to if we want to generate the correct distribution. We are restricting here to systems of no explicit time dependence.¹

A non-Hamiltonian system of equations

$$\frac{dx}{dt} = \xi(x) \quad (5.48)$$

will be expressed as an operator equations

$$\frac{dx}{dt} = iLx, \quad (5.49)$$

¹The Liouville operator formalism can be extended to the case of explicit time dependence (which is also the framework of this thesis)

where the action of the generalized Liouville operator looks as:

$$iL = \xi(x) \cdot \nabla_x. \quad (5.50)$$

Here the x represents the full phase-space vector

$$x = (\vec{r}_1, \dots, \vec{r}_N, \eta, \vec{p}_1, \dots, \vec{p}_N, p_\eta) \quad (5.51)$$

The Liouville operator can be written as

$$iL = iL_{\text{NH}} + iL_q + iL_p, \quad (5.52)$$

where iL_q and iL_p were already defined previously as (4.13) and (4.14) respectively. These two terms together represent our physical system - the Hamiltonian one. The new term is

$$iL_{\text{NH}} = - \sum_{i=1}^N \frac{p_\eta}{Q} \vec{p}_i \cdot \frac{\partial}{\partial \vec{p}_i} + \frac{p_\eta}{Q} \frac{\partial}{\partial \eta} + G \frac{\partial}{\partial p_\eta}, \quad (5.53)$$

where

$$G = \sum_{i=1}^N \frac{\vec{p}_i^2}{m_i} - dNk_B T. \quad (5.54)$$

We will proceed the same way as for the Hamiltonian case. The solution formally looks $x_t = \exp(iLt)x_0$, which is the same as for the Hamiltonian system. Factorization of the propagator $\exp(iL\Delta t)$ for a single time step using the Trotter expansion can look as:

$$e^{iL\Delta t} = e^{iL_{\text{NH}}\Delta t/2} e^{iL_p\Delta t/2} e^{iL_q\Delta t} e^{iL_p\Delta t/2} e^{iL_{\text{NH}}\Delta t/2} + \mathcal{O}(\Delta t^3) \quad (5.55)$$

This kind of factorization, where in the middle we have three operators that would on its own generate Velocity-Verlet algorithm, and on the ends, we have a non-Hamiltonian part of the Liouville operator, is called an "end" scheme.² In this work, we have decided to use the Leapfrog integrator with the Nosé-Hoover thermostat. The propagator for this case looks as:

$$\exp(iL\Delta t) = \exp(iL_q\Delta t) \exp(iL_{\text{NH}}\Delta t/2) \exp(iL_p\Delta t) \exp(iL_{\text{NH}}\Delta t/2) + \mathcal{O}(t^3) \quad (5.56)$$

From this, it is possible to derive a propagation algorithm [81].

In GROMACS's implementation of the Nosé-Hoover thermostat a new parameter is introduced - the period of the oscillations of kinetic energy between the system and the reservoir τ_T . This parameter is used to determine Q

$$Q = \frac{\tau_T T}{4\pi^2}, \quad (5.57)$$

²An alternative "middle" scheme, where the Liouville propagator for the Nosé-Hoover thermostat is in the middle, is inferior in the case when the studied system is a harmonic oscillator in terms of errors in the configurational distribution.

which describes the system-bath coupling strength. Since Q depends on temperature, it is more intuitive to use τ_T , which is independent of the system size and reference temperature. Nosé-Hoover thermostat produces an oscillatory relaxation to the selected temperature. The relaxation time is much larger than the period of the oscillations that we select [82].

To bring the system to a selected temperature in the equilibration part of the simulation, different, much simpler thermostats are used, e.g. the velocity rescale thermostat, which produces a strongly damped exponential relaxation. These types of thermostats are not suitable for the production run itself, only for the equilibration part, since they do not generate the correct ensemble.

A disadvantage of a simple Nosé-Hoover thermostat is that it can lead to non-ergodic simulation in certain cases, such as a collection of harmonic oscillators. Because of this, a better thermostat, Nosé-Hoover chains, has been developed, where variables that represent the thermostat have their own thermostat, and so on. This is where the "chain" name comes from. In the limit of an infinite chain of thermostats, the dynamics is ergodic, but even a chain of 10 thermostats improves the ergodicity. Unfortunately, it still does not produce an ergodic system [74].

In this work, we wanted to opt for the Nosé-Hoover chain thermostat, but unfortunately GROMACS simulation package has not implemented the combination of Leapfrog integrator with Nosé-Hoover chains yet. That is why we have decided to use a more simple Nosé-Hoover thermostat, which still has the advantage of the extended system thermostats.

5.4 Pressure coupling

To simulate an NPT (isothermal-isobaric) ensemble, one must introduce fluctuations in the volume of the system such that the pressure remains constant. In the case of the Parrinello-Rahman barostat, simulation box vectors represented by a matrix \mathbf{b} obey the following equation:

$$\frac{d^2\mathbf{b}}{dt^2} = V\mathbf{W}^{-1}\mathbf{b}^{\top-1}(\mathbf{P} - \mathbf{P}_{\text{ref}}), \quad (5.58)$$

where V denotes the box volume, \mathbf{W} is a matrix of strength coupling parameters and defines how can the box be deformed. \mathbf{P} and \mathbf{P}_{ref} are matrices representing immediate pressure and reference pressure, respectively. The coupling strength matrix is calculated as follows:

$$\left(\mathbf{W}^{-1}\right)_{ij} = \frac{4\pi^2\beta_{ij}}{3\tau_p^2L}. \quad (5.59)$$

It is more convenient not to think about this matrix dependence on the box length vector L , therefore GROMACS automatically calculates this matrix when the isothermal compressibilities β_{ij} and the pressure time constant τ_p are provided in the GROMACS input file.

Implementation of the Parrinello-Rahman barostat without thermostating leads to the modified Hamiltonian

$$\mathcal{H}_{\text{universe}} = \mathcal{H}_{\text{system}} + V \sum_i P_{ii} + \sum_{i,j} \frac{1}{2} W_{ij} \left(\frac{db_{ij}}{dt} \right)^2 \quad (5.60)$$

which yields the following equations of motion:

$$\frac{d\mathbf{p}_i}{dt} = \mathbf{F}_i - \mathbf{M}\mathbf{p}_i, \quad (5.61)$$

where

$$\mathbf{M} = \mathbf{b}^{-1} \left[\mathbf{b} \frac{d\mathbf{b}^\top}{dt} + \frac{d\mathbf{b}}{dt} \mathbf{b}^\top \right] \mathbf{b}^{\top-1} \quad (5.62)$$

As can be seen from these equations, this barostat gives us the option to apply anisotropic pressure.

Similar to the Nosé-Hoover thermostat, the Parrinello-Rahman barostat is suitable for use when the system is already in equilibrium. If the pressure of the system is too far from the equilibrium, the Parrinello-Rahman coupling can cause large box oscillations and the simulation can even crash. For bringing the system to the desired temperature and pressure the weak-coupling scheme, such as the Berendsen pressure coupling scheme, is preferred [82]. To see the combined Nosé-Hoover thermostat with the Parrinello-Rahman barostat and its derivation in the realm of Liouville formalism, we kindly ask the reader to check [83]

6. Simulation workflow

In this Chapter, we will describe what steps were taken before the actual production run, i.e. the simulation of the tubulin dimer with an external electric field (EEF) of different frequencies. We have decided to use the GROMACS simulation package due to the previous use of this package by other colleagues. Computing infrastructure Metacentrum was used for the calculations [84]. Jobs were submitted on `gpu.long` queue, dedicated to long simulations up to 336 hours. On average, each production run simulation took 300 real-life hours to compute.

6.1 PDB structure and Solvation

As a model system of tubulin dimer, we used the 3J6E microtubule structure obtained from the Protein Data Bank (PDB). This structure contains 2 stabilizing Mg^{2+} cations, GTP molecule and G2P¹ molecule. For our purposes, we exchanged the G2P for the GTP molecule. C-termini were added to this structure because they are important to the biological functions of the tubulin. The importance of C-termini was already discussed in 1.3. Due to quite a huge size of our system of interest (598 949 atoms), a large simulation box was needed to simulate the system properly. As such, a box with an 18 nm side length was used.

Solvation had been done with GROMACS function `gmx solvate`, where we chose the TIP3P model of water, which is a 3-point model. 195 018 water molecules were added. Since the tubulin dimer is a charged structure (-59 e) and there are 2 additional Mg^{2+} cations, 55 sodium cations needed to be added to neutralize the system with the GROMACS function `gmx genion`.

6.2 Minimization

A crucial step is to bring the system to the energy minimum before the simulation itself. A proper way to do this is to use an efficient but not that thorough minimization algorithm such as the steepest descent algorithm first,

$$\mathbf{r}_{n+1} = \mathbf{r}_n + \frac{\mathbf{F}_n}{\max(|\mathbf{F}_n|)} h_n, \quad (6.1)$$

where \mathbf{r}_n is the vector of all $3N$ coordinates, h_n is the maximum displacement and \mathbf{F}_n is the force, all at timestep n . $\max(|\mathbf{F}_n|)$ denotes the largest scalar force on any atom. At the beginning ($n=0$), the maximum displacement has to be given (0.01 nm). For new positions, forces and energy are calculated, and if the energy decreases, the new positions are accepted and $h_{n+1} = 1.2h_n$; otherwise, they are rejected and $h_{n+1} = 0.2h_n$. This algorithm continues until a maximum force on any atom is less than the user-specified value or the maximum number of steps is reached. This algorithm goes to the well of minimal energy rather quickly but is slow to find the really precise minimum inside this well. That is why another algorithm is usually used after the first one. We have chosen to use a conjugate

¹phosphomethylphosphonic acid guanylate ester

gradient algorithm.

The results of these minimizations are provided in table 6.1 and 6.2. As you can see, the steepest descent algorithm was not sufficient to find the proper minimum and the conjugate gradient algorithm was necessary to reach a goal $F_{\max} < 100\text{kJmol}^{-1}\text{nm}^{-1}$.

The steepest descent algorithm reached the following values after 10427 steps.

Potential Energy	= -9.9837920×10^6 kJmol ⁻¹
Maximum force	= 1.2158622×10^3 kJmol ⁻¹ nm ⁻¹ on atom 13765

Table 6.1: Values reached in the minimization step by the steepest descent algorithm in 10427 steps

The conjugate gradients converged to $F_{\max} < 100\text{kJmol}^{-1}\text{nm}^{-1}$ in 1143 steps.

Potential Energy	= -1.0623572×10^7 kJmol ⁻¹
Maximum force	= 9.7807320×10^1 kJmol ⁻¹ nm ⁻¹ on atom 112650

Table 6.2: Values reached in the minimization step by the conjugate gradient algorithm in 1143 steps

Minimization parameter files can be found in the Appendix 10.1.

6.3 Equilibration

Parameters of the equilibration steps can be found in the parameter files in Appendix 10.1.2, 10.1.3, and 10.1.4. Integration step was 1 fs. Trajectories were saved every 10 ps.

In this part of the system preparation, random velocities from a Maxwell-Boltzmann distribution for a certain temperature T are assigned to all of the atoms of the system. After this point, all the consequent simulations are deterministic, and “in theory”, we would always get the same outcome of the next steps. We say “in theory” because computational hardware and settings can slightly influence the outcome of the simulation. Since the simulation is deterministic in nature, to get some statistics, we need to prepare more repetitions of our minimized system that would differ only in random velocities assigned to the atoms at the beginning of the equilibration. Therefore, we pre-prepared four systems that were equilibrated as follows.

After the system has been minimized, it needs to be brought to the desired temperature and pressure; in other words, it needs to be equilibrated. The velocities were assigned randomly, and even though they represent the correct temperature at time $t = 0$ in the next steps, the simulation can blow up due to randomness, since the energy is not distributed evenly. The equilibration step is needed to spread the energy correctly.

It is commonly suggested to equilibrate the solvent around the protein first. Therefore, protein needs to be restrained during this phase.

First, we chose to equilibrate the system to the target temperature (300K) and reach a canonical (NVT) ensemble. This equilibration simulation with restrained protein lasted 10 ns, and the thermostat of choice for this was V-rescale, which is a suitable thermostat for bringing the system to the equilibrium, even though it is not suitable to be used for a production run due to not being able to sample the chosen ensemble correctly.

Since the experiment is done under usual conditions, where the pressure and temperature are approximately constant during the measurement, the solvent needed to be also equilibrated to reach the correct pressure and, therefore, the correct isobaric-isothermal (NPT) ensemble using C-rescale barostat. The chosen pressure was 100 kPa, which is approximately a normal atmospheric pressure. In this part of the equilibration, the thermostat was changed to Nose-Hoover, which samples the canonical ensemble much better than V-rescale but is not that suitable to be used in NVT equilibration itself, as was already mentioned. This choice is valid since the system is already equilibrated to the chosen temperature. The NPT equilibration step lasted an additional 10 ns, and the protein was still restrained.

As a result of these two steps, the solvent (in our case, water) should have been equilibrated by then, and thus, it was time to do the “equilibration” of the whole system with protein being finally unrestrained. We put the quotation marks there since the terminology for this step is not generally recognized. The idea behind this “equilibration” step is that the native structure of the protein does not always match the PDB structure, which is usually determined from the crystallized protein by X-ray crystallography. Here, the target temperature and pressure from the previous steps were left unchanged. This NPT equilibration with unrestrained protein lasted for 100 ns. To verify whether the system is equilibrated, we checked a RMSD plot. Since the protein goes through different conformations even when it is equilibrated, it is sometimes hard to tell whether we have reached a proper equilibrated state.

6.4 Production run

We have prepared three systems following the previous steps - solvation, minimization, velocity generation, and equilibration. After that, production runs started where electric fields 10 - 150 GHz with 10 increment were applied in 6 different directions. The amplitude of the field was 100 MV/m = 0.1 V/nm. Due to periodic boundary conditions, the real magnitude of the electric field inside the simulation box is probably larger. It is assumed that the correct field felt by the protein inside the simulation box is the specified value times dielectric constant of the box [85].

We simulate the effect of EF for 100 ns, while the integration step was held at 1 fs. Trajectories were saved every 1 ps; therefore, this yielded 100 000 frames per trajectory. Each initial condition with subsequent production runs is called a batch. To understand this workflow fully, it is probably better to visualize it, and so we tried - see Figure 6.1. The initial conformations of each “batch” can be viewed in Figures 6.2a, 6.2b, and 6.2c.

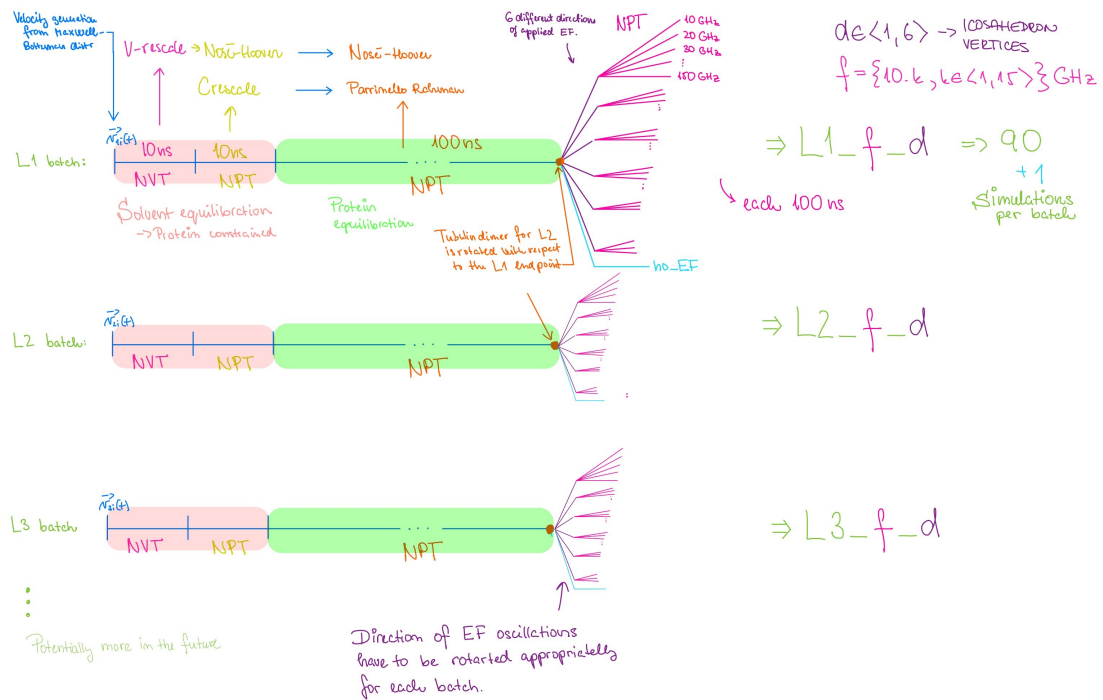


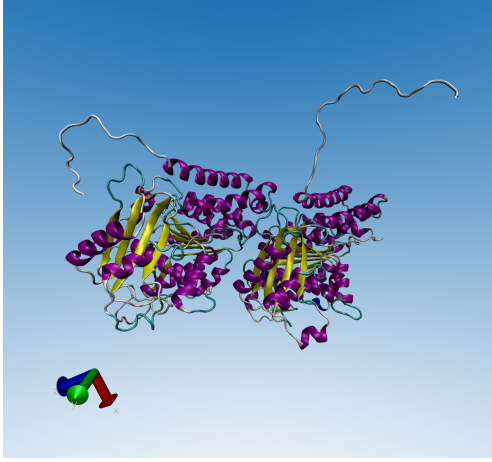
Figure 6.1: Workflow scheme; L_i represents batch i , d directions, f frequency; no EF - case of no electric field; v_{0j} represent the generated velocities

6.4.1 Directions of applied Electric Field

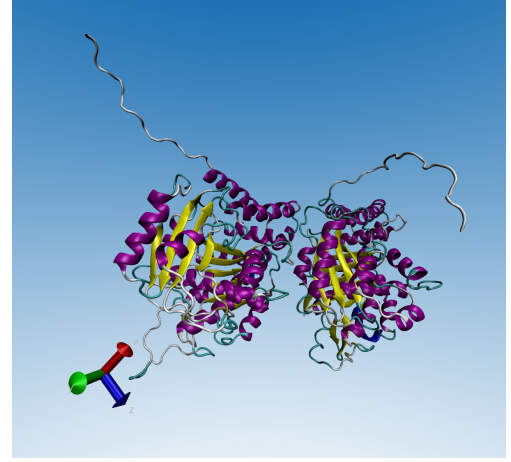
Since the assigned velocities at the beginning of the first equilibration steps are different for each repetition (=batches with different velocities generated and assigned to the atoms before the equilibration), the final frames of the last equilibration step will have a protein in a different conformation. Most importantly, protein will be rotated. The snapshots of the tubulin dimer at the last frame before the electric field is applied can be seen in Figure 6.2. We can see that the tubulin is in a different starting conformation.

We want to apply an external oscillating electric field in 6 different directions, trying to mimic a real-life situation where tubulin dimers are randomly rotated in a sample. For an already computationally heavy system, choosing 6 directions should be quite enough of a sampling. Since we want the applied electric field directions to be uniformly distributed in 3D, the best way to do it is to find a uniform distribution of points on the sphere. This can be a task in itself, but since it is well-known that platonic solids have their vertices uniformly distributed on a circumscribed sphere, we choose icosahedron vertices to define the 6 unique directions of the electric field. Icosahedron has 12 vertices, 6 of which inverse to the other 6.

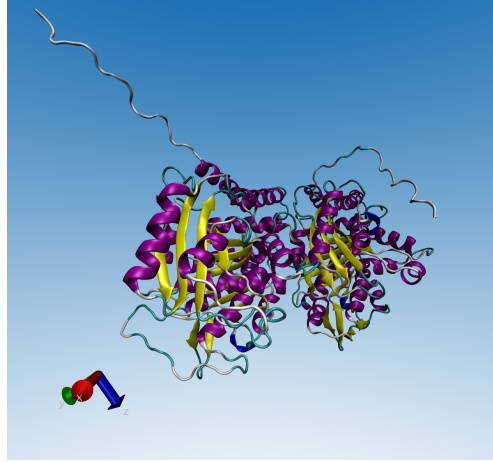
$$\begin{aligned} & \pm (1, 0, 0) \\ & \pm \left(\frac{1}{\sqrt{5}}, \frac{2}{\sqrt{5}}, 0 \right) \\ & \pm \left(\frac{1}{\sqrt{5}}, \frac{1 - \frac{1}{\sqrt{5}}}{2}, \pm \sqrt{\frac{1 + \frac{1}{\sqrt{5}}}{2}} \right) \end{aligned}$$



(a) Initial conformation of the batch 1 simulations



(b) Initial conformation of the batch 2 simulations



(c) Initial conformation of the batch 3 simulations

Figure 6.2: Initial conformations for the production runs

$$\pm \left(\frac{1}{\sqrt{5}}, \frac{-1 - \frac{1}{\sqrt{5}}}{2}, \pm \sqrt{\frac{1 - \frac{1}{\sqrt{5}}}{2}} \right)$$

Let us assume we have vectors that connect the origin (the centre of the icosahedron) with its vertices, then

$$\vec{v}_i = -\vec{v}_j,$$

where $i = 1 \dots 6, j = 7 \dots 12$. However, since we have an oscillating electric field, an oscillation in direction \vec{v}_i is (up to the phase) the same as an oscillation in direction \vec{v}_j . That is why we have chosen \vec{v}_i with + to be directions of the oscillation of the applied external electric field.

For the first batch (repetition), these exact directions have been used. For the second batch, the protein is rotated in the last frame of protein equilibration with respect to the protein in the first batch. Therefore, we have written and implemented a Python code that determines the two axes of rotation and corresponding angles and, consequently, rotates the vertices vectors in such a way

that the external electric field is applied to the tubulin in approximately the same direction. The centre-point of the program is a Rodriguez rotational formula for axes.

6.4.2 Rotation of icosahedron program

Program consists of 3 parts.

1. Determination of the tubulin orientation in a box in the last frame of protein equilibration for each batch.
2. Calculation of the angles of rotations of tubulin initial conformation (which is the last frame of the equilibration) of each batch with respect to the 1st batch.
3. Rotation of the icosahedron vertices for the second and the third batch, such that they cross the tubulin in the same direction for each batch.

The corresponding program can be found in the Appendix in 10.2.

The electric-field oscillation directions with respect to the tubulin structure are shown in Figure 6.3.

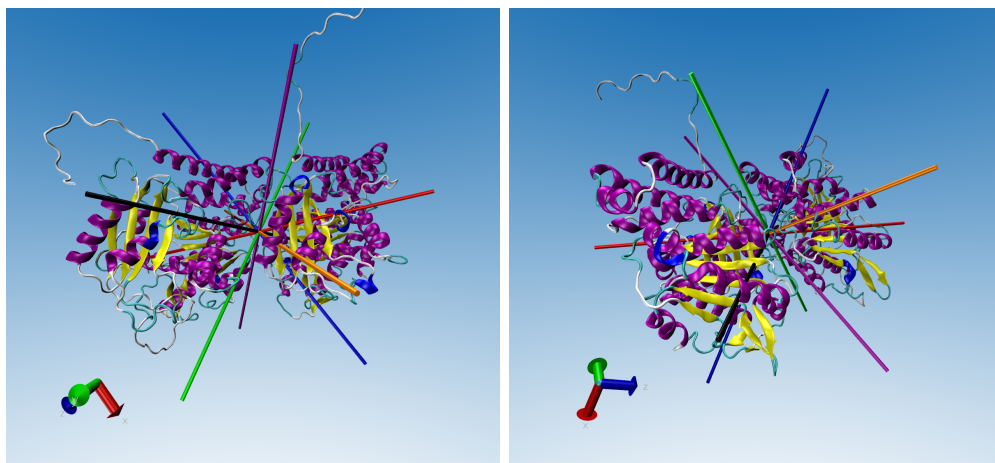


Figure 6.3: Directions of the electric field oscillations, colour-coded. Blue - d1; orange - d2; green - d3; red - d4; purple - d5; black - d6; shown for initial frame of production run for batch 1. The program rotates these vertices for the next two batches in such a way that they will have the same relative direction with respect to the protein structure; two different points of view on the structure

6.5 Trajectory conversion

During the simulation tubulin is subjected to diffusion, therefore it tends to move and cross the border of the simulation box. In order to proceed further with the analysis of the trajectories, we must first take care of this and move the protein back into the simulation box. For this, a GROMACS function `gmx trjconv` was used. There can be a lot done with this function, but we have mainly used it

to centre or rotationally and translationally fit the tubulin dimer to its desired previous position. The centring process is not that easy for multimeric proteins, and since the documentation is not that clear on what the individual parameters of this function do, it was quite a long process to find the right combination of commands to provide us with correct results, where the tubulin heterodimer is together and not separated on the opposite sites of the box. In 10.3, we provide one of the many scripts used for trajectory conversion, where you can see the use of different functions, such as `make_ndx`, whose role is to create new index groups - parts of the structure. In this way, we have created index groups for specific residues or their atoms that make up different parts of the tubulin heterodimer, such as C-termini or binding sites.

7. Methods

Root Mean Square Deviation (RMSD) and Root Mean Square Fluctuation (RMSF) of the system’s coordinates are fundamental tools in the analysis of molecular dynamics simulations, each serving distinct purposes in evaluating the behaviour and stability of molecular systems.

7.1 Root Mean Square Deviation (RMSD)

RMSD quantifies the average deviation of a set of coordinates from a reference set over time. In the context of MD simulations, the reference typically represents the system’s starting configuration ($t = 0$). The first step of the RMSD calculation is to align the current-frame structure to the reference structure to eliminate the translational and rotational motion of the protein. This is done for all frames. Then, the calculation of the RMSD itself is done by taking the square root of the average of the squared deviations of the atomic positions from the reference coordinates. Mathematically, for a system with N atoms, RMSD at time t is given by:

$$\text{RMSD}(t) = \sqrt{\frac{1}{N} \sum_{i=1}^N (\vec{r}_i(t) - \vec{r}_i(0))^2}, \quad (7.1)$$

where $\vec{r}_i(t)$ is the position of the i -th atom at time t , and $\vec{r}_i(0)$ is the reference structure of the i -th atom.

By plotting RMSD versus time, one can observe how the molecular structure evolves relative to its initial configuration. Significant deviations indicate conformational changes, while smaller deviations suggest structural stability.

7.2 Root Mean Square Fluctuations (RMSF)

RMSF, on the other hand, measures the flexibility of individual atoms or residues over the entire simulation trajectory. RMSF of atom i is calculated as follows:

$$\text{RMSF}(i) = \sqrt{\frac{1}{T} \sum_{j=1}^T (\vec{r}_i(t_j) - \langle \vec{r}_i(t_j) \rangle)^2}, \quad (7.2)$$

where $\langle \vec{r}_i(t_j) \rangle$ is the average position of the atom i over the simulation time T . For every frame, the structure is fitted to the average structure so that we truly calculate the fluctuations of the atoms. We can always determine which part of the protein will be used for the fitting procedure. Usually, only the most stable atoms are considered, such as protein backbone or C_α atoms. After this fitting part, the RMSF of all the atoms or residues is calculated.

Usually, RMSF is plotted against residue number. The RMSF of a residue is calculated as the mean value of the RMSF of each atom that the residuum

consists of.

The analysis of RMSF is useful for understanding the dynamic behaviour of different parts of the molecule, such as identifying flexible loops or stable cores. High RMSF values correspond to the regions of the molecule with high flexibility, whereas rigid parts of the molecule have low RMSF values.

RMSD and RMSF provide complementary insights. RMSD vs time tracks the overall conformational stability and changes of the entire protein or selected regions (e.g., backbone, side chains, or other) over time. It is useful for identifying periods of equilibrium and major structural transitions, whereas RMSF gives us the fluctuations of individual residues.

7.3 Rotational analysis

To study the rotational motion of the tubulin dimer in the presence of the external electric field, a new Python code has been written. The MDAnalysis package was used to load the trajectories to Python.

From the RMSF data, we had to determine which residues are the most stable, from which we consequently had to choose two atoms that would represent the longitudinal axis of the tubulin dimer. Each of these atoms should have been ideally from the different tubulin monomer and relatively far from each other. We chose atoms with indexes 88 and 7863 to be used for this. These atoms defined the vector, which represents the longitudinal axis of our tubulin dimer. Then we studied the rotation of this axis with respect to the external electric field direction of oscillation. We calculated the dot product between this vector and the corresponding direction of oscillation for that simulation. An explanation of what are the exact directions of the oscillation can be found in Chapter 4. Angle θ between the vector representing longitudinal axis \vec{a} and the unit vector corresponding to the axis of electric field oscillation \vec{e} , which is a unit vector, was determined

$$\theta(t) = \arccos\left(\frac{\vec{e}(t) \cdot \vec{a}(t)}{|\vec{a}(t)|}\right). \quad (7.3)$$

We provide a part of the code that has been used in this analysis in the Appendix: 10.4.

7.4 Analysis of dipole moment dynamics

The tubulin heterodimer possesses a substantially large permanent dipole moment. Our investigation aims to determine how this dipole moment responds to the influence of an electric field ranging from 10 to 150 GHz in frequency. We examined the evolution of the dipole moment for both the entire tubulin dimer and also for the dimer without the C-termini.

Dipole moment serves as an approximation to the charge distribution in space, representing the second term in the multipole expansion. Consequently, excluding a segment of the protein could potentially yield non-representative outcomes, given its role in describing spatial charges. Our rationale for computing the dipole

moment of the tubulin dimer without the C-termini stems from their typically unstructured and freely moving nature, often not in close proximity to the protein bulk. Although occasionally interacting with the structured region of tubulin, they reside externally. Thus, our approach remains valid.

Our structure, the tubulin dimer, has a nonzero charge (-59 e), which means that the dipole moment is not invariant under the translation of the point of reference. The best way to calculate the dipole moment is with respect to the centre of charge. We developed custom code for this analysis due to the limitation of the GROMACS package, which does not facilitate dipole moment calculations for specific segments of molecules. To load the trajectories, we have again used the MDAnalysis Python package. The code that calculated the dipole moment components, its magnitude and its projection onto the direction of electric field oscillations for the whole tubulin dimer can be found in the Appendix 10.5.

8. Results

In this chapter, we will present and describe the results. There will also be comments on how they were calculated in practice. The potential consequences of the effects found will be discussed in the next chapter.

8.1 Outline

We will start with the presentation of the Root mean square deviations - RMSD data of the whole tubulin, tubulin without very flexible unstructured C-termini and the RMSD of the C-termini alone. Then, we will proceed with the root mean square fluctuation (RMSF) data. We specifically concentrated on the RMSF of the residues that form binding sites of several anti-tubulin drugs. What follows is the analysis of the rotational movement of the tubulin dimer. At last, we will present the data of the calculated time series of dipole moment magnitudes and their projections onto the electric field oscillation axes.

8.2 RMSD Analysis

We present here the results of the RMSD analysis. Besides the time series of RMSD, histograms (distributions) of the RMSD are also plotted. They help us to determine how long the tubulin stayed in one conformation. In each graph, corresponding to different frequencies and batches, there are RMSD data for simulations with 6 different directions of the electric-field oscillation, together with the RMSD of the tubulin, when no electric field is applied (as a reference). By looking at the graphs, we can see that for certain combinations of initial conformation, frequency of EF and direction of EF, tubulin ended up exploring quite different parts of the phase space. There is a huge overall difference in the RMSD of the third batch. To remind the reader, batches differ by different initial conformation of tubulin. You can view these initial conformations here: 6.2. For the initial conformations 1 and 2 (batch 1 and 2), the RMSD is much higher overall than for the initial conformation 3, regardless of whether the electric field is applied or not. Initial conformation of batch 3 is therefore much more stable conformation than the ones of batch 1 or 2.

8.2.1 RMSD - Batch 1

First, we will discuss batch 1. The case of no EF is rather interesting here, too. We can see that around the time 40 ns, the RMSD got quite high, and the tubulin ended up having a rather stable conformation. This is caused by the change in the C-termini state, as can be seen by the comparison of the whole-tubulin RMSD vs. C-termini RMSD vs. tubulin-without-C-termini RMSD.

Similar **RMSD fluctuation change of C-termini of batch 1** was also achieved when the following combination of frequency and direction of electric

field was applied to our structure:

- 10 GHz - d2
- 20 GHz - d3 and d4 - even the same mean RMSD, therefore the same stable conformation of C-termini
- 30 GHz - d3 - also the same mean RMSD,
- 40 GHz - d1 - also the same mean RMSD; and d5,
- 50 GHz - d4, d5 (not that stable),
- 60 GHz - d3,
- 70 GHz - d1 and d6 - also the same mean RMSD,
- 80 GHz - d1 - also the same mean RMSD,
- 90 GHz - d1 and d5 - also the same mean RMSD,
- 100 GHz - d1 and d2 - also the same mean RMSD,
- 110 GHz - d6 - - also the same mean RMSD; d3 only for a short period of time (10 ns)
- 120 GHz - d4, d5 and d6 - also the same mean RMSD
- 130 GHz - d2 - also the same mean RMSD,
- 140 GHz - d2 and d6; d5 shortly
- 150 GHz - d1, d2, d3 - also the same mean RMSD

When we compare the RMSD of the whole tubulin vs the ones for the tubulin without C-termini (bulk tubulin) or just the C-termini, we can also observe conformational changes in the bulk of the tubulin dimer.

A distinct changes in conformations of the bulk are caused by the following electric fields of specific directions:

- 10 GHz
 - d3 - larger RMSD for the first 20 ns
 - d5 - larger RMSD around 30-60 ns
 - d1, d3 and d6 - RMSD is larger in the last 10 ns
- 20 GHz
 - d2 - Really big fluctuations in RMSD between 20 - 60 ns, then stable conformation
 - d4 - Distinctively different stable conformation after 60 ns of electric field application

- 30 GHz
 - d2 - higher RMSD fluctuation in the end of the simulation and around 50 ns
 - d6 - transiently higher RMSD around 50 ns
- 40 GHz
 - d4 and d5 - Different stable conformation reached around 70 ns and 20 ns, respectively
- 50 GHz
 - d4 - different stable conformation reached around 70 ns
- 70 GHz
 - d5 - different stable conformation
- 80 GHz
 - d2 - stable conformation hopping in the first 40 ns
 - d4 - different conformation in the last 30 ns
- 100 GHz
 - d1, d2, d4 - different stable conformation
- 110 GHz
 - d2, d3, d6 - different stable conformation
- 120 GHz
 - d1, d2, d3 and d5 - slightly different - higher RMSD - different stable conformation
 - d4 - higher RMSD that fluctuates a lot - not a stable conformation
- 130 GHz
 - d2 - slightly higher mean RMSD for the whole simulation - different stable conformation
 - d3, d4, d5 - even higher mean RMSD than for d2
- 140 GHz
 - d3 - higher RMSD, not that stable
- 150 GHz
 - d1, d6 - higher mean RMSD

There can also be seen more subtle changes in the conformation of the bulk of tubulin; in the previous list, we only wrote out the most obvious ones.

RMSD of the whole tubulin dimer - Batch 1

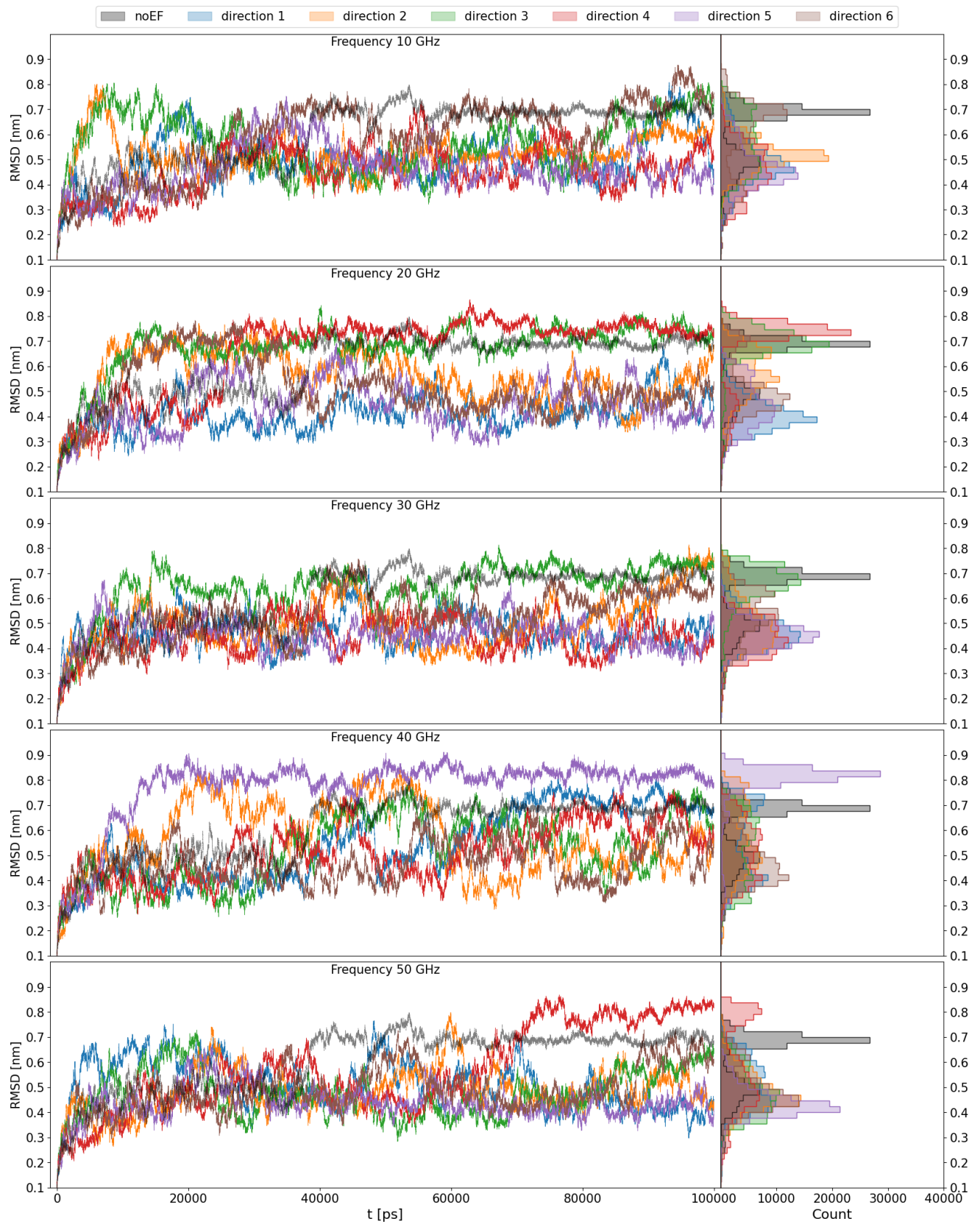


Figure 8.1: RMSD of the tubulin dimer - Batch 1 - Part 1

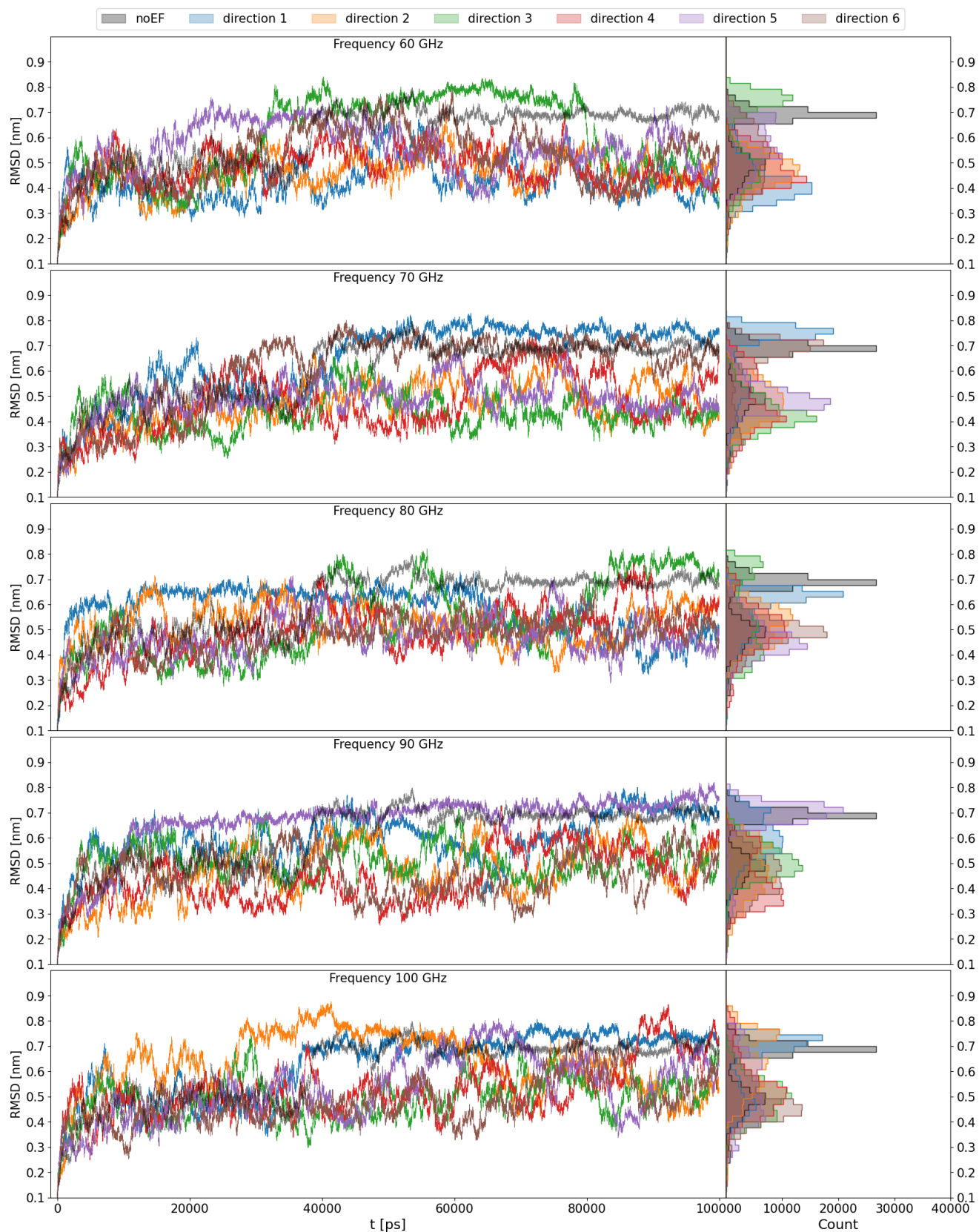


Figure 8.2: RMSD of the tubulin dimer - Batch 1 - Part 2

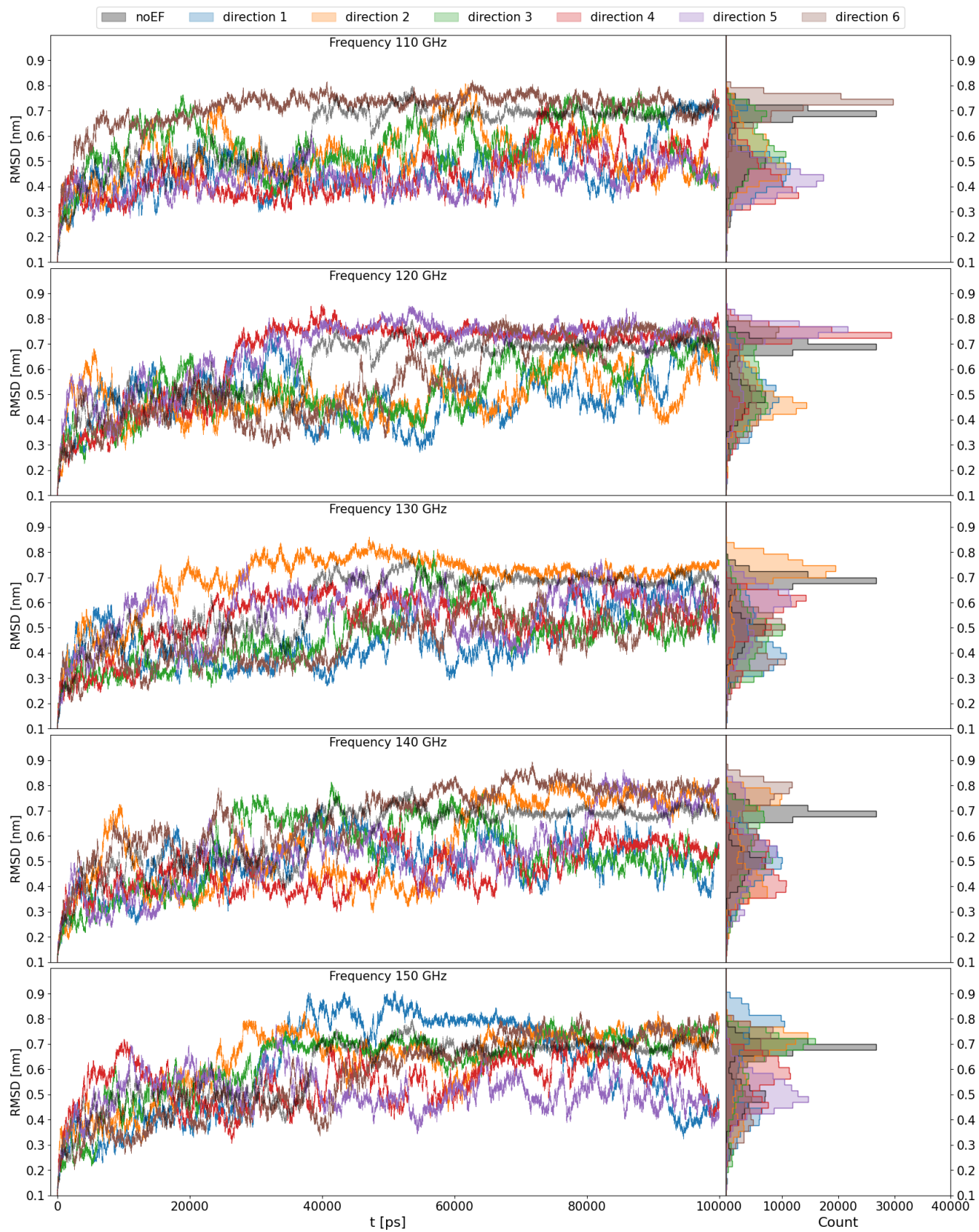


Figure 8.3: RMSD of the tubulin dimer - Batch 1 - Part 3

RMSD of the tubulin dimer without the C-termini - Batch 1

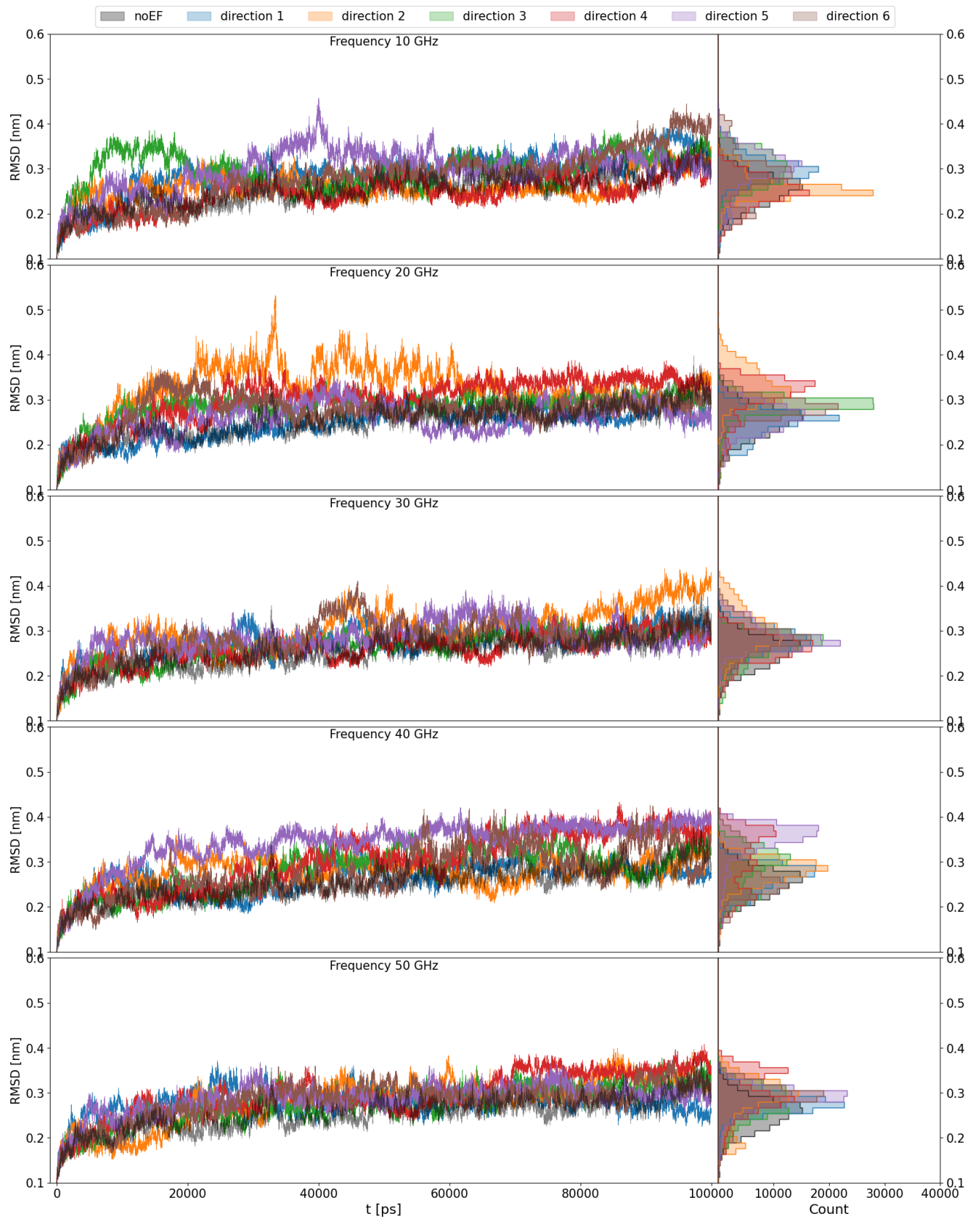


Figure 8.4: RMSD of the tubulin dimer without the C-termini - Batch 1 - Part 1

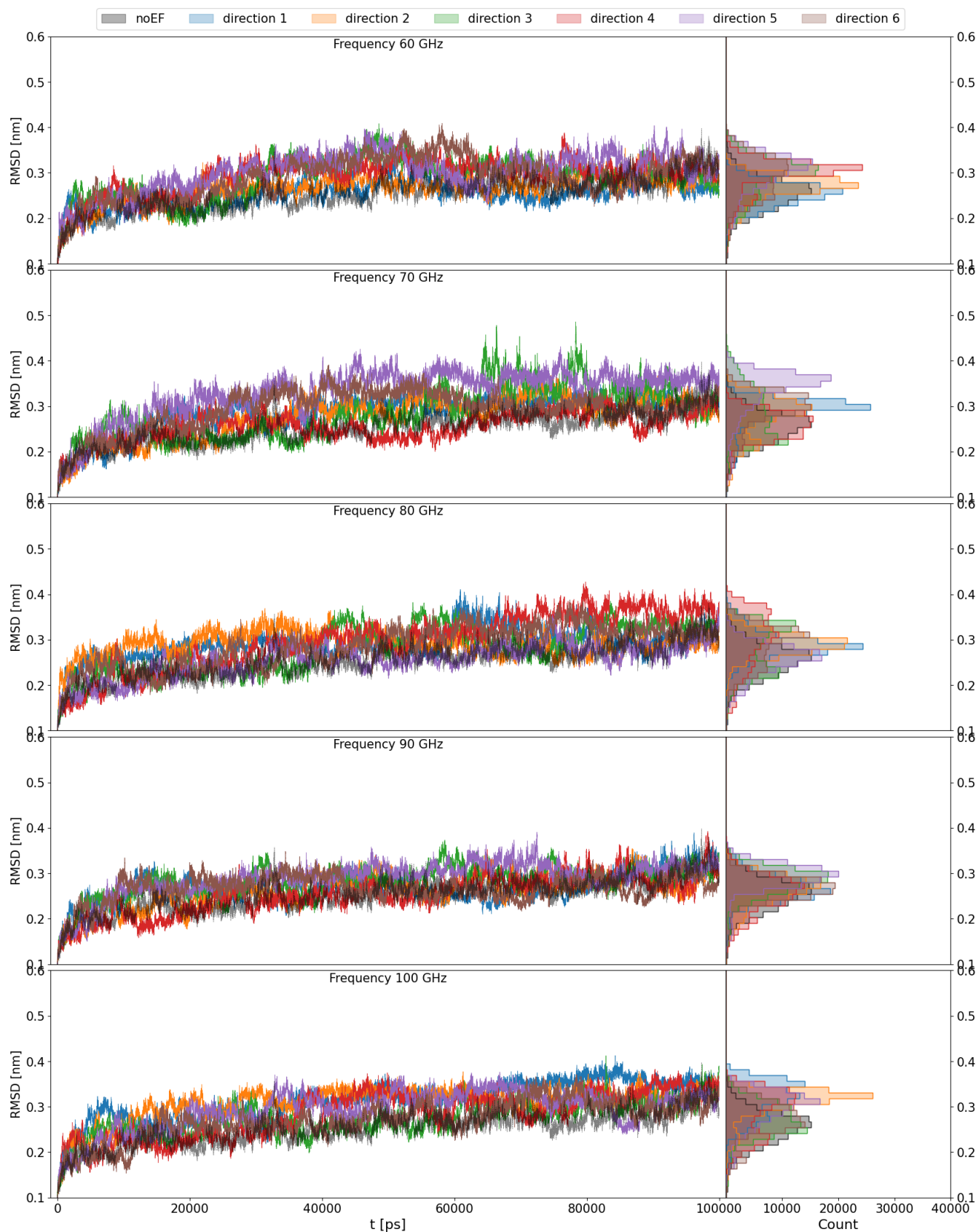


Figure 8.5: RMSD of the tubulin dimer without the C-termini - Batch 1 - Part 2

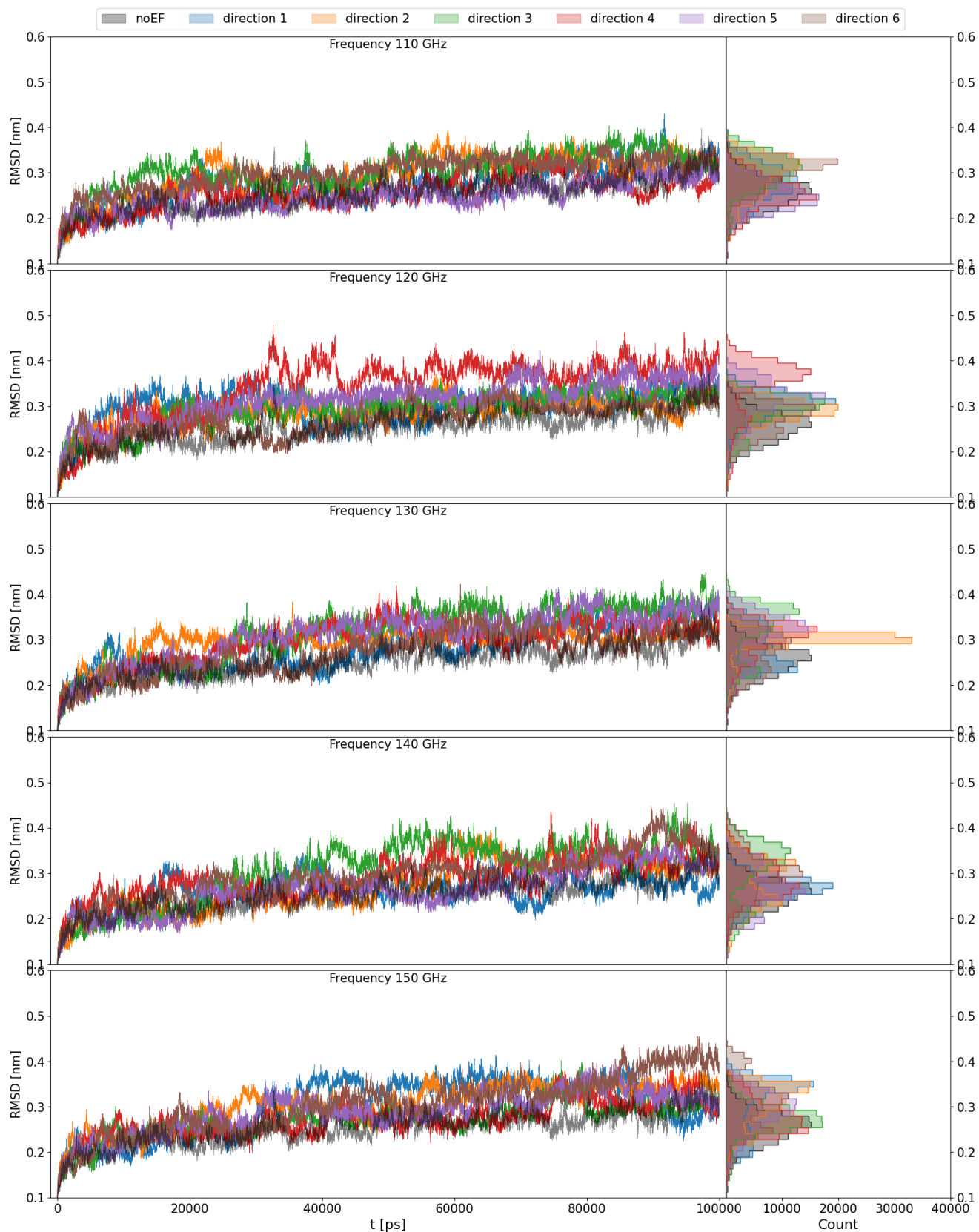


Figure 8.6: RMSD of the tubulin dimer without the C-termini - Batch 1 - Part 3

RMSD of the C-termini - Batch 1

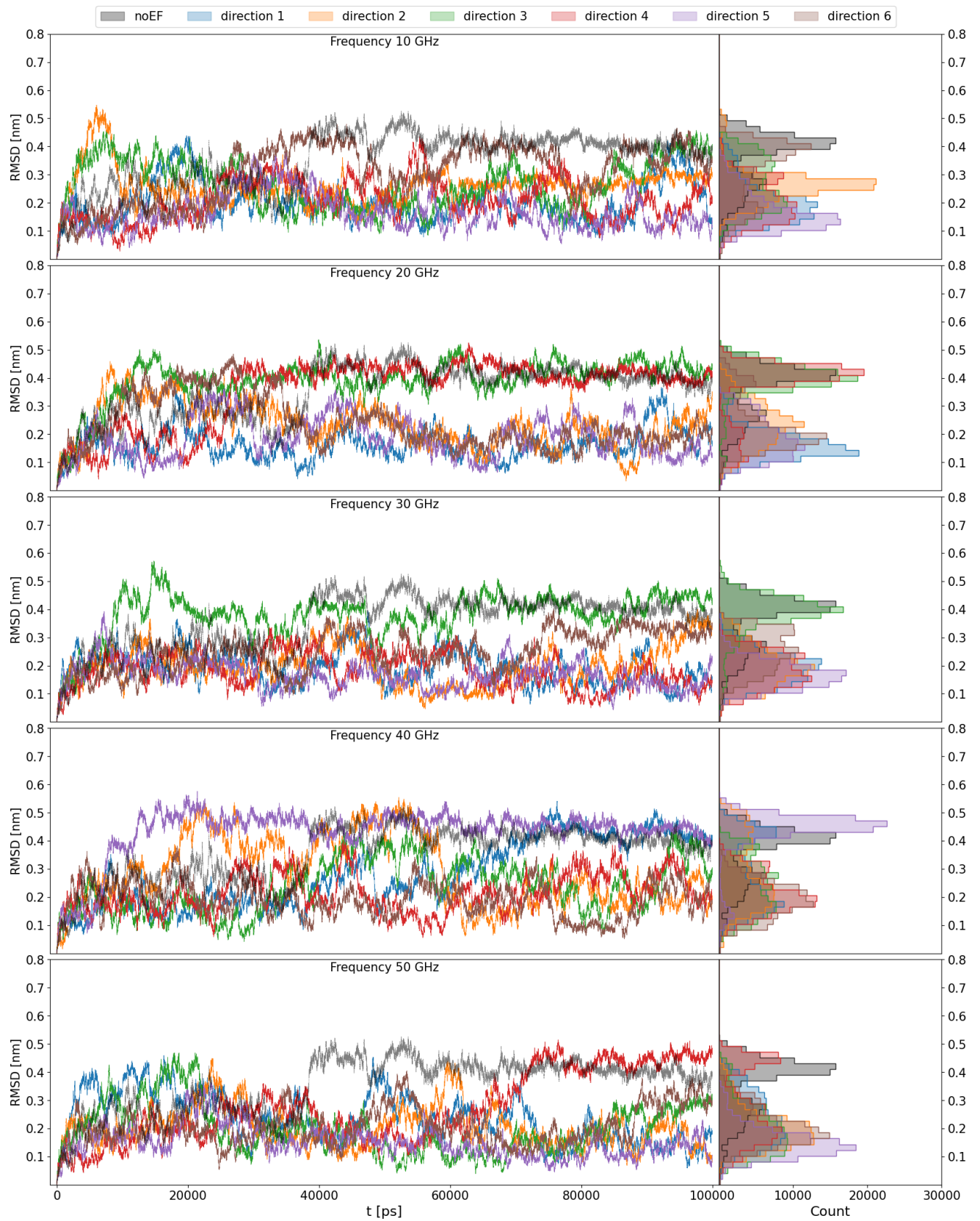


Figure 8.7: RMSD of the C-termini of the tubulin dimer - Batch 1 - Part 1

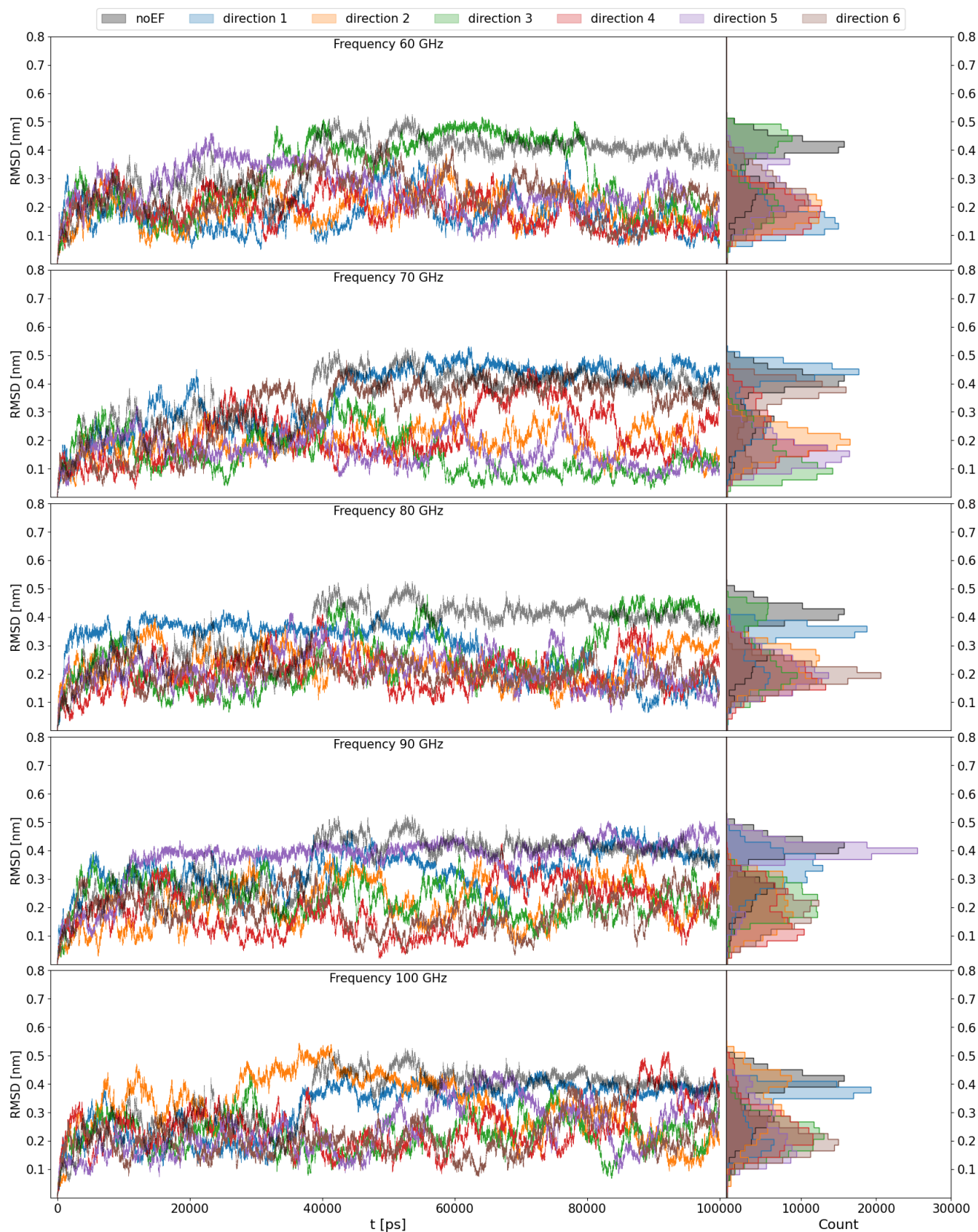


Figure 8.8: RMSD of the C-termini of the tubulin dimer - Batch 1 - Part 2

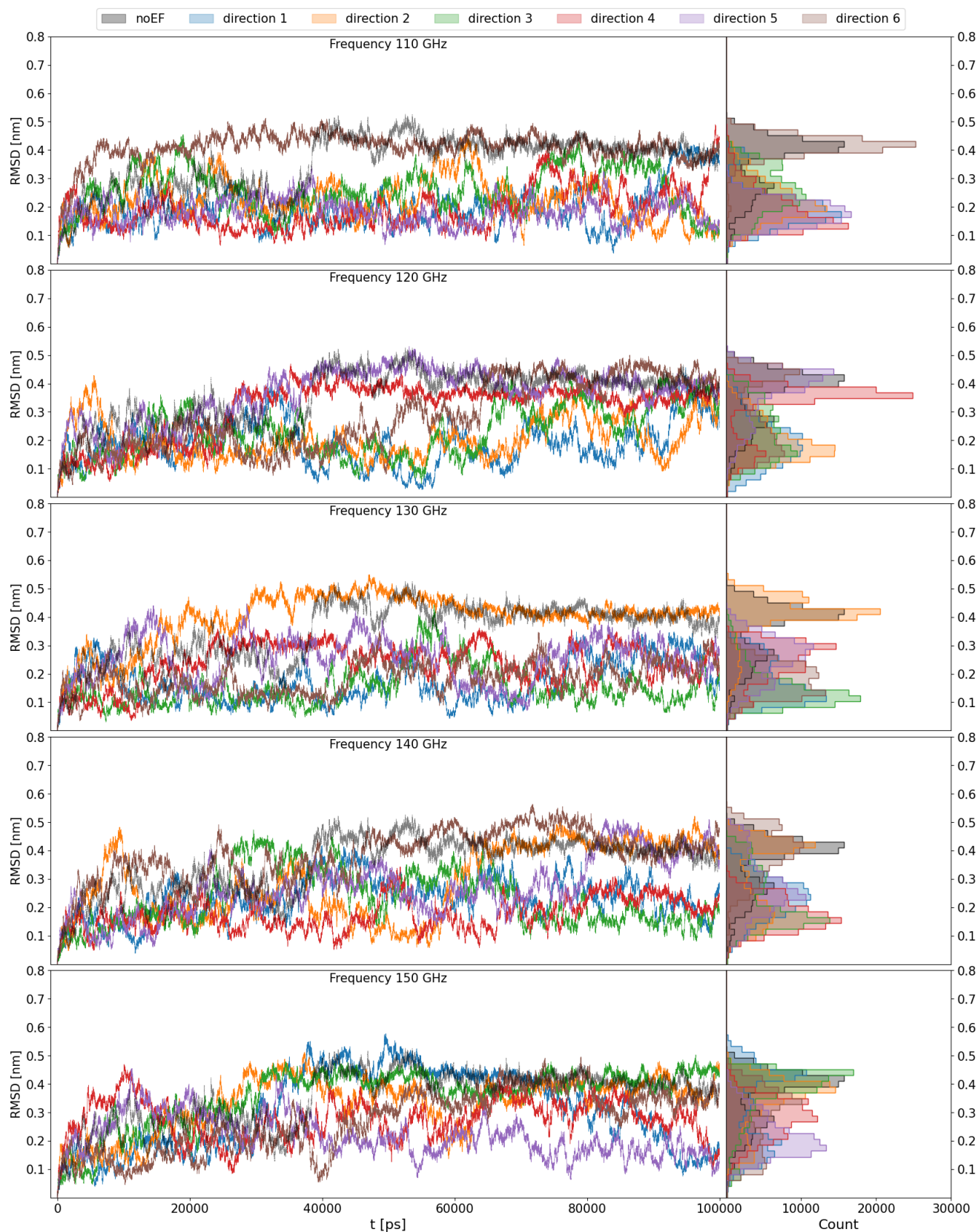


Figure 8.9: RMSD of the C-termini of the tubulin dimer - Batch 1 - Part 3

8.2.2 RMSD - Batch 2

The no EF trajectory of the batch 2 has stable RMSD of the bulk tubulin around 0.21 nm. However, the C-termini in this no EF simulation of batch 2 is completely flexible - it has high fluctuations of RMSD.

First, we will comment on the bulk tubulin RMSD. There can be seen rather large RMSD fluctuations of tubulin bulk for some electric fields. We also observe a change of tubulin conformation to more stable ones under the effect of electric fields. Overall, the bulk RMSD is higher in the cases with EF. However, the RMSD of C-termini is overall lower.

Effect of EF on the bulk of tubulin dimer

- 10 GHz
 - d1 - high RMSD and high RMSD fluctuations for the majority of simulation
 - d6 - switch to a higher RMSD between 65-90 ns
- 20 GHz
 - d2, d4, d5 - higher fluctuations of RMSD
- 30 GHz
 - Rather stable conformations except for a 10 ns for d2.
- 40 GHz
 - d1 - Different stable conformation with low fluctuation
- 50 GHz
 - d2, d4, d5 - higher RMSD fluctuations
- 60 GHz
 - d6 - different stable conformation
- 70 GHz
 - d1 - different rather stable conformation of a larger RMSD compared to no EF case.
- 80 GHz
 - d4 - very large RMSD fluctuations
 - d2 - very large RMSD fluctuations for a short period of time
- 90 GHz
 - d1, d3 - higher mean RMSD
 - d4 - between 20 - 60 ns a larger RMSD, which fluctuates, but not as much as for 80 GHz

- 100 GHz
 - d1, d4, d4, d5 - higher mean RMSD and bit higher fluctuations of RMSD
- 110 GHz
 - d1 - a very large change of RMSD to a higher value (0.4 nm). Fluctuations are larger but the conformation seems rather stable.
 - d2, d4, d6 - a larger mean RMD
- 120 GHz
 - d2,d5 - higher fluctuations of RMSD in some parts of the simulation
- 130 GHz
 - d3 - a large change of mean RMSD and also large fluctuations
- 140 GHz
 - d2, d4 - slightly higher RMSD, d4 has also high RMSD change around 45 ns, but comes back to lower RMSD
- 150 GHz
 - d5 - different stable conformation throughout the whole simulation

Effect of EF on the C-termini part of the tubulin dimer When it comes to the C-termini part of the tubulin, the effect of the electric field on the batch 2 has some stabilizing properties, especially these combinations of frequency and directions:

- 10 GHz - d5 - low mean RMSD (0.15 nm), still fluctuates
- 20 GHz - d3 - very low mean RMSD (0.1 nm), intermediate fluctuations
- 30 GHz - d1, d4, d6 - very low fluctuations of RMSD, additionally d6 -very low mean RMSD
- 40 GHz - d2 - low RMSD, intermediate fluctuations, d5 - very low mean RMSD, intermediate fluctuations
- 50 GHz - d1, d3 - very low mean RMSD, intermediate fluctuations
- 60 GHz - d3, d6 - very low mean RMSD, low fluctuations
- 70 GHz - d1 - very low mean RMSD, very low fluctuations, d6 - very low mean RMSD, intermediate fluctuations, d3 - low mean RMSD, very low fluctuations
- 80 GHz - d2, d4 - very low mean RMSD, intermediate fluctuations
- 90 GHz - d4, d5 - low mean RMSD, intermediate fluctuations, d6 low (0.2 nm) mean RMSD and very low fluctuations

- 100 GHz - d2 and d6 - very low mean RMSD, intermediate fluctuations
- 110 GHz - d2 and d3 - low mean RMSD, intermediate fluctuations, d5 - low mean RMSD (0.2 nm), very low fluctuations
- 120 GHz - d1 - low mean RMSD (0.2 nm), low fluctuations
- 130 GHz - d2 and d6 - very low mean RMSD, intermediate fluctuations
- 140 GHz - d1, d3 and d5 - very low mean RMSD, low fluctuations
- 150 GHz - d4, d6 - low mean RMSD, intermediate fluctuations, d5 - high RMSD, very low fluctuations at some longer intervals

Also, other combinations of parameters showed lower RMSD and stabilizing actions; we only mentioned the most obvious ones. To get more insight, please check the following Figures: 8.16, 8.17, and 8.18

RMSD of the whole tubulin dimer - Batch 2

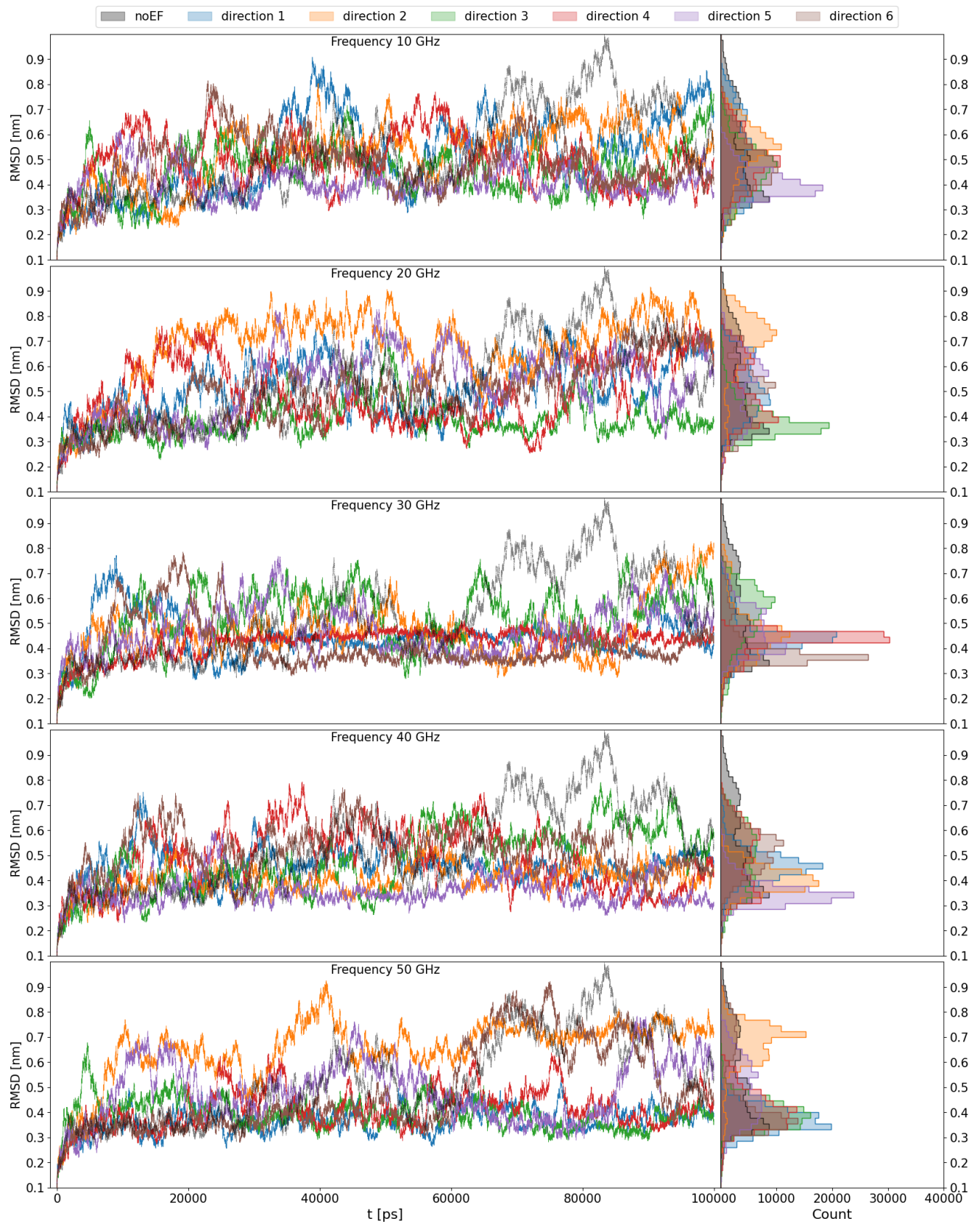


Figure 8.10: RMSD of the tubulin dimer - Batch 2 - Part 1

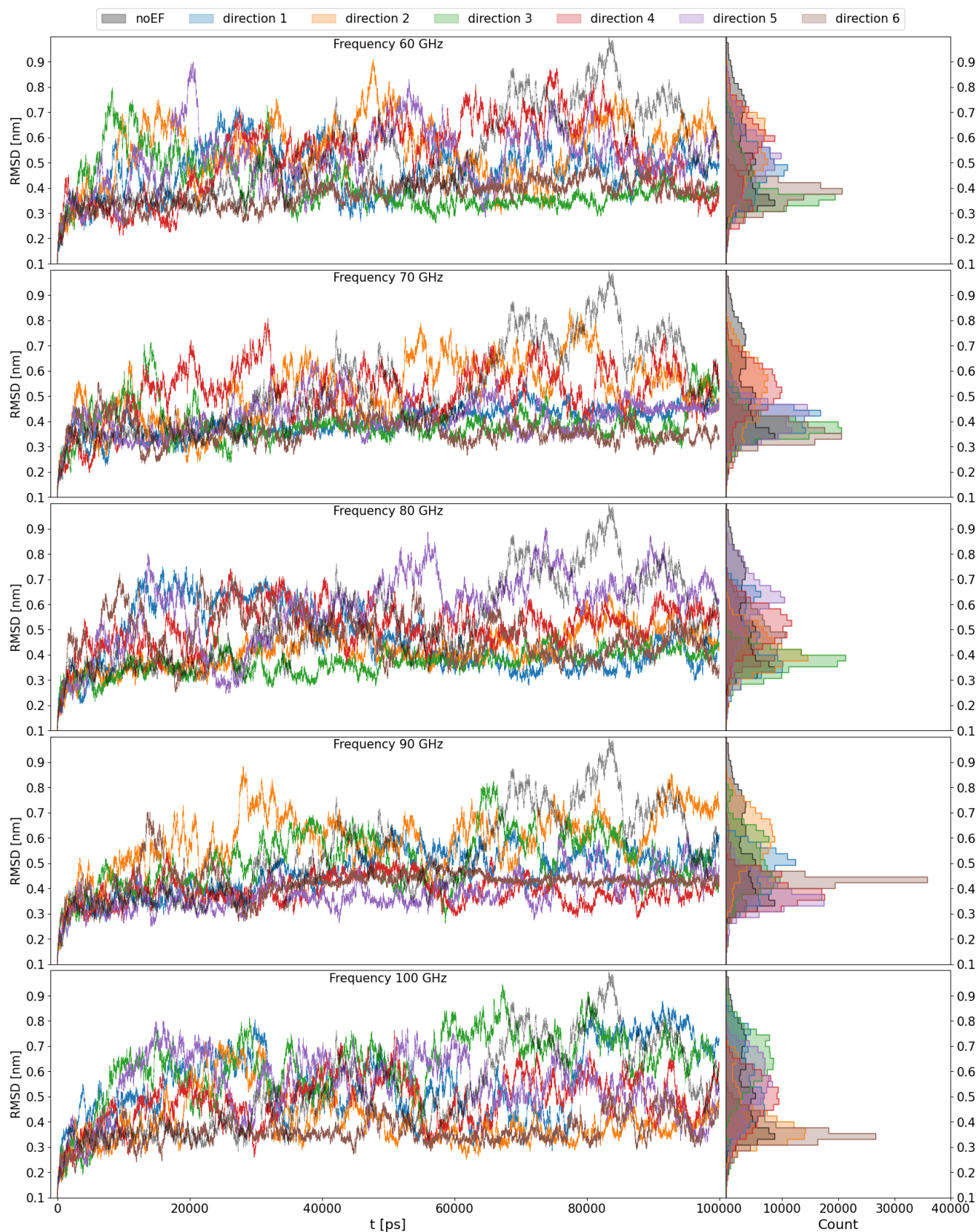


Figure 8.11: RMSD of the tubulin dimer - Batch 2 - Part 2

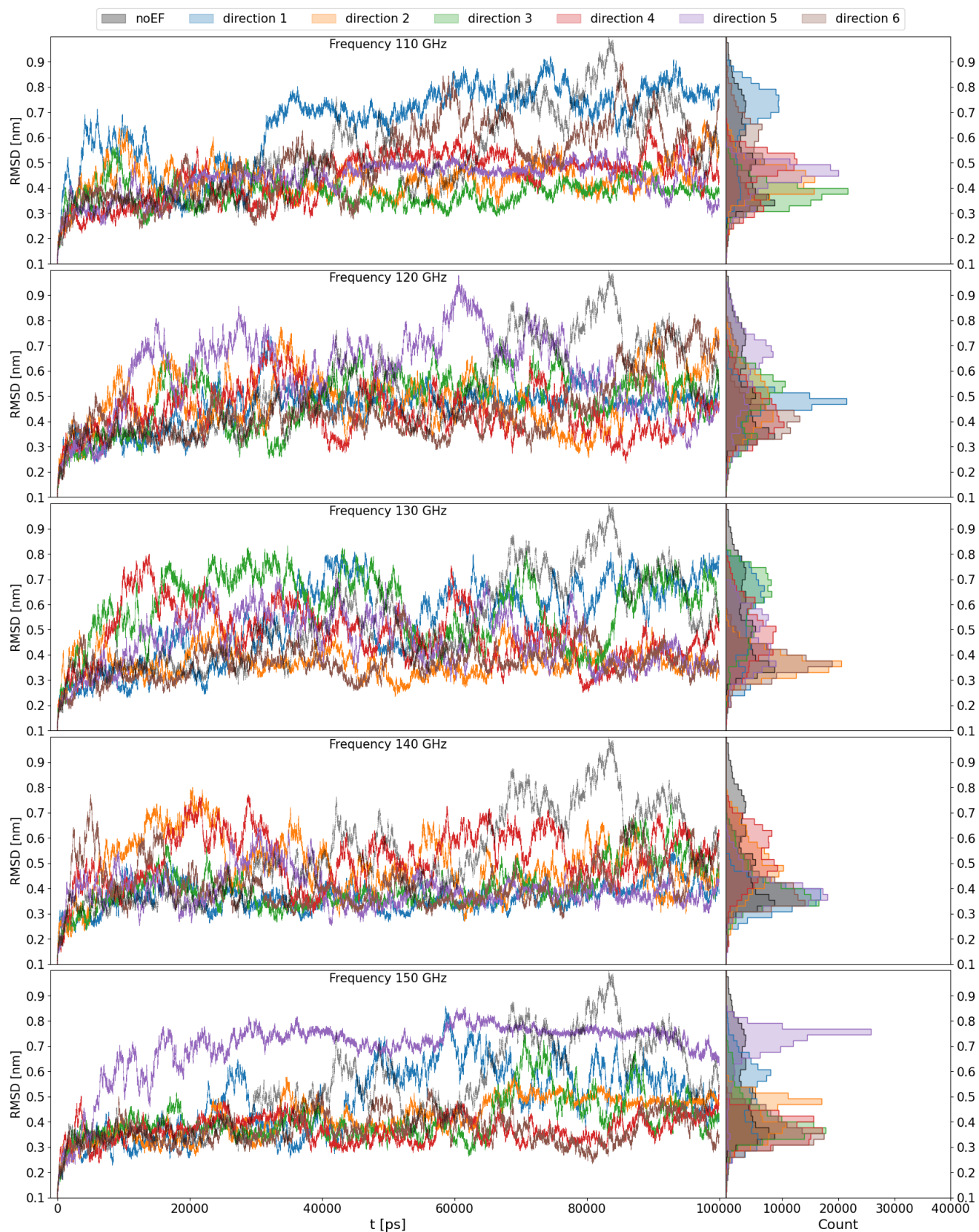


Figure 8.12: RMSD of the tubulin dimer - Batch 2 - Part 3

RMSD of the tubulin dimer without the C-termini - Batch 2

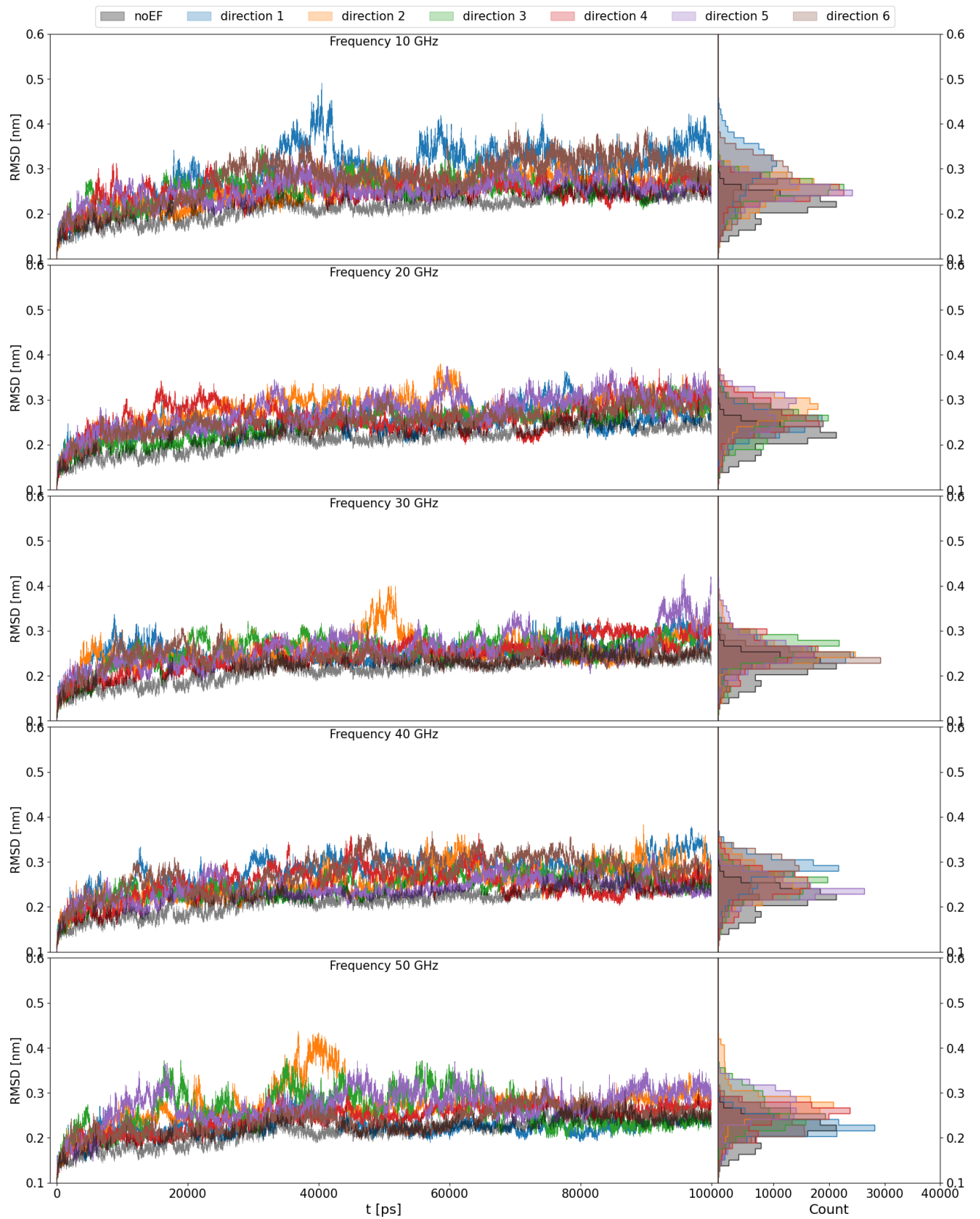


Figure 8.13: RMSD of the tubulin dimer without the C-termini - Batch 2 - Part 1

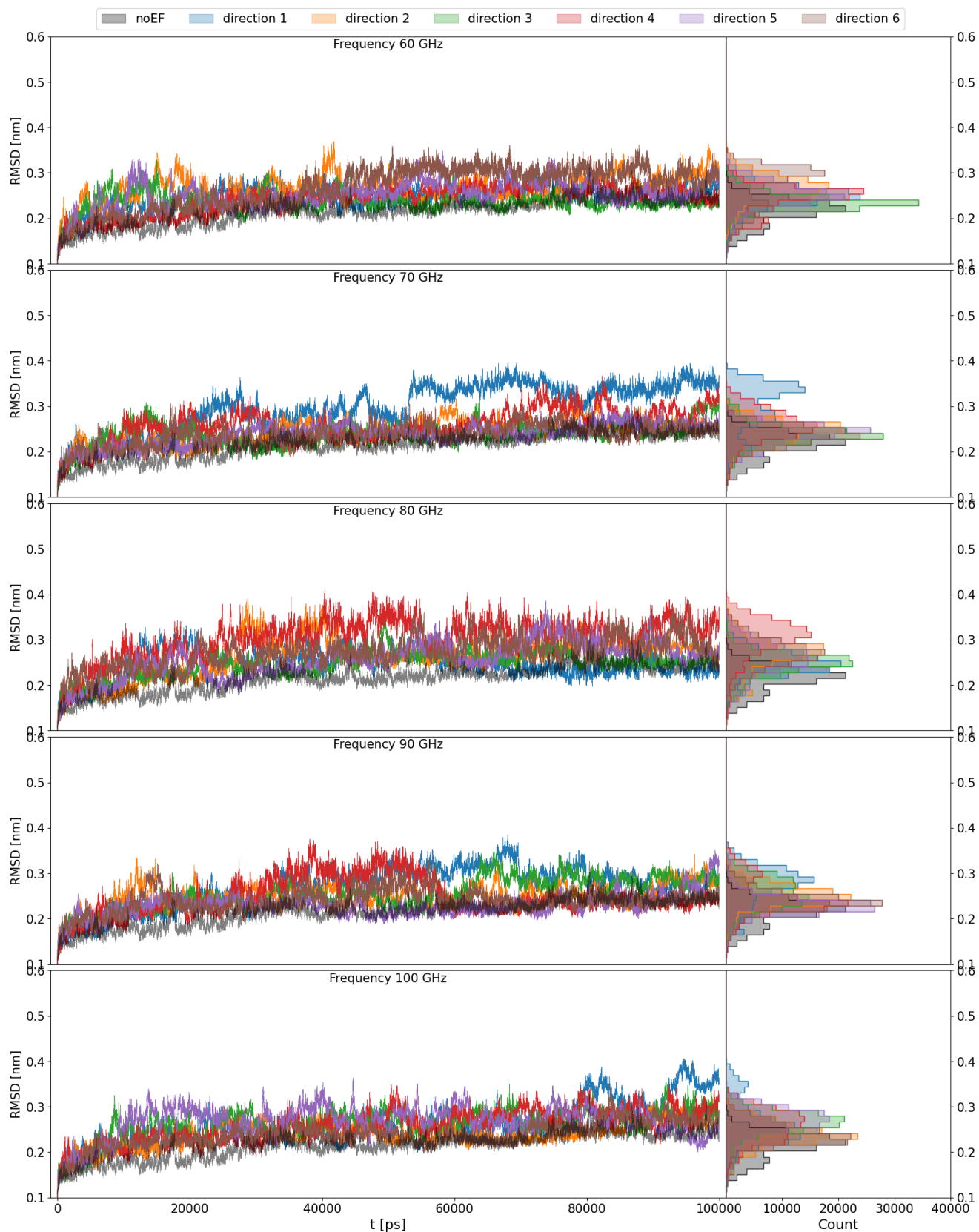


Figure 8.14: RMSD of the tubulin dimer without the C-termini - Batch 2 - Part 2



Figure 8.15: RMSD of the tubulin dimer without the C-termini - Batch 2 - Part 3

RMSD of the C-termini - Batch 2

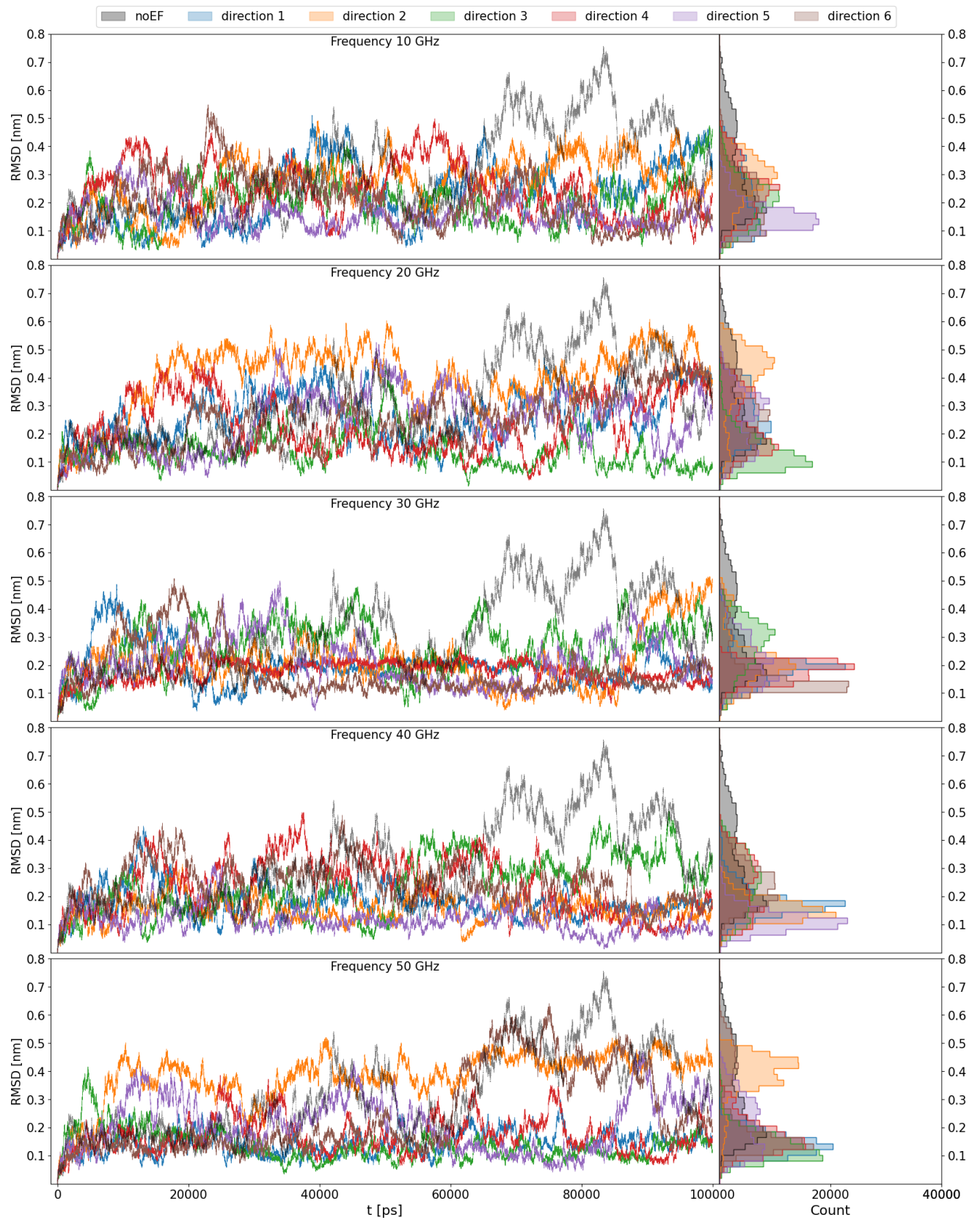


Figure 8.16: RMSD of the C-termini of the tubulin dimer - Batch 2 - Part 1

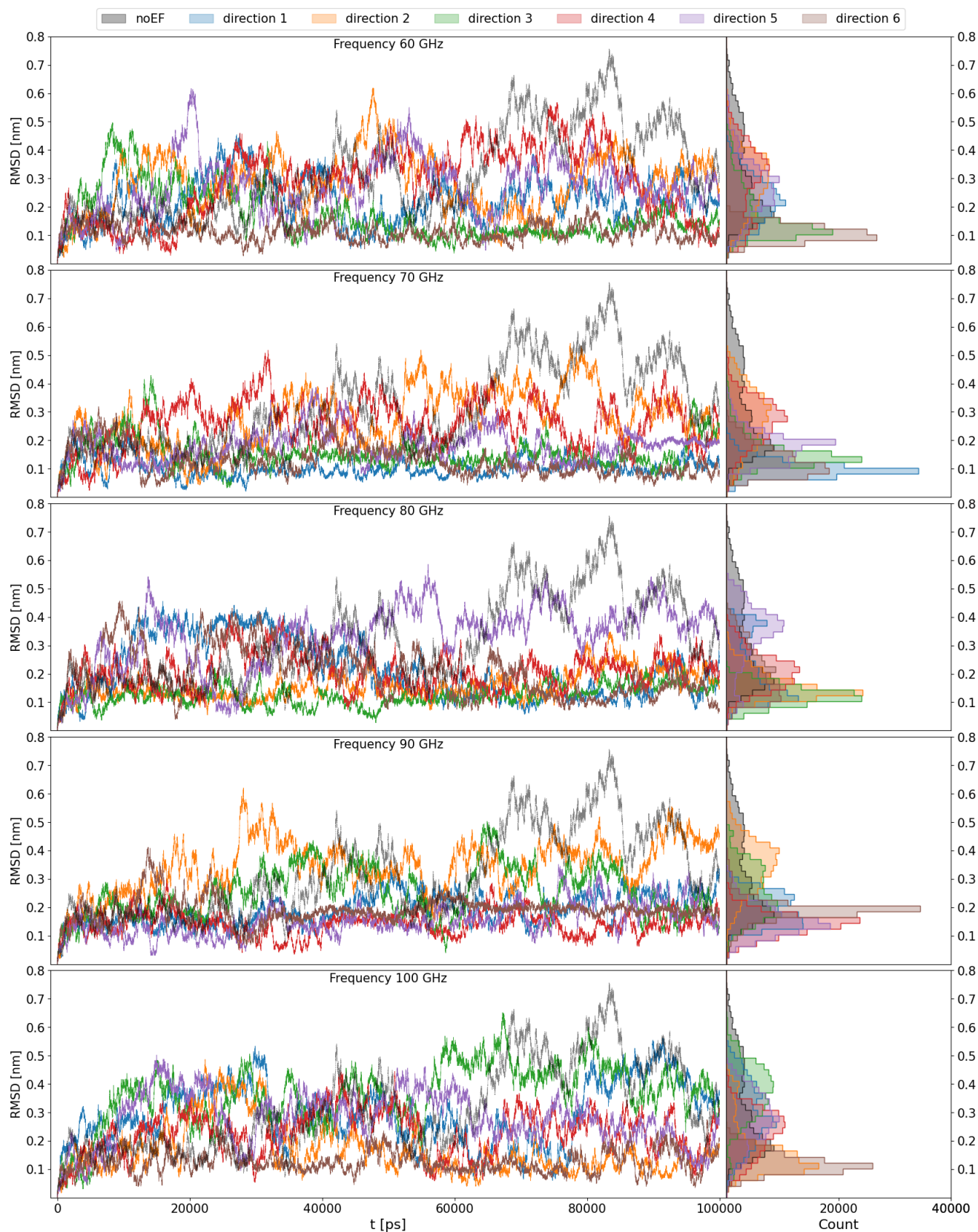


Figure 8.17: RMSD of the C-termini of the tubulin dimer - Batch 2 - Part 2

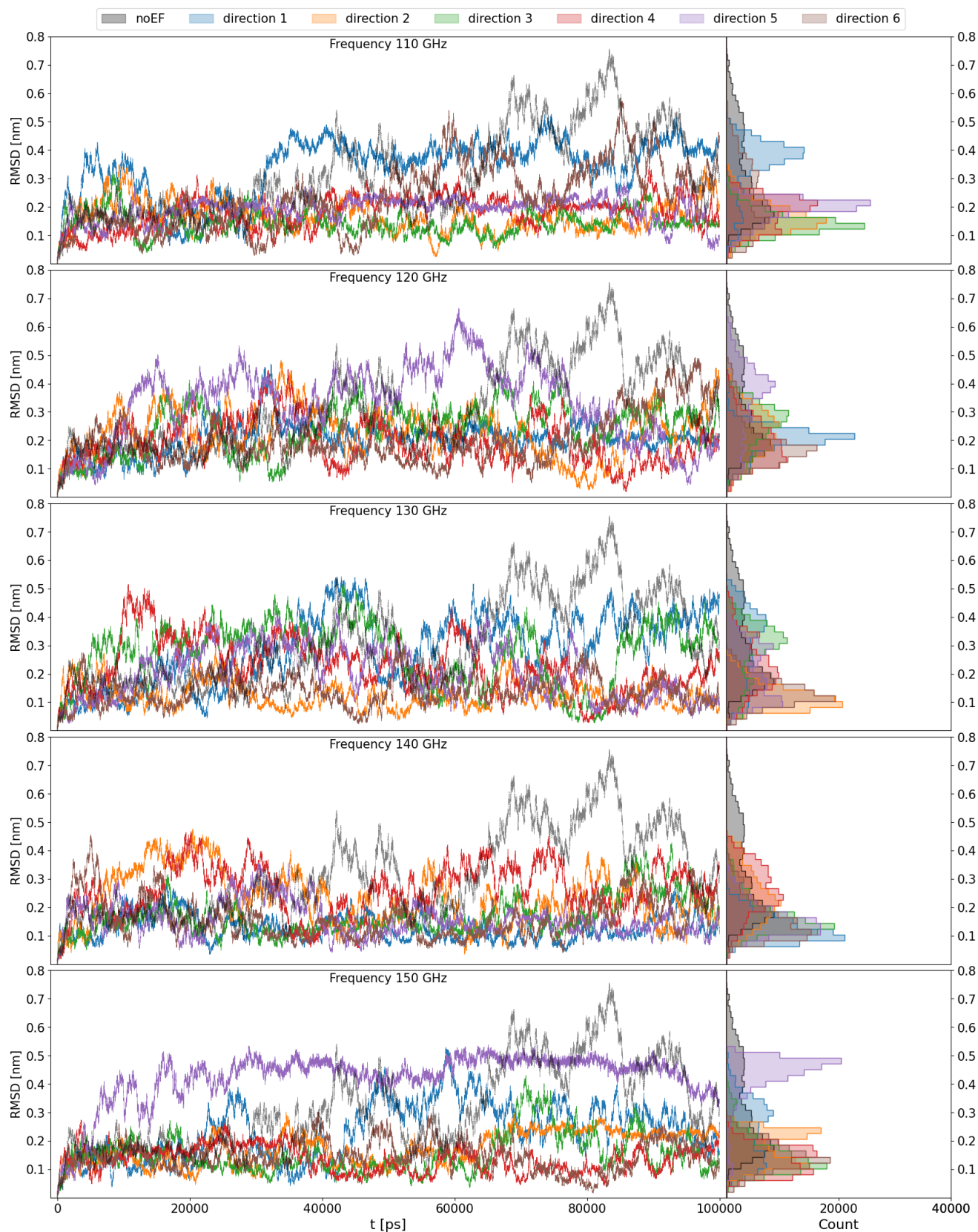


Figure 8.18: RMSD of the C-termini of the tubulin dimer - Batch 2 - Part 3

8.2.3 RMSD - Batch 3

The RMSD for the third batch is much lower for nearly all of the directions and frequencies than for the first two batches. After the equilibration, tubulin must have found a pretty stable conformation. However, for certain frequencies and directions of an electric field, we see that the tubulin ended up getting out of that conformation. To see the state of this initial conformation, we loaded it to VMD and realized that the C-termini of tubulin β is in close proximity to the bulk of tubulin (“connected”).

Comparing the graphs for the whole protein, protein without C-termini, and for only C-termini, we can say that the majority of the changes in the conformation state of tubulin for the third batch are caused by C-termini movement.

We can see the change of the C-termini state to a more flexible one for the electric field of 10 GHz and direction d2, 20 GHz and directions d1, d3 and d4.

For 30 GHz, we can see a similar behaviour for direction d1, but interestingly, for direction d4, the C-termini found another even more stable conformation since the fluctuations of RMSD were even smaller and around a different value: 0.2 nm. This happened around 20 ns. By checking this concrete trajectory in VMD, we realised this is because also the second C-terminus of tubulin α got stuck in close proximity to the bulk (is “connected” to the bulk).

The second C-terminus getting in the stable conformation also happened for the 40 GHz and direction d2, but at a later time. We can also see a change in RMSD for d3, but the C-termini does not cause it.

For the electric field of 50 GHz applied in directions d3, d4, and d6, the RMSD after 60 ns got quite high for this batch. Again, it is caused by the change in the conformation of the C-terminus. It moved from a stable state to a flexible one, where it goes through some conformational ensemble rather quickly.

The 60 GHz electric field introduced only slightly higher RMSD for d1, d4 and d5. In the last 10 ns of the simulation with 60 GHz applied in direction d4, the RMSD got quite high and oscillated a lot.

70 GHz electric field in the direction d4 caused a change of conformation of the C-terminus during the first 25 ns that corresponded to the transient, more flexible conformations.

When 80 GHz electric field was applied, we saw a significant conformational change of C-termini only for the direction d3. The fluctuation of the deviations was quite high, therefore corresponding to more flexible conformations, where neither of the C-termini is connected to the tubulin bulk.

For the electric field of 90 GHz and direction d6 and d4 we saw C-termini switching to another stable conformation around 22 ns and 60 ns, respectively. This means the second C-terminus is connected to the bulk.

100 GHz applied in direction d1 also caused this switch to another stable conformation, but around 75 ns, both C-termini got out of this conformation, and the RMSD rose to a higher value - 0.8 nm; and around 90 ns it dropped to 0.6 nm. This frequency of EF applied in direction d3 also caused the RMSD to rise (around the time 70 ns).

For 110 GHz we have not seen any major deviation from the case of no electric field.

The 120 GHz applied in direction d6 caused a switch to a different conformation of C-termini - where both C-termini are free moving through a certain

conformational ensemble.

The electric field of 130 GHz and 140 GHz applied in the direction d5 yielded conformation where both C-termini are connected to the bulk and are, therefore, more stable. Additionally, the EF of 140 GHz in the direction d2 also led to this switch.

For 150 GHz, only if applied in direction d1, we could see the change in the conformation, which again is caused by the C-terminus getting out of the stable configuration to the free-moving one.

RMSD of the whole tubulin dimer - Batch 3

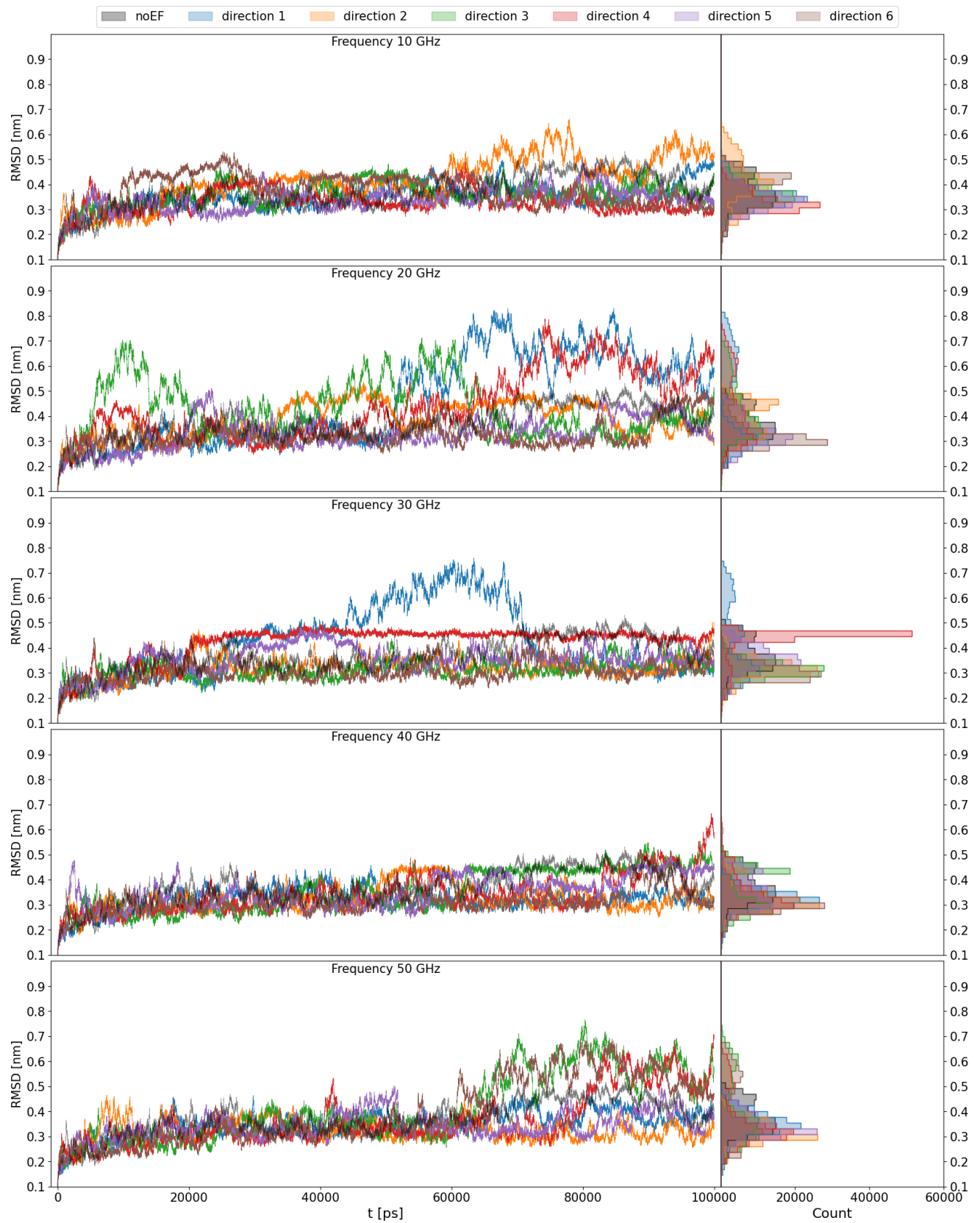


Figure 8.19: RMSD of the tubulin dimer - Batch 3 - Part 1

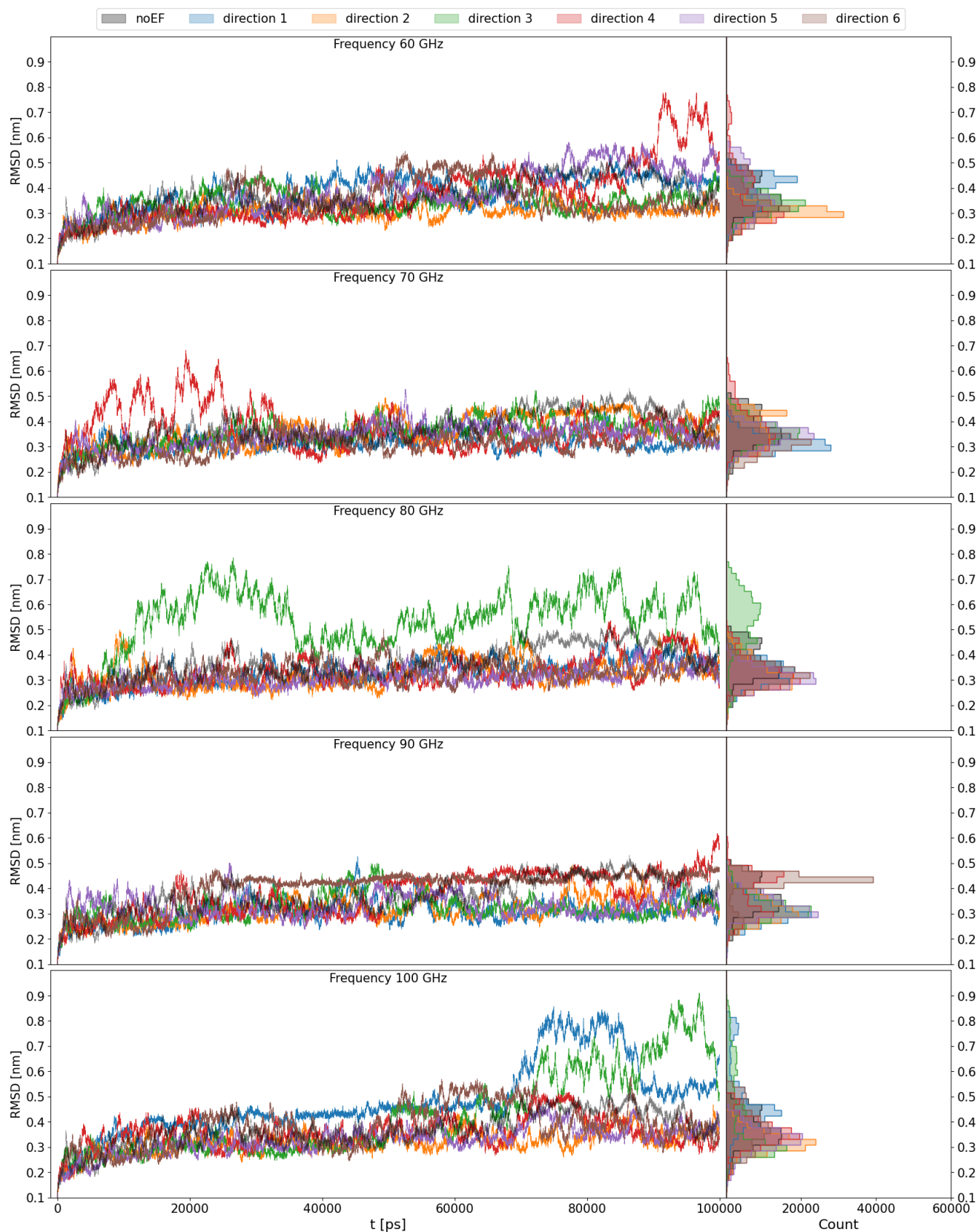


Figure 8.20: RMSD of the tubulin dimer - Batch 3 - Part 2

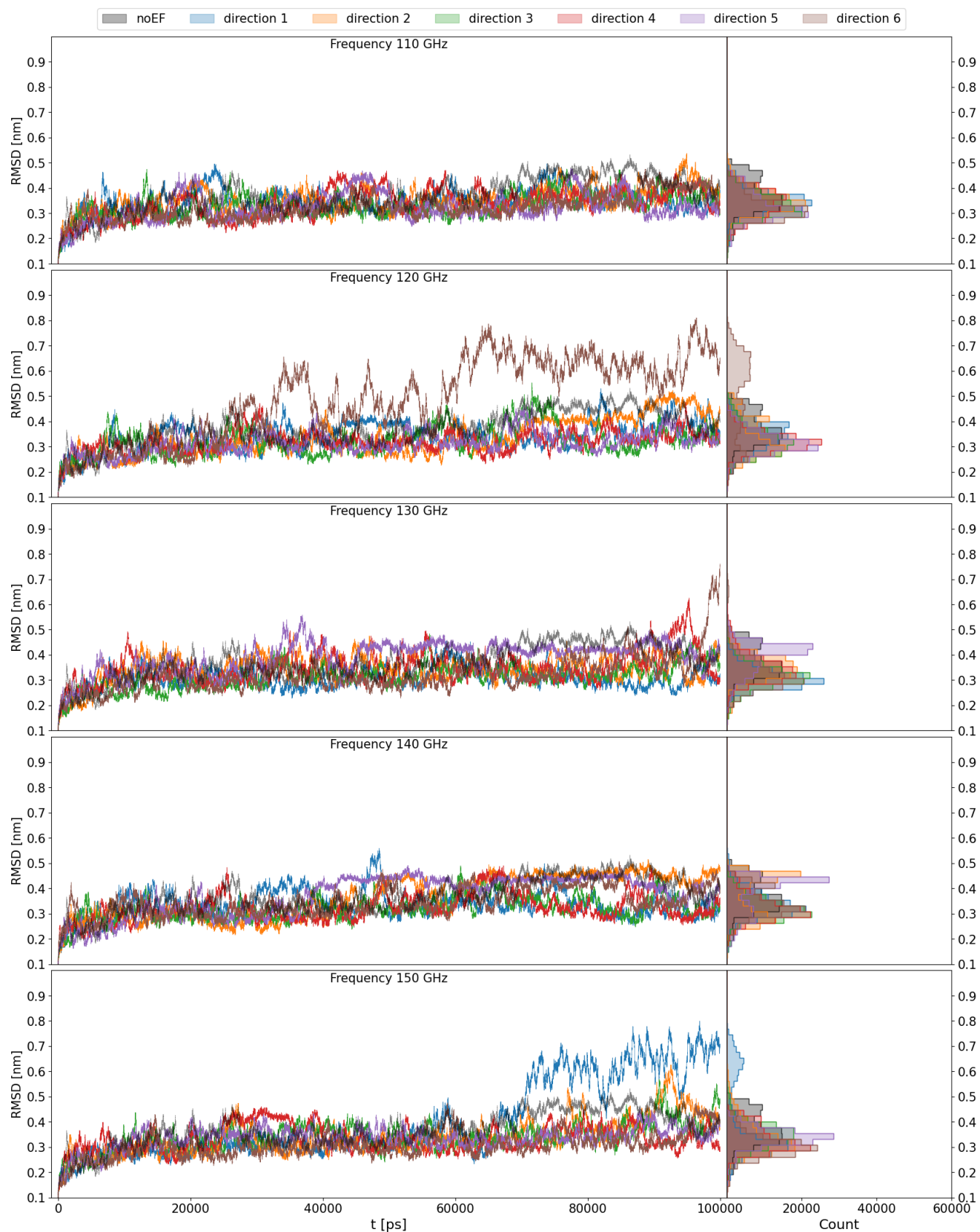


Figure 8.21: RMSD of the tubulin dimer - Batch 3 - Part 3

RMSD of the tubulin dimer without the C-termini - Batch 3

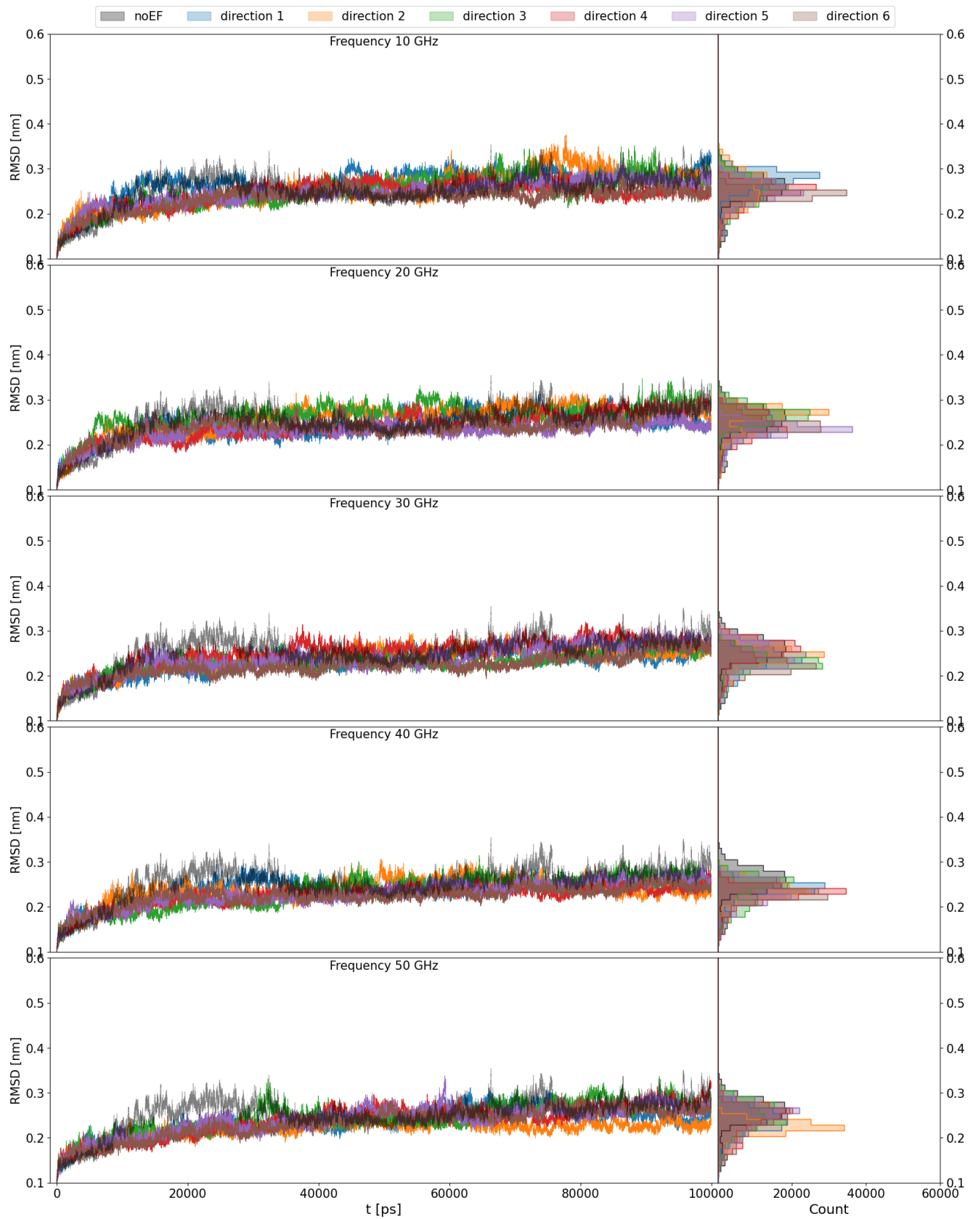


Figure 8.22: RMSD of the tubulin dimer without the C-termini - Batch 3 - Part 1

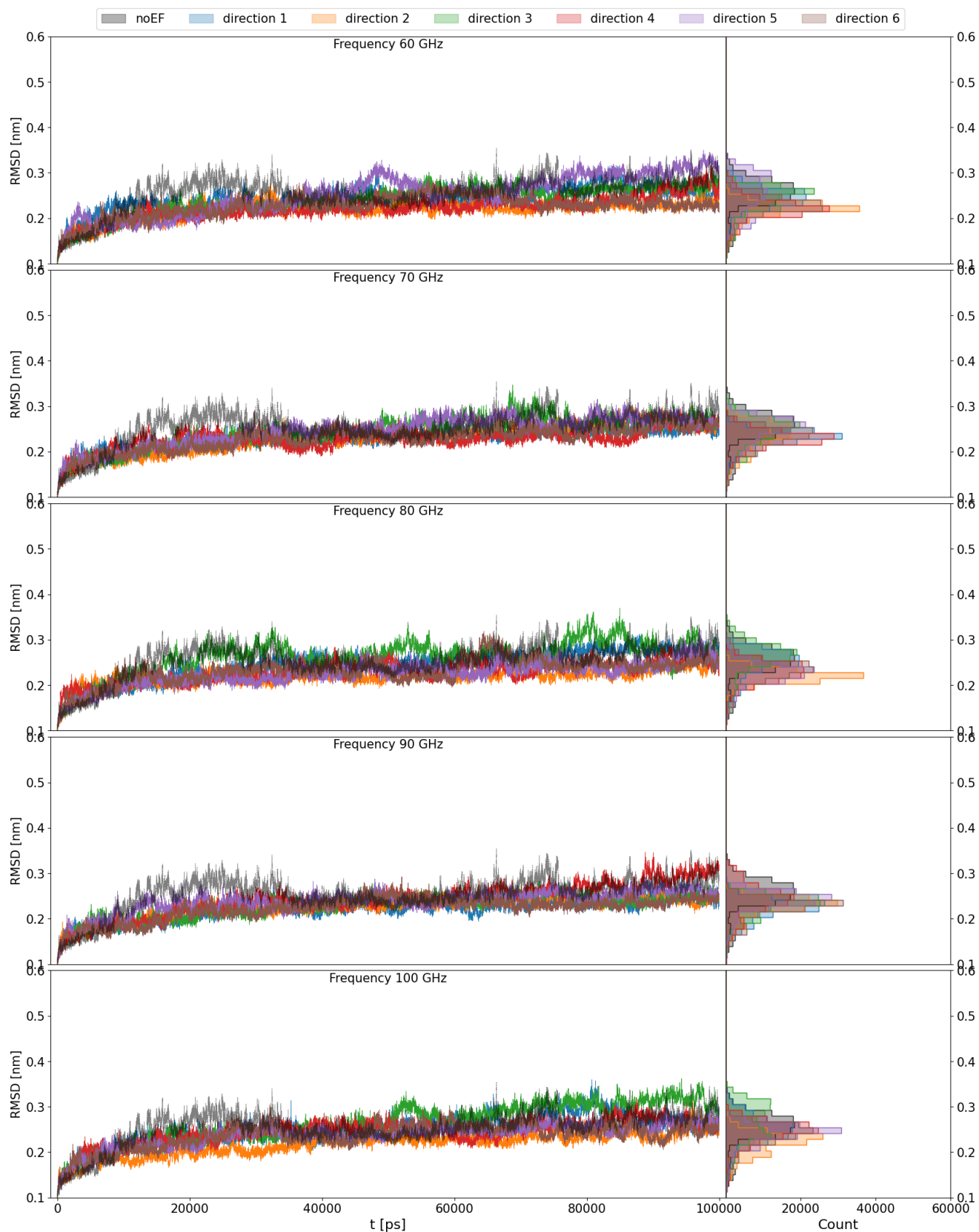


Figure 8.23: RMSD of the tubulin dimer without the C-termini - Batch 3 - Part 2

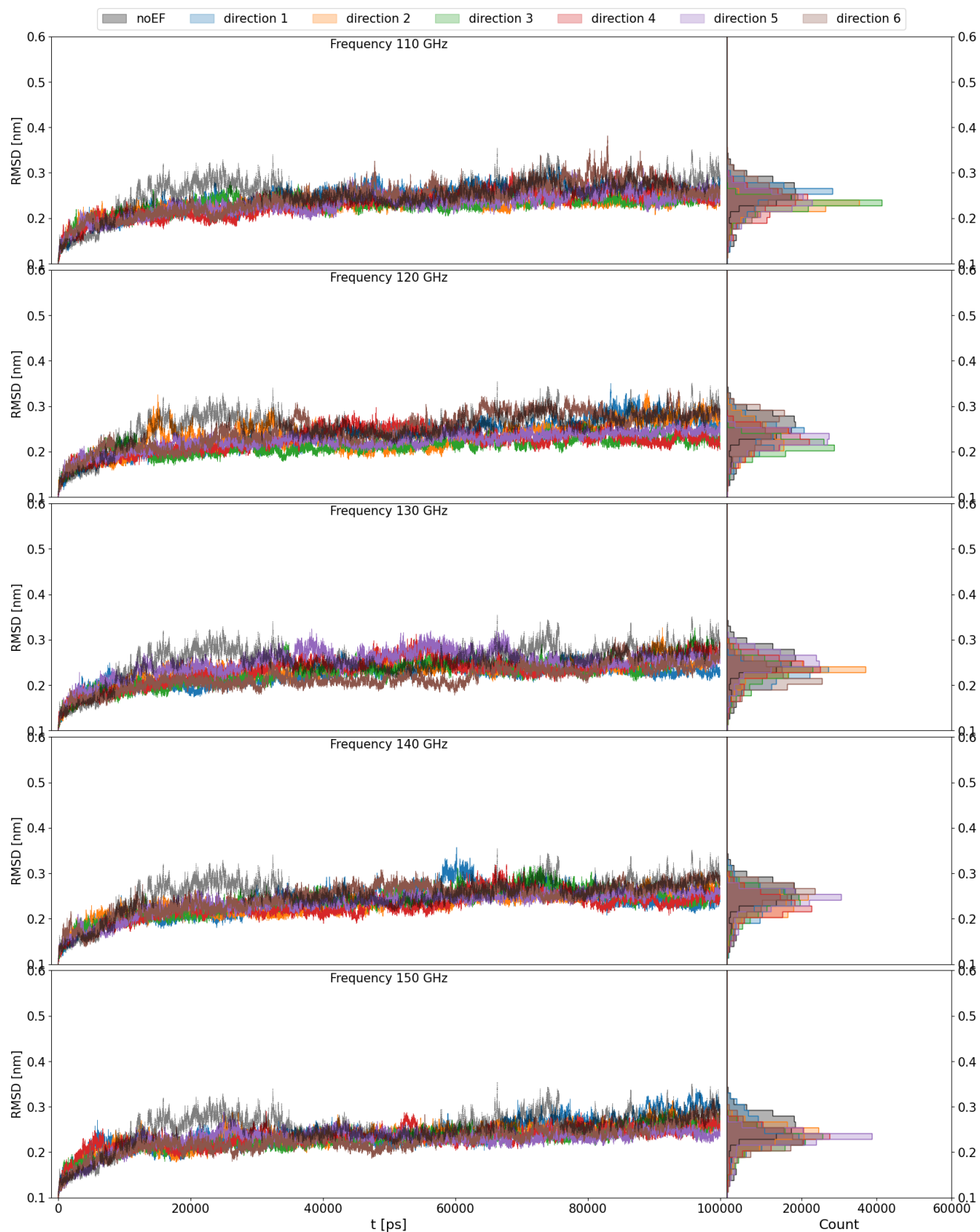


Figure 8.24: RMSD of the tubulin dimer without the C-termini - Batch 3 - Part 3

RMSD of the C-termini - Batch 3

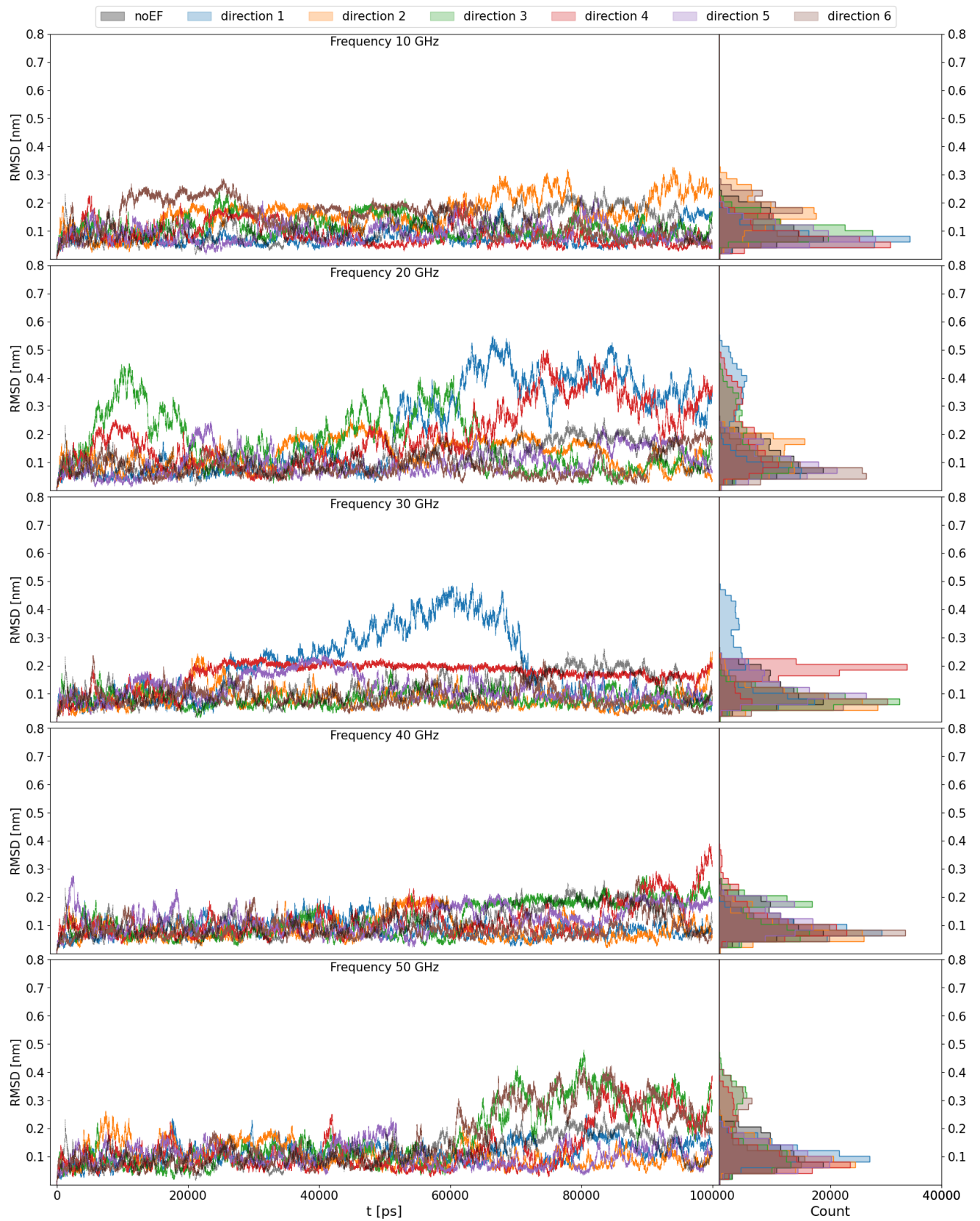


Figure 8.25: RMSD of the C-termini of the tubulin dimer - Batch 3 - Part 1

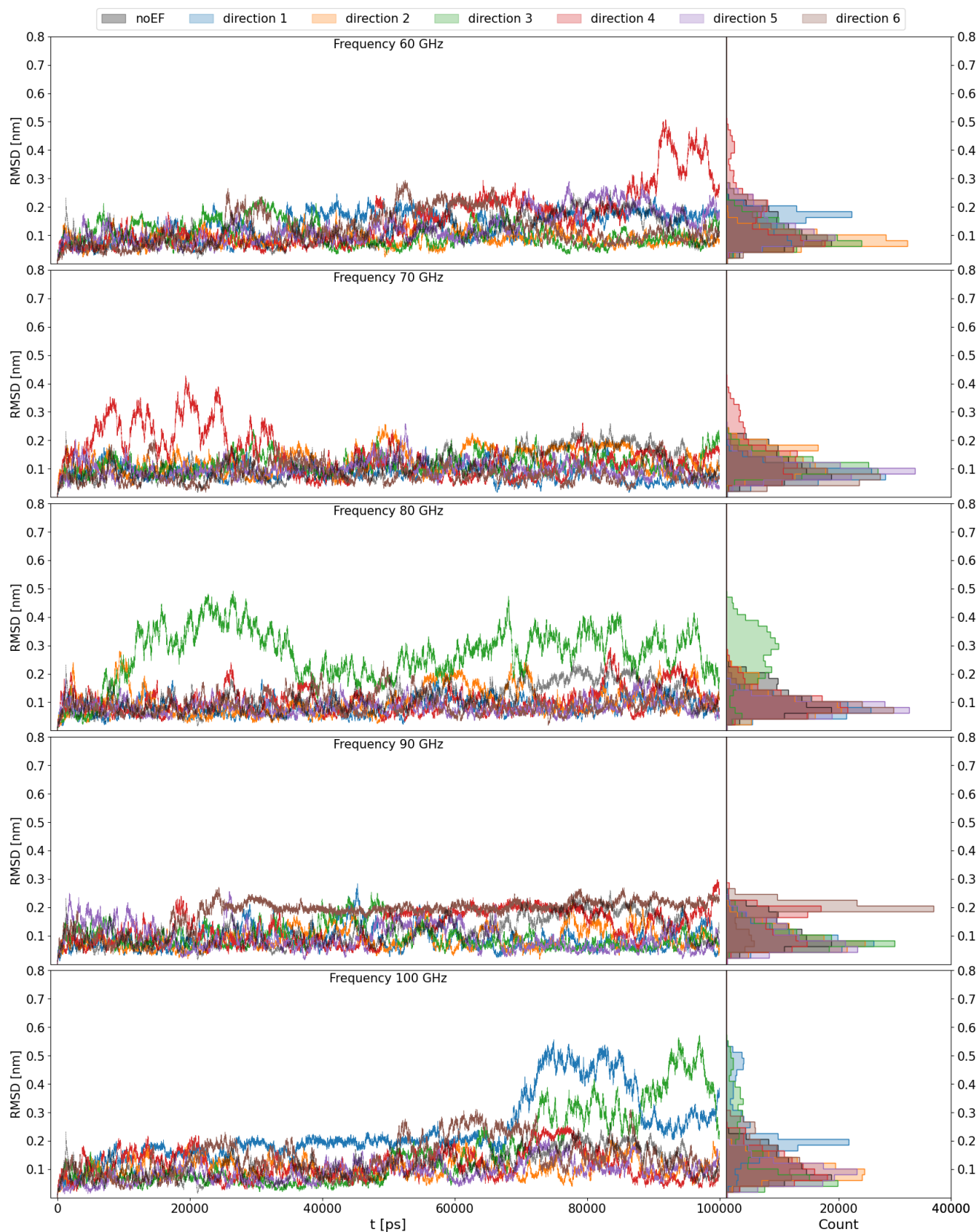


Figure 8.26: RMSD of the C-termini of the tubulin dimer - Batch 3 - Part 2

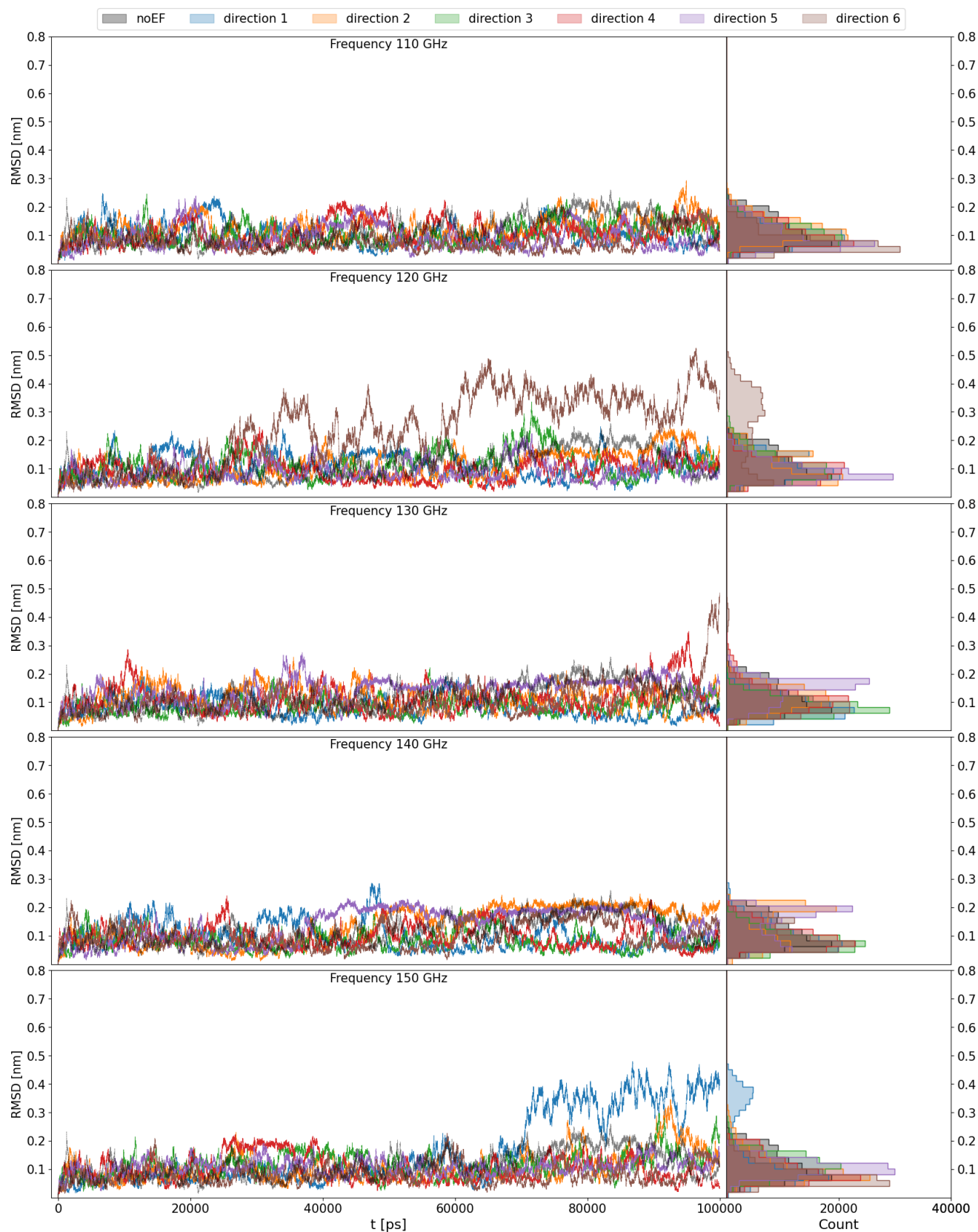


Figure 8.27: RMSD of the C-termini of the tubulin dimer - Batch 3 - Part 3

8.3 RMSF of residues

Due to a vast amount of RMSF-related graphs, we present only some examples in this section, and the rest can be found in the Appendix 10.9. RMSF of residues of tubulin α and tubulin β are plotted separately to have a good resolution.

First, we show the difference graphs calculated as

$$\text{RMSF}_{\text{diff}}(i) = \text{RMSF}(i) - \text{RMSF}_{\text{noEF}}(i) \quad (8.1)$$

for each batch, frequency and direction of the electric field; i denotes the residue index. The residues which show negative $\text{RMSF}_{\text{diff}}$ are more stable under the electric field condition in comparison with the case of no electric field. The parts with $\text{RMSF}_{\text{diff}}$ being larger than 0 correspond to the parts of the tubulin, which are more flexible when an electric field of particular frequency and direction is applied.

We have also plotted averages through these values across either directions or batches or both. Unfortunately, this averaging hides the outcomes of different directions or starting conformations (batches). We cannot truly have a definitive answer as to how a particular frequency acts on some part of the tubulin since for different directions or batches (different starting configuration of tubulin), the $\text{RMSF}_{\text{diff}}$ can be drastically different - the electric field of the same frequency but different starting configuration or direction can lead to both a stabilizing or destabilizing effect. This huge dependence on the starting position and direction of the applied EF oscillation was already seen in the RMSD analysis. However, from the statistical point of view, the averaging would show us the true response of an ensemble of tubulins to such an external perturbation, if our statistics was larger. We have only 3 true repetitions (different starting conformation), which is a rather small sampling, even though for each frequency and starting conformation we have 6 different directions of electric field oscillation.

However, we can definitely see (from individual or averaged graphs) that the electric field has a huge impact on some parts of the structure. For tubulin α , those are the residues 25-60, 240-260, 270-290, 305-315, and of course in C-terminus. To showcase spatially where these residues reside in the tubulin dimer, we have included the visualisation pictures done in VMD 8.28. On average, the electric fields cause an increase in their flexibility, but if looked at specific trajectories, we can also see a stabilizing effect for some combination of initial conformation and electric-field oscillation direction.

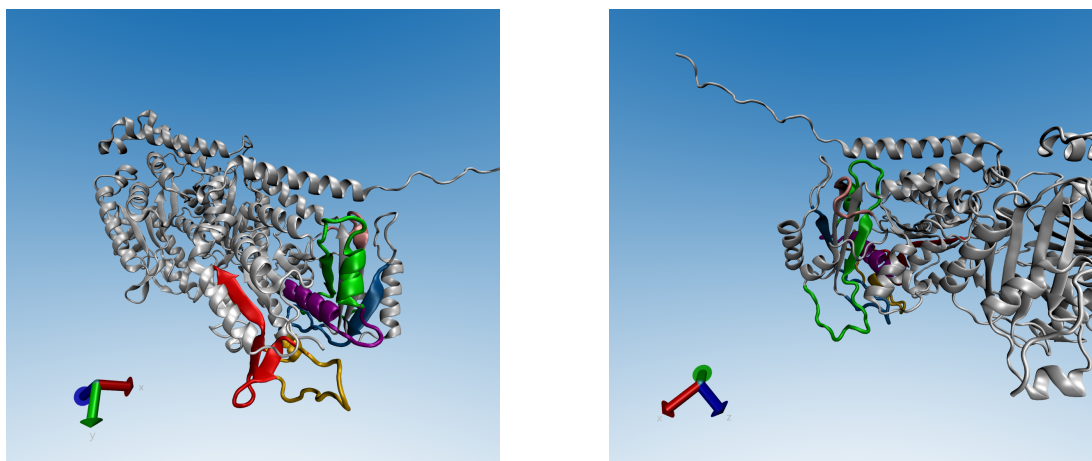


Figure 8.28: Tubulin alpha residues affected the most by electric fields colour-coded as follows: 25-50 orange; 50-70 red; 230-250 purple; 250-286 green; 305-313 pink; 350-370 blue (structure is obtained from the simulation of 30 GHz in direction d4 - batch 1 at 70 ns)

For tubulin β , the biggest changes of RMSF can be seen for residues 25-100, 160-180 and 265-285. Again, to see where these residues lie in the tubulin beta, see the visualisations from VMD 8.29. Residues 270-290 form the S7-H9 loop or the so-called "M-loop", which is important for lateral interactions between tubulin protofilaments that form a microtubule. Almost all electric fields cause an increase in flexibility of this region. On the other hand, the effect of the electric field on the residues 160-180 is, for the most part, stabilizing.

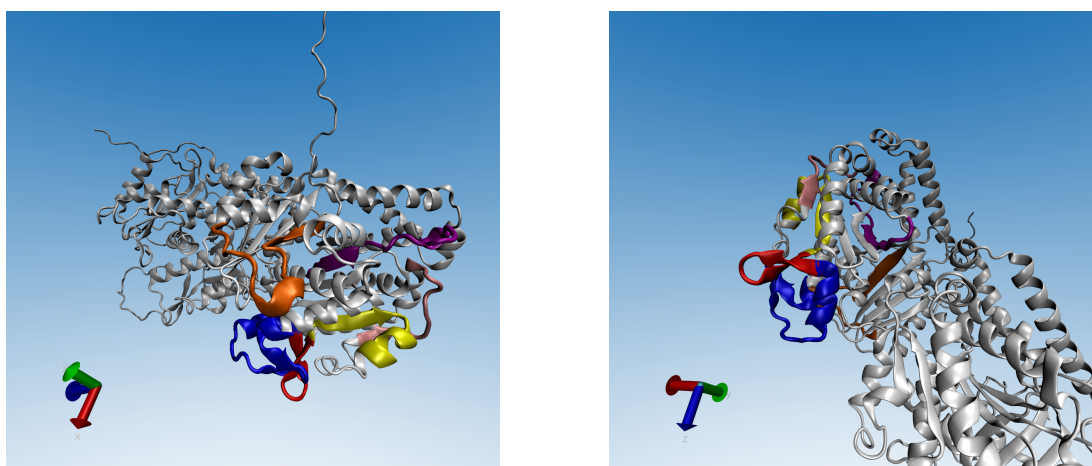


Figure 8.29: Tubulin beta residues affected the most by electric fields colour-coded as follows: 25-50 blue, 50-60 red; 60-75 yellow; 90-100 pink; 160-180 purple; 265-285 orange (structure is obtained from the simulation of 10 GHz in direction d1 - batch 1 at 100ns)

Since again the amount of data is enormous, we advise the reader to check all these graphs in the RMSF section in Appendix: the non-averaged $\text{RMSF}_{\text{diff}}$ graphs 10.91-10.180; the $\text{RMSF}_{\text{diff}}$ averaged 10.181-10.210; the $\text{RMSF}_{\text{diff}}$ averaged only through initial conditions 10.211-10.240. Here in this section we only show an example for each batch and for one frequency only - 20 GHz. See 10.92, 10.107,

10.122 - residue RMSF of tubulin α . 10.137, 10.152, 10.167 - residue RMSF of tubulin β .

In this chapter, we also show the averaged $\text{RMSF}_{\text{diff}}$ over directions and initial conformations for 20 GHz only 10.182, 10.197. The rest can be again seen in Appendix 10.10.

Additionally, RMSF graphs (not the differential ones are also plotted in Appendix) 10.8.

8.3.1 Tubulin α

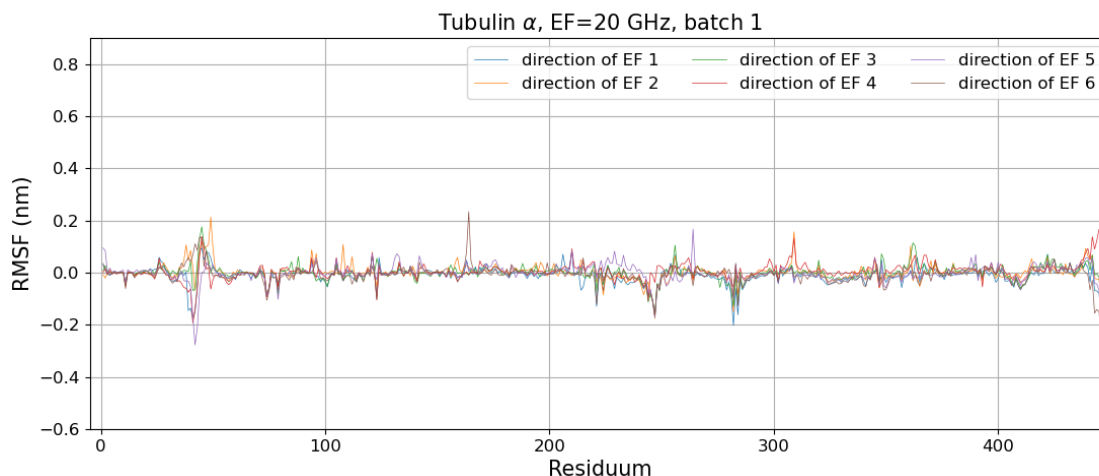


Figure 8.30: $\text{RMSF}_{\text{diff}}$ of the residues of the tubulin α subjected to the electric field of frequency 20 GHz, Batch 1

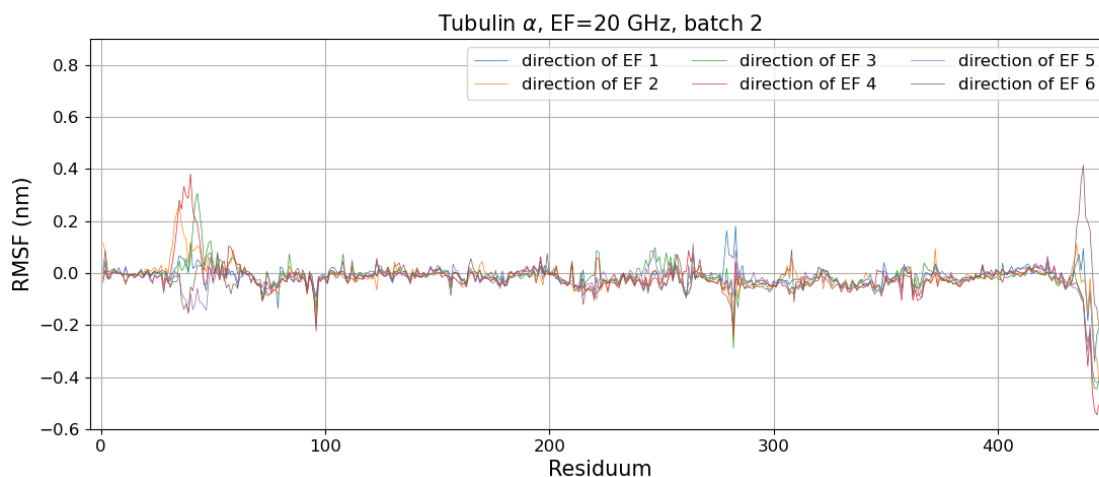


Figure 8.31: $\text{RMSF}_{\text{diff}}$ of the residues of the tubulin α subjected to the electric field of frequency 20 GHz, Batch 2

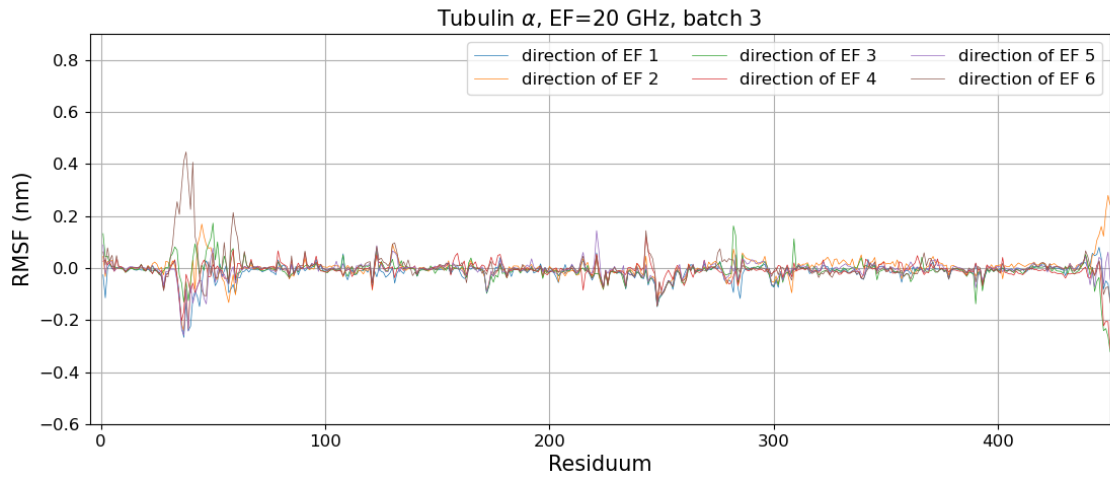


Figure 8.32: $\text{RMSF}_{\text{diff}}$ of the residues of the tubulin α subjected to the electric field of frequency 20 GHz, Batch 3

8.3.2 Tubulin β

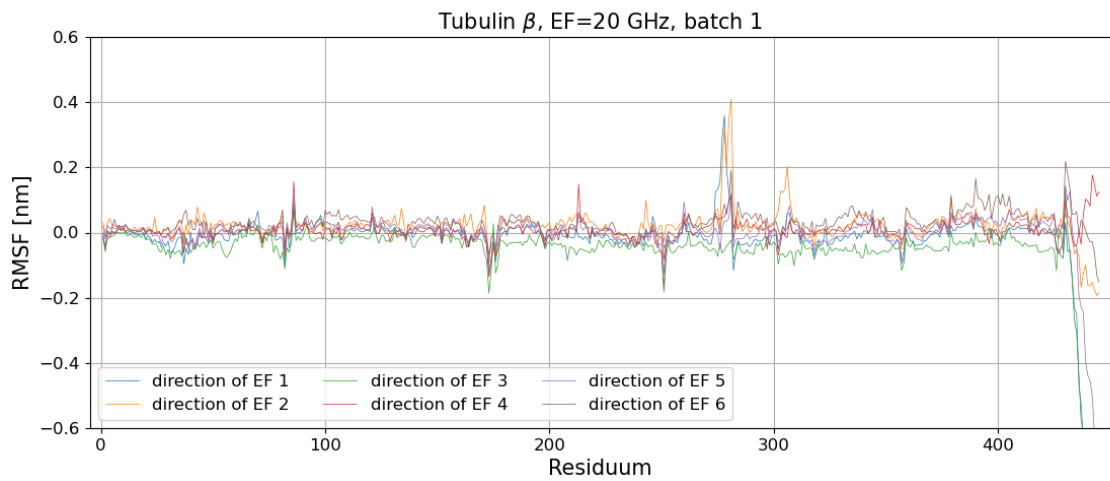


Figure 8.33: $\text{RMSF}_{\text{diff}}$ of the residues of the tubulin β subjected to the electric field of frequency 20 GHz, Batch 1

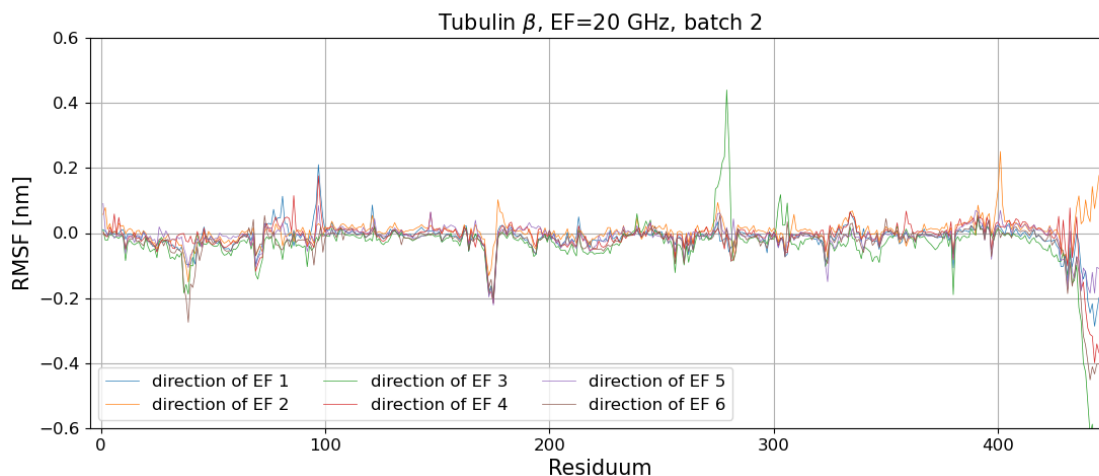


Figure 8.34: $\text{RMSF}_{\text{diff}}$ of the residues of the tubulin β subjected to the electric field of frequency 20 GHz, Batch 2

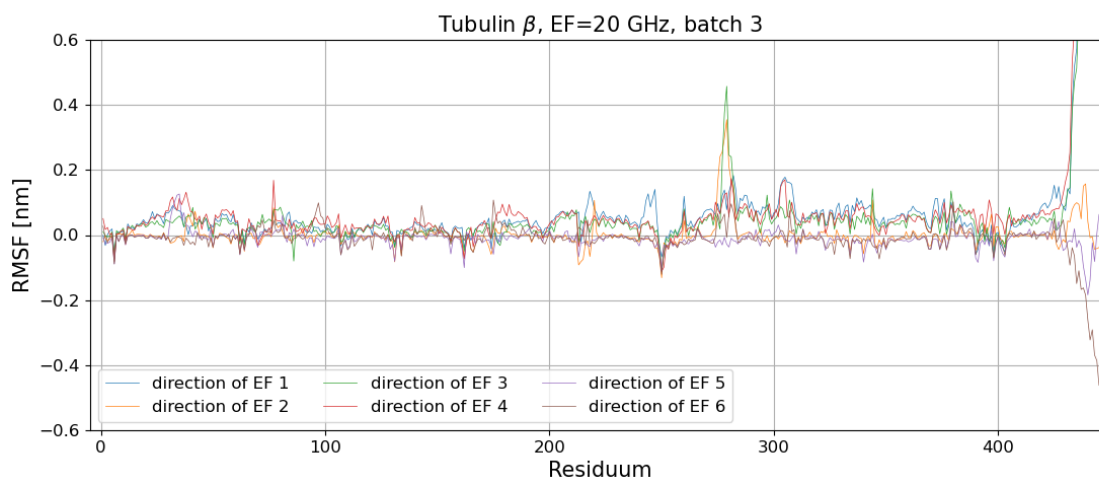


Figure 8.35: $\text{RMSF}_{\text{diff}}$ of the residues of the tubulin β subjected to the electric field of frequency 20 GHz, Batch 3

8.4 RMSF of residue - averaged over whole batches (initial conformations and directions)

$\text{RMSF}_{\text{diff}}$ of residues subjected to electric fields of different frequencies and directions, averaged over batches (initial conformations and directions) can be found in the Appendix 10.10.

8.4.1 Tubulin α

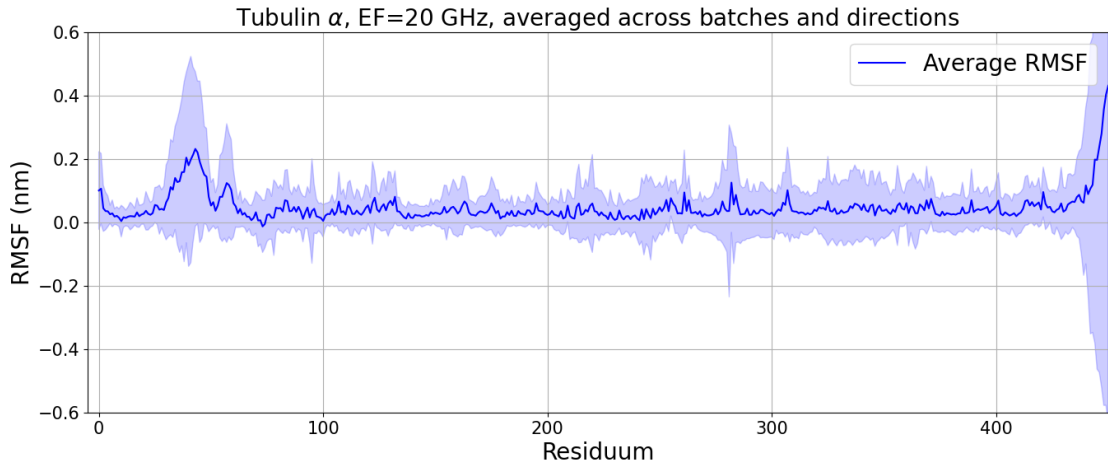


Figure 8.36: Average of $\text{RMSF}_{\text{diff}}$ of the residues of the α tubulin subjected to the electric field of frequency 20 GHz

8.4.2 Tubulin β

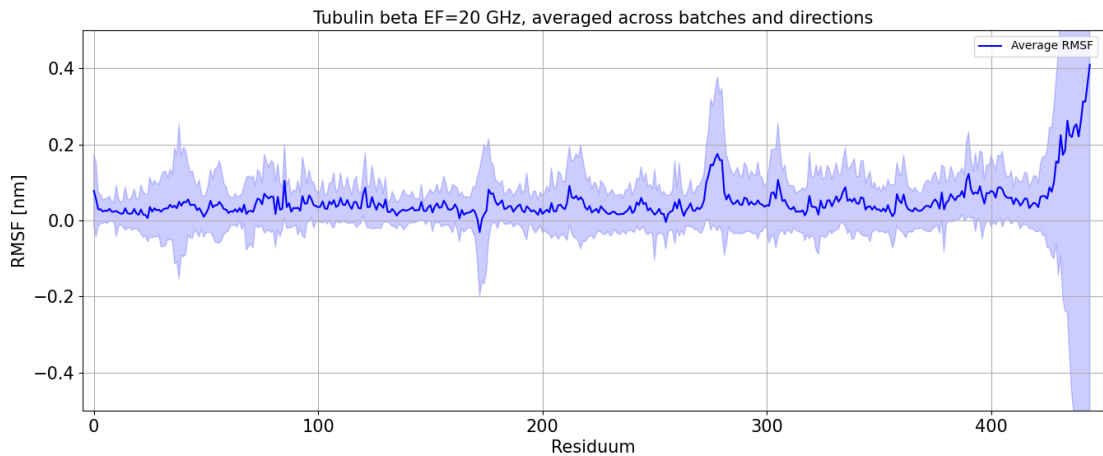


Figure 8.37: Average of $\text{RMSF}_{\text{diff}}$ of the residues of the β tubulin subjected to the electric field of frequency 20 GHz

$\text{RMSF}_{\text{diff}}$ of residues subjected to electric fields of different frequencies and directions, averaged only over initial conditions, can be found in the Appendix 10.11.

8.5 RMSF of selected residues that make up a binding site

It can be seen across the different batches (even for no EF case) that the majority of residues have drastically different RMSF values. We inform the reader that the y-axes are of a different range in each graph in this section.

Binding site of vinca alkaloids

The vinca alkaloid binding site consists of the residues 325, 329, 351 and 353 of tubulin α and the residues 173, 174, 175, 177, 212, 218, 220, 221 and 225 on the tubulin β . Vinca binding site does not reside in the middle of the tubulin dimer but between two different tubulin dimers in a protofilament of a microtubule - see Figure 1.6.

Tubulin α

When it comes to the residues on tubulin α , which facilitate the binding to vinca alkaloids, electric fields of different directions of oscillation and different frequencies affect this binding site differently. However, when we average over all directions and batches, we can see that there is a small stabilizing effect overall, mainly when we apply the electric field of the following frequencies: 20, 70, 130 and 140 GHz. See Figures: 8.39, 8.41, 8.43, and 8.45. The stabilizing effect is mostly seen for the batch 2 initial conformation.

Tubulin β

In the case of the residues of tubulin β , which bind to the vinca alkaloids, we can see a dramatic stabilizing effect of an electric field of all frequencies for the residues 173 (Figure 8.47) and 174 (Figure 8.49) especially. On average, the RMSF of all residues under the effect of EF is lower than for the no EF case, except for the residue 177 (Figure 10.242). In the case of residue 173, the electric fields of 90 GHz and 110 GHz lead to the drop of RMSF to such an extent that the standard deviation from the mean does not overlap with the deviation of the mean of the no EF case. This is nearly true also for the 20, 60 and 120 GHz for the residue 173 and for 20, 50 and 110 GHz for the residue 174. The stabilization of this binding site is the most evident in the case of batch 2 initial conformation and a bit in the case of the batch 1 initial conformation.

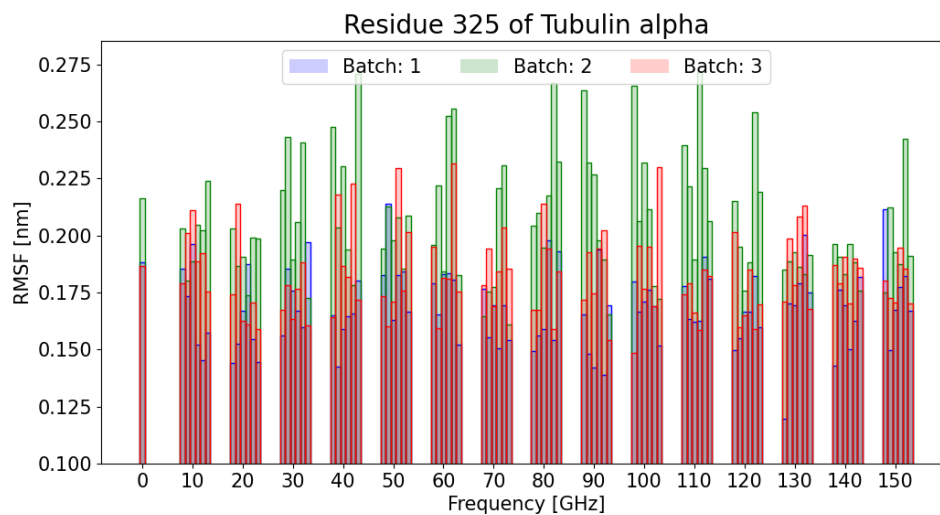


Figure 8.38: RMSF of residue 325 of tubulin alpha - different directions and batches; the bars for 0 GHz mean that no EF is applied

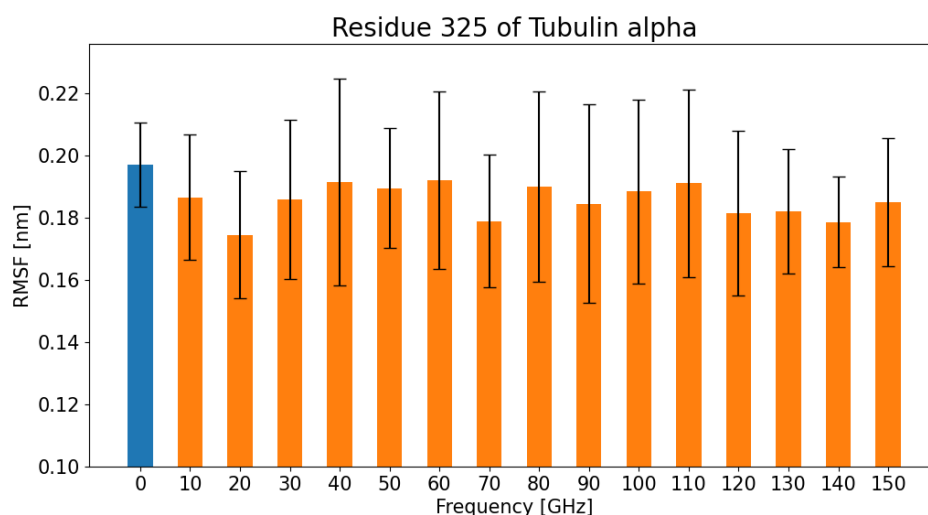


Figure 8.39: RMSF of residue 325 of tubulin alpha - averaged over directions and batches; the bars for 0 GHz mean that no EF is applied

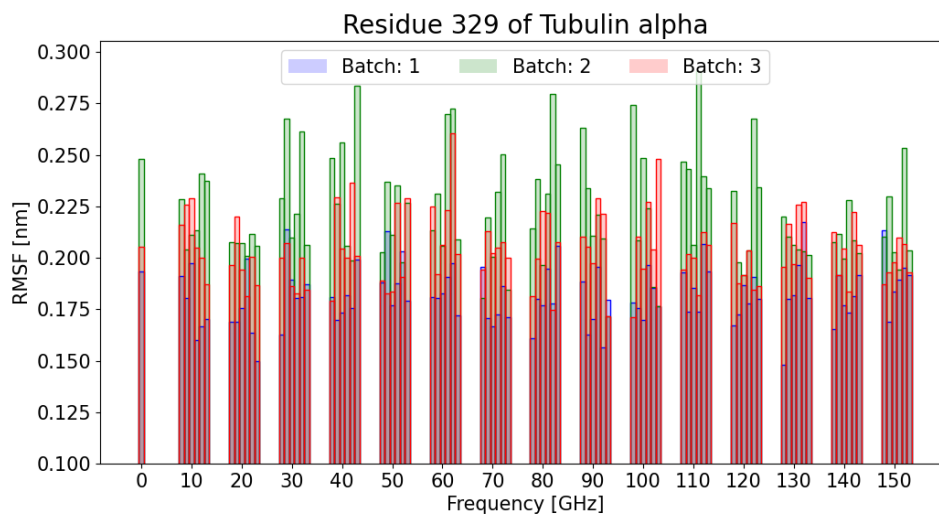


Figure 8.40: RMSF of residue 329 of tubulin alpha - different directions and batches; the bars for 0 GHz mean that no EF is applied

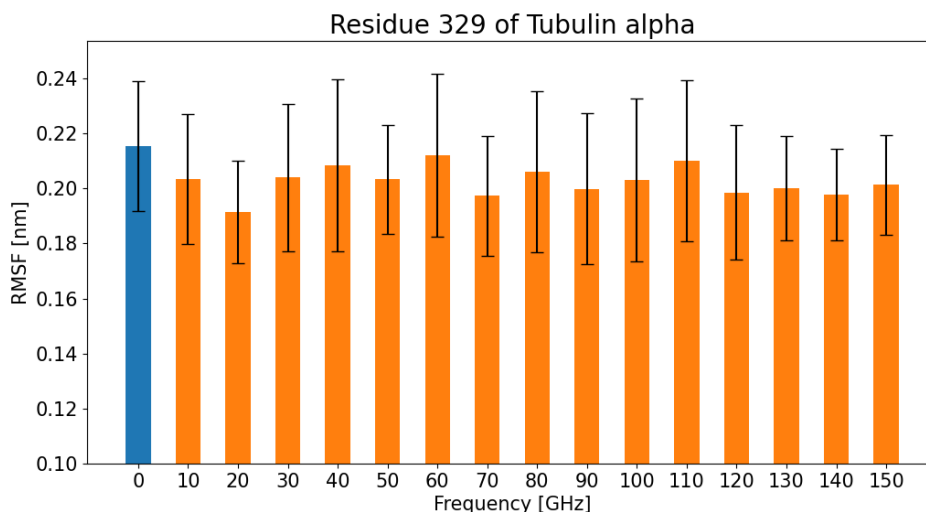


Figure 8.41: RMSF of residue 329 of tubulin alpha - averaged over directions and batches; the bars for 0 GHz mean that no EF is applied

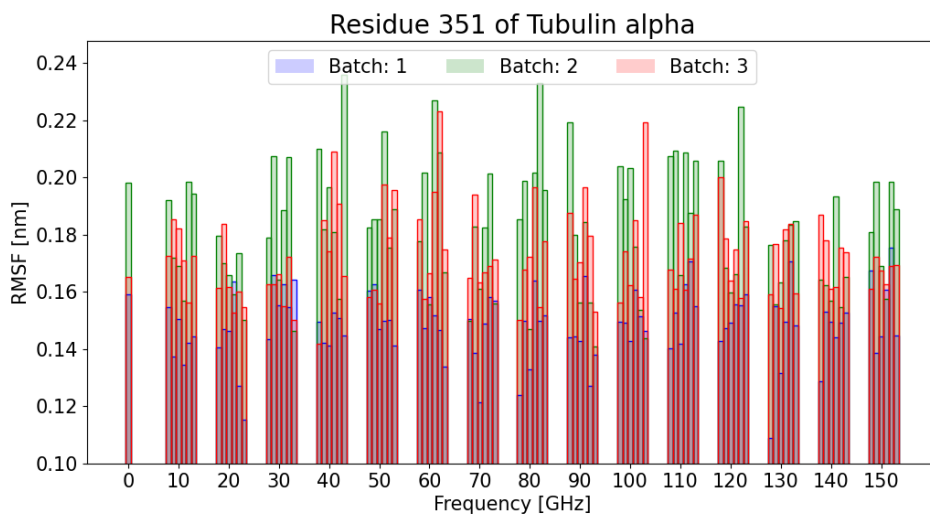


Figure 8.42: RMSF of residue 351 of tubulin alpha - different directions and batches; the bars for 0 GHz mean that no EF is applied

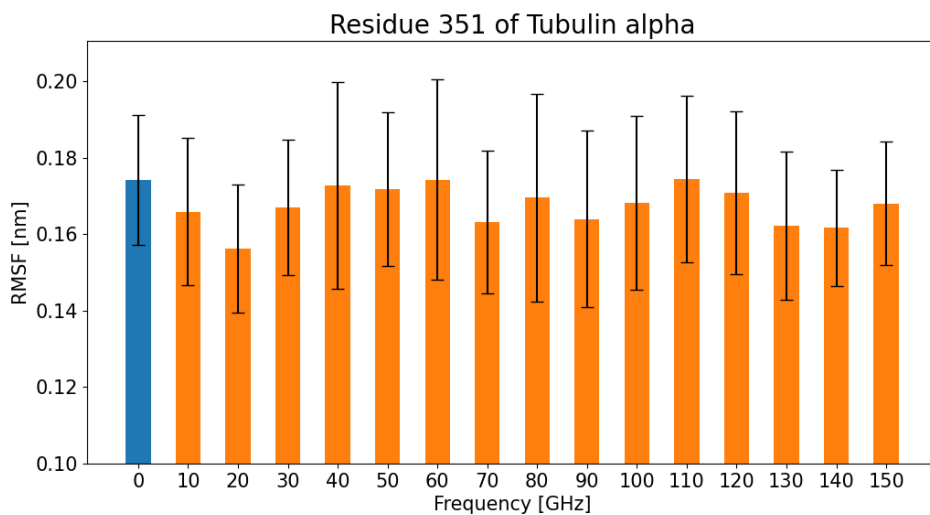


Figure 8.43: RMSF of residue 351 of tubulin alpha - averaged over directions and batches; the bars for 0 GHz mean that no EF is applied

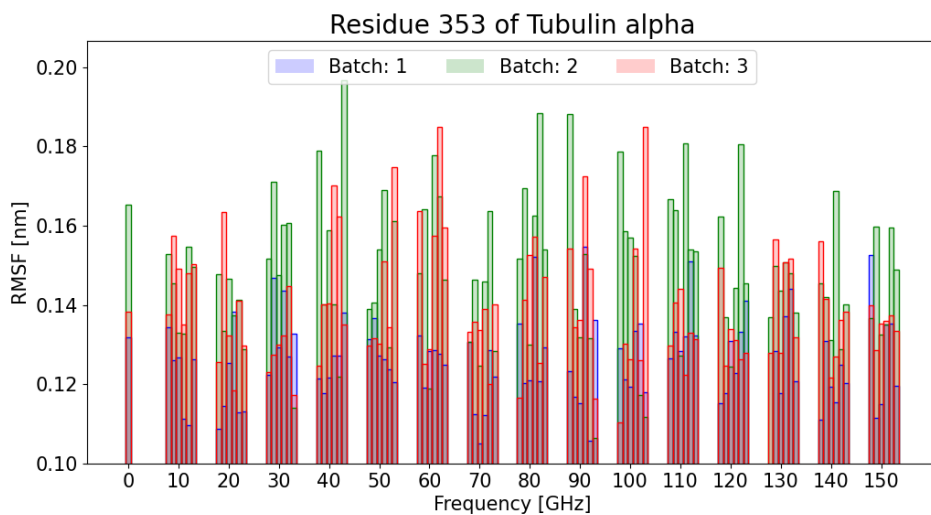


Figure 8.44: RMSF of residue 353 of tubulin alpha - different directions and batches; the bars for 0 GHz mean that no EF is applied

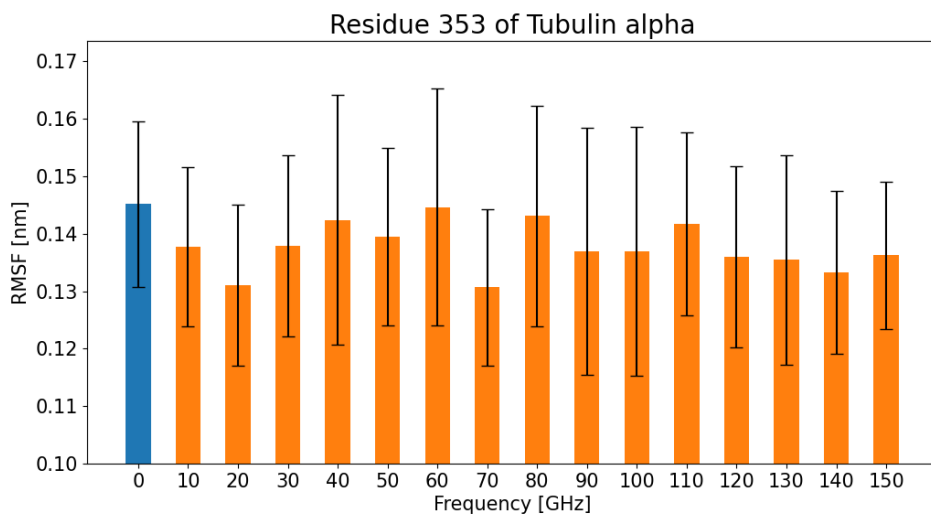


Figure 8.45: RMSF of residue 353 of tubulin alpha - averaged over directions and batches; the bars for 0 GHz mean that no EF is applied

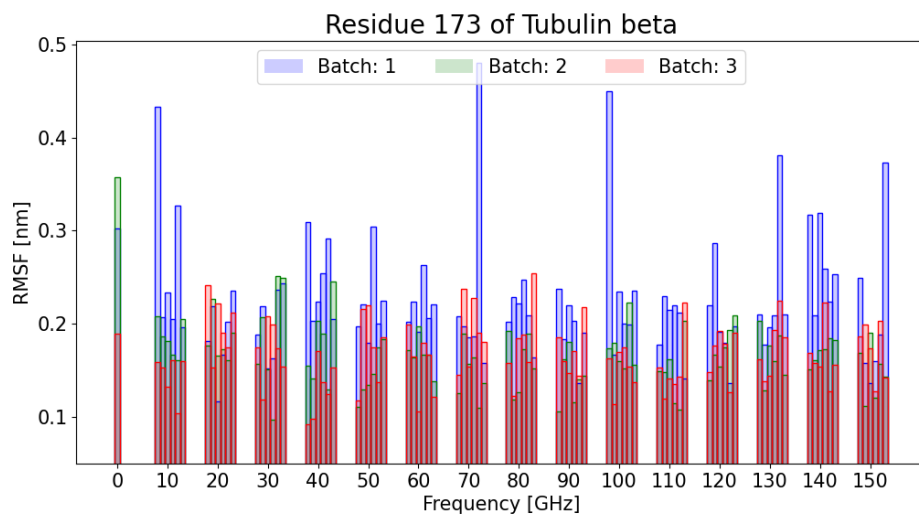


Figure 8.46: RMSF of residue 173 of tubulin beta - different directions and batches; the bars for 0 GHz mean that no EF is applied

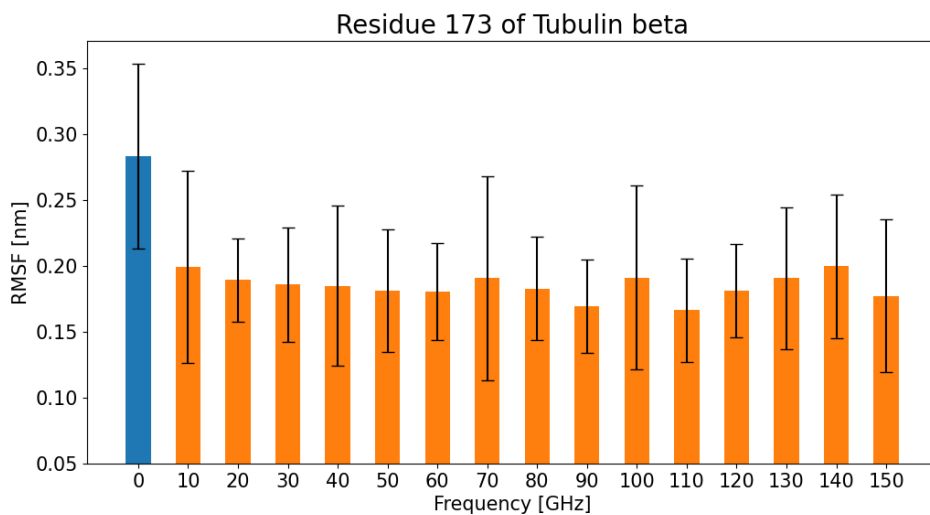


Figure 8.47: RMSF of residue 173 of tubulin beta - averaged over directions and batches; the bars for 0 GHz mean that no EF is applied

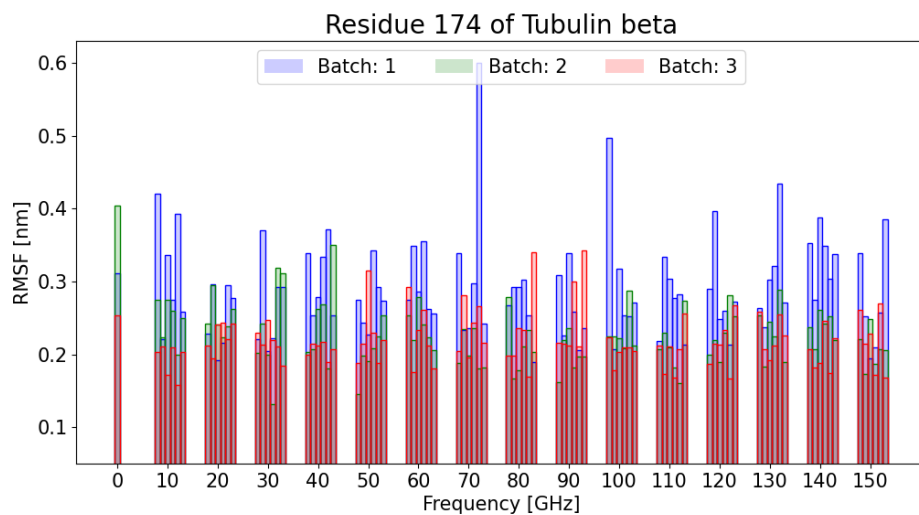


Figure 8.48: RMSF of residue 174 of tubulin beta - different directions and batches; the bars for 0 GHz mean that no EF is applied

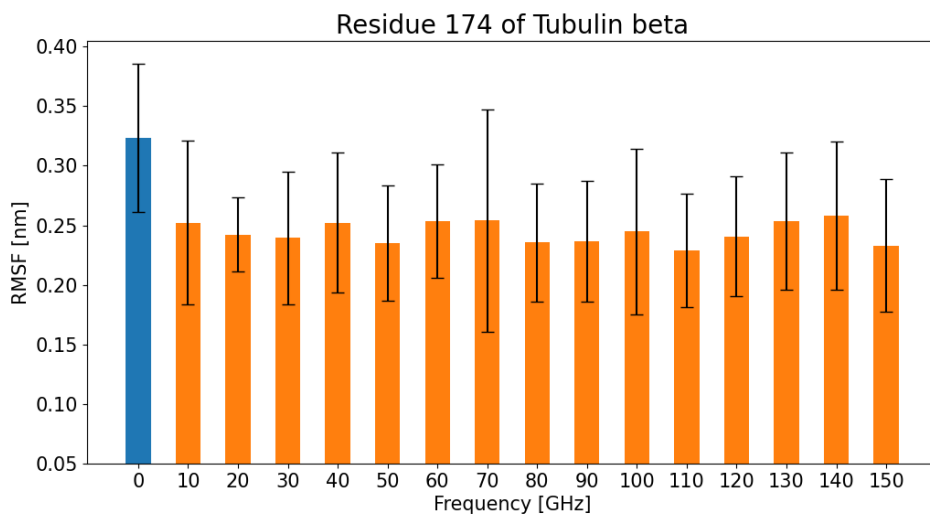


Figure 8.49: RMSF of residue 174 of tubulin beta - averaged over directions and batches; the bars for 0 GHz mean that no EF is applied

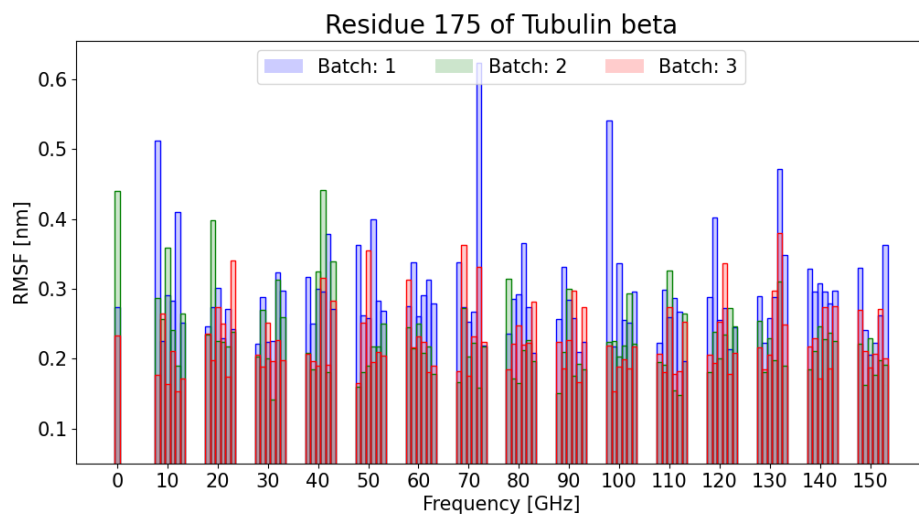


Figure 8.50: RMSF of residue 175 of tubulin beta - different directions and batches; the bars for 0 GHz mean that no EF is applied

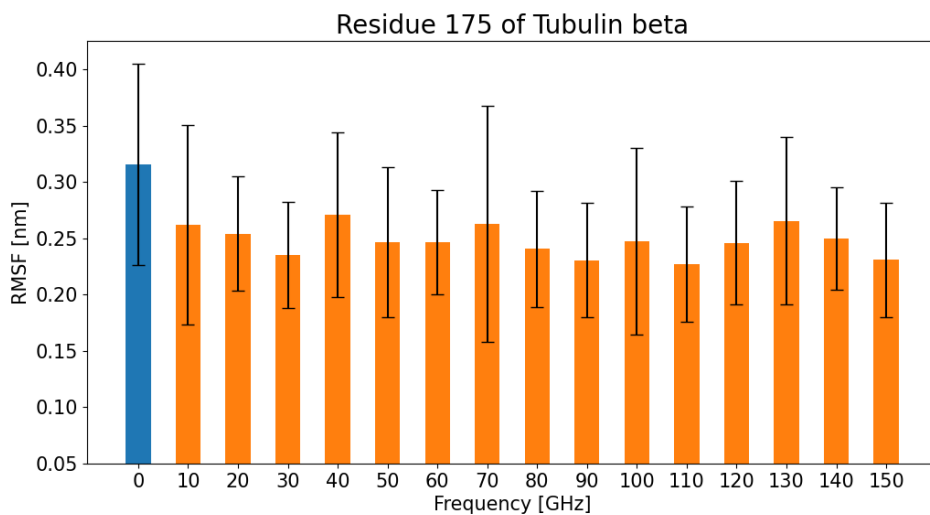


Figure 8.51: RMSF of residue 175 of tubulin beta - averaged over directions and batches; the bars for 0 GHz mean that no EF is applied

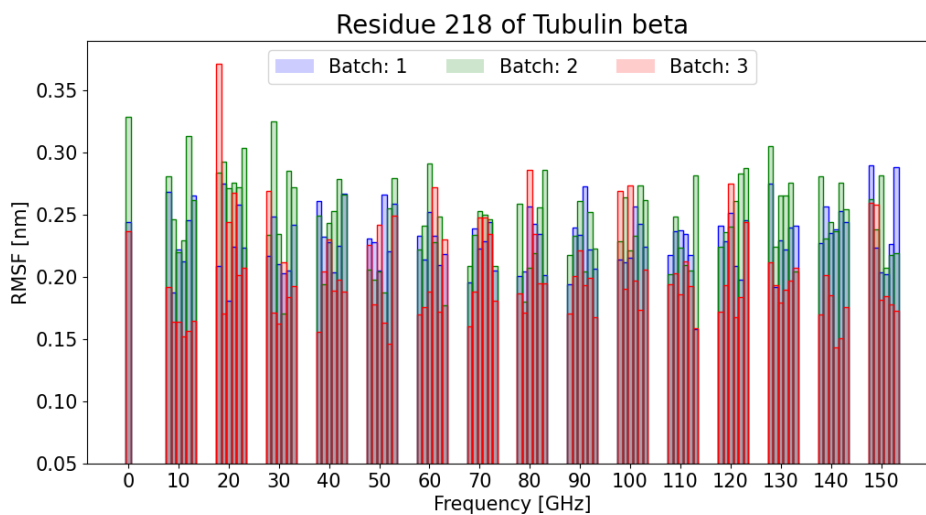


Figure 8.52: RMSF of residue 218 of tubulin beta - different directions and batches; the bars for 0 GHz mean that no EF is applied

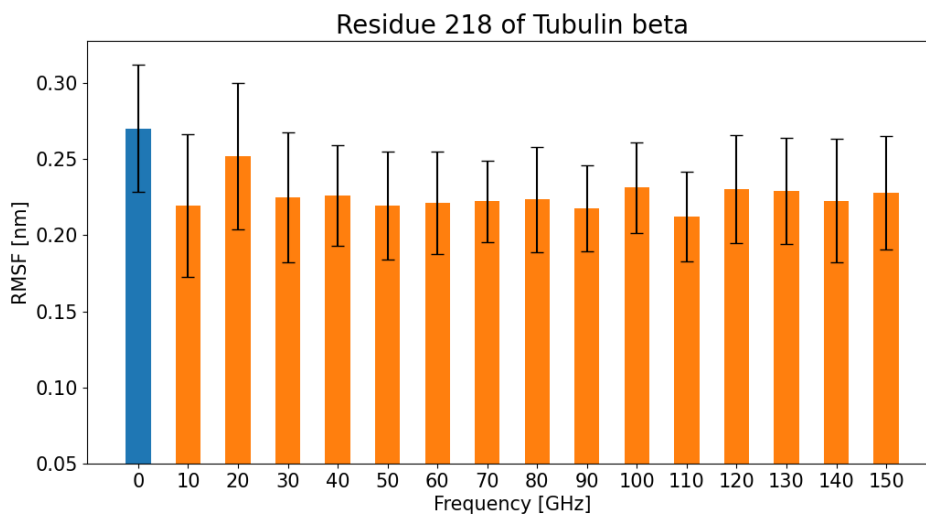


Figure 8.53: RMSF of residue 218 of tubulin beta - averaged over directions and batches; the bars for 0 GHz mean that no EF is applied

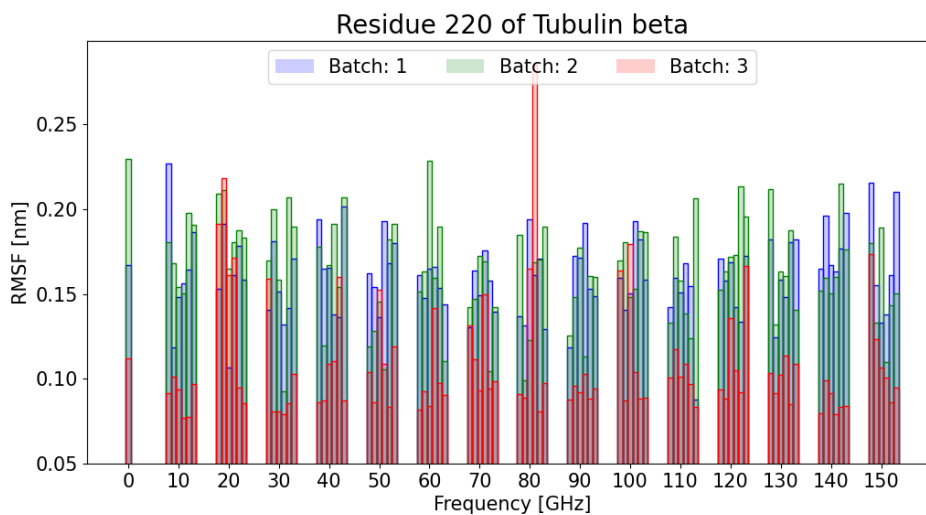


Figure 8.54: RMSF of residue 220 of tubulin beta - different directions and batches; the bars for 0 GHz mean that no EF is applied

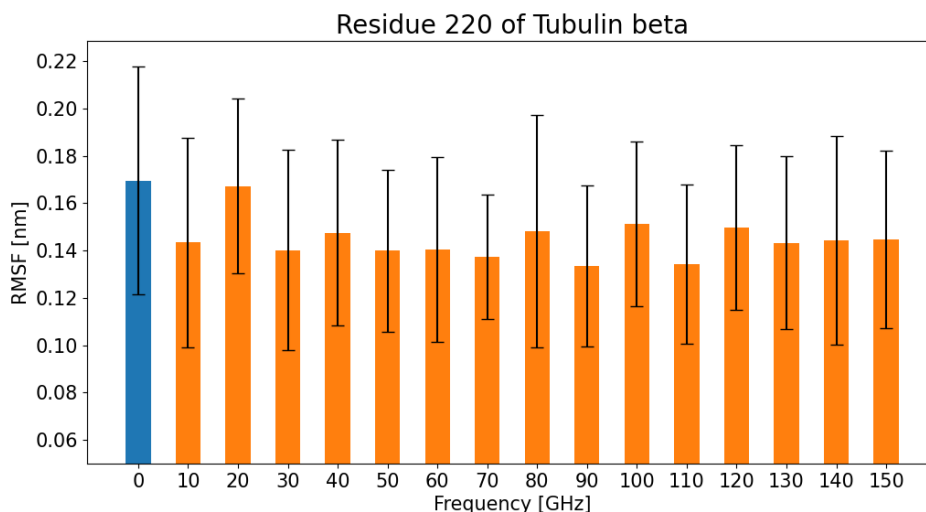


Figure 8.55: RMSF of residue 220 of tubulin beta - averaged over directions and batches; the bars for 0 GHz mean that no EF is applied

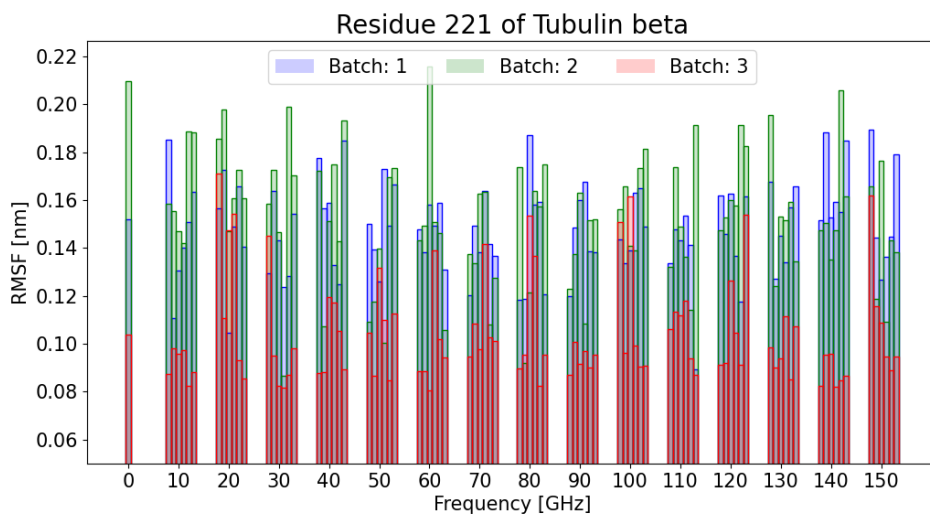


Figure 8.56: RMSF of residue 221 of tubulin beta - different directions and batches; the bars for 0 GHz mean that no EF is applied

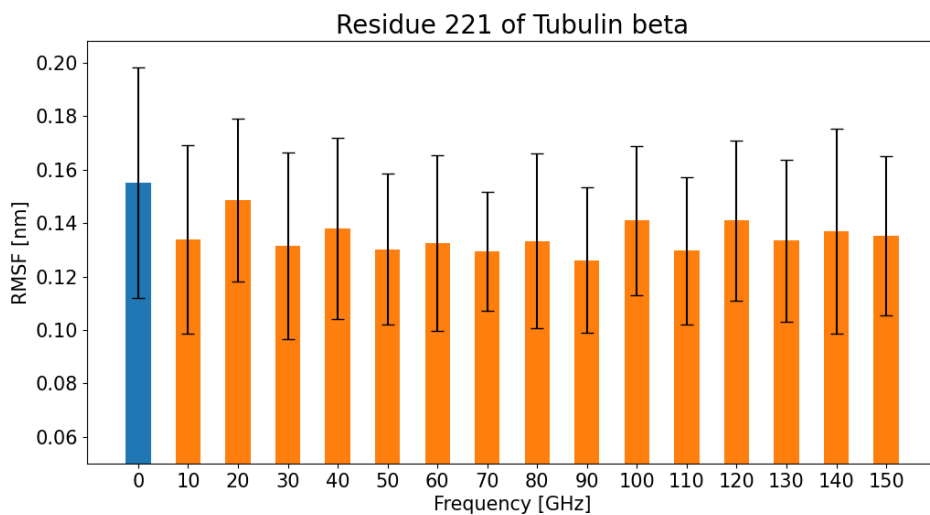


Figure 8.57: RMSF of residue 221 of tubulin beta - averaged over directions and batches; the bars for 0 GHz mean that no EF is applied

8.5.1 Binding site of colchicine

The colchicine binding site on microtubule consists of the residues 178, 179, 180 and 181 on tubulin α and of the residues 236, 239, 246, 248, 253, 256, 257, 313, 314 and 350 on tubulin β subunit. The residue RMSF again highly depends, besides the frequency, on the initial conformation and the external electric-field oscillation direction. To see an effect of electric fields of the specific oscillations and on concrete structures, please check the following graphs: 10.249, 10.251, 8.58, 8.60, 8.62, 10.253, 8.64, 8.66, 8.68, 8.70, 8.72, 10.255, 8.74, 10.257. Due to taking too much space, some of them are located in the Appendix.

Tubulin α

By averaging through batches and directions, we cannot see any major influence of electric field on the residues 178 (Figure 10.250) and 179 (Figure 10.252). However, we see an effect on the residues 180 (Figure 8.59) and 181 (Figure 8.61). Clearly, they have become more stable on average under the influence of electric fields in the range of 10 -150 GHz, but mainly under 20 GHz. On the other hand, residue 178 becomes slightly more unstable under the influence of 30 - 80 GHz, 110-130 GHz on average. Similarly, residue 179 becomes more flexible under the influence of 30-60, 80, and 100-130 GHz. When we look at the graphs of RMSF of residues 178 and 179, where the effect of individual directions and batches are displayed (10.249, 10.251), we see that the spread of RMSF is quite high for each frequency.

Tubulin β

Effects of contradicting nature are seen at tubulin β residues. The averaged RMSF graphs hide that for the different initial conformations, the effect is either stabilizing or the complete opposite.

Residue 236 in the batch 3 (See Figure 8.62) becomes very flexible for all 15 frequencies, whereas this residue in the batch 1 and 2 becomes more stable.

Residue 239 (10.253) flexibility is not changed much on average, maybe only for the 150 GHz, where it becomes a lot more flexible for batch 1.

Residue 246 (8.64) on average does not show any major change of flexibility, but again, in a specific simulation of a specific direction of electric field causes a dramatic effect of this residue flexibility.

Residue 248 (8.66) is, on average, stabilized under the influence of all-electric fields. Only for some directions of EF we see a dramatically opposite effect.

Residue 253 (8.68) is truly stabilized for the majority of combinations of electric field and starting conformation. 10 GHz and 70 GHz electric fields have the biggest stabilizing effect on it. However, this stabilizing effect is very evident across all frequencies since for the majority of them, the deviation from the mean does not overlap with the deviation of the mean of no EF case.

Residue 256 (8.70) is also dramatically stabilized for batch 2 starting conformation.

Residue 257 (8.72) is also stabilised for batch 3 for all frequencies besides 50 and 100 GHz and also for batch 2 for again nearly all frequencies. On average 70, 90 and 110 GHz cause the biggest lowering of RMSF.

Residues' 313 (10.255) and 314 (8.74) stability depends on the specific direction of EF application and on the initial conformation of the protein.
 Residue 350 (10.257) stability hugely depends on the specific direction of EF application and on the initial conformation of the protein.

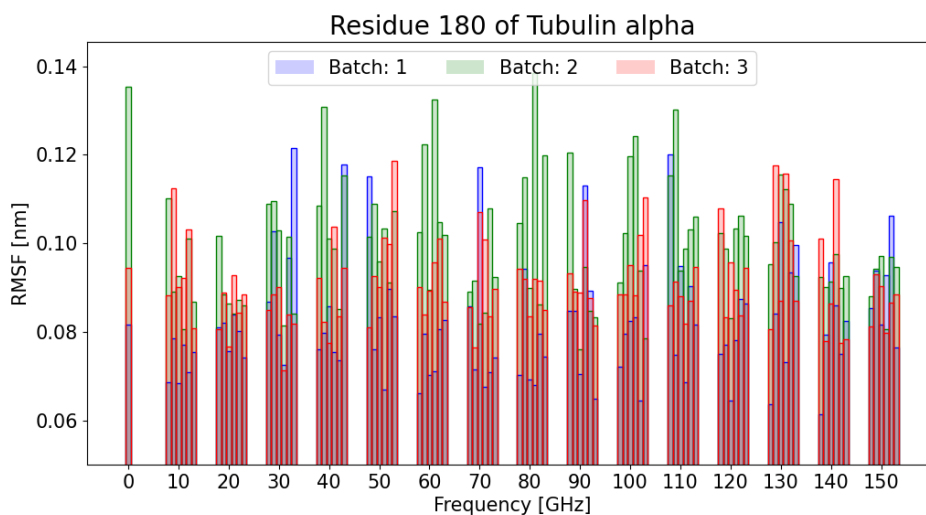


Figure 8.58: RMSF of residue 180 of tubulin alpha - different directions and batches; the bars for 0 GHz mean that no EF is applied

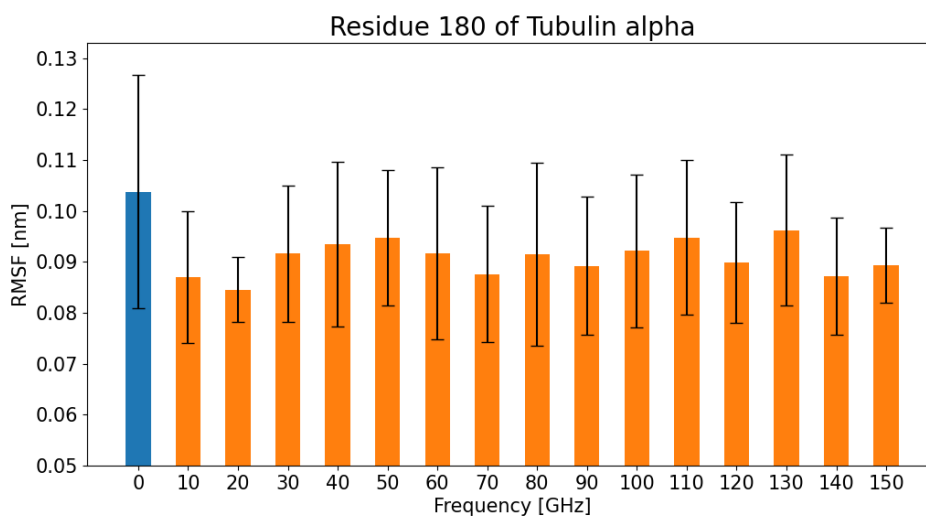


Figure 8.59: RMSF of residue 180 of tubulin alpha - averaged over directions and batches; the bars for 0 GHz mean that no EF is applied

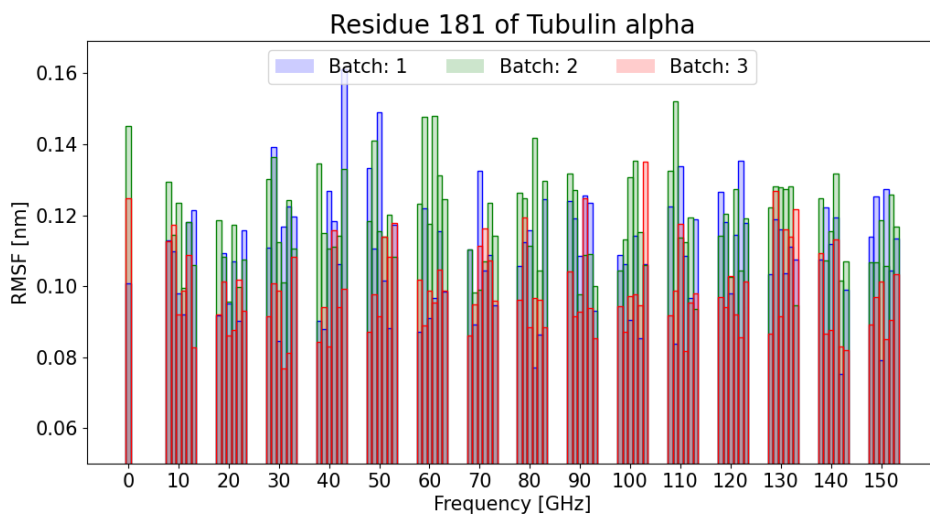


Figure 8.60: RMSF of residue 181 of tubulin alpha - different directions and batches; the bars for 0 GHz mean that no EF is applied

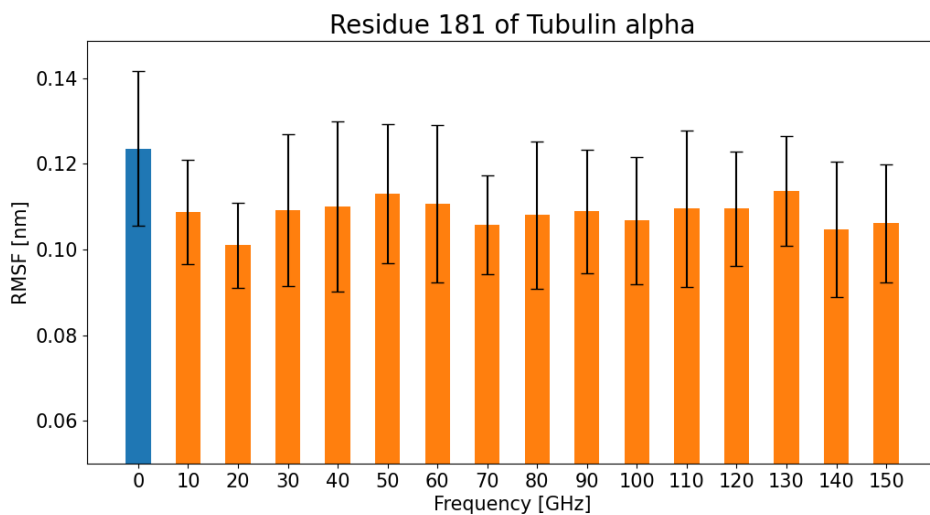


Figure 8.61: RMSF of residue 181 of tubulin alpha - averaged over directions and batches; the bars for 0 GHz mean that no EF is applied

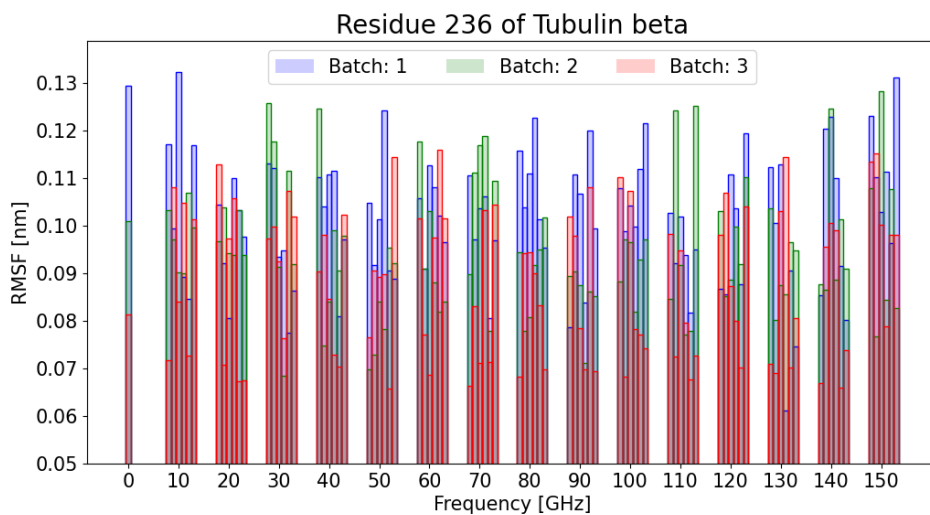


Figure 8.62: RMSF of residue 236 of tubulin beta - different directions and batches; the bars for 0 GHz mean that no EF is applied

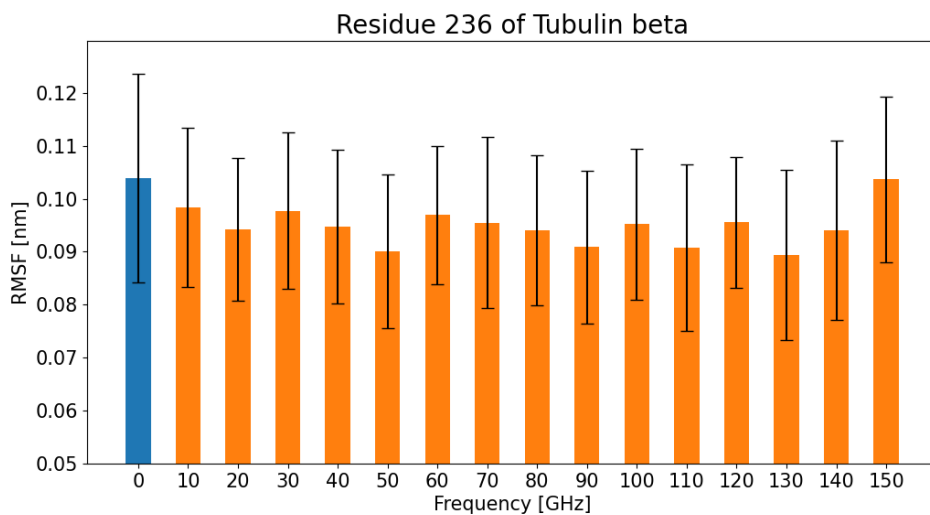


Figure 8.63: RMSF of residue 236 of tubulin beta - averaged over directions and batches; the bars for 0 GHz mean that no EF is applied

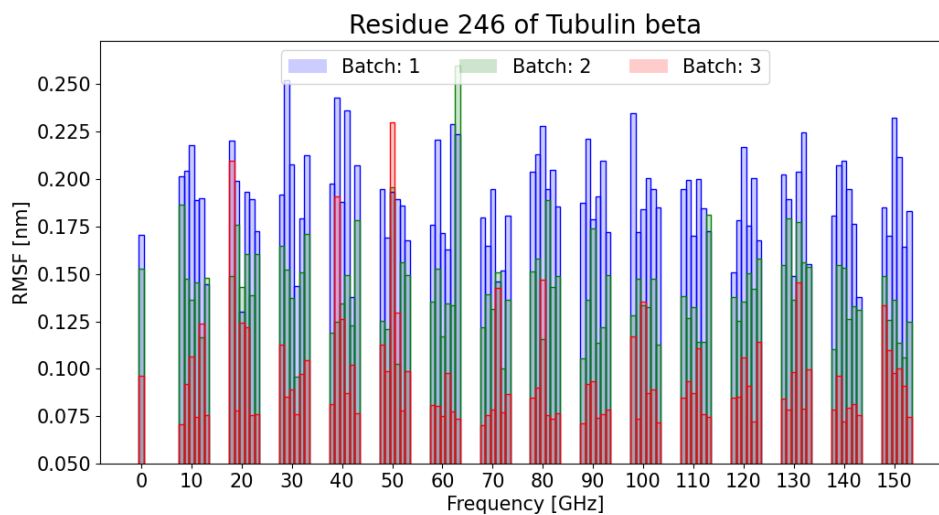


Figure 8.64: RMSF of residue 246 of tubulin beta - different directions and batches; the bars for 0 GHz mean that no EF is applied

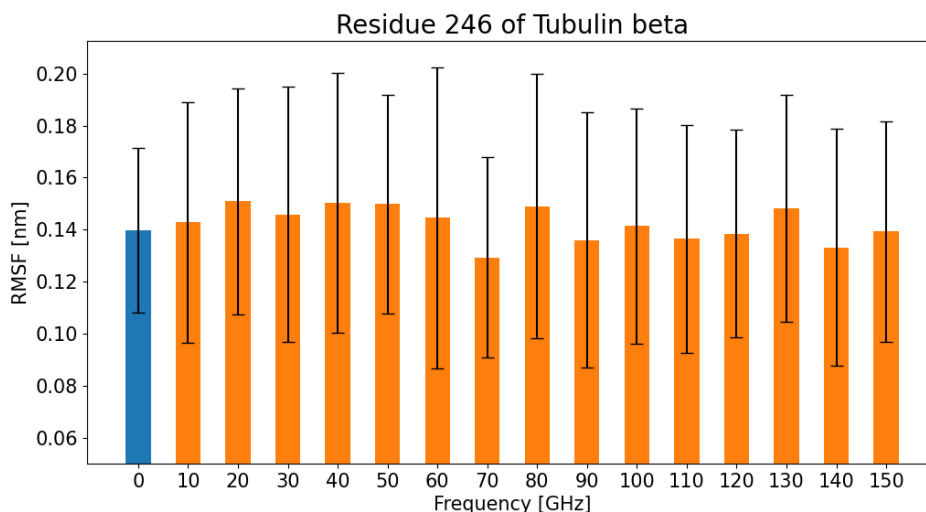


Figure 8.65: RMSF of residue 246 of tubulin beta - averaged over directions and batches; the bars for 0 GHz mean that no EF is applied

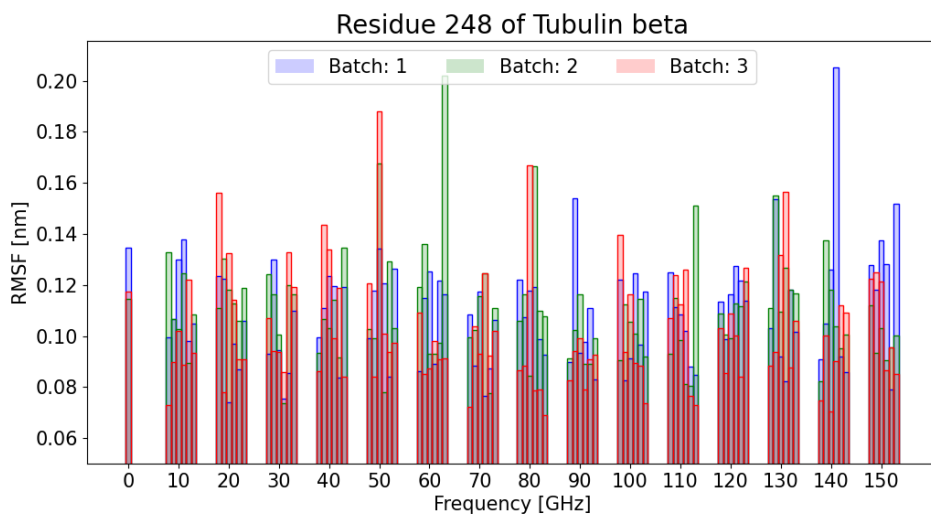


Figure 8.66: RMSF of residue 248 of tubulin beta - different directions and batches; the bars for 0 GHz mean that no EF is applied

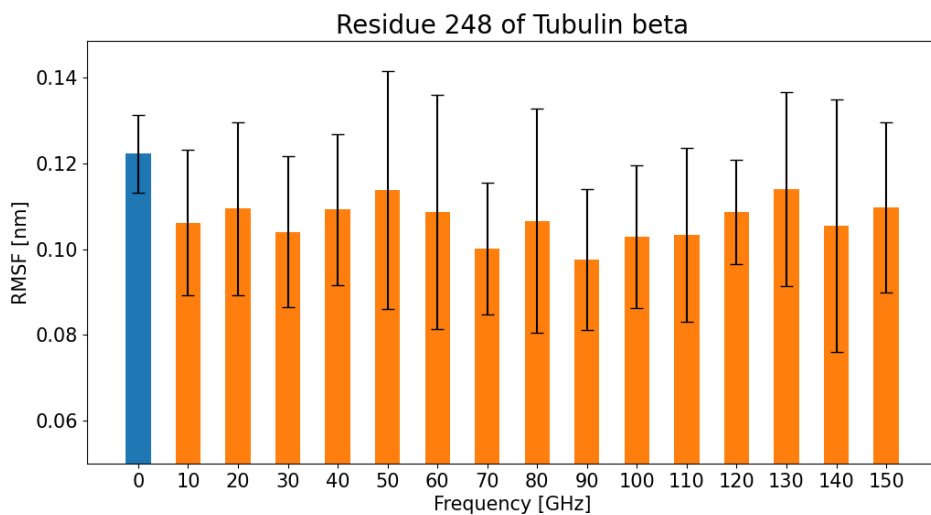


Figure 8.67: RMSF of residue 248 of tubulin beta - averaged over directions and batches; the bars for 0 GHz mean that no EF is applied

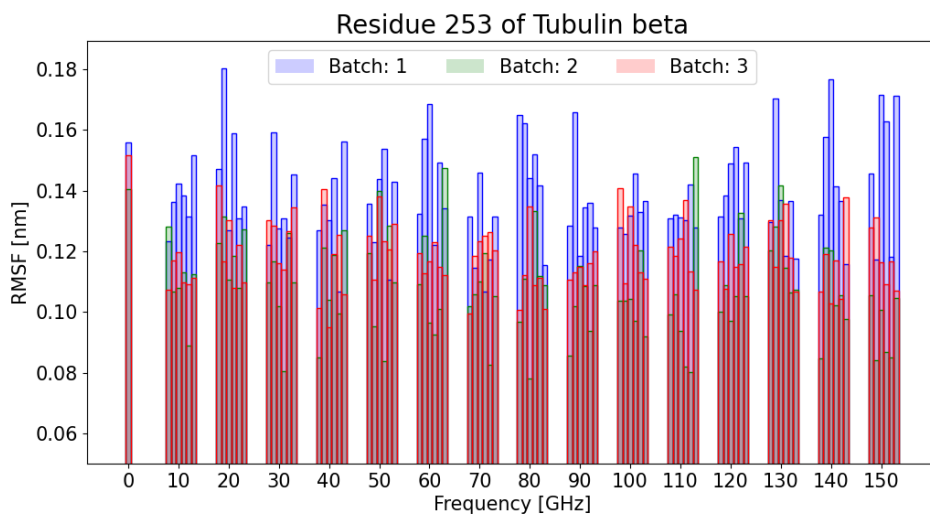


Figure 8.68: RMSF of residue 253 of tubulin beta - different directions and batches; the bars for 0 GHz mean that no EF is applied

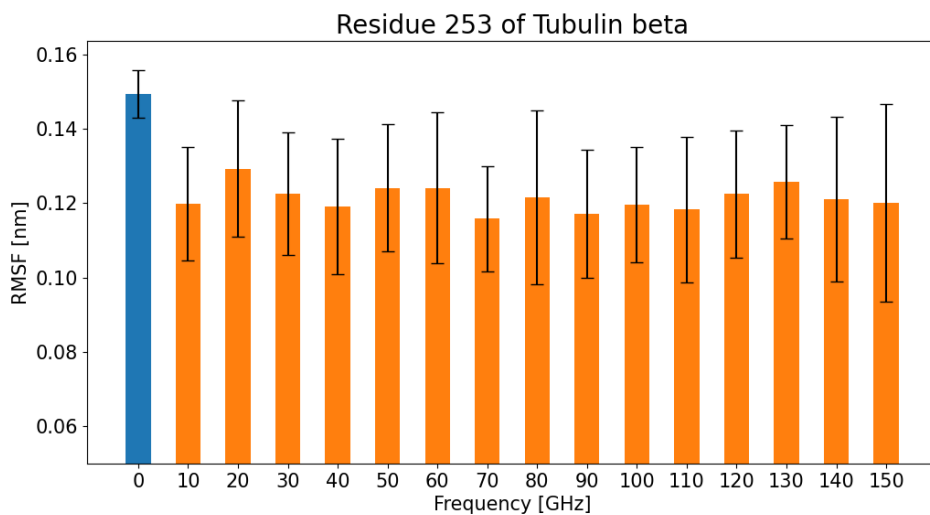


Figure 8.69: RMSF of residue 253 of tubulin beta - averaged over directions and batches; the bars for 0 GHz mean that no EF is applied

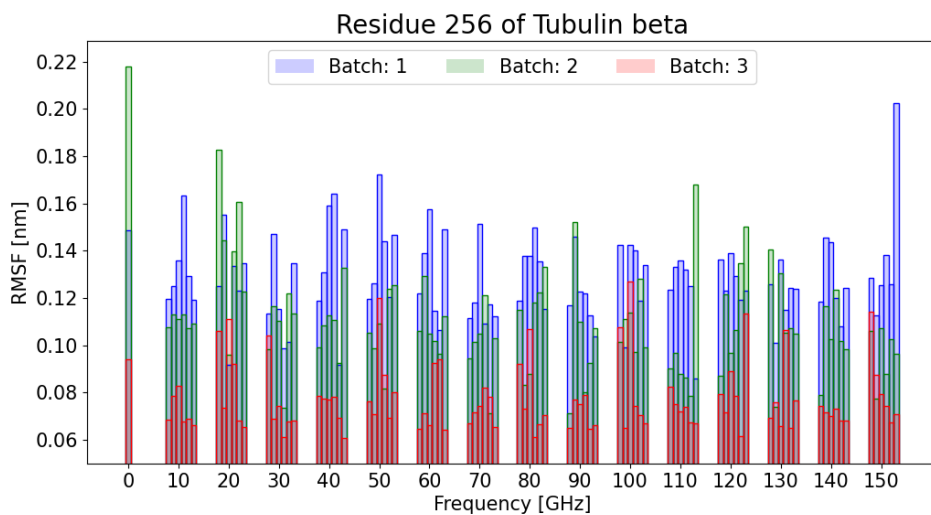


Figure 8.70: RMSF of residue 256 of tubulin beta - different directions and batches; the bars for 0 GHz mean that no EF is applied

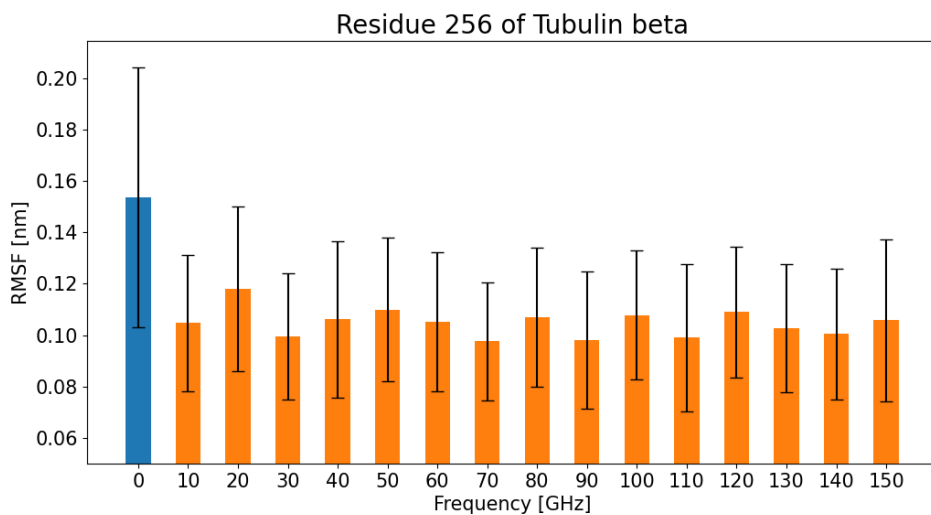


Figure 8.71: RMSF of residue 256 of tubulin beta - averaged over directions and batches; the bars for 0 GHz mean that no EF is applied

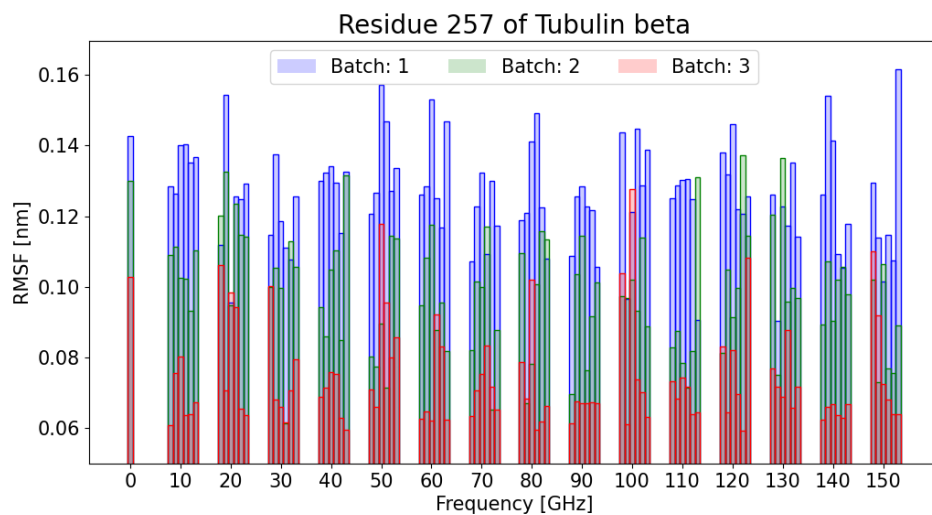


Figure 8.72: RMSF of residue 257 of tubulin beta - different directions and batches; the bars for 0 GHz mean that no EF is applied

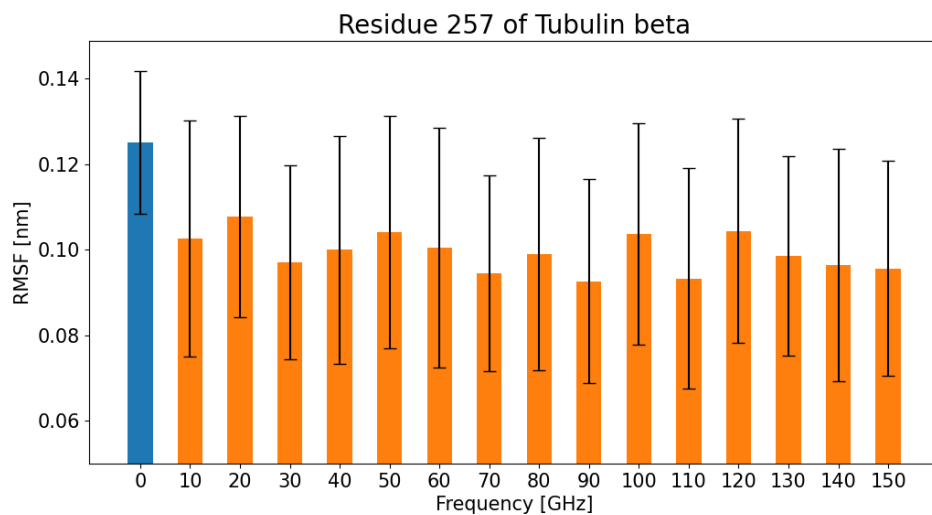


Figure 8.73: RMSF of residue 257 of tubulin beta - averaged over directions and batches; the bars for 0 GHz mean that no EF is applied

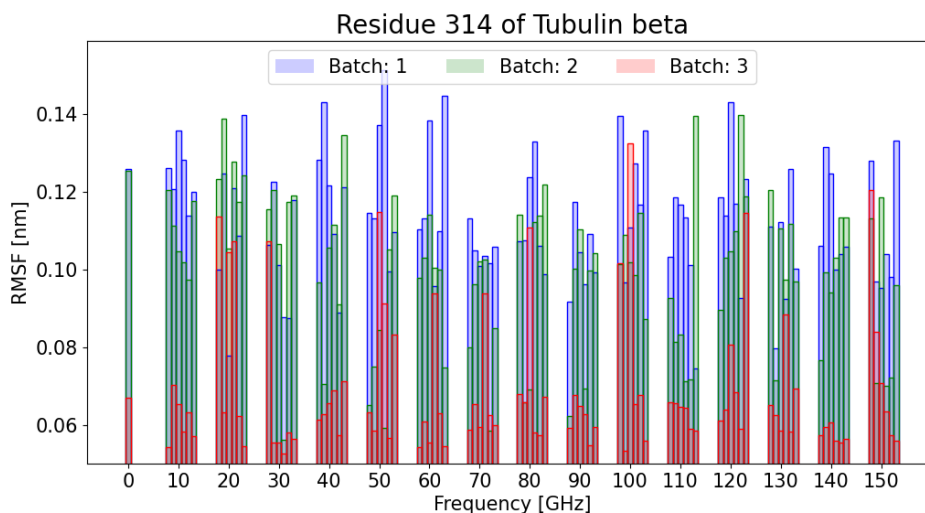


Figure 8.74: RMSF of residue 314 of tubulin beta - different directions and batches; the bars for 0 GHz mean that no EF is applied

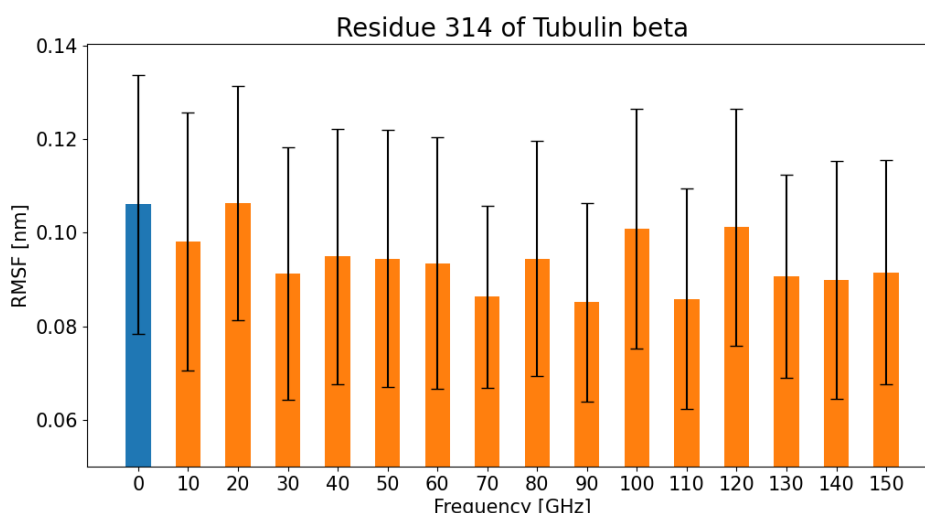


Figure 8.75: RMSF of residue 314 of tubulin beta - averaged over directions and batches; the bars for 0 GHz mean that no EF is applied

8.5.2 Binding site of Paclitaxel

Tubulin β

Paclitaxel binds to the tubulin β only, where residues 23, 26, 27, 215, 227, 228, 231, 234, 270, 272, 273, 274, 276, 280, 358, 359, 360, 361 mediate this interaction. Again, some of those graphs are displayed in Appendix 10.14 due to a high number of graphs. Stabilization by electric field of all frequencies was seen in some of them - 215, 228, 231, 272 (averaged result). See Figures 8.77, 8.81, 10.266, and 8.83.

On the other hand, a few of them became more flexible under all frequencies of EF (averaged result) - 274 (Figure 8.85), 276 (8.87), 280 (8.89) and 359 (8.93). But again the results differed quite a lot for different directions of the electric field or the initial conformation.

Residues 23 (Figure 10.260), 26 (10.262) and 27 (10.264) did not show a big

change of RMSF on average, since the outcomes really depended on the initial conformation. For example, for the batch 3 initial conformation, we saw these three residues become a lot more flexible in the case of 20 and 100 GHz (for some directions of oscillation).

10 and 110 GHz had a stabilizing effect on residue 215 (Figure 8.77).

A similar effect of 90 GHz and 110 GHz was seen on residue 272 (8.83); however, this residue experienced higher fluctuations for 20 and 100 GHz mainly in the batch 3 conformation.

An increase in the fluctuations due to 20 and 100 GHz electric fields was also observed in residues 273 (10.272) and 274 (8.85). Residue 274 also had higher fluctuations for 10 and 110 GHz electric fields.

Residues 276 (8.87) and 280 (8.89) became more flexible under the influence of all electric fields, but mainly 10, 30, 40 and 90 GHz (and 130 GHz for res 280).

Flexibilities of the residues 358 (8.91), 359 (8.93), 360 (8.95) and 361 (8.97) highly depend on the direction of EF and initial conformation. Residue 358 became more rigid under the majority of conditions, whereas residue 359 was more flexible.

We have not provided references here for all residues that are in the appendix, so we advise the reader, if interested, to see the corresponding part of the appendix: 10.14

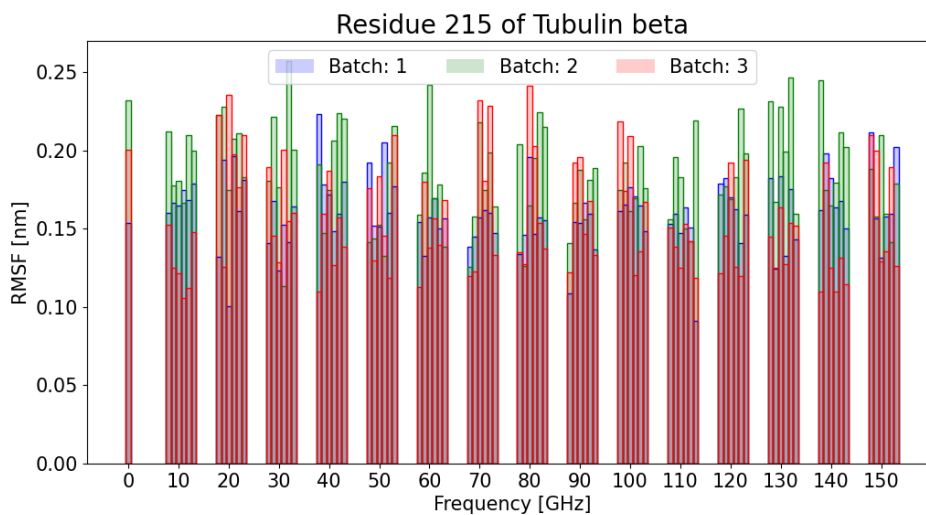


Figure 8.76: RMSF of residue 215 of tubulin beta - different directions and batches; the bars for 0 GHz mean that no EF is applied

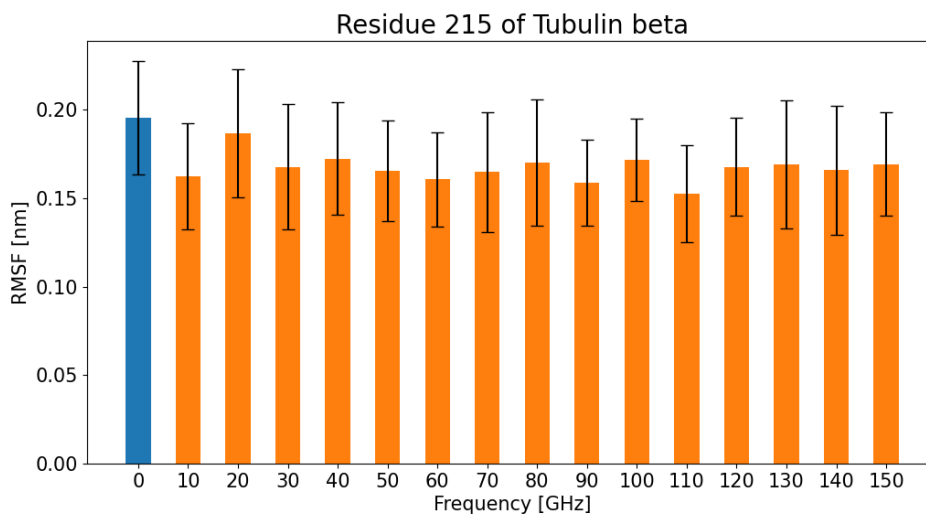


Figure 8.77: RMSF of residue 215 of tubulin beta - averaged over directions and batches; the bars for 0 GHz mean that no EF is applied

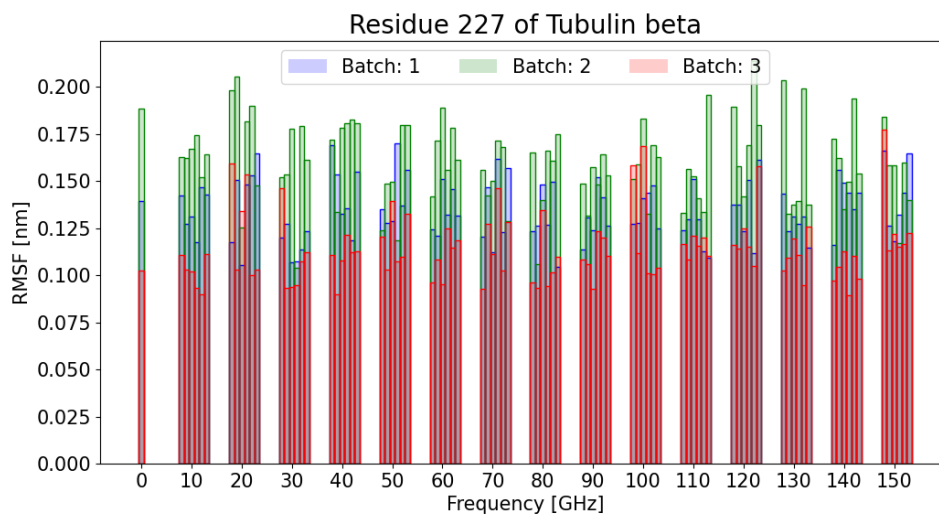


Figure 8.78: RMSF of residue 227 of tubulin beta - different directions and batches; the bars for 0 GHz mean that no EF is applied

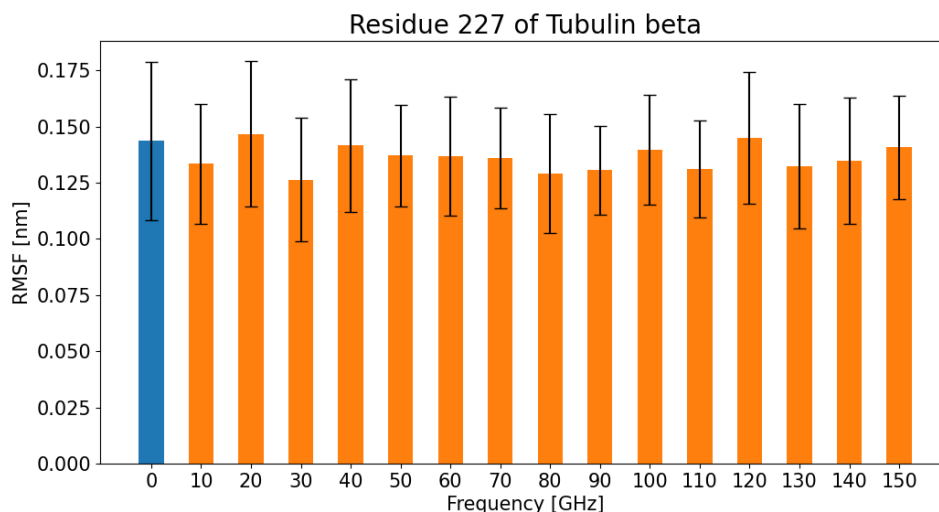


Figure 8.79: RMSF of residue 227 of tubulin beta - averaged over directions and batches; the bars for 0 GHz mean that no EF is applied

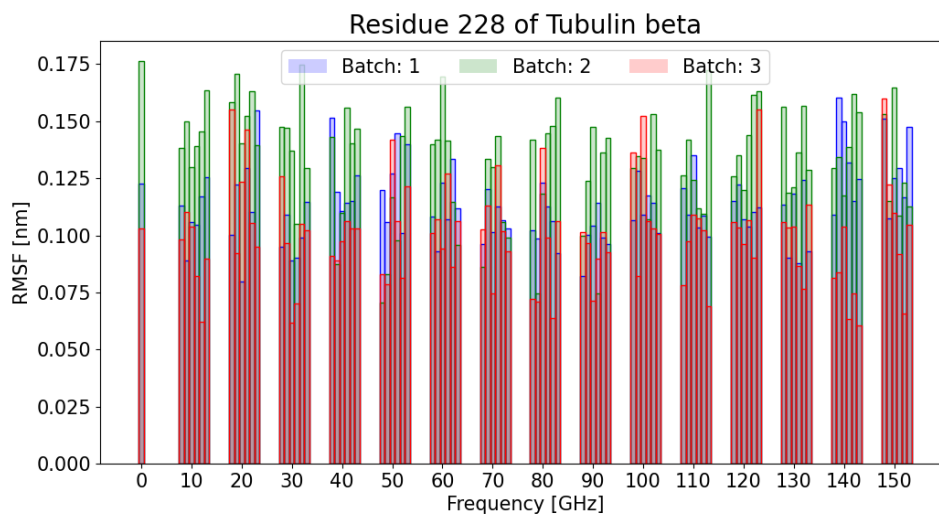


Figure 8.80: RMSF of residue 228 of tubulin beta - different directions and batches; the bars for 0 GHz mean that no EF is applied

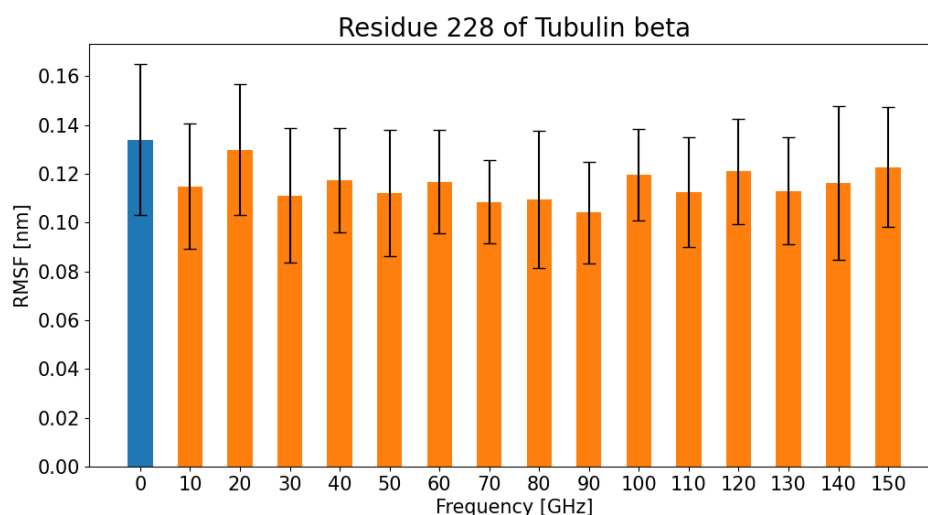


Figure 8.81: RMSF of residue 228 of tubulin beta - averaged over directions and batches; the bars for 0 GHz mean that no EF is applied

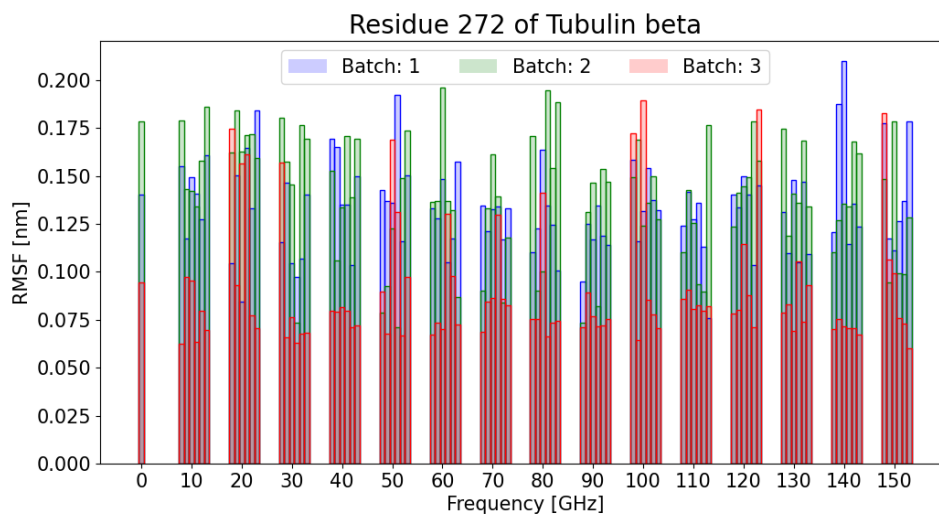


Figure 8.82: RMSF of residue 272 of tubulin beta - different directions and batches; the bars for 0 GHz mean that no EF is applied

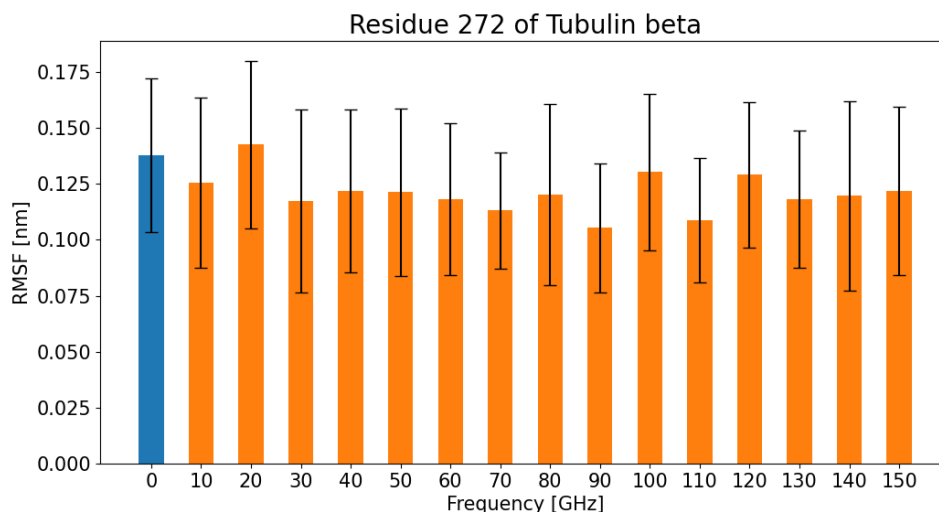


Figure 8.83: RMSF of residue 272 of tubulin beta - averaged over directions and batches; the bars for 0 GHz mean that no EF is applied

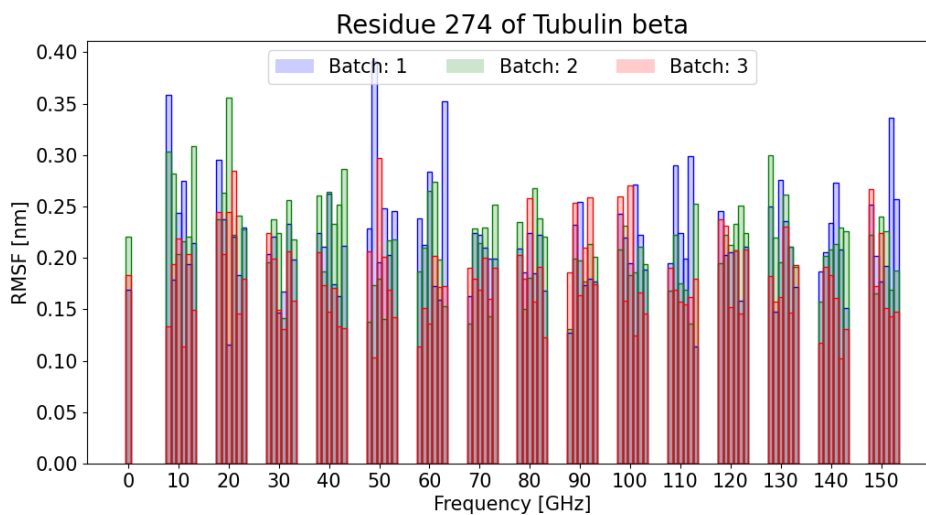


Figure 8.84: RMSF of residue 274 of tubulin beta - different directions and batches; the bars for 0 GHz mean that no EF is applied

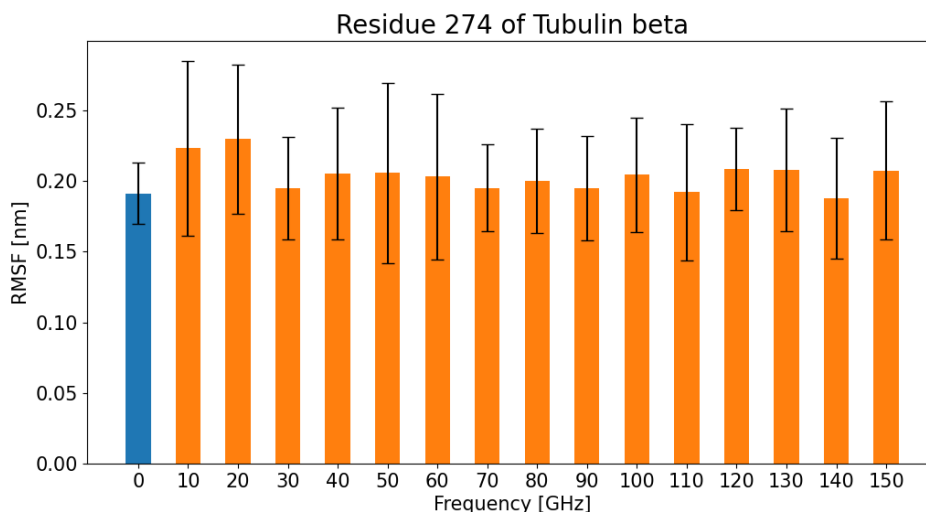


Figure 8.85: RMSF of residue 274 of tubulin beta - averaged over directions and batches; the bars for 0 GHz mean that no EF is applied

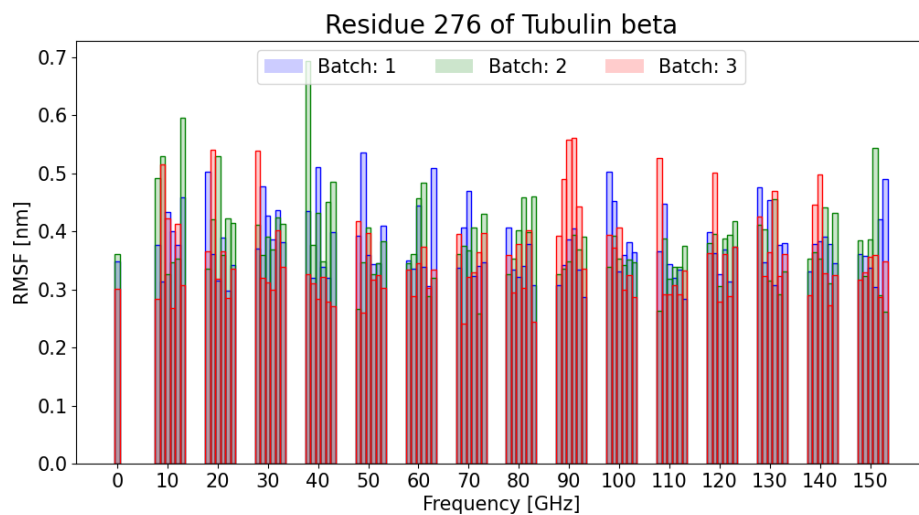


Figure 8.86: RMSF of residue 276 of tubulin beta - different directions and batches; the bars for 0 GHz mean that no EF is applied

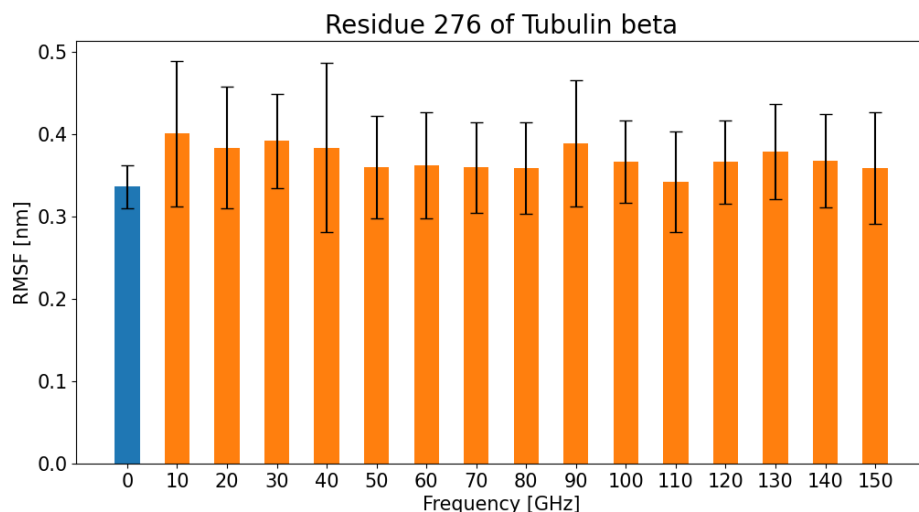


Figure 8.87: RMSF of residue 276 of tubulin beta - averaged over directions and batches; the bars for 0 GHz mean that no EF is applied

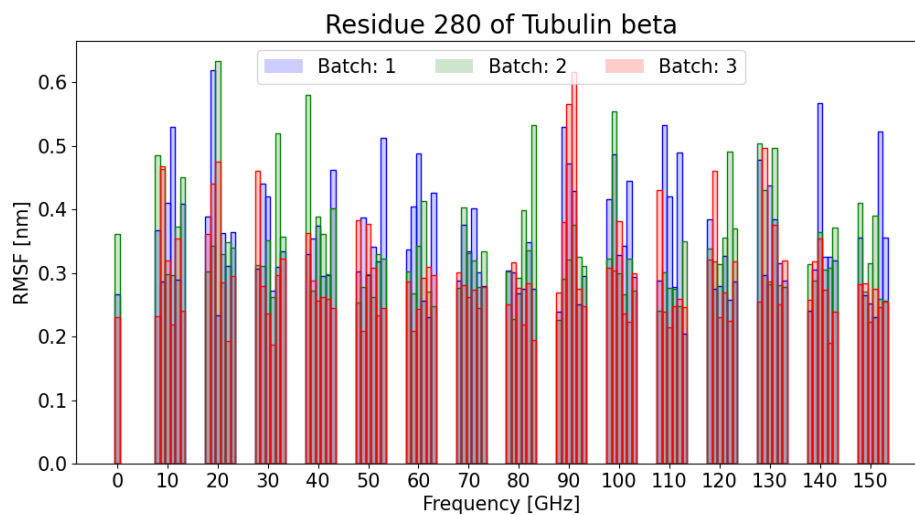


Figure 8.88: RMSF of residue 280 of tubulin beta - different directions and batches; the bars for 0 GHz mean that no EF is applied

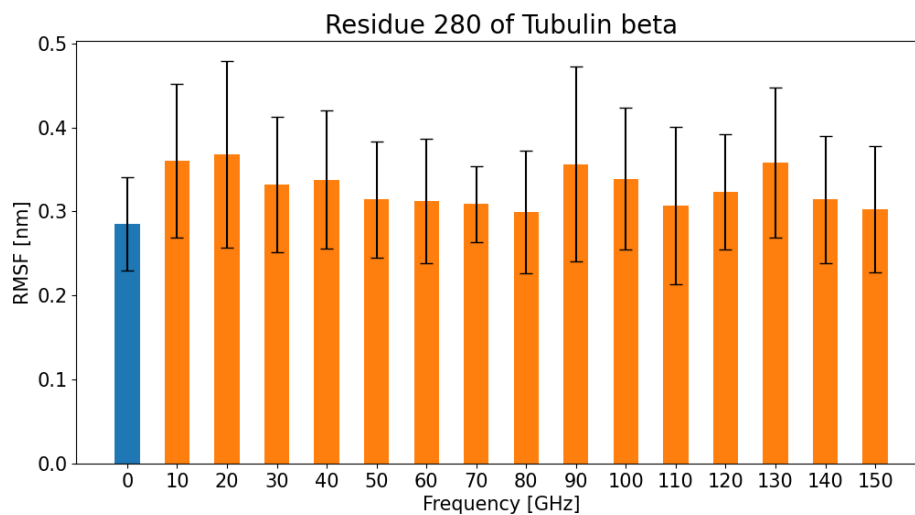


Figure 8.89: RMSF of residue 280 of tubulin beta - averaged over directions and batches; the bars for 0 GHz mean that no EF is applied

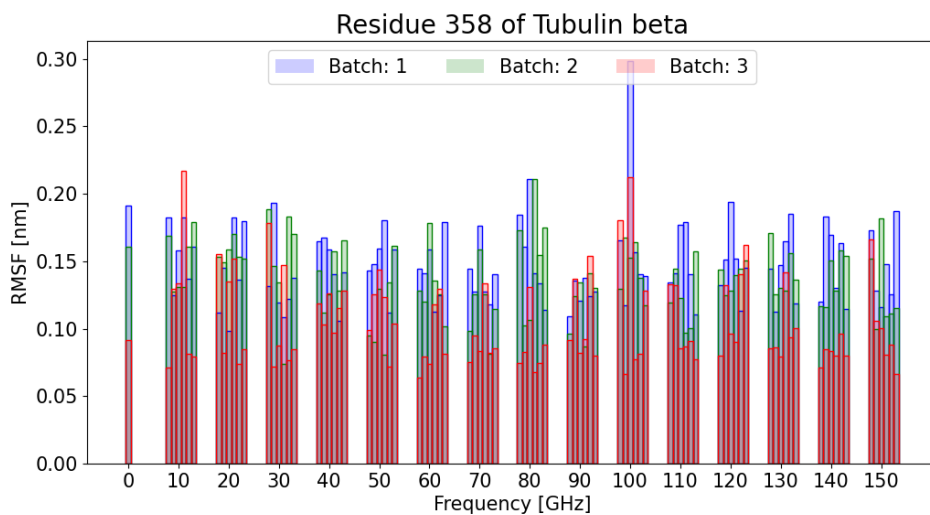


Figure 8.90: RMSF of residue 358 of tubulin beta - different directions and batches; the bars for 0 GHz mean that no EF is applied

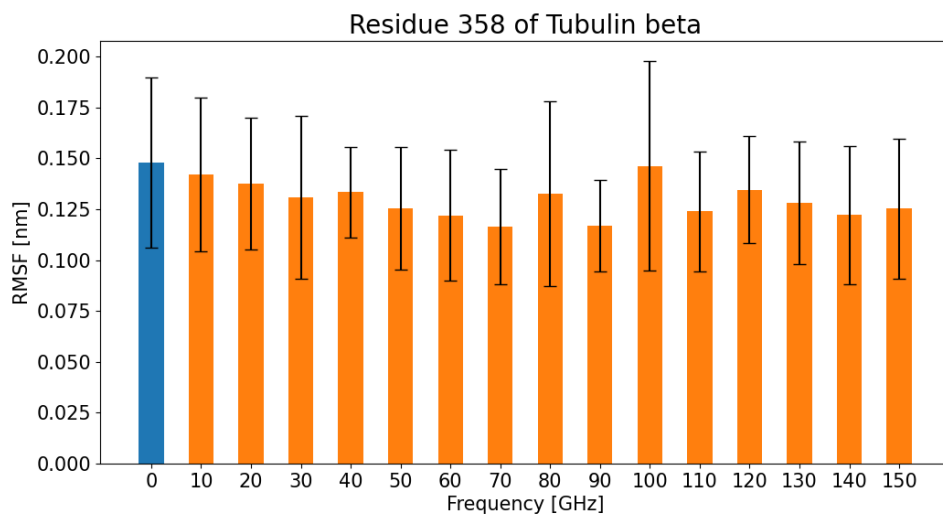


Figure 8.91: RMSF of residue 358 of tubulin beta - averaged over directions and batches; the bars for 0 GHz mean that no EF is applied

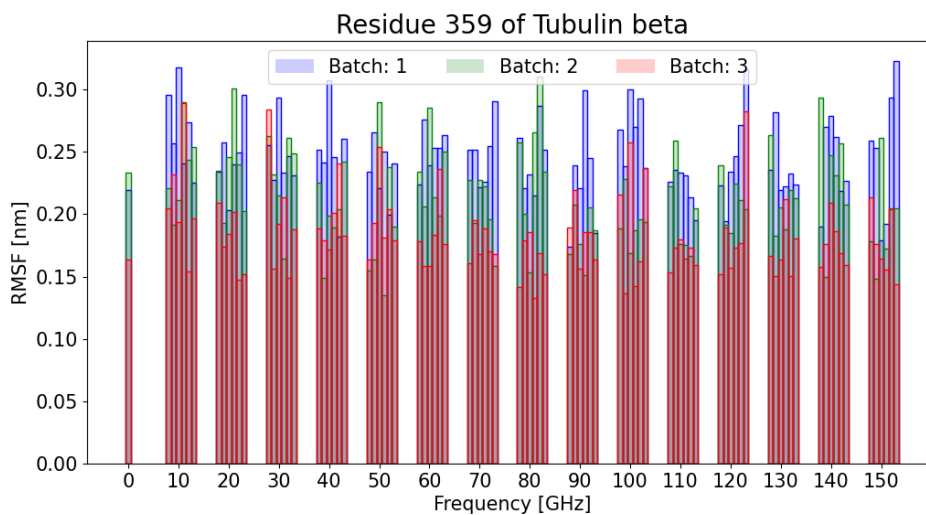


Figure 8.92: RMSF of residue 359 of tubulin beta - different directions and batches; the bars for 0 GHz mean that no EF is applied

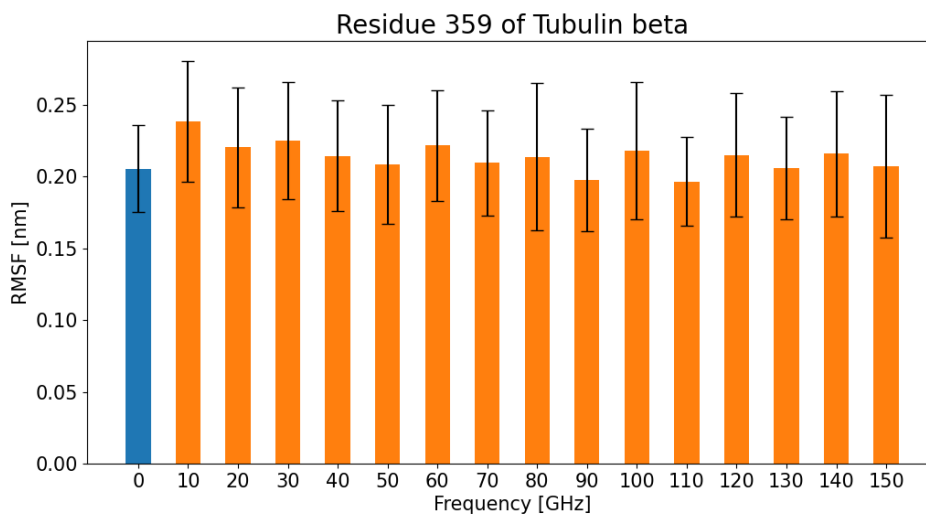


Figure 8.93: RMSF of residue 359 of tubulin beta - averaged over directions and batches; the bars for 0 GHz mean that no EF is applied

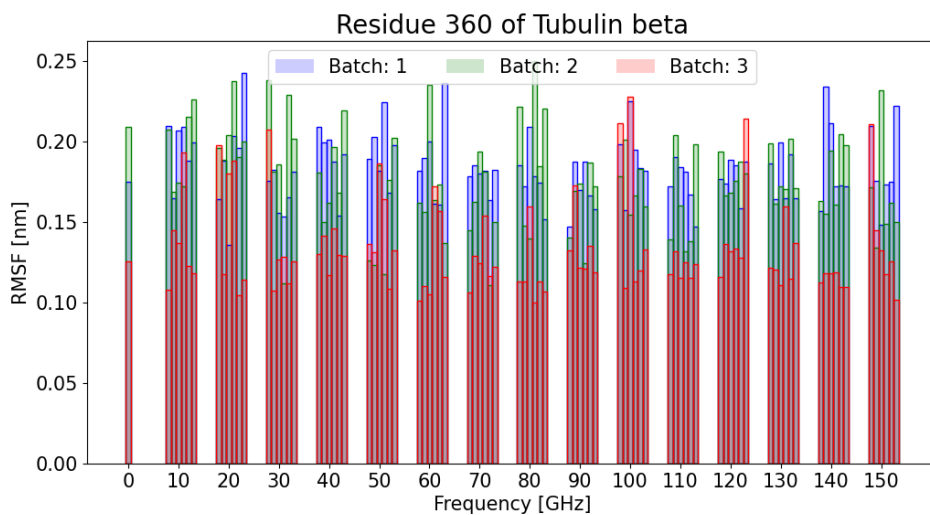


Figure 8.94: RMSF of residue 360 of tubulin beta - different directions and batches; the bars for 0 GHz mean that no EF is applied

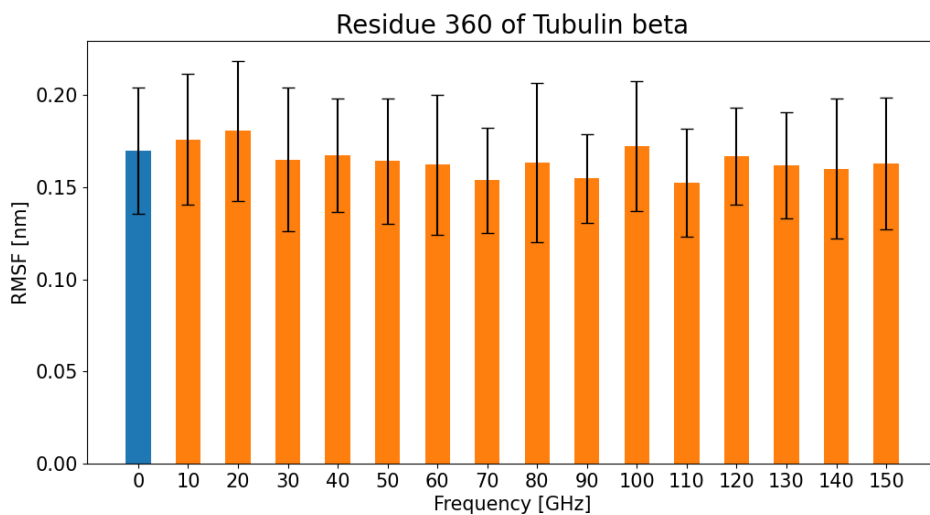


Figure 8.95: RMSF of residue 360 of tubulin beta - averaged over directions and batches; the bars for 0 GHz mean that no EF is applied

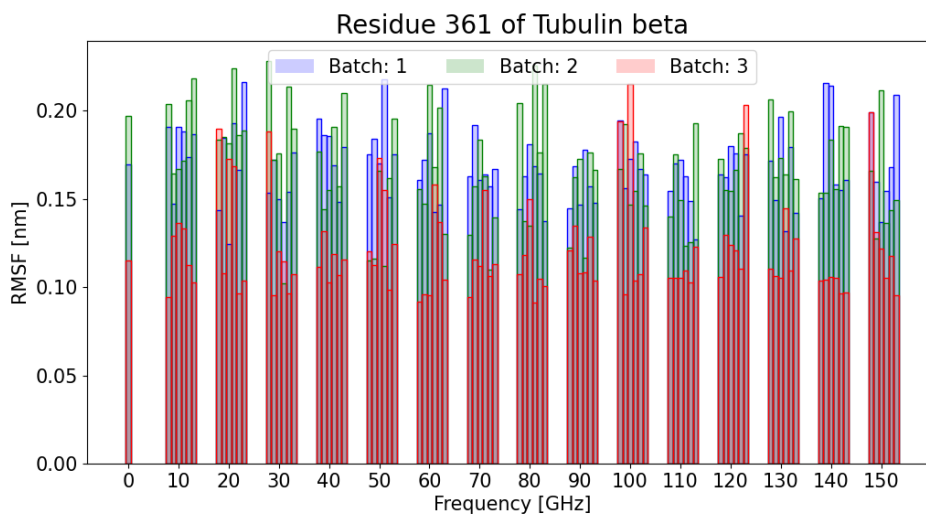


Figure 8.96: RMSF of residue 361 of tubulin beta - different directions and batches; the bars for 0 GHz mean that no EF is applied

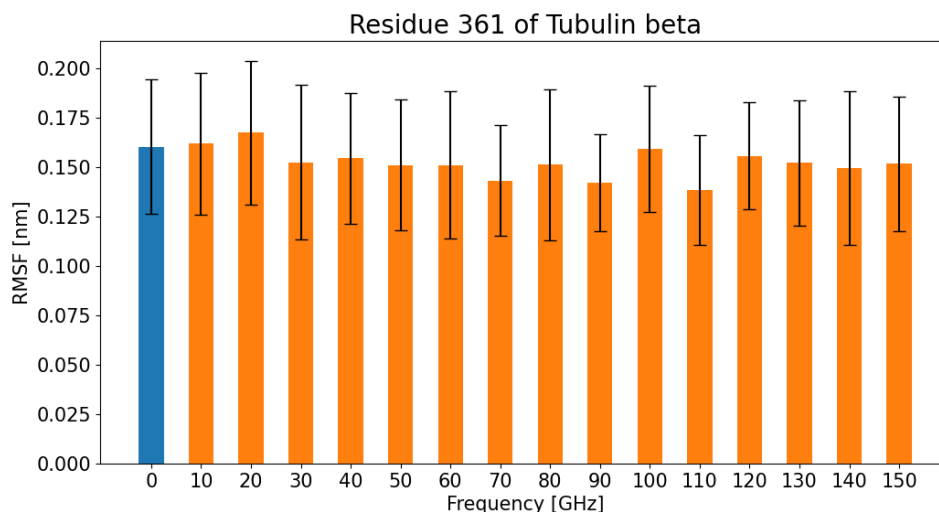


Figure 8.97: RMSF of residue 361 of tubulin beta - averaged over directions and batches; the bars for 0 GHz mean that no EF is applied

8.6 Rotational analysis

Rotational diffusion is normal for proteins in solution, therefore we wanted to know whether the applied oscillating electric field in the range of 10 - 150 GHz would disrupt this natural behaviour and whether we would see a rotational effect due to the electric field. Indeed, this was observed for frequencies 10, 20, 30 and 40 GHz - protein rotated until its longitudinal axis was approximately parallel to the electric-field oscillation direction. This was initially rather unintuitive since the dipole moment of the tubulin is approximately perpendicular to the longitudinal axis (highly depends on the C-termini conformations). Hence, the electric field exhibits the largest torque onto the dipole moment in this oriented state. We will discuss the physics behind this in the Discussion Chapter 9.2.

The time it took for the tubulin to rotate was really small for the electric field of frequencies 10 - 40 GHz. Afterwards, the longitudinal axis of tubulin stayed oriented approximately parallel to the electric-field oscillations. At higher frequencies up until 70 GHz, the tubulin dimer is also being oriented in the same fashion, but the orientation is not that fast and not that stable. The angle between the tubulin longitudinal axis and the axis of the electric-field oscillation direction is changing much more. For higher frequencies, the distributions of the angles become more chaotic, and we do not observe this orientational effect.

Batch 1

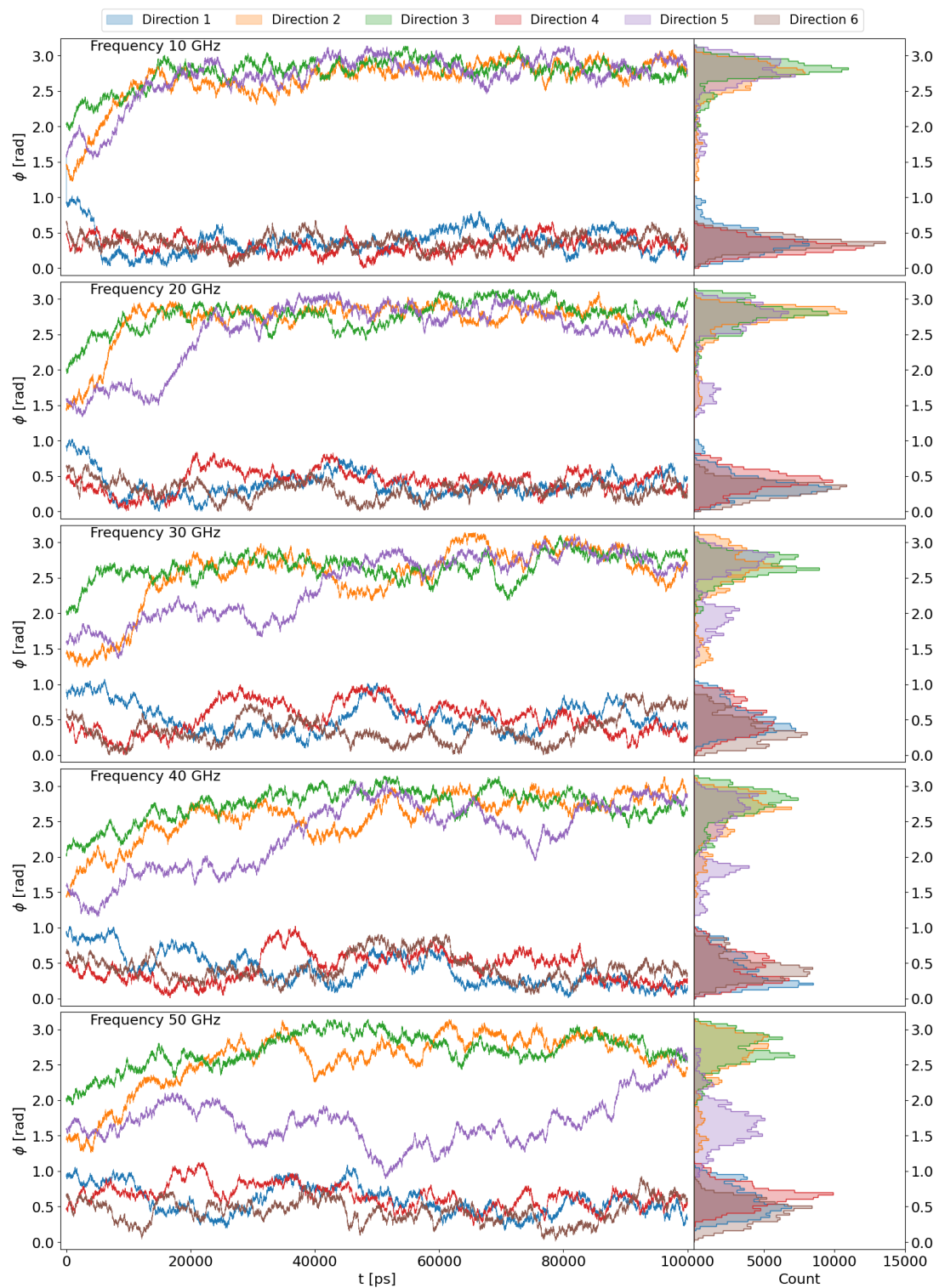


Figure 8.98: Angle between longitudinal axis of tubulin heterodimer and electric field direction - batch 1. part 1 (frequencies 10-50 GHz)

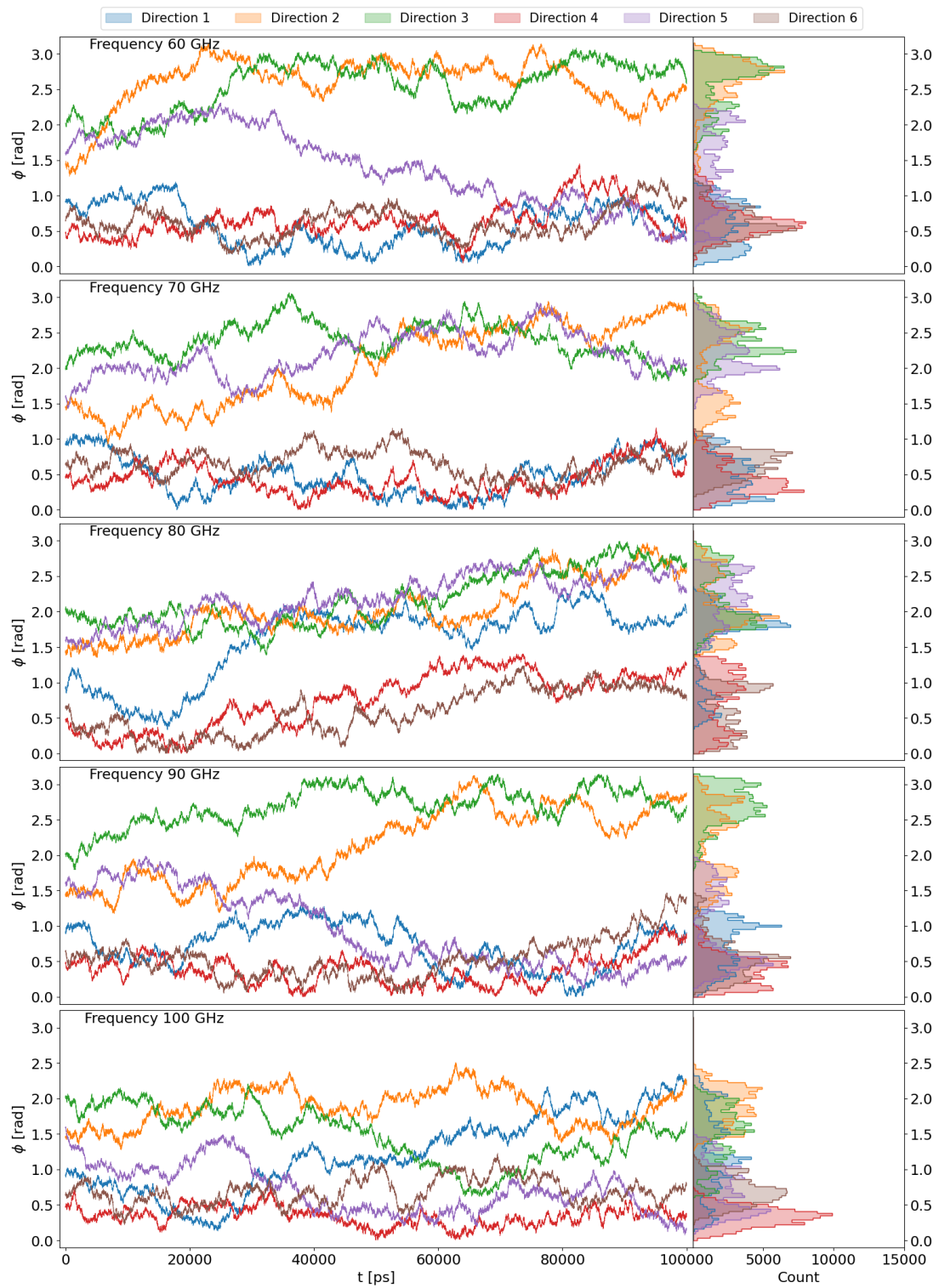


Figure 8.99: Angle between longitudinal axis of tubulin heterodimer and electric field direction - batch 1. part 2 (frequencies 60-100 GHz)

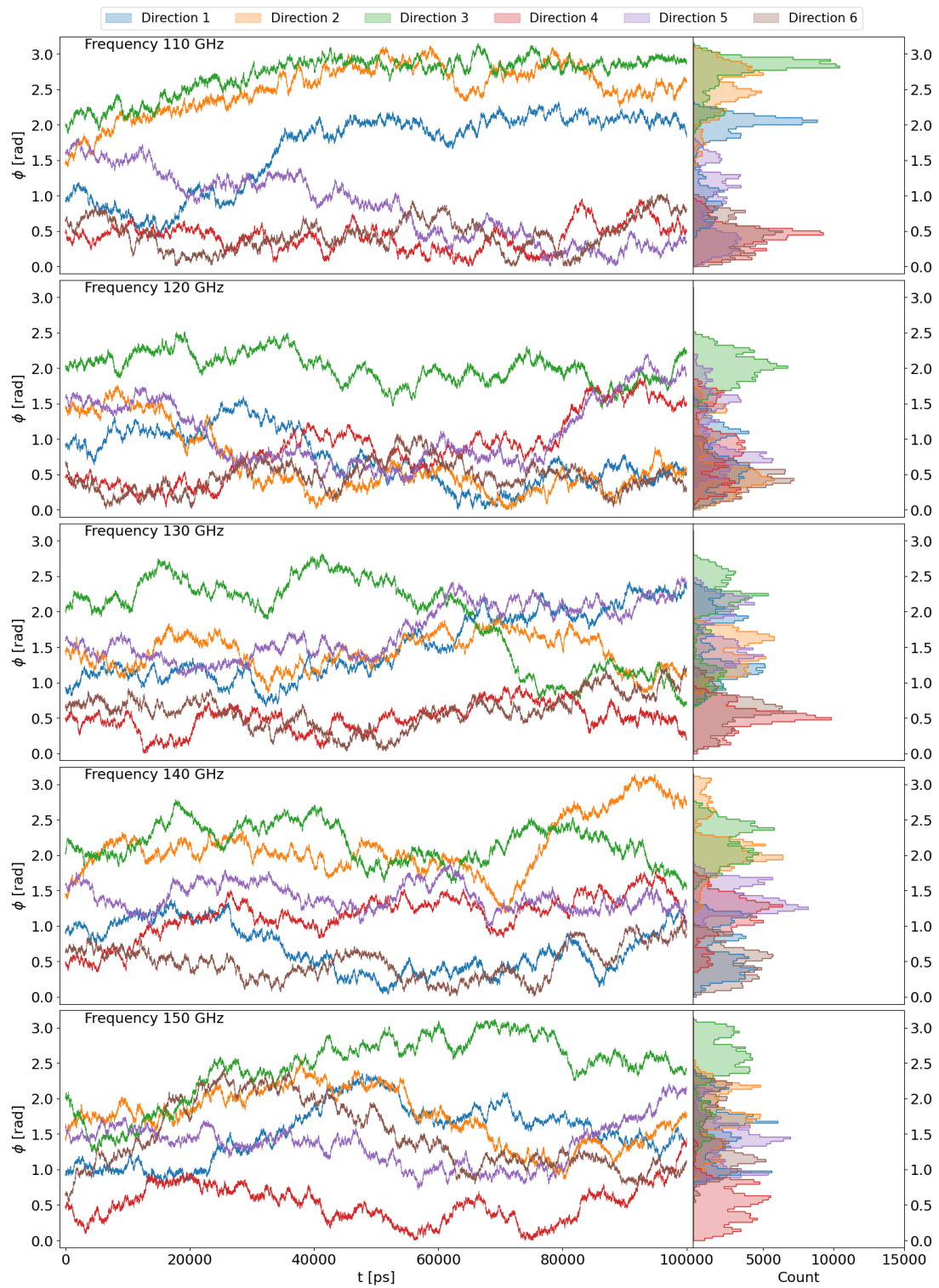


Figure 8.100: Angle between longitudinal axis of tubulin heterodimer and electric field direction - batch 1. part 3 (frequencies 110-150 GHz)

Batch 2

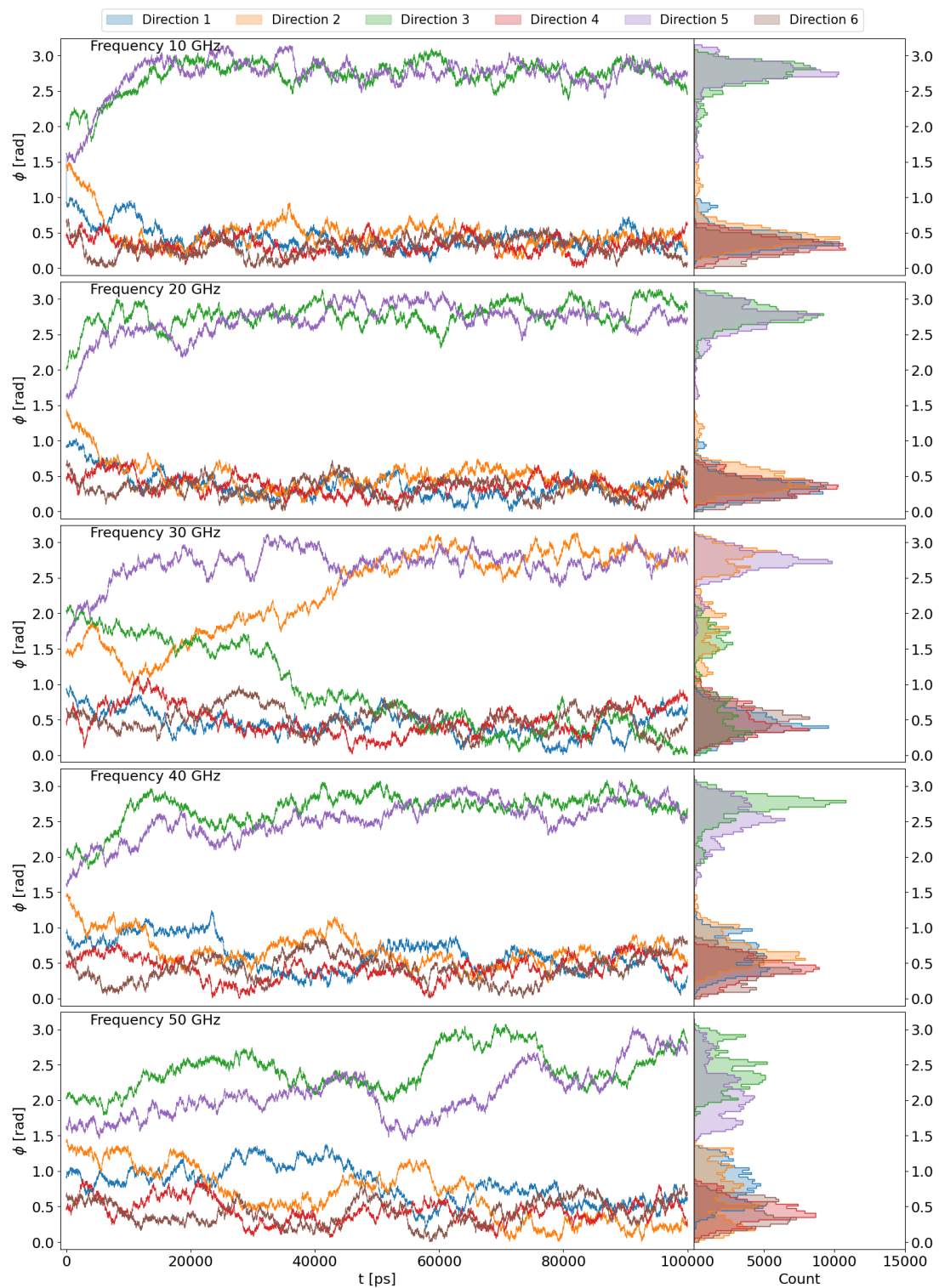


Figure 8.101: Angle between longitudinal axis of tubulin heterodimer and electric field direction - batch 2. 1 (frequencies 10-50 GHz)

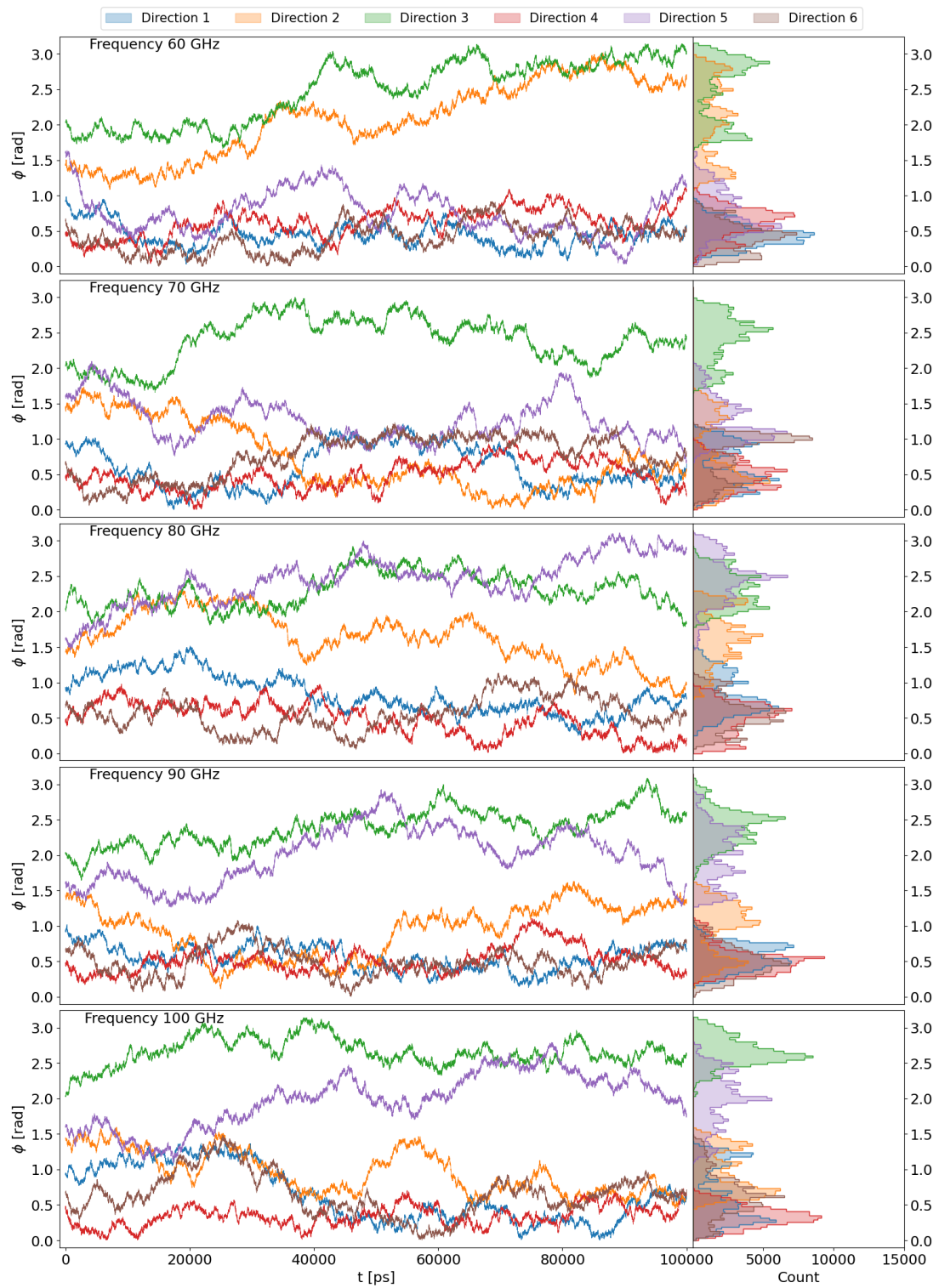


Figure 8.102: Angle between longitudinal axis of tubulin heterodimer and electric field direction - batch 2. 2 (frequencies 60-100 GHz)

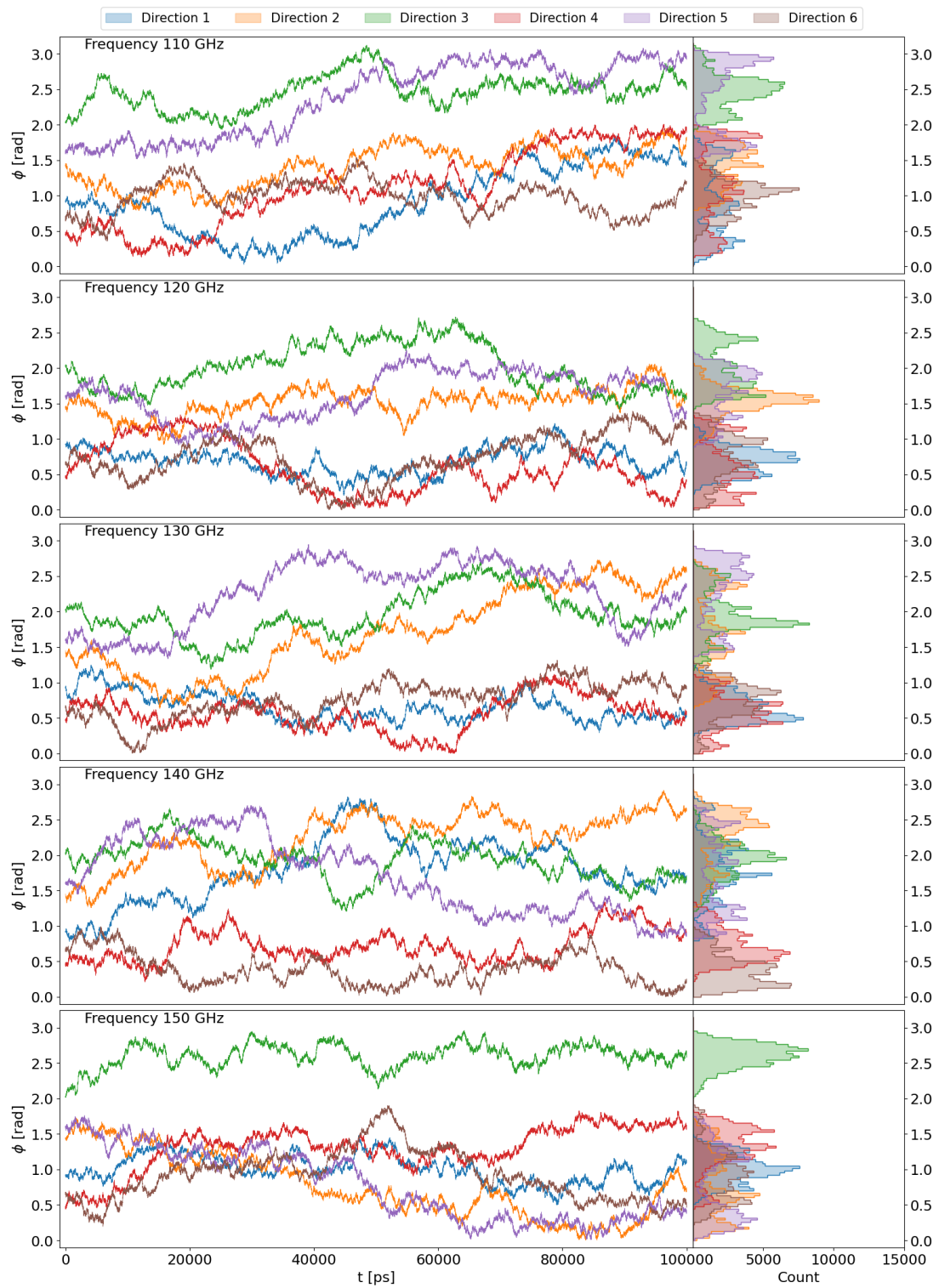


Figure 8.103: Angle between longitudinal axis of tubulin heterodimer and electric field direction - batch 2. 3 (frequencies 110-150 GHz)

Batch 3

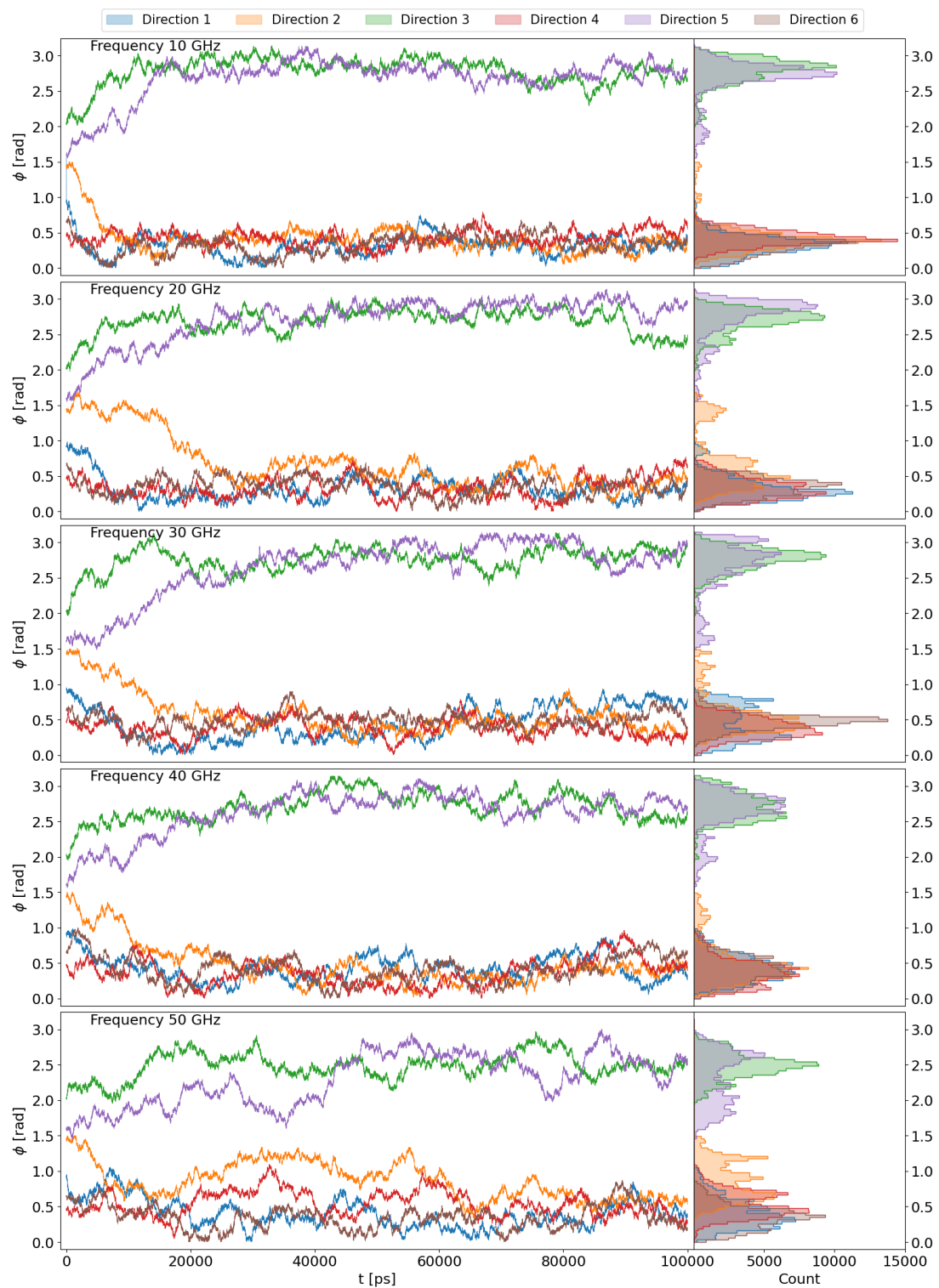


Figure 8.104: Angle between longitudinal axis of tubulin heterodimer and electric field direction - batch 3. 1 (frequencies 10-50 GHz)

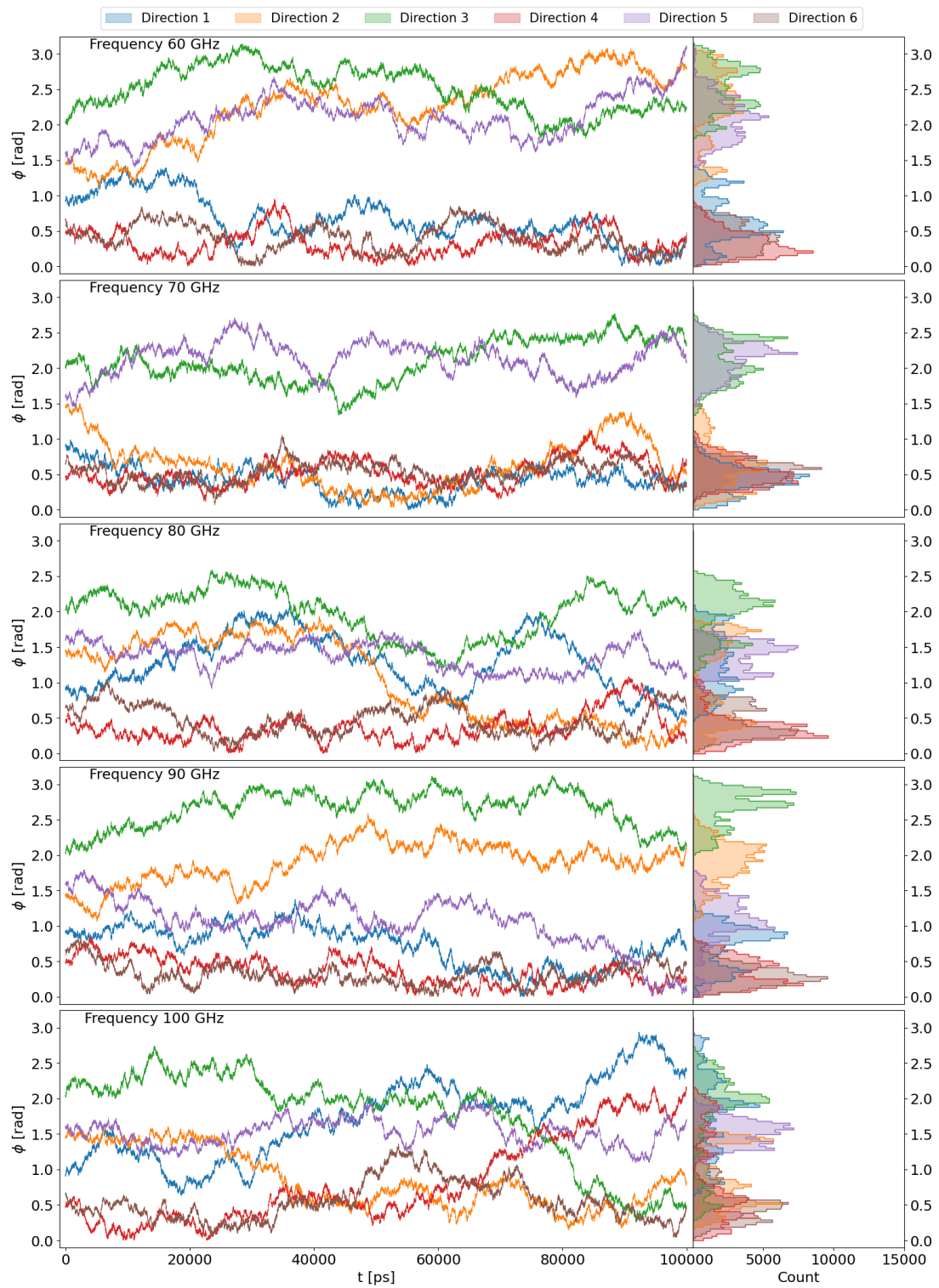


Figure 8.105: Angle between longitudinal axis of tubulin heterodimer and electric field direction - batch 3. 2 (frequencies 60-100 GHz)

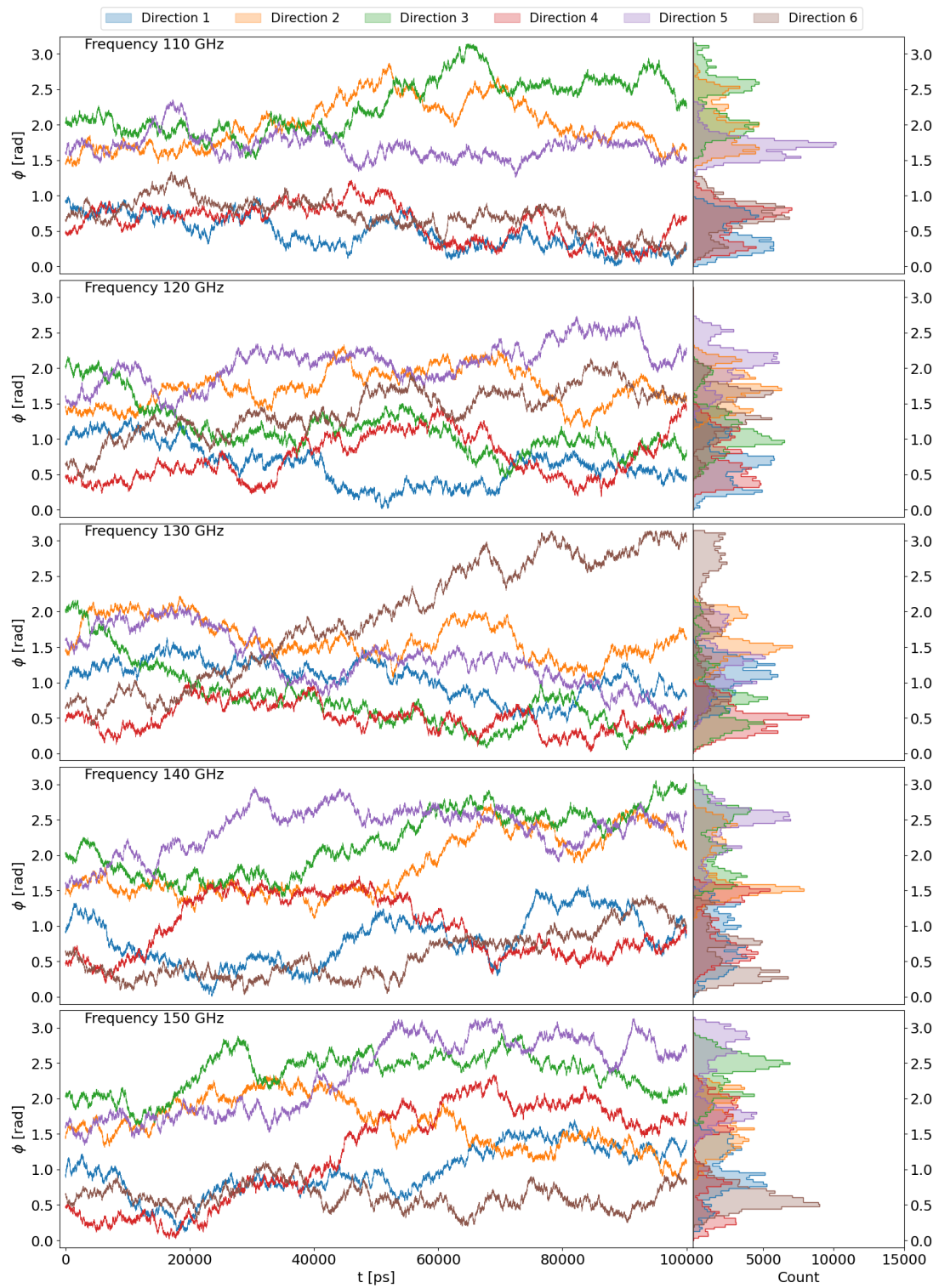


Figure 8.106: Angle between longitudinal axis of tubulin heterodimer and electric field direction - batch 3. 3 (frequencies 110-150 GHz)

Time spent oriented parallel to the electric-field direction of oscillation

Here, we present the data regarding the amount of time the tubulin spent oriented in the fashion explained in the previous section. The limiting value of the angle for which we would still consider the tubulin to be "oriented" was chosen to be $\approx 40^\circ$, since the tubulin stable orientation does not completely coincide with longitudinal axis. The stable orientation is around 0.4 rad, therefore this means that if the angle ϕ is smaller than 40° , the limiting value is actually 20° . The graphs of the counts (of the tubulin being oriented) depending on the frequency of the electric field that is applied, are showcased below only for the first batch 8.107-8.112. The graphs of the second and third batch are displayed in Appendix 10.15. The colour of the bars in these bar graphs represents the length of the data considered. The blue, orange and green correspond to the counts calculated from 100 ns, the last 75 ns and the last 50 ns, respectively. This is done to showcase the trend of the orientation process. We see again from the graphs below that electric fields of frequencies 10, 20, 30 or 40 GHz (regardless of their directions of oscillation with respect to the tubulin) rotate the tubulin (regardless of its initial conformation). However, when it comes to the other frequencies, the rotational effect of the electric field strongly depends on the direction of electric-field oscillations and on the initial conformation of the tubulin. After the non-averaged bar graphs follow the ones that showcase the average values of these oriented time counts either over directions 8.113, batches (initial conformations) 8.114 or both 8.115.

Time spent oriented - Batch 1

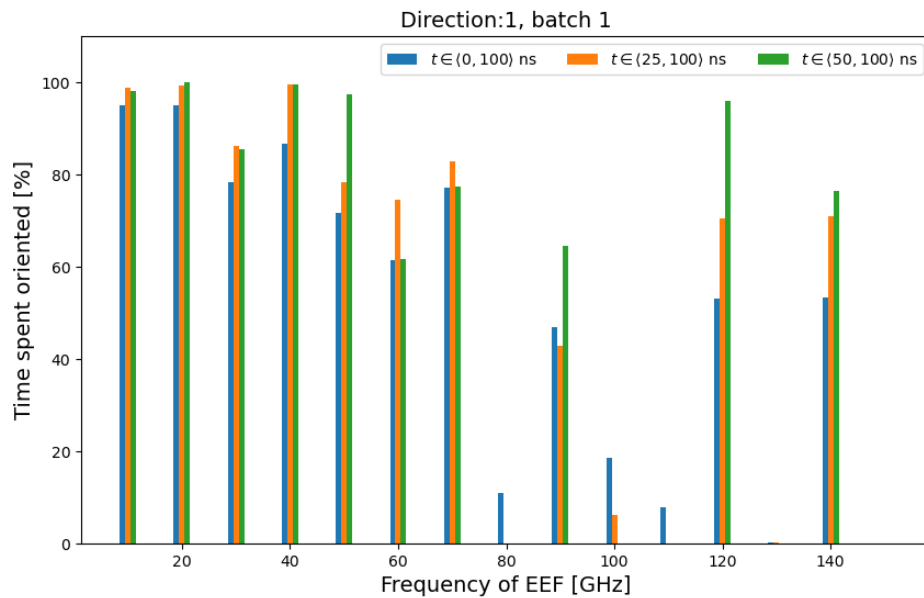


Figure 8.107: Time spent approximately parallel to the electric field direction of oscillation - batch 1, direction 1

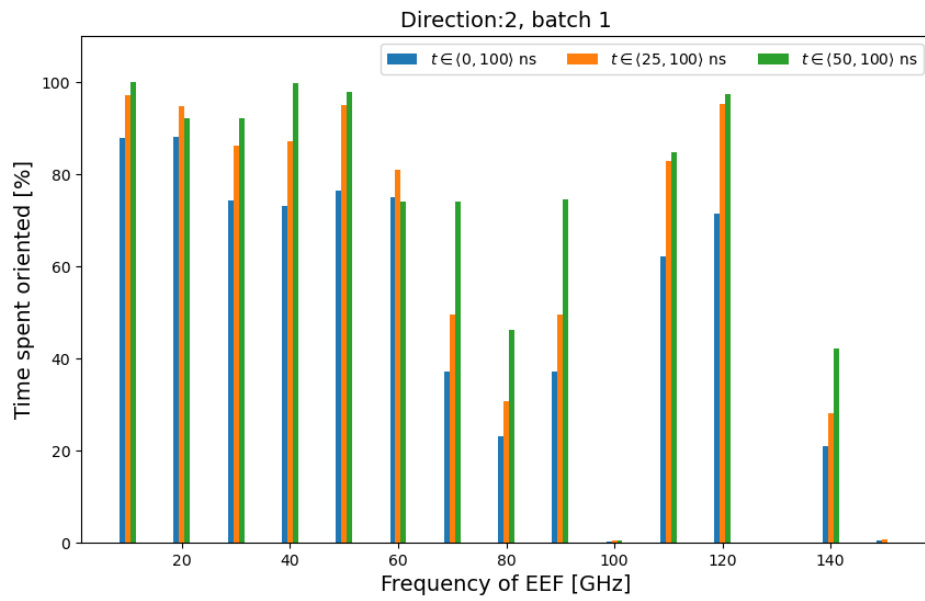


Figure 8.108: Time spent approximately parallel to the electric field direction of oscillation - batch 1, direction 2

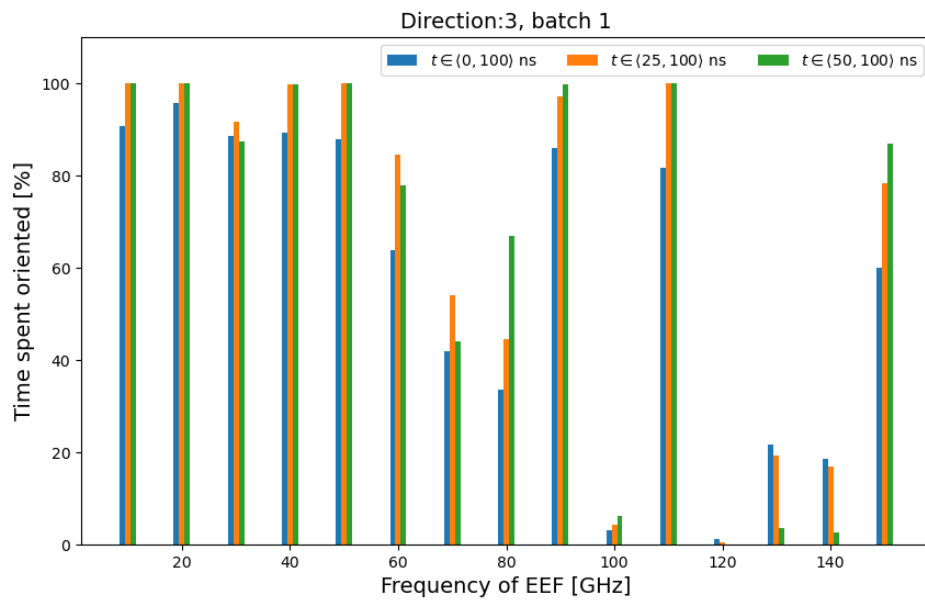


Figure 8.109: Time spent approximately parallel to the electric field direction of oscillation - batch 1, direction 3

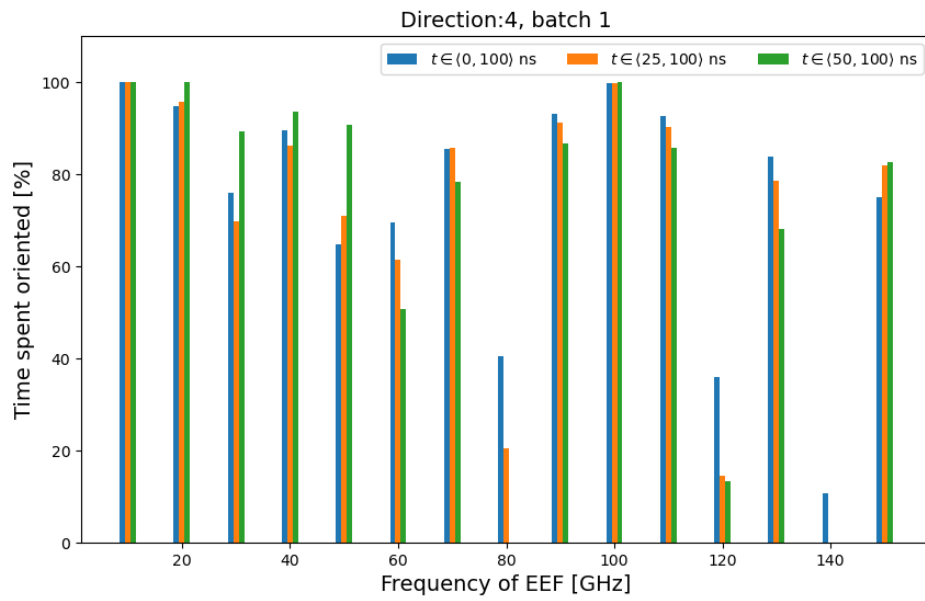


Figure 8.110: Time spent approximately parallel to the electric field direction of oscillation - batch 1, direction 4

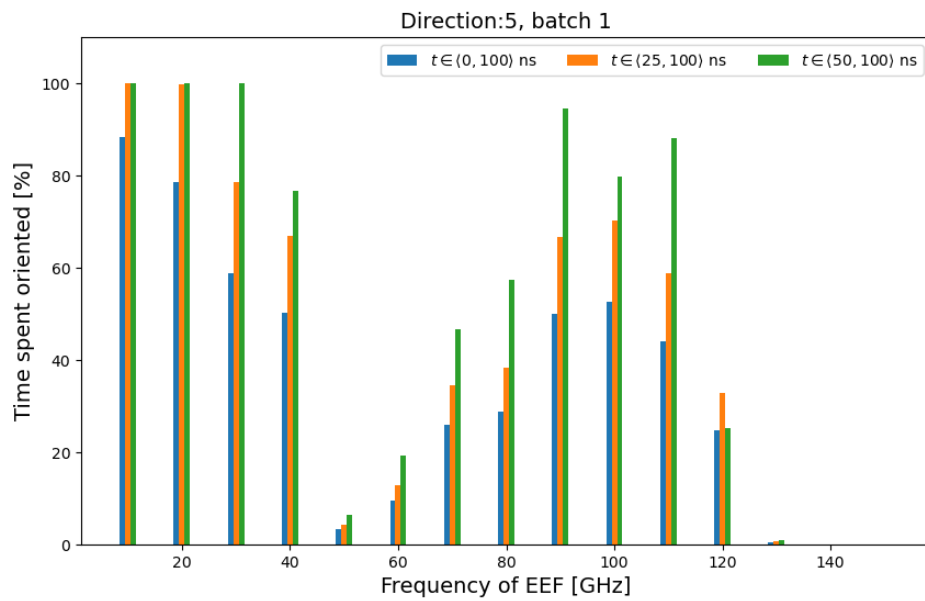


Figure 8.111: Time spent approximately parallel to the electric field direction of oscillation - batch 1, direction 5

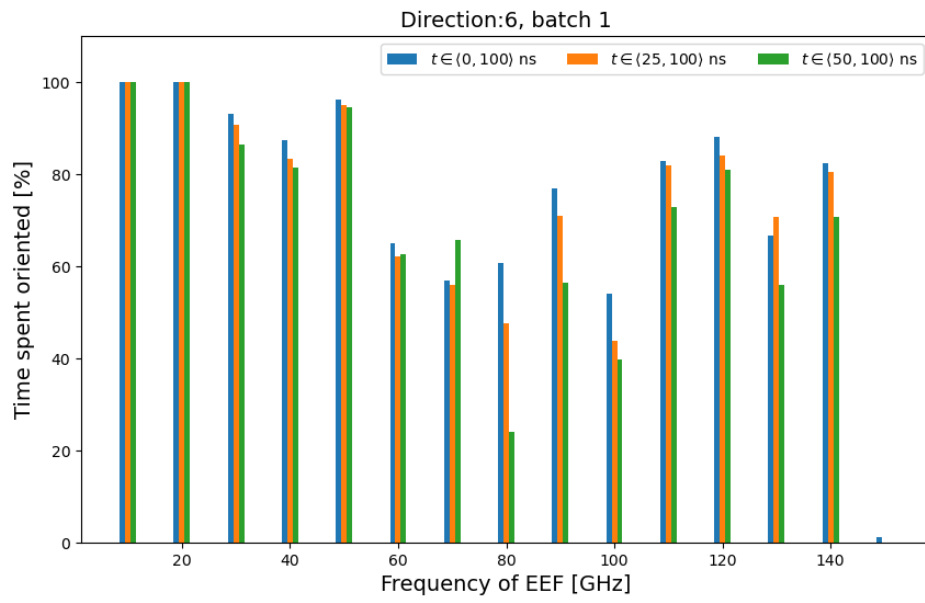


Figure 8.112: Time spent approximately parallel to the electric field direction of oscillation - batch 1, direction 6

Time spent oriented - Averaged over directions

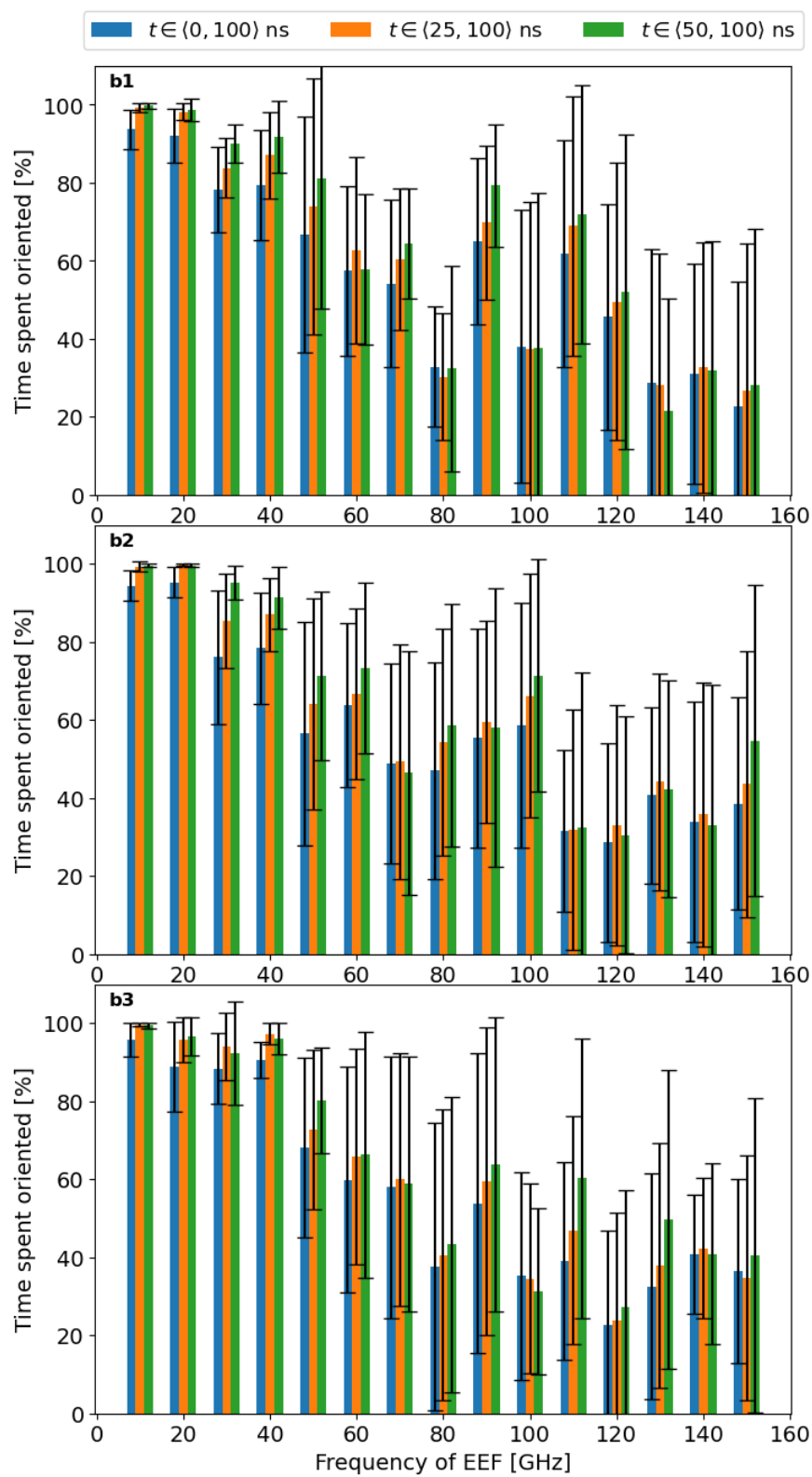


Figure 8.113: Time spent approximately parallel to the electric field direction of oscillation - averaged over different directions; b1 - b3 represent different batches (initial conformations)

Time spent oriented - Averaged over batches

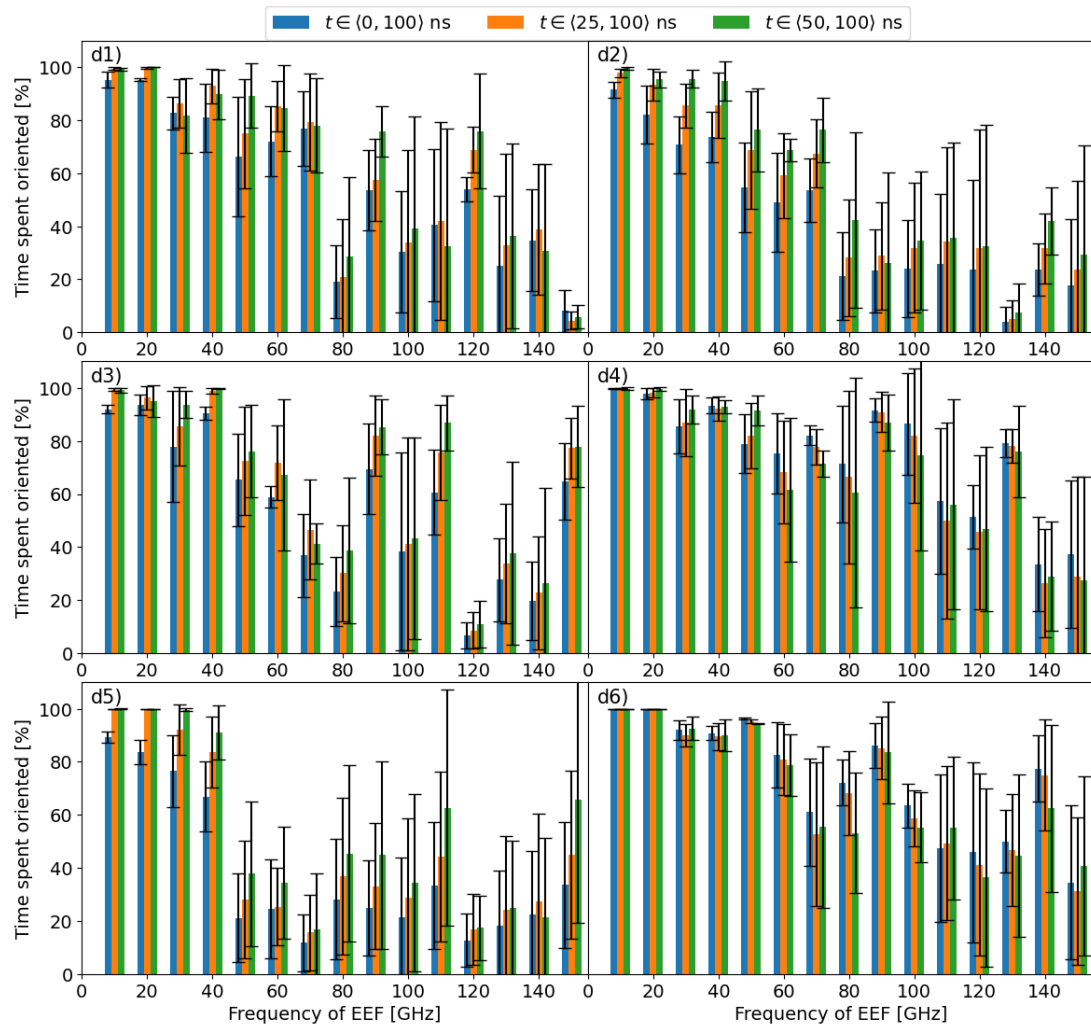


Figure 8.114: Time spent approximately parallel to the electric field direction of oscillation - averaged over batches; d1) - d6) represents 6 different directions of oscillations

Time spent oriented - Averaged over batches and directions

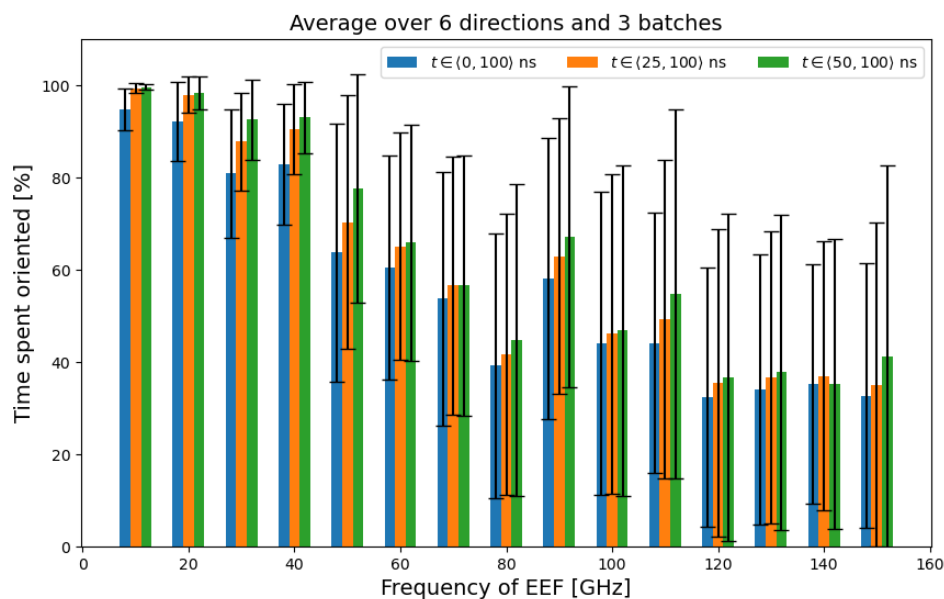


Figure 8.115: Time spent approximately parallel to the electric field direction of oscillation - averaged over batches and directions

8.7 Dipole Moment Analysis

In this section, we present the time series data of the magnitude of the total dipole moment and the projection of the dipole moment onto the axis of electric field oscillation. Next to this dipole moment time series, a histogram is plotted that shows the concatenated data into the distributions. The calculation was done for the whole tubulin dimer and for the tubulin dimer without C-termini. As we have mentioned in the 7.4, the Python code was written to calculate the dipole moments, which were subsequently used in this analysis and can be found in Appendix 10.5.

8.7.1 Dipole moments of the whole tubulin dimer

First, we will comment on the no EF (batch 1) case, where we can see quite a big drop in the magnitude of the dipole moment. When we check the RMSD of noEF for the first batch, we know that this corresponds to the change of conformation - more precisely the the change in the C-terminus, which is being stabilized by the interactions with the bulk. This leads to the low dipole moment that we see here. Similar changes in the dipole moment can also be seen for other simulations with different directions of EF and different frequencies, such as: 20 GHz - d3, d4; 30 GHz - d3; 40 GHz - d1, d5; 50 GHz - d4; 60 GHz - d3; 70 GHz - d1, d4, d5; . . . end so on for other frequencies. If we check the RMSD data, we can see that all these changes of dipole moments are caused by the C-terminus connecting to the bulk of tubulin. Therefore, the dipole moment analysis, together with RMSD analysis, shed insight into the different conformations (flexible or stable)

of the highly negatively charged C-termini.

Batch 2 and 3 can be found in the Appendix 10.16

Time series and distributions of the magnitude of the dipole moment of tubulin dimer - Batch 1

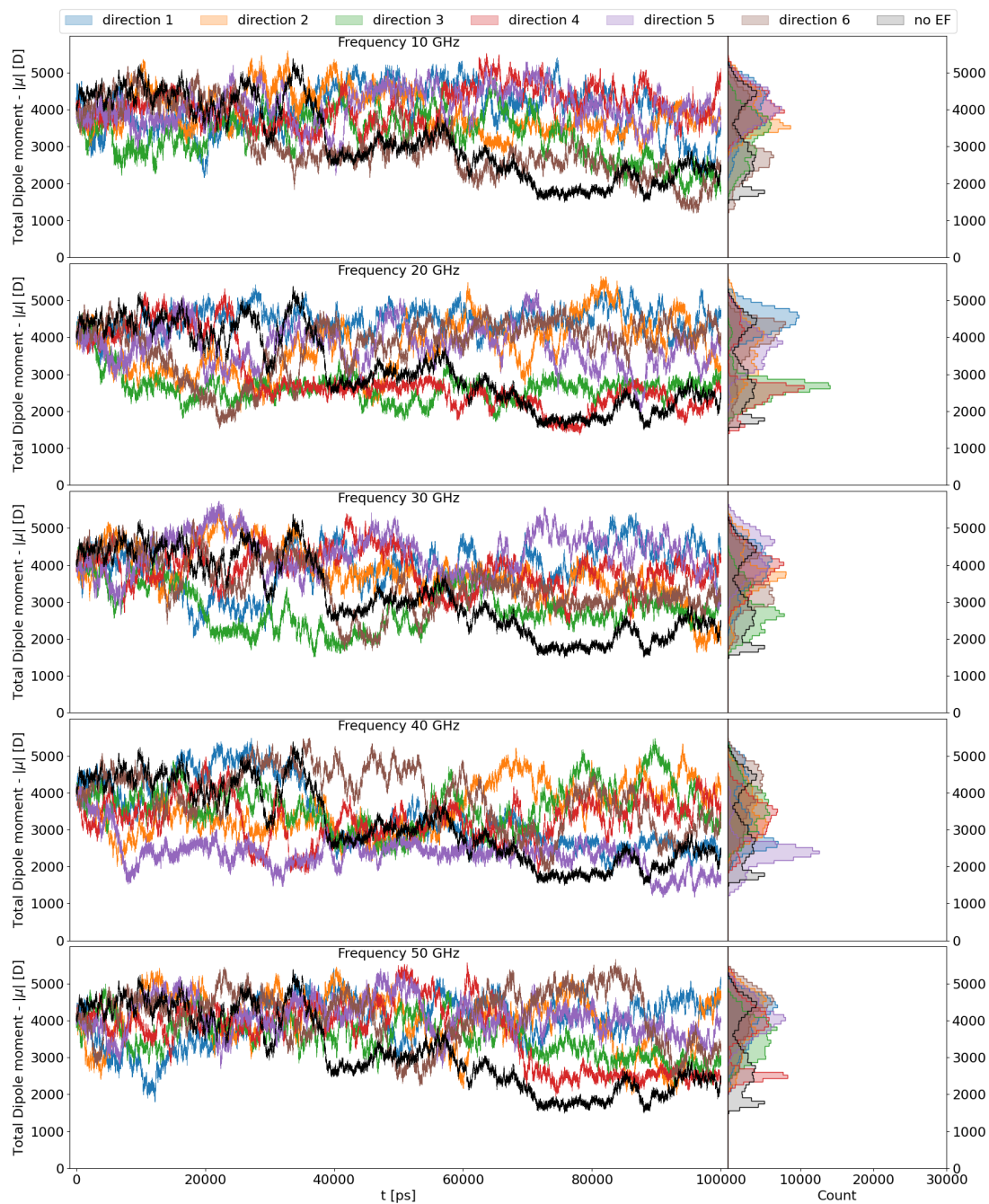


Figure 8.116: Magnitude of the dipole moment of tubulin heterodimer - time series and distributions - batch 1, Frequencies 10-50 GHz

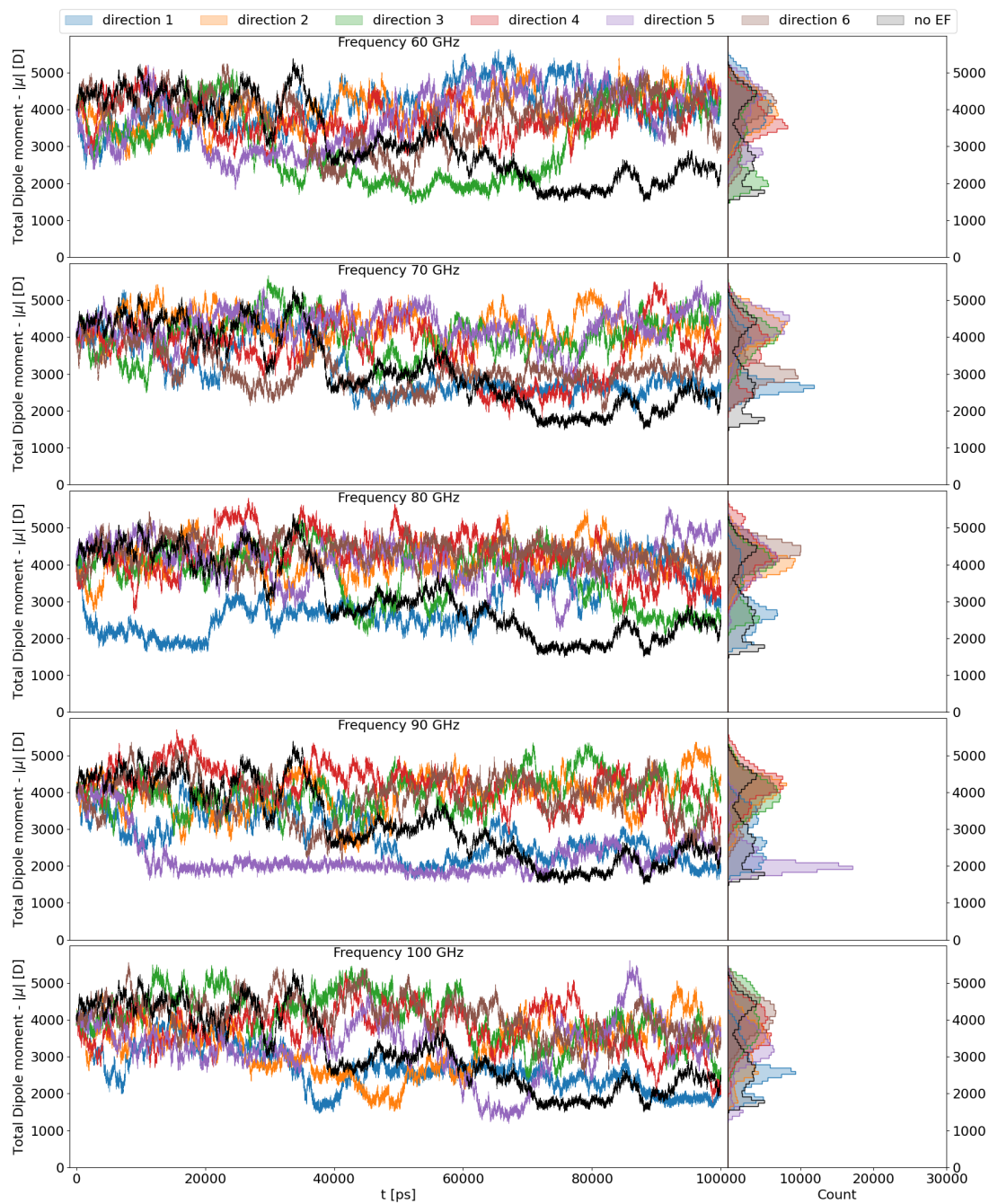


Figure 8.117: Magnitude of the dipole moment of tubulin heterodimer - time series and distributions - batch 1, Frequencies 60-100 GHz

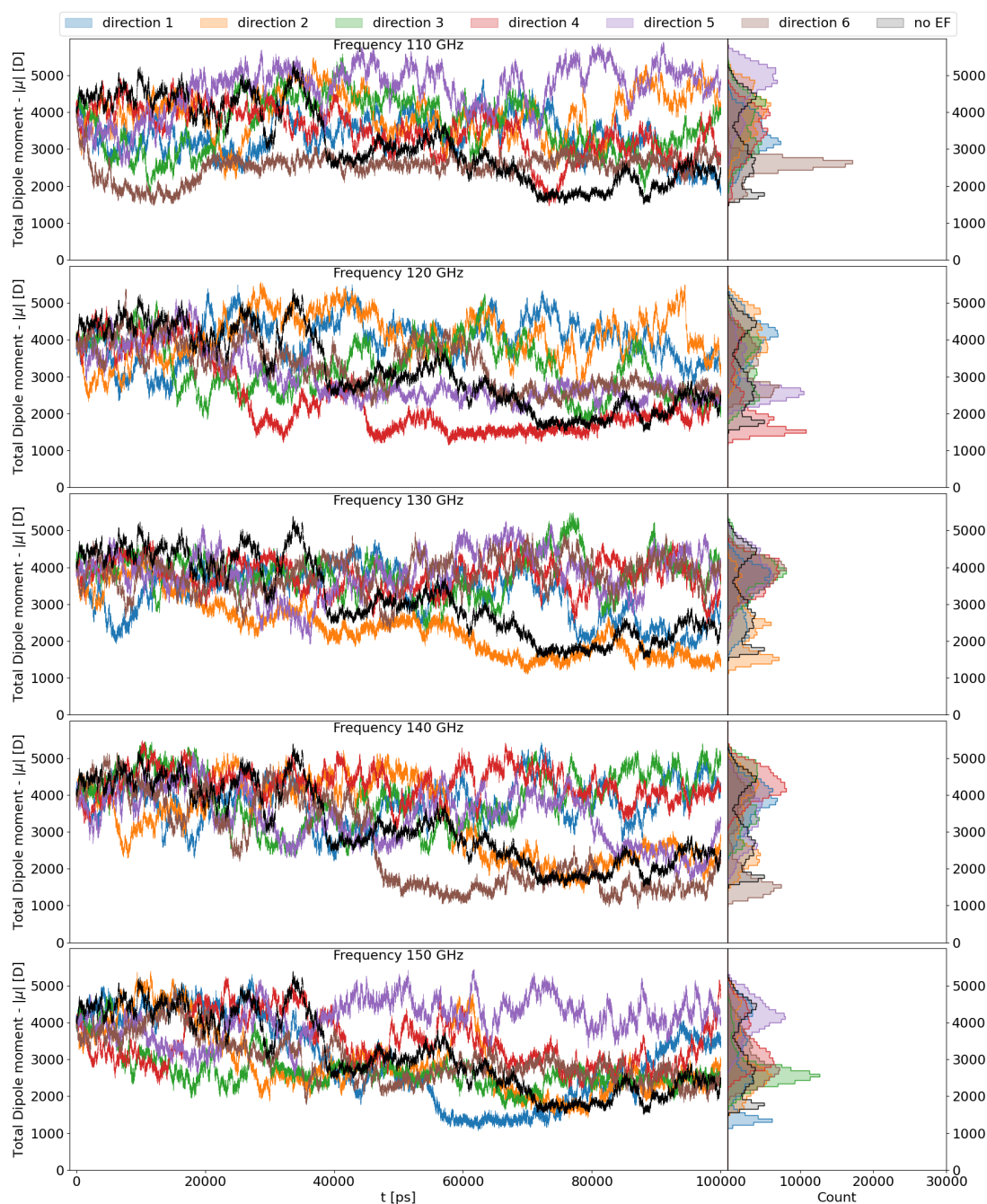


Figure 8.118: Magnitude of the dipole moment of tubulin heterodimer - time series and distributions - batch 1, Frequencies 110-150 GHz

Projection of the total dipole moment onto the axis of electric field oscillation

The following graphs of the projection of the total dipole moment onto the axis of electric field oscillation give us similar info to rotational analysis data (that will be present in the next section) since the dipole moment is approximately perpendicular to the longitudinal axis. Only this time, here we also see the effect of the C-termini conformations, whereas, in rotational analysis, this was not a concern.

We will show here only the batch 1, due to a high number of graphs. The

other two batches can be found in appendix 10.16, 10.16.

Time series and distributions of the projection of the dipole moment - Batch 1

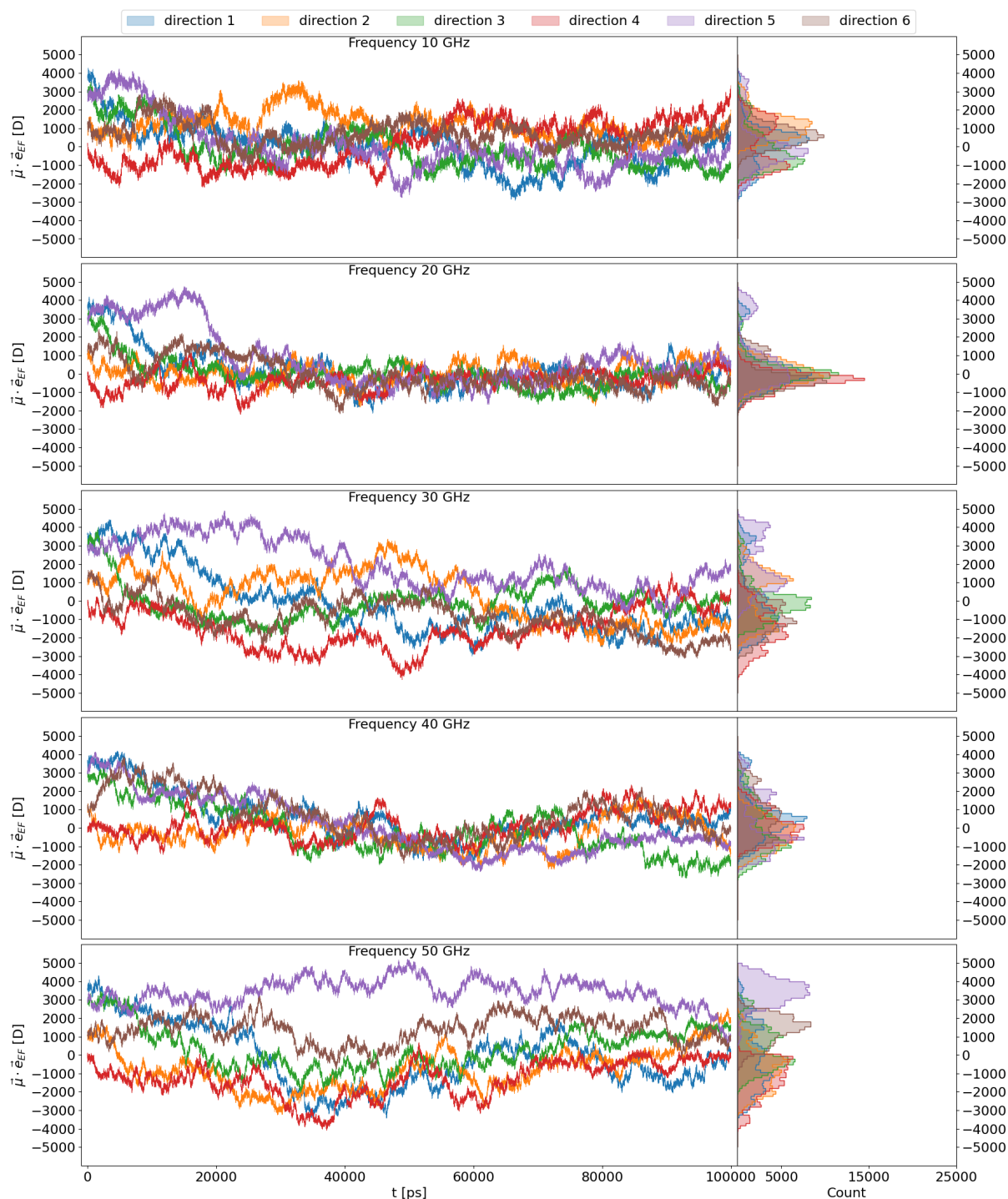


Figure 8.119: Time series and distributions of the projection of dipole moment of tubulin dimer onto the axis of electric field oscillations - batch 1, Frequencies 10-50 GHz

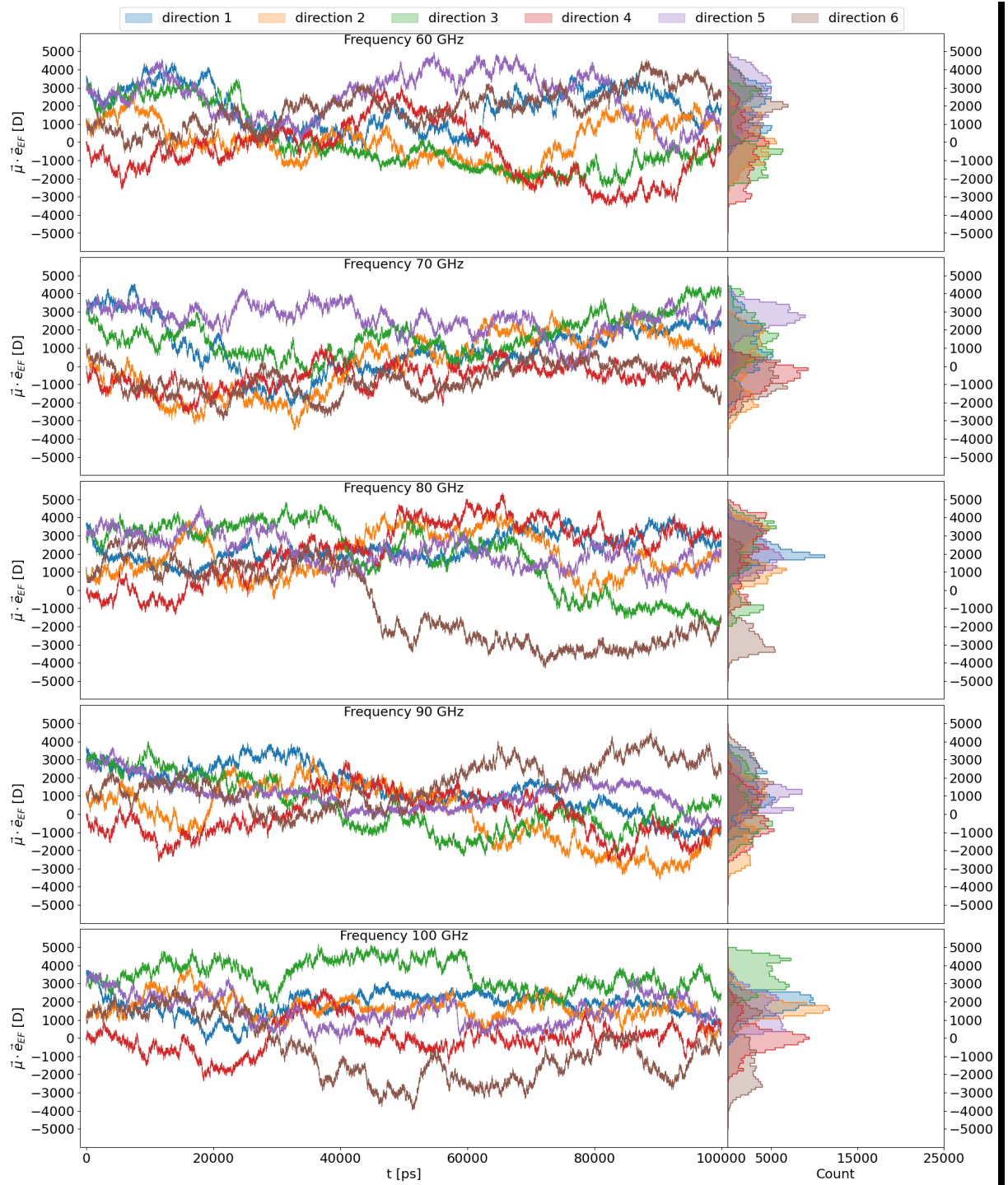


Figure 8.120: Time series and distributions of the projection of dipole moment of tubulin dimer onto the axis of electric field oscillations - batch 1, Frequencies 60-100 GHz

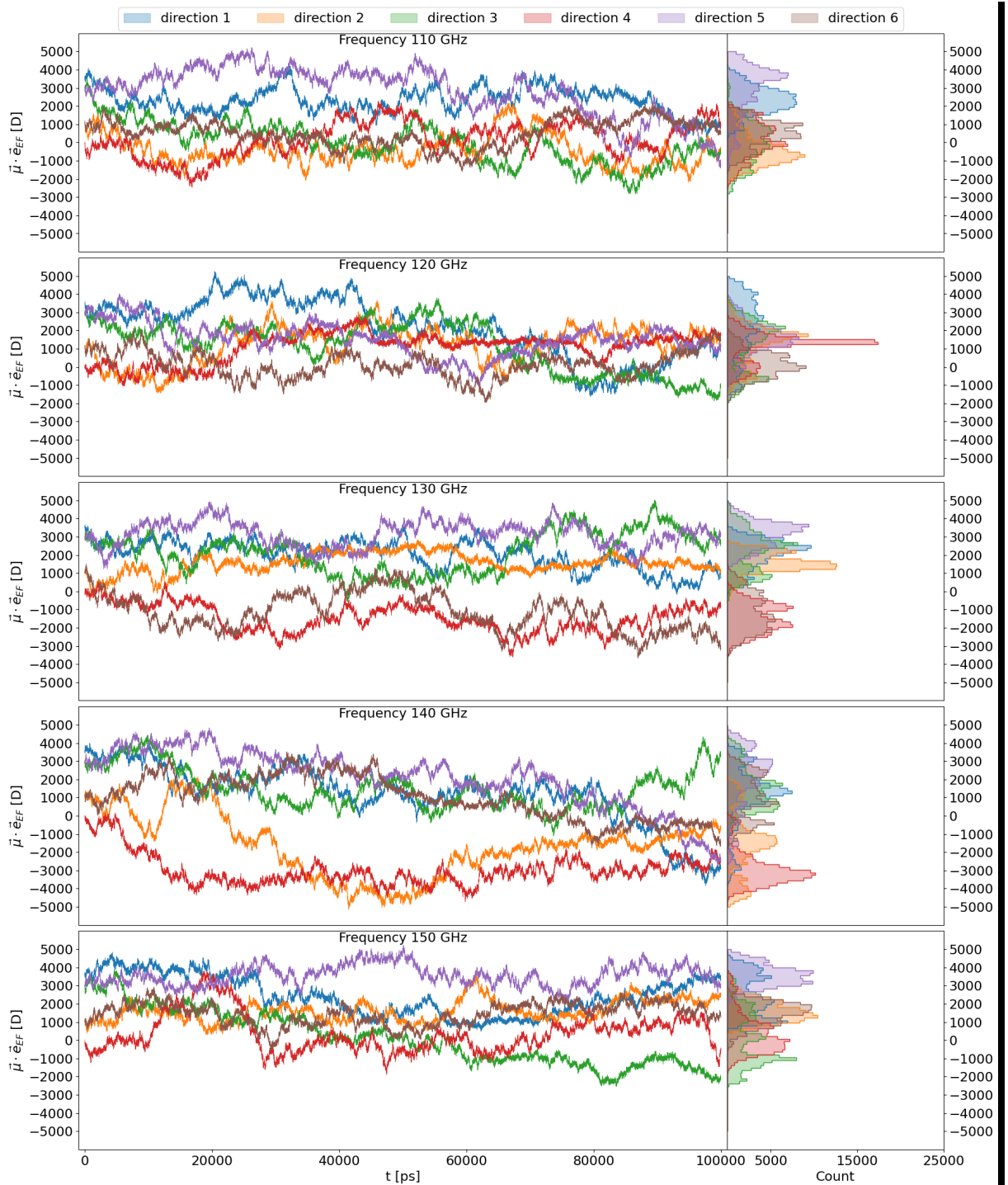


Figure 8.121: Time series and distributions of the projection of dipole moment of tubulin dimer onto the axis of electric field oscillations - batch 1, Frequencies 110-150 GHz

8.7.2 Dipole moments of the tubulin dimer without C-termini

We present here probability distributions of dipole moment calculated for the bulk tubulin (wo C-termini). EF of different frequencies and direction of application affected the dipole moment of the bulk of the tubulin differently.

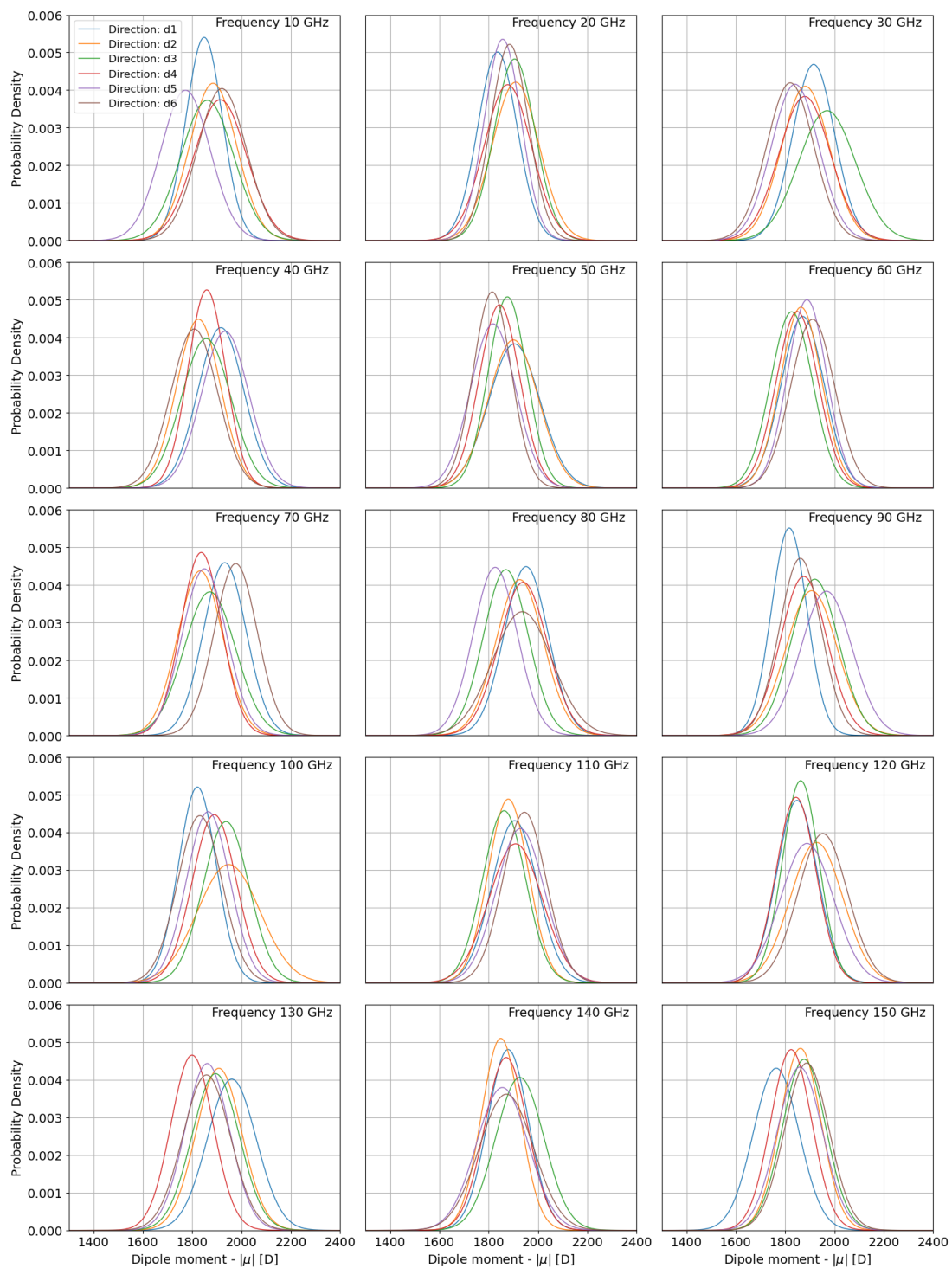


Figure 8.122: Propability distributions of dipole moment calculated for the bulk tubulin (wo C-termini); Batch 1

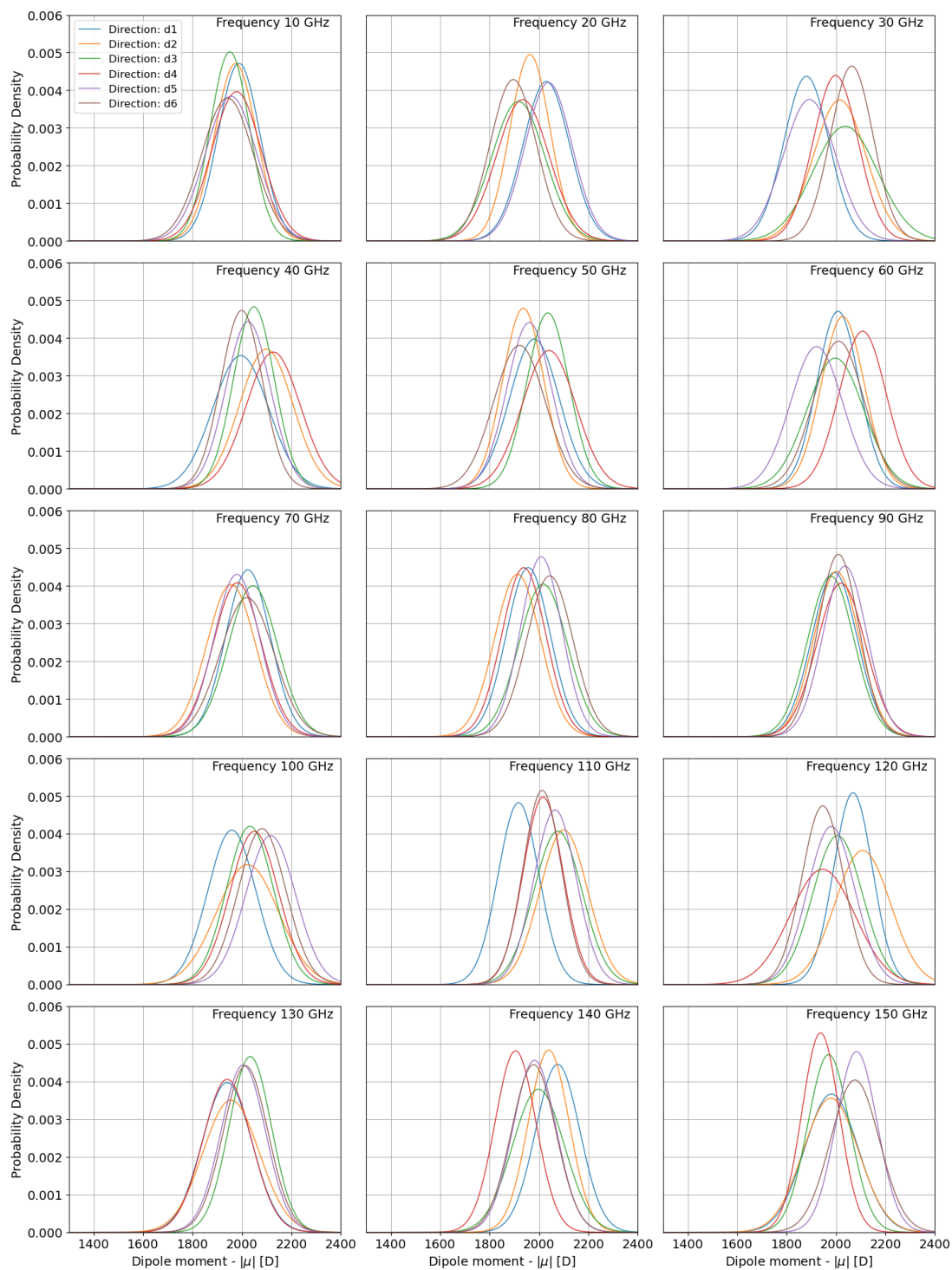


Figure 8.123: Propability distributions of dipole moment calculated for the bulk tubulin (wo C-termini); Batch 2

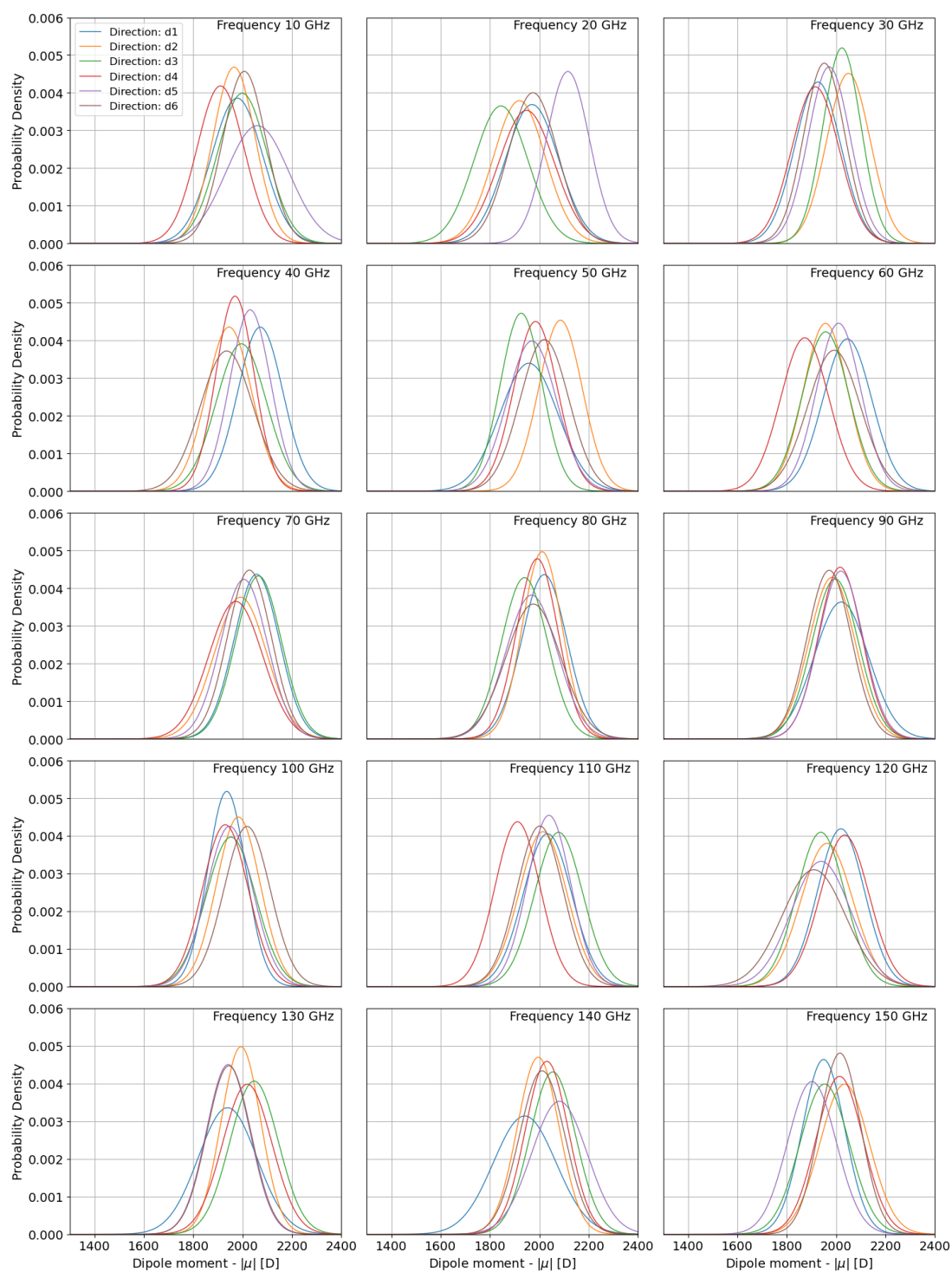


Figure 8.124: Propability distributions of dipole moment calculated for the bulk tubulin (wo C-termini); Batch 3

9. Discussion

9.1 Conformational changes

In the Result section, we have thoroughly analysed the RMSD graphs, where we have determined which directions of the applied electric field of a specific frequency (10-150 GHz) result in a change of mean of RMSD or its fluctuations. The lowering of the fluctuations indicates a more stable configuration, such as the C-terminus being in close proximity to the tubulin bulk or a more stable conformation of the loops. The thorough examinations of some of the trajectories in VMD really confirmed the theory that the very low fluctuations of RMSD correspond to the conformation, where one or two C-termini are connected to the tubulin bulk. These very low fluctuations of the RMSD mean those are very stable conformations, whereas high fluctuations of tubulin RMSD indicate a lot of flexibility. In most cases, these higher fluctuations of RMSD are caused by free-moving C-termini, but from Figures of the RMSD of tubulin without C-termini (bulk) (8.4-8.24) we can really see that it is not always the case.

It is important to note that we are dealing with deterministic simulations, where, besides the machine roundup error, we get the same outcomes for the same initial conditions. Simulations corresponding to one batch have the same initial conformation, and only the presence of an electric field changes the outcome. Without the field, all 90 simulations (6 directions x 15 frequencies) would look approximately the same. As we can see, the presence of an electric field in the explored frequency range causes real conformational changes in the structure.

The dipole moment data nicely complement the results of RMSD since the change of the C-termini conformational ensemble reflects on the dipole moment vector due to carrying a large charge. Since C-termini are intrinsically disordered, the dipole moment will change rapidly until they find a stable ("connected") conformation. Therefore, when the fluctuations are low, a specific value of the mean RMSD and mean dipole moment correspond to one of the stable connected conformations of C-termini.

Dissecting the trajectory

By observing some of the trajectories in VMD, we know that each C-terminus can end up in a variety of stable conformations where it is connected to the bulk. For no particular reason besides seeing probable different conformations of the C-terminus from the dipole moment graph and RMSD graph, we have decided to check the batch 2, frequency 15, direction 2 (Dipole moment graph: 10.287, for visualisations see Figures 9.1-9.7) and direction 5 (Dipole moment graph: 10.287, for visualisations see Figure 9.8). In either of them, both C-termini eventually connected to the structure. However, the stable conformations are different. This

can be seen from both RMSD and dipole moments, where both properties end up having low fluctuations, but the mean values are dramatically different.

For the direction 2 at 7 ns (see Figure 9.1), we observe that the tubulin β C-terminus is partially connected to the bulk but still rather unstable. At 20 ns, we can see that the β C-terminus is approaching its stable conformation. At 24 ns (see Figure 9.2), we can see that it disconnects for a very brief amount of time (few ns). During that time, the tubulin α C-terminus is in very close proximity to the bulk. At 36 ns (9.4), it is truly in one of the connected conformations, where it stays until the end of the simulation.

Tubulin α is free moving until about 65 ns (9.5), when it starts to connect to the bulk and then around 73 ns (9.6) it becomes fully connected - it is in a stable conformation. Both C-termini stay connected until the end of the trajectory (9.7). This can be again very nicely seen in the Magnitude of dipole moment graph 10.287 and RMSD graph 8.18. The batch 2 direction 2 of 150 GHz EF:



Figure 9.1: C-termini conformation at 7 ns of Batch 2 simulation with 150 GHz EF in direction 2; α C-terminus is coloured red, β C-terminus is coloured green

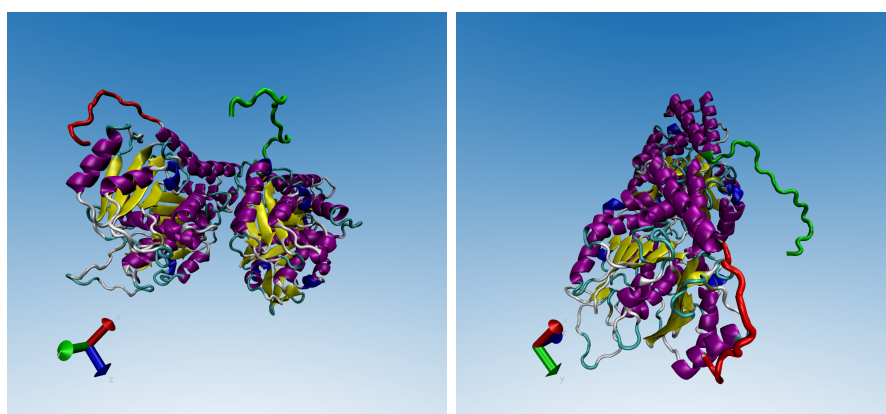


Figure 9.2: C-termini conformation at 24 ns of Batch 2 simulation with 150 GHz EF in direction 2; α C-terminus is coloured red, β C-terminus is coloured green

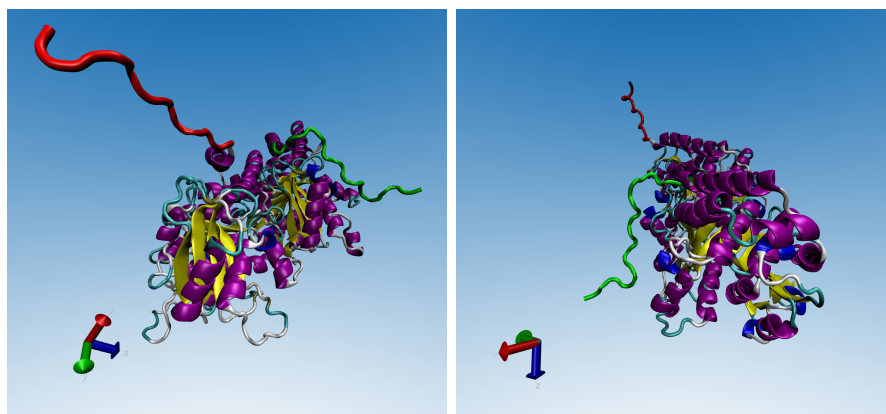


Figure 9.3: C-termini conformation at 31 ns of Batch 2 simulation with 150 GHz EF in direction 2; α C-terminus is coloured red, β C-terminus is coloured green

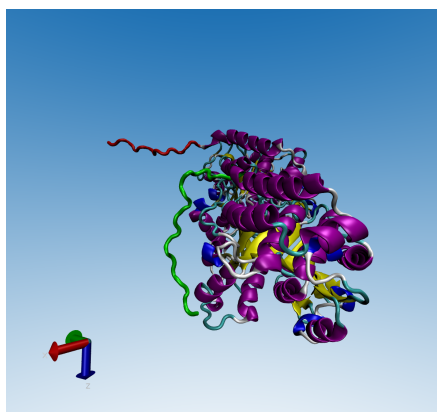


Figure 9.4: C-termini conformation at 36 ns of Batch 2 simulation with 150 GHz EF in direction 2; α C-terminus is coloured red, β C-terminus is coloured green

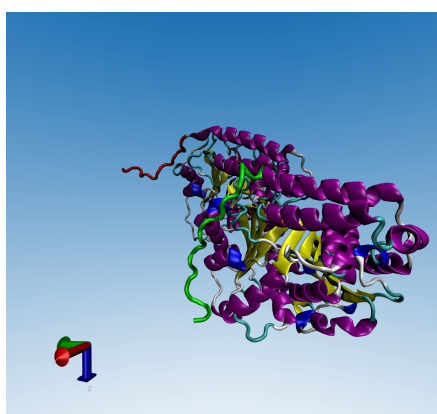


Figure 9.5: C-termini conformation at 65 ns of Batch 2 simulation with 150 GHz EF in direction 2; α C-terminus is coloured red, β C-terminus is coloured green

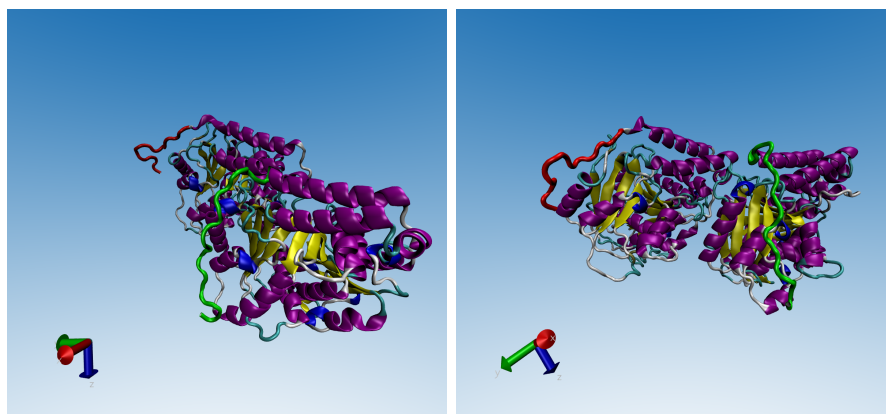


Figure 9.6: C-termini conformation at 73 ns of Batch 2 simulation with 150 GHz EF in direction 2; α C-terminus is coloured red, β C-terminus is coloured green



Figure 9.7: C-termini conformation at 100 ns of Batch 2 simulation with 150 GHz EF in direction 2; α C-terminus is coloured red, β C-terminus is coloured green

To compare with the outcome of different direction (The batch 2 direction 5 of 150 GHz EF), it can be seen from the following visualisations, that the C-termini indeed ended up in different stable conformation (see the left Figure 9.8). In this simulation, the tubulin α C-terminus ended up disconnecting from the bulk, which has, of course, impacted the dipole moment and RMSD and, therefore, can be visible in the corresponding graphs.

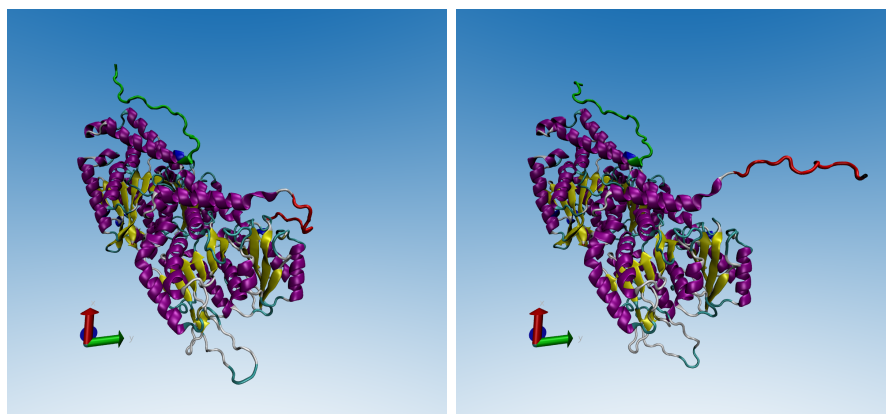


Figure 9.8: C-termini conformation at 88 ns (left) and 100 ns (right) of Batch 2 simulation with 150 GHz EF in direction 5; α C-terminus is coloured red, β C-terminus is coloured green

As we can see, the magnitude of the dipole moment of tubulin heterodimer and RMSD graphs really follow what we see in VMD. It makes sense that this analysis will be most sensitive to the C-termini since they are very flexible unless stuck in stable conformations (connected to the bulk) and are highly negatively charged. Therefore, the distributions of dipole moments can help us distinguish between different conformations of the C-termini. For example, if the mean dipole moment in the batch 2 (Figures 10.285, 10.286, and 10.287) has the value of 1700 D and low oscillations, it means that the tubulin has both C-termini connected and presumably in a similar fashion to 150 GHz in direction 2 trajectory (See visualisation 9.7. Electric fields that probably cause a similar stable conformational state of C-termini are:

- 30 GHz - directions d1, d4 and d6
- 40 GHz - d1
- 90 GHz - d1, d4 and d6
- 110 GHz - d4 and d5
- 120 GHz - d1
- 150 GHz - d2

Impact of the initial conformation

Really important was also the initial conformation of each batch of simulations 6.2a, 6.2b, and 6.2c. The batch 3 initial conformation already has one C-terminus (on tubulin β) in close proximity to the bulk of tubulin. This is the reason why this batch has very different outcomes for RMSD and RMSF analysis since the initial conformation is quite different from the first two batches. The other differences lie mainly in the unstructured loops due to their higher flexibility compared to the structured part of the tubulin.

Potential lateral binding of tubulins disruption

Regarding the bulk of the tubulin, in some cases (mostly for the batch 1), we have seen the change of the conformational state even in this part. Thus, to complement the RMSD analysis, RMSF graphs of each residue were calculated to see which parts of the tubulin cause these rapid fluctuations. The bulk parts that are influenced the most by the electric field are predominantly unstructured loops and secondly, some helices or strands of beta-sheet motif 8.28, 8.29. Still, it is evident that the C-termini of the tubulin are the most affected parts.¹ The difference graphs of RMSF have given us information regarding how much the RMSF of a certain residuum under the influence of our electric fields differs from the no EF case. Very noticeable fluctuations were induced in important parts of the tubulin dimer - the β :M-loop (S7-H9 loop, consisting of the residues 279-287), and α :H1-B2 loop (residues 29-62), both of which ensure lateral interaction between microtubule protofilaments. Thus, disrupting the native rigidity of these loops could lead to defects in microtubules and cause their depolymerization. This potential disruption of microtubule dynamics could ultimately lead to biological effects, such as cell death.

Changes in the anti-tubulin binding sites

We also concentrated on the residues that form the binding sites of pharmacologically important drugs, such as vinca alkaloids, colchicine or paclitaxel. We have observed visible effects of electric fields on the majority of these residues. For some simulations of the combination of variables (frequency and direction of EF oscillations, initial conformation of tubulin) the effect turned up to be stabilizing and for other combinations destabilizing. On average, we saw that the effect of EF on vinca alkaloid binding-site residues is mostly stabilizing for the majority of frequencies of EF, but especially for 20, 50, 60, 70, 90, 110, or 120 GHz electric fields (different frequencies for different residues). Residues 173 and 174 were very stabilized for all combinations of parameters (frequency,...). This stabilization means a more rigid binding site, which could potentially inhibit its binding ability.

The average effect of electric field on colchicine is mixed. Some residues became a lot more rigid for all frequencies, and some became a bit more flexible, and for some, it depended on the frequency applied. Again, these are averaged data through all directions and initial conformations. Therefore, they do not reflect the fact that for a specific direction of EF and initial conformation, the effect was drastically different. Nevertheless, the influence of electric fields was really obvious, and again, this could have a negative impact on the binding activity of colchicine to the tubulin. A thorough analysis of these changes in this region is written in Chapter Results.

When looking at averaged data of paclitaxel binding site RMSF, some of the residues became a lot more rigid under the influence of EF - those are 215, 228, 231 and 272. Oppositely, some of the residues became more flexible due to the electric field being applied - those are 274, 276, 280 and 359. Different frequencies

¹Due to a huge amount of data, the majority of the graphs can be found in Appendix 10.9

caused different amount of change.

Flexibility changes of these residues could impact the binding ability of tubulin to these drugs and could potentially disrupt their therapeutic effect. More studies, where electric fields would be applied to the tubulin while an anti-tubulin drug is present, are needed to explore this idea fully. On the other hand, maybe the specific electric fields could induce such changes to the tubulin structure that mimic the effect of these drugs, therefore having a therapeutic potential themselves. In the end, a change in the rigidity of tubulin heterodimer overall can affect the speed of straight-to-curved conformation transitions of the protofilaments of microtubules, which could disrupt the microtubule dynamics. For example, paclitaxel's main effect on microtubules is making them more rigid, which disrupts the native microtubule dynamics and causes its malfunction. This leads to cell death. Our findings, the change of rigidity of different parts of the tubulin due to the effect of the electric fields in this subTHz region, could lead to similar disruption and consequent biological effects. To prove that this will indeed happen, experiments or simulations of more tubulin dimers (ideally a part of the microtubule) will be needed.

9.2 Rotational movement

We have shown the rotational effect of predominantly 10 - 40 GHz electric field on the tubulin dimer. Here, we will try to explain the physics behind this.

First, we will mention that our simulations are all-atom molecular dynamics simulations, where each atom is assigned a partial charge, which does not reflect the real physical charge. Charges are parameters in the force-field that are fitted either to quantum mechanical data or the empirical ones. There exist polarizable force-fields, which take into consideration the polarisation of individual atoms, but we have not worked with these force-fields, since they are very computationally demanding, and our simulations were already very computationally expensive due to a huge system size. Therefore, our results do not reflect the polarizability of tubulin quite right. Each partial charge "feels" the electric field, but this charge is fixed on the atom coordinate. Therefore, the effect of the specific electric field could be a bit different if the polarizable force-field was used.

The charge distribution is connected to the structure firmly, therefore electric field that interacts with these charges causes the atoms to move. Hence an induced dipole can emerge in the tubulin (which already has a permanent dipole moment). Therefore, there is still some form of polarisation present in the all-atom MD.

If we do not take into consideration the C-termini of our structure, tubulin has the form of a prolate ellipsoid. There is a whole field that studies the effect of DC or AC fields on the dielectric particles in medium [86, 87, 88, 89]. In [89], it was shown theoretically and even experimentally that non-spherical particles in the medium of a different complex permittivity start rotating themselves in the presence of an alternating electrical field until they reach the stable orientation, which is determined by the geometry of the particle, by the permittivity of such particle and by the frequency of the applied electric field. There is one and only

one direction of stable orientation, which depends on the frequency of the electric field. However, for the very high frequencies, the longest axis will be oriented parallel to the field [89], which is also the case in our simulations.

We see that this rotational action of electric field ceases to be consistent across all directions and batches for the frequencies above 40 GHz. This is because the value of relative permittivity of TIP3P water model drops down from $\epsilon_r(0) = 100$ to the value of $\epsilon_r(40\text{GHz}) = 25$ for 40 GHz and even further to the value 10 for the frequencies higher than 100 GHz. The high-frequency limit of relative permittivity of tubulin dimer was determined to be $\epsilon_r^{\text{tub}}(\infty) = 8.41$ by [90]. Since this rotational effect happens only when there is a difference between the relative permittivity of the solution and solute, we are not observing it for higher frequencies.

9.3 Our decisions throughout this work

Many molecular dynamics studies of tubulin heterodimer do not contain unstructured C-terminal tails in their structures. This is because it can sometimes complicate the simulation or analysis workflow. For example, due to having these highly flexible unstructured C-termini in our tubulin dimer, we had to use a bigger simulation box, which meant simulating a lot more water molecules. This in turn caused the simulation to run much longer. If we had saved the data regarding water molecules also, it would have taken up a really huge amount of disc space.

We have already mentioned in Chapter 1 that the C-terminal ends impact the intrinsic properties of tubulin heterodimer and are important for binding microtubule-associated proteins. Therefore, we have decided to use them in our simulation despite the problems. As we can see, this turned out to be a good decision since both RMSD and RMSF showed a huge impact of electric field on this part of the tubulin, where we observed the C-terminal ends to fully connect to the bulk structure of the tubulin, which corresponds to the lowering of the fluctuations of these residues.

Conclusion

In this thesis, the conformational and dynamic changes of tubulin dimer under the influence of electric field in the range of 10-150 GHz were explored. The analysis of RMSD and RMSF revealed that electric fields influence the stability and flexibility of tubulin dimer. The parts of the tubulin that were affected the most were intrinsically unstructured freely moving C-terminal ends (C-termini). There we observed that different conformational ensembles were visited depending on the frequency and direction of the electric field. For some electric field parameters, we observed the C-termini to either freely move, which corresponds to high fluctuations of the RMSD and dipole moment magnitude, and for some electric fields, we observed the C-termini to find a stable conformation, where they are in very close proximity to the structured bulk of the tubulin (“connected”). To fully determine the effects of specific electric fields on C-termini, more simulations with different starting conformations need to be done in the future since 3 is probably not enough.

Even though the changes of RMSD were linked to conformational switching in C-termini in the majority of times, it was not a universal rule, as some bulk regions also showed variability. Therefore, to see the effect of EF on the specific parts of the tubulin we looked at how the RMSF differs from no EF case. Differential RMSF graphs showed that there are indeed parts of the bulk that are affected a lot. The parts of the tubulin that either became more flexible or more rigid under the influence of specific field can be seen in Figures 8.28 and 8.29. Those are mainly unstructured loops, but not exclusively. M-loop, which is crucial for lateral interactions in microtubules, is one of those parts, whose rigidity was influenced. Therefore microtubule stability could be impacted if exposed to electric fields of 10 - 150 GHz. Having some parts of the microtubule more flexible and some more stiff can lead to the strain in the microtubule and potentially to its collapse. Therefore, these EF may bias tubulin towards depolymerization.

Further, our study highlighted the impact of electric fields on critical residues involved in drug binding sites for vinca alkaloids, colchicine, and paclitaxel. The electric fields induced both stabilizing and destabilizing effects on these residues, depending on the frequency and direction of the field, as well as the initial conformation of the tubulin. This suggests potential applications in modulating drug binding efficacy or a possible mimicking of the effects of these drugs through targeted electric field applications.

Additionally, the rotational movements induced by lower frequency electric fields (10-40 GHz) were observed, showing how electric fields can align the tubulin longitudinal axis with the direction of the electric-field oscillations. This happens due to a difference between the relative permittivity of the solvent and solute-tubulin. This rotational effect diminishes at higher frequencies due to a rapid change in the relative permittivity of the water model.

Overall, our research demonstrates that electric fields can significantly influence tubulin structure, rigidity and dynamics. These effects need further exploration. Future *in silico* studies should aim to refine our understanding of these interactions by incorporating polarizable force-fields to capture the tubulin response to electric fields properly. If our preliminary results are found to be solid

and consequently also proven experimentally, research into potential therapeutic applications of subTHz electric fields will be of great importance.

Bibliography

- [1] Gary J. Brouhard and Luke M. Rice. Microtubule dynamics: an interplay of biochemistry and mechanics. *Nature Reviews Molecular Cell Biology*, 19(7):451–463, July 2018.
- [2] Caitlin Simpson and Yohei Yamauchi. Microtubules in influenza virus entry and egress. *Viruses*, 12:117, 01 2020.
- [3] Antonina Roll-Mecak. The tubulin code in microtubule dynamics and information encoding. *Developmental Cell*, 54(1):7–20, 2020.
- [4] Vadym Sulimenko, Zuzana Hájková, Anastasiya Klebanovych, and Pavel Dráber. Regulation of microtubule nucleation mediated by γ -tubulin complexes. *Protoplasma*, 254(3):1187–1199, 2017.
- [5] Ju Zhou, Anhui Wang, Yinlong Song, Nan Liu, Jia Wang, Yan Li, Xin Liang, Guohui Li, Huiying Chu, and Hong-Wei Wang. Structural insights into the mechanism of gtp initiation of microtubule assembly. *Nature Communications*, 14(1):5980, 2023.
- [6] Yeshitila Gebremichael, Jih-Wei Chu, and Gregory A. Voth. Intrinsic bending and structural rearrangement of tubulin dimer: Molecular dynamics simulations and coarse-grained analysis. *Biophysical Journal*, 95(5):2487–2499, September 2008. Open Archive.
- [7] Dorota Wloga, Ewa Joachimiak, and Hanna Fabczak. Tubulin post-translational modifications and microtubule dynamics. *International Journal of Molecular Sciences*, 18(10), 2017.
- [8] Peter Tompa and Monika Fuxreiter. Fuzzy complexes: polymorphism and structural disorder in protein-protein interactions. *Trends in Biochemical Sciences*, 33(1):2–8, Jan 2008.
- [9] Monika Borg, Tanja Mittag, Tony Pawson, Michael Tyers, Julie D. Forman-Kay, and Hue Sun Chan. Polyelectrostatic interactions of disordered ligands suggest a physical basis for ultrasensitivity. *Proceedings of the National Academy of Sciences of the United States of America*, 104(23):9650–9655, Jun 2007.
- [10] Jeremy Aiken, David Sept, Michael Costanzo, Charles Boone, John A. Cooper, and Jason K. Moore. Genome-wide analysis reveals novel and discrete functions for tubulin carboxy-terminal tails. *Current Biology*, 24(12):1295–1303, Jun 2014.
- [11] Danuta Wloga, Diana M. Webster, Krzysztof Rogowski, Marie-Hélène Bré, Nicole Levilliers, Małgorzata Jerka-Dziadosz, Carsten Janke, Stuart T. Dougan, and Jacek Gaertig. Ttl3 is a tubulin glycine ligase that regulates the assembly of cilia. *Developmental Cell*, 16(6):867–876, Jun 2009.

- [12] Li Xia, Baozhen Hai, Yan Gao, Dylan Burnette, Radhika Thazhath, Jing Duan, Marie-Hélène Bré, Nicole Levilliers, Martin A. Gorovsky, and Jacek Gaertig. Polyglycylation of tubulin is essential and affects cell motility and division in *tetrahymena thermophila*. *Journal of Cell Biology*, 149(5):1097–1106, May 2000.
- [13] Gregory M. Alushin, Varun Musinipally, David Matson, John Tooley, Paul T. Stukenberg, and Eva Nogales. Multimodal microtubule binding by the ndc80 kinetochore complex. *Nature Structural Molecular Biology*, 19(11):1161–1167, Nov 2012.
- [14] Christopher P. Garnham, Arunangshu Vemu, Elizabeth M. Wilson-Kubalek, Isabel Yu, Agnieszka Szyk, Gabriel C. Lander, Ronald A. Milligan, and Antonina Roll-Mecak. Multivalent microtubule recognition by tubulin tyrosine ligase-like family glutamylases. *Cell*, 161(5):1112–1123, May 2015.
- [15] Agnieszka Szyk, Alexandra M. Deaconescu, Grzegorz Piszczek, and Antonina Roll-Mecak. Tubulin tyrosine ligase structure reveals adaptation of an ancient fold to bind and modify tubulin. *Nature Structural Molecular Biology*, 18(11):1250–1258, Oct 2011.
- [16] Helena Pérez-Peña, Anne-Catherine Abel, Maxim Shevelev, Andrea E. Prota, Stefano Pieraccini, and Dragos Horvath. Computational approaches to the rational design of tubulin-targeting agents. *Biomolecules*, 13(2), 2023.
- [17] Tobias Mühlethaler, Dario Gioia, Andrea E. Prota, May E. Sharpe, Andrea Cavalli, and Michel O. Steinmetz. Comprehensive analysis of binding sites in tubulin. *Angewandte Chemie International Edition*, 60(24):13331–13342, 2021.
- [18] C. Elie-Caille, F. Severin, J. Helenius, J. Howard, D. J. Muller, A. A. Hyman, and G. Straight. Gdp-tubulin protofilaments form in the presence of taxol. *Current Biology*, 17:1765–1770, 2007.
- [19] J. Lowe, H. Li, K. Downing, and E. Nogales. Refined structure of alpha-beta tubulin at 3.5 Å resolution. *Journal of Molecular Biology*, 313:1045–1057, 2001.
- [20] D. A. Brito, Z. Yang, and C. L. Rieder. Microtubules do not promote mitotic slippage when the spindle assembly checkpoint cannot be satisfied. *Journal of Cell Biology*, 182:623–629, 2008.
- [21] B. Rajnish and Y. Hongtao. The spindle checkpoint, aneuploidy, and cancer. *Oncogene*, 23:2016–2027, 2004.
- [22] Peter W. Baas, Anand N. Rao, Andrew J. Matamoros, and Lanfranco Leo. Stability properties of neuronal microtubules. *Cytoskeleton*, 73(9):442–460, 2016.
- [23] P. W. Baas, M. M. Black, and G. A. Banker. Changes in microtubule polarity orientation during the development of hippocampal neurons in culture. *J Cell Biol*, 109(6):3085–3094, Dec 1989.

- [24] P. W. Baas, J. S. Deitch, M. M. Black, and G. A. Banker. Polarity orientation of microtubules in hippocampal neurons: uniformity in the axon and nonuniformity in the dendrite. *Proc Natl Acad Sci USA*, 85(21):8335–8339, Nov 1988.
- [25] Peter W. Baas and Shen Lin. Hooks and comets: The story of microtubule polarity orientation in the neuron. *Developmental Neurobiology*, 71(6):403–418, Dec 2010.
- [26] Peter W. Baas and M. M. Black. Individual microtubules in the axon consist of domains that differ in both composition and stability. *Journal of Cell Biology*, 111(2):495–509, Aug 1990.
- [27] Peter W. Baas and Olga I. Mozgova. A novel role for retrograde transport of microtubules in the axon. *Cytoskeleton*, 69(7):416–425, Feb 2012.
- [28] Pengyu Ren, Jaehun Chun, Dennis G. Thomas, Michael J. Schnieders, Marcelo Marucho, Jiajing Zhang, and Nathan A. Baker. Biomolecular electrostatics and solvation: a computational perspective. *Quarterly Reviews of Biophysics*, 45(4):427–491, 2012.
- [29] Thomas Simonson. Electrostatics and dynamics of proteins. *Reports on Progress in Physics*, 66:737, 2003.
- [30] Min-Yeh Tsai, Weihua Zheng, D. Balamurugan, Nicholas P. Schafer, Bobby L. Kim, Margaret S. Cheung, and Peter G. Wolynes. Electrostatics, structure prediction, and the energy landscapes for protein folding and binding. *Protein Science*, 25(1):255–269, 2016.
- [31] A. Budi, F. S. Legge, H. Treutlein, and I. Yarovsky. Electric field effects on insulin chain-b conformation. *The Journal of Physical Chemistry B*, 109(46):22641–22648, 2005.
- [32] A. Budi, F. S. Legge, H. Treutlein, and I. Yarovsky. Effect of frequency on insulin response to electric field stress. *The Journal of Physical Chemistry B*, 111:5748–5756, 2007.
- [33] X. Wang, Y. Li, X. He, S. Chen, and J. Z. H. Zhang. Effect of strong electric field on the conformational integrity of insulin. *The Journal of Physical Chemistry A*, 118:8942–8952, 2014.
- [34] N. J. English and D. A. Mooney. Denaturation of hen egg white lysozyme in electromagnetic fields: A molecular dynamics study. *The Journal of Chemical Physics*, 126:091105, 2007.
- [35] N. J. English, G. Y. Solomentsev, and P. O’Brien. Nonequilibrium molecular dynamics study of electric and low-frequency microwave fields on hen egg white lysozyme. *The Journal of Chemical Physics*, 131:035106, 2009.
- [36] G. Y. Solomentsev, N. J. English, and D. A. Mooney. Hydrogen bond perturbation in hen egg white lysozyme by external electromagnetic fields: A nonequilibrium molecular dynamics study. *The Journal of Chemical Physics*, 133:235102, 2010.

- [37] N. Todorova, A. Bentvelzen, N. J. English, and I. Yarovsky. Electromagnetic-field effects on structure and dynamics of amyloidogenic peptides. *The Journal of Chemical Physics*, 144:085101, 2016.
- [38] F. Toschi, F. Lugli, F. Biscarini, and F. Zerbetto. Effects of electric field stress on a α -amyloid peptide. *The Journal of Physical Chemistry B*, 113:369–376, 2009.
- [39] F. Lugli, F. Toschi, F. Biscarini, and F. Zerbetto. Electric field effects on short fibrils of $\alpha\beta$ amyloid peptides. *Journal of Chemical Theory and Computation*, 6:3516–3526, 2010.
- [40] P. Marracino, F. Apollonio, M. Liberti, G. d’Inzeo, and A. Amadei. Effect of high exogenous electric pulses on protein conformation: Myoglobin as a case study. *The Journal of Physical Chemistry B*, 117:2273–2279, 2013.
- [41] P. Marracino. Technology of high-intensity electric-field pulses: A way to control protein unfolding. *Journal of Physical Chemistry & Biophysics*, 3, 2013.
- [42] X. S. Qian, J. Q. Zhang, and C. Q. Ru. Wave propagation in orthotropic microtubules. *J. Appl. Phys.*, 101:084702, 2007.
- [43] J. Pokorný. Conditions for coherent vibrations in the cytoskeleton. *Bioelectrochem. Bioenerg.*, 48:267–271, 1999.
- [44] M. Jibu, S. Hagan, S. R. Hameroff, K. H. Pribram, and K. Yasue. Quantum optical coherence in cytoskeletal microtubules: implications for brain function. *Biosystems*, 32:195–209, 1994.
- [45] S. Hameroff, A. Nip, M. Porter, and J. Tuszynski. Conduction pathways in microtubules, biological quantum computation, and consciousness. *Biosystems*, 64:149–168, 2002.
- [46] J. Pokorný. Excitation of vibrations in microtubules in living cell. *Bioelectrochemistry*, 63:321–326, 2004.
- [47] M. Cifra, D. Havelka, and M. A. Deriu. Electric field generated by longitudinal axial microtubule vibration modes with high spatial resolution microtubule model. *J. Phys. Conf. Ser.*, 329:012013, 2011.
- [48] S. Sahu, S. Ghosh, D. Fujita, and A. Bandyopadhyay. Live visualizations of single isolated tubulin protein self-assembly via tunneling current: effect of electromagnetic pumping during spontaneous growth of microtubule. *Sci. Rep.*, 4:7303, 2014.
- [49] Cameron M. Hough, David N. Purschke, Clayton Bell, Aarat P. Kalra, Patricia J. Oliva, Chenxi Huang, Jack A. Tuszynski, Brad J. Warkentin, and Frank A. Hegmann. Disassembly of microtubules by intense terahertz pulses. *Biomed Opt Express*, 12(9):5812–5828, Sep 2021.

- [50] Djamel Eddine Chafai, Vadym Sulimenko, Daniel Havelka, Lucie Kubínová, Pavel Dráber, and Michal Cifra. Reversible and irreversible modulation of tubulin self-assembly by intense nanosecond pulsed electric fields. *Advanced Materials*, 31(39):1903636, 2019.
- [51] Djamel Eddine Chafai, František Vostárek, Eduarda Dráberová, Daniel Havelka, Delia Arnaud-Cormos, Philippe Leveque, Jiří Janáček, Lucie Kubínová, Michal Cifra, and Pavel Dráber. Microtubule cytoskeleton remodeling by nanosecond pulsed electric fields. *Advanced Biosystems*, 4(7), 2020.
- [52] Dong Yin, Wangrong G. Yang, Jack Weissberg, Catherine B. Goff, Weikai Chen, Yoshio Kuwayama, Amanda Leiter, Hongtao Xing, Antonie Meixel, Daria Gaut, Fikret Kirkbir, David Sawcer, P. Thomas Vernier, and H. Phillip Koeffler. Cutaneous papilloma and squamous cell carcinoma therapy utilizing nanosecond pulsed electric fields (nspef). *PLOS One*, 7(8):e43891, 2012.
- [53] Eilon D. Kirson, Vladimír Dbalý, Frantisek Tovarys, Josef Vymazal, Jean F. Soustiel, Aviran Itzhaki, Daniel Mordechovich, Shirley Steinberg-Shapira, Zoya Gurvich, Rosa Schneiderman, Yoram Wasserman, Marc Salzberg, Bernhard Ryffel, Dorit Goldsher, Erez Dekel, and Yoram Palti. Alternating electric fields arrest cell proliferation in animal tumor models and human brain tumors. *Proceedings of the National Academy of Sciences of the United States of America*, 104(24):10152–10157, 2007. Epub 2007 Jun 5.
- [54] Ola Rominiyi, Aurelie Vanderlinden, Susan Jane Clenton, Caroline Bridgewater, Yahia Al-Tamimi, and Spencer James Collis. Tumour treating fields therapy for glioblastoma: current advances and future directions. *British Journal of Cancer*, 124(4):697–709, 2021.
- [55] Roger Stupp, Eric T Wong, Andrew A Kanner, David Steinberg, Herbert Engelhard, Volkmar Heidecke, Eilon D Kirson, Sophie Taillibert, Frank Liebermann, Vladimir Dbalý, Zvi Ram, J Lee Villano, Nikolai Rainov, Uri Weinberg, David Schiff, Lara Kunschner, Jeffrey Raizer, Jerome Honnorat, Andrew Sloan, Mark Malkin, Joseph C Landolfi, Franz Payer, Maximilian Mehdorn, Robert J Weil, Susan C Pannullo, Manfred Westphal, Martin Smrcka, Lawrence Chin, Herwig Kostron, Silvia Hofer, Jeffrey Bruce, Rees Cosgrove, Nina Paleologous, Yoram Palti, and Philip H Gutin. Novotf-100a versus physician’s choice chemotherapy in recurrent glioblastoma: a randomised phase iii trial of a novel treatment modality. *European Journal of Cancer*, 48(14):2192–2202, 2012.
- [56] Roger Stupp, Sophie Taillibert, Andrew A Kanner, Santosh Kesari, David M Steinberg, Stuart A Toms, Leland P Taylor, Frank Lieberman, Arrigo Silvani, Kurt L Fink, Gene H Barnett, James J Zhu, John W Henson, Herbert H Engelhard, Thomas C Chen, Donald D Tran, Jakub Sroubek, Ngoc D Tran, Andreas F Hottinger, Joseph Landolfi, Raj Desai, Mario Caroli, Yoon-Jin Kew, Jerome Honnorat, Ahmed Idbaih, Eilon D Kirson, Uri Weinberg, Yoram Palti, Monika E Hegi, and Zvi Ram. Maintenance therapy with tumor-treating fields plus temozolomide vs temozolomide alone for glioblastoma: A randomized clinical trial. *JAMA*, 314(23):2535–2543, 2015.

- [57] Roger Stupp, Sophie Taillibert, Andrew Kanner, William Read, David Steinberg, Benoit Lhermitte, Stuart Toms, Ahmed Idbaih, Manmeet S Ahluwalia, Kurt Fink, Francesco Di Meo, Frank Lieberman, James J Zhu, Giuseppe Stragliotto, Donald Tran, Steven Brem, Andreas Hottinger, Eilon D Kirson, Gitit Lavy-Shahaf, Uri Weinberg, Changyoung Kim, Sun Ha Paek, Graham Nicholas, Jordi Bruna, Hans Hirte, Michael Weller, Yoram Palti, Monika E Hegi, and Zvi Ram. Effect of tumor-treating fields plus maintenance temozolomide vs maintenance temozolomide alone on survival in patients with glioblastoma: A randomized clinical trial. *JAMA*, 318(23):2306–2316, 2017. Erratum in: *JAMA*. 2018 May 1;319(17):1824. doi: 10.1001/jama.2018.3431.
- [58] Joshua J. Timmons, Jordane Preto, Jack A. Tuszynski, and Eric T. Wong. Tubulin’s response to external electric fields by molecular dynamics simulations. *PLOS ONE*, 13(9):1–17, 09 2018.
- [59] H. R. Saeidi, A. Lohrasebi, and K. Mahnam. External electric field effects on the mechanical properties of the α -tubulin dimer of microtubules: a molecular dynamics study. *Journal of Molecular Modeling*, 20(8):2395, 2014.
- [60] S. S. Setayandeh and A. Lohrasebi. The effects of external electric fields of 900 mhz and 2450 mhz frequencies on α -tubulin dimer stabilized by paclitaxel: Molecular dynamics approach. *Journal of Theoretical and Computational Chemistry*, 15(2):1650010, 2016. 10 pages.
- [61] S. S. Setayandeh and A. Lohrasebi. Influence of ghz electric fields on the mechanical properties of a microtubule. *Journal of Molecular Modeling*, 21(4):85, 2015.
- [62] A.I. Vakis, V.A. Yastrebov, J. Scheibert, L. Nicola, D. Dini, C. Minfray, A. Almqvist, M. Paggi, S. Lee, G. Limbert, J.F. Molinari, G. Anciaux, R. Aghababaei, S. Echeverri Restrepo, A. Papangelo, A. Cammarata, P. Nicolini, C. Putignano, G. Carbone, S. Stupkiewicz, J. Lengiewicz, G. Costagliola, F. Bosia, R. Guarino, N.M. Pugno, M.H. Müser, and M. Ciavarella. Modeling and simulation in tribology across scales: An overview. *Tribology International*, 125:169–199, 2018.
- [63] B. R. Brooks, C. L. Brooks 3rd, A. D. Mackerell Jr., L. Nilsson, R. J. Petrella, B. Roux, Y. Won, G. Archontis, C. Bartels, S. Boresch, A. Caffisch, L. Caves, Q. Cui, A. R. Dinner, M. Feig, S. Fischer, J. Gao, M. Hodoseck, W. Im, K. Kuczera, T. Lazaridis, J. Ma, V. Ovchinnikov, E. Paci, R. W. Pastor, C. B. Post, J. Z. Pu, M. Schaefer, B. Tidor, R. M. Venable, H. L. Woodcock, X. Wu, W. Yang, D. M. York, and M. Karplus. CHARMM: The biomolecular simulation program. *J Comput Chem*, 30(10):1545–1614, 2009.
- [64] Jason M. Swails. *Free Energy Simulations of Complex Biological Systems at Constant pH*. PhD thesis, University of Florida, 2013. A dissertation presented to the Graduate School of the University of Florida in partial fulfillment of the requirements for the degree of Doctor of Philosophy.
- [65] Wikibooks contributors. The lennard-jones potential. https://en.wikibooks.org/wiki/Molecular_Simulation/The_Lennard-Jones_Potential. Accessed: 2024-07-18.

- [66] GROMACS reference manual: Periodic boundary conditions. <https://manual.gromacs.org/current/reference-manual/algorithms/periodic-boundary-conditions.html#periodic-boundary-conditions>. Accessed on April 7, 2024.
- [67] Wikimedia Commons. Minimum image convention. https://commons.wikimedia.org/wiki/File:Minimum_Image_Convention.png. Accessed: 2024-07-18.
- [68] M. Bhandarkar, Robert Brunner, Chris Chipot, A. Dalke, Surjit Dixit, P. Grayson, J. Gullingsrud, Attila Gursoy, David Hardy, W. Humphrey, David Hurwitz, and Neal Krawetz. NAMD molecular dynamics software non-exclusive, noncommercial use license, 01 2000.
- [69] GROMACS reference manual: Long-range electrostatics. <https://manual.gromacs.org/documentation/2019-rc1/reference-manual/functions/long-range-electrostatics.html>. Accessed on April 8, 2024.
- [70] Xiongwu Wu and B. Brooks. *Molecular Simulation with Discrete Fast Fourier Transform*, pages 137–164. 05 2012.
- [71] S. Henninger. Wärmetransformation mit zeolith/wasser-systemen – monte carlo simulationen zur materialoptimierung. Master’s thesis, University of Freiburg, Faculty of Physics, Freiburg, Germany, 2002. Diploma thesis.
- [72] Tom Darden, Darrin York, and Lee Pedersen. Particle mesh Ewald: An $N \log(N)$ method for Ewald sums in large systems. *The Journal of Chemical Physics*, 98(12):10089–10092, 06 1993.
- [73] Compute Canada. Molecular dynamics theory: Electrostatics, 2024. Accessed: 2024-07-14.
- [74] Mark E. Tuckerman. *Title of the Book*. Oxford University Press, Great Clarendon Street, Oxford, OX2 6DP, United Kingdom, second edition, 2023. First Edition published in 2010.
- [75] Ben Cooke and Scott C. Schmidler. Preserving the Boltzmann ensemble in replica-exchange molecular dynamics. *The Journal of Chemical Physics*, 129(16):164112, 10 2008.
- [76] Mark Tuckerman and Glenn Martyna. Understanding modern molecular dynamics: Techniques and applications. *Journal of Physical Chemistry B*, 104:159–178, 01 2000.
- [77] Mark E. Tuckerman, Yi Liu, Giovanni Ciccotti, and Glenn J. Martyna. Non-Hamiltonian molecular dynamics: Generalizing Hamiltonian phase space principles to non-Hamiltonian systems. *The Journal of Chemical Physics*, 115(4):1678–1702, 07 2001.
- [78] M. E. Tuckerman, C. J. Mundy, and G. J. Martyna. On the classical statistical mechanics of non-hamiltonian systems. *Europhysics Letters*, 45(2):149, jan 1999.

- [79] William G. Hoover. Canonical dynamics: Equilibrium phase-space distributions. *Phys. Rev. A*, 31:1695–1697, Mar 1985.
- [80] Glenn J. Martyna, Michael L. Klein, and Mark Tuckerman. Nosé–Hoover chains: The canonical ensemble via continuous dynamics. *The Journal of Chemical Physics*, 97(4):2635–2643, 08 1992.
- [81] Glenn J. Martyna, Mark E. Tuckerman, Douglas J. Tobias, and Michael L. Klein. Explicit reversible integrators for extended systems dynamics. *Molecular Physics*, 87(5):1117–1157, 1996.
- [82] GROMACS Development Team. Gromacs molecular dynamics reference manual. <https://manual.gromacs.org/2021/reference-manual/algorithms/molecular-dynamics.html>. Accessed: 2024-07-18.
- [83] Simone Melchionna. Constrained systems and statistical distribution. *Physical Review E*, 61(6):6165–6177, June 2000. Received 3 May 1999; revised manuscript received 11 February 2000.
- [84] Metacentrum (metavo) - virtual organization. <https://metavo.metacentrum.cz/en/index.html>. Accessed: 2024-07-18.
- [85] GROMACS Development Team. *Electric Fields*, 2024. Accessed: 2024-07-14.
- [86] Thomas B. Jones. *Electromechanics of Particles*. Library of Congress Cataloguing in Publication data. Cambridge University Press, Cambridge, New York, Melbourne, Madrid, Cape Town, Singapore, Sao Paulo, 1995. First published 1995. This digitally printed first paperback version 2005. A catalogue record for this publication is available from the British Library.
- [87] R. D. Miller and T. B. Jones. Electro-orientation of ellipsoidal erythrocytes. theory and experiment. *Biophysical Journal*, 64:1588–1595, 1993.
- [88] Nidhi M. Diwakar, Golak Kunti, Touvia Miloh, Gilad Yossifon, and Orlin D. Velev. Ac electrohydrodynamic propulsion and rotation of active particles of engineered shape and asymmetry. *Current Opinion in Colloid Interface Science*, 59:101586, 2022.
- [89] Gerhard Schwarz, Masao Saito, and Herman P. Schwan. On the Orientation of Nonspherical Particles in an Alternating Electrical Field. *The Journal of Chemical Physics*, 43(10):3562–3569, 11 1965.
- [90] A. Mershin, A.A. Kolomenski, H.A. Schuessler, and D.V. Nanopoulos. Tubulin dipole moment, dielectric constant and quantum behavior: computer simulations, experimental results and suggestions. *Biosystems*, 77(1):73–85, 2004.

List of Figures

1.1	A - Tubulin dimer consisting of α and β tubulin subunits can form microtubule - tubular structures made of usually 13 protofilaments. There is another special form of tubulin called γ that is used to anchor the minus ends of microtubules to MTOCs; B - A model of a cell. In the cytoplasm, microtubules create dynamic networks that are stably anchored at MTOCs, such as the centrosome and Golgi apparatus; the illustration taken from [2]	5
1.2	A - A depiction of the different post-translational modifications of tubulin in a neuron model; also, kinesin and dynein “walking” on these microtubules are also shown here. B - A depiction of mitosis, where kinesin is connected to the chromosome and walks along the microtubule. C - A flagella is depicted, we can again see the movement of cargo via kinesin and dynein along the microtubule; the illustration is taken from [3]	6
1.3	Human osteosarcoma cells in different phases of mitosis - a interphase, b metaphase, c anaphase, d telophase. α tubulins are stained with polyclonal antibody (green), γ tubulin with monoclonal antibody TU-30 (red) and DNA by DAPI(blue). Bars = 10 μm ; the illustration is taken from [4]	7
1.4	Dynamic instability of microtubules, during the catastrophe, the rate of phosphate release from the GTP cap is higher than the addition of new GTP tubulins. During the rescue, it is vice versa; the illustration is taken from [3]	8
1.5	Post-translational modifications of tubulins; the illustration is taken from [3]	9
1.6	Antitubulin agents and their binding sites; the illustration is taken from [16]	11
2.1	Atomic force microscopy images of structures formed from B) untreated tubulin, C) treated tubulin by 200 pulses, D) treated tubulin by 800 pulses. In D) the schematic representations of those structures are depicted; [50]	15
3.1	Timescales and lengthscales accessible by different types of physical system simulations; the illustration taken from [62]	18
3.2	Degrees of freedom of the individual force-field potentials; the illustration taken from [64]	20
3.3	Lennard-Jones potential; ε is ε_{AB} in our notation, R_{\min} is R_{AB}^{\min} in our notation; the illustration taken from [65]	21
3.4	Minimum Image Convention; the illustration taken from [67]	23
3.5	Switch function used for the truncation of the van der Waals interactions; [68]	24
3.6	Screening in the Ewald summation, [71]	26

3.7	Particle Mesh Ewald interpolation diagram for the evaluation of long-range electrostatics in molecular dynamics simulation; the illustration taken from [73]	27
6.1	Workflow scheme; L_i represents batch i , d directions, f frequency; no EF - case of no electric field; v_{0j} represent the generated velocities	49
6.2	Initial conformations for the production runs	50
6.3	Directions of the electric field oscillations, colour-coded. Blue - d1; orange - d2; green - d3; red - d4; purple - d5; black - d6; shown for initial frame of production run for batch 1. The program rotates these vertices for the next two batches in such a way that they will have the same relative direction with respect to the protein structure; two different points of view on the structure	51
8.1	RMSD of the tubulin dimer - Batch 1 - Part 1	59
8.2	RMSD of the tubulin dimer - Batch 1 - Part 2	60
8.3	RMSD of the tubulin dimer - Batch 1 - Part 3	61
8.4	RMSD of the tubulin dimer without the C-termini - Batch 1 - Part 1	62
8.5	RMSD of the tubulin dimer without the C-termini - Batch 1 - Part 2	63
8.6	RMSD of the tubulin dimer without the C-termini - Batch 1 - Part 3	64
8.7	RMSD of the C-termini of the tubulin dimer - Batch 1 - Part 1 .	65
8.8	RMSD of the C-termini of the tubulin dimer - Batch 1 - Part 2 .	66
8.9	RMSD of the C-termini of the tubulin dimer - Batch 1 - Part 3 .	67
8.10	RMSD of the tubulin dimer - Batch 2 - Part 1	71
8.11	RMSD of the tubulin dimer - Batch 2 - Part 2	72
8.12	RMSD of the tubulin dimer - Batch 2 - Part 3	73
8.13	RMSD of the tubulin dimer without the C-termini - Batch 2 - Part 1	74
8.14	RMSD of the tubulin dimer without the C-termini - Batch 2 - Part 2	75
8.15	RMSD of the tubulin dimer without the C-termini - Batch 2 - Part 3	76
8.16	RMSD of the C-termini of the tubulin dimer - Batch 2 - Part 1 .	77
8.17	RMSD of the C-termini of the tubulin dimer - Batch 2 - Part 2 .	78
8.18	RMSD of the C-termini of the tubulin dimer - Batch 2 - Part 3 .	79
8.19	RMSD of the tubulin dimer - Batch 3 - Part 1	82
8.20	RMSD of the tubulin dimer - Batch 3 - Part 2	83
8.21	RMSD of the tubulin dimer - Batch 3 - Part 3	84
8.22	RMSD of the tubulin dimer without the C-termini - Batch 3 - Part 1	85
8.23	RMSD of the tubulin dimer without the C-termini - Batch 3 - Part 2	86
8.24	RMSD of the tubulin dimer without the C-termini - Batch 3 - Part 3	87
8.25	RMSD of the C-termini of the tubulin dimer - Batch 3 - Part 1 .	88
8.26	RMSD of the C-termini of the tubulin dimer - Batch 3 - Part 2 .	89
8.27	RMSD of the C-termini of the tubulin dimer - Batch 3 - Part 3 .	90
8.28	Tubulin alpha residues affected the most by electric fields colour-coded as follows: 25-50 orange; 50-70 red; 230-250 purple; 250-286 green; 305-313 pink; 350-370 blue (structure is obtained from the simulation of 30 GHz in direction d4 - batch 1 at 70 ns	92
8.29	Tubulin beta residues affected the most by electric fields colour-coded as follows: 25-50 blue, 50-60 red; 60-75 yellow; 90-100 pink; 160-180 purple; 265-285 orange (structure is obtained from the simulation of 10 GHz in direction d1 - batch 1 at 100ns)	92

8.30	RMSF _{diff} of the residues of the tubulin α subjected to the electric field of frequency 20 GHz, Batch 1	93
8.31	RMSF _{diff} of the residues of the tubulin α subjected to the electric field of frequency 20 GHz, Batch 2	93
8.32	RMSF _{diff} of the residues of the tubulin α subjected to the electric field of frequency 20 GHz, Batch 3	94
8.33	RMSF _{diff} of the residues of the tubulin β subjected to the electric field of frequency 20 GHz, Batch 1	94
8.34	RMSF _{diff} of the residues of the tubulin β subjected to the electric field of frequency 20 GHz, Batch 2	95
8.35	RMSF _{diff} of the residues of the tubulin β subjected to the electric field of frequency 20 GHz, Batch 3	95
8.36	Average of RMSF _{diff} of the residues of the α tubulin subjected to the electric field of frequency 20 GHz	96
8.37	Average of RMSF _{diff} of the residues of the β tubulin subjected to the electric field of frequency 20 GHz	96
8.38	RMSF of residue 325 of tubulin alpha - different directions and batches; the bars for 0 GHz mean that no EF is applied	98
8.39	RMSF of residue 325 of tubulin alpha - averaged over directions and batches; the bars for 0 GHz mean that no EF is applied	98
8.40	RMSF of residue 329 of tubulin alpha - different directions and batches; the bars for 0 GHz mean that no EF is applied	99
8.41	RMSF of residue 329 of tubulin alpha - averaged over directions and batches; the bars for 0 GHz mean that no EF is applied	99
8.42	RMSF of residue 351 of tubulin alpha - different directions and batches; the bars for 0 GHz mean that no EF is applied	100
8.43	RMSF of residue 351 of tubulin alpha - averaged over directions and batches; the bars for 0 GHz mean that no EF is applied	100
8.44	RMSF of residue 353 of tubulin alpha - different directions and batches; the bars for 0 GHz mean that no EF is applied	101
8.45	RMSF of residue 353 of tubulin alpha - averaged over directions and batches; the bars for 0 GHz mean that no EF is applied	101
8.46	RMSF of residue 173 of tubulin beta - different directions and batches; the bars for 0 GHz mean that no EF is applied	102
8.47	RMSF of residue 173 of tubulin beta - averaged over directions and batches; the bars for 0 GHz mean that no EF is applied	102
8.48	RMSF of residue 174 of tubulin beta - different directions and batches; the bars for 0 GHz mean that no EF is applied	103
8.49	RMSF of residue 174 of tubulin beta - averaged over directions and batches; the bars for 0 GHz mean that no EF is applied	103
8.50	RMSF of residue 175 of tubulin beta - different directions and batches; the bars for 0 GHz mean that no EF is applied	104
8.51	RMSF of residue 175 of tubulin beta - averaged over directions and batches; the bars for 0 GHz mean that no EF is applied	104
8.52	RMSF of residue 218 of tubulin beta - different directions and batches; the bars for 0 GHz mean that no EF is applied	105
8.53	RMSF of residue 218 of tubulin beta - averaged over directions and batches; the bars for 0 GHz mean that no EF is applied	105

8.54	RMSF of residue 220 of tubulin beta - different directions and batches; the bars for 0 GHz mean that no EF is applied	106
8.55	RMSF of residue 220 of tubulin beta - averaged over directions and batches; the bars for 0 GHz mean that no EF is applied	106
8.56	RMSF of residue 221 of tubulin beta - different directions and batches; the bars for 0 GHz mean that no EF is applied	107
8.57	RMSF of residue 221 of tubulin beta - averaged over directions and batches; the bars for 0 GHz mean that no EF is applied	107
8.58	RMSF of residue 180 of tubulin alpha - different directions and batches; the bars for 0 GHz mean that no EF is applied	109
8.59	RMSF of residue 180 of tubulin alpha - averaged over directions and batches; the bars for 0 GHz mean that no EF is applied	109
8.60	RMSF of residue 181 of tubulin alpha - different directions and batches; the bars for 0 GHz mean that no EF is applied	110
8.61	RMSF of residue 181 of tubulin alpha - averaged over directions and batches; the bars for 0 GHz mean that no EF is applied	110
8.62	RMSF of residue 236 of tubulin beta - different directions and batches; the bars for 0 GHz mean that no EF is applied	111
8.63	RMSF of residue 236 of tubulin beta - averaged over directions and batches; the bars for 0 GHz mean that no EF is applied	111
8.64	RMSF of residue 246 of tubulin beta - different directions and batches; the bars for 0 GHz mean that no EF is applied	112
8.65	RMSF of residue 246 of tubulin beta - averaged over directions and batches; the bars for 0 GHz mean that no EF is applied	112
8.66	RMSF of residue 248 of tubulin beta - different directions and batches; the bars for 0 GHz mean that no EF is applied	113
8.67	RMSF of residue 248 of tubulin beta - averaged over directions and batches; the bars for 0 GHz mean that no EF is applied	113
8.68	RMSF of residue 253 of tubulin beta - different directions and batches; the bars for 0 GHz mean that no EF is applied	114
8.69	RMSF of residue 253 of tubulin beta - averaged over directions and batches; the bars for 0 GHz mean that no EF is applied	114
8.70	RMSF of residue 256 of tubulin beta - different directions and batches; the bars for 0 GHz mean that no EF is applied	115
8.71	RMSF of residue 256 of tubulin beta - averaged over directions and batches; the bars for 0 GHz mean that no EF is applied	115
8.72	RMSF of residue 257 of tubulin beta - different directions and batches; the bars for 0 GHz mean that no EF is applied	116
8.73	RMSF of residue 257 of tubulin beta - averaged over directions and batches; the bars for 0 GHz mean that no EF is applied	116
8.74	RMSF of residue 314 of tubulin beta - different directions and batches; the bars for 0 GHz mean that no EF is applied	117
8.75	RMSF of residue 314 of tubulin beta - averaged over directions and batches; the bars for 0 GHz mean that no EF is applied	117
8.76	RMSF of residue 215 of tubulin beta - different directions and batches; the bars for 0 GHz mean that no EF is applied	119
8.77	RMSF of residue 215 of tubulin beta - averaged over directions and batches; the bars for 0 GHz mean that no EF is applied	119

8.78	RMSF of residue 227 of tubulin beta - different directions and batches; the bars for 0 GHz mean that no EF is applied	120
8.79	RMSF of residue 227 of tubulin beta - averaged over directions and batches; the bars for 0 GHz mean that no EF is applied	120
8.80	RMSF of residue 228 of tubulin beta - different directions and batches; the bars for 0 GHz mean that no EF is applied	121
8.81	RMSF of residue 228 of tubulin beta - averaged over directions and batches; the bars for 0 GHz mean that no EF is applied	121
8.82	RMSF of residue 272 of tubulin beta - different directions and batches; the bars for 0 GHz mean that no EF is applied	122
8.83	RMSF of residue 272 of tubulin beta - averaged over directions and batches; the bars for 0 GHz mean that no EF is applied	122
8.84	RMSF of residue 274 of tubulin beta - different directions and batches; the bars for 0 GHz mean that no EF is applied	123
8.85	RMSF of residue 274 of tubulin beta - averaged over directions and batches; the bars for 0 GHz mean that no EF is applied	123
8.86	RMSF of residue 276 of tubulin beta - different directions and batches; the bars for 0 GHz mean that no EF is applied	124
8.87	RMSF of residue 276 of tubulin beta - averaged over directions and batches; the bars for 0 GHz mean that no EF is applied	124
8.88	RMSF of residue 280 of tubulin beta - different directions and batches; the bars for 0 GHz mean that no EF is applied	125
8.89	RMSF of residue 280 of tubulin beta - averaged over directions and batches; the bars for 0 GHz mean that no EF is applied	125
8.90	RMSF of residue 358 of tubulin beta - different directions and batches; the bars for 0 GHz mean that no EF is applied	126
8.91	RMSF of residue 358 of tubulin beta - averaged over directions and batches; the bars for 0 GHz mean that no EF is applied	126
8.92	RMSF of residue 359 of tubulin beta - different directions and batches; the bars for 0 GHz mean that no EF is applied	127
8.93	RMSF of residue 359 of tubulin beta - averaged over directions and batches; the bars for 0 GHz mean that no EF is applied	127
8.94	RMSF of residue 360 of tubulin beta - different directions and batches; the bars for 0 GHz mean that no EF is applied	128
8.95	RMSF of residue 360 of tubulin beta - averaged over directions and batches; the bars for 0 GHz mean that no EF is applied	128
8.96	RMSF of residue 361 of tubulin beta - different directions and batches; the bars for 0 GHz mean that no EF is applied	129
8.97	RMSF of residue 361 of tubulin beta - averaged over directions and batches; the bars for 0 GHz mean that no EF is applied	129
8.98	Angle between longitudinal axis of tubulin heterodimer and electric field direction - batch 1. part 1 (frequencies 10-50 GHz)	131
8.99	Angle between longitudinal axis of tubulin heterodimer and electric field direction - batch 1. part 2 (frequencies 60-100 GHz)	132
8.100	Angle between longitudinal axis of tubulin heterodimer and electric field direction - batch 1. part 3 (frequencies 110-150 GHz)	133
8.101	Angle between longitudinal axis of tubulin heterodimer and electric field direction - batch 2. 1 (frequencies 10-50 GHz)	134

8.102	Angle between longitudinal axis of tubulin heterodimer and electric field direction - batch 2. 2 (frequencies 60-100 GHz)	135
8.103	Angle between longitudinal axis of tubulin heterodimer and electric field direction - batch 2. 3 (frequencies 110-150 GHz)	136
8.104	Angle between longitudinal axis of tubulin heterodimer and electric field direction - batch 3. 1 (frequencies 10-50 GHz)	137
8.105	Angle between longitudinal axis of tubulin heterodimer and electric field direction - batch 3. 2 (frequencies 60-100 GHz)	138
8.106	Angle between longitudinal axis of tubulin heterodimer and electric field direction - batch 3. 3 (frequencies 110-150 GHz)	139
8.107	Time spent approximately parallel to the electric field direction of oscillation - batch 1, direction 1	140
8.108	Time spent approximately parallel to the electric field direction of oscillation - batch 1, direction 2	141
8.109	Time spent approximately parallel to the electric field direction of oscillation - batch 1, direction 3	141
8.110	Time spent approximately parallel to the electric field direction of oscillation - batch 1, direction 4	142
8.111	Time spent approximately parallel to the electric field direction of oscillation - batch 1, direction 5	142
8.112	Time spent approximately parallel to the electric field direction of oscillation - batch 1, direction 6	143
8.113	Time spent approximately parallel to the electric field direction of oscillation - averaged over different directions; b1 - b3 represent different batches (initial conformations)	144
8.114	Time spent approximately parallel to the electric field direction of oscillation - averaged over batches; d1) - d6) represents 6 different directions of oscillations	145
8.115	Time spent approximately parallel to the electric field direction of oscillation - averaged over batches and directions	146
8.116	Magnitude of the dipole moment of tubulin heterodimer - time series and distributions - batch 1, Frequencies 10-50 GHz	148
8.117	Magnitude of the dipole moment of tubulin heterodimer - time series and distributions - batch 1, Frequencies 60-100 GHz	149
8.118	Magnitude of the dipole moment of tubulin heterodimer - time series and distributions - batch 1, Frequencies 110-150 GHz	150
8.119	Time series and distributions of the projection of dipole moment of tubulin dimer onto the axis of electric field oscillations - batch 1, Frequencies 10-50 GHz	152
8.120	Time series and distributions of the projection of dipole moment of tubulin dimer onto the axis of electric field oscillations - batch 1, Frequencies 60-100 GHz	153
8.121	Time series and distributions of the projection of dipole moment of tubulin dimer onto the axis of electric field oscillations - batch 1, Frequencies 110-150 GHz	154
8.122	Propability distributions of dipole moment calculated for the bulk tubulin (wo C-termini); Batch 1	155

8.123	Propability distributions of dipole moment calculated for the bulk tubulin (wo C-termini); Batch 2	156
8.124	Propability distributions of dipole moment calculated for the bulk tubulin (wo C-termini); Batch 3	157
9.1	C-termini conformation at 7 ns of Batch 2 simulation with 150 GHz EF in direction 2; α C-terminus is coloured red, β C-terminus is coloured green	159
9.2	C-termini conformation at 24 ns of Batch 2 simulation with 150 GHz EF in direction 2; α C-terminus is coloured red, β C-terminus is coloured green	159
9.3	C-termini conformation at 31 ns of Batch 2 simulation with 150 GHz EF in direction 2; α C-terminus is coloured red, β C-terminus is coloured green	160
9.4	C-termini conformation at 36 ns of Batch 2 simulation with 150 GHz EF in direction 2; α C-terminus is coloured red, β C-terminus is coloured green	160
9.5	C-termini conformation at 65 ns of Batch 2 simulation with 150 GHz EF in direction 2; α C-terminus is coloured red, β C-terminus is coloured green	160
9.6	C-termini conformation at 73 ns of Batch 2 simulation with 150 GHz EF in direction 2; α C-terminus is coloured red, β C-terminus is coloured green	161
9.7	C-termini conformation at 100 ns of Batch 2 simulation with 150 GHz EF in direction 2; α C-terminus is coloured red, β C-terminus is coloured green	161
9.8	C-termini conformation at 88 ns (left) and 100 ns (right) of Batch 2 simulation with 150 GHz EF in direction 5; α C-terminus is coloured red, β C-terminus is coloured green	162
10.1	RMSF of tubulin α residues subjected to the electric field of frequency 10 GHz; Batch 1	218
10.2	RMSF of tubulin α residues subjected to the electric field of frequency 20 GHz; Batch 1	218
10.3	RMSF of tubulin α residues subjected to the electric field of frequency 30 GHz; Batch 1	219
10.4	RMSF of tubulin α residues subjected to the electric field of frequency 40 GHz; Batch 1	219
10.5	RMSF of tubulin α residues subjected to the electric field of frequency 50 GHz; Batch 1	220
10.6	RMSF of tubulin α residues subjected to the electric field of frequency 60 GHz; Batch 1	220
10.7	RMSF of tubulin α residues subjected to the electric field of frequency 70 GHz; Batch 1	221
10.8	RMSF of tubulin α residues subjected to the electric field of frequency 80 GHz; Batch 1	221
10.9	RMSF of tubulin α residues subjected to the electric field of frequency 90 GHz; Batch 1	222

10.10RMSF of tubulin α residues subjected to the electric field of frequency 100 GHz; Batch 1	222
10.11RMSF of tubulin α residues subjected to the electric field of frequency 110 GHz; Batch 1	223
10.12RMSF of tubulin α residues subjected to the electric field of frequency 120 GHz; Batch 1	223
10.13RMSF of tubulin α residues subjected to the electric field of frequency 130 GHz; Batch 1	224
10.14RMSF of tubulin α residues subjected to the electric field of frequency 140 GHz; Batch 1	224
10.15RMSF of tubulin α residues subjected to the electric field of frequency 150 GHz; Batch 1	225
10.16RMSF of tubulin α residues subjected to the electric field of frequency 10 GHz; Batch 2	225
10.17RMSF of tubulin α residues subjected to the electric field of frequency 20 GHz; Batch 2	226
10.18RMSF of tubulin α residues subjected to the electric field of frequency 30 GHz; Batch 2	226
10.19RMSF of tubulin α residues subjected to the electric field of frequency 40 GHz; Batch 2	227
10.20RMSF of tubulin α residues subjected to the electric field of frequency 50 GHz; Batch 2	227
10.21RMSF of tubulin α residues subjected to the electric field of frequency 60 GHz; Batch 2	228
10.22RMSF of tubulin α residues subjected to the electric field of frequency 70 GHz; Batch 2	228
10.23RMSF of tubulin α residues subjected to the electric field of frequency 80 GHz; Batch 2	229
10.24RMSF of tubulin α residues subjected to the electric field of frequency 90 GHz; Batch 2	229
10.25RMSF of tubulin α residues subjected to the electric field of frequency 100 GHz; Batch 2	230
10.26RMSF of tubulin α residues subjected to the electric field of frequency 110 GHz; Batch 2	230
10.27RMSF of tubulin α residues subjected to the electric field of frequency 120 GHz; Batch 2	231
10.28RMSF of tubulin α residues subjected to the electric field of frequency 130 GHz; Batch 2	231
10.29RMSF of tubulin α residues subjected to the electric field of frequency 140 GHz; Batch 2	232
10.30RMSF of tubulin α residues subjected to the electric field of frequency 150 GHz; Batch 2	232
10.31RMSF of tubulin α residues subjected to the electric field of frequency 10 GHz; Batch 3	233
10.32RMSF of tubulin α residues subjected to the electric field of frequency 20 GHz; Batch 3	233
10.33RMSF of tubulin α residues subjected to the electric field of frequency 30 GHz; Batch 3	234

10.34RMSF of tubulin α residues subjected to the electric field of frequency 40 GHz; Batch 3	234
10.35RMSF of tubulin α residues subjected to the electric field of frequency 50 GHz; Batch 3	235
10.36RMSF of tubulin α residues subjected to the electric field of frequency 60 GHz; Batch 3	235
10.37RMSF of tubulin α residues subjected to the electric field of frequency 70 GHz; Batch 3	236
10.38RMSF of tubulin α residues subjected to the electric field of frequency 80 GHz; Batch 3	236
10.39RMSF of tubulin α residues subjected to the electric field of frequency 90 GHz; Batch 3	237
10.40RMSF of tubulin α residues subjected to the electric field of frequency 100 GHz; Batch 3	237
10.41RMSF of tubulin α residues subjected to the electric field of frequency 110 GHz; Batch 3	238
10.42RMSF of tubulin α residues subjected to the electric field of frequency 120 GHz; Batch 3	238
10.43RMSF of tubulin α residues subjected to the electric field of frequency 130 GHz; Batch 3	239
10.44RMSF of tubulin α residues subjected to the electric field of frequency 140 GHz; Batch 3	239
10.45RMSF of tubulin α residues subjected to the electric field of frequency 150 GHz; Batch 3	240
10.46RMSF of tubulin β residues subjected to the electric field of frequency 10 GHz; Batch 1	240
10.47RMSF of tubulin β residues subjected to the electric field of frequency 20 GHz; Batch 1	241
10.48RMSF of tubulin β residues subjected to the electric field of frequency 30 GHz; Batch 1	241
10.49RMSF of tubulin β residues subjected to the electric field of frequency 40 GHz; Batch 1	242
10.50RMSF of tubulin β residues subjected to the electric field of frequency 50 GHz; Batch 1	242
10.51RMSF of tubulin β residues subjected to the electric field of frequency 60 GHz; Batch 1	243
10.52RMSF of tubulin β residues subjected to the electric field of frequency 70 GHz; Batch 1	243
10.53RMSF of tubulin β residues subjected to the electric field of frequency 80 GHz; Batch 1	244
10.54RMSF of tubulin β residues subjected to the electric field of frequency 90 GHz; Batch 1	244
10.55RMSF of tubulin β residues subjected to the electric field of frequency 100 GHz; Batch 1	245
10.56RMSF of tubulin β residues subjected to the electric field of frequency 110 GHz; Batch 1	245
10.57RMSF of tubulin β residues subjected to the electric field of frequency 120 GHz; Batch 1	246

10.58RMSF of tubulin β residues subjected to the electric field of frequency 130 GHz; Batch 1	246
10.59RMSF of tubulin β residues subjected to the electric field of frequency 140 GHz; Batch 1	247
10.60RMSF of tubulin β residues subjected to the electric field of frequency 150 GHz; Batch 1	247
10.61RMSF of tubulin β residues subjected to the electric field of frequency 10 GHz; Batch 2	248
10.62RMSF of tubulin β residues subjected to the electric field of frequency 20 GHz; Batch 2	248
10.63RMSF of tubulin β residues subjected to the electric field of frequency 30 GHz; Batch 2	249
10.64RMSF of tubulin β residues subjected to the electric field of frequency 40 GHz; Batch 2	249
10.65RMSF of tubulin β residues subjected to the electric field of frequency 50 GHz; Batch 2	250
10.66RMSF of tubulin β residues subjected to the electric field of frequency 60 GHz; Batch 2	250
10.67RMSF of tubulin β residues subjected to the electric field of frequency 70 GHz; Batch 2	251
10.68RMSF of tubulin β residues subjected to the electric field of frequency 80 GHz; Batch 2	251
10.69RMSF of tubulin β residues subjected to the electric field of frequency 90 GHz; Batch 2	252
10.70RMSF of tubulin β residues subjected to the electric field of frequency 100 GHz; Batch 2	252
10.71RMSF of tubulin β residues subjected to the electric field of frequency 110 GHz; Batch 2	253
10.72RMSF of tubulin β residues subjected to the electric field of frequency 120 GHz; Batch 2	253
10.73RMSF of tubulin β residues subjected to the electric field of frequency 130 GHz; Batch 2	254
10.74RMSF of tubulin β residues subjected to the electric field of frequency 140 GHz; Batch 2	254
10.75RMSF of tubulin β residues subjected to the electric field of frequency 150 GHz; Batch 2	255
10.76RMSF of tubulin β residues subjected to the electric field of frequency 10 GHz; Batch 3	255
10.77RMSF of tubulin β residues subjected to the electric field of frequency 20 GHz; Batch 3	256
10.78RMSF of tubulin β residues subjected to the electric field of frequency 30 GHz; Batch 3	256
10.79RMSF of tubulin β residues subjected to the electric field of frequency 40 GHz; Batch 3	257
10.80RMSF of tubulin β residues subjected to the electric field of frequency 50 GHz; Batch 3	257
10.81RMSF of tubulin β residues subjected to the electric field of frequency 60 GHz; Batch 3	258

10.82RMSF of tubulin β residues subjected to the electric field of frequency 70 GHz; Batch 3	258
10.83RMSF of tubulin β residues subjected to the electric field of frequency 80 GHz; Batch 3	259
10.84RMSF of tubulin β residues subjected to the electric field of frequency 90 GHz; Batch 3	259
10.85RMSF of tubulin β residues subjected to the electric field of frequency 100 GHz; Batch 3	260
10.86RMSF of tubulin β residues subjected to the electric field of frequency 110 GHz; Batch 3	260
10.87RMSF of tubulin β residues subjected to the electric field of frequency 120 GHz; Batch 3	261
10.88RMSF of tubulin β residues subjected to the electric field of frequency 130 GHz; Batch 3	261
10.89RMSF of tubulin β residues subjected to the electric field of frequency 140 GHz; Batch 3	262
10.90RMSF of tubulin β residues subjected to the electric field of frequency 150 GHz; Batch 3	262
10.91RMSF _{diff} of the residues of the tubulin α subjected to the electric field of frequency 10 GHz, Batch 1	263
10.92RMSF _{diff} of the residues of the tubulin α subjected to the electric field of frequency 20 GHz, Batch 1	263
10.93RMSF _{diff} of the residues of the tubulin α subjected to the electric field of frequency 30 GHz, Batch 1	264
10.94RMSF _{diff} of the residues of the tubulin α subjected to the electric field of frequency 40 GHz, Batch 1	264
10.95RMSF _{diff} of the residues of the tubulin α subjected to the electric field of frequency 50 GHz, Batch 1	265
10.96RMSF _{diff} of the residues of the tubulin α subjected to the electric field of frequency 60 GHz, Batch 1	265
10.97RMSF _{diff} of the residues of the tubulin α subjected to the electric field of frequency 70 GHz, Batch 1	266
10.98RMSF _{diff} of the residues of the tubulin α subjected to the electric field of frequency 80 GHz, Batch 1	266
10.99RMSF _{diff} of the residues of the tubulin α subjected to the electric field of frequency 90 GHz, Batch 1	267
10.100RMSF _{diff} of the residues of the tubulin α subjected to the electric field of frequency 100 GHz, Batch 1	267
10.101RMSF _{diff} of the residues of the tubulin α subjected to the electric field of frequency 110 GHz, Batch 1	268
10.102RMSF _{diff} of the residues of the tubulin α subjected to the electric field of frequency 120 GHz, Batch 1	268
10.103RMSF _{diff} of the residues of the tubulin α subjected to the electric field of frequency 130 GHz, Batch 1	269
10.104RMSF _{diff} of the residues of the tubulin α subjected to the electric field of frequency 140 GHz, Batch 1	269
10.105RMSF _{diff} of the residues of the tubulin α subjected to the electric field of frequency 150 GHz, Batch 1	270

10.106	RMSF _{diff} of the residues of the tubulin α subjected to the electric field of frequency 10 GHz, Batch 2	270
10.107	RMSF _{diff} of the residues of the tubulin α subjected to the electric field of frequency 20 GHz, Batch 2	271
10.108	RMSF _{diff} of the residues of the tubulin α subjected to the electric field of frequency 30 GHz, Batch 2	271
10.109	RMSF _{diff} of the residues of the tubulin α subjected to the electric field of frequency 40 GHz, Batch 2	272
10.110	RMSF _{diff} of the residues of the tubulin α subjected to the electric field of frequency 50 GHz, Batch 2	272
10.111	RMSF _{diff} of the residues of the tubulin α subjected to the electric field of frequency 60 GHz, Batch 2	273
10.112	RMSF _{diff} of the residues of the tubulin α subjected to the electric field of frequency 70 GHz, Batch 2	273
10.113	RMSF _{diff} of the residues of the tubulin α subjected to the electric field of frequency 80 GHz, Batch 2	274
10.114	RMSF _{diff} of the residues of the tubulin α subjected to the electric field of frequency 90 GHz, Batch 2	274
10.115	RMSF _{diff} of the residues of the tubulin α subjected to the electric field of frequency 100 GHz, Batch 2	275
10.116	RMSF _{diff} of the residues of the tubulin α subjected to the electric field of frequency 110 GHz, Batch 2	275
10.117	RMSF _{diff} of the residues of the tubulin α subjected to the electric field of frequency 120 GHz, Batch 2	276
10.118	RMSF _{diff} of the residues of the tubulin α subjected to the electric field of frequency 130 GHz, Batch 2	276
10.119	RMSF _{diff} of the residues of the tubulin α subjected to the electric field of frequency 140 GHz, Batch 2	277
10.120	RMSF _{diff} of the residues of the tubulin α subjected to the electric field of frequency 150 GHz, Batch 2	277
10.121	RMSF _{diff} of the residues of the tubulin α subjected to the electric field of frequency 10 GHz, Batch 3	278
10.122	RMSF _{diff} of the residues of the tubulin α subjected to the electric field of frequency 20 GHz, Batch 3	278
10.123	RMSF _{diff} of the residues of the tubulin α subjected to the electric field of frequency 30 GHz, Batch 3	279
10.124	RMSF _{diff} of the residues of the tubulin α subjected to the electric field of frequency 40 GHz, Batch 3	279
10.125	RMSF _{diff} of the residues of the tubulin α subjected to the electric field of frequency 50 GHz, Batch 3	280
10.126	RMSF _{diff} of the residues of the tubulin α subjected to the electric field of frequency 60 GHz, Batch 3	280
10.127	RMSF _{diff} of the residues of the tubulin α subjected to the electric field of frequency 70 GHz, Batch 3	281
10.128	RMSF _{diff} of the residues of the tubulin α subjected to the electric field of frequency 80 GHz, Batch 3	281
10.129	RMSF _{diff} of the residues of the tubulin α subjected to the electric field of frequency 90 GHz, Batch 3	282

10.130	RMSF _{diff} of the residues of the tubulin α subjected to the electric field of frequency 100 GHz, Batch 3	282
10.131	RMSF _{diff} of the residues of the tubulin α subjected to the electric field of frequency 110 GHz, Batch 3	283
10.132	RMSF _{diff} of the residues of the tubulin α subjected to the electric field of frequency 120 GHz, Batch 3	283
10.133	RMSF _{diff} of the residues of the tubulin α subjected to the electric field of frequency 130 GHz, Batch 3	284
10.134	RMSF _{diff} of the residues of the tubulin α subjected to the electric field of frequency 140 GHz, Batch 3	284
10.135	RMSF _{diff} of the residues of the tubulin α subjected to the electric field of frequency 150 GHz, Batch 3	285
10.136	RMSF _{diff} of the residues of the tubulin β subjected to the electric field of frequency 10 GHz, Batch 1	285
10.137	RMSF _{diff} of the residues of the tubulin β subjected to the electric field of frequency 20 GHz, Batch 1	286
10.138	RMSF _{diff} of the residues of the tubulin β subjected to the electric field of frequency 30 GHz, Batch 1	286
10.139	RMSF _{diff} of the residues of the tubulin β subjected to the electric field of frequency 40 GHz, Batch 1	287
10.140	RMSF _{diff} of the residues of the tubulin β subjected to the electric field of frequency 50 GHz, Batch 1	287
10.141	RMSF _{diff} of the residues of the tubulin β subjected to the electric field of frequency 60 GHz, Batch 1	288
10.142	RMSF _{diff} of the residues of the tubulin β subjected to the electric field of frequency 70 GHz, Batch 1	288
10.143	RMSF _{diff} of the residues of the tubulin β subjected to the electric field of frequency 80 GHz, Batch 1	289
10.144	RMSF _{diff} of the residues of the tubulin β subjected to the electric field of frequency 90 GHz, Batch 1	289
10.145	RMSF _{diff} of the residues of the tubulin β subjected to the electric field of frequency 100 GHz, Batch 1	290
10.146	RMSF _{diff} of the residues of the tubulin β subjected to the electric field of frequency 110 GHz, Batch 1	290
10.147	RMSF _{diff} of the residues of the tubulin β subjected to the electric field of frequency 120 GHz, Batch 1	291
10.148	RMSF _{diff} of the residues of the tubulin β subjected to the electric field of frequency 130 GHz, Batch 1	291
10.149	RMSF _{diff} of the residues of the tubulin β subjected to the electric field of frequency 140 GHz, Batch 1	292
10.150	RMSF _{diff} of the residues of the tubulin β subjected to the electric field of frequency 150 GHz, Batch 1	292
10.151	RMSF _{diff} of the residues of the tubulin β subjected to the electric field of frequency 10 GHz, Batch 2	293
10.152	RMSF _{diff} of the residues of the tubulin β subjected to the electric field of frequency 20 GHz, Batch 2	293
10.153	RMSF _{diff} of the residues of the tubulin β subjected to the electric field of frequency 30 GHz, Batch 2	294

10.154	RMSF _{diff} of the residues of the tubulin β subjected to the electric field of frequency 40 GHz, Batch 2	294
10.155	RMSF _{diff} of the residues of the tubulin β subjected to the electric field of frequency 50 GHz, Batch 2	295
10.156	RMSF _{diff} of the residues of the tubulin β subjected to the electric field of frequency 60 GHz, Batch 2	295
10.157	RMSF _{diff} of the residues of the tubulin β subjected to the electric field of frequency 70 GHz, Batch 2	296
10.158	RMSF _{diff} of the residues of the tubulin β subjected to the electric field of frequency 80 GHz, Batch 2	296
10.159	RMSF _{diff} of the residues of the tubulin β subjected to the electric field of frequency 90 GHz, Batch 2	297
10.160	RMSF _{diff} of the residues of the tubulin β subjected to the electric field of frequency 100 GHz, Batch 2	297
10.161	RMSF _{diff} of the residues of the tubulin β subjected to the electric field of frequency 110 GHz, Batch 2	298
10.162	RMSF _{diff} of the residues of the tubulin β subjected to the electric field of frequency 120 GHz, Batch 2	298
10.163	RMSF _{diff} of the residues of the tubulin β subjected to the electric field of frequency 130 GHz, Batch 2	299
10.164	RMSF _{diff} of the residues of the tubulin β subjected to the electric field of frequency 140 GHz, Batch 2	299
10.165	RMSF _{diff} of the residues of the tubulin β subjected to the electric field of frequency 150 GHz, Batch 2	300
10.166	RMSF _{diff} of the residues of the tubulin β subjected to the electric field of frequency 10 GHz, Batch 3	300
10.167	RMSF _{diff} of the residues of the tubulin β subjected to the electric field of frequency 20 GHz, Batch 3	301
10.168	RMSF _{diff} of the residues of the tubulin β subjected to the electric field of frequency 30 GHz, Batch 3	301
10.169	RMSF _{diff} of the residues of the tubulin β subjected to the electric field of frequency 40 GHz, Batch 3	302
10.170	RMSF _{diff} of the residues of the tubulin β subjected to the electric field of frequency 50 GHz, Batch 3	302
10.171	RMSF _{diff} of the residues of the tubulin β subjected to the electric field of frequency 60 GHz, Batch 3	303
10.172	RMSF _{diff} of the residues of the tubulin β subjected to the electric field of frequency 70 GHz, Batch 3	303
10.173	RMSF _{diff} of the residues of the tubulin β subjected to the electric field of frequency 80 GHz, Batch 3	304
10.174	RMSF _{diff} of the residues of the tubulin β subjected to the electric field of frequency 90 GHz, Batch 3	304
10.175	RMSF _{diff} of the residues of the tubulin β subjected to the electric field of frequency 100 GHz, Batch 3	305
10.176	RMSF _{diff} of the residues of the tubulin β subjected to the electric field of frequency 110 GHz, Batch 3	305
10.177	RMSF _{diff} of the residues of the tubulin β subjected to the electric field of frequency 120 GHz, Batch 3	306

10.178	RMSF _{diff} of the residues of the tubulin β subjected to the electric field of frequency 130 GHz, Batch 3	306
10.179	RMSF _{diff} of the residues of the tubulin β subjected to the electric field of frequency 140 GHz, Batch 3	307
10.180	RMSF _{diff} of the residues of the tubulin β subjected to the electric field of frequency 150 GHz, Batch 3	307
10.181	Average of RMSF _{diff} of the residues of the α tubulin subjected to the electric field of frequency 10 GHz	308
10.182	Average of RMSF _{diff} of the residues of the α tubulin subjected to the electric field of frequency 20 GHz	308
10.183	Average of RMSF _{diff} of the residues of the α tubulin subjected to the electric field of frequency 30 GHz	309
10.184	Average of RMSF _{diff} of the residues of the α tubulin subjected to the electric field of frequency 40 GHz	309
10.185	Average of RMSF _{diff} of the residues of the α tubulin subjected to the electric field of frequency 50 GHz	310
10.186	Average of RMSF _{diff} of the residues of the α tubulin subjected to the electric field of frequency 60 GHz	310
10.187	Average of RMSF _{diff} of the residues of the α tubulin subjected to the electric field of frequency 70 GHz	311
10.188	Average of RMSF _{diff} of the residues of the α tubulin subjected to the electric field of frequency 80 GHz	311
10.189	Average of RMSF _{diff} of the residues of the α tubulin subjected to the electric field of frequency 90 GHz	312
10.190	Average of RMSF _{diff} of the residues of the α tubulin subjected to the electric field of frequency 100 GHz	312
10.191	Average of RMSF _{diff} of the residues of the α tubulin subjected to the electric field of frequency 110 GHz	313
10.192	Average of RMSF _{diff} of the residues of the α tubulin subjected to the electric field of frequency 120 GHz	313
10.193	Average of RMSF _{diff} of the residues of the α tubulin subjected to the electric field of frequency 130 GHz	314
10.194	Average of RMSF _{diff} of the residues of the α tubulin subjected to the electric field of frequency 140 GHz	314
10.195	Average of RMSF _{diff} of the residues of the α tubulin subjected to the electric field of frequency 150 GHz	315
10.196	Average of RMSF _{diff} of the residues of the β tubulin subjected to the electric field of frequency 10 GHz	315
10.197	Average of RMSF _{diff} of the residues of the β tubulin subjected to the electric field of frequency 20 GHz	316
10.198	Average of RMSF _{diff} of the residues of the β tubulin subjected to the electric field of frequency 30 GHz	316
10.199	Average of RMSF _{diff} of the residues of the β tubulin subjected to the electric field of frequency 40 GHz	317
10.200	Average of RMSF _{diff} of the residues of the β tubulin subjected to the electric field of frequency 50 GHz	317
10.201	Average of RMSF _{diff} of the residues of the β tubulin subjected to the electric field of frequency 60 GHz	318

10.202	Average of $\text{RMSF}_{\text{diff}}$ of the residues of the β tubulin subjected to the electric field of frequency 70 GHz	318
10.203	Average of $\text{RMSF}_{\text{diff}}$ of the residues of the β tubulin subjected to the electric field of frequency 80 GHz	319
10.204	Average of $\text{RMSF}_{\text{diff}}$ of the residues of the β tubulin subjected to the electric field of frequency 90 GHz	319
10.205	Average of $\text{RMSF}_{\text{diff}}$ of the residues of the β tubulin subjected to the electric field of frequency 100 GHz	320
10.206	Average of $\text{RMSF}_{\text{diff}}$ of the residues of the β tubulin subjected to the electric field of frequency 110 GHz	320
10.207	Average of $\text{RMSF}_{\text{diff}}$ of the residues of the β tubulin subjected to the electric field of frequency 120 GHz	321
10.208	Average of $\text{RMSF}_{\text{diff}}$ of the residues of the β tubulin subjected to the electric field of frequency 130 GHz	321
10.209	Average of $\text{RMSF}_{\text{diff}}$ of the residues of the β tubulin subjected to the electric field of frequency 140 GHz	322
10.210	Average of $\text{RMSF}_{\text{diff}}$ of the residues of the β tubulin subjected to the electric field of frequency 150 GHz	322
10.211	$\text{RMSF}_{\text{diff}}$ difference graphs of tubulin α with 10 GHz EF - averaged over batches	324
10.212	$\text{RMSF}_{\text{diff}}$ difference graphs of tubulin α with 20 GHz EF - averaged over batches	325
10.213	$\text{RMSF}_{\text{diff}}$ difference graphs of tubulin α with 30 GHz EF - averaged over batches	326
10.214	$\text{RMSF}_{\text{diff}}$ difference graphs of tubulin α with 40 GHz EF - averaged over batches	327
10.215	$\text{RMSF}_{\text{diff}}$ difference graphs of tubulin α with 50 GHz EF - averaged over batches	328
10.216	$\text{RMSF}_{\text{diff}}$ difference graphs of tubulin α with 60 GHz EF - averaged over batches	329
10.217	$\text{RMSF}_{\text{diff}}$ difference graphs of tubulin α with 70 GHz EF - averaged over batches	330
10.218	$\text{RMSF}_{\text{diff}}$ difference graphs of tubulin α with 80 GHz EF - averaged over batches	331
10.219	$\text{RMSF}_{\text{diff}}$ difference graphs of tubulin α with 90 GHz EF - averaged over batches	332
10.220	$\text{RMSF}_{\text{diff}}$ difference graphs of tubulin α with 100 GHz EF - averaged over batches	333
10.221	$\text{RMSF}_{\text{diff}}$ difference graphs of tubulin α with 110 GHz EF - averaged over batches	334
10.222	$\text{RMSF}_{\text{diff}}$ difference graphs of tubulin α with 120 GHz EF - averaged over batches	335
10.223	$\text{RMSF}_{\text{diff}}$ difference graphs of tubulin α with 130 GHz EF - averaged over batches	336
10.224	$\text{RMSF}_{\text{diff}}$ difference graphs of tubulin α with 140 GHz EF - averaged over batches	337
10.225	$\text{RMSF}_{\text{diff}}$ difference graphs of tubulin α with 150 GHz EF - averaged over batches	338

10.22	5	RMSF _{diff} difference graphs of tubulin β with 10 GHz EF - averaged over batches	339
10.22	7	RMSF _{diff} difference graphs of tubulin β with 20 GHz EF - averaged over batches	340
10.22	8	RMSF _{diff} difference graphs of tubulin β with 30 GHz EF - averaged over batches	341
10.22	9	RMSF _{diff} difference graphs of tubulin β with 40 GHz EF - averaged over batches	342
10.23	0	RMSF _{diff} difference graphs of tubulin β with 50 GHz EF - averaged over batches	343
10.23	1	RMSF _{diff} difference graphs of tubulin β with 60 GHz EF - averaged over batches	344
10.23	2	RMSF _{diff} difference graphs of tubulin β with 70 GHz EF - averaged over batches	345
10.23	3	RMSF _{diff} difference graphs of tubulin β with 80 GHz EF - averaged over batches	346
10.23	4	RMSF _{diff} difference graphs of tubulin β with 90 GHz EF - averaged over batches	347
10.23	5	RMSF _{diff} difference graphs of tubulin β with 100 GHz EF - averaged over batches	348
10.23	6	RMSF _{diff} difference graphs of tubulin β with 110 GHz EF - averaged over batches	349
10.23	7	RMSF _{diff} difference graphs of tubulin β with 120 GHz EF - averaged over batches	350
10.23	8	RMSF _{diff} difference graphs of tubulin β with 130 GHz EF - averaged over batches	351
10.23	9	RMSF _{diff} difference graphs of tubulin β with 140 GHz EF - averaged over batches	352
10.24	0	RMSF _{diff} difference graphs of tubulin β with 150 GHz EF - averaged over batches	353
10.24	1	RMSF of residue 177 of tubulin beta - different directions and batches; the bars for 0 GHz mean that no EF is applied	354
10.24	2	RMSF of residue 177 of tubulin beta - averaged over directions and batches; the bars for 0 GHz mean that no EF is applied	354
10.24	3	RMSF of residue 208 of tubulin beta - different directions and batches; the bars for 0 GHz mean that no EF is applied	355
10.24	4	RMSF of residue 208 of tubulin beta - averaged over directions and batches; the bars for 0 GHz mean that no EF is applied	355
10.24	5	RMSF of residue 212 of tubulin beta - different directions and batches; the bars for 0 GHz mean that no EF is applied	356
10.24	6	RMSF of residue 212 of tubulin beta - averaged over directions and batches; the bars for 0 GHz mean that no EF is applied	356
10.24	7	RMSF of residue 225 of tubulin beta - different directions and batches; the bars for 0 GHz mean that no EF is applied	357
10.24	8	RMSF of residue 225 of tubulin beta - averaged over directions and batches; the bars for 0 GHz mean that no EF is applied	357
10.24	9	RMSF of residue 178 of tubulin alpha - different directions and batches; the bars for 0 GHz mean that no EF is applied	358

10.250	RMSF of residue 178 of tubulin alpha - averaged over directions and batches; the bars for 0 GHz mean that no EF is applied	358
10.251	RMSF of residue 179 of tubulin alpha - different directions and batches; the bars for 0 GHz mean that no EF is applied	359
10.252	RMSF of residue 179 of tubulin alpha - averaged over directions and batches; the bars for 0 GHz mean that no EF is applied	359
10.253	RMSF of residue 239 of tubulin beta - different directions and batches; the bars for 0 GHz mean that no EF is applied	360
10.254	RMSF of residue 239 of tubulin beta - averaged over directions and batches; the bars for 0 GHz mean that no EF is applied	360
10.255	RMSF of residue 313 of tubulin beta - different directions and batches; the bars for 0 GHz mean that no EF is applied	361
10.256	RMSF of residue 313 of tubulin beta - averaged over directions and batches; the bars for 0 GHz mean that no EF is applied	361
10.257	RMSF of residue 350 of tubulin beta - different directions and batches; the bars for 0 GHz mean that no EF is applied	362
10.258	RMSF of residue 350 of tubulin beta - averaged over directions and batches; the bars for 0 GHz mean that no EF is applied	362
10.259	RMSF of residue 23 of tubulin beta - different directions and batches; the bars for 0 GHz mean that no EF is applied	363
10.260	RMSF of residue 23 of tubulin beta - averaged over directions and batches; the bars for 0 GHz mean that no EF is applied	363
10.261	RMSF of residue 26 of tubulin beta - different directions and batches; the bars for 0 GHz mean that no EF is applied	364
10.262	RMSF of residue 26 of tubulin beta - averaged over directions and batches; the bars for 0 GHz mean that no EF is applied	364
10.263	RMSF of residue 27 of tubulin beta - different directions and batches; the bars for 0 GHz mean that no EF is applied	365
10.264	RMSF of residue 27 of tubulin beta - averaged over directions and batches; the bars for 0 GHz mean that no EF is applied	365
10.265	RMSF of residue 231 of tubulin beta - different directions and batches; the bars for 0 GHz mean that no EF is applied	366
10.266	RMSF of residue 231 of tubulin beta - averaged over directions and batches; the bars for 0 GHz mean that no EF is applied	366
10.267	RMSF of residue 234 of tubulin beta - different directions and batches; the bars for 0 GHz mean that no EF is applied	367
10.268	RMSF of residue 234 of tubulin beta - averaged over directions and batches; the bars for 0 GHz mean that no EF is applied	367
10.269	RMSF of residue 270 of tubulin beta - different directions and batches; the bars for 0 GHz mean that no EF is applied	368
10.270	RMSF of residue 270 of tubulin beta - averaged over directions and batches; the bars for 0 GHz mean that no EF is applied	368
10.271	RMSF of residue 273 of tubulin beta - different directions and batches; the bars for 0 GHz mean that no EF is applied	369
10.272	RMSF of residue 273 of tubulin beta - averaged over directions and batches; the bars for 0 GHz mean that no EF is applied	369
10.273	Time spent approximately parallel to the electric field direction of oscillation - batch 2, direction 1	371

10.274	Time spent approximately parallel to the electric field direction of oscillation - batch 2, direction 2	371
10.275	Time spent approximately parallel to the electric field direction of oscillation - batch 2, direction 3	372
10.276	Time spent approximately parallel to the electric field direction of oscillation - batch 2, direction 4	372
10.277	Time spent approximately parallel to the electric field direction of oscillation - batch 2, direction 5	373
10.278	Time spent approximately parallel to the electric field direction of oscillation - batch 2, direction 6	373
10.279	Time spent approximately parallel to the electric field direction of oscillation - batch 3, direction 1	374
10.280	Time spent approximately parallel to the electric field direction of oscillation - batch 3, direction 2	374
10.281	Time spent approximately parallel to the electric field direction of oscillation - batch 3, direction 3	375
10.282	Time spent approximately parallel to the electric field direction of oscillation - batch 3, direction 4	375
10.283	Time spent approximately parallel to the electric field direction of oscillation - batch 3, direction 5	376
10.284	Time spent approximately parallel to the electric field direction of oscillation - batch 3, direction 6	376
10.285	Magnitude of the dipole moment of tubulin heterodimer - time series and distributions - batch 2, Frequencies 10-50 GHz	377
10.286	Magnitude of the dipole moment of tubulin heterodimer - time series and distributions - batch 2, Frequencies 60-100 GHz	378
10.287	Magnitude of the dipole moment of tubulin heterodimer - time series and distributions - batch 2, Frequencies 110-150 GHz	379
10.288	Magnitude of the dipole moment of tubulin heterodimer - time series and distributions - batch 3, Frequencies 10-50 GHz	380
10.289	Magnitude of the dipole moment of tubulin heterodimer - time series and distributions - batch 3, Frequencies 60-100 GHz	381
10.290	Magnitude of the dipole moment of tubulin heterodimer - time series and distributions - batch 3, Frequencies 110-150 GHz	382
10.291	Time series and distributions of the projection of dipole moment of tubulin dimer onto the axis of electric field oscillations - batch 2, Frequencies 10-50 GHz	383
10.292	Time series and distributions of the projection of dipole moment of tubulin dimer onto the axis of electric field oscillations - batch 2, Frequencies 60-100 GHz	384
10.293	Time series and distributions of the projection of dipole moment of tubulin dimer onto the axis of electric field oscillations - batch 2, Frequencies 110-150 GHz	385
10.294	Time series and distributions of the projection of dipole moment of tubulin dimer onto the axis of electric field oscillations - batch 3, Frequencies 10-50 GHz	386

10.293	Time series and distributions of the projection of dipole moment of tubulin dimer onto the axis of electric field oscillations - batch 3, Frequencies 60-100 GHz	387
10.296	Time series and distributions of the projection of dipole moment of tubulin dimer onto the axis of electric field oscillations - batch 3, Frequencies 110-150 GHz	388

List of Tables

6.1	Values reached in the minimization step by the steepest descent algorithm in 10427 steps	47
6.2	Values reached in the minimization step by the conjugate gradient algorithm in 1143 steps	47

10. Appendix

10.1 Input parameter files

10.1.1 Energy Minimization parameter files

Steepest descent algorithm

```
integrator = steep          ; Algorithm (steep = steepest descent
minimization)
emtol      = 100.0         ; Stop minimization when the maximum force <
1000.0 kJ/mol/nm
emstep     = 0.01         ; Minimization step size
nsteps     = 500000       ; Maximum number of (minimization) steps to
perform

nstlist    = 10           ; Frequency to update the neighbor list and
long range forces
cutoff-scheme = Verlet    ; Buffered neighbor searching
ns_type     = grid        ; Method to determine neighbor list (simple,
grid)
coulombtype = PME         ; Treatment of long range electrostatic
interactions
rcoulomb    = 1.0         ; Short-range electrostatic cut-off
rvdw        = 1.0         ; Short-range Van der Waals cut-off
ewald-rtol  = 1e-5
fourierspacing = 0.12
pme-order   = 4
pbc         = xyz         ; Periodic Boundary Conditions in all 3
dimensions
```

Conjugate gradient algorithm

```
integrator = cg
emtol      = 10.0         ; Stop minimization when the maximum force < 10.0
kJ/mol/nm
emstep     = 0.01         ; Minimization step size
nsteps     = 500000       ; Maximum number of (minimization) steps to
perform
define     = -DFLEXIBLE

nstlist    = 10           ; Frequency to update the neighbor list and
long range forces
cutoff-scheme = Verlet    ; Buffered neighbor searching
ns_type     = grid        ; Method to determine neighbor list (simple,
grid)
coulombtype = PME         ; Treatment of long range electrostatic
```

```

interactions
rcoulomb      = 1.0      ; Short-range electrostatic cut-off
rvdw          = 1.0      ; Short-range Van der Waals cut-off
ewald-rtol    = 1e-5
fourierspacing = 0.12
pme-order     = 4
pbc           = xyz      ; Periodic Boundary Conditions in all 3
dimensions

```

10.1.2 NVT solvent equilibration parameter file

Run input file nvt.tpr generated from this parameter nvt.mdp file by the following command line:

```

gmx_21.3gpu grompp -f nvt.mdp -c min_CG_emptol10.gro
-p topol.top -r min_CG_emptol10.gro -o nvt.tpr -po min2nvt.mdp

```

The position of tubulin is restrained here in nvt.mdp:

```

title                = TubulinDimerEquilibration

define               = -DPOSRES ; position restrain the protein

; Run parameters

integrator           = md        ; Leap-frog
nsteps               = 500000    ; 2 * 50000 = 1 ns
dt                   = 0.002     ; 2 fs

; Output control

nstxout              = 5000      ; save coordinates every 10.0 ps
nstvout              = 5000      ; save velocities every 10.0 ps
nstenergy            = 5000      ; save energies every 10.0 ps
nstlog               = 5000      ; update log file every 10.0 ps

; Bond parameters

continuation         = no        ; first dynamics run
constraint_algorithm = lincs     ; holonomic constraints
constraints          = h-bonds   ; bonds involving H are constrained
lincs_iter           = 1        ; accuracy of LINCS
lincs_order          = 4        ; also related to accuracy

; Nonbonded settings

cutoff-scheme        = Verlet    ; Buffered neighbor searching
ns_type              = grid      ; search neighboring grid cells
nstlist              = 10       ; 20 fs, largely irrelevant with Verlet

; Coulomb

coulombtype = PME

```

```

rcoulomb          = 1.2          ; short-range electrostatic cutoff (in
nm)
pme_order = 4
fourierspacing = 0.12

; van der Waals

vdwtype = cutoff
vdw-modifier = force-switch
rvdw = 1.2
rvdw-switch = 1.0
DispCorr          = no          ; account for cut-off vdW scheme

; Temperature coupling is on

nsttcouple = 1
tcoupl           = V-rescale      ; modified Berendsen
thermostat
tc-grps          = Protein Non-Protein ; two coupling groups - more
accurate
tau_t            = 0.1          0.1          ; time constant, in ps
ref_t            = 300          300          ; reference temperature, one
for each group, in K

; Pressure coupling is off

pcoupl           = no            ; no pressure coupling in NVT

; Periodic boundary conditions

pbc              = xyz           ; 3-D PBC

; Velocity generation

gen_vel          = yes           ; assign velocities from Maxwell distribution
gen_temp         = 300           ; temperature for Maxwell
distribution
gen_seed         = -1            ; generate a random seed

```

10.1.3 NPT solvent equilibration parameter file

By the use of the parameter file and command line below, run input file npt.tpr was generated.

```

gmx_21.3gpu grompp -f npt_Nika_2.mdp -c nvt.gro -r nvt.gro
-t nvt.cpt -p topol.top -o npt.tpr -po nvt2npt.mdp -pp 2npt.top

```

The position of tubulin is restrained here:

```

title           = NPT equilibration
define          = -DPOSRES      ; position restrain the protein

; Run parameters
integrator      = md            ; leap-frog
nsteps         = 500000         ; 2 * 50000 = 1 ns
dt             = 0.002          ; 2 fs

```

```

; Output control

nstxout          = 5000      ; save coordinates every 10 ps
nstvout          = 5000      ; save velocities every 10 ps
nstenergy        = 5000      ; save energies every 10 ps
nstlog           = 5000      ; update log file every 10 ps

; Bond parameters

continuation     = yes       ; Restarting after NVT
constraint_algorithm = lincs  ; holonomic constraints
constraints      = h-bonds   ; bonds involving H are constrained
lincs_iter       = 1         ; accuracy of LINCS
lincs_order      = 4         ; also related to accuracy

; Nonbonded settings

cutoff-scheme    = Verlet    ; Buffered neighbor searching
ns_type          = grid      ; search neighboring grid cells
nstlist          = 10        ; 20 fs, largely irrelevant with
Verlet scheme

;Coulomb

rcoulomb         = 1.2       ; short-range electrostatic cutoff
(in nm)
coulombtype      = PME       ; Particle Mesh Ewald for long-range
electrostatics
pme_order        = 4         ; cubic interpolation
fourierspacing   = 0.12     ; grid spacing for FFT

; vdW

vdwtype = cutoff
vdw-modifier = force-switch
rvdw = 1.2
rvdw-switch = 1.0
DispCorr = no

; Temperature coupling is on

tcoupl           = Nose-Hoover
tc-grps          = Protein Non-Protein ; two coupling groups -
more accurate
tau_t            = 0.4      0.4      ; time constant, in ps
ref_t            = 300      300      ; reference temperature,
one for each group, in K

; Pressure coupling is on

pcoupl           = C-rescale ; Pressure coupling on in NPT
pcoupltype       = isotropic ; uniform scaling of box
vectors
tau_p            = 2.0      ; time constant, in ps
ref_p            = 1.0      ; reference pressure, in bar
compressibility   = 4.5e-5   ; isothermal compressibility
of water, bar^-1

```

```

refcoord_scaling      = com
; Periodic boundary conditions
pbc                   = xyz           ; 3-D PBC
; Velocity generation
gen_vel               = no           ; Velocity generation is off

```

10.1.4 NPT - equilibration of unrestrained protein

We have used the following command to get the run input file `prot_eq.tpr` that is shown below:

```

gmx_21.3gpu grompp -f prot_eq.mdp -c npt.gro -t npt.cpt -p topol.top
-o prot_eq_4.tpr -po npt2proteq.mdp

```

```

title                 = NPT

; Run parameters
integrator            = md           ; leap-frog
nsteps               = 50000000     ; 2 * 5000000 = 100 ns
dt                   = 0.002       ; 2 fs

; Output control
nstxout              = 5000         ; save coordinates every 10 ps
nstvout              = 5000         ; save velocities every 10 ps
nstenergy            = 5000         ; save energies every 10 ps
nstlog               = 5000         ; update log file every 10 ps

; Bond parameters
continuation         = yes          ; Restarting after NVT
constraint_algorithm = lincs        ; holonomic constraints
constraints          = h-bonds      ; bonds involving H are constrained
lincs_iter           = 1            ; accuracy of LINCS
lincs_order          = 4            ; also related to accuracy

; Nonbonded settings
cutoff-scheme        = Verlet       ; Buffered neighbor searching
ns_type              = grid         ; search neighboring grid cells
nstlist              = 10           ; 20 fs, largely irrelevant with Verlet
scheme

;Coulomb
rcoulomb             = 1.2          ; short-range electrostatic cutoff (in
nm)
coulombtype          = PME          ; Particle Mesh Ewald for long-range
electrostatics
pme_order            = 4            ; cubic interpolation
fourierspacing       = 0.12        ; grid spacing for FFT

; vdW
vdwtype = cutoff
vdw-modifier = force-switch

```

```

rvdw = 1.2
rvdw-switch = 1.0
DispCorr = no

; Temperature coupling is on

tcoupl          = Nose-Hoover
tc-grps         = Protein Non-Protein ; two coupling groups - more
accurate
tau_t           = 0.4    0.4          ; time constant, in ps
ref_t           = 300    300          ; reference temperature, one
for each group, in K

; Pressure coupling is on

pcoupl          = Parrinello-Rahman ; Pressure coupling on in NPT
pcoupltype     = isotropic          ; uniform scaling of box
vectors
tau_p           = 2.0              ; time constant, in ps
ref_p           = 1.0              ; reference pressure, in bar
compressibility = 4.5e-5           ; isothermal compressibility
of water, bar^-1
refcoord_scaling = com
; Periodic boundary conditions
pbc             = xyz              ; 3-D PBC
; Velocity generation
gen_vel         = no              ; Velocity generation is off

```

10.1.5 Simulation with electric field

Here we provide an example of the parameter file for the simulation with an electric field. For different batch and different direction of electric field oscillation, the parameters for the electric field must be of course changed. In the next section ?? we have written a new code that calculates the correct electric field direction. Bash script that automatizes the rewriting process in mdp file was written. Here is the mdp file example:

```

          title                = Production run
; Run parameters
integrator      = md          ; leap-frog integrator
nsteps         = 50000000    ; 2 * 50000000 = 100000 ps (100 ns)
dt             = 0.002      ; 2 fs
; Output control
nstxout        = 500         ; suppress bulky .trr file by
specifying
nstvout        = 500         ; 0 for output frequency of nstxout,
nstfout        = 500         ; nstvout, and nstfout
nstenergy      = 500         ; save energies every 10.0 ps
nstlog         = 50000       ; update log file every 100.0 ps
nstxout-compressed = 5000    ; save compressed coordinates every 10.0
ps
compressed-x-grps = System   ; save the whole system
; Bond parameters
continuation    = yes        ; Restarting after NPT

```

```

constraint_algorithm = lincs      ; holonomic constraints
constraints          = h-bonds    ; bonds involving H are constrained
lincs_iter          = 1          ; accuracy of LINCS
lincs_order         = 4          ; also related to accuracy
; Neighborsearching
cutoff-scheme       = Verlet     ; Buffered neighbor searching
ns_type             = grid       ; search neighboring grid cells
nstlist             = 10        ; 20 fs, largely irrelevant with Verlet scheme
; Electrostatics
coulombtype         = PME        ; Particle Mesh Ewald for long-range
electrostatics
rcoulomb = 1.2
vdw-type = cutoff
vdw-modifier = force-switch
rvdw = 1.2
rvdw-switch = 1.0
pme_order           = 4          ; cubic interpolation
fourierspacing      = 0.12      ; grid spacing for FFT
; Temperature coupling is on
tcoupl              = nose-hoover
tc-grps             = Protein Non-Protein ; two coupling groups - more
accurate
tau_t               = 0.5        0.5          ; time constant, in ps
ref_t               = 300        300          ; reference temperature, one
for each group, in K
; Pressure coupling is on
pcoupl              = Parrinello-Rahman ; Pressure coupling on in NPT
pcoupltype          = isotropic    ; uniform scaling of box
vectors
tau_p               = 2.0        ; time constant, in ps
ref_p               = 1.0        ; reference pressure, in bar
compressibility      = 4.5e-5     ; isothermal compressibility
of water, bar^-1
; Periodic boundary conditions
pbc                 = xyz        ; 3-D PBC
; Dispersion correction
DispCorr            = no         ; account for cut-off vdW scheme
; Velocity generation
gen_vel             = no         ; Velocity generation is off

;Electric Field

electric-field-x     = -0.0843623 0.376991 0 0
electric-field-y     = 0.0439523 0.376991 0 0
electric-field-z     = -0.0308414 0.376991 0 0

```

10.2 Rotation of icosahedron vertices - program

```

import numpy as np
import matplotlib.pyplot as plt
import MDAnalysis

from math import acos
from math import sqrt
from math import pi

```

```

from random import random
import os
cwd = os.getcwd()

#-----ICOSAHEDRON-VERTICES-----#

def generate_icosahedron_vertices():

    phi_plus = (1 + 1/np.sqrt(5)) / 2
    phi_minus = (1 - 1/np.sqrt(5)) / 2
    vertices = np.array([
        [1, 0, 0],
        [1/np.sqrt(5), 2/np.sqrt(5), 0],
        [1/np.sqrt(5), phi_minus, np.sqrt(phi_plus)],
        [1/np.sqrt(5), phi_minus, -np.sqrt(phi_plus)],
        [1/np.sqrt(5), -phi_plus, np.sqrt(phi_minus)],
        [1/np.sqrt(5), -phi_plus, -np.sqrt(phi_minus)],
    ])
    vertices /= np.linalg.norm(vertices, axis=1, keepdims=True)

    return vertices

#-----COORDINATES-----#

def get_atom_coordinates(u, atom_index):

    atom = u.atoms[atom_index]
    atom_coords = atom.position

    return atom_coords

#-----CALCULATE-VECTOR-----#

def calculate_vector(atom1_coords, atom2_coords):

    return atom2_coords - atom1_coords

#-----ROTATION-AXIS-AND-ORIENTED-ANGLE-CALCULATION-----#

def calculate_angle_and_axis(tub1, tub2):

    #.....CROSS_and_DOT_product.....#

    cross_product = np.cross(tub1, tub2)
    dot_product = np.dot(tub1, tub2)

    #.....ROTATION_AXIS.....#
    if np.dot(ref_axis, cross_product) < 0:
        cross_product = -cross_product
    n = cross_product / np.linalg.norm(cross_product)

    #.....ORIENTED_ANGLE.....#

    theta = np.arctan2(np.linalg.norm(cross_product), dot_product)
    print('theta before:', theta)

```

```

    if np.dot(tub1, np.cross(tub2, cross_product)) < 0:
        theta = -theta
    print('theta after:', theta)

    return cross_product, dot_product, theta, n

def calculate_angle_and_axis2(tub1, tub2):

    #.....CROSS_and_DOT_product.....#

    cross_product = np.cross(tub1, tub2)
    dot_product = np.dot(tub1, tub2)

    #.....ROTATION_AXIS.....#

    n = cross_product / np.linalg.norm(cross_product)

    #.....ORIENTED_ANGLE.....#

    theta = np.arctan2(np.linalg.norm(cross_product), dot_product)
    print('theta before:', theta)
    if np.dot(tub1, np.cross(tub2, cross_product)) < 0:
        theta = -theta
    print('theta after:', theta)

    return cross_product, dot_product, theta, n

def rotate_vertex(vertex, angle, axis):
    cos_theta = np.cos(angle)
    sin_theta = np.sin(angle)
    rotated_vertex = vertex * cos_theta + np.cross(axis, vertex) * sin_theta + axis * np.dot

    return rotated_vertex

#-----LOAD-GROMACS-FILES-----#

gro_files = ['../Last_frames_proteq_for_analysis/prot_eq_1.gro',
             '../Last_frames_proteq_for_analysis/prot_eq_2.gro',
             '../Last_frames_proteq_for_analysis/prot_eq_3.gro',
             '../Last_frames_proteq_for_analysis/prot_eq_4.gro',
             '../Last_frames_proteq_for_analysis/prot_eq_5.gro',
             '../Last_frames_proteq_for_analysis/prot_eq_6.gro',
             '../Last_frames_proteq_for_analysis/prot_eq_8.gro'
            ]

xtc_files = ['../Last_frames_proteq_for_analysis/last_frame_prot_eq_1.xtc',
             '../Last_frames_proteq_for_analysis/last_frame_prot_eq_2.xtc',
             '../Last_frames_proteq_for_analysis/last_frame_prot_eq_3.xtc',
             '../Last_frames_proteq_for_analysis/last_frame_prot_eq_4.xtc',
             '../Last_frames_proteq_for_analysis/last_frame_prot_eq_5.xtc',
             '../Last_frames_proteq_for_analysis/last_frame_prot_eq_6.xtc',
             '../Last_frames_proteq_for_analysis/last_frame_prot_eq_8.xtc',
            ]

#-----INICIALIZATION_OF_THE_PROTEIN_AXIS_LIST-----#

```

```

protein_axis_list = []

#-----WHICH_ATOMS_MAKE_THE_AXIS_OF_PROTEIN?-----

atom_index_1 = 4828
atom_index_2 = 9002

atom_index_3 = 8000

#-----LOAD THE FRAMES-AND CALCULATE THE VECTOR-----

for traj_num, (xtc_file, gro_file) in enumerate(zip(xtc_files, gro_files), start=1):
    u = MDAnalysis.Universe(topology=gro_file, trajectory=xtc_file)

    frame_number = 0
    u.trajectory[frame_number]

    atom1_coords = get_atom_coordinates(u, atom_index_1)
    atom2_coords = get_atom_coordinates(u, atom_index_2)
    atom3_coords = get_atom_coordinates(u, atom_index_3)

    protein_axis = calculate_vector(atom1_coords, atom2_coords)

#-----Normalization of the vector - axis of tubulin-----

    protein_axis /= np.linalg.norm(protein_axis)

#-----SAVING OF PROTEIN AXES FOR ALL EQ-----

    protein_axis_list.append(protein_axis)

#-----PRINT IT-----

    print(f"Trajectory {traj_num}: Initial Protein Axis for the First Conformation:
    {protein_axis}")

#print(protein_axes_list)
#print(protein_axis_list[0])

#-----GENERATE_ICOSAHEDRON_VERTICES-----

icosahedron_vertices = generate_icosahedron_vertices()

#-----VERTICES_FOR_THE_FIRST_CONFORMATION-----

```

```

icosahedron_vertices_first_conformation = icosahedron_vertices

#-----INITIALIZE_ARRAYS-----
protein_axis_2_list = []
rotated_protein_axis_2_list = []

rotated_vertices = np.zeros((len(protein_axis_list),
len(icosahedron_vertices), 3))
rotated_vertices_2 = np.zeros((len(protein_axis_list),
len(rotated_vertices[1]), 3))

a_coord = np.zeros((len(protein_axis_list), 3))
v2 = np.zeros((len(protein_axis_list), 3))
p2 = np.zeros((len(protein_axis_list), 3))
dot_product_v2_p1 = np.zeros((7))

ang = np.zeros(len(protein_axis_list))
ax = np.zeros((len(protein_axis_list), 3))
cross = np.zeros((len(protein_axis_list), 3))
dot = np.zeros(len(protein_axis_list))
cross2 = np.zeros((len(protein_axis_list), 3))
dot2 = np.zeros(len(protein_axis_list))

#-----REFERENCE_AXIS-FIRST_CONFORMATION_AXIS-----

ref_axis = protein_axis_list[0]
a = 1

rotated_p_axis = np.zeros((len(protein_axis_list),3))
rotated_p2_axis = np.zeros((len(protein_axis_list),3))

kolme_list=[]

#-----CALCULATE_ROTATED_VERTICES-----

for i, p_axis in enumerate(protein_axis_list):
    cross[i], dot[i], angle, axis = calculate_angle_and_axis(ref_axis, p_axis)
    rotated_vertices[i] = np.array([rotate_vertex(vertex, angle, axis)
    for vertex in icosahedron_vertices])

#-----PO_TADETO_FUNKCNE_1_ROTACIA-----

    rotated_p_axis[i] = np.array([rotate_vertex(p_axis, -angle, axis)])

    a_coord[i] = atom1_coords + a*p_axis
    #point on the first axis
    v2[i] = calculate_vector(a_coord[i], atom3_coords)
    #vector starting at axis point and ends in 3rd point
    dot_product_v2_p1[i] = np.dot(protein_axis_list[i],v2[i])
    #dot product of this new vector with protein axis 1
    p2[i] = v2[i] - dot_product_v2_p1[i]*protein_axis_list[i]
    #calculation of protein axis 2 that is perpendicular to the first protein axis
    p2[i] /= np.linalg.norm(p2)
    #nomralization of the axis

```

```

kolme_list.append(np.dot(p2[i],protein_axis_list[i]))
#test if they are perpendicular
protein_axis_2_list.append(p2[i])
#list of the 2nd protein axes

rotated_p2_axis[i] = np.array([rotate_vertex(p2[i], -angle, axis)])
rotated_protein_axis_2_list.append(rotated_p2_axis[i])

#-----Save the angles and axes-----

    ang[i] = angle
    ax[i] = axis

#####PRINT#####
#   print('angle:',angle)
#   print('axis:',axis)

#-----PRINT KOLME P1 a P2?-----
for i, p_axis in enumerate(protein_axis_list):
    print('-----')
    print('p1:',protein_axis_list[i])
    print('p2:',protein_axis_2_list[i])
    print('angle between p1 and p2',kolme_list[i])

    print('-----')
#-----

print('cross1:',cross)
print('dot1:',dot)
print('rotated_vertices shape:',rotated_vertices.shape)
print('-----')
print('-----')
print('rotated_PROTEIN_AXIS_2:',rotated_protein_axis_2_list)
print('-----')
print('-----')
#####ENDPRINT#####

ref2_axis = protein_axis_2_list[0]
print('REFERENCE 2 AXIS:',ref2_axis)
print('rotated_vertices shape:', rotated_vertices.shape)
print('rotated_vertices_2 shape:', rotated_vertices_2.shape)
for i, p2_axis in enumerate(rotated_protein_axis_2_list):

    cross2, dot2, angle2, axis2 = calculate_angle_and_axis(ref2_axis,
rotated_protein_axis_2_list[i])
    print('axis2 between rotated vertices and p2 axis:',axis2)
    print(cross2.shape)
    print('cross2:',cross2)
    print('dot2:',dot2)
    #if cross2[1] < 0:
        #   angle2 = -angle2
    print('angle2 for rotated vertices and p2 axis:',angle2)
    rotated_vertices_2[i] = np.array([rotate_vertex(vertex2, angle2,
protein_axis_list[i]) for vertex2 in rotated_vertices[i]])

```

```

print('-----')
print('-----')
print('-----')
#print('TEST:'np.cross(
#-----PRINTING_THE_RESULTS-----

#print('angles:', ang)
#print('axes:', ax)
#print('rotated vertices:',rotated_vertices)

#print('completely rotated vertices:', rotated_vertices_2)

#-----CHECK IF IT WORKS-----

final=np.zeros((7,6))
dot_pr=np.zeros((6))

print('-----FINALLY ROTATED VERTICES - 1ST AXIS-----')
for i, p_axis in enumerate(protein_axis_list):
    #print(i,'st protein axis:', p_axis)
    #print('vertices-rotated:', rotated_vertices[i])
    for j, rotated_vertex in enumerate(rotated_vertices_2[i]):
        dot_pr[j] = np.dot(p_axis, rotated_vertex)
        print(dot_pr[j])
        final[i,j]=dot_pr[j]
print(final)
print('-----FINALLY ROTATED VERTICES - 2ND AXIS-----')
for i, p_axis in enumerate(protein_axis_2_list):
    for j, rotated_vertex in enumerate(rotated_vertices_2[i]):
        dot_pr[j] = np.dot(p_axis, rotated_vertex)
        print(dot_pr[j])
        final[i,j]=dot_pr[j]
print(final)

print(rotated_vertices_2)
rotated_vertices_2.shape

#-----INICIALIZATION OF ARRAYS FOR NORMALIZATION-----
norm_rot_vertices_final=np.zeros((rotated_vertices_2.shape[0],
rotated_vertices_2.shape[1],rotated_vertices_2.shape[2]))
#-----NORMALIZATION OF VERTICES-----

for i in range(rotated_vertices_2.shape[0]):
    for j in range(rotated_vertices_2.shape[1]):
        vertex_rotated = rotated_vertices_2[i, j, :]
        vertex_rotated /= np.linalg.norm(vertex_rotated)
        norm_rot_vertices_final[i,j,:] = vertex_rotated[:]

norm_rot_vertices_final.shape
print('Normalized rotated vertices:',norm_rot_vertices_final)
#-----AMPLITUDA EL POLA = 0.1V.m-1-----

EF = 0.1*norm_rot_vertices_final
print('Rotated directions of EF:', EF)

#-----PRINT TO TEXT FILE-----

```

```

for i in range(EF.shape[0]):
    slice = EF[i,:,:]
    filename = f"EFxyz_amplitudes_for_prot_eq{i}.txt"

    with open(filename, "w") as file:
        for row in slice:
            # Write each row as a comma-separated string
            row_str = " ".join(map(str, row))
            file.write(row_str + "\n")

```

10.3 Trajectory conversion script

```

#!/bin/bash
p=1
gmx=gmx
storage=/mnt/qnap/veronika/FF_CHARM_MORE_OUTPUT/Leapfrog${p}

for freq in {1..15};
do
    for d in {1..6};
    do
        NAME="${storage}/L${p}_${freq}_${d}/EF_freq${freq}
_in_dir${d}_after_prot_eq${p}"
        OUT="${storage}/L${p}_${freq}_${d}/EF_freq${freq}
_in_dir${d}_after_prot_eq${p}_NOWATER"
        NOWATER="${storage}/L${p}_${freq}_${d}/NOWATER"
        NOSOD="${storage}/L${p}_${freq}_${d}/NOSOD"

        echo "22" | ${gmx} trjconv -f ${NAME}.gro -s ${NAME}.gro -o
        ${OUT}.gro

        #spravi 20-tu index group
        ${gmx} make_ndx -f ${OUT}.gro -o $NOWATER.ndx << EOF
1 | 13 | 14|17|18
q
EOF

        echo "20" | ${gmx} trjconv -f ${OUT}.trr -s ${OUT}.gro -o ${OUT}
        _NOSOD.trr -n $NOWATER.ndx

        echo "20" | ${gmx} trjconv -f ${OUT}.gro -s ${OUT}.gro -o ${OUT}
        _NOSOD.gro -n $NOWATER.ndx

        echo "20" | ${gmx} convert-tpr -s ${NAME}.tpr -o ${OUT}
        _NOSOD.tpr -n $NOWATER.ndx

        ${gmx} make_ndx -f ${OUT}_NOSOD.gro -o $NOSOD.ndx << EOF
20
q
EOF
PROT_EQ=${storage}/prot_eq_1_NOWATER.tpr

#-----PBC WHOLE A CENTER-----

```

```

echo "0" | ${gmx} trjconv -f ${OUT}_NOSOD.trr -s ${PROT_EQ} -o
${OUT}_NOSOD-nj-prot_eq.trr -n $NOSOD.ndx -pbc nojump

echo "1 0" | ${gmx} trjconv -f ${OUT}_NOSOD-nj-prot_eq.trr -s
${PROT_EQ} -o ${OUT}_NOSOD-nj-center-prot_eq.trr -n $NOSOD.ndx -
pbc mol -center -ur compact

#-----1st frame DUMP from centered trajectory-----

${gmx} trjconv -f ${OUT}_NOSOD-nj-center-prot_eq.trr -o ${OUT}
_NOSOD-nj-center_1st_frame-prot_eq.trr -dump 0

#-----centered gro 1st frame-----

echo "0" | ${gmx} trjconv -f ${OUT}_NOSOD-nj-center_1st_frame-
prot_eq.trr -s ${OUT}_NOSOD.tpr -o ${OUT}_NOSOD-nj-
center_1st_frame-prot_eq.gro

#-----generation of centered tpr-----

${gmx} grompp -f /mnt/qnap/veronika/FF_CHARM_MORE_OUTPUT/
md_noEF.mdp -c ${OUT}_NOSOD-nj-center_1st_frame-prot_eq.gro -p
${storage}/topol_NOWATER_NOSOD.top -o ${OUT}_NOSOD-nj-
center_1st_frame-prot_eq.tpr -maxwarn 1

#-----ROTTRANS, TRANS FIT-----

echo "4 0" | ${gmx} trjconv -f ${OUT}_NOSOD-nj-prot_eq.trr -s
${OUT}_NOSOD-nj-center_1st_frame-prot_eq.tpr -o ${OUT}_NOSOD-nj-
rottrans.trr -n $NOSOD.ndx -fit rot+trans

echo "4 0" | ${gmx} trjconv -f ${OUT}_NOSOD-nj.trr -s ${OUT}
_NOSOD-wh-center_1st_frame.tpr -o ${OUT}_NOSOD-nj-
trans_1st_frame.trr -n $NOSOD.ndx -fit trans

done
done

```

10.4 Rotational analysis - Python script

Here we provide one of the Python scripts for rotational analysis:

```

import numpy as np
import matplotlib.pyplot as plt
import MDAnalysis as mda

from math import acos
from math import sqrt
from math import pi
from random import random
import os
os.getcwd()

```

```

atom_index_1 = 88
atom_index_2 = 7863

#-----COORDINATES-----#

def get_atom_coordinates(u, atom_index):

    atom = u.atoms[atom_index]
    atom_coords = atom.position

    return atom_coords

#-----CALCULATE-VECTOR-----#

def calculate_vector(atom1_coords, atom2_coords):

    return atom2_coords - atom1_coords

#-----ICOSAHEDRON-VERTICES-----#

def generate_icosahedron_vertices():

    phi_plus = (1 + 1/np.sqrt(5)) / 2
    phi_minus = (1 - 1/np.sqrt(5)) / 2
    vertices = np.array([
        [1, 0, 0],
        [1/np.sqrt(5), 2/np.sqrt(5), 0],
        [1/np.sqrt(5), phi_minus, np.sqrt(phi_plus)],
        [1/np.sqrt(5), phi_minus, -np.sqrt(phi_plus)],
        [1/np.sqrt(5), -phi_plus, np.sqrt(phi_minus)],
        [1/np.sqrt(5), -phi_plus, -np.sqrt(phi_minus)],
    ])
    vertices /= np.linalg.norm(vertices, axis=1, keepdims=True)

    return vertices

icos = np.zeros((7, 6, 3))

for p in range(7):
    file_name = f"./EFxyz_amplitudes_for_pr_eq{p+1}_new.txt"
    print(p)
    if p==0:
        icos[p,:,:]=generate_icosahedron_vertices()
    else:
        with open(file_name, 'r') as file:
            for d in range(6):
                line = file.readline().strip().split()
                for x in range(3):
                    icos[p, d, x] = float(line[x])*10

#-----LOAD THE FRAMES-AND CALCULATE THE VECTOR-----#
batches=3
p_range=range(batches)
f_range=range(15)
d_range=range(6)
x_range=range(3)

```

```

protein_axis = np.empty((100001,batches,15,6,3))
prot_axis_projection = np.empty((100001,batches,15,6))
cos = np.empty((100001,batches,15,6))
pa_norm = np.empty((100001,batches,15,6))

#for p in p_range:
p=2
for f in f_range:
    for d in d_range:
        print(f'starting freq:{f} dir:{d}')
        if p==0 or p==1:
            gro_file = f'./Leapfrog{p+1}/L{p+1}_{f+1}_{d+1}/EF_freq{f+1}
_in_dir{d+1}_after_prot_eq{p+1}_NOWATER_NOSOD-nj-
center_1st_frame-prot_eq.tpr'

            xtc_file = f'./Leapfrog{p+1}/L{p+1}_{f+1}_{d+1}/EF_freq{f+1}
_in_dir{d+1}_after_prot_eq{p+1}_NOWATER_NOSOD-nj-center-
all_from_trr.xtc'
        else:
            gro_file = f'/mnt/qnap2/Leapfrog{p+1}/L{p+1}_{f+1}_{d+1}/
EF_freq{f+1}_in_dir{d+1}_after_prot_eq{p+1}_NOWATER_NOSOD-nj-
center_1st_frame-prot_eq.tpr'

            xtc_file = f'/mnt/qnap2/Leapfrog{p+1}/L{p+1}_{f+1}_{d+1}/
EF_freq{f+1}_in_dir{d+1}_after_prot_eq{p+1}_NOWATER_NOSOD-nj-
center-all_from_trr.xtc'

        if not os.path.isfile(gro_file):
            print(f"File {gro_file} not found. Skipping...")
        else:
            u = mda.Universe(gro_file, xtc_file)
            for ts in u.trajectory:
                atom1_coords = get_atom_coordinates(u, atom_index_1)
                atom2_coords = get_atom_coordinates(u, atom_index_2)
                atom3_coords = get_atom_coordinates(u, atom_index_3)

                protein_axis[ts.frame,p,f,d,:] =
                calculate_vector(atom1_coords, atom2_coords)

                pa_norm[ts.frame,p,f,d] =
                np.linalg.norm(protein_axis[ts.frame,p,f,d,:])

                prot_axis_projection[ts.frame,p,f,d]=np.dot(icos[p,d,:],
                protein_axis[ts.frame, p, f, d, :])
                cos[ts.frame,p,f,d] =
                prot_axis_projection[ts.frame,p,f,d]/
                pa_norm[ts.frame,p,f,d]
            print(f'ending freq:{f} dir:{d}')

import numpy as np
p_range=range(batches)
f_range=range(15)
d_range=range(6)
x_range=range(3)
p=2
cos_file_path = f"cos_values_{p+1}_new.txt"

```

```

with open(cos_file_path, 'w') as file:
    file.write("time p f d cos")
    for f in f_range:
        for d in d_range:
            for ts in range(cos.shape[0]):
                cos_value = cos[ts, p, f, d]
                line = f"{ts} {p} {f} {d} {cos_value}\n"
                file.write(line)

import numpy as np

min_rad = 0.7
max_rad = 3.14-min_rad

angle_plus_min = min_rad
angle_plus_max = max_rad

angle_t = np.empty((100001,3,15,6))
oriented = np.empty((len(p_range), len(f_range), len(d_range)))
angle_t = np.arccos(cos)
for p in p_range:
    for f in f_range:
        for d in d_range:
            for t in range(100001):

                if (np.abs(angle_t[t,p,f,d]) <=
                    angle_plus_min) or (angle_minus_max <=
                    np.abs(angle_t[t,p,f,d])) :
                    oriented[p, f, d] += 1

```

10.5 Dipole moment analysis - Python script

Here is the example of one of the dipole moment analysis scripts

```

import numpy as np
import MDAnalysis as mda
import os

p_range=range(3)
f_range=range(15)
d_range=range(6)
x_range=range(3)

q = []
pdb = "partial_charges.pdb"
with open(pdb, "r") as pdb_file:
    lines= pdb_file.readlines()[4:-2]
    for line in lines:
        parts = line.split()
        if len(parts) == 12:
            q.append(float(parts[10]))

q_array = np.array(q)

```

```

print(q_array)

icos = np.zeros((7, 6, 3))

def generate_icosahedron_vertices():

    phi_plus = (1 + 1/np.sqrt(5)) / 2
    phi_minus = (1 - 1/np.sqrt(5)) / 2
    vertices = np.array([
        [1, 0, 0],
        [1/np.sqrt(5), 2/np.sqrt(5), 0],
        [1/np.sqrt(5), phi_minus, np.sqrt(phi_plus)],
        [1/np.sqrt(5), phi_minus, -np.sqrt(phi_plus)],
        [1/np.sqrt(5), -phi_plus, np.sqrt(phi_minus)],
        [1/np.sqrt(5), -phi_plus, -np.sqrt(phi_minus)],
    ])
    vertices /= np.linalg.norm(vertices, axis=1, keepdims=True)

    return vertices

for p in range(7):
    file_name = f"./EFxyz_amplitudes_for_pr_eq{p+1}_new.txt"
    print(p)
    if p==0:
        icos[p, :, :] = generate_icosahedron_vertices()
    else:
        with open(file_name, 'r') as file:
            for d in range(6):
                line = file.readline().strip().split()
                for x in range(3):
                    icos[p, d, x] = float(line[x])*10

import os
import MDAnalysis as mda
import numpy as np

#-----LOADING THE CHARGES FROM PDB-----
q = []
pdb = "partial_charges.pdb"
with open(pdb, "r") as pdb_file:
    lines = pdb_file.readlines()[4:-2]
    for line in lines:
        parts = line.split()
        if len(parts) == 12:
            q.append(float(parts[10]))

q_array = np.array(q)

#-----ARRAYS INICIALIZATION-----
num_frames = 100001
dipole_moments = np.empty((num_frames, 3, 15, 6, 3))
tot_dipole_moments = np.empty((num_frames, 3, 15, 6))
dip_collinear_magnitude = np.empty((num_frames, 3, 15, 6))

p_range = range(3)
f_range = range(15)
d_range = range(6)

```

```

#-----LOADING THE TRAJECTORIES-----
for p in p_range:
    for f in f_range:
        for d in d_range:
            if p == 0 or p == 1:
                traj_file = f'./Leapfrog{p+1}/L{p+1}_{f+1}_{d+1}/
                EF_freq{f+1}_in_dir{d+1}_after_prot_eq{p+1}
                _NOWATER_NOSOD-nj-center-all_from_trr.xtc'

                topology_file = f'./Leapfrog{p+1}/L{p+1}_{f+1}_{d+1}/
                EF_freq{f+1}_in_dir{d+1}_after_prot_eq{p+1}
                _NOWATER_NOSOD-nj-center_1st_frame-prot_eq.tpr'
            else:
                traj_file = f'/mnt/qnap2/Leapfrog{p+1}/L{p+1}_{f+1}
                _{d+1}/EF_freq{f+1}_in_dir{d+1}_after_prot_eq{p+1}
                _NOWATER_NOSOD-nj-center-all_from_trr.xtc'

                topology_file = f'/mnt/qnap2/Leapfrog{p+1}/L{p+1}_{f+1}
                _{d+1}/EF_freq{f+1}_in_dir{d+1}_after_prot_eq{p+1}
                _NOWATER_NOSOD-nj-center_1st_frame-prot_eq.tpr'

            if not os.path.isfile(traj_file):
                print(f"File {traj_file} not found. Skipping...")
            else:
                min_file_size = 5200000000
                max_file_size = 5300000000
                file_size = os.path.getsize(traj_file)
                if not (min_file_size <= file_size <= max_file_size):
                    print(f"File {traj_file} is not within the
                    acceptable size range. Size: {file_size} bytes.
                    (Min: {min_file_size}, Max: {max_file_size})")

                u = mda.Universe(topology_file, traj_file)
                num_frames = len(u.trajectory)

#-----SELECTING ATOMS-----
protein_atoms = u.select_atoms('protein')

#-----CALCULATION-----
print(f'starting p={p} f={f} d={d}')

with open(f'center_of_charge_p{p}_f{f}_d{d}.txt', 'w')
as f_out:
    for ts in u.trajectory:
        charges = protein_atoms.charges
        coordinates = protein_atoms.positions

        num_x = np.sum(np.abs(charges) * coordinates[:,
        0])
        num_y = np.sum(np.abs(charges) * coordinates[:,
        1])
        num_z = np.sum(np.abs(charges) * coordinates[:,
        2])

        denominator = np.sum(np.abs(charges))

        center_of_charge_x = num_x / denominator
        center_of_charge_y = num_y / denominator

```

```

center_of_charge_z = num_z / denominator

f_out.write(f"Frame {ts.frame}:
{center_of_charge_x} {center_of_charge_y}
{center_of_charge_z}\n")

dipole_moments[ts.frame, p, f, d, 0] =
np.sum((protein_atoms.positions[:, 0] -
center_of_charge_x) * q_array)
dipole_moments[ts.frame, p, f, d, 1] =
np.sum((protein_atoms.positions[:, 1] -
center_of_charge_y) * q_array)

dipole_moments[ts.frame, p, f, d, 2] =
np.sum((protein_atoms.positions[:, 2] -
center_of_charge_z) * q_array)

dip_collinear_magnitude[ts.frame, p, f, d] =
np.dot(icos[p, d, :], dipole_moments[ts.frame,
p, f, d, :])
tot_dipole_moments[ts.frame, p, f, d] = np.sqrt(
    dipole_moments[ts.frame, p, f, d, 0] ** 2 +
    dipole_moments[ts.frame, p, f, d, 1] ** 2 +
    dipole_moments[ts.frame, p, f, d, 2] ** 2
)

```

-----OUTPUT-----

```

for p in p_range:
    for f in f_range:
        for d in d_range:
            dipoles_file = f"dipoles_WHOLE_PROT_COC_xyz_L{p+1}_{f+1}
_{d+1}.txt"
            with open(dipoles_file, 'w') as file:
                #file.write("time p f d dip_x dip_y dip_z tot_dip
collinear_dip")
                for ts in range(dipole_moments.shape[0]):
                    dip_x = dipole_moments[ts, p, f, d, 0]
                    dip_y = dipole_moments[ts, p, f, d, 1]
                    dip_z = dipole_moments[ts, p, f, d, 2]

                    line = f"{ts} {dip_x} {dip_y} {dip_z}\n"
                    file.write(line)

for p in p_range:
    for f in f_range:
        for d in d_range:
            dipoles_file = f"dipoles_WHOLE_PROT_COC_tot_corr_L{p+1}_{f+1}
_{d+1}.txt"
            with open(dipoles_file, 'w') as file:
                #file.write("time p f d dip_x dip_y dip_z tot_dip
collinear_dip")
                for ts in range(dipole_moments.shape[0]):
                    dip_tot = tot_dipole_moments[ts, p, f, d]
                    dip_col = dip_collinear_magnitude[ts, p, f, d]

                    line = f"{ts} {dip_tot} {dip_col}\n"
                    file.write(line)

```

10.6 RMSF of residues - original data

10.6.1 Tubulin α - Batch 1

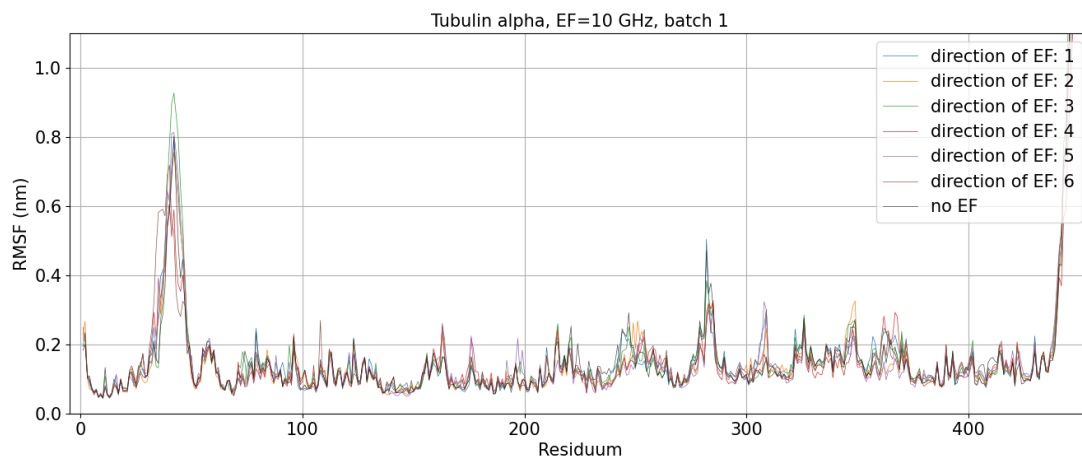


Figure 10.1: RMSF of tubulin α residues subjected to the electric field of frequency 10 GHz; Batch 1

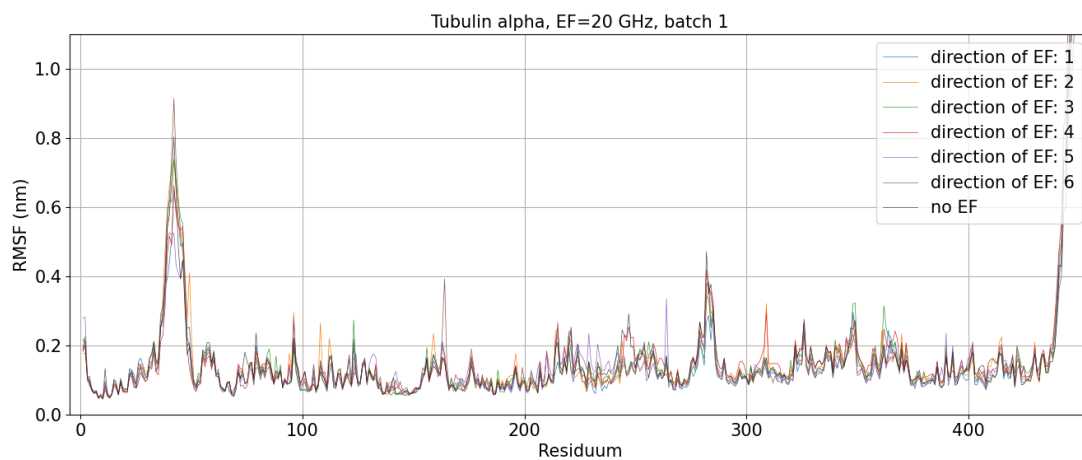


Figure 10.2: RMSF of tubulin α residues subjected to the electric field of frequency 20 GHz; Batch 1

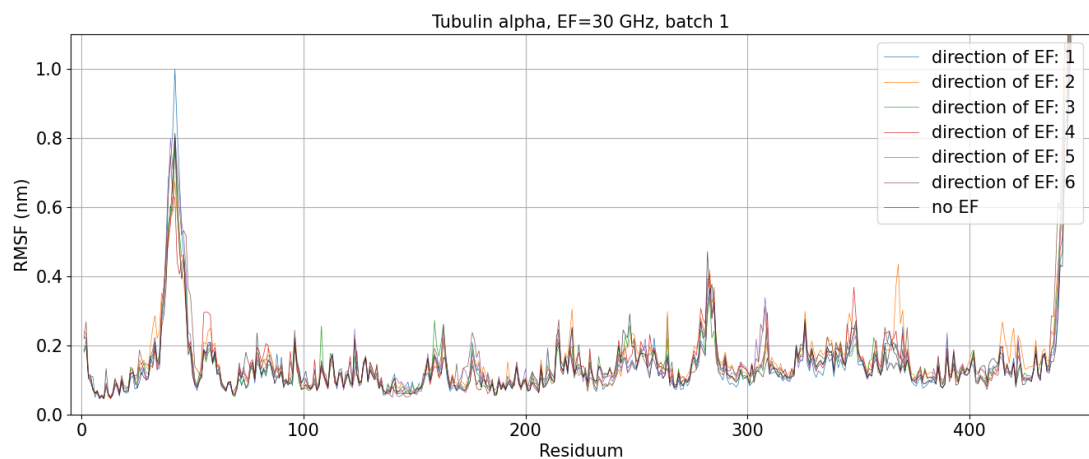


Figure 10.3: RMSF of tubulin α residues subjected to the electric field of frequency 30 GHz; Batch 1

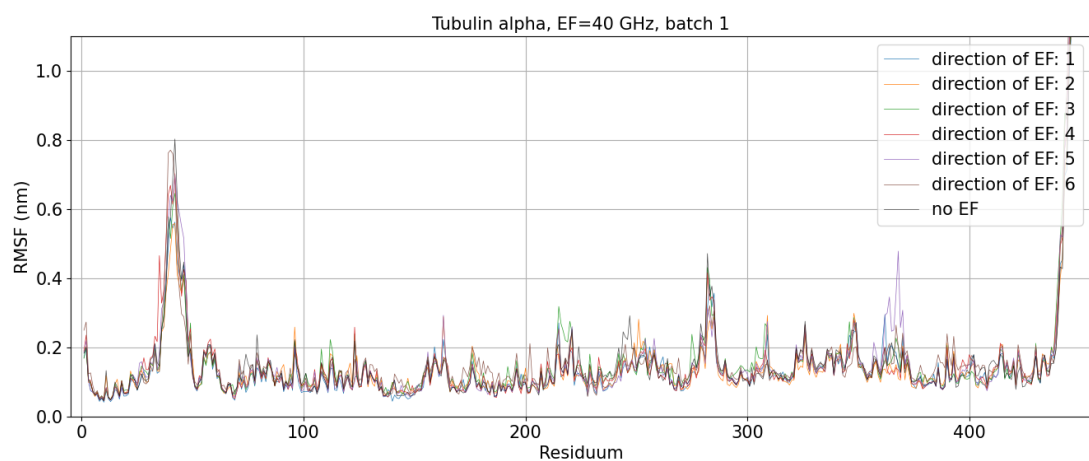


Figure 10.4: RMSF of tubulin α residues subjected to the electric field of frequency 40 GHz; Batch 1

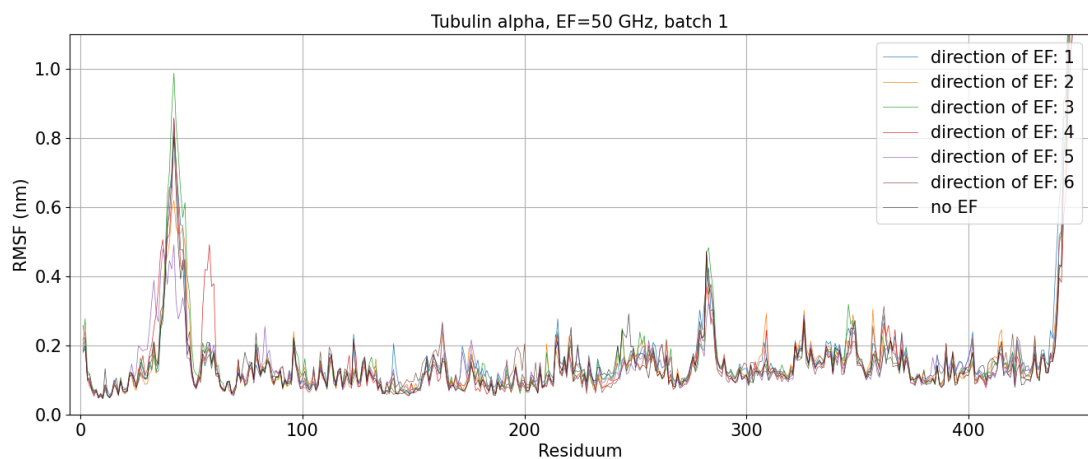


Figure 10.5: RMSF of tubulin α residues subjected to the electric field of frequency 50 GHz; Batch 1

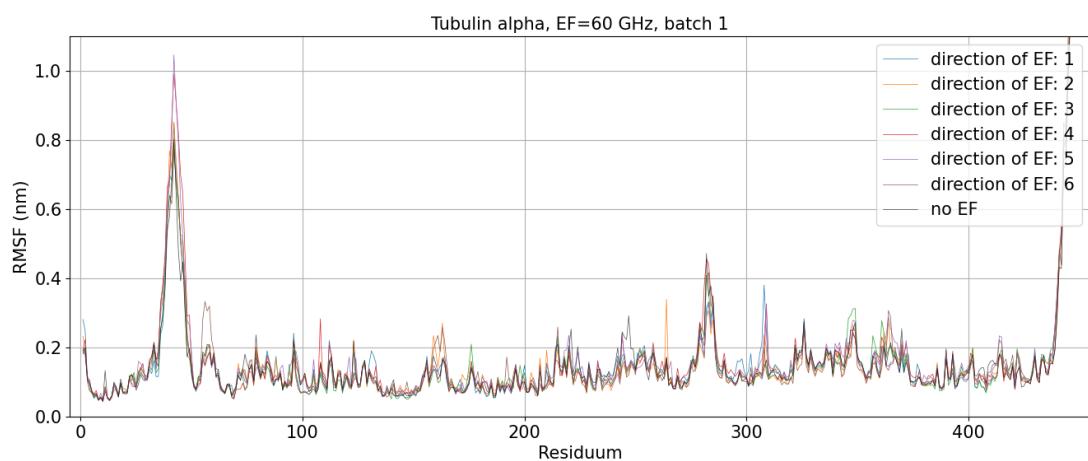


Figure 10.6: RMSF of tubulin α residues subjected to the electric field of frequency 60 GHz; Batch 1

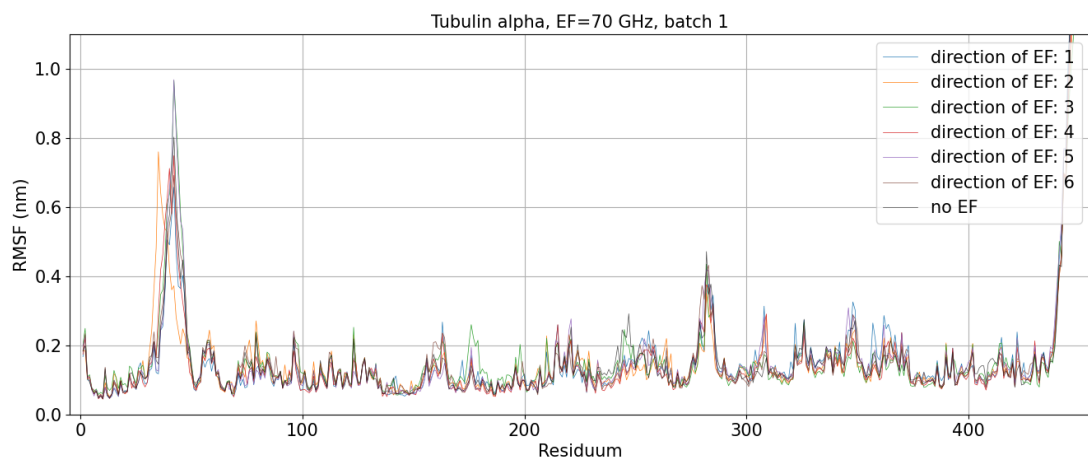


Figure 10.7: RMSF of tubulin α residues subjected to the electric field of frequency 70 GHz; Batch 1

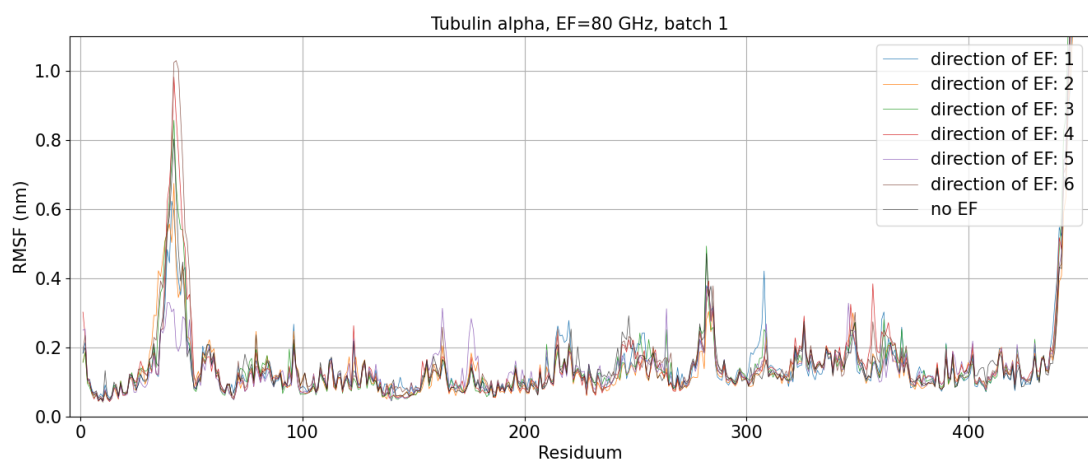


Figure 10.8: RMSF of tubulin α residues subjected to the electric field of frequency 80 GHz; Batch 1

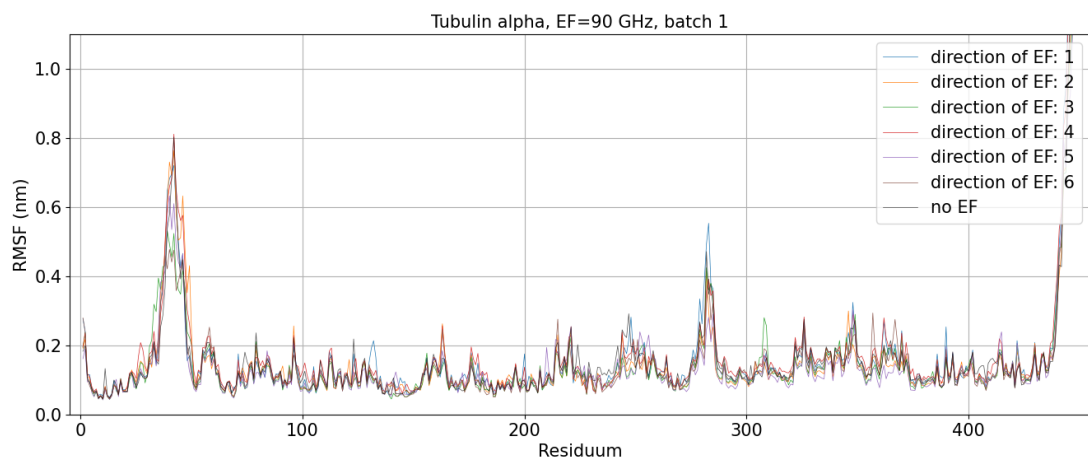


Figure 10.9: RMSF of tubulin α residues subjected to the electric field of frequency 90 GHz; Batch 1

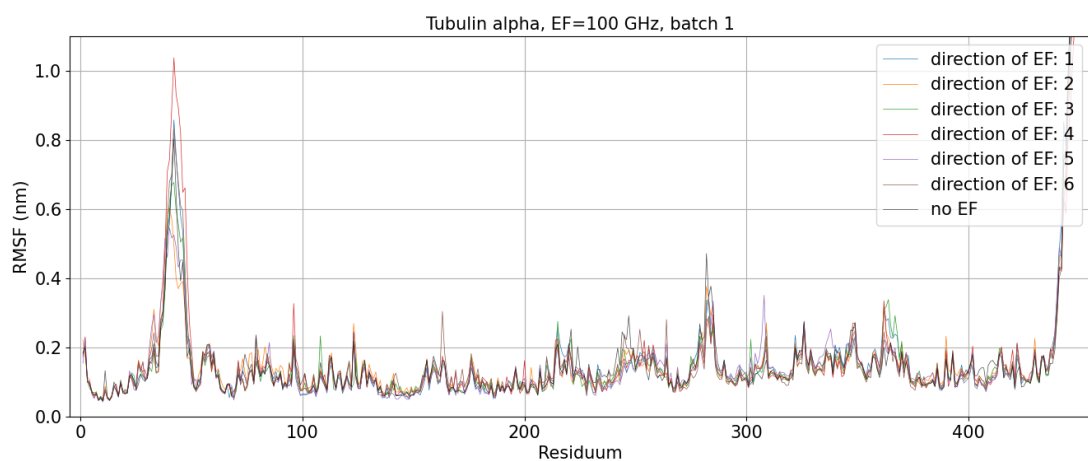


Figure 10.10: RMSF of tubulin α residues subjected to the electric field of frequency 100 GHz; Batch 1

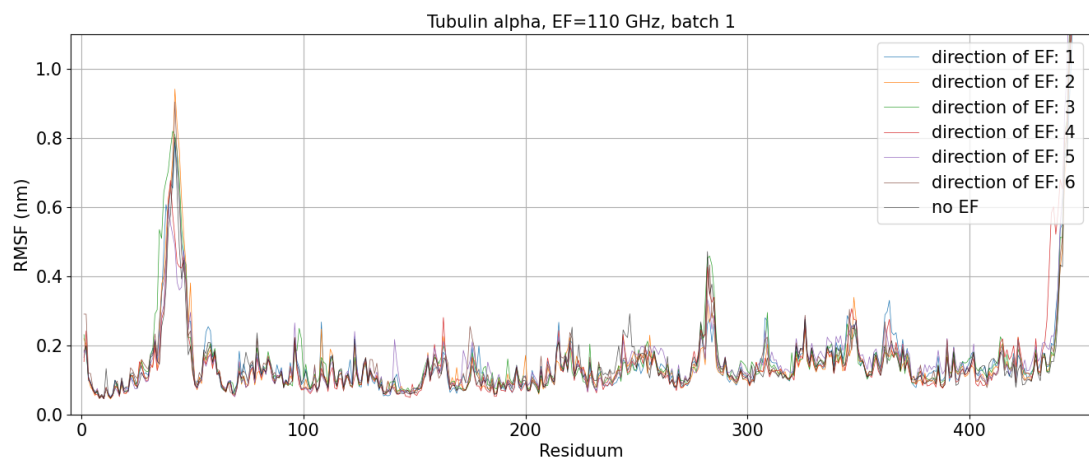


Figure 10.11: RMSF of tubulin α residues subjected to the electric field of frequency 110 GHz; Batch 1

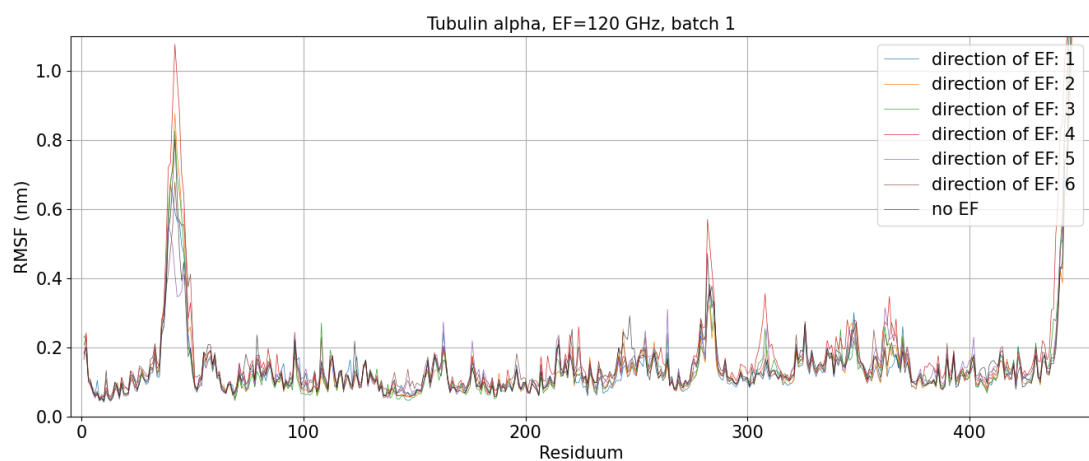


Figure 10.12: RMSF of tubulin α residues subjected to the electric field of frequency 120 GHz; Batch 1

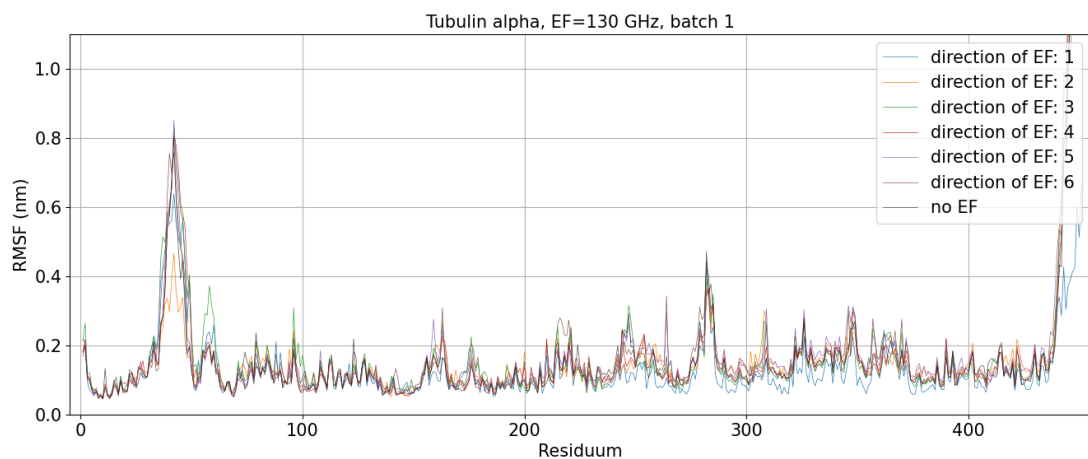


Figure 10.13: RMSF of tubulin α residues subjected to the electric field of frequency 130 GHz; Batch 1

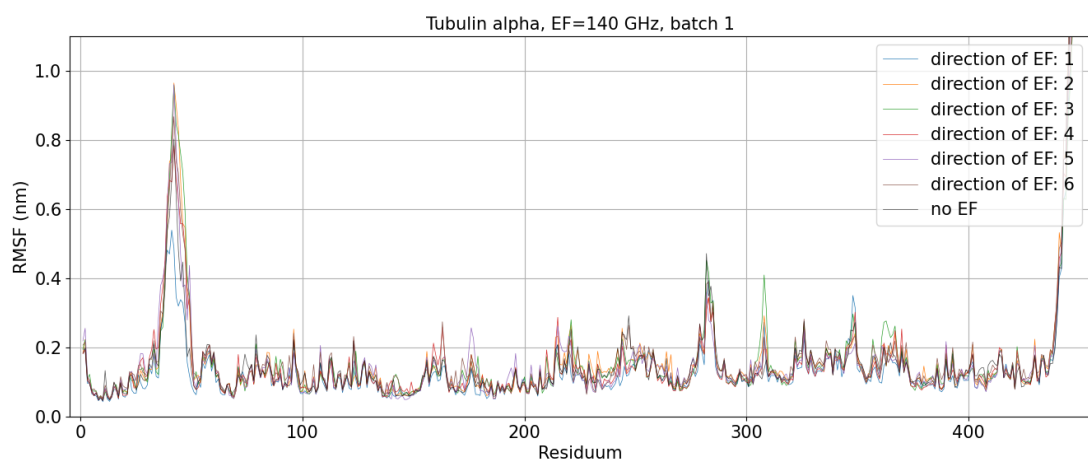


Figure 10.14: RMSF of tubulin α residues subjected to the electric field of frequency 140 GHz; Batch 1

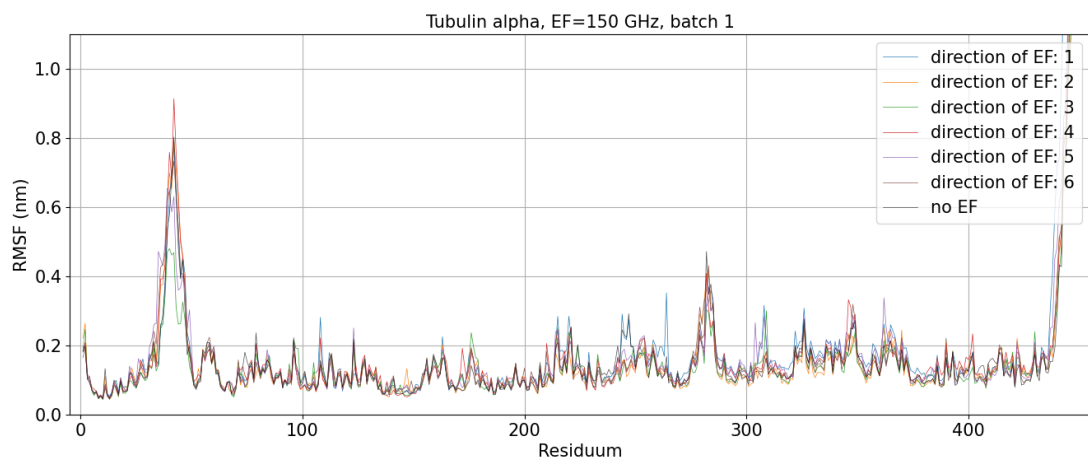


Figure 10.15: RMSF of tubulin α residues subjected to the electric field of frequency 150 GHz; Batch 1

10.6.2 Tubulin α - Batch 2

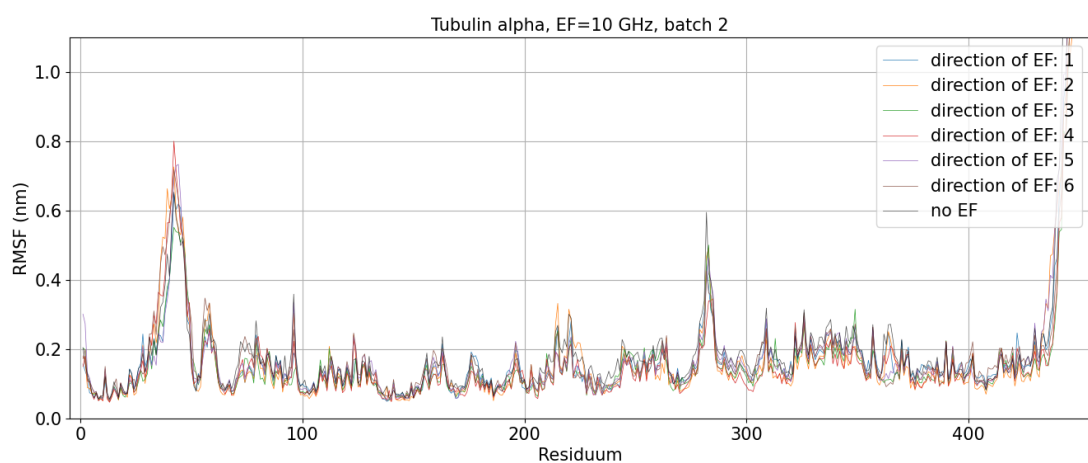


Figure 10.16: RMSF of tubulin α residues subjected to the electric field of frequency 10 GHz; Batch 2

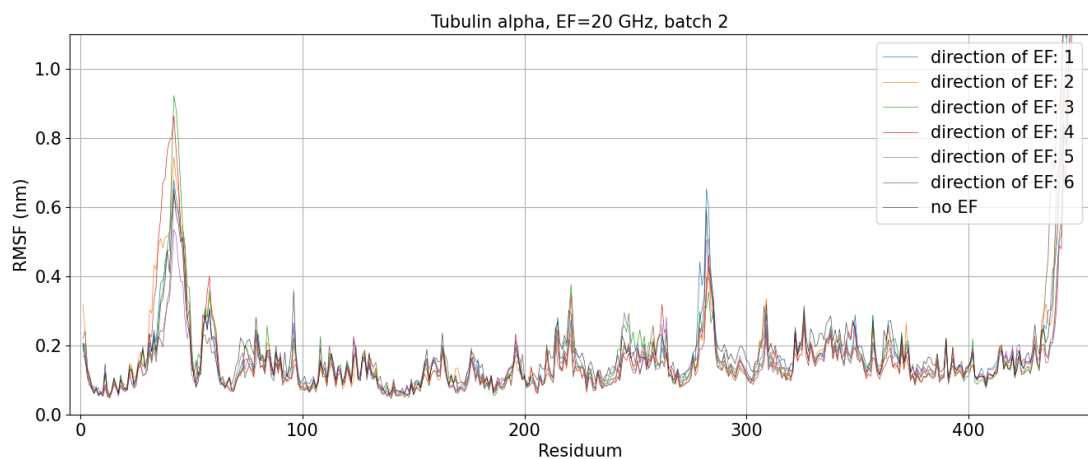


Figure 10.17: RMSF of tubulin α residues subjected to the electric field of frequency 20 GHz; Batch 2

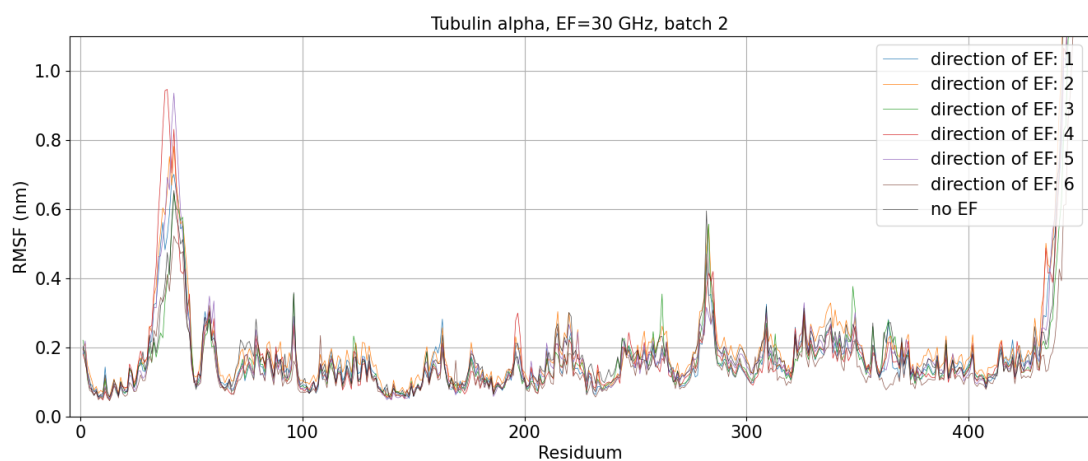


Figure 10.18: RMSF of tubulin α residues subjected to the electric field of frequency 30 GHz; Batch 2

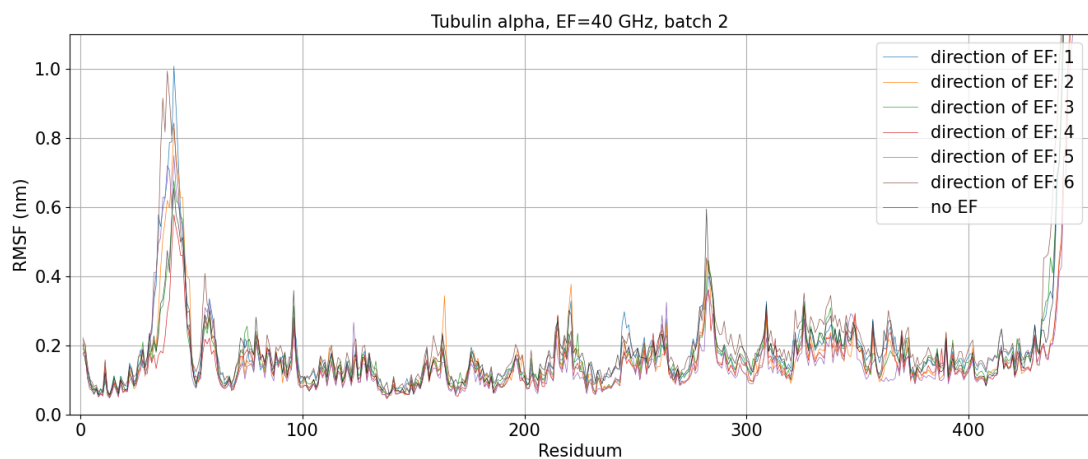


Figure 10.19: RMSF of tubulin α residues subjected to the electric field of frequency 40 GHz; Batch 2

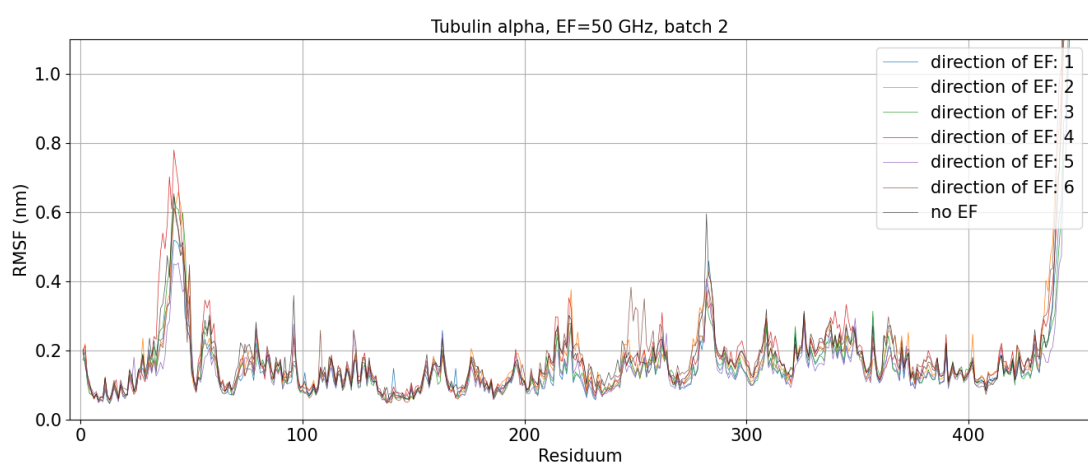


Figure 10.20: RMSF of tubulin α residues subjected to the electric field of frequency 50 GHz; Batch 2

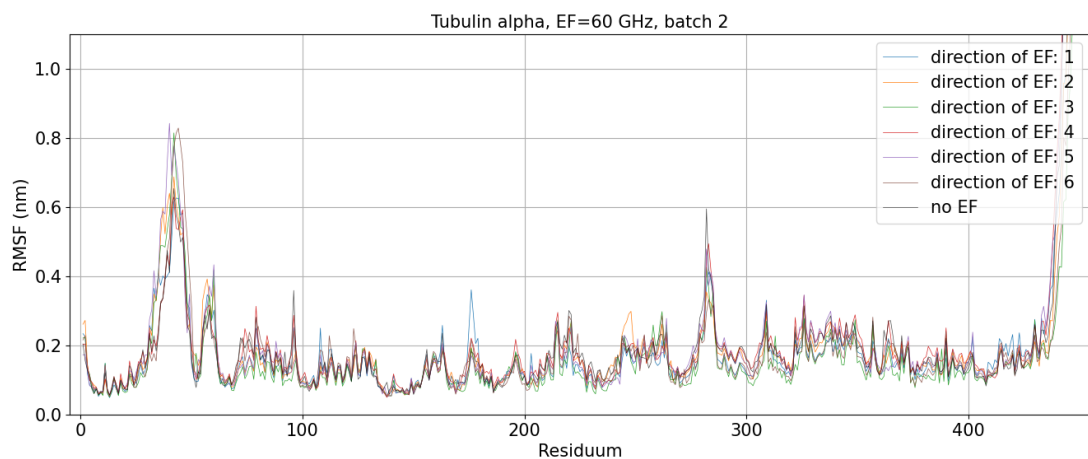


Figure 10.21: RMSF of tubulin α residues subjected to the electric field of frequency 60 GHz; Batch 2

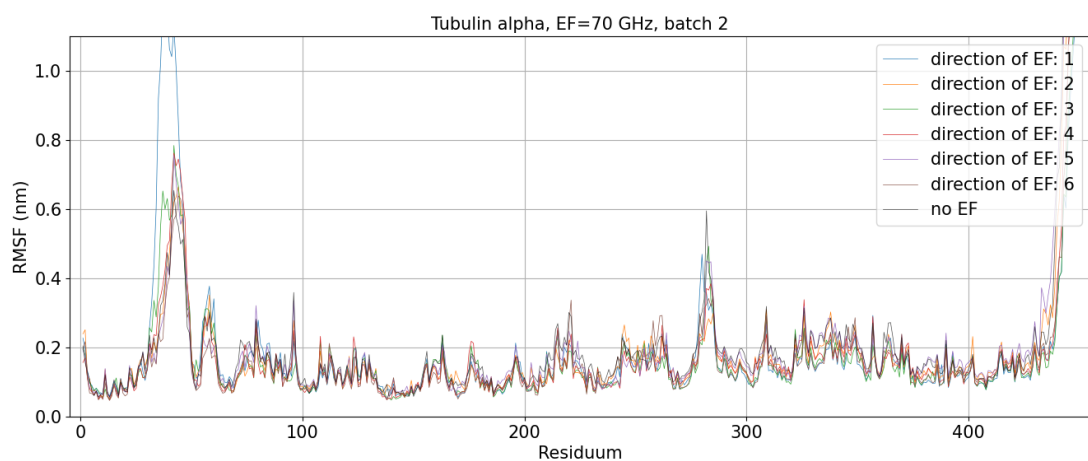


Figure 10.22: RMSF of tubulin α residues subjected to the electric field of frequency 70 GHz; Batch 2

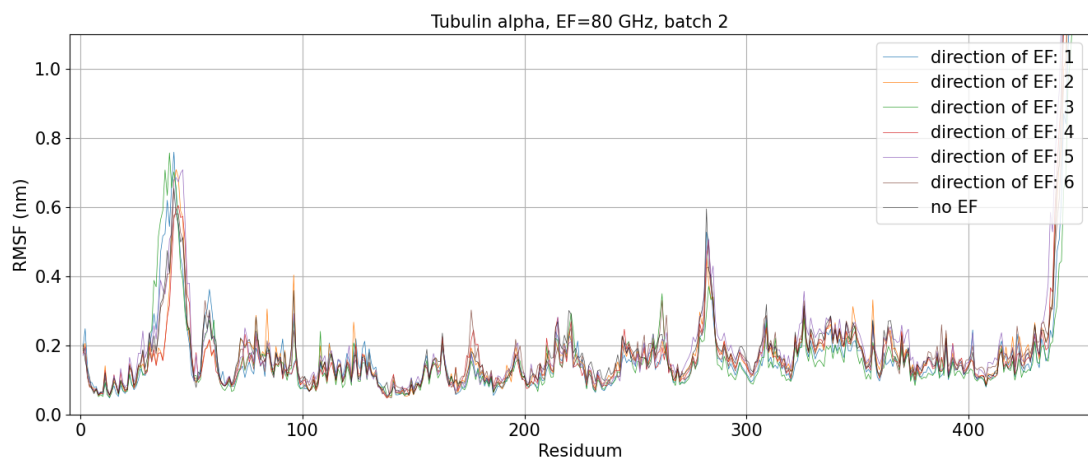


Figure 10.23: RMSF of tubulin α residues subjected to the electric field of frequency 80 GHz; Batch 2

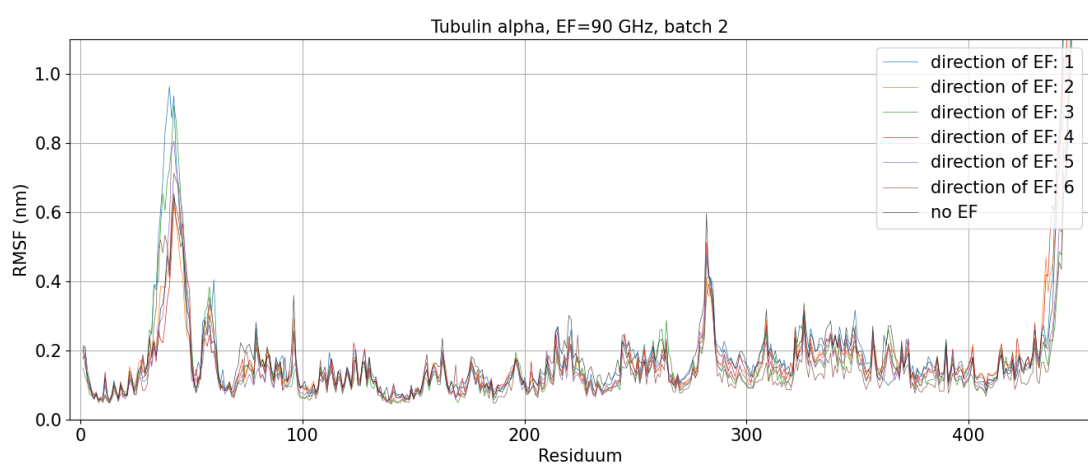


Figure 10.24: RMSF of tubulin α residues subjected to the electric field of frequency 90 GHz; Batch 2

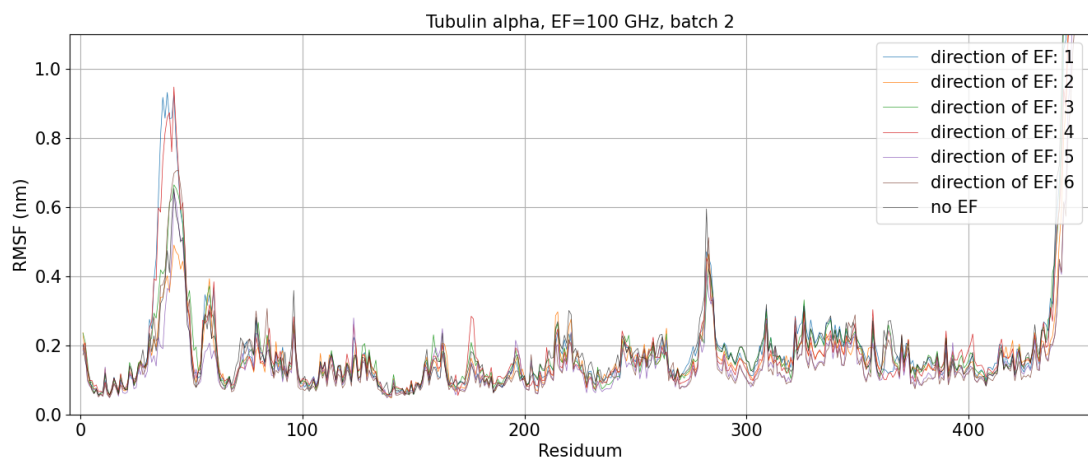


Figure 10.25: RMSF of tubulin α residues subjected to the electric field of frequency 100 GHz; Batch 2

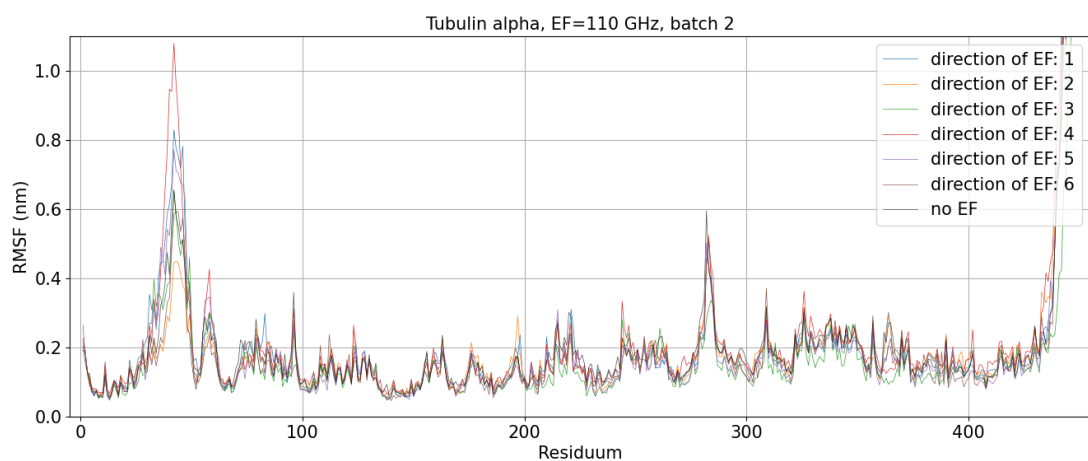


Figure 10.26: RMSF of tubulin α residues subjected to the electric field of frequency 110 GHz; Batch 2

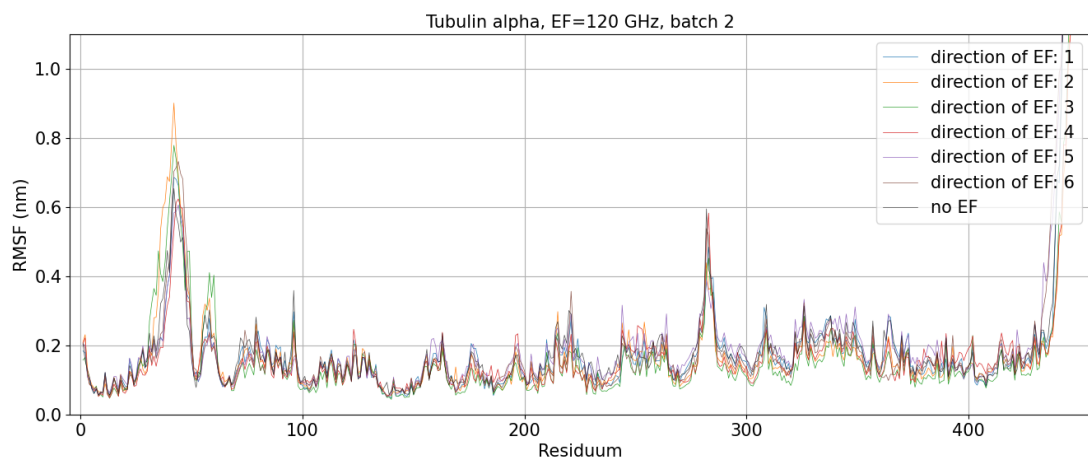


Figure 10.27: RMSF of tubulin α residues subjected to the electric field of frequency 120 GHz; Batch 2

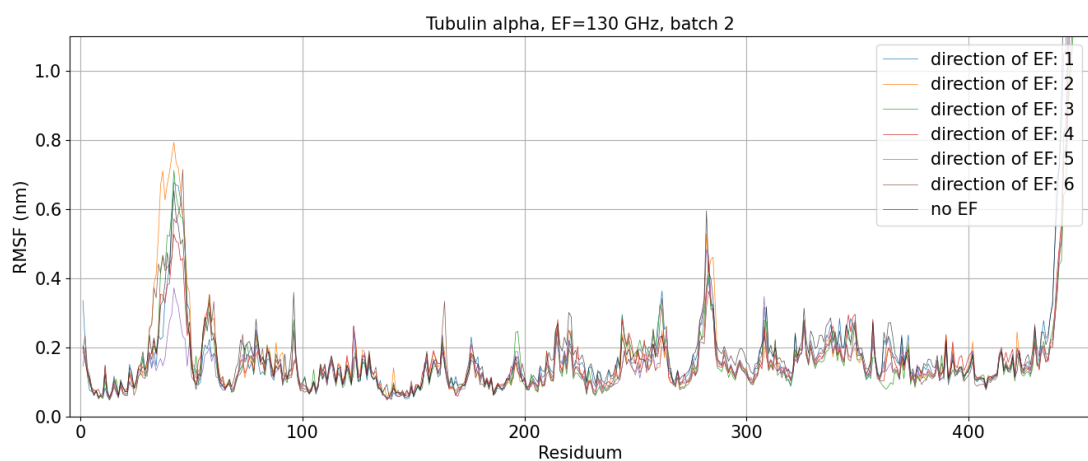


Figure 10.28: RMSF of tubulin α residues subjected to the electric field of frequency 130 GHz; Batch 2

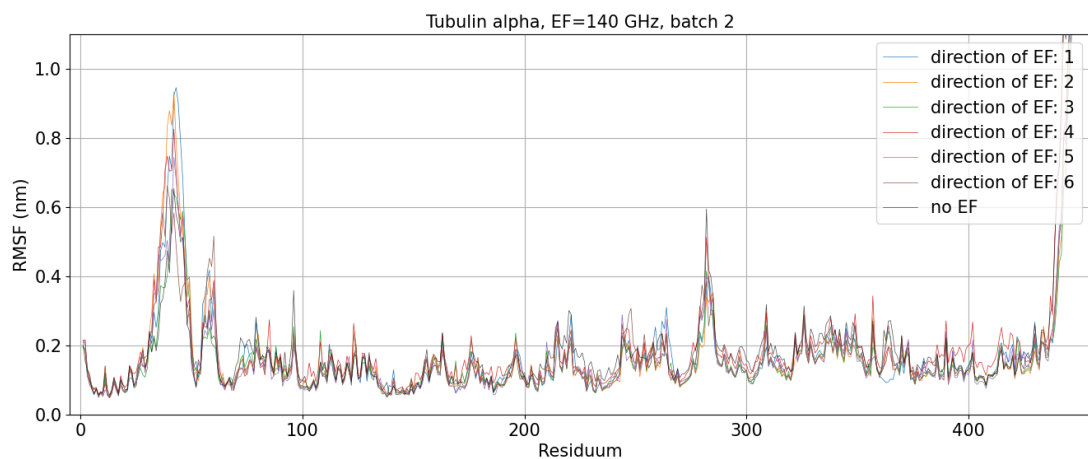


Figure 10.29: RMSF of tubulin α residues subjected to the electric field of frequency 140 GHz; Batch 2

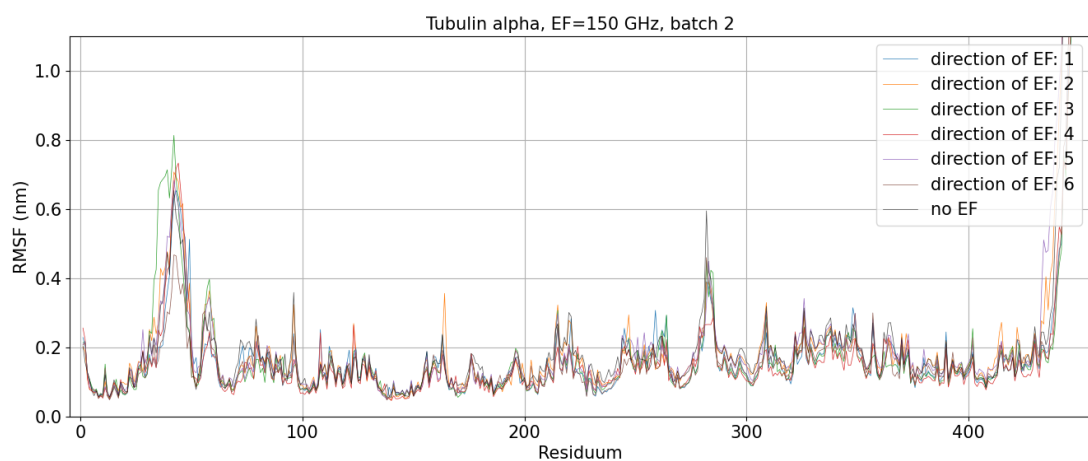


Figure 10.30: RMSF of tubulin α residues subjected to the electric field of frequency 150 GHz; Batch 2

10.6.3 Tubulin α - Batch 3

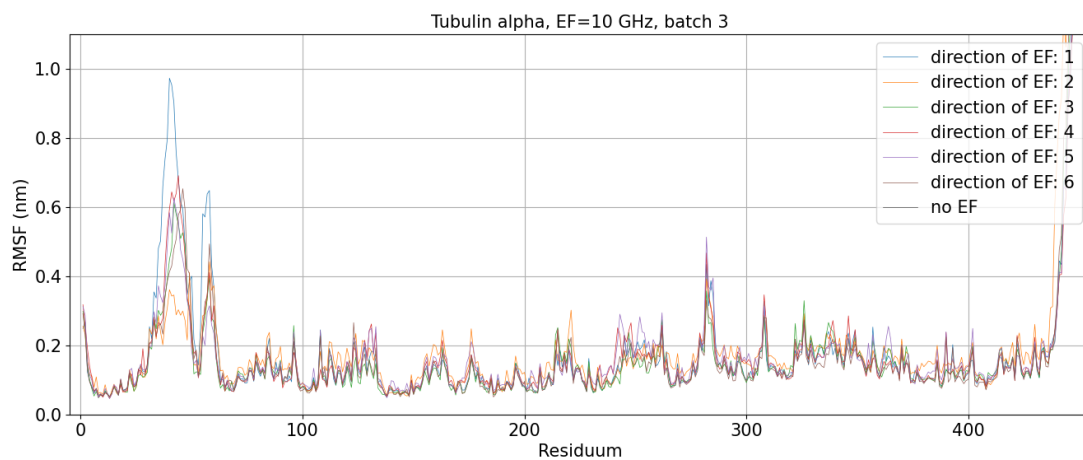


Figure 10.31: RMSF of tubulin α residues subjected to the electric field of frequency 10 GHz; Batch 3

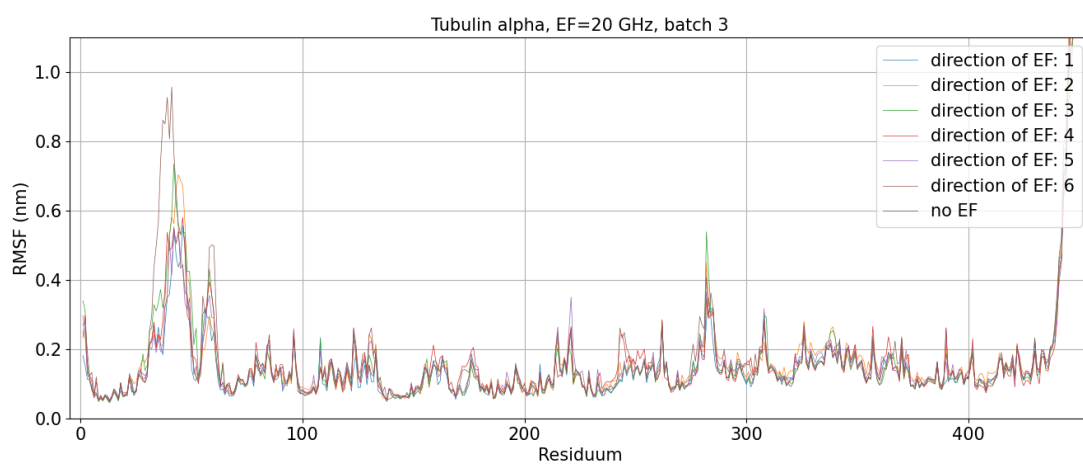


Figure 10.32: RMSF of tubulin α residues subjected to the electric field of frequency 20 GHz; Batch 3

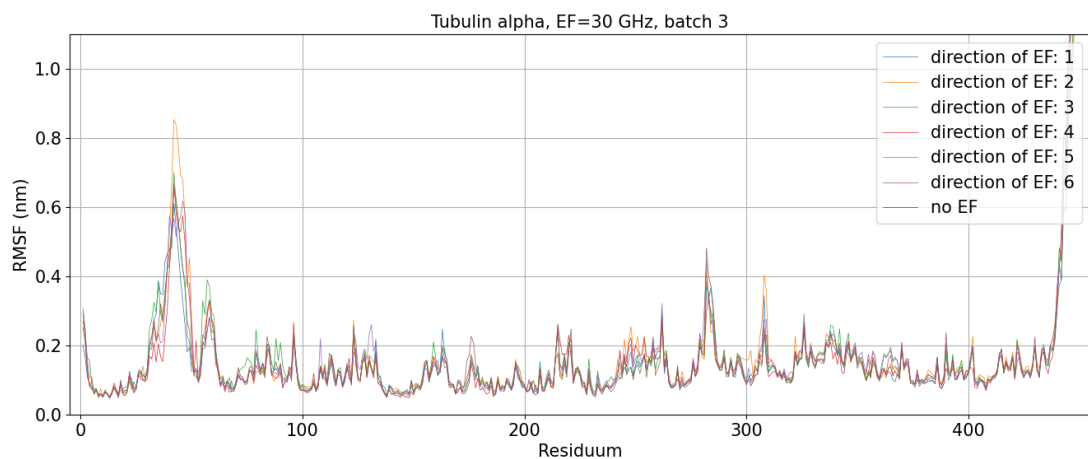


Figure 10.33: RMSF of tubulin α residues subjected to the electric field of frequency 30 GHz; Batch 3

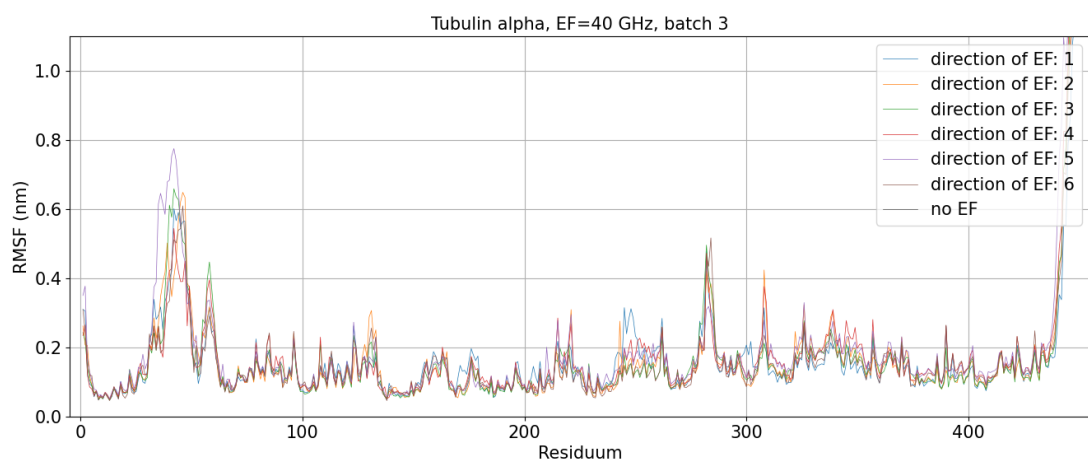


Figure 10.34: RMSF of tubulin α residues subjected to the electric field of frequency 40 GHz; Batch 3

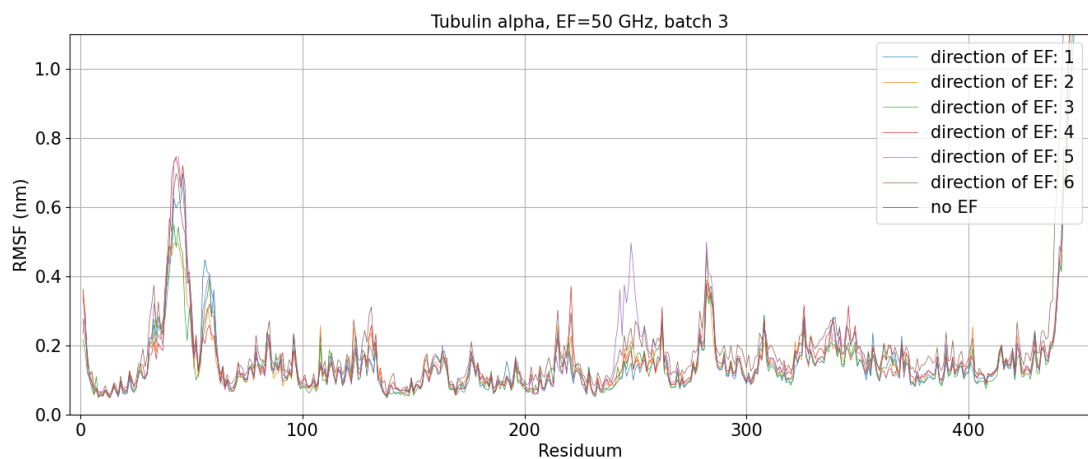


Figure 10.35: RMSF of tubulin α residues subjected to the electric field of frequency 50 GHz; Batch 3

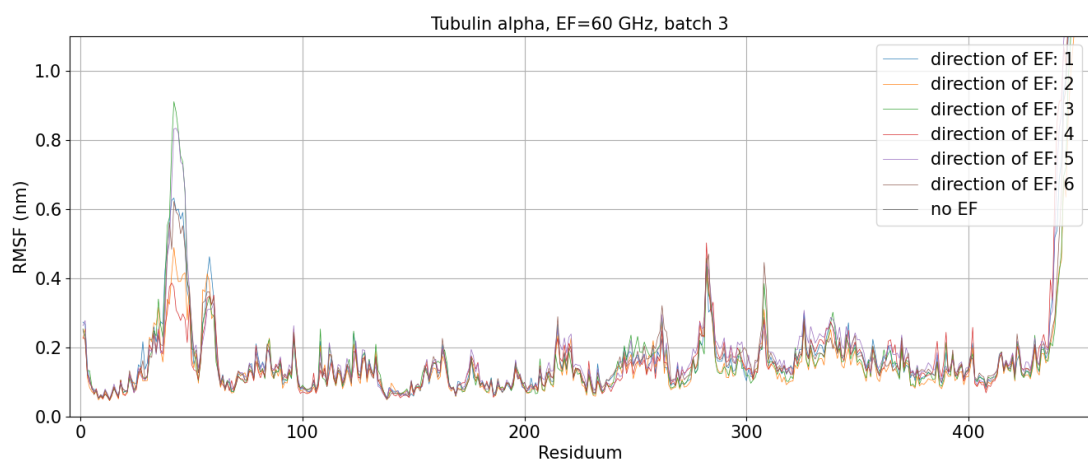


Figure 10.36: RMSF of tubulin α residues subjected to the electric field of frequency 60 GHz; Batch 3

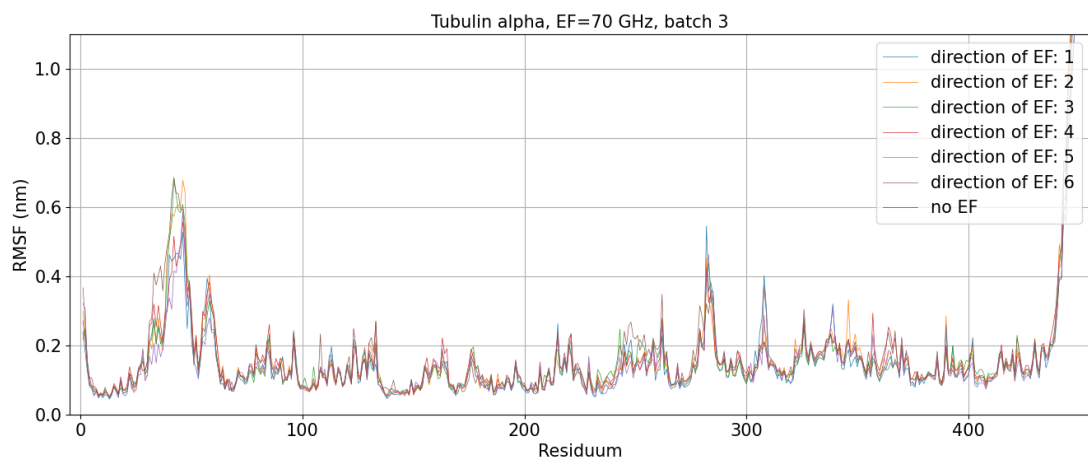


Figure 10.37: RMSF of tubulin α residues subjected to the electric field of frequency 70 GHz; Batch 3

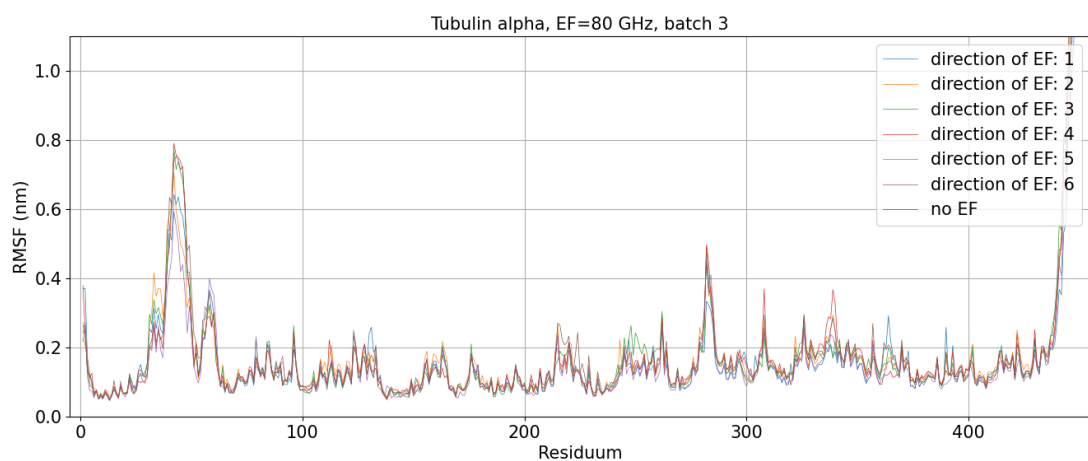


Figure 10.38: RMSF of tubulin α residues subjected to the electric field of frequency 80 GHz; Batch 3

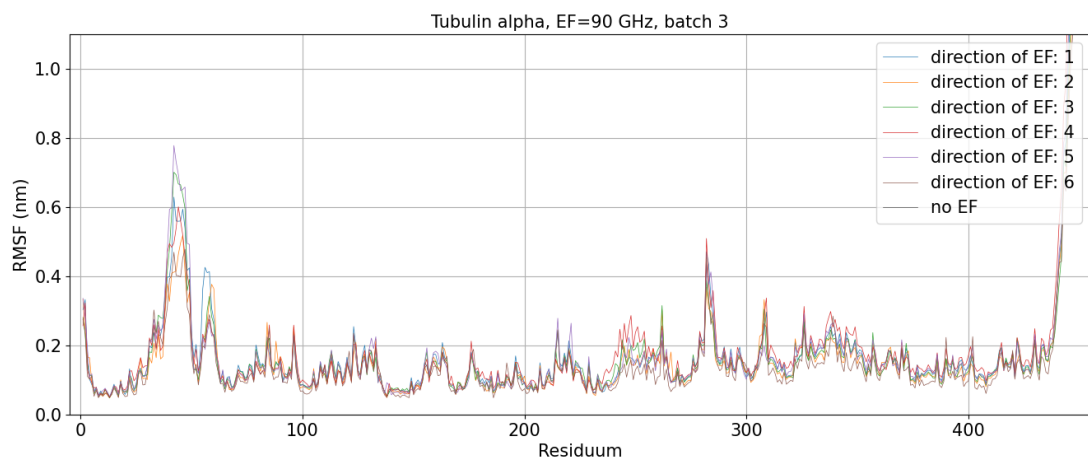


Figure 10.39: RMSF of tubulin α residues subjected to the electric field of frequency 90 GHz; Batch 3

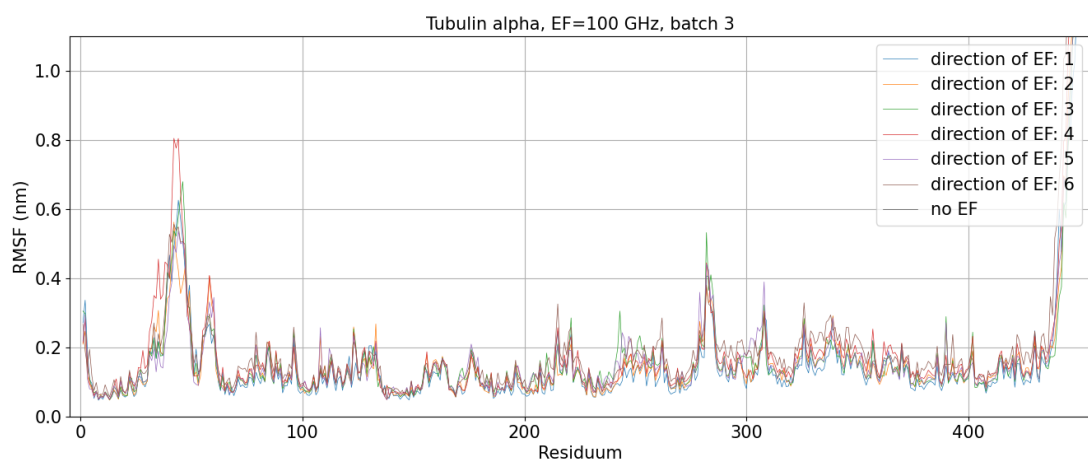


Figure 10.40: RMSF of tubulin α residues subjected to the electric field of frequency 100 GHz; Batch 3

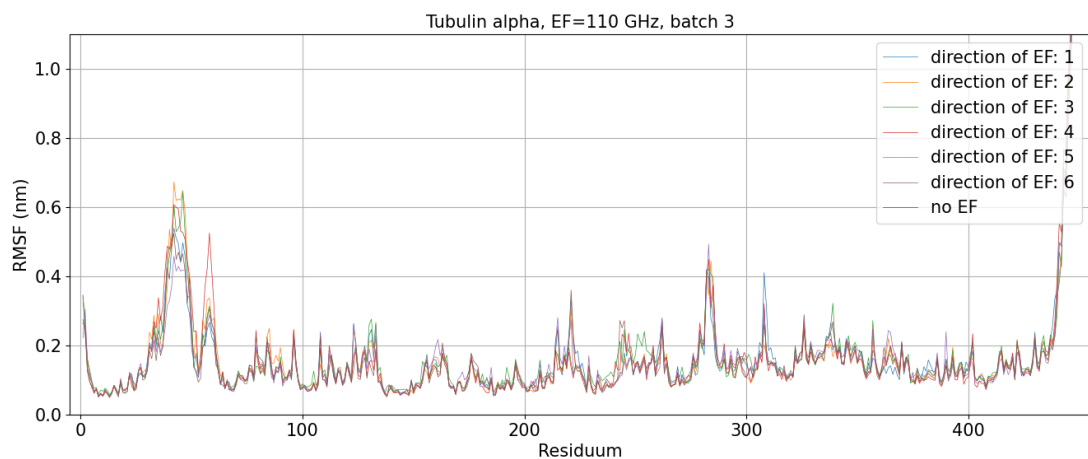


Figure 10.41: RMSF of tubulin α residues subjected to the electric field of frequency 110 GHz; Batch 3

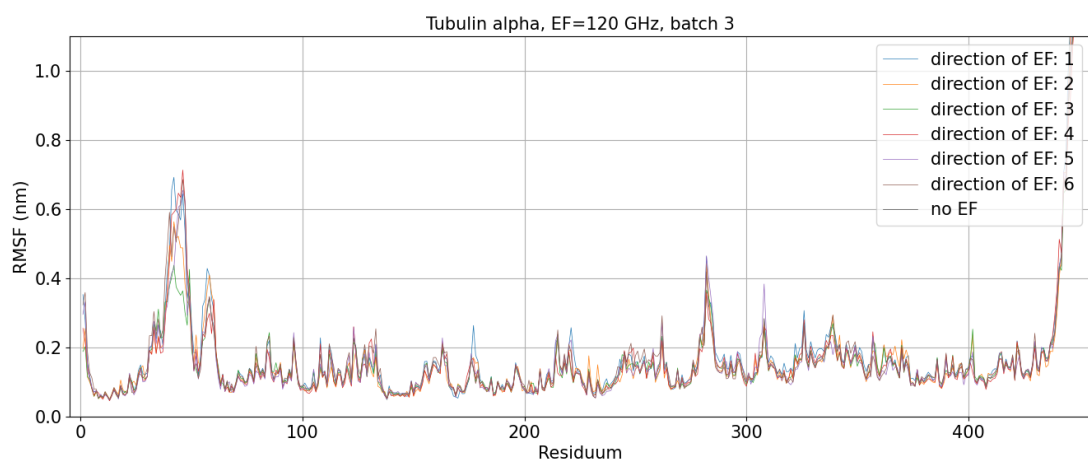


Figure 10.42: RMSF of tubulin α residues subjected to the electric field of frequency 120 GHz; Batch 3

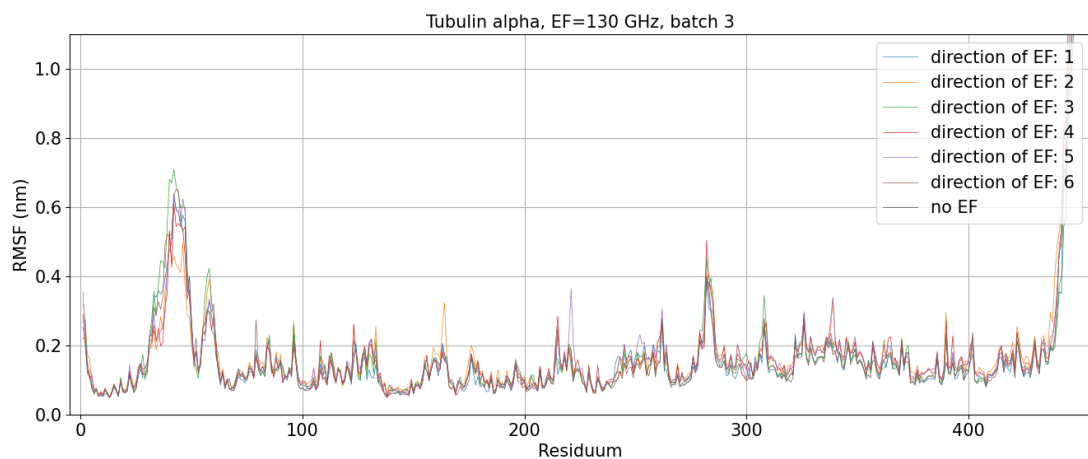


Figure 10.43: RMSF of tubulin α residues subjected to the electric field of frequency 130 GHz; Batch 3

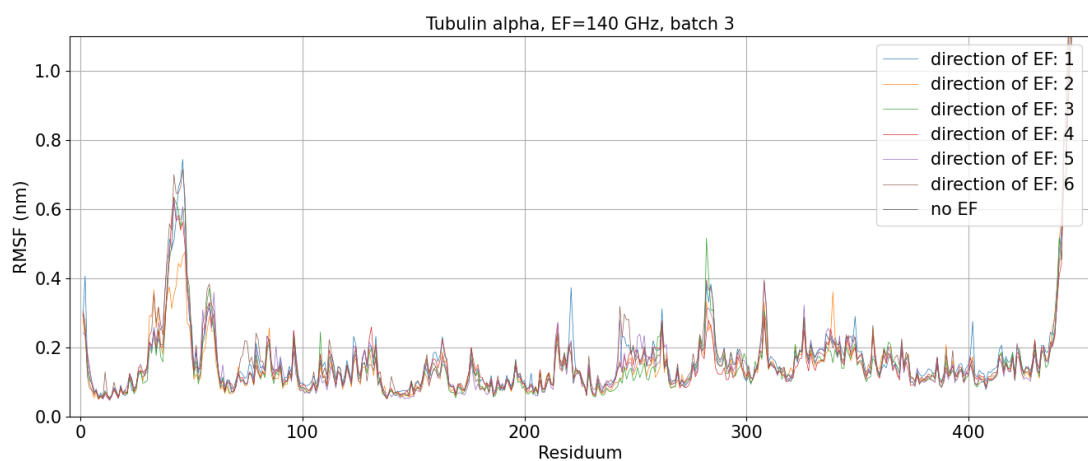


Figure 10.44: RMSF of tubulin α residues subjected to the electric field of frequency 140 GHz; Batch 3

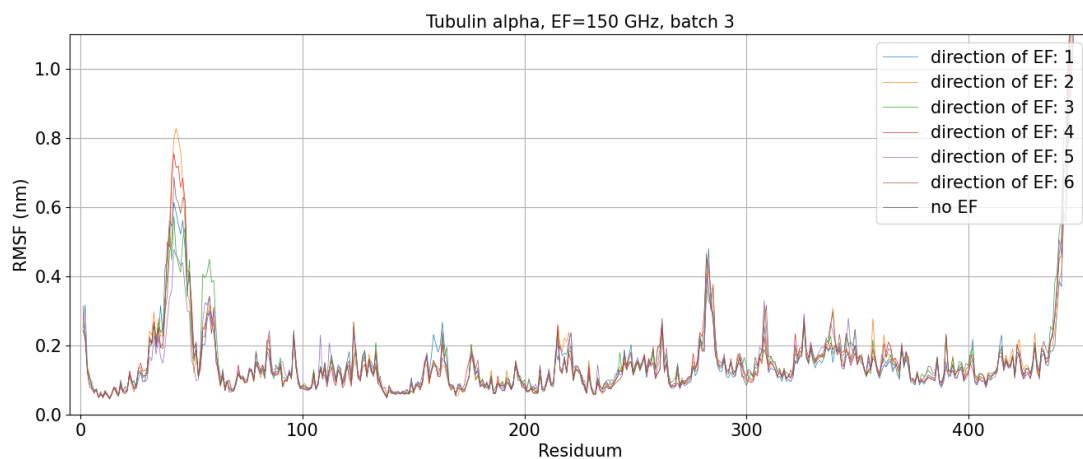


Figure 10.45: RMSF of tubulin α residues subjected to the electric field of frequency 150 GHz; Batch 3

10.7 RMSF of residues - original data

10.7.1 Tubulin β - Batch 1

10.8 RMSF of residues - original data

10.8.1 Tubulin β - Batch 1

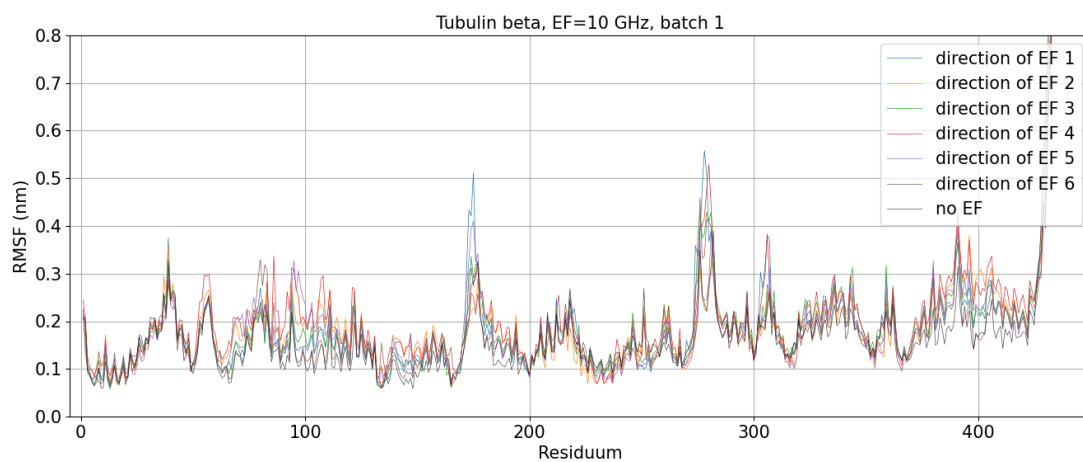


Figure 10.46: RMSF of tubulin β residues subjected to the electric field of frequency 10 GHz; Batch 1

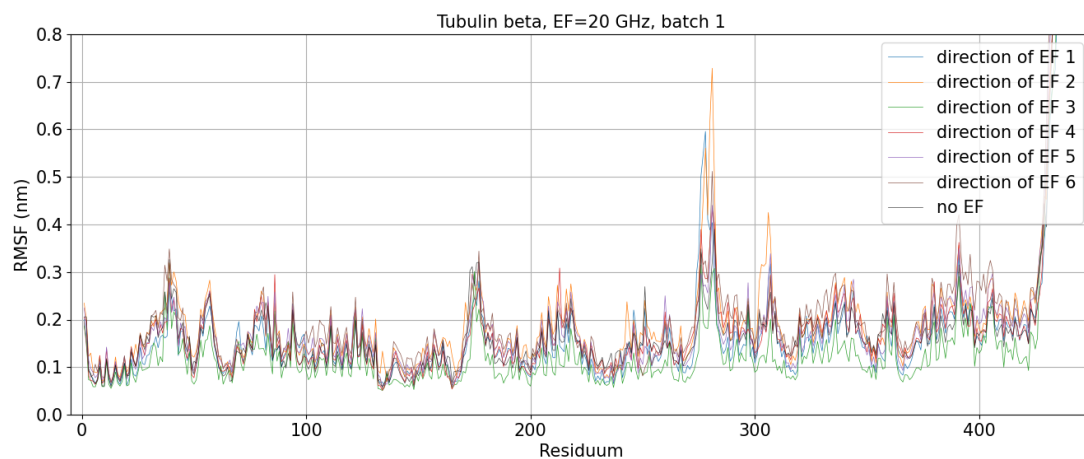


Figure 10.47: RMSF of tubulin β residues subjected to the electric field of frequency 20 GHz; Batch 1

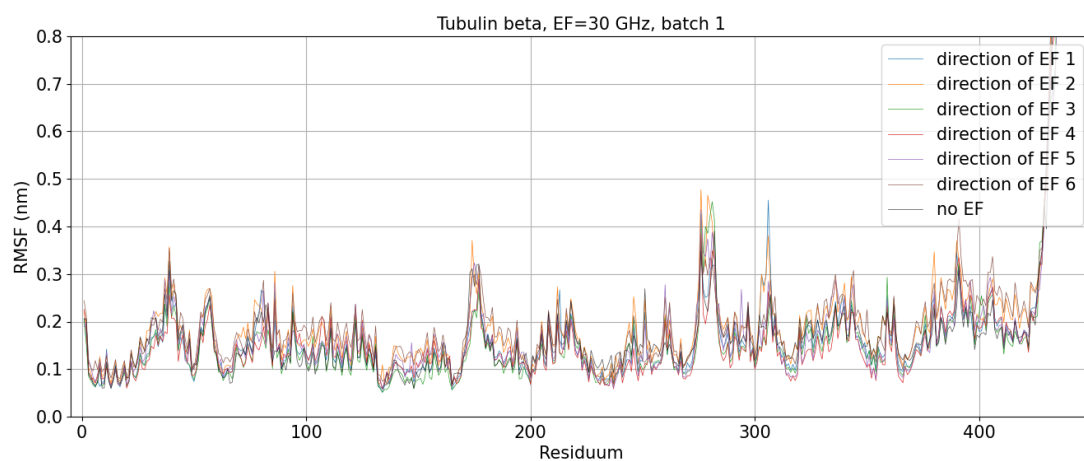


Figure 10.48: RMSF of tubulin β residues subjected to the electric field of frequency 30 GHz; Batch 1

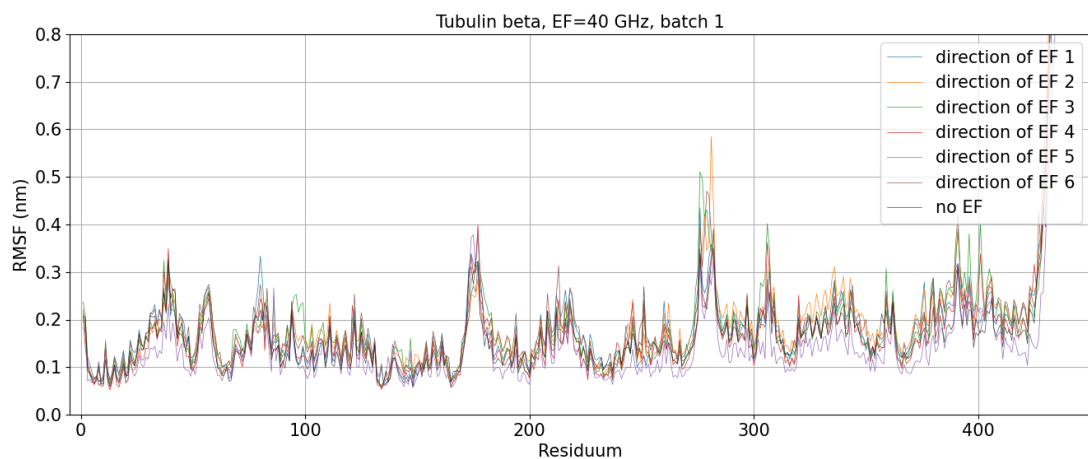


Figure 10.49: RMSF of tubulin β residues subjected to the electric field of frequency 40 GHz; Batch 1

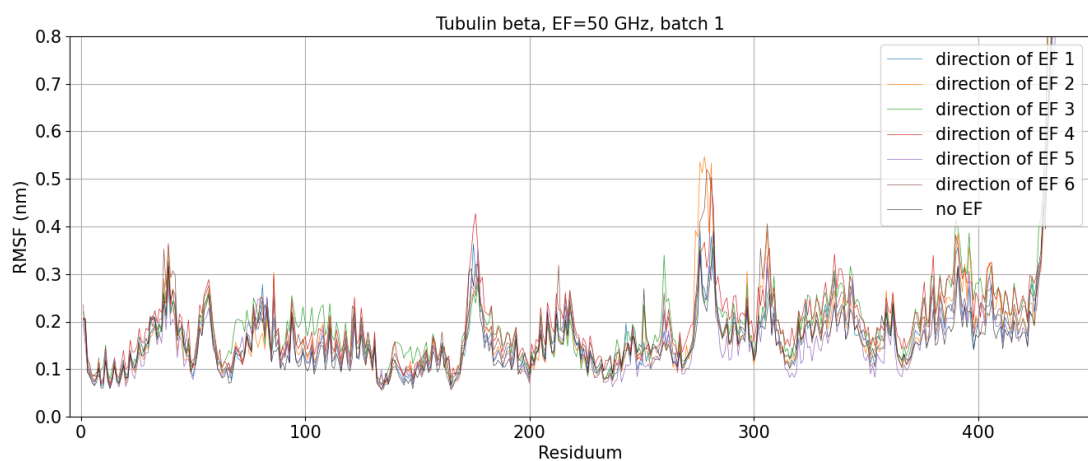


Figure 10.50: RMSF of tubulin β residues subjected to the electric field of frequency 50 GHz; Batch 1

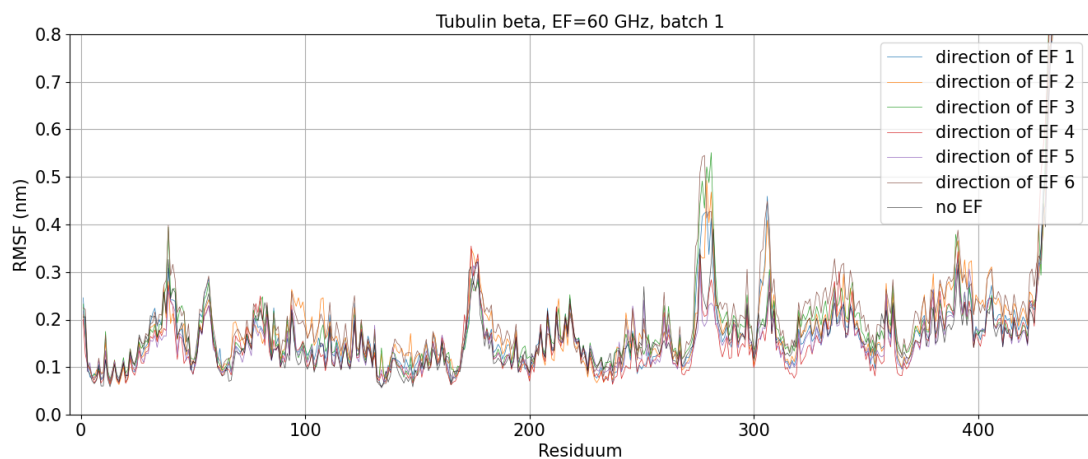


Figure 10.51: RMSF of tubulin β residues subjected to the electric field of frequency 60 GHz; Batch 1

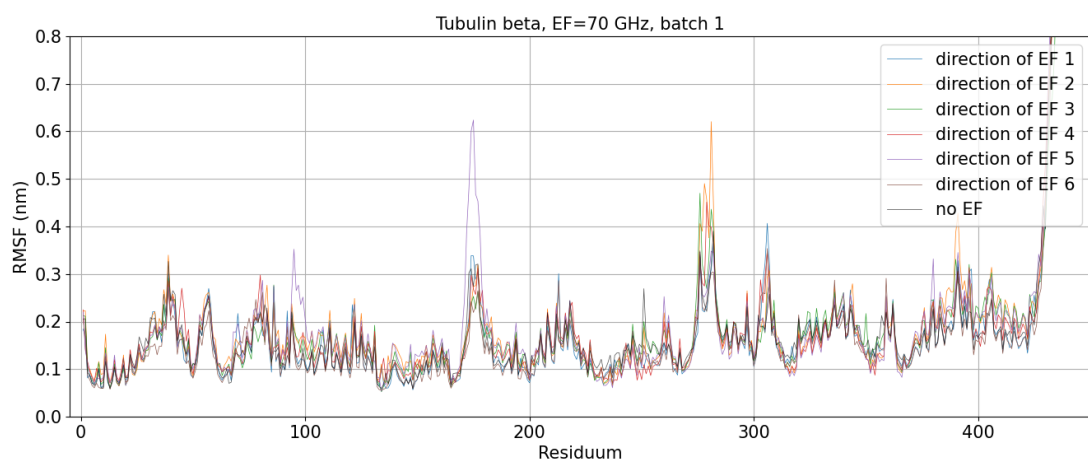


Figure 10.52: RMSF of tubulin β residues subjected to the electric field of frequency 70 GHz; Batch 1

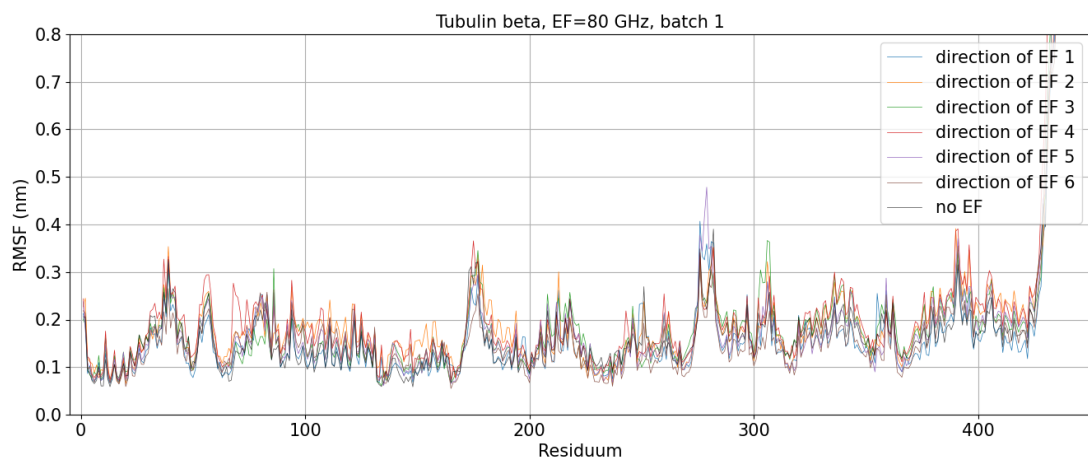


Figure 10.53: RMSF of tubulin β residues subjected to the electric field of frequency 80 GHz; Batch 1

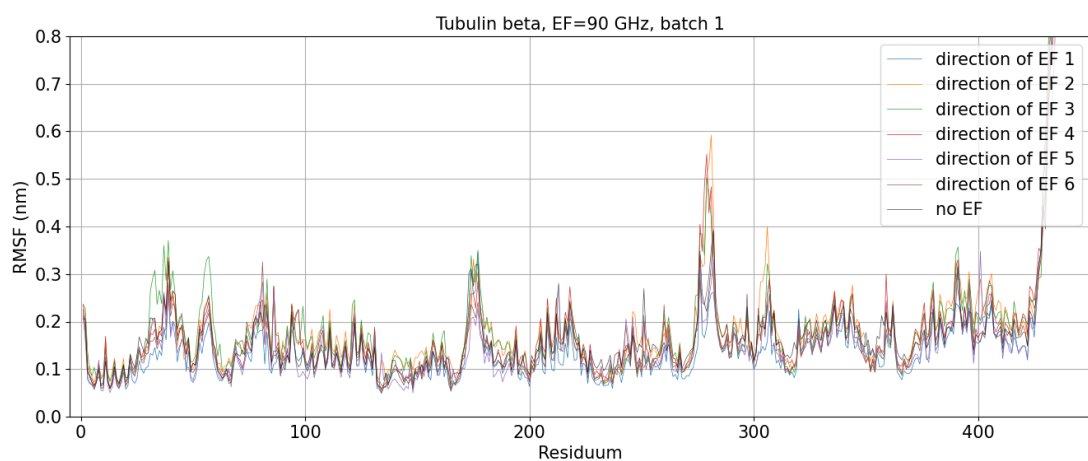


Figure 10.54: RMSF of tubulin β residues subjected to the electric field of frequency 90 GHz; Batch 1

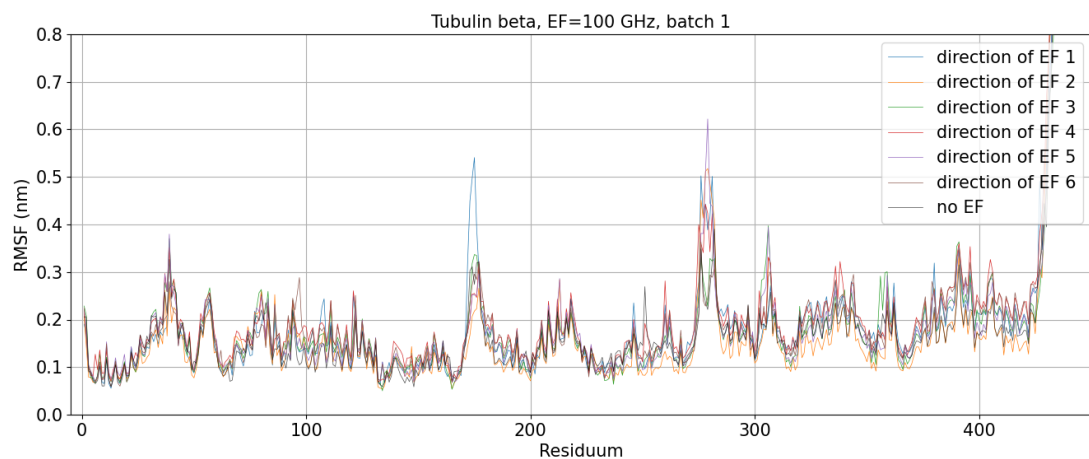


Figure 10.55: RMSF of tubulin β residues subjected to the electric field of frequency 100 GHz; Batch 1

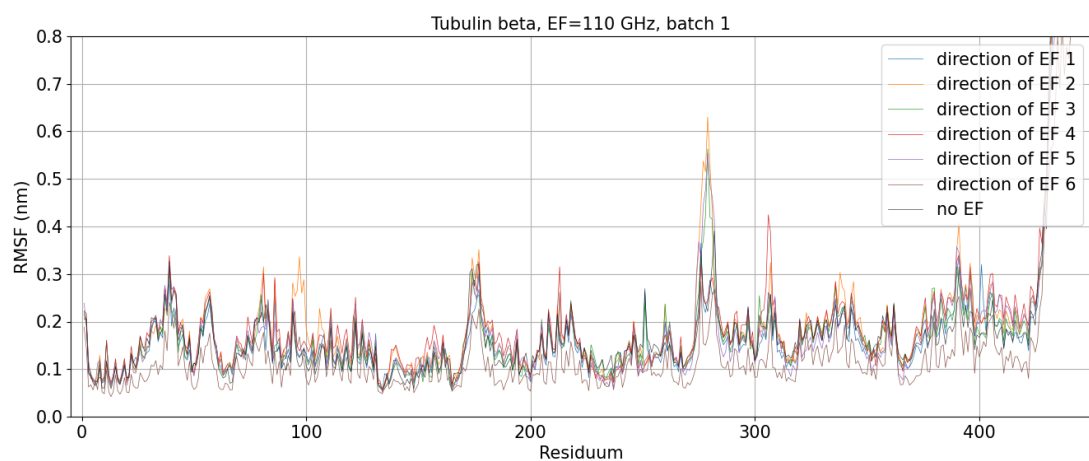


Figure 10.56: RMSF of tubulin β residues subjected to the electric field of frequency 110 GHz; Batch 1

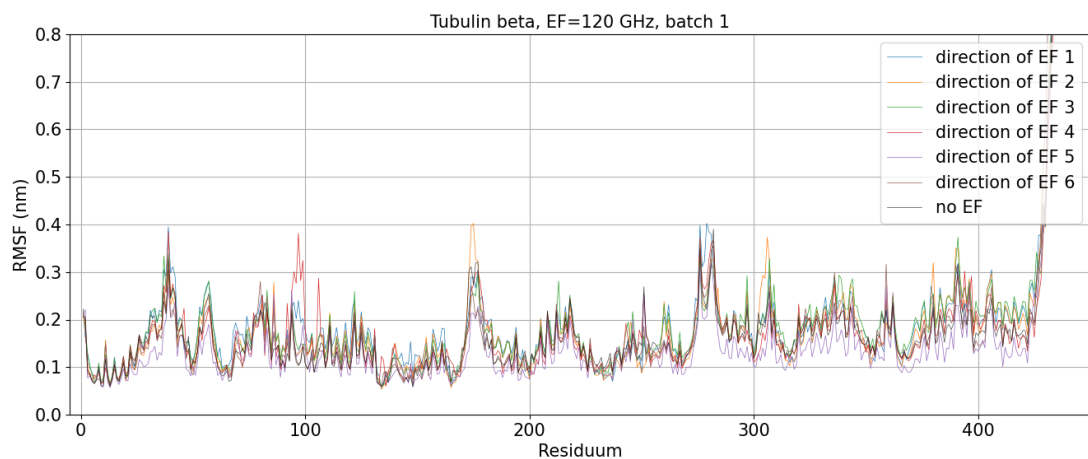


Figure 10.57: RMSF of tubulin β residues subjected to the electric field of frequency 120 GHz; Batch 1

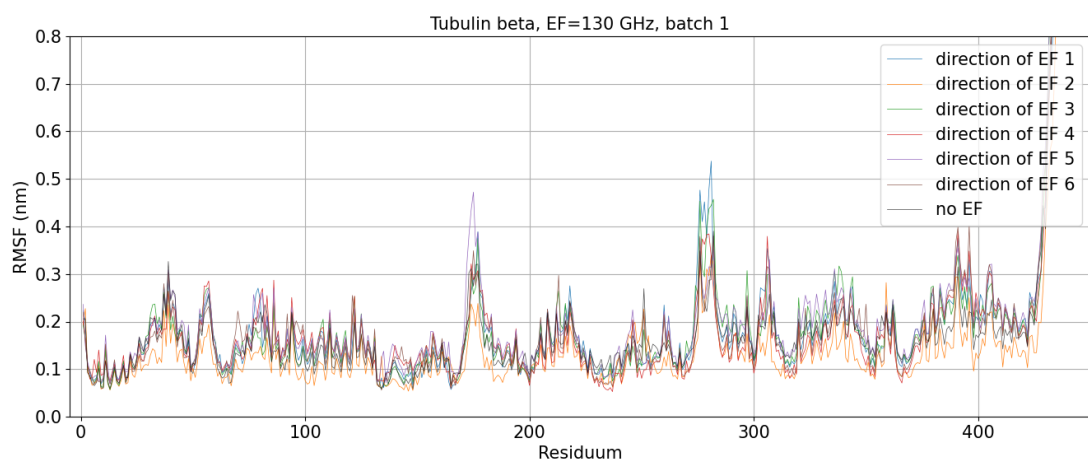


Figure 10.58: RMSF of tubulin β residues subjected to the electric field of frequency 130 GHz; Batch 1

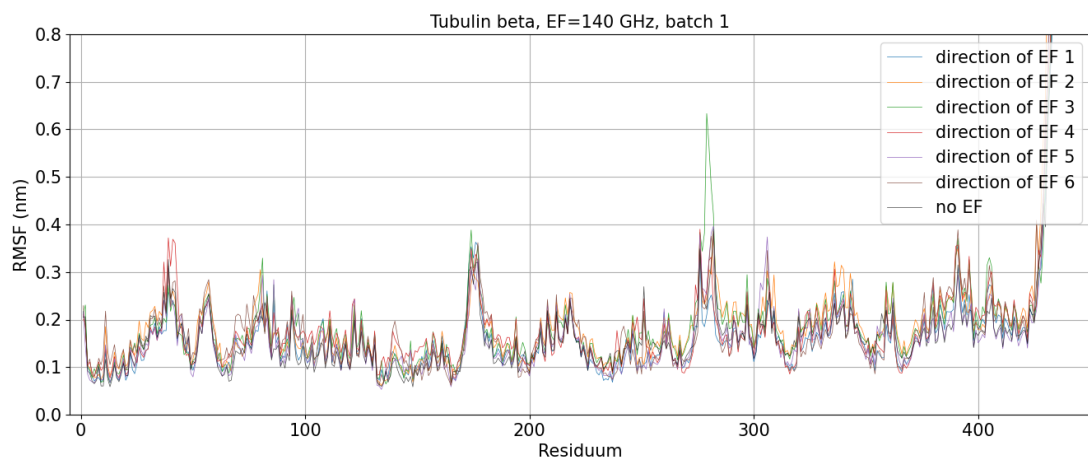


Figure 10.59: RMSF of tubulin β residues subjected to the electric field of frequency 140 GHz; Batch 1

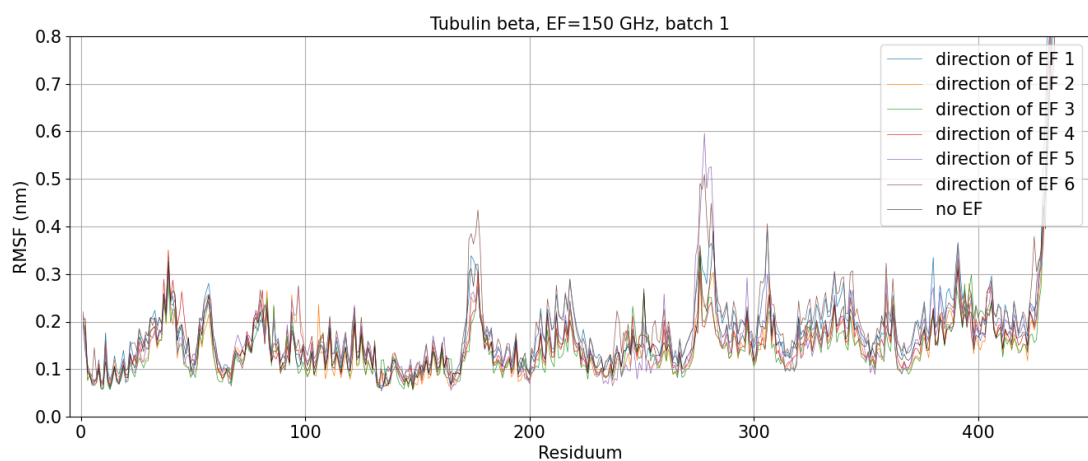


Figure 10.60: RMSF of tubulin β residues subjected to the electric field of frequency 150 GHz; Batch 1

10.8.2 Tubulin β - Batch 2

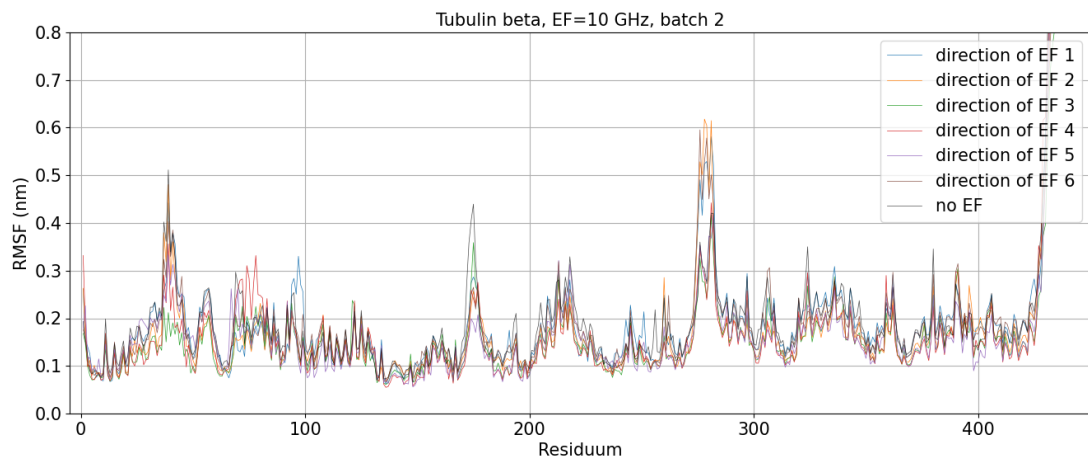


Figure 10.61: RMSF of tubulin β residues subjected to the electric field of frequency 10 GHz; Batch 2

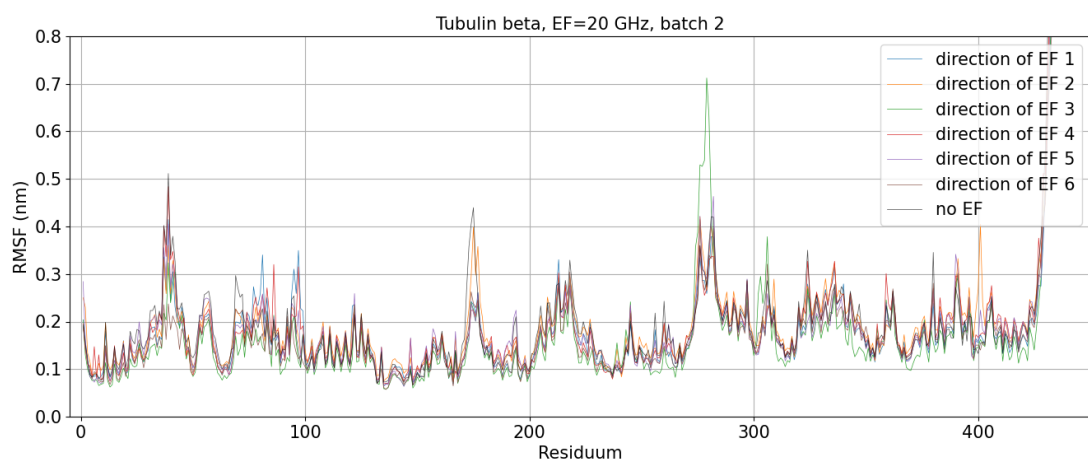


Figure 10.62: RMSF of tubulin β residues subjected to the electric field of frequency 20 GHz; Batch 2

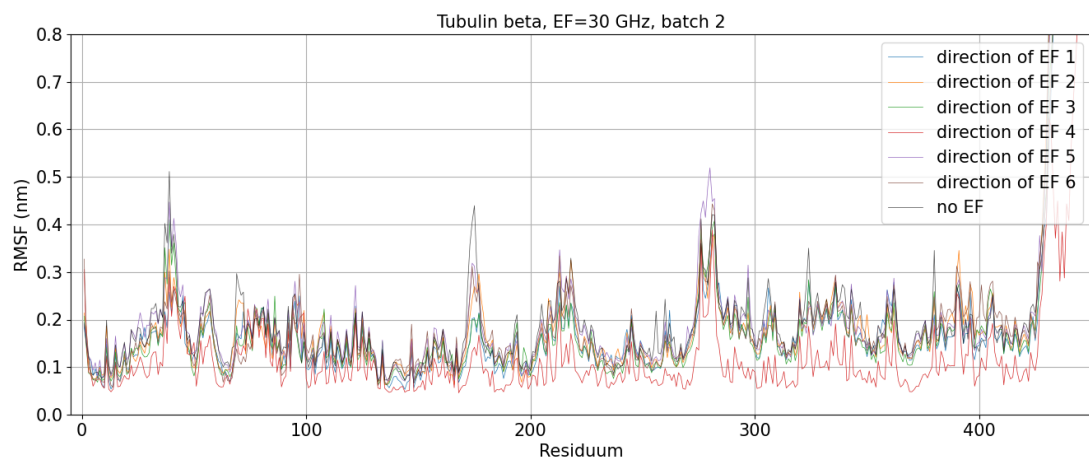


Figure 10.63: RMSF of tubulin β residues subjected to the electric field of frequency 30 GHz; Batch 2

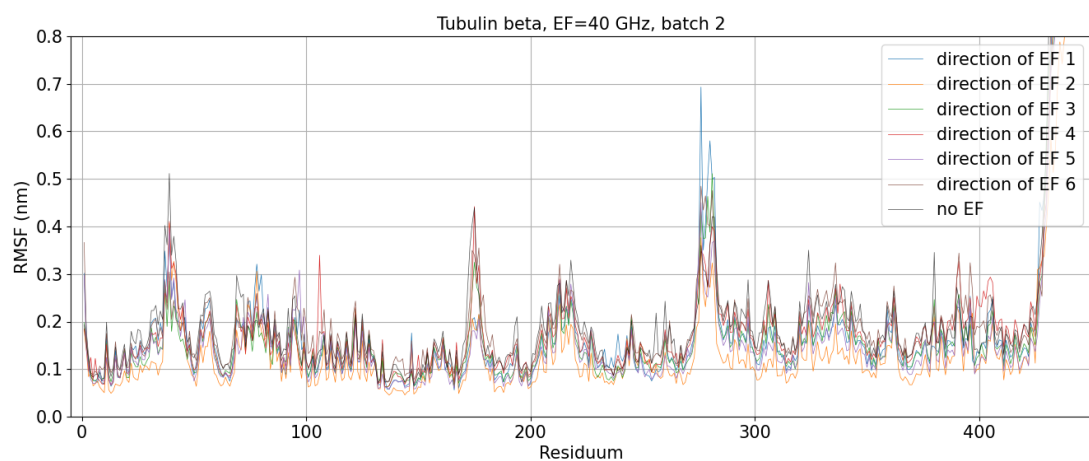


Figure 10.64: RMSF of tubulin β residues subjected to the electric field of frequency 40 GHz; Batch 2

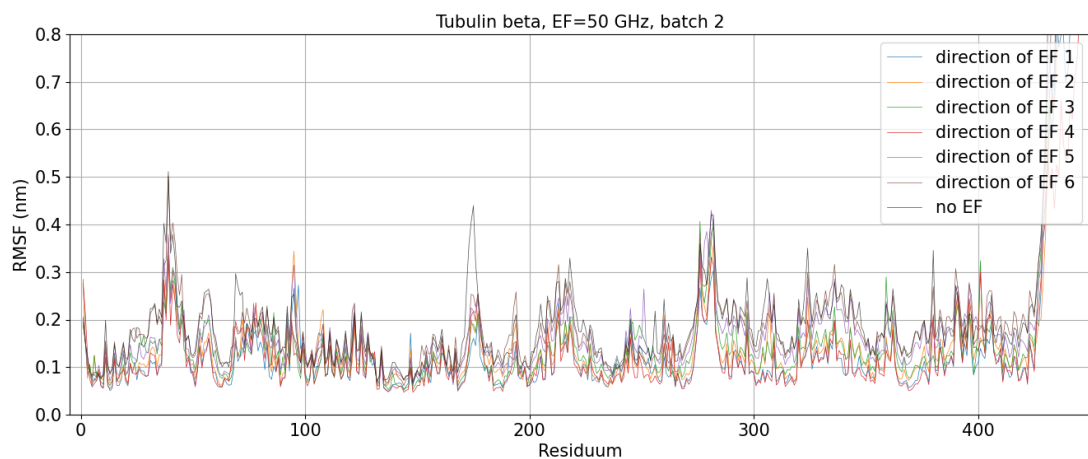


Figure 10.65: RMSF of tubulin β residues subjected to the electric field of frequency 50 GHz; Batch 2

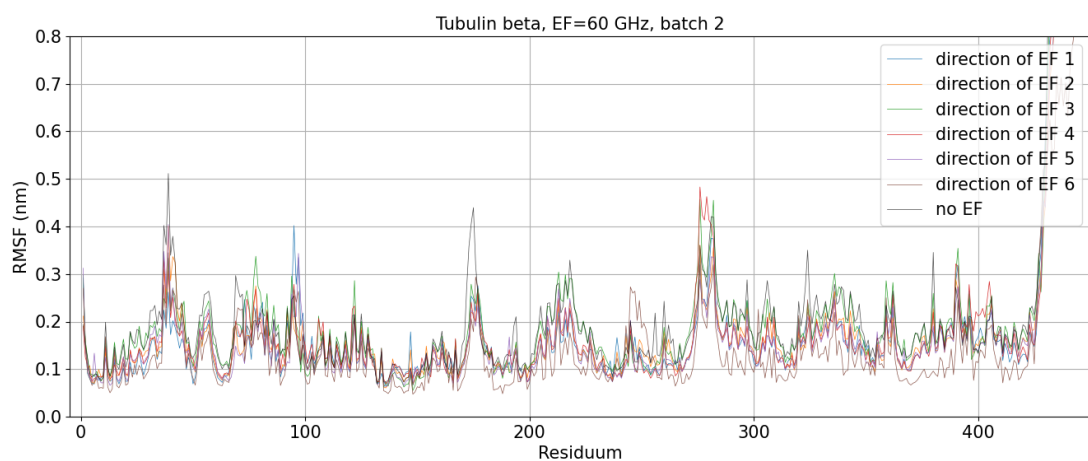


Figure 10.66: RMSF of tubulin β residues subjected to the electric field of frequency 60 GHz; Batch 2

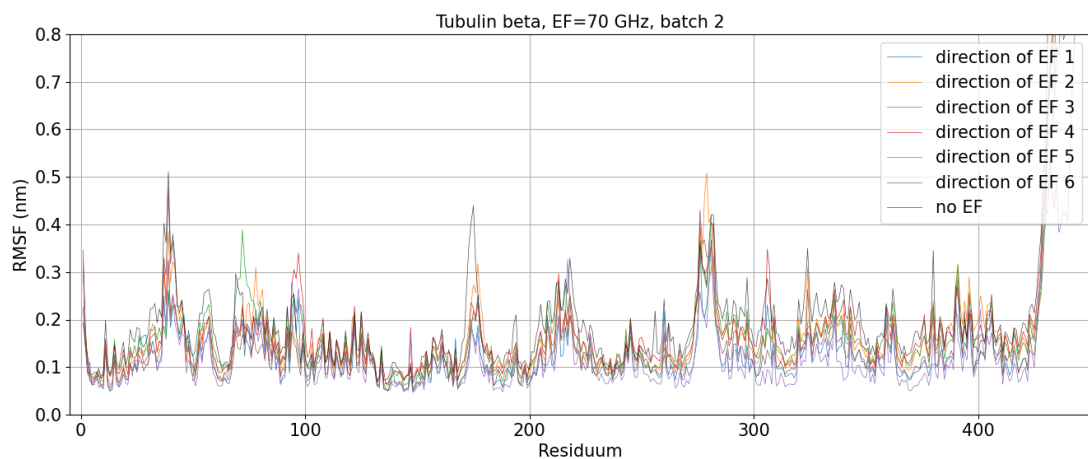


Figure 10.67: RMSF of tubulin β residues subjected to the electric field of frequency 70 GHz; Batch 2

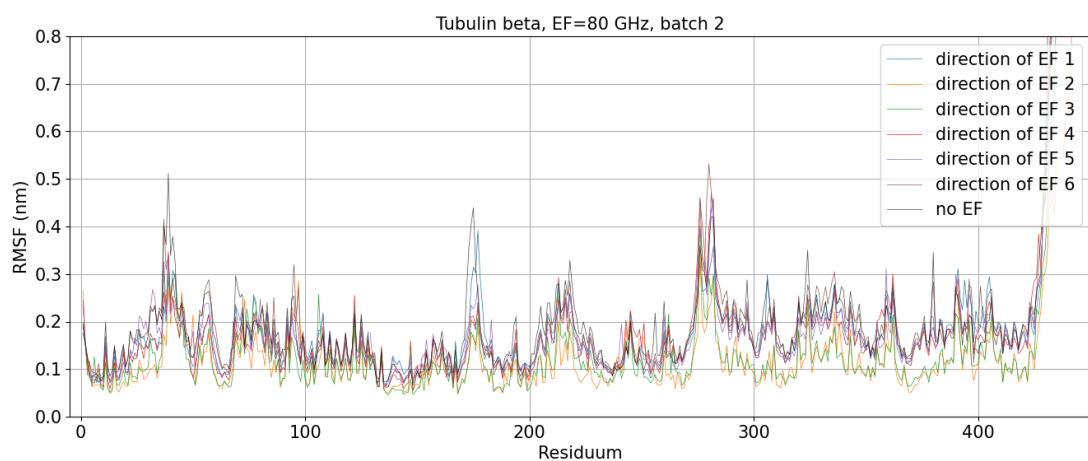


Figure 10.68: RMSF of tubulin β residues subjected to the electric field of frequency 80 GHz; Batch 2

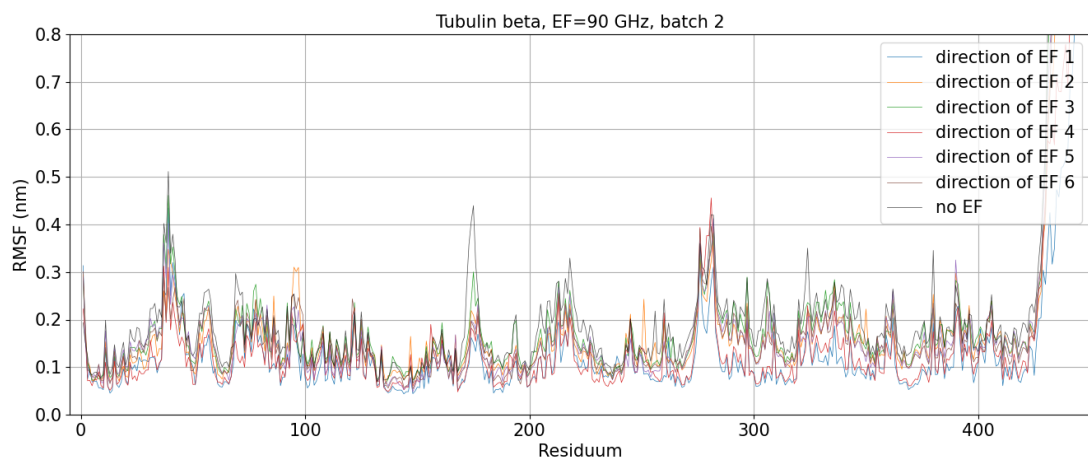


Figure 10.69: RMSF of tubulin β residues subjected to the electric field of frequency 90 GHz; Batch 2

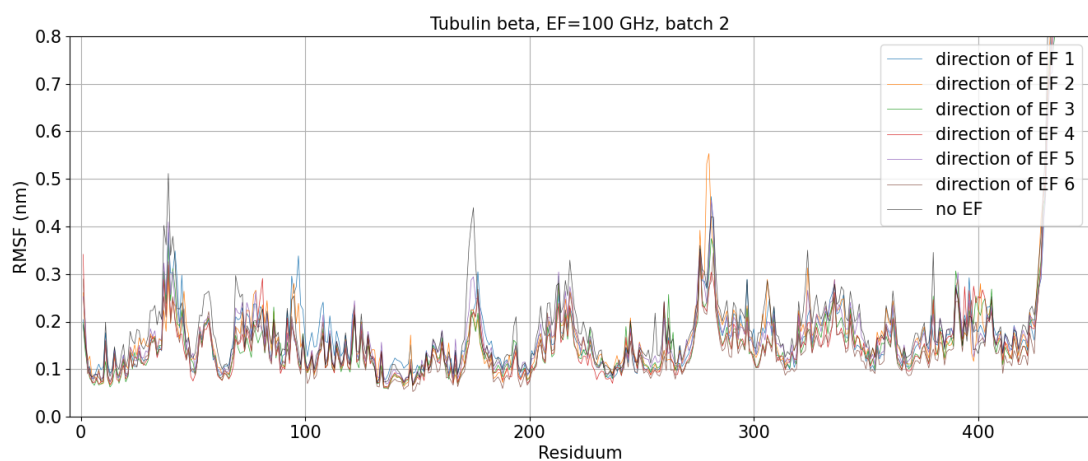


Figure 10.70: RMSF of tubulin β residues subjected to the electric field of frequency 100 GHz; Batch 2

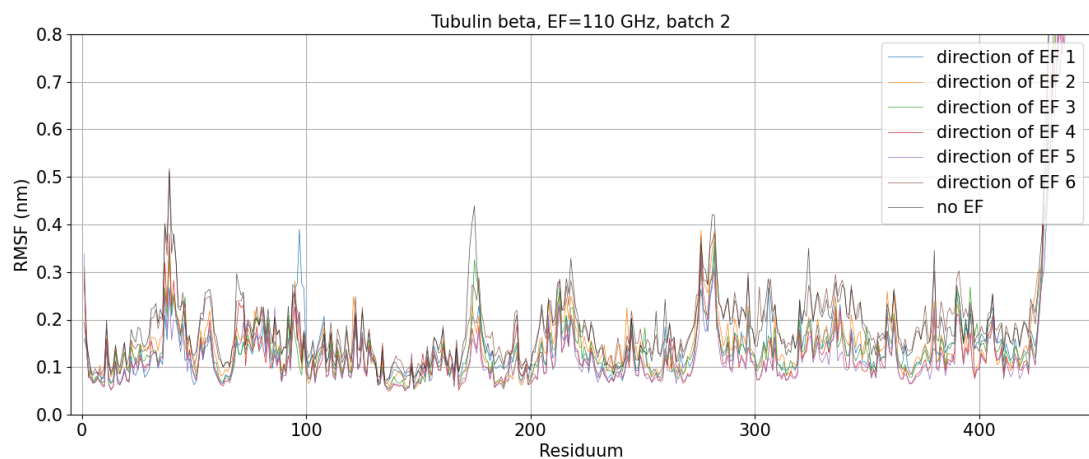


Figure 10.71: RMSF of tubulin β residues subjected to the electric field of frequency 110 GHz; Batch 2

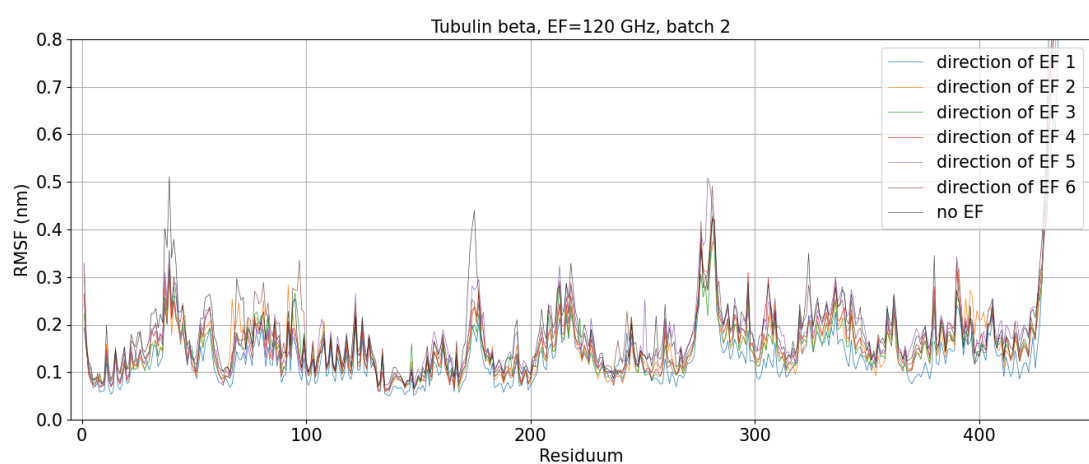


Figure 10.72: RMSF of tubulin β residues subjected to the electric field of frequency 120 GHz; Batch 2

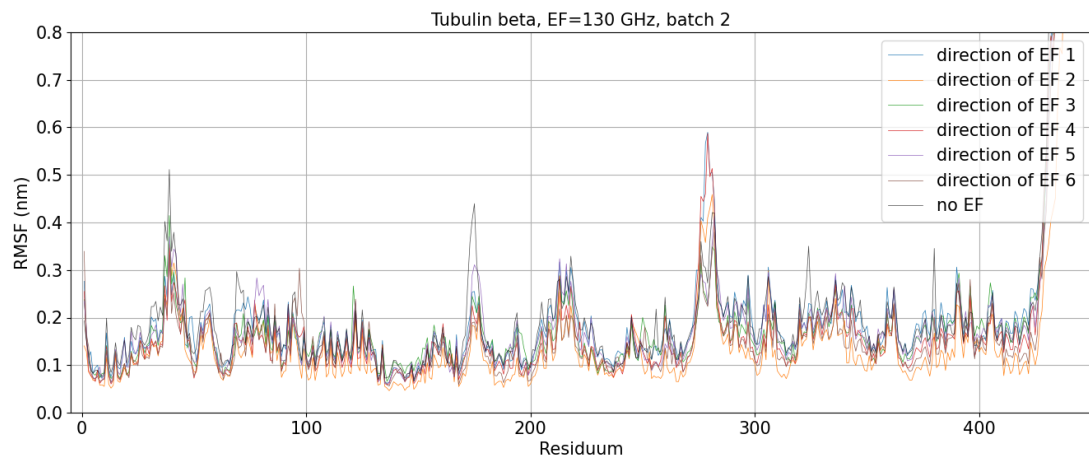


Figure 10.73: RMSF of tubulin β residues subjected to the electric field of frequency 130 GHz; Batch 2

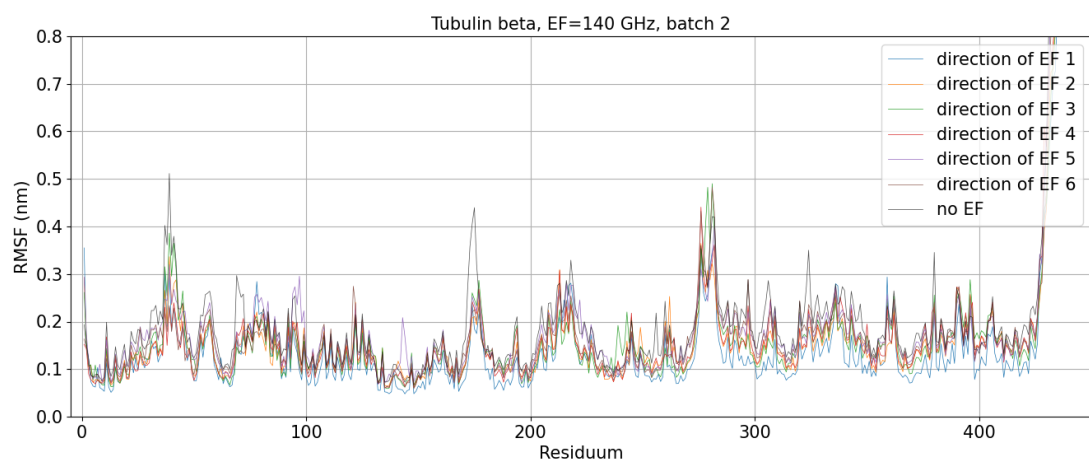


Figure 10.74: RMSF of tubulin β residues subjected to the electric field of frequency 140 GHz; Batch 2

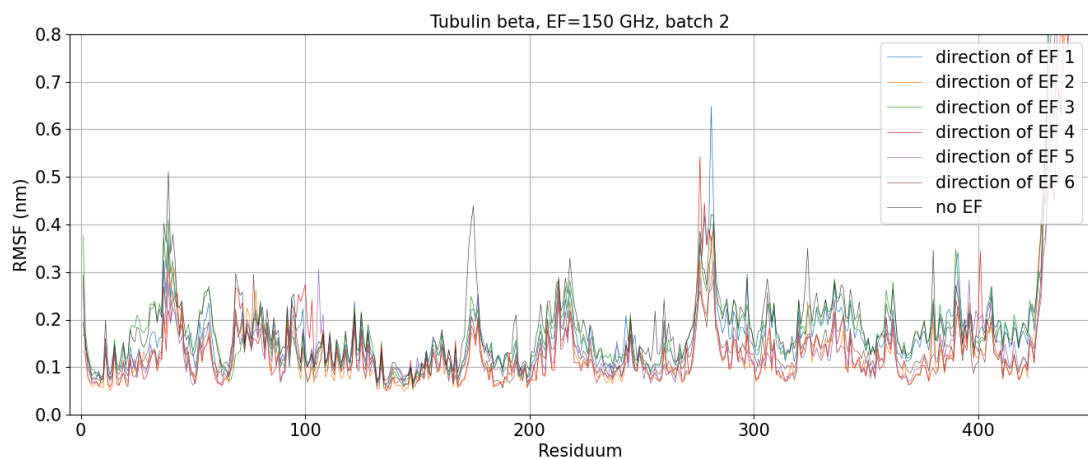


Figure 10.75: RMSF of tubulin β residues subjected to the electric field of frequency 150 GHz; Batch 2

10.8.3 Tubulin β - Batch 3

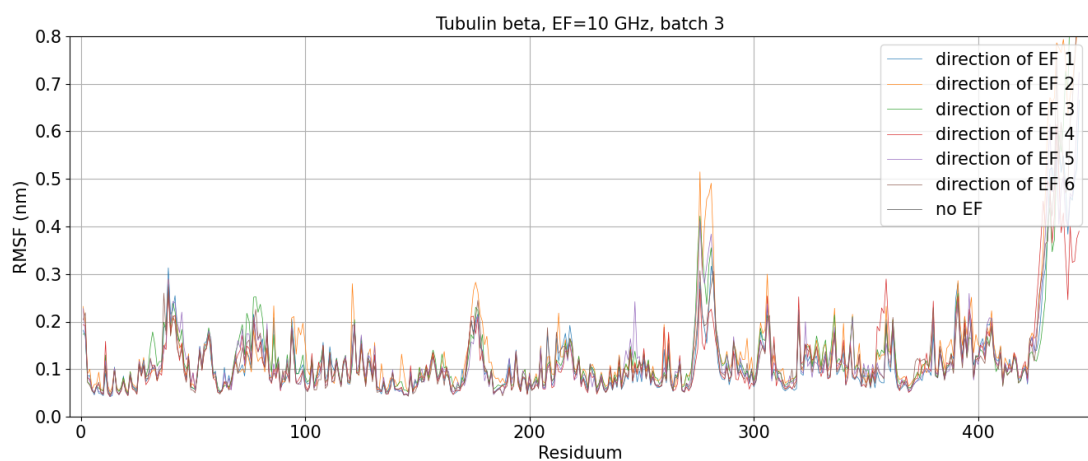


Figure 10.76: RMSF of tubulin β residues subjected to the electric field of frequency 10 GHz; Batch 3

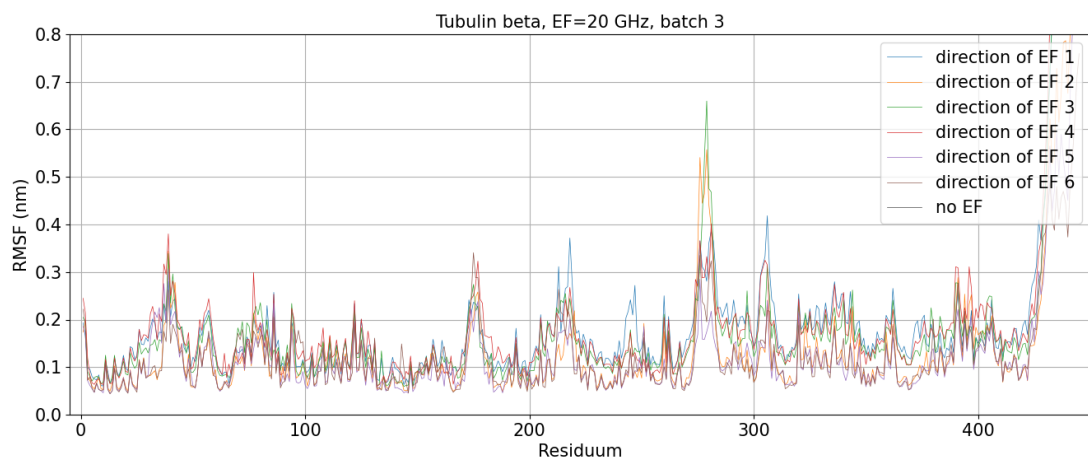


Figure 10.77: RMSF of tubulin β residues subjected to the electric field of frequency 20 GHz; Batch 3

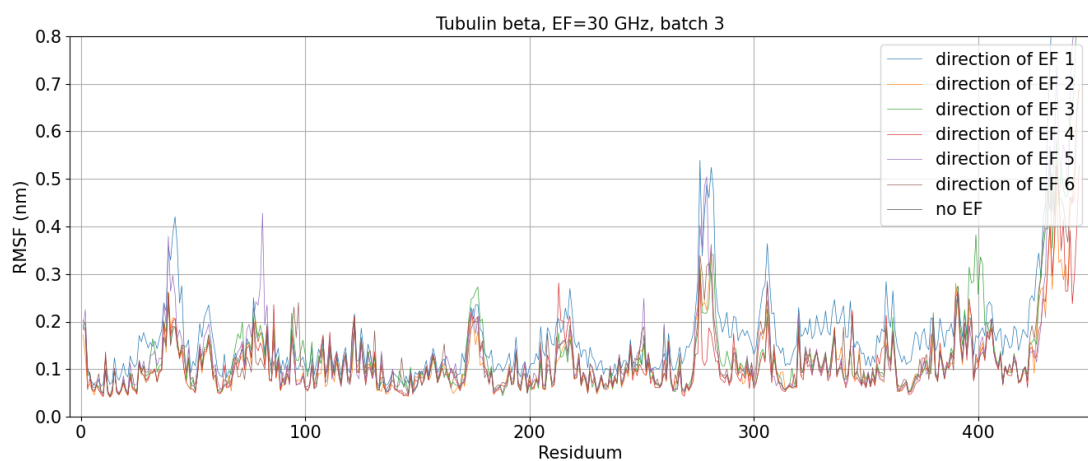


Figure 10.78: RMSF of tubulin β residues subjected to the electric field of frequency 30 GHz; Batch 3

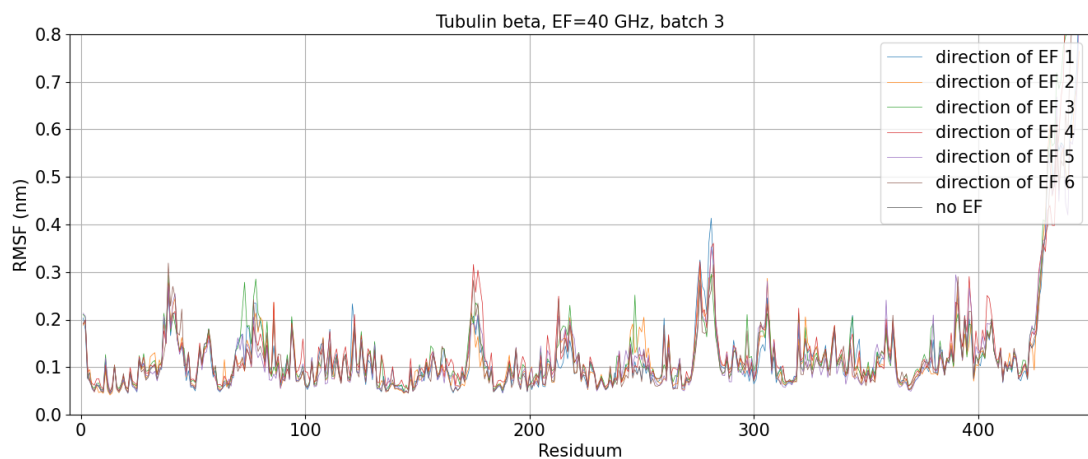


Figure 10.79: RMSF of tubulin β residues subjected to the electric field of frequency 40 GHz; Batch 3

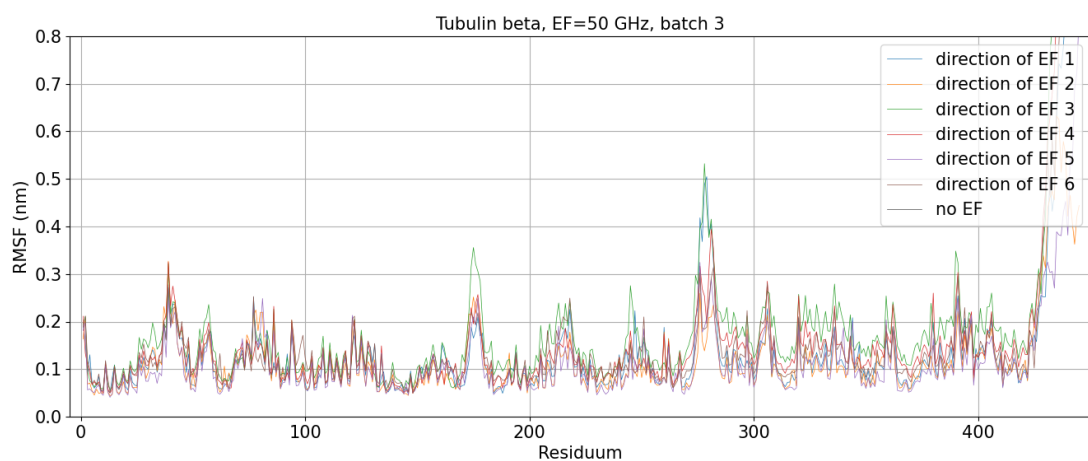


Figure 10.80: RMSF of tubulin β residues subjected to the electric field of frequency 50 GHz; Batch 3

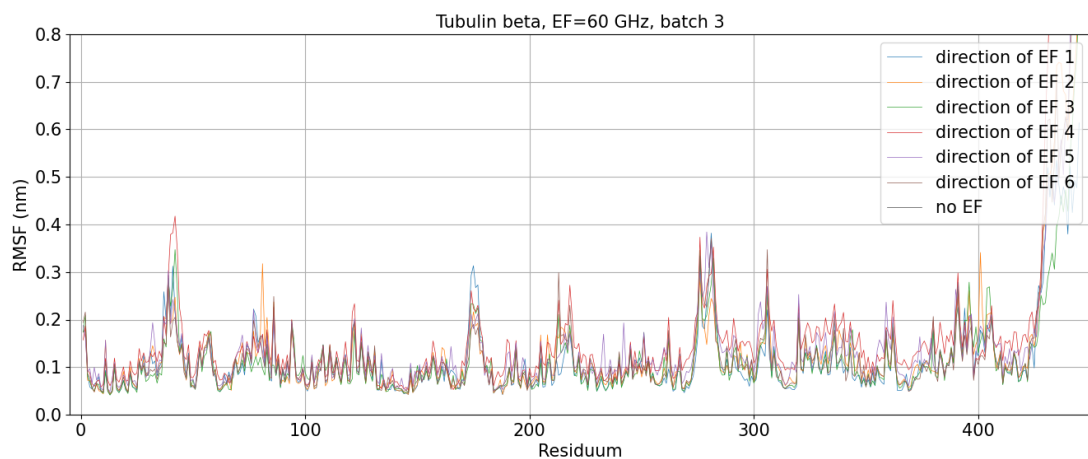


Figure 10.81: RMSF of tubulin β residues subjected to the electric field of frequency 60 GHz; Batch 3

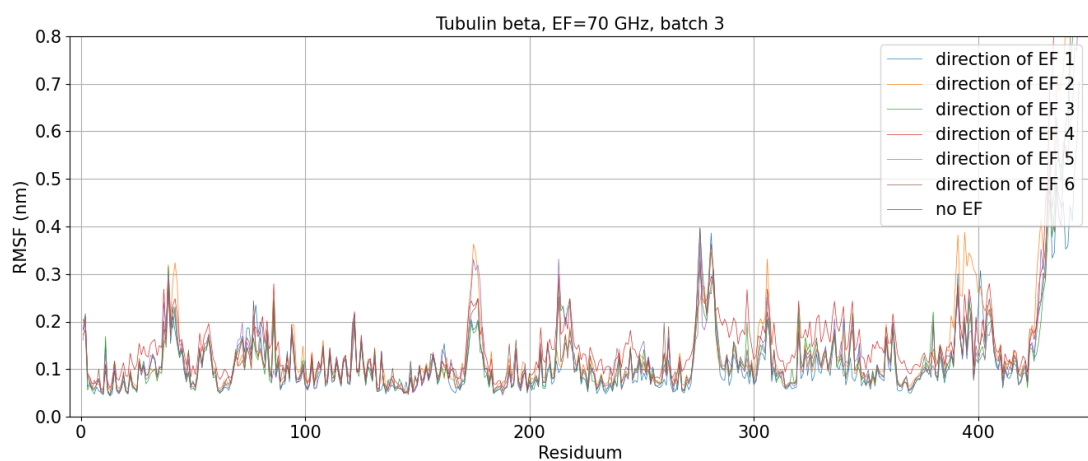


Figure 10.82: RMSF of tubulin β residues subjected to the electric field of frequency 70 GHz; Batch 3

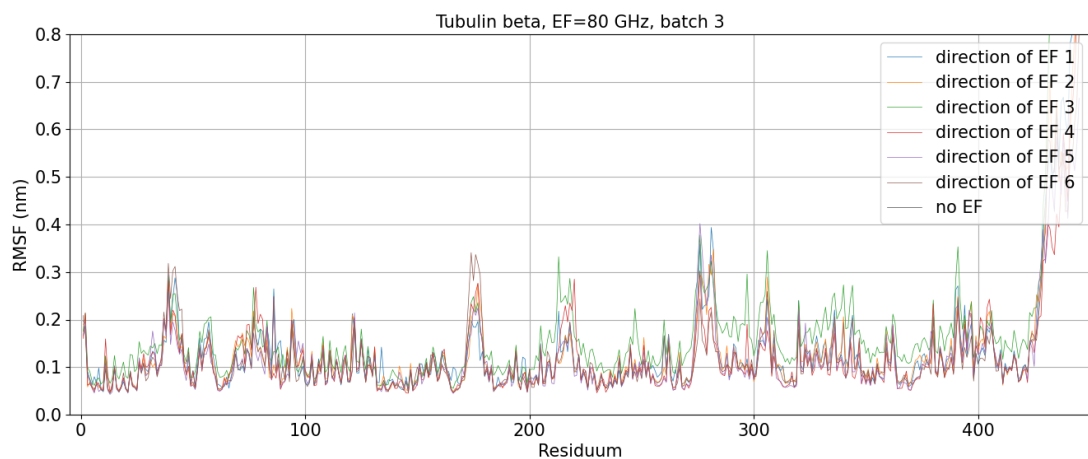


Figure 10.83: RMSF of tubulin β residues subjected to the electric field of frequency 80 GHz; Batch 3

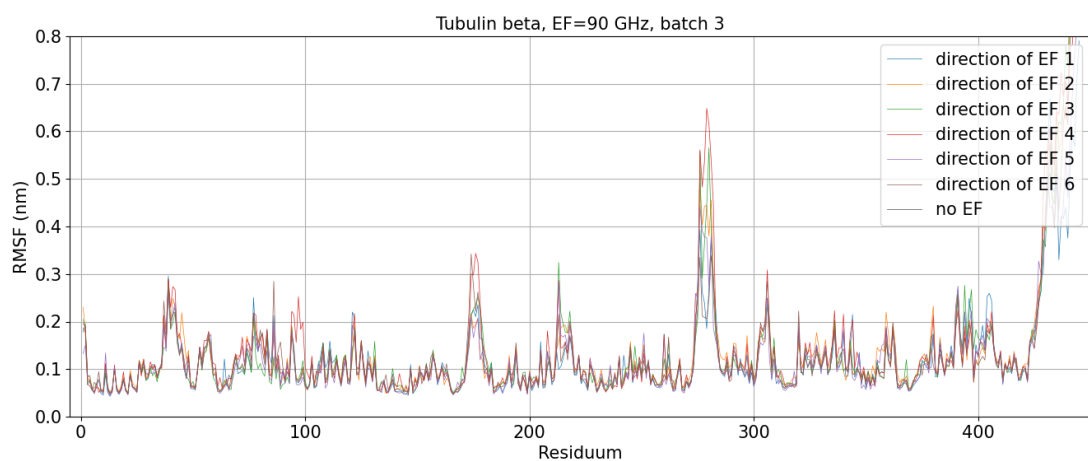


Figure 10.84: RMSF of tubulin β residues subjected to the electric field of frequency 90 GHz; Batch 3

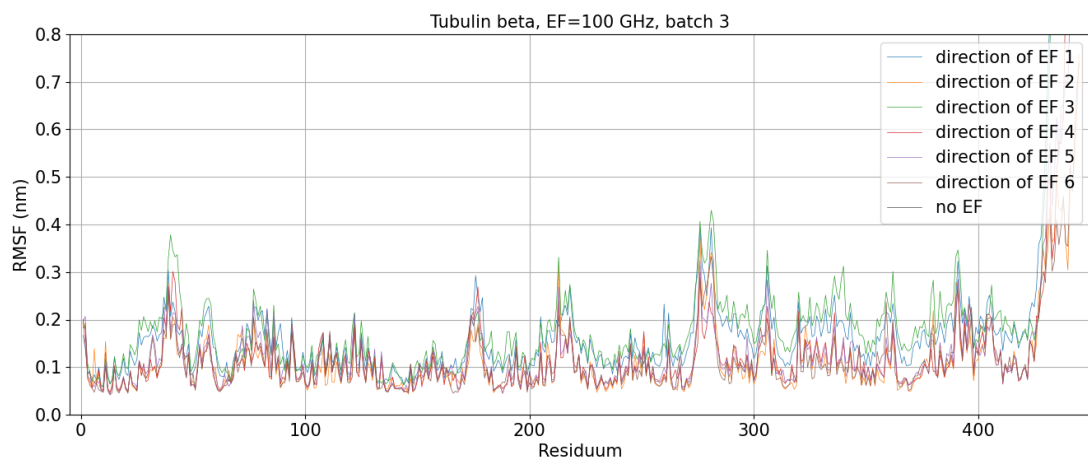


Figure 10.85: RMSF of tubulin β residues subjected to the electric field of frequency 100 GHz; Batch 3

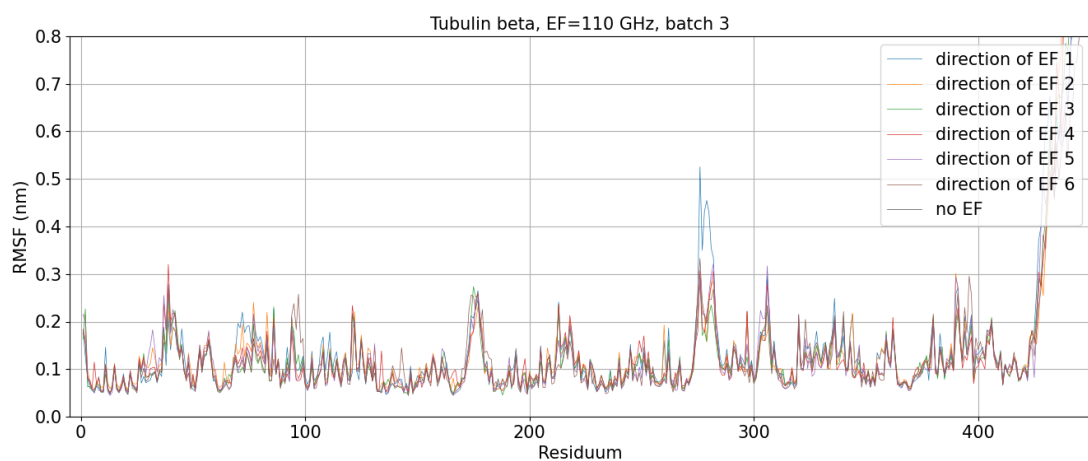


Figure 10.86: RMSF of tubulin β residues subjected to the electric field of frequency 110 GHz; Batch 3

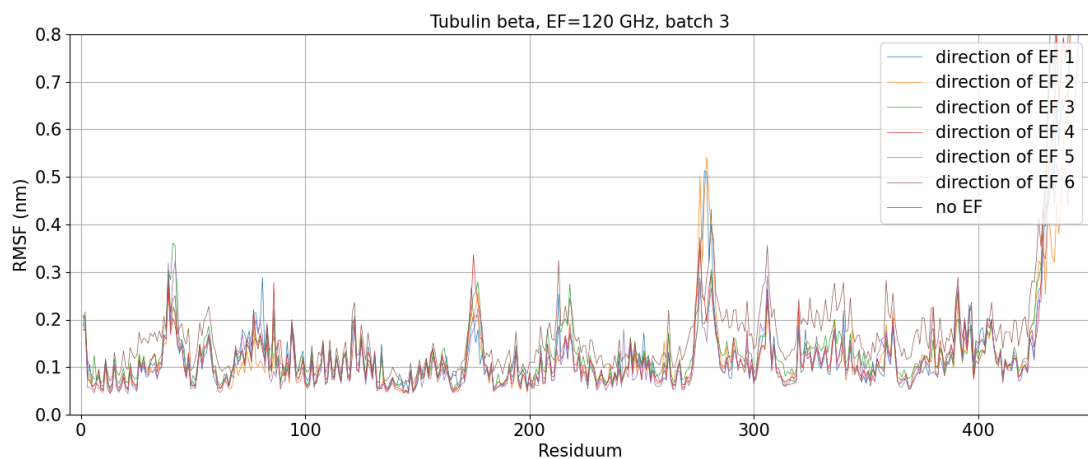


Figure 10.87: RMSF of tubulin β residues subjected to the electric field of frequency 120 GHz; Batch 3

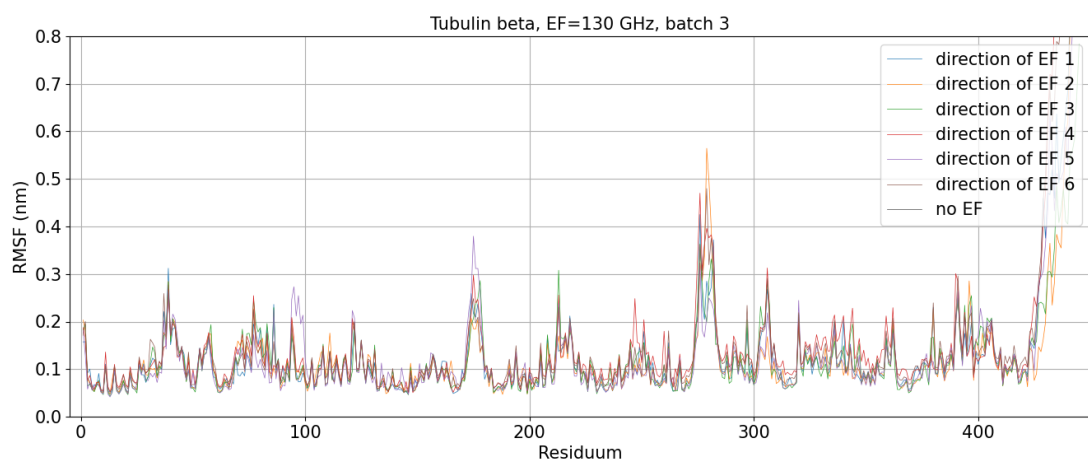


Figure 10.88: RMSF of tubulin β residues subjected to the electric field of frequency 130 GHz; Batch 3

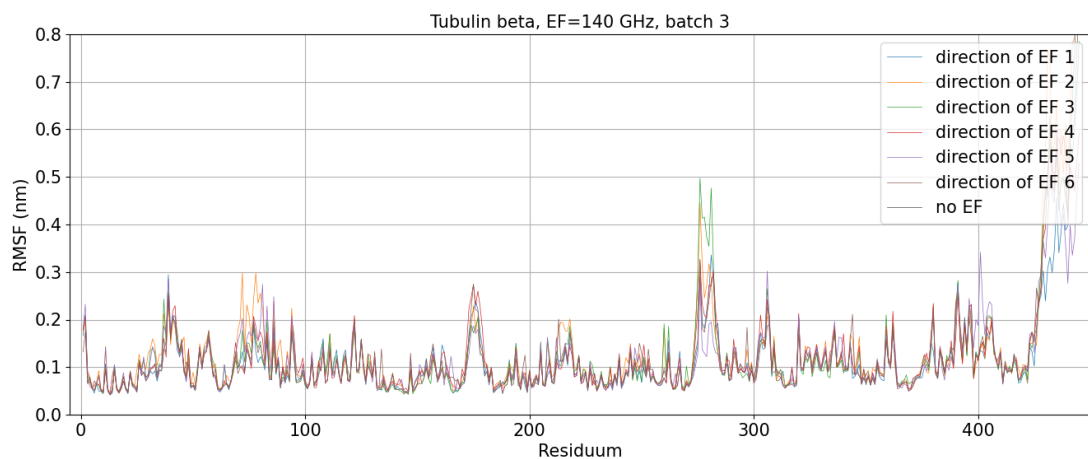


Figure 10.89: RMSF of tubulin β residues subjected to the electric field of frequency 140 GHz; Batch 3

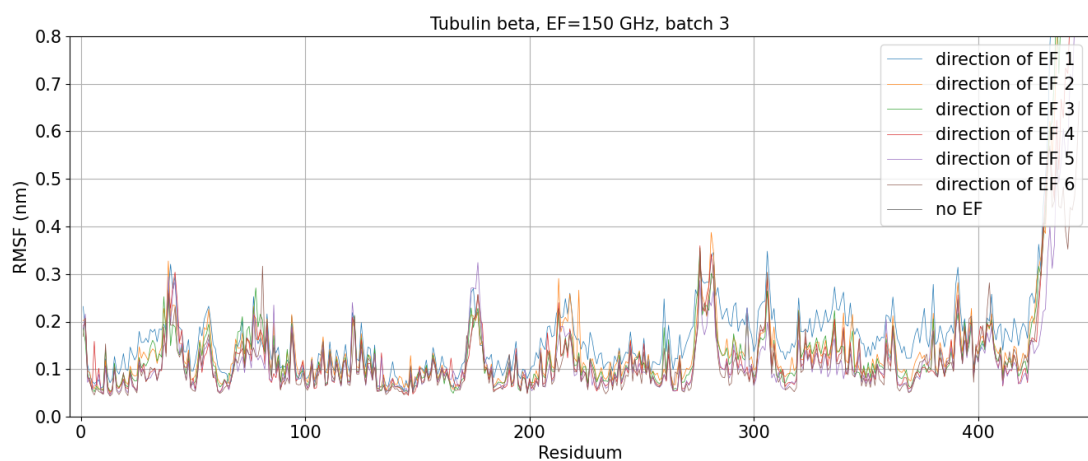


Figure 10.90: RMSF of tubulin β residues subjected to the electric field of frequency 150 GHz; Batch 3

10.9 RMSF_{diff} of residues - individual simulations

10.9.1 Tubulin α - Batch 1

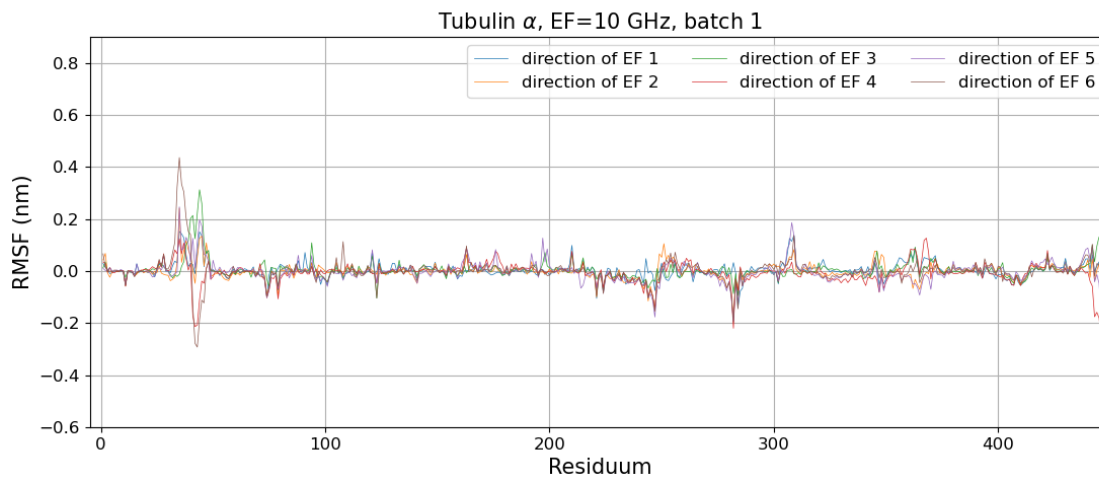


Figure 10.91: RMSF_{diff} of the residues of the tubulin α subjected to the electric field of frequency 10 GHz, Batch 1

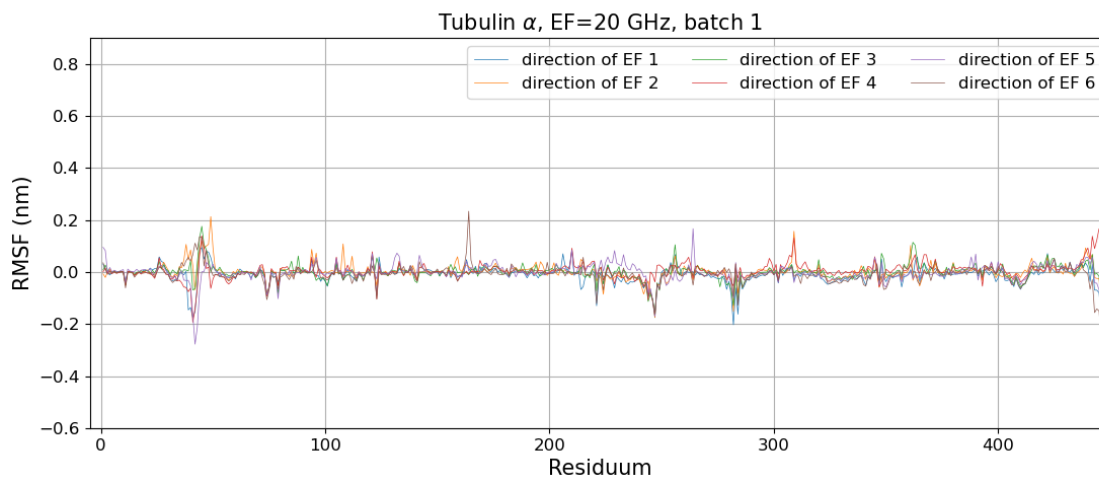


Figure 10.92: RMSF_{diff} of the residues of the tubulin α subjected to the electric field of frequency 20 GHz, Batch 1

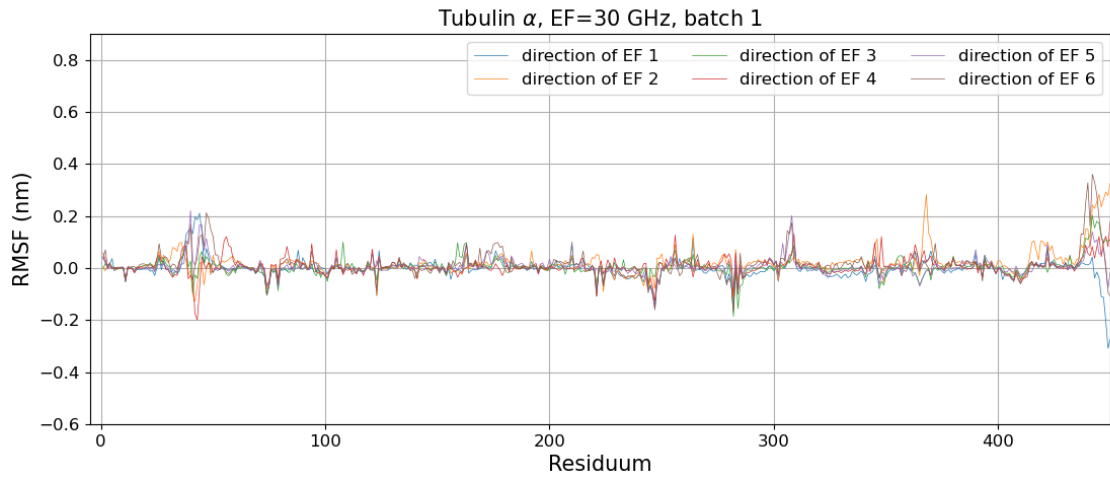


Figure 10.93: $\text{RMSF}_{\text{diff}}$ of the residues of the tubulin α subjected to the electric field of frequency 30 GHz, Batch 1

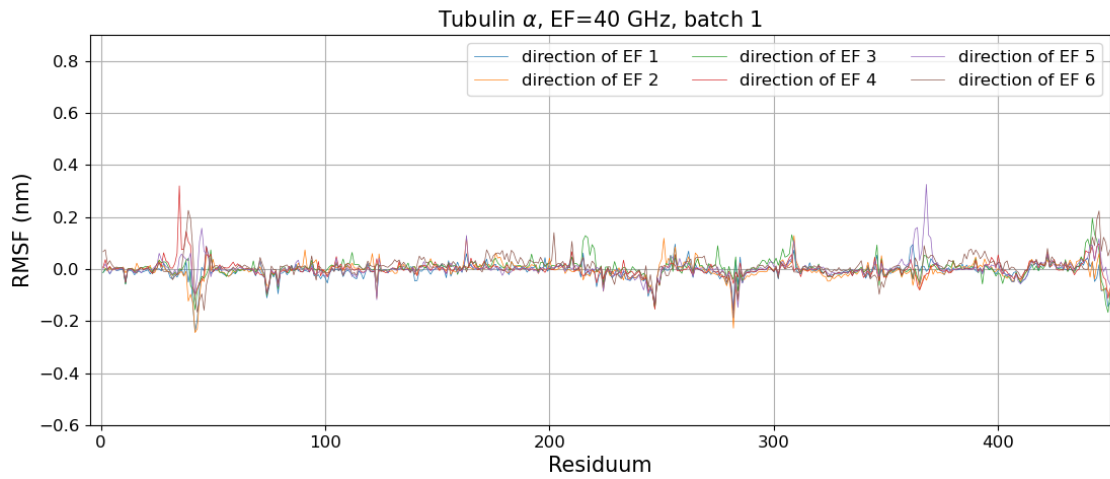


Figure 10.94: $\text{RMSF}_{\text{diff}}$ of the residues of the tubulin α subjected to the electric field of frequency 40 GHz, Batch 1

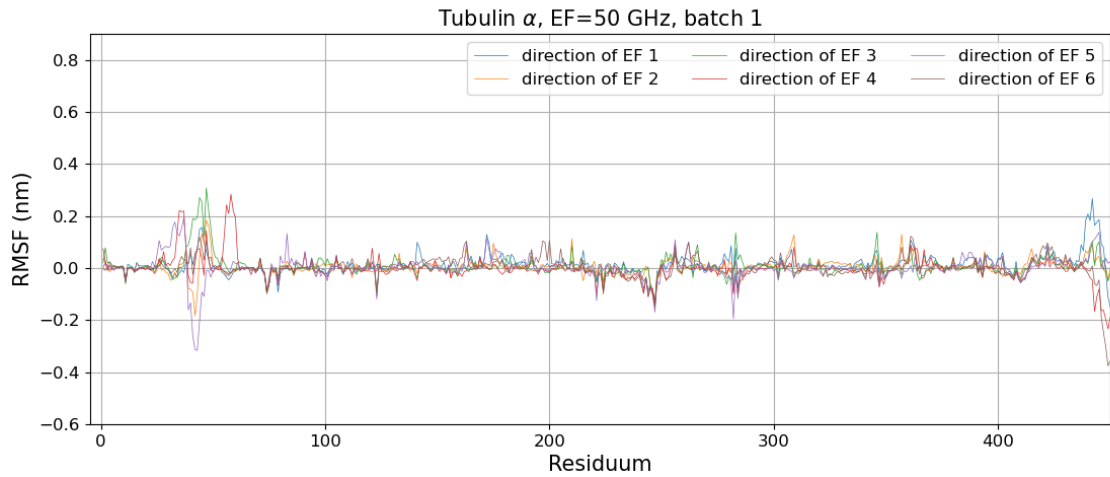


Figure 10.95: $\text{RMSF}_{\text{diff}}$ of the residues of the tubulin α subjected to the electric field of frequency 50 GHz, Batch 1

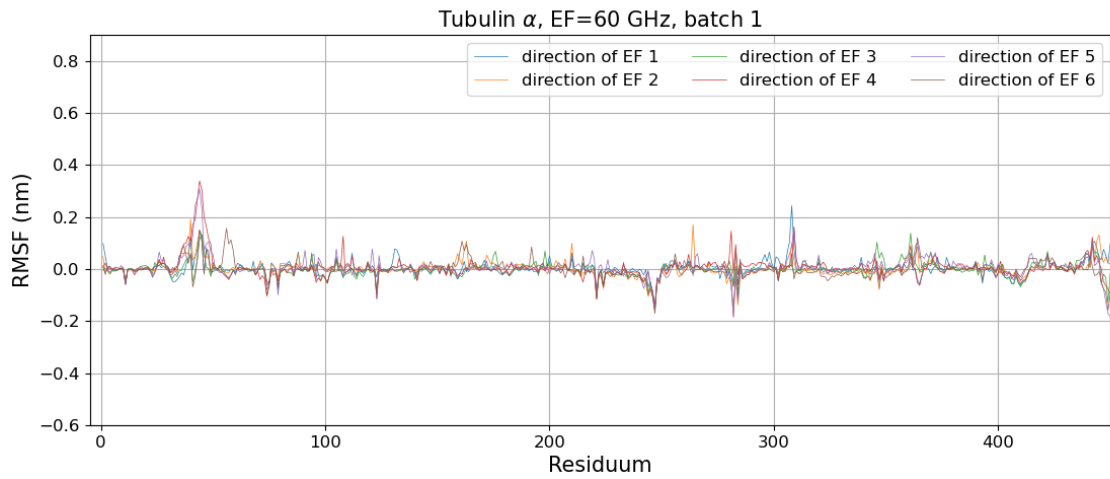


Figure 10.96: $\text{RMSF}_{\text{diff}}$ of the residues of the tubulin α subjected to the electric field of frequency 60 GHz, Batch 1

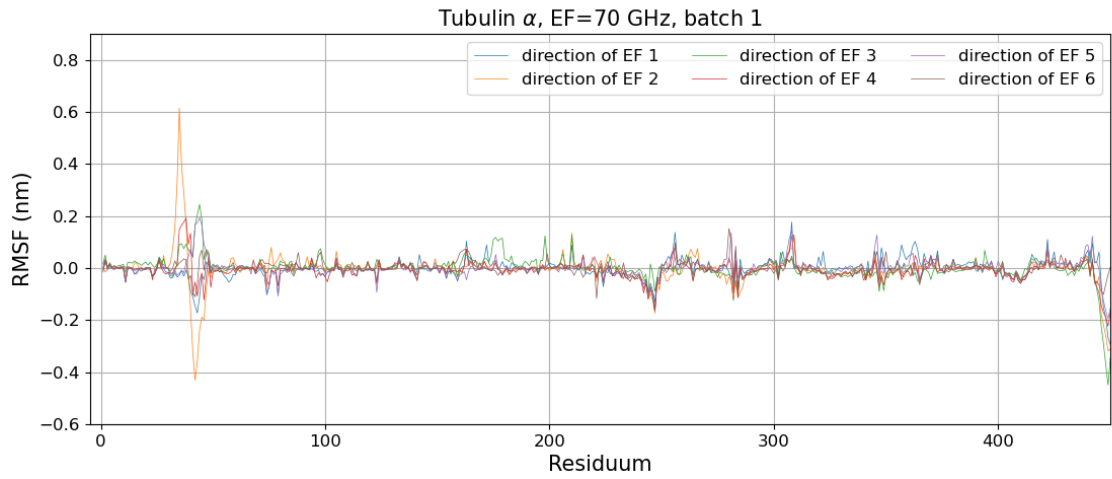


Figure 10.97: $\text{RMSF}_{\text{diff}}$ of the residues of the tubulin α subjected to the electric field of frequency 70 GHz, Batch 1

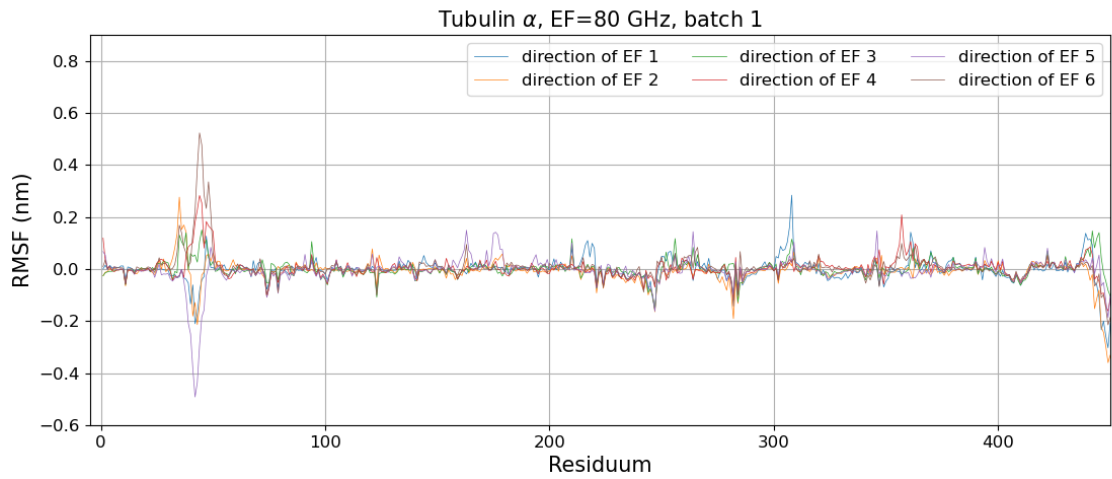


Figure 10.98: $\text{RMSF}_{\text{diff}}$ of the residues of the tubulin α subjected to the electric field of frequency 80 GHz, Batch 1

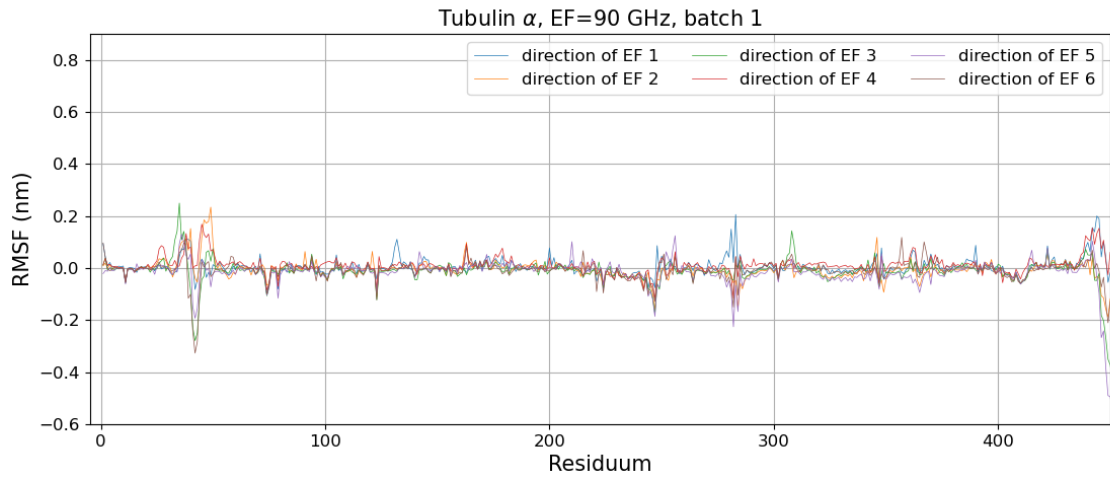


Figure 10.99: $\text{RMSF}_{\text{diff}}$ of the residues of the tubulin α subjected to the electric field of frequency 90 GHz, Batch 1

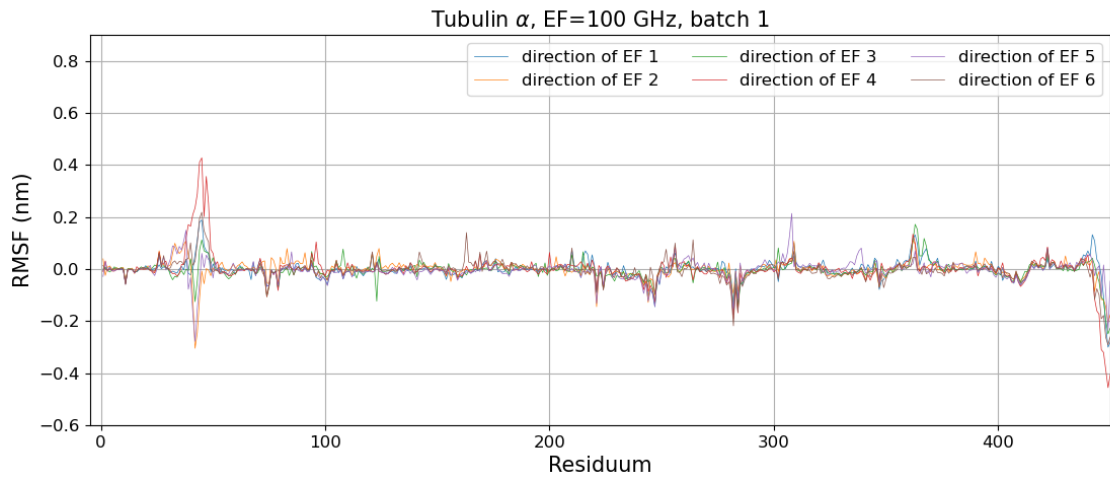


Figure 10.100: $\text{RMSF}_{\text{diff}}$ of the residues of the tubulin α subjected to the electric field of frequency 100 GHz, Batch 1

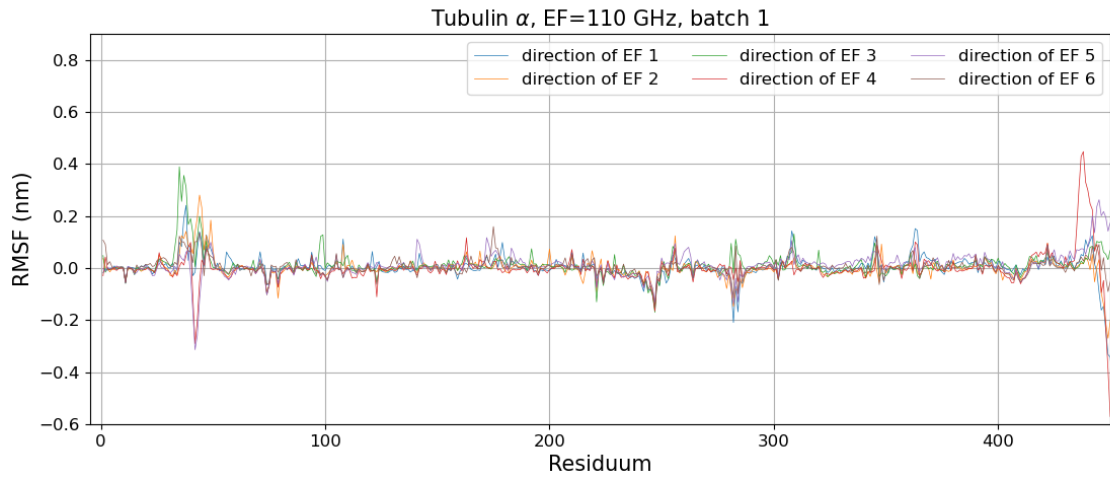


Figure 10.101: $\text{RMSF}_{\text{diff}}$ of the residues of the tubulin α subjected to the electric field of frequency 110 GHz, Batch 1

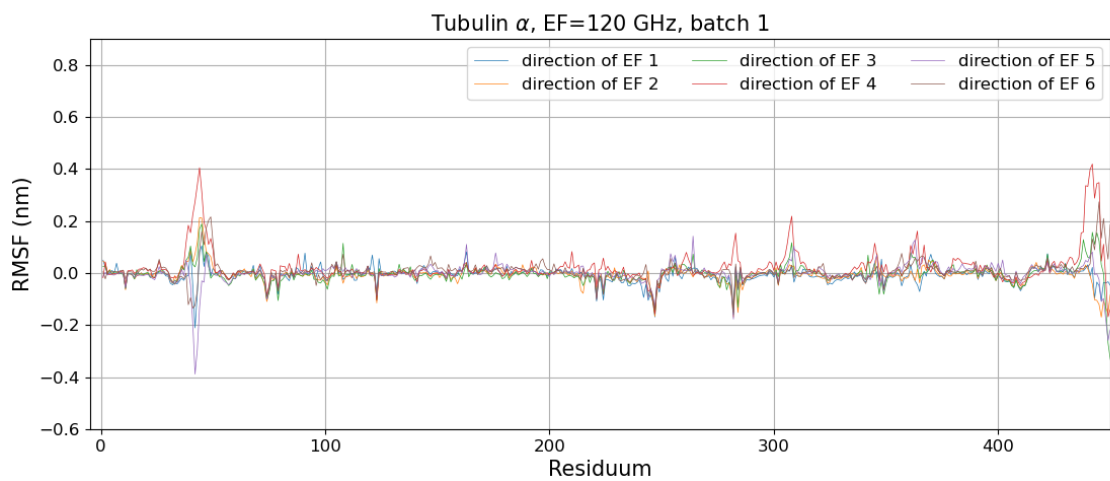


Figure 10.102: $\text{RMSF}_{\text{diff}}$ of the residues of the tubulin α subjected to the electric field of frequency 120 GHz, Batch 1

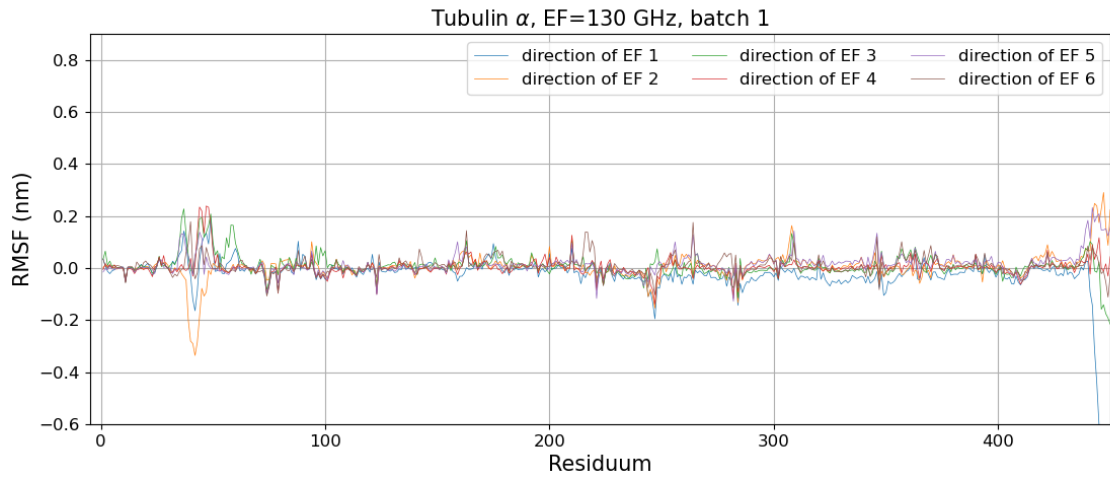


Figure 10.103: $\text{RMSF}_{\text{diff}}$ of the residues of the tubulin α subjected to the electric field of frequency 130 GHz, Batch 1

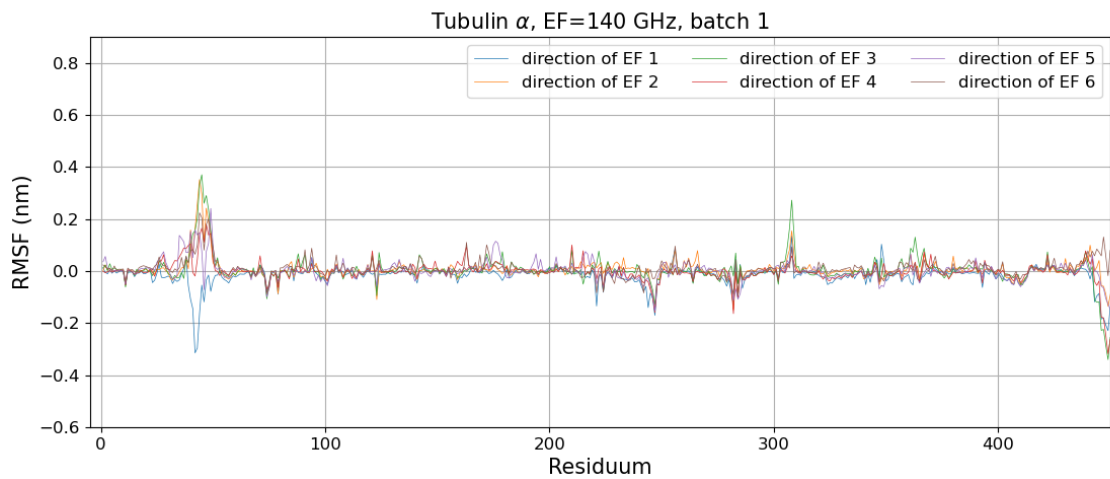


Figure 10.104: $\text{RMSF}_{\text{diff}}$ of the residues of the tubulin α subjected to the electric field of frequency 140 GHz, Batch 1

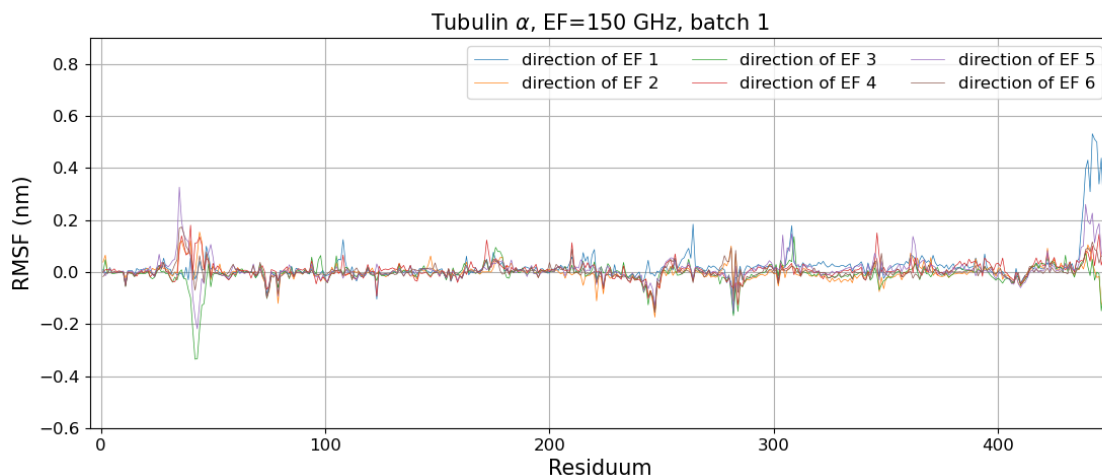


Figure 10.105: $\text{RMSF}_{\text{diff}}$ of the residues of the tubulin α subjected to the electric field of frequency 150 GHz, Batch 1

10.9.2 Tubulin α - Batch 2

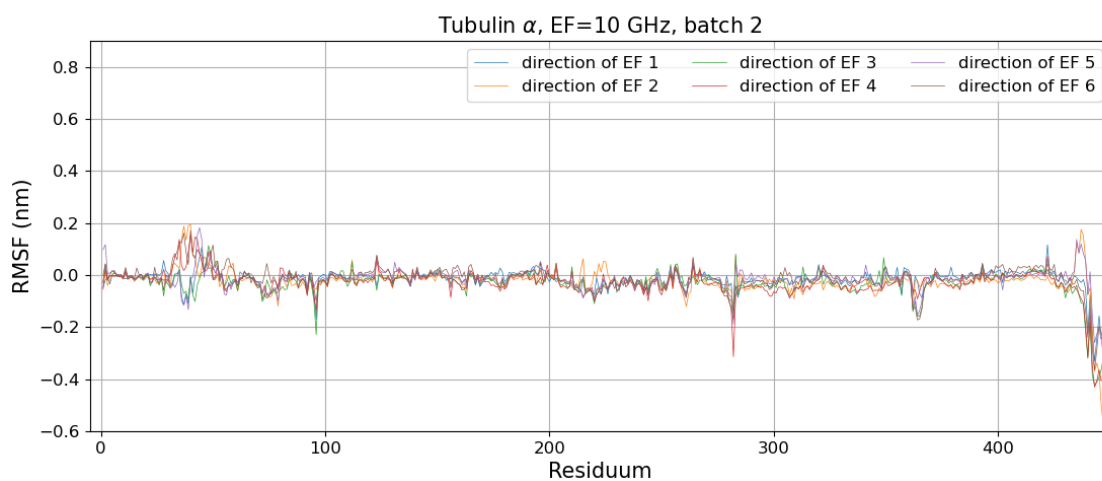


Figure 10.106: $\text{RMSF}_{\text{diff}}$ of the residues of the tubulin α subjected to the electric field of frequency 10 GHz, Batch 2

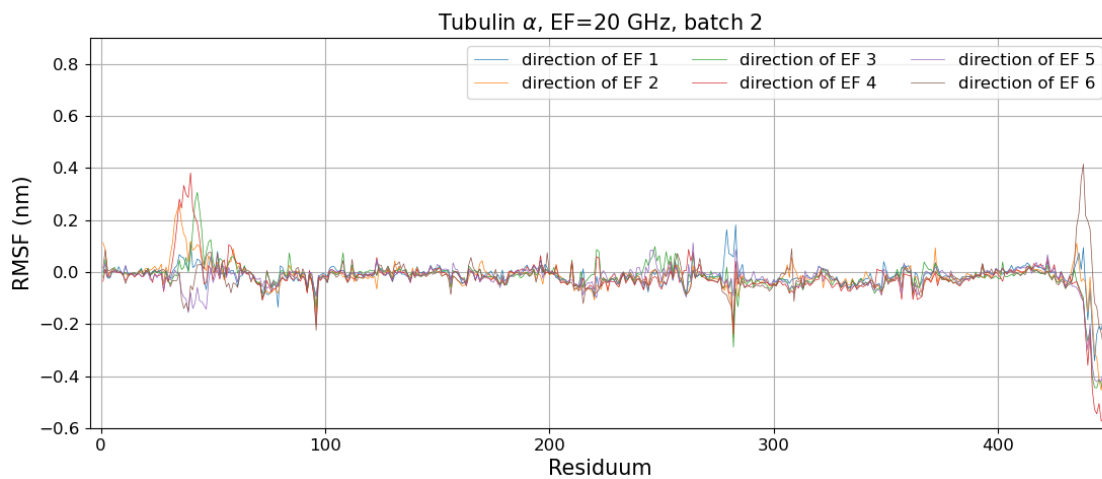


Figure 10.107: $\text{RMSF}_{\text{diff}}$ of the residues of the tubulin α subjected to the electric field of frequency 20 GHz, Batch 2

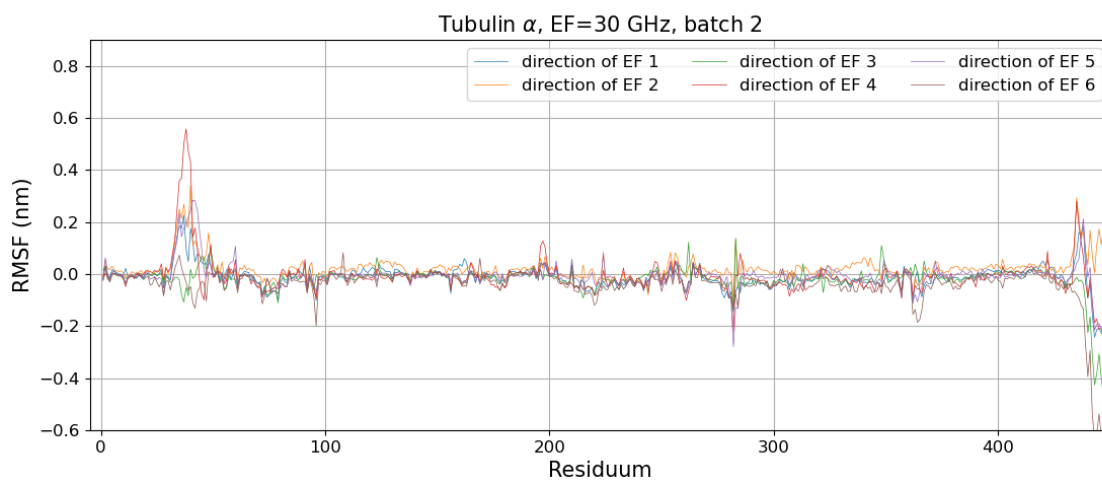


Figure 10.108: $\text{RMSF}_{\text{diff}}$ of the residues of the tubulin α subjected to the electric field of frequency 30 GHz, Batch 2

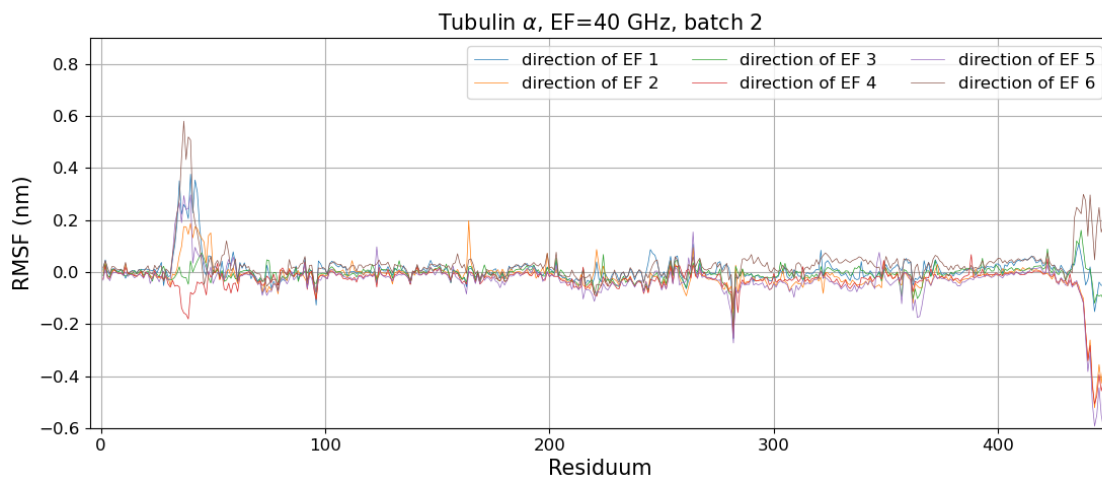


Figure 10.109: $\text{RMSF}_{\text{diff}}$ of the residues of the tubulin α subjected to the electric field of frequency 40 GHz, Batch 2



Figure 10.110: $\text{RMSF}_{\text{diff}}$ of the residues of the tubulin α subjected to the electric field of frequency 50 GHz, Batch 2

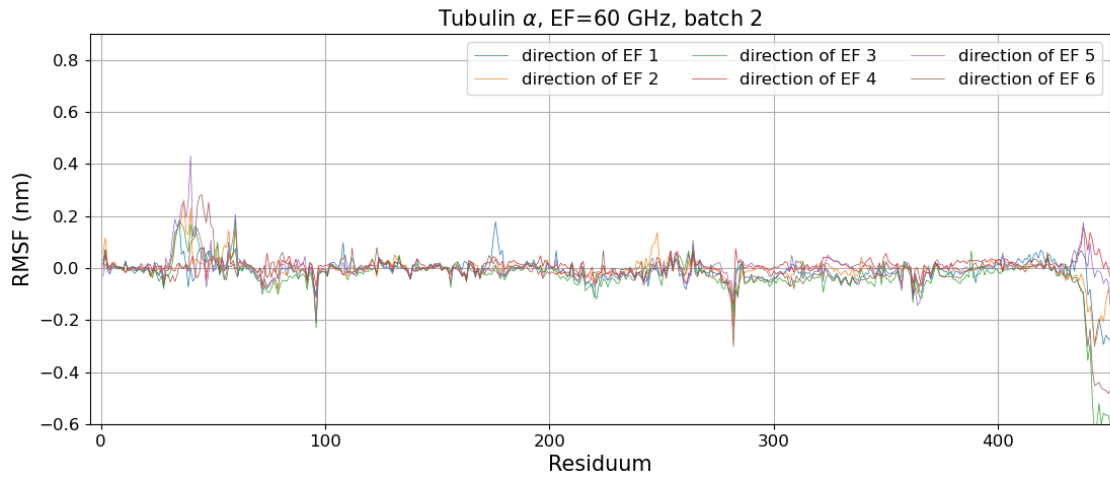


Figure 10.111: $\text{RMSF}_{\text{diff}}$ of the residues of the tubulin α subjected to the electric field of frequency 60 GHz, Batch 2

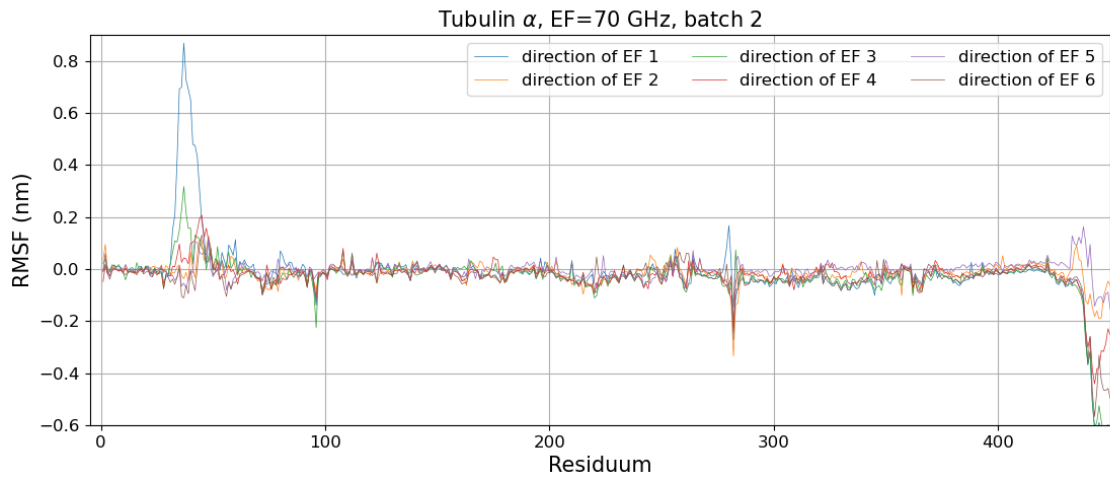


Figure 10.112: $\text{RMSF}_{\text{diff}}$ of the residues of the tubulin α subjected to the electric field of frequency 70 GHz, Batch 2

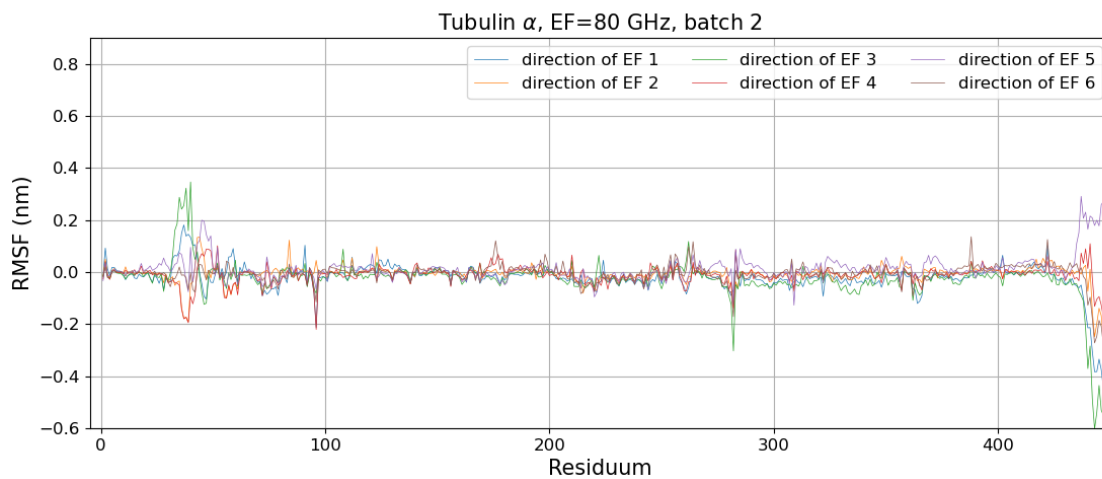


Figure 10.113: $\text{RMSF}_{\text{diff}}$ of the residues of the tubulin α subjected to the electric field of frequency 80 GHz, Batch 2

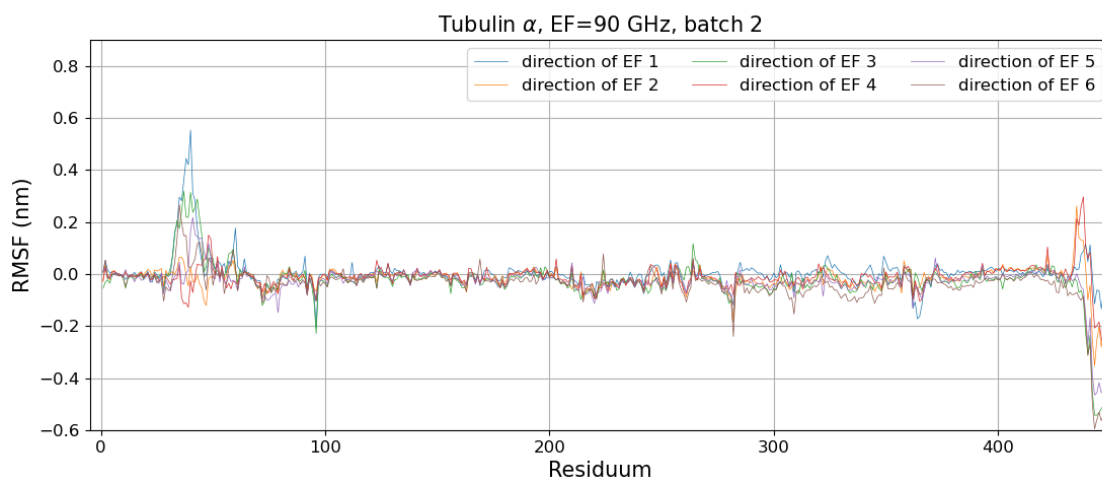


Figure 10.114: $\text{RMSF}_{\text{diff}}$ of the residues of the tubulin α subjected to the electric field of frequency 90 GHz, Batch 2

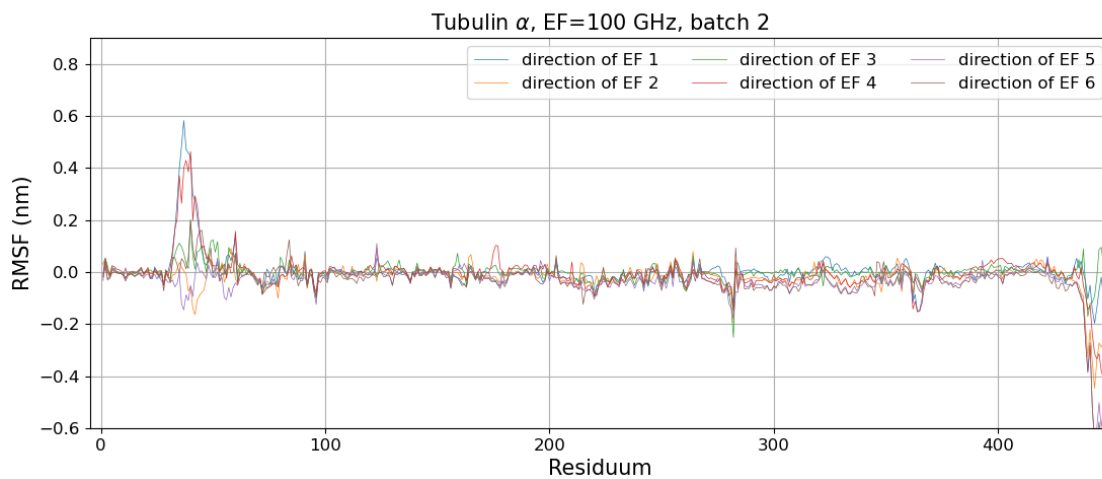


Figure 10.115: $\text{RMSF}_{\text{diff}}$ of the residues of the tubulin α subjected to the electric field of frequency 100 GHz, Batch 2

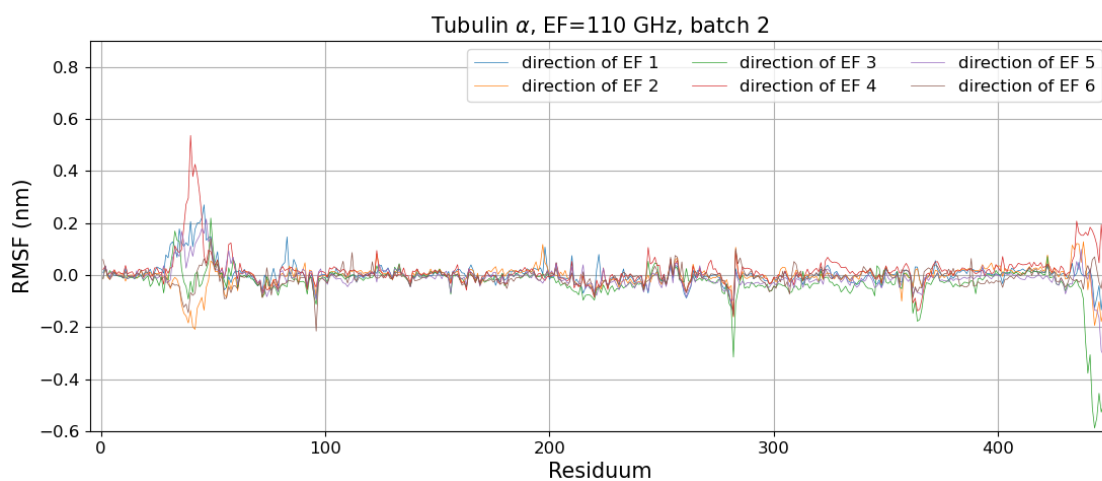


Figure 10.116: $\text{RMSF}_{\text{diff}}$ of the residues of the tubulin α subjected to the electric field of frequency 110 GHz, Batch 2

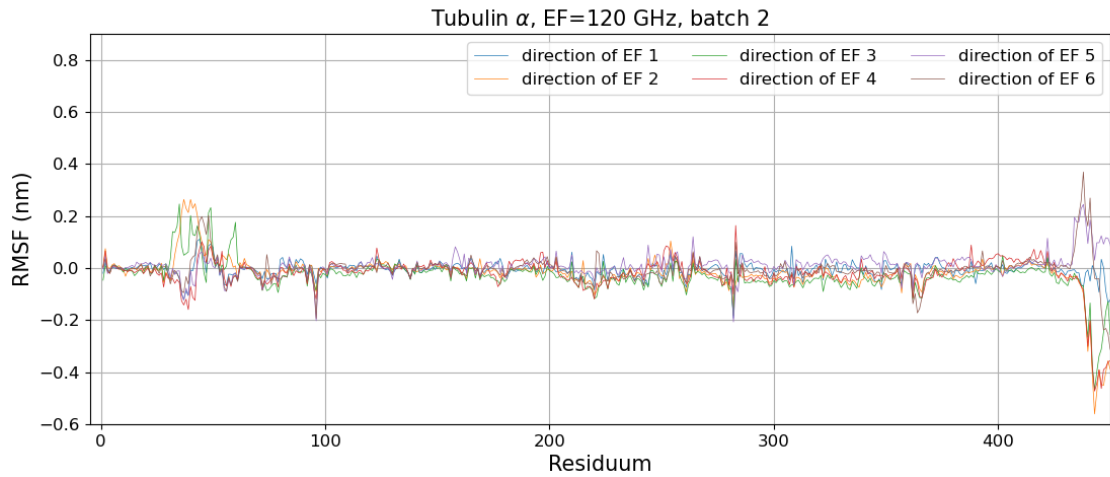


Figure 10.117: $\text{RMSF}_{\text{diff}}$ of the residues of the tubulin α subjected to the electric field of frequency 120 GHz, Batch 2

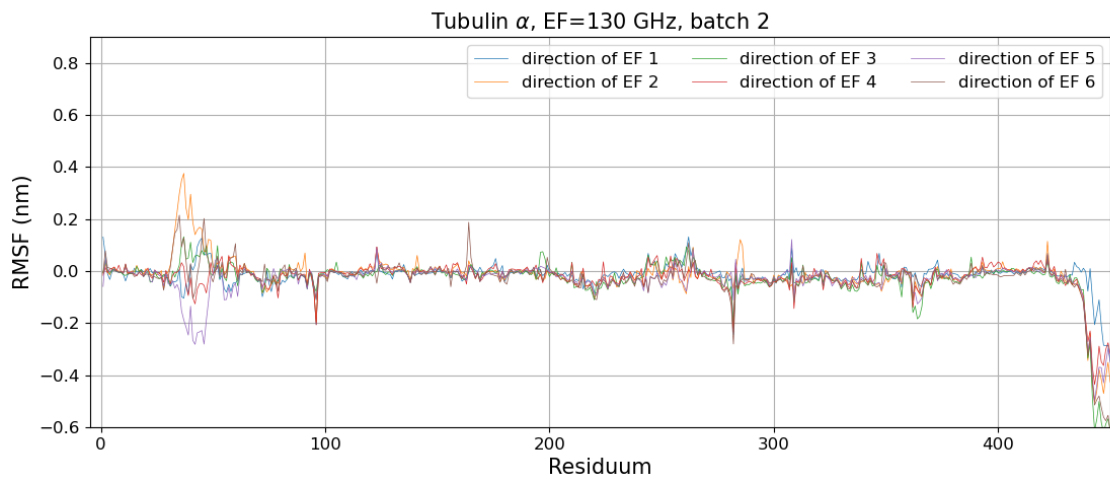


Figure 10.118: $\text{RMSF}_{\text{diff}}$ of the residues of the tubulin α subjected to the electric field of frequency 130 GHz, Batch 2

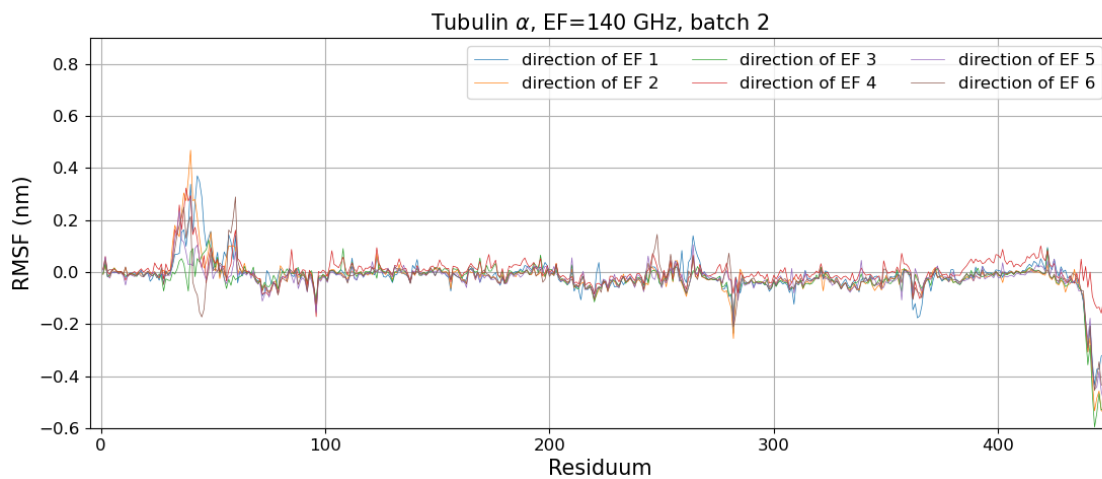


Figure 10.119: $\text{RMSF}_{\text{diff}}$ of the residues of the tubulin α subjected to the electric field of frequency 140 GHz, Batch 2

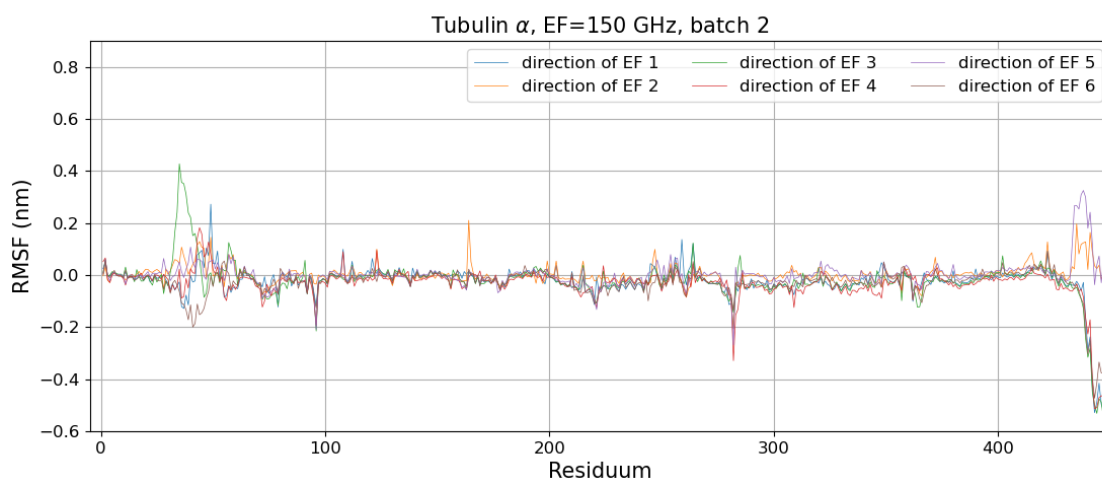


Figure 10.120: $\text{RMSF}_{\text{diff}}$ of the residues of the tubulin α subjected to the electric field of frequency 150 GHz, Batch 2

10.9.3 Tubulin α - Batch 3

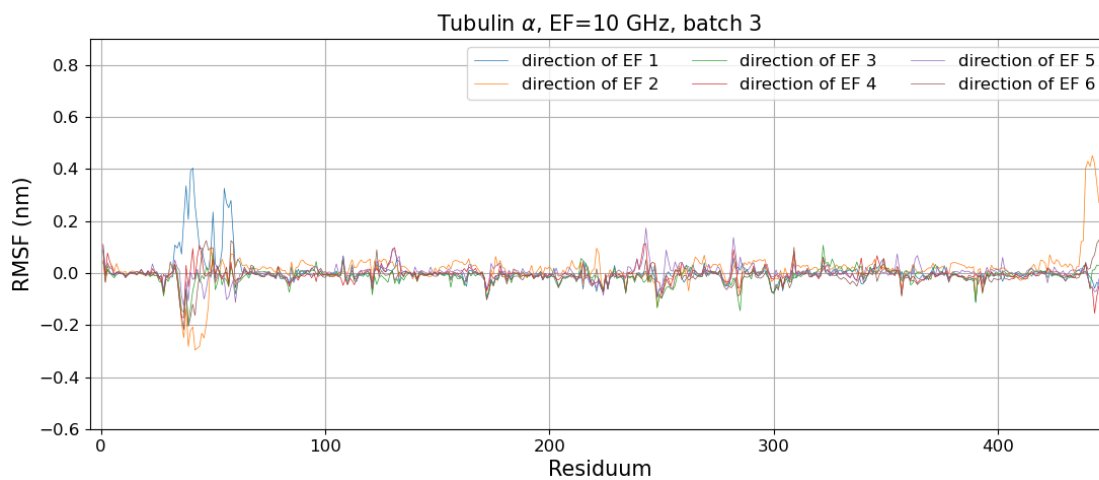


Figure 10.121: $\text{RMSF}_{\text{diff}}$ of the residues of the tubulin α subjected to the electric field of frequency 10 GHz, Batch 3

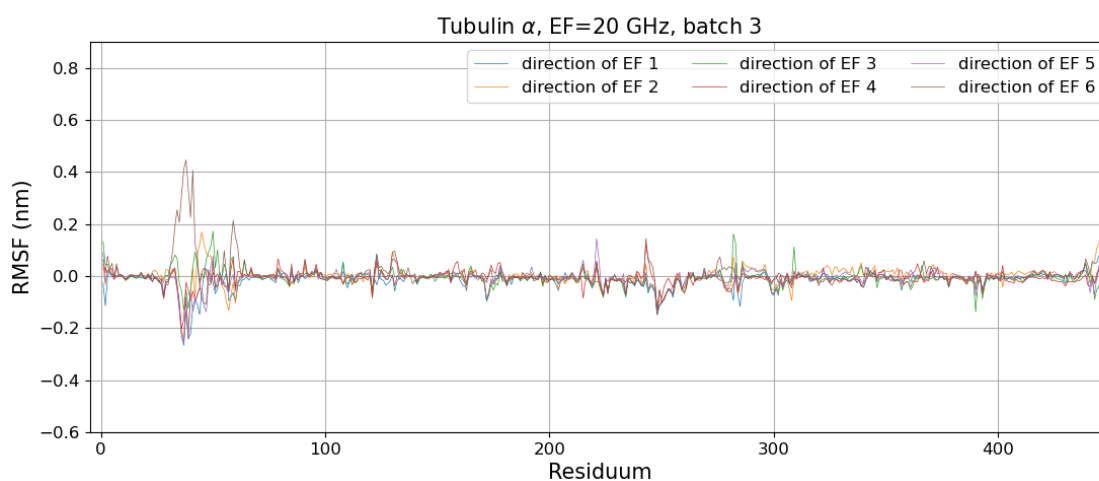


Figure 10.122: $\text{RMSF}_{\text{diff}}$ of the residues of the tubulin α subjected to the electric field of frequency 20 GHz, Batch 3

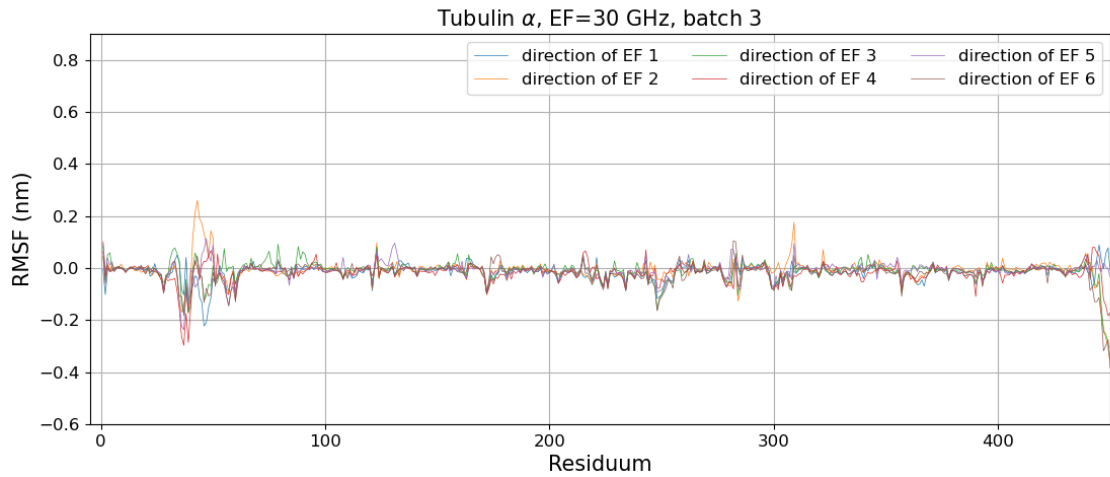


Figure 10.123: $\text{RMSF}_{\text{diff}}$ of the residues of the tubulin α subjected to the electric field of frequency 30 GHz, Batch 3

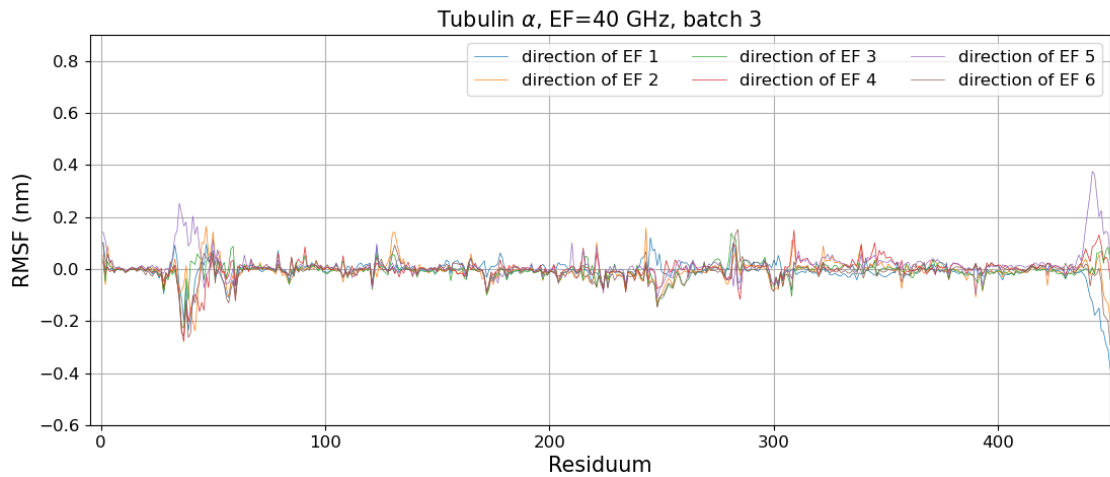


Figure 10.124: $\text{RMSF}_{\text{diff}}$ of the residues of the tubulin α subjected to the electric field of frequency 40 GHz, Batch 3

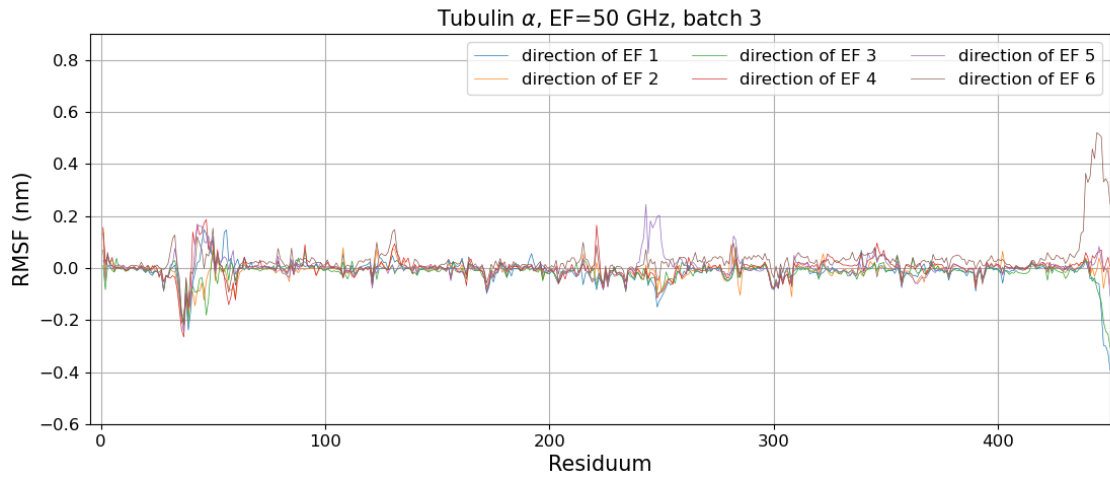


Figure 10.125: $\text{RMSF}_{\text{diff}}$ of the residues of the tubulin α subjected to the electric field of frequency 50 GHz, Batch 3

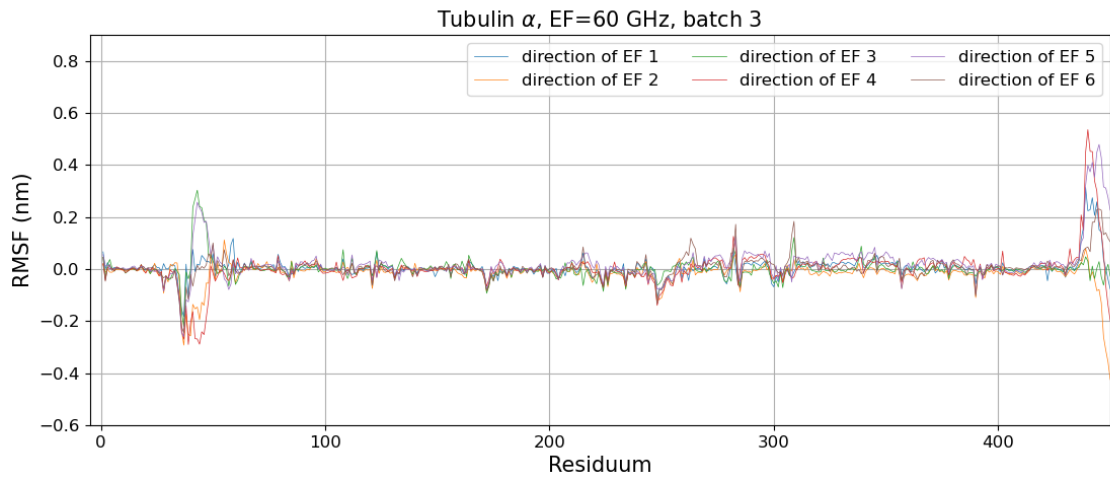


Figure 10.126: $\text{RMSF}_{\text{diff}}$ of the residues of the tubulin α subjected to the electric field of frequency 60 GHz, Batch 3

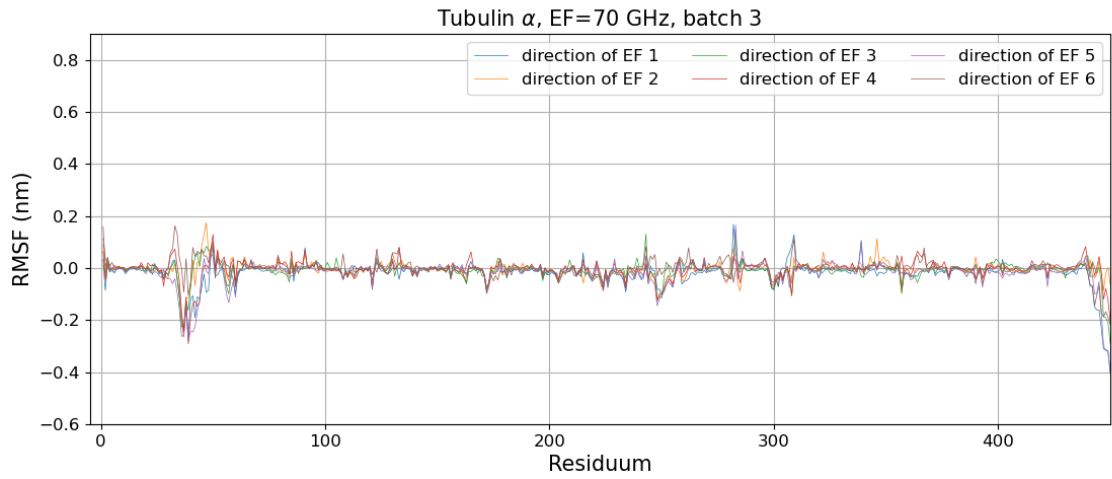


Figure 10.127: $\text{RMSF}_{\text{diff}}$ of the residues of the tubulin α subjected to the electric field of frequency 70 GHz, Batch 3

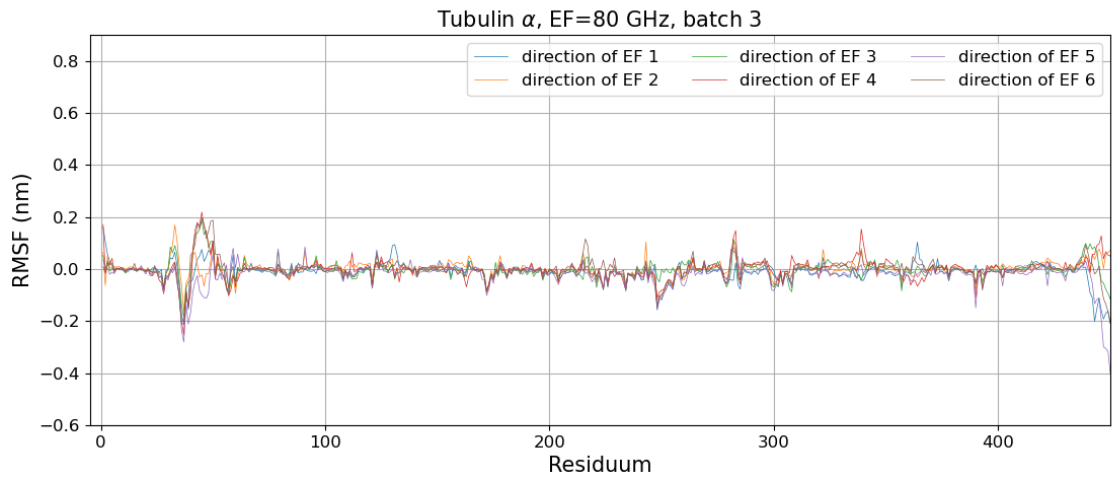


Figure 10.128: $\text{RMSF}_{\text{diff}}$ of the residues of the tubulin α subjected to the electric field of frequency 80 GHz, Batch 3

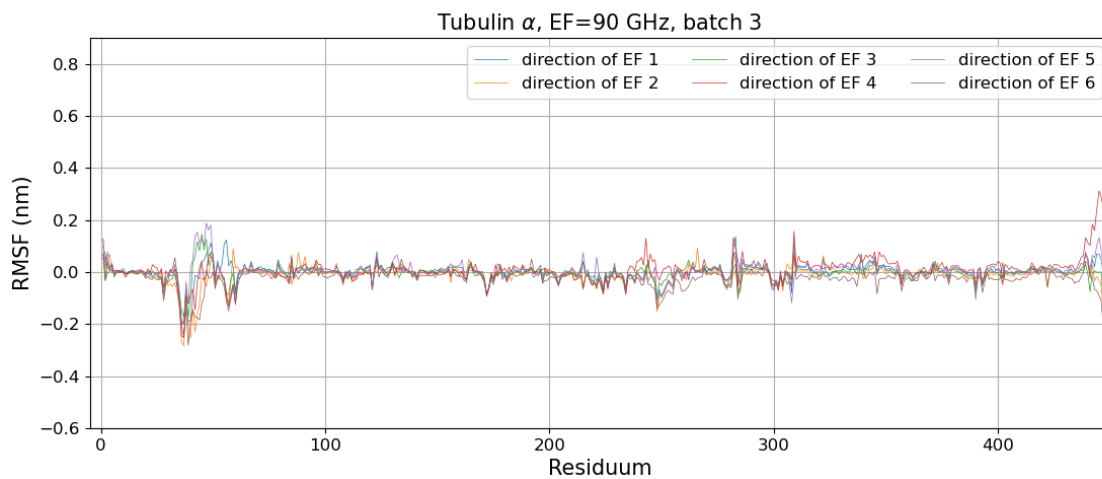


Figure 10.129: $\text{RMSF}_{\text{diff}}$ of the residues of the tubulin α subjected to the electric field of frequency 90 GHz, Batch 3

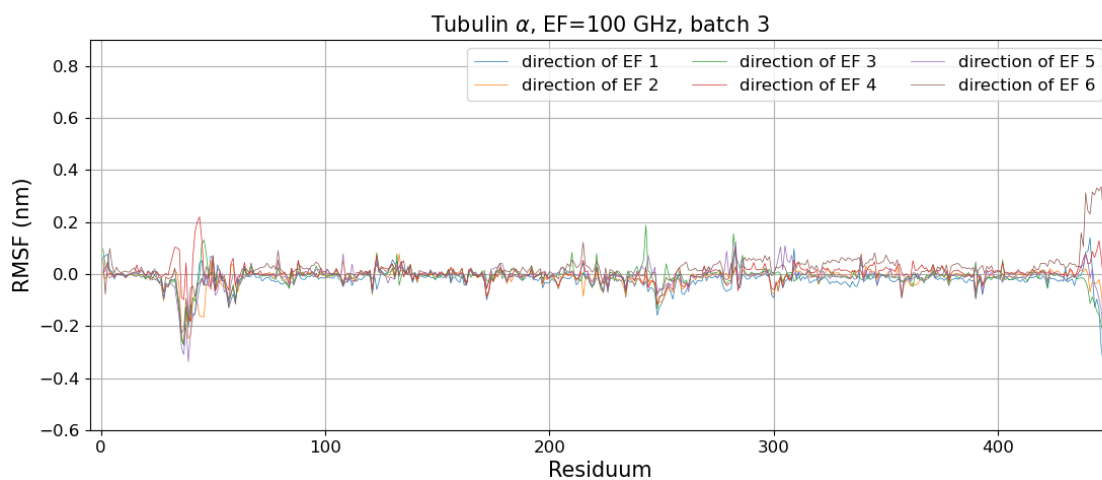


Figure 10.130: $\text{RMSF}_{\text{diff}}$ of the residues of the tubulin α subjected to the electric field of frequency 100 GHz, Batch 3

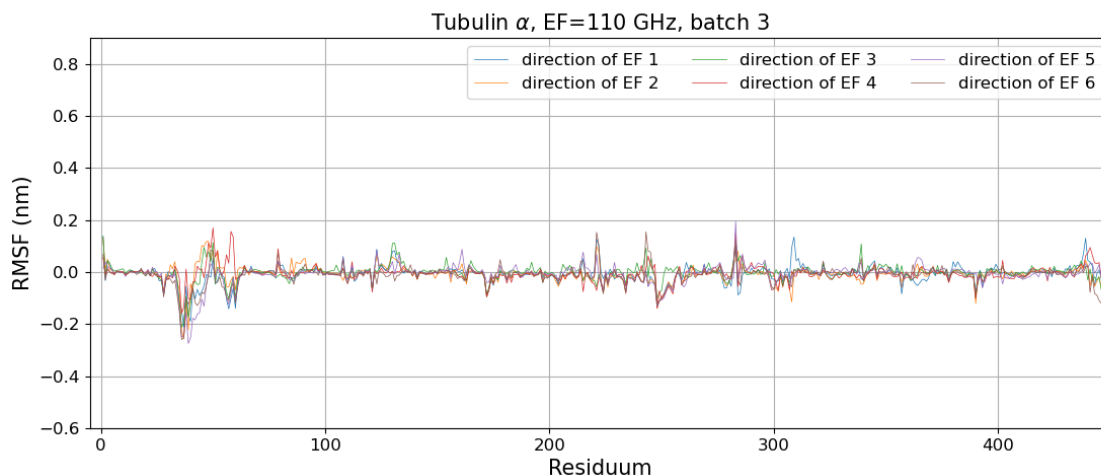


Figure 10.131: $\text{RMSF}_{\text{diff}}$ of the residues of the tubulin α subjected to the electric field of frequency 110 GHz, Batch 3

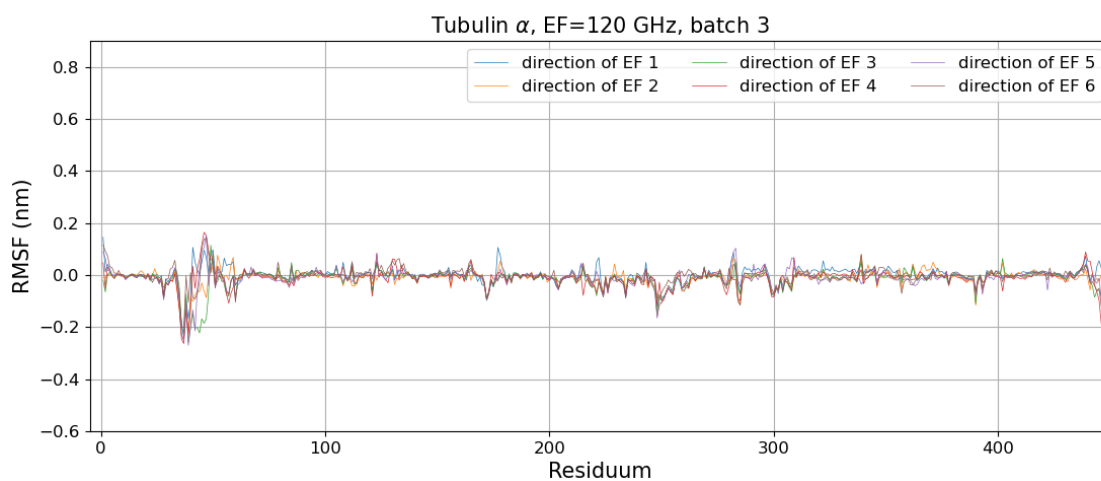


Figure 10.132: $\text{RMSF}_{\text{diff}}$ of the residues of the tubulin α subjected to the electric field of frequency 120 GHz, Batch 3

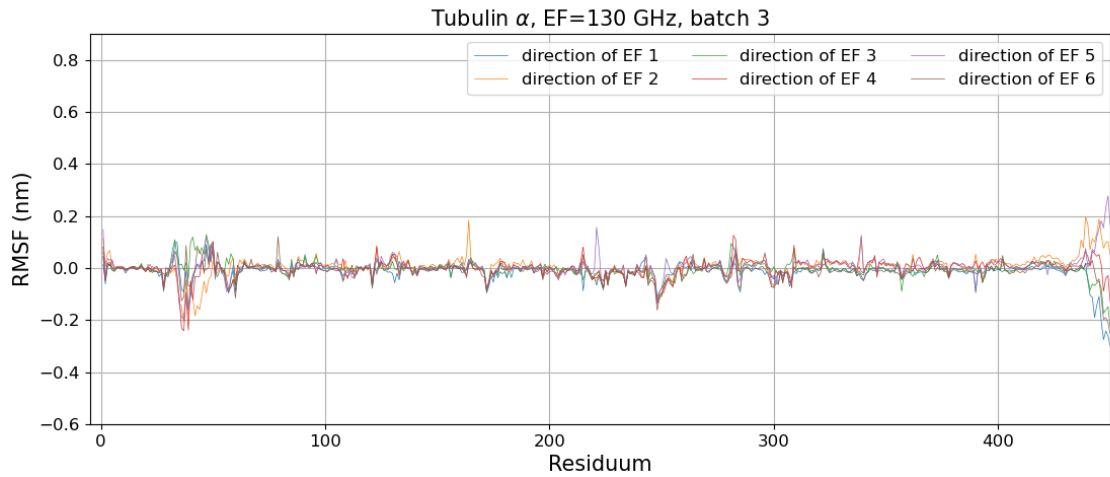


Figure 10.133: $\text{RMSF}_{\text{diff}}$ of the residues of the tubulin α subjected to the electric field of frequency 130 GHz, Batch 3

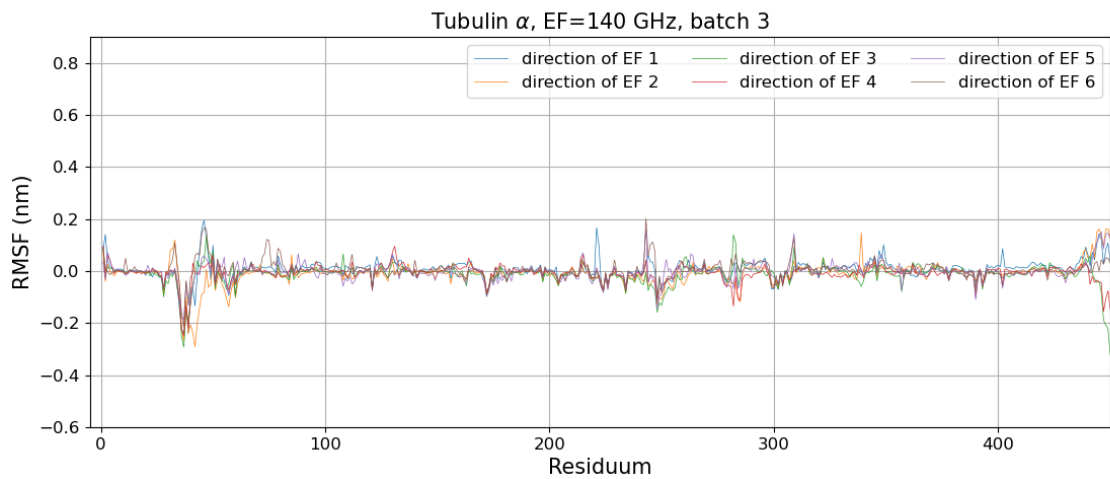


Figure 10.134: $\text{RMSF}_{\text{diff}}$ of the residues of the tubulin α subjected to the electric field of frequency 140 GHz, Batch 3

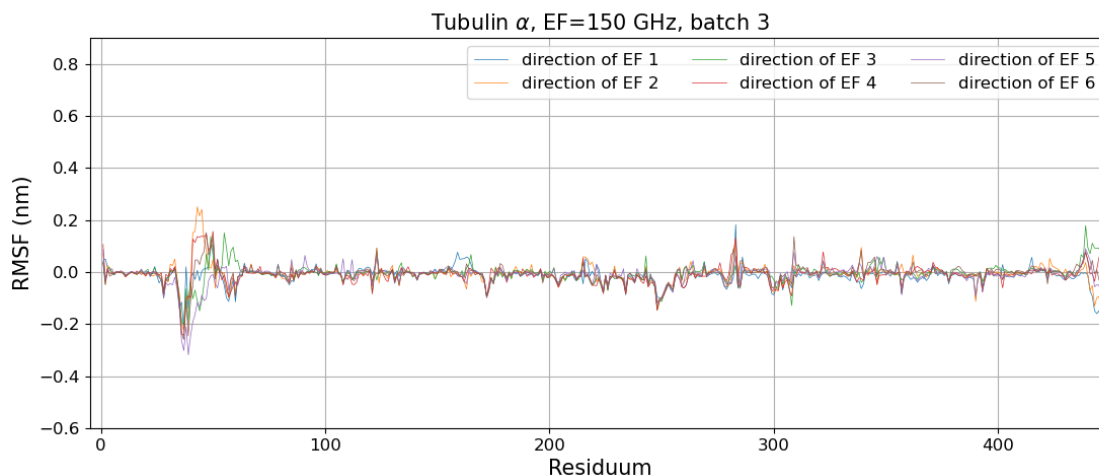


Figure 10.135: $\text{RMSF}_{\text{diff}}$ of the residues of the tubulin α subjected to the electric field of frequency 150 GHz, Batch 3

10.9.4 Tubulin β - Batch 1

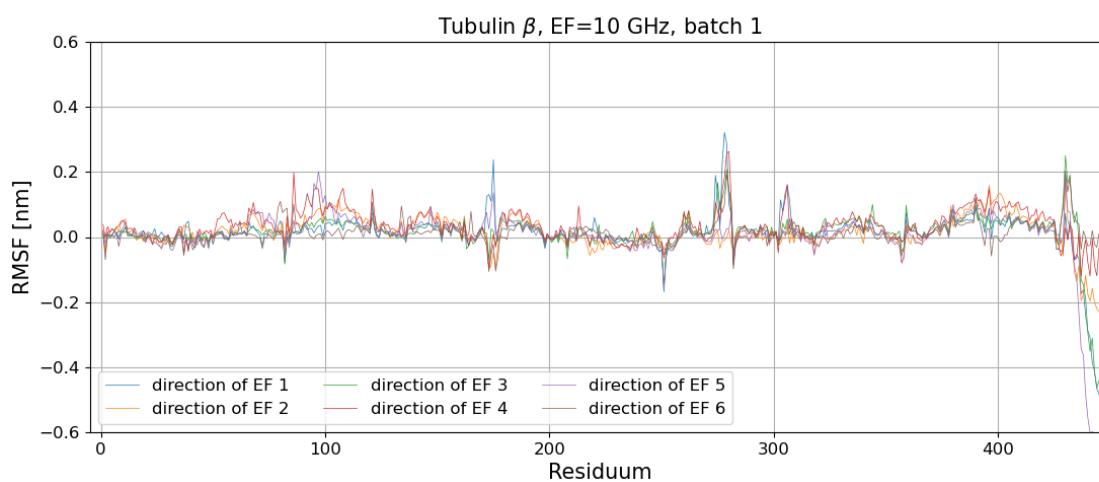


Figure 10.136: $\text{RMSF}_{\text{diff}}$ of the residues of the tubulin β subjected to the electric field of frequency 10 GHz, Batch 1

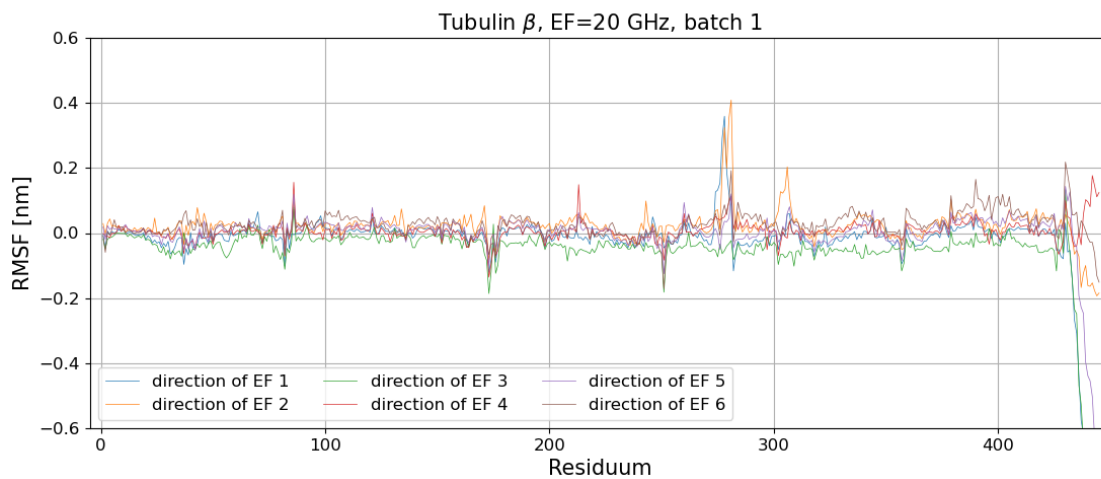


Figure 10.137: $\text{RMSF}_{\text{diff}}$ of the residues of the tubulin β subjected to the electric field of frequency 20 GHz, Batch 1

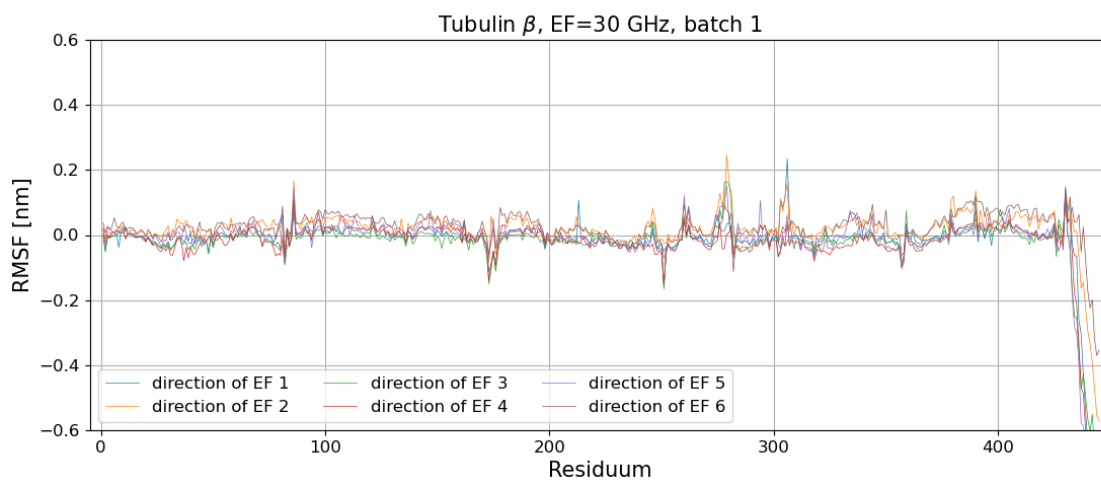


Figure 10.138: $\text{RMSF}_{\text{diff}}$ of the residues of the tubulin β subjected to the electric field of frequency 30 GHz, Batch 1

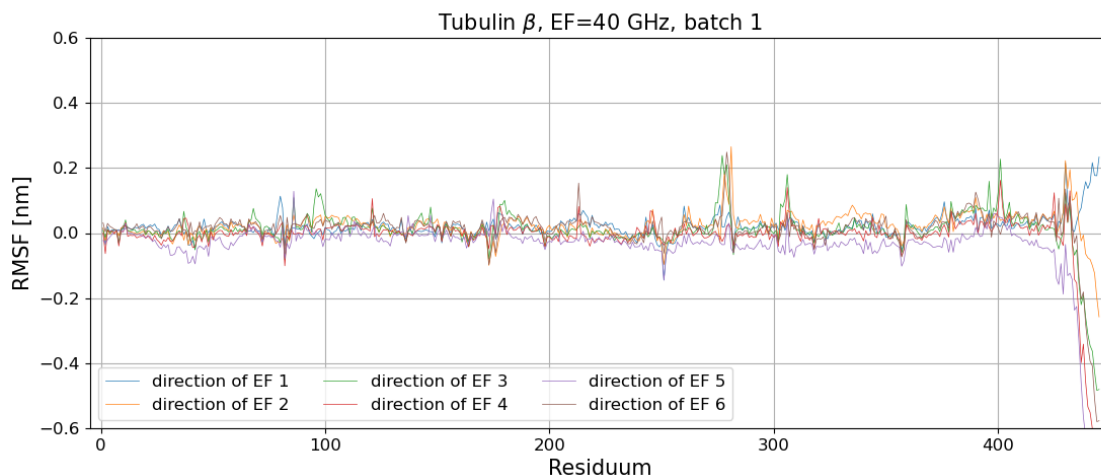


Figure 10.139: $\text{RMSF}_{\text{diff}}$ of the residues of the tubulin β subjected to the electric field of frequency 40 GHz, Batch 1

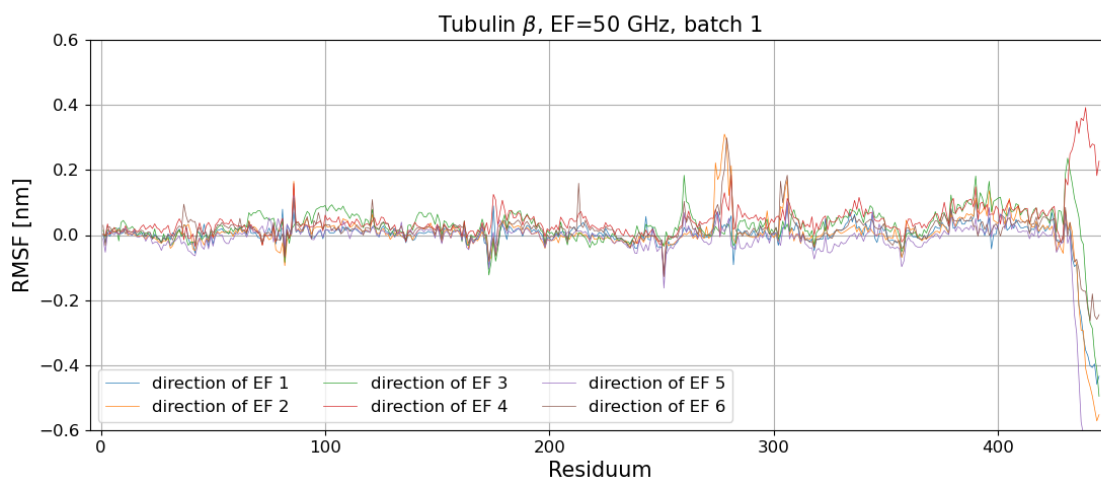


Figure 10.140: $\text{RMSF}_{\text{diff}}$ of the residues of the tubulin β subjected to the electric field of frequency 50 GHz, Batch 1

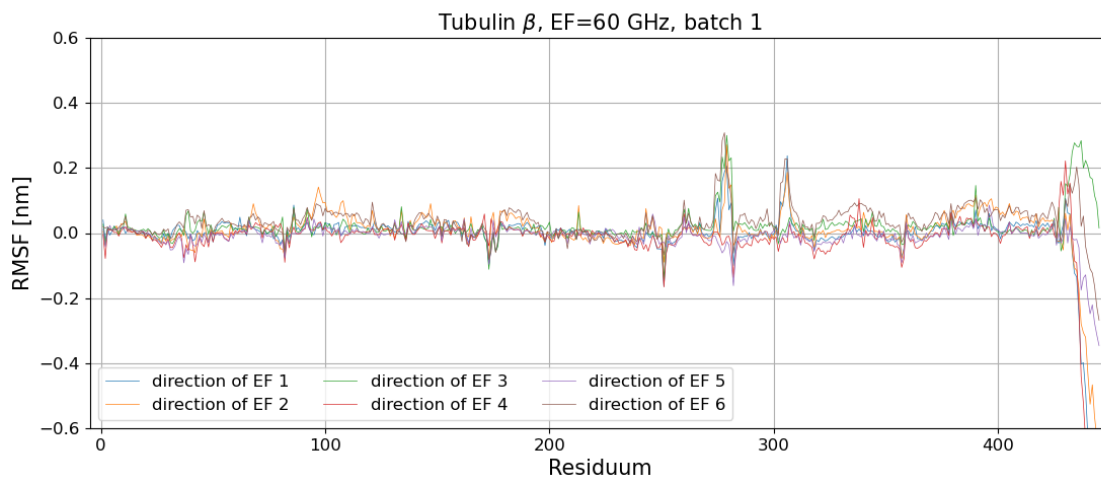


Figure 10.141: $\text{RMSF}_{\text{diff}}$ of the residues of the tubulin β subjected to the electric field of frequency 60 GHz, Batch 1

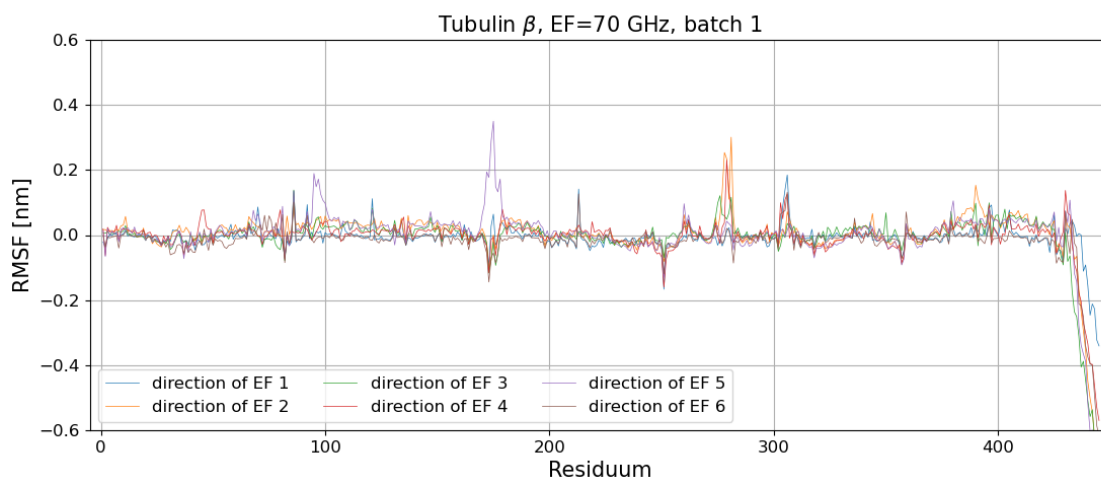


Figure 10.142: $\text{RMSF}_{\text{diff}}$ of the residues of the tubulin β subjected to the electric field of frequency 70 GHz, Batch 1

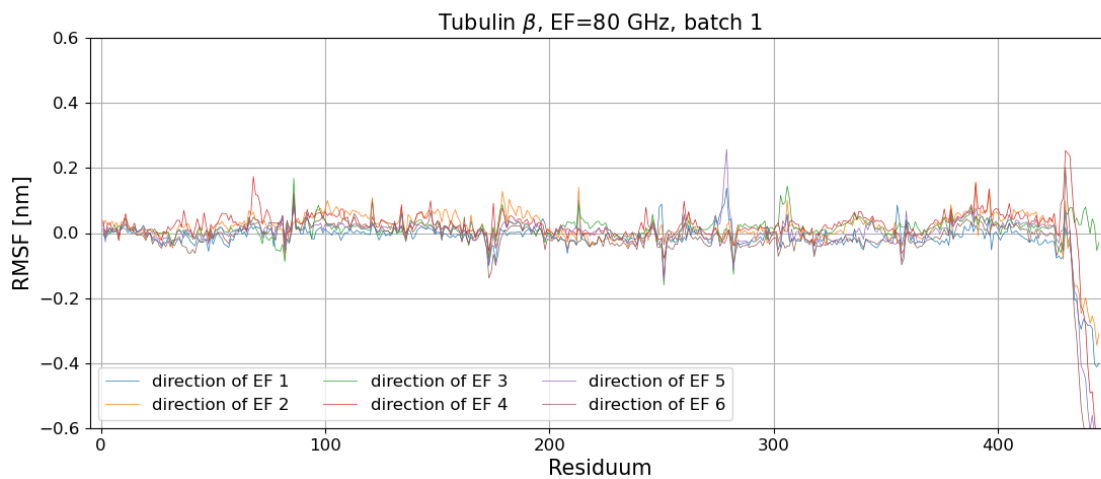


Figure 10.143: $\text{RMSF}_{\text{diff}}$ of the residues of the tubulin β subjected to the electric field of frequency 80 GHz, Batch 1

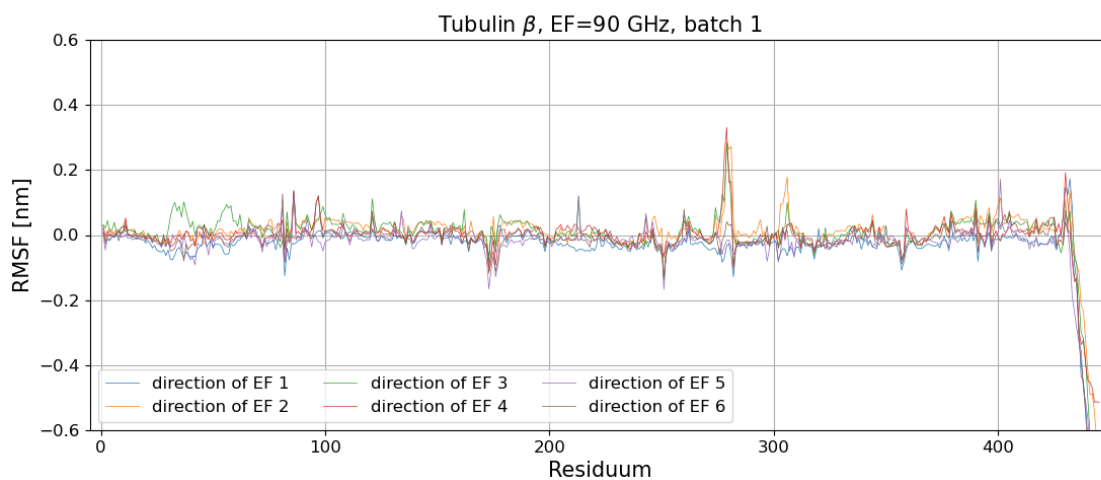


Figure 10.144: $\text{RMSF}_{\text{diff}}$ of the residues of the tubulin β subjected to the electric field of frequency 90 GHz, Batch 1

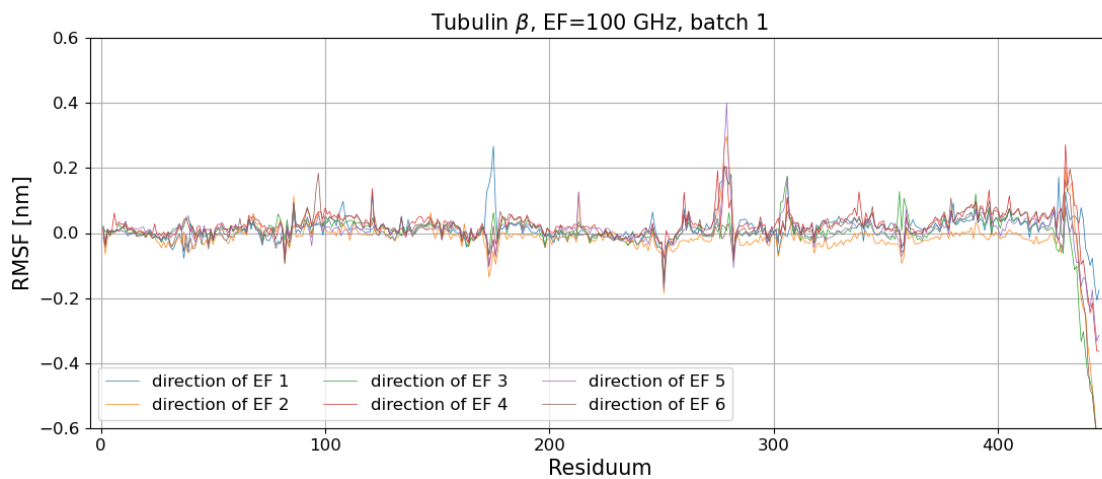


Figure 10.145: $\text{RMSF}_{\text{diff}}$ of the residues of the tubulin β subjected to the electric field of frequency 100 GHz, Batch 1

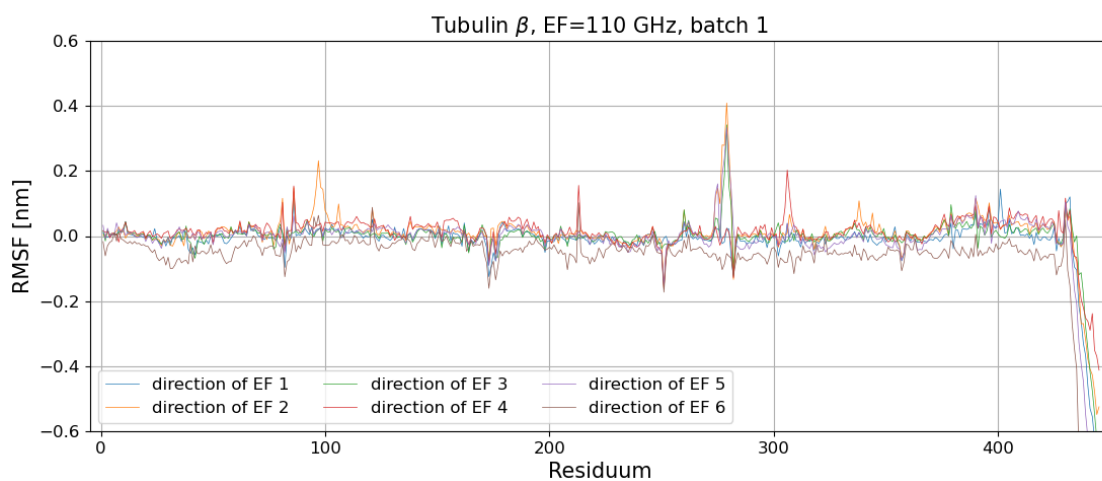


Figure 10.146: $\text{RMSF}_{\text{diff}}$ of the residues of the tubulin β subjected to the electric field of frequency 110 GHz, Batch 1

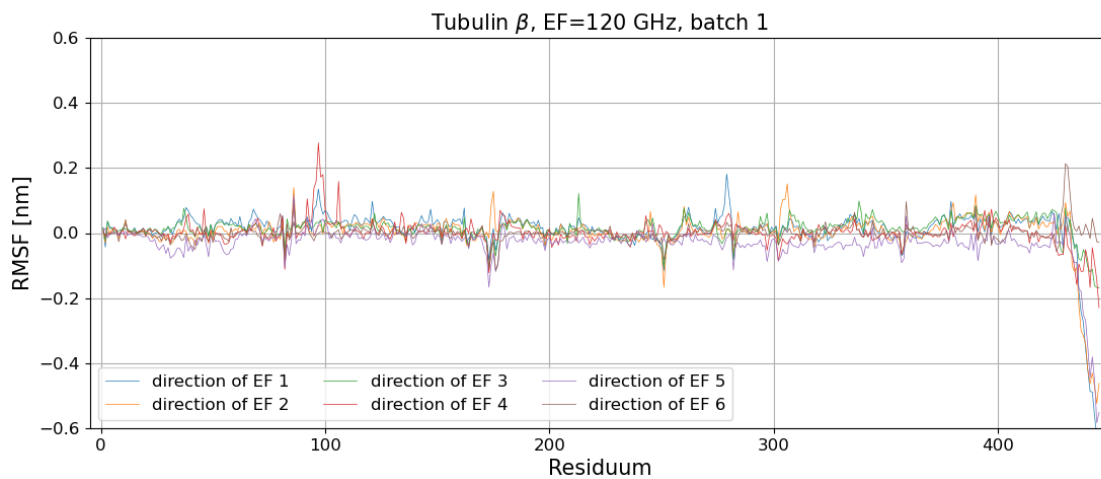


Figure 10.147: $\text{RMSF}_{\text{diff}}$ of the residues of the tubulin β subjected to the electric field of frequency 120 GHz, Batch 1

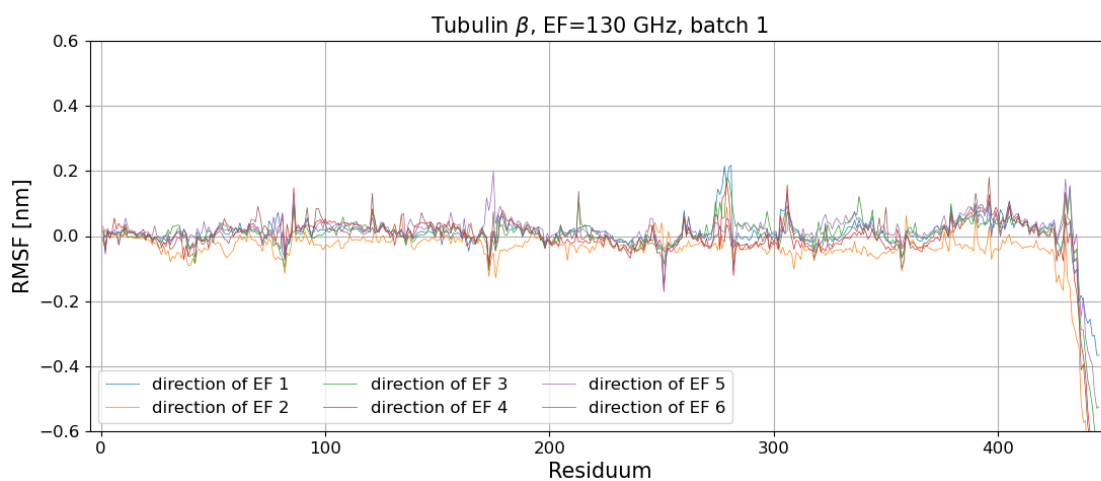


Figure 10.148: $\text{RMSF}_{\text{diff}}$ of the residues of the tubulin β subjected to the electric field of frequency 130 GHz, Batch 1

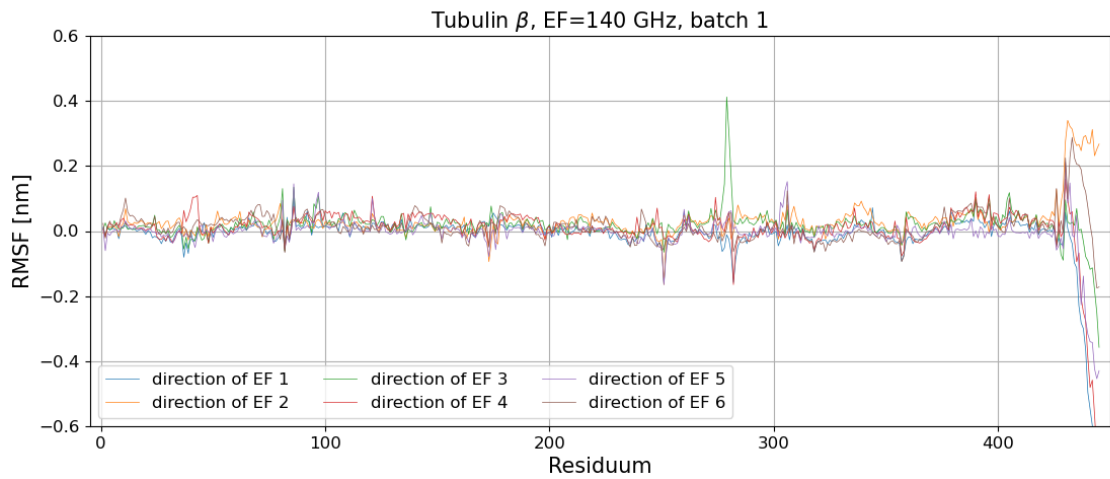


Figure 10.149: $\text{RMSF}_{\text{diff}}$ of the residues of the tubulin β subjected to the electric field of frequency 140 GHz, Batch 1

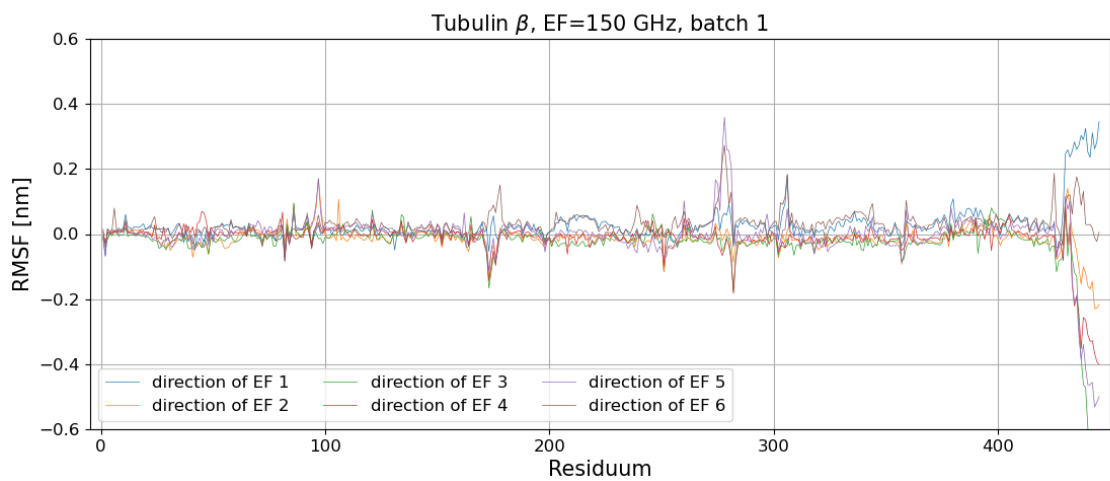


Figure 10.150: $\text{RMSF}_{\text{diff}}$ of the residues of the tubulin β subjected to the electric field of frequency 150 GHz, Batch 1

10.9.5 Tubulin β - Batch 2

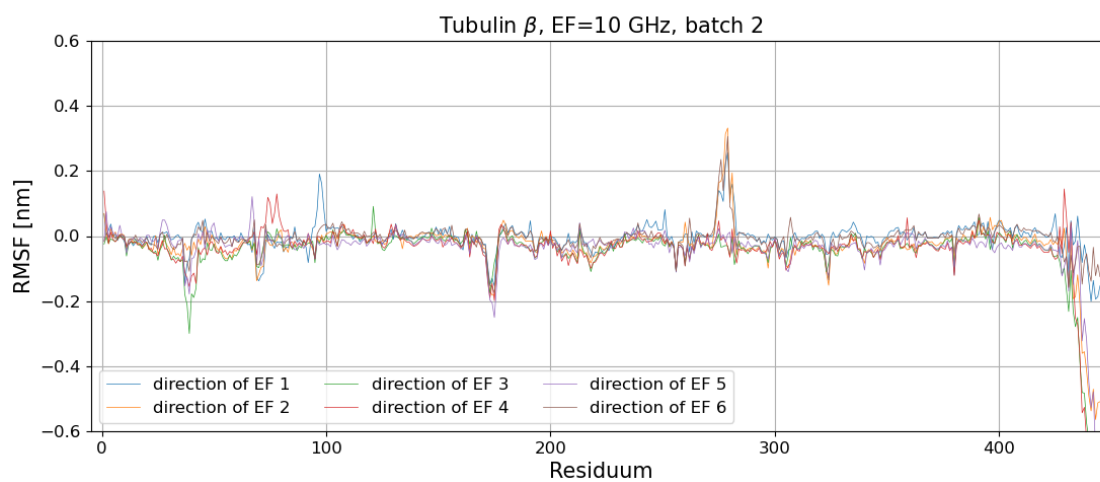


Figure 10.151: $\text{RMSF}_{\text{diff}}$ of the residues of the tubulin β subjected to the electric field of frequency 10 GHz, Batch 2

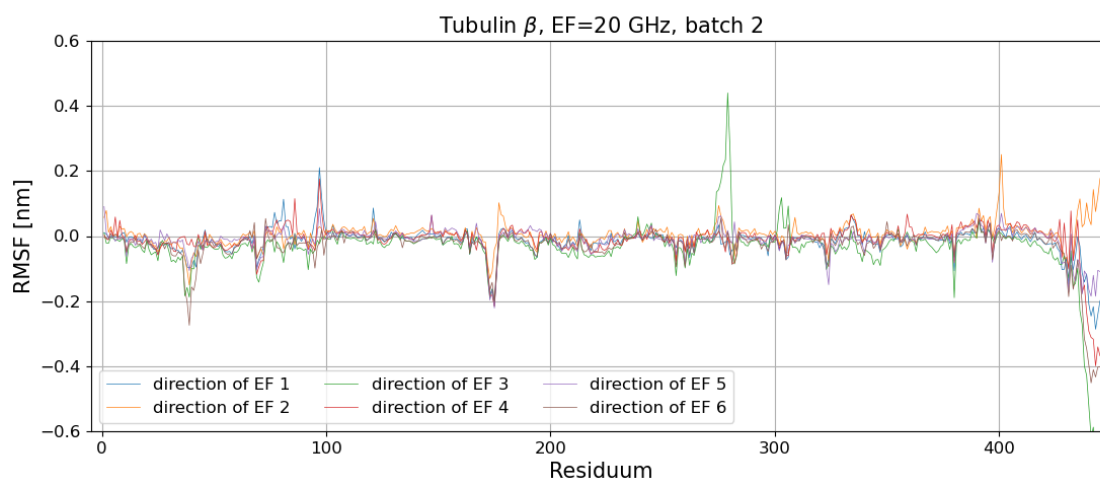


Figure 10.152: $\text{RMSF}_{\text{diff}}$ of the residues of the tubulin β subjected to the electric field of frequency 20 GHz, Batch 2

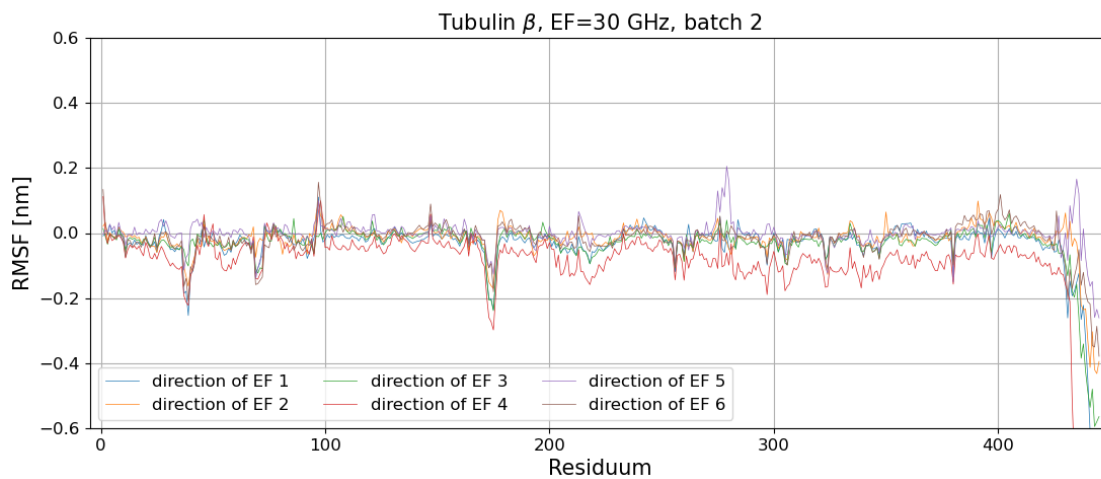


Figure 10.153: $\text{RMSF}_{\text{diff}}$ of the residues of the tubulin β subjected to the electric field of frequency 30 GHz, Batch 2

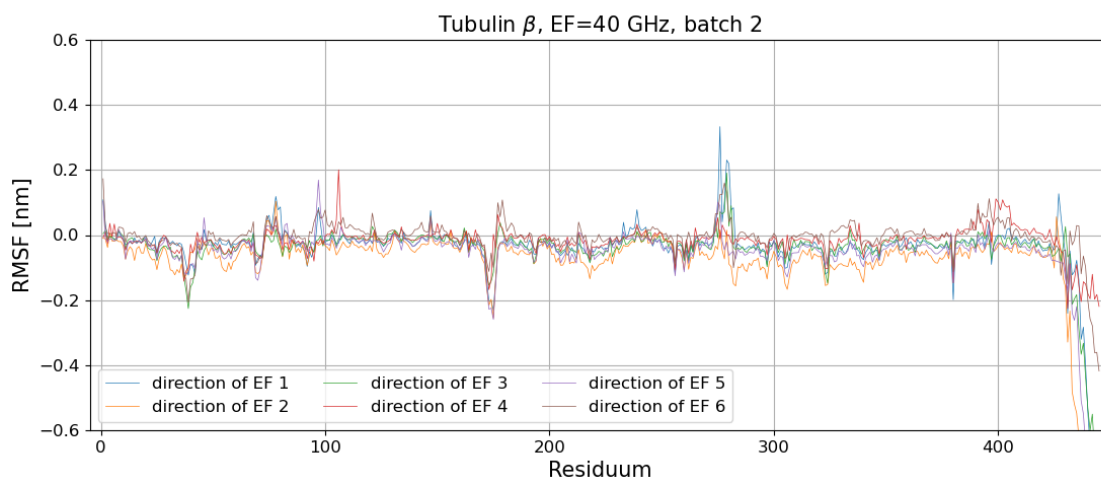


Figure 10.154: $\text{RMSF}_{\text{diff}}$ of the residues of the tubulin β subjected to the electric field of frequency 40 GHz, Batch 2

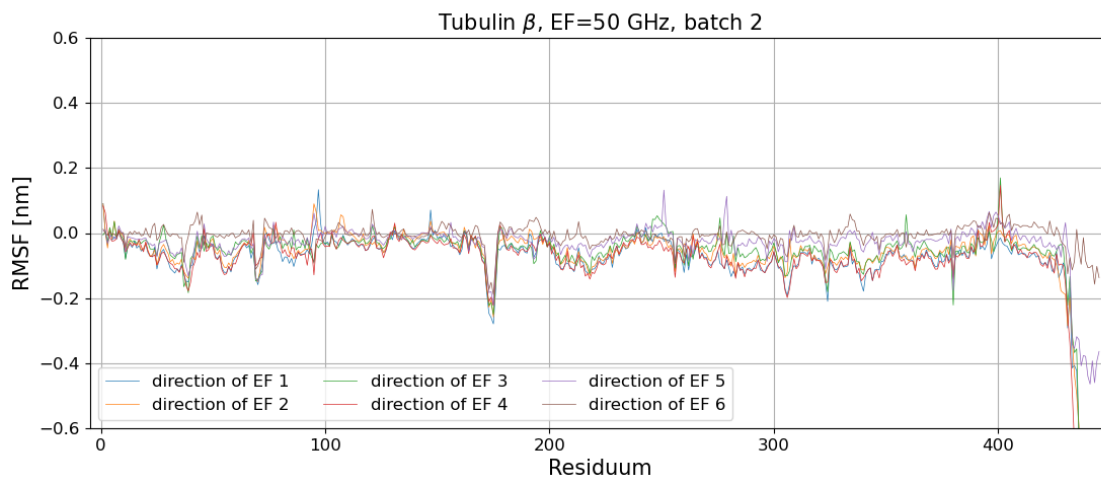


Figure 10.155: $\text{RMSF}_{\text{diff}}$ of the residues of the tubulin β subjected to the electric field of frequency 50 GHz, Batch 2

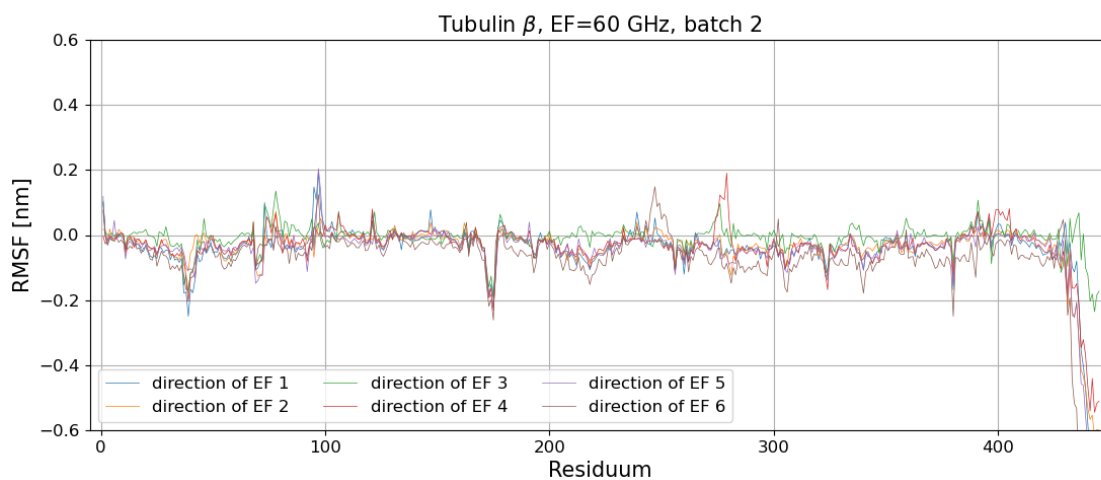


Figure 10.156: $\text{RMSF}_{\text{diff}}$ of the residues of the tubulin β subjected to the electric field of frequency 60 GHz, Batch 2

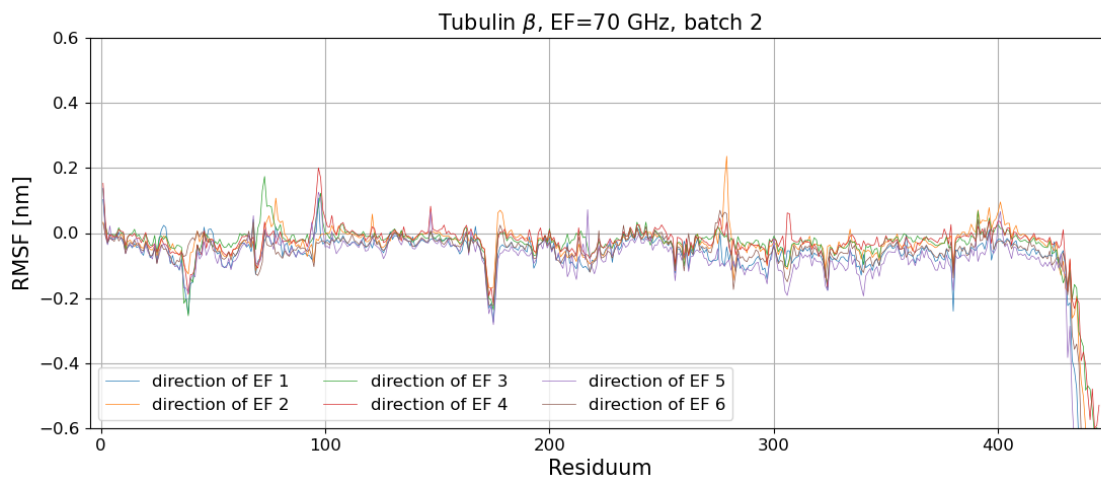


Figure 10.157: $\text{RMSF}_{\text{diff}}$ of the residues of the tubulin β subjected to the electric field of frequency 70 GHz, Batch 2

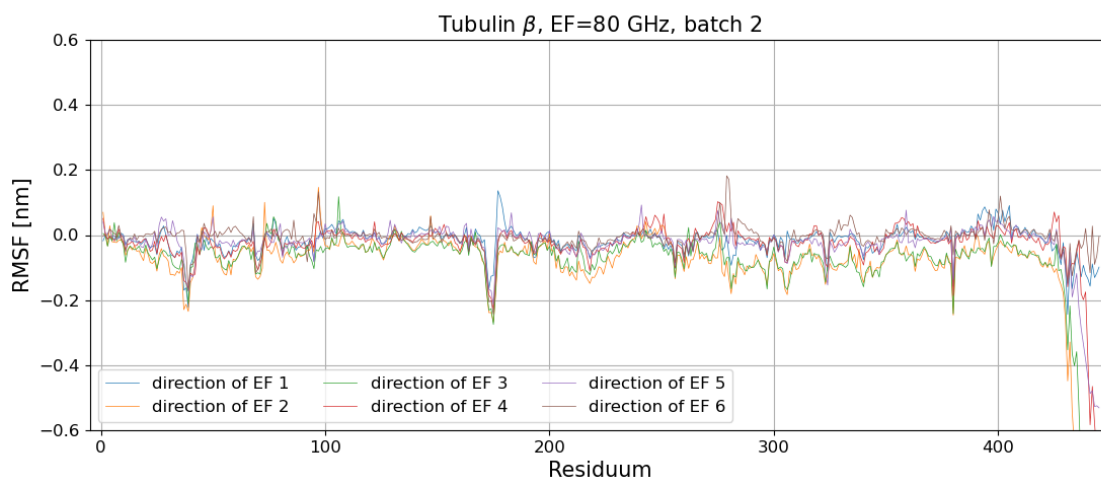


Figure 10.158: $\text{RMSF}_{\text{diff}}$ of the residues of the tubulin β subjected to the electric field of frequency 80 GHz, Batch 2

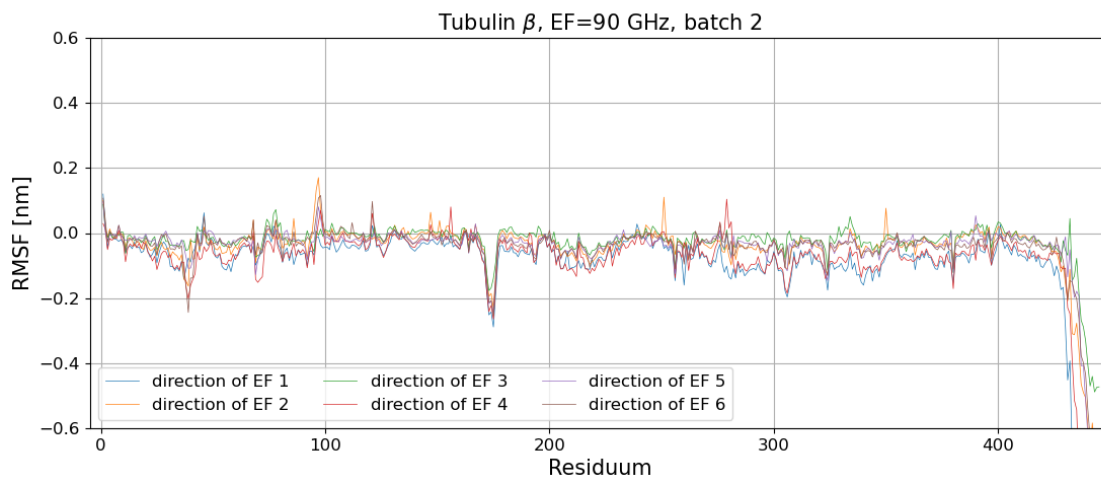


Figure 10.159: $\text{RMSF}_{\text{diff}}$ of the residues of the tubulin β subjected to the electric field of frequency 90 GHz, Batch 2

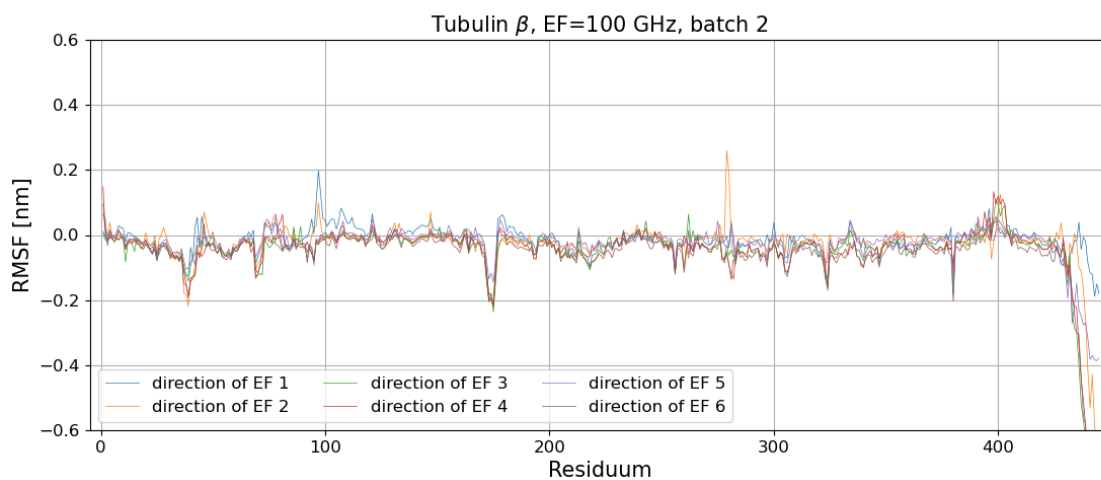


Figure 10.160: $\text{RMSF}_{\text{diff}}$ of the residues of the tubulin β subjected to the electric field of frequency 100 GHz, Batch 2

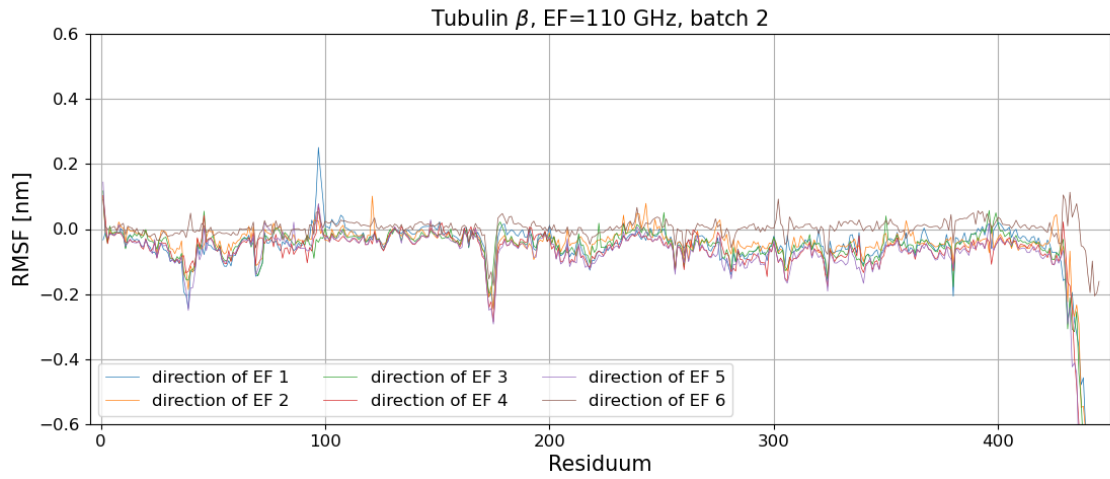


Figure 10.161: $\text{RMSF}_{\text{diff}}$ of the residues of the tubulin β subjected to the electric field of frequency 110 GHz, Batch 2

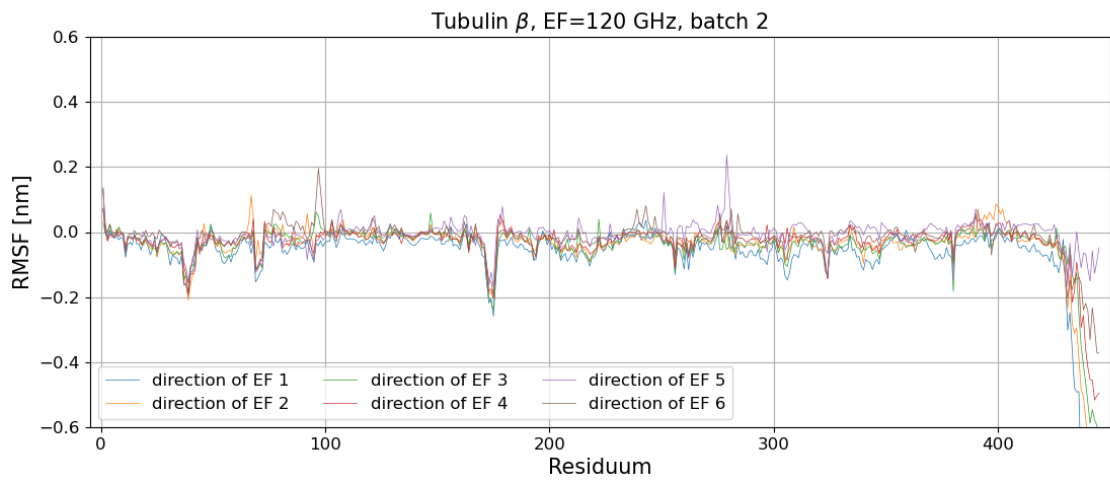


Figure 10.162: $\text{RMSF}_{\text{diff}}$ of the residues of the tubulin β subjected to the electric field of frequency 120 GHz, Batch 2

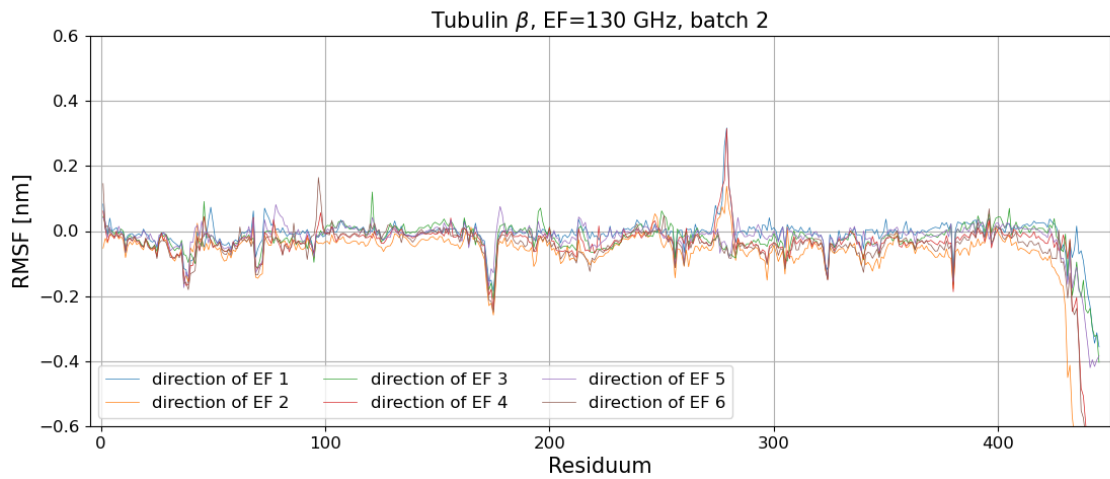


Figure 10.163: $\text{RMSF}_{\text{diff}}$ of the residues of the tubulin β subjected to the electric field of frequency 130 GHz, Batch 2

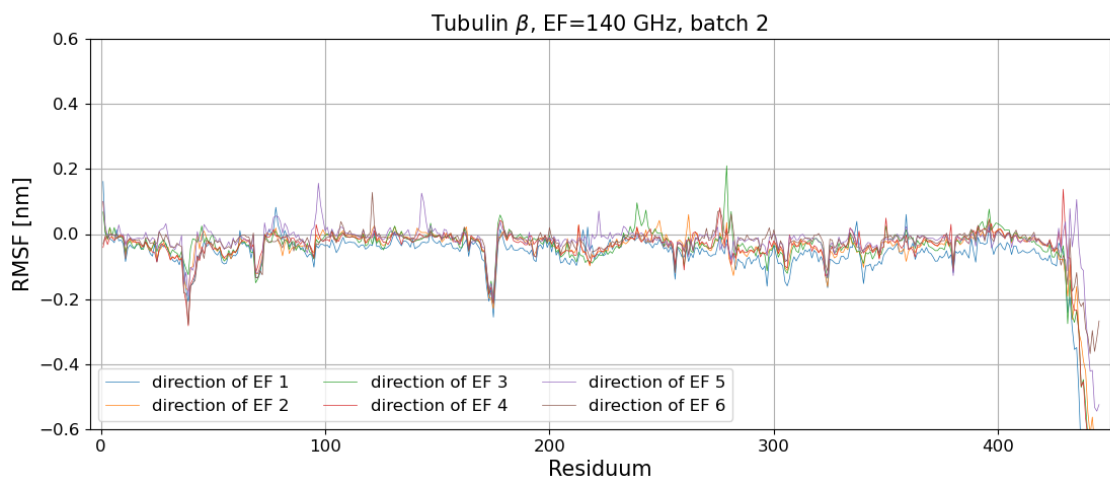


Figure 10.164: $\text{RMSF}_{\text{diff}}$ of the residues of the tubulin β subjected to the electric field of frequency 140 GHz, Batch 2

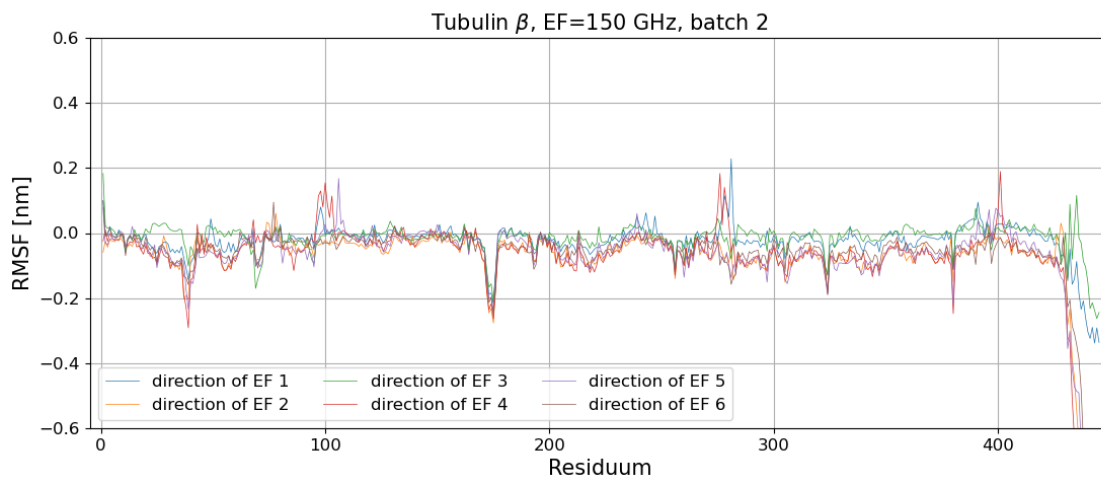


Figure 10.165: $\text{RMSF}_{\text{diff}}$ of the residues of the tubulin β subjected to the electric field of frequency 150 GHz, Batch 2

10.9.6 Tubulin β - Batch 3

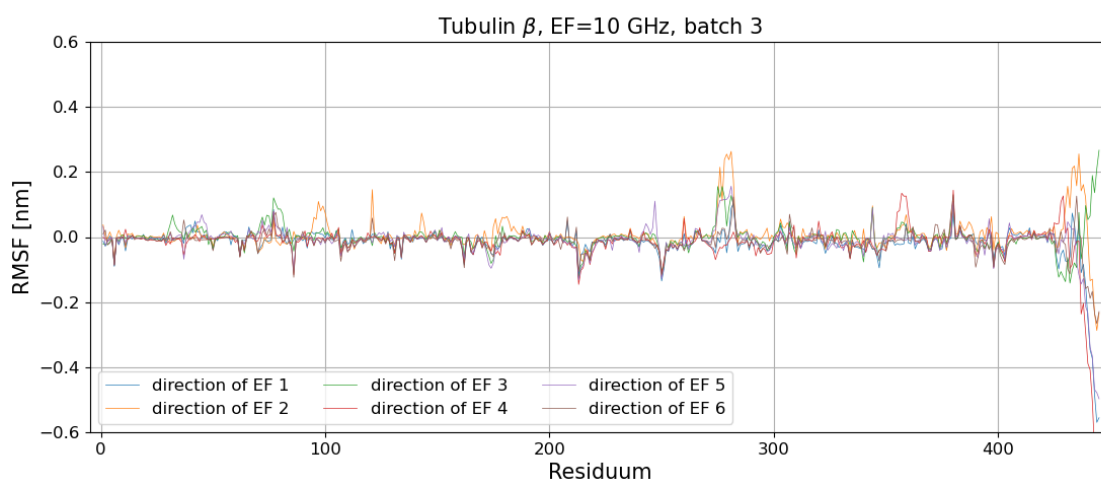


Figure 10.166: $\text{RMSF}_{\text{diff}}$ of the residues of the tubulin β subjected to the electric field of frequency 10 GHz, Batch 3

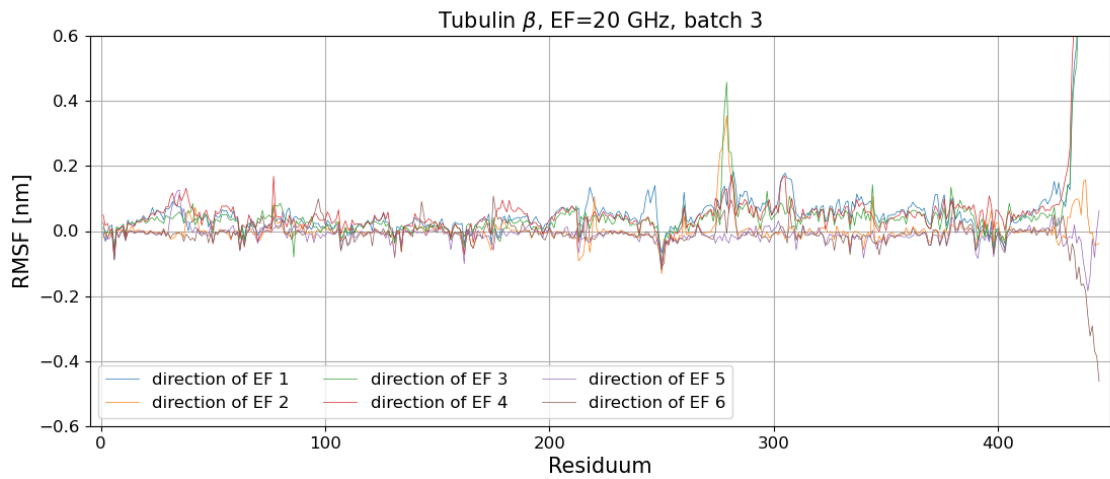


Figure 10.167: $\text{RMSF}_{\text{diff}}$ of the residues of the tubulin β subjected to the electric field of frequency 20 GHz, Batch 3

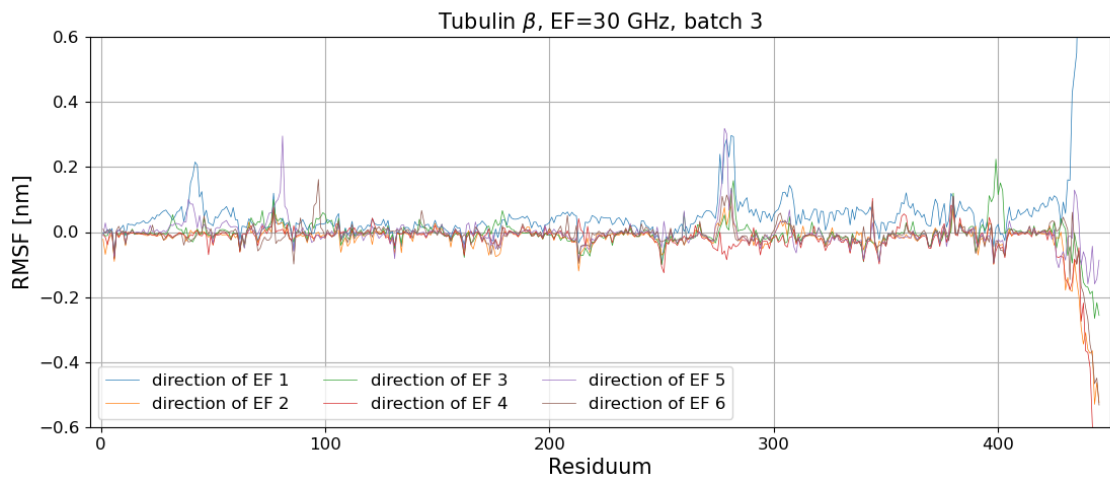


Figure 10.168: $\text{RMSF}_{\text{diff}}$ of the residues of the tubulin β subjected to the electric field of frequency 30 GHz, Batch 3

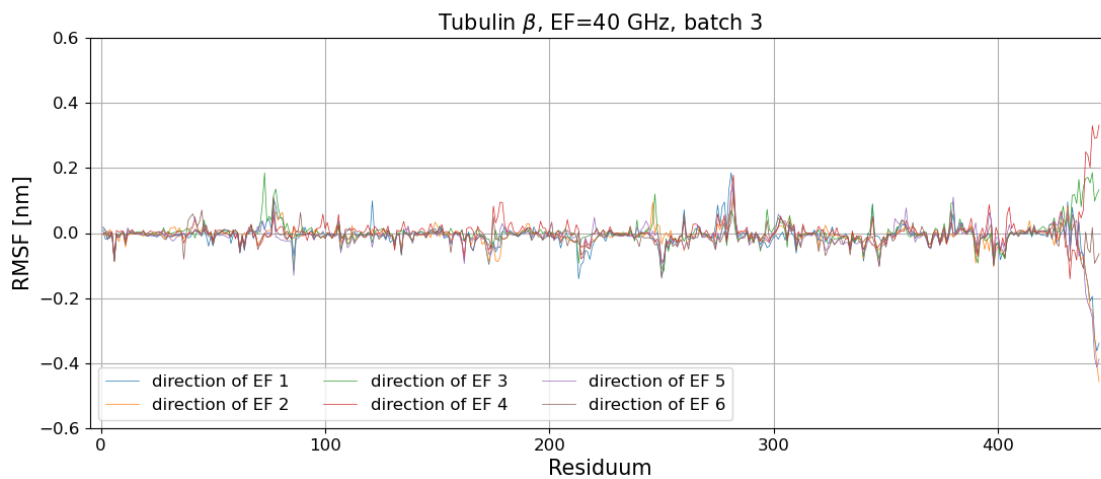


Figure 10.169: $\text{RMSF}_{\text{diff}}$ of the residues of the tubulin β subjected to the electric field of frequency 40 GHz, Batch 3

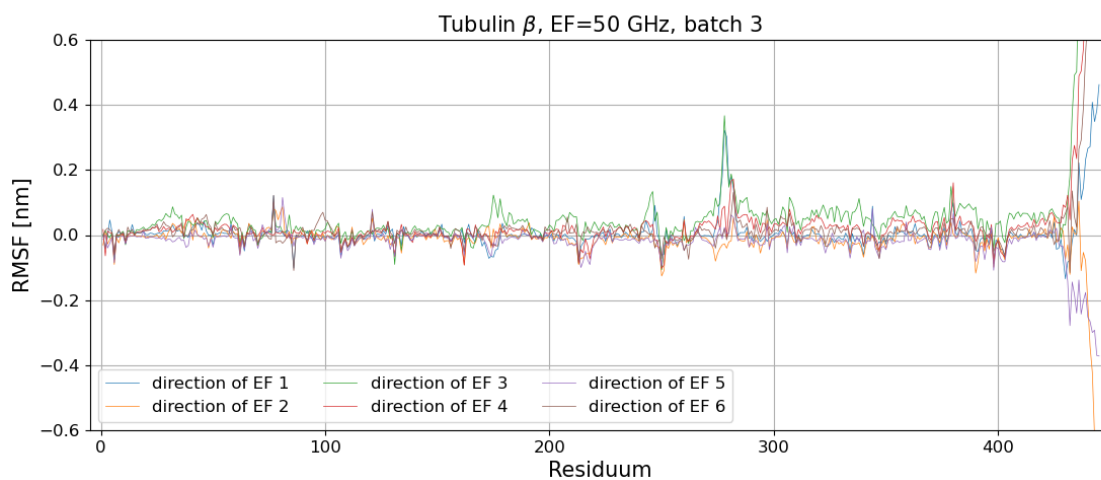


Figure 10.170: $\text{RMSF}_{\text{diff}}$ of the residues of the tubulin β subjected to the electric field of frequency 50 GHz, Batch 3

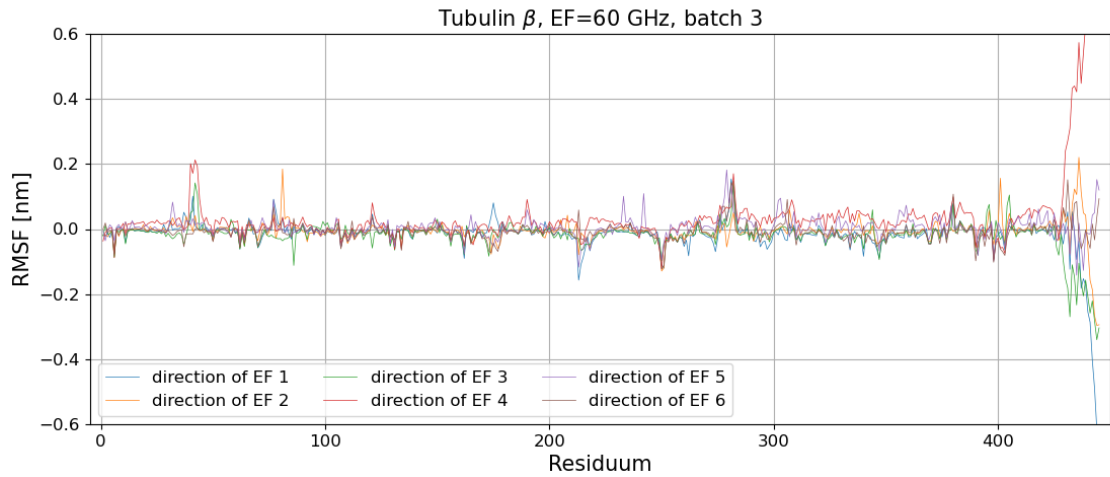


Figure 10.171: $\text{RMSF}_{\text{diff}}$ of the residues of the tubulin β subjected to the electric field of frequency 60 GHz, Batch 3

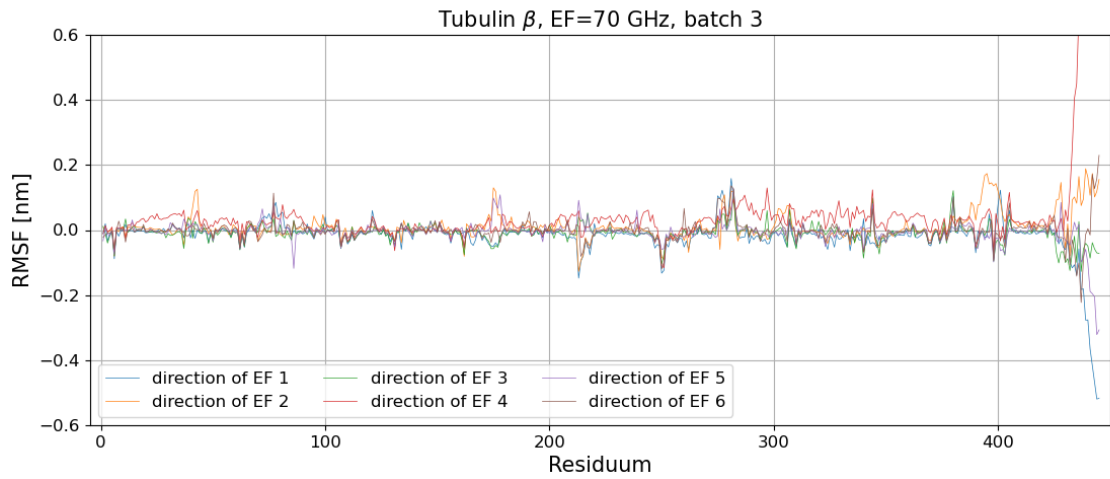


Figure 10.172: $\text{RMSF}_{\text{diff}}$ of the residues of the tubulin β subjected to the electric field of frequency 70 GHz, Batch 3

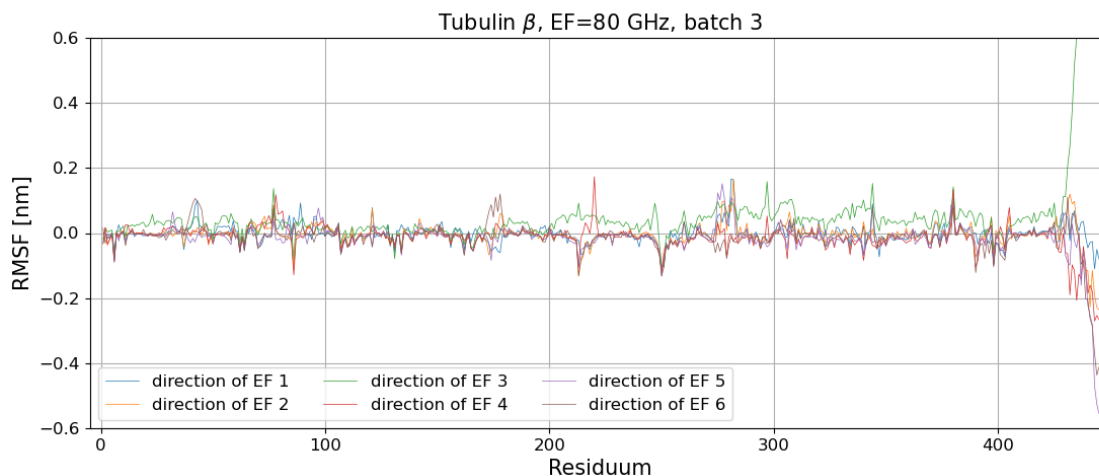


Figure 10.173: $\text{RMSF}_{\text{diff}}$ of the residues of the tubulin β subjected to the electric field of frequency 80 GHz, Batch 3

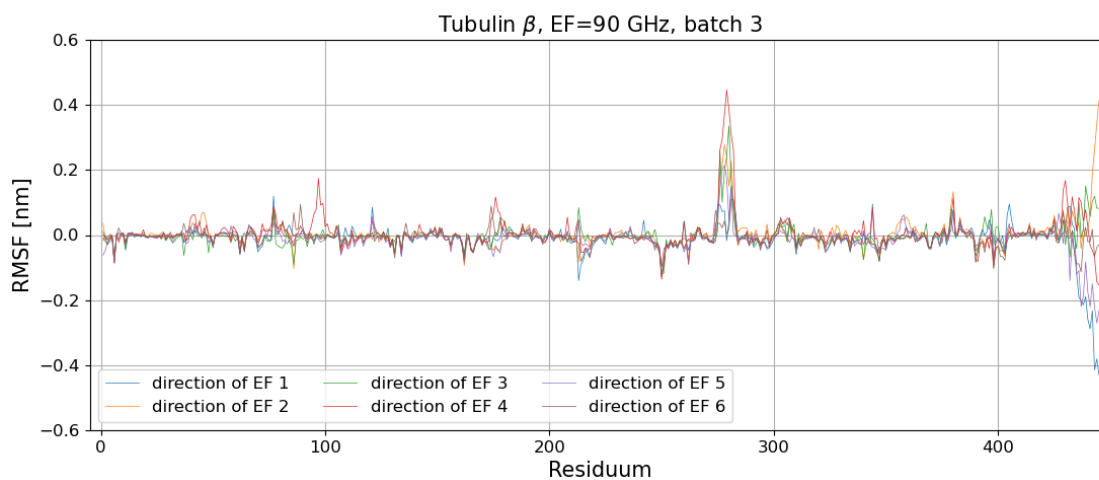


Figure 10.174: $\text{RMSF}_{\text{diff}}$ of the residues of the tubulin β subjected to the electric field of frequency 90 GHz, Batch 3

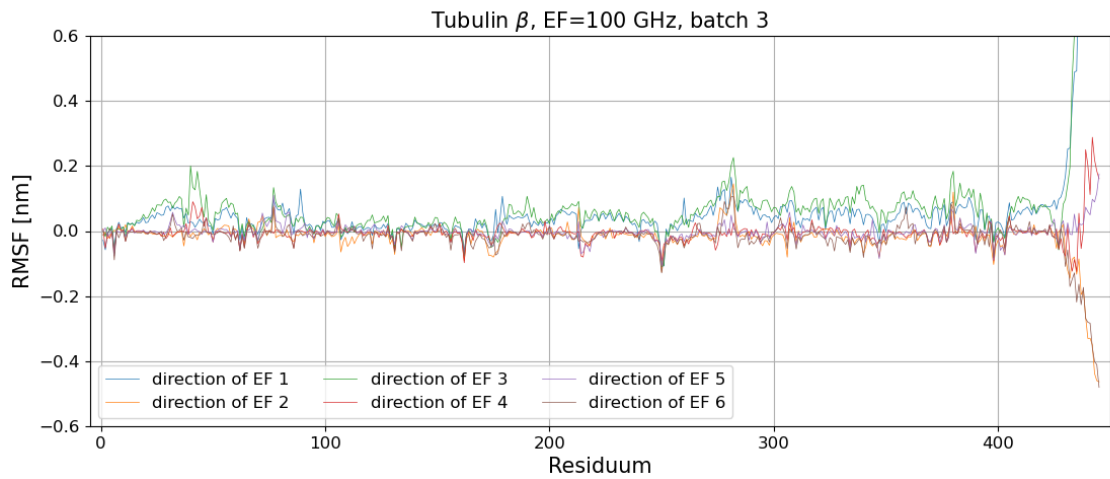


Figure 10.175: $\text{RMSF}_{\text{diff}}$ of the residues of the tubulin β subjected to the electric field of frequency 100 GHz, Batch 3

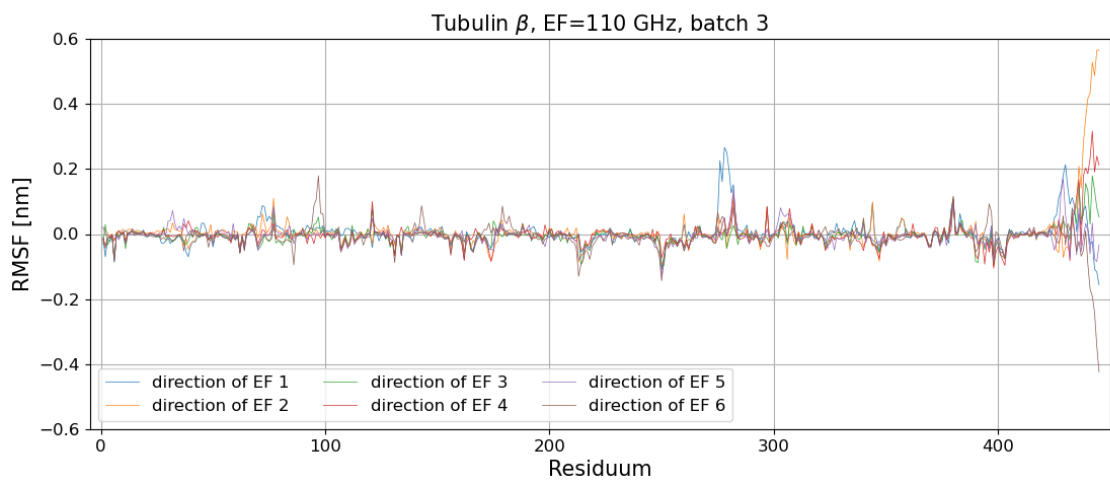


Figure 10.176: $\text{RMSF}_{\text{diff}}$ of the residues of the tubulin β subjected to the electric field of frequency 110 GHz, Batch 3

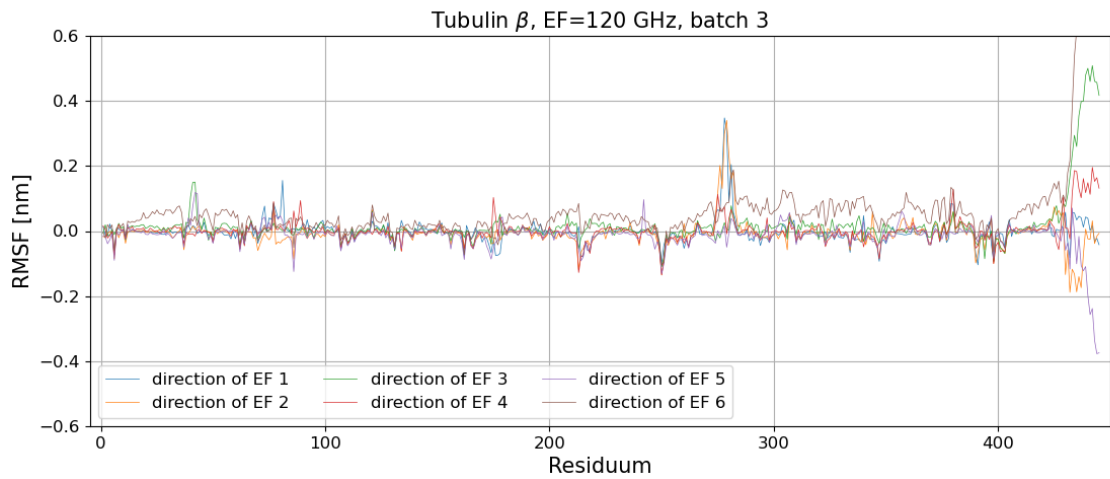


Figure 10.177: $\text{RMSF}_{\text{diff}}$ of the residues of the tubulin β subjected to the electric field of frequency 120 GHz, Batch 3

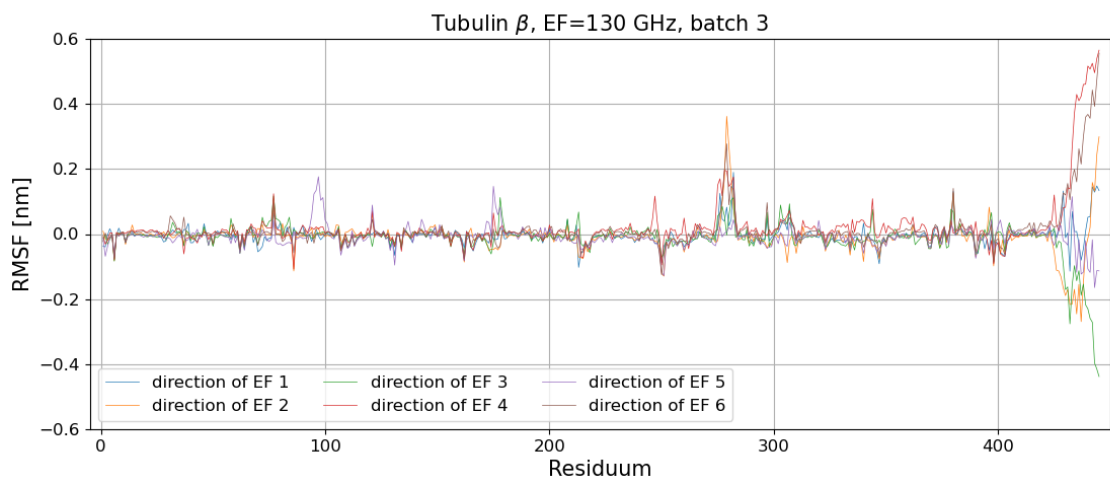


Figure 10.178: $\text{RMSF}_{\text{diff}}$ of the residues of the tubulin β subjected to the electric field of frequency 130 GHz, Batch 3

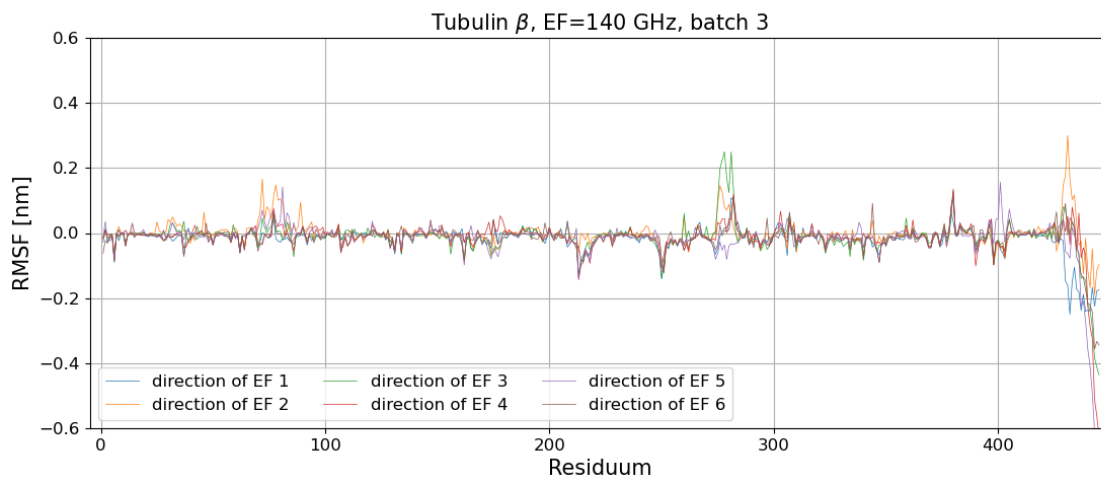


Figure 10.179: $\text{RMSF}_{\text{diff}}$ of the residues of the tubulin β subjected to the electric field of frequency 140 GHz, Batch 3

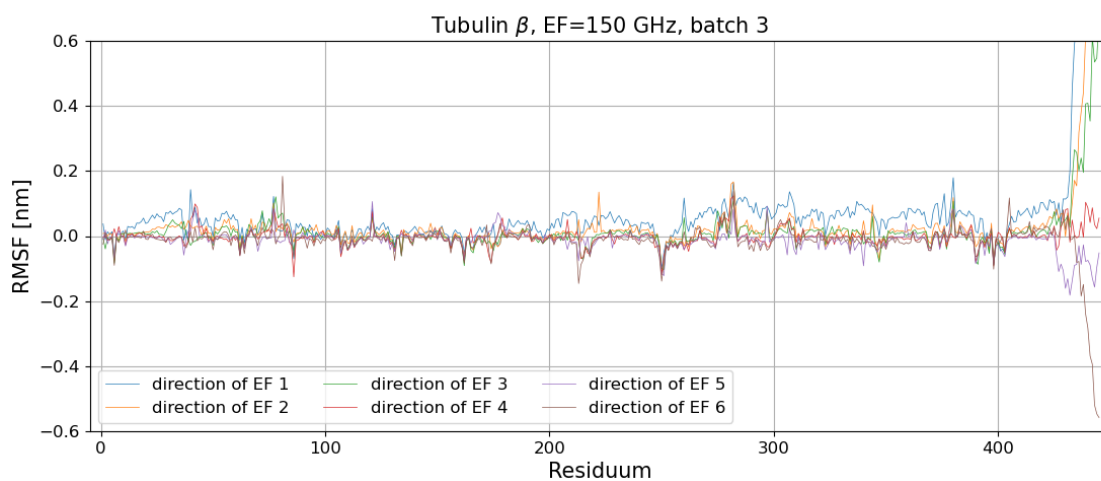


Figure 10.180: $\text{RMSF}_{\text{diff}}$ of the residues of the tubulin β subjected to the electric field of frequency 150 GHz, Batch 3

10.10 Averaged $\text{RMSF}_{\text{diff}}$ over all batches (initial conditions and direction of EF)

10.10.1 Tubulin α

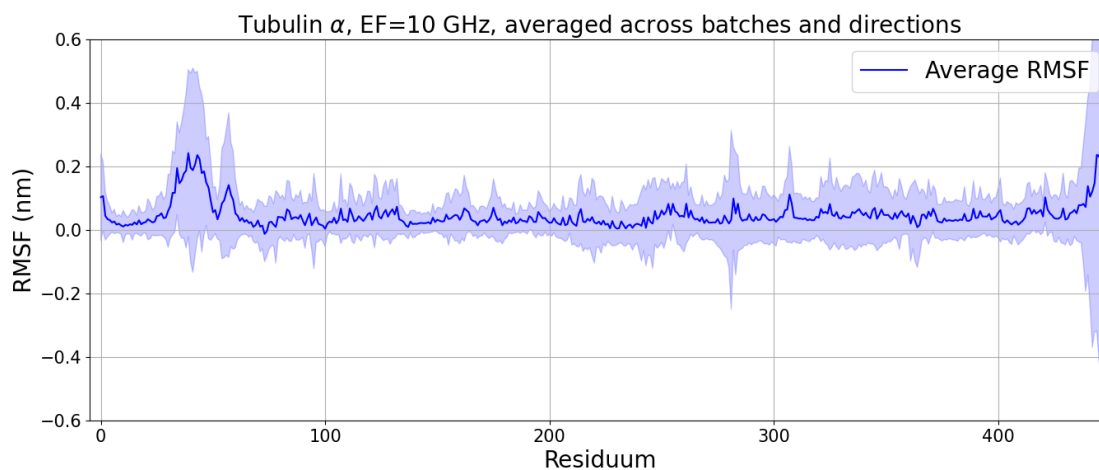


Figure 10.181: Average of $\text{RMSF}_{\text{diff}}$ of the residues of the α tubulin subjected to the electric field of frequency 10 GHz

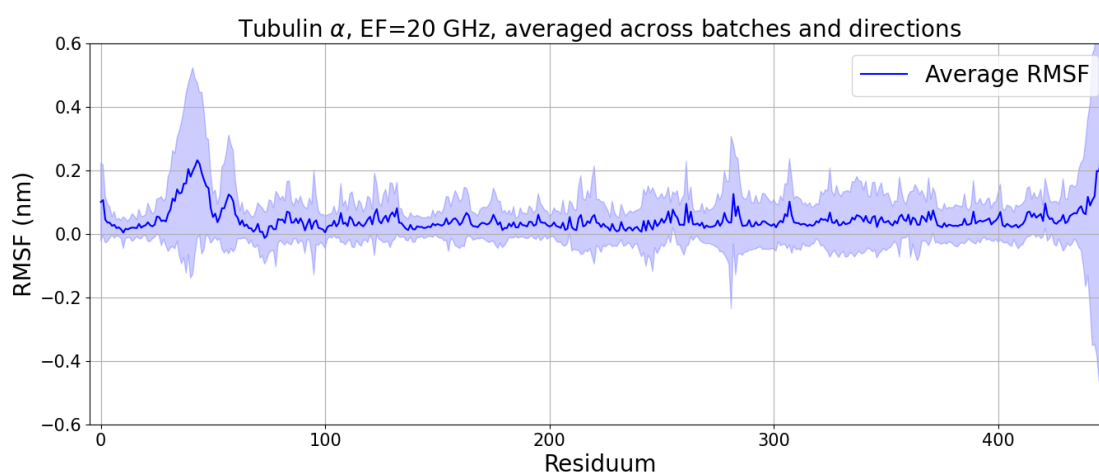


Figure 10.182: Average of $\text{RMSF}_{\text{diff}}$ of the residues of the α tubulin subjected to the electric field of frequency 20 GHz

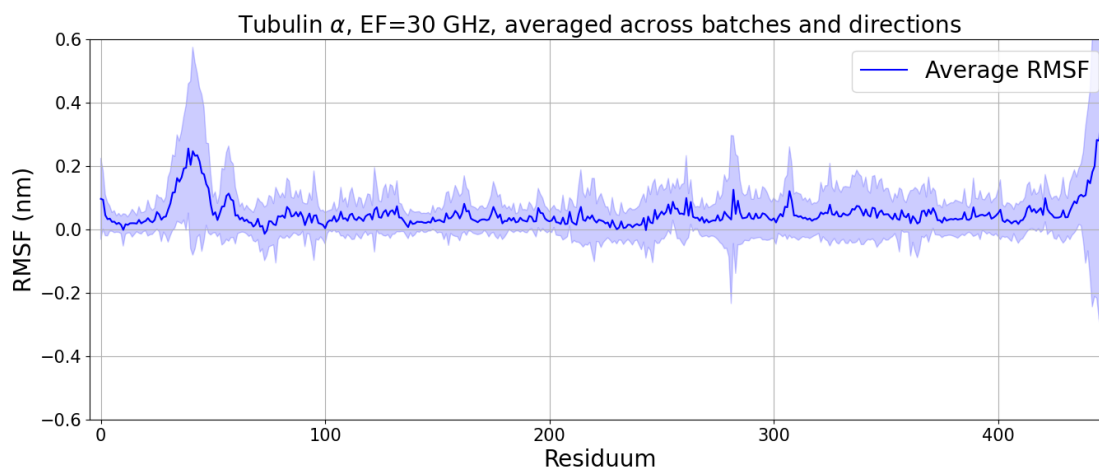


Figure 10.183: Average of $\text{RMSF}_{\text{diff}}$ of the residues of the α tubulin subjected to the electric field of frequency 30 GHz

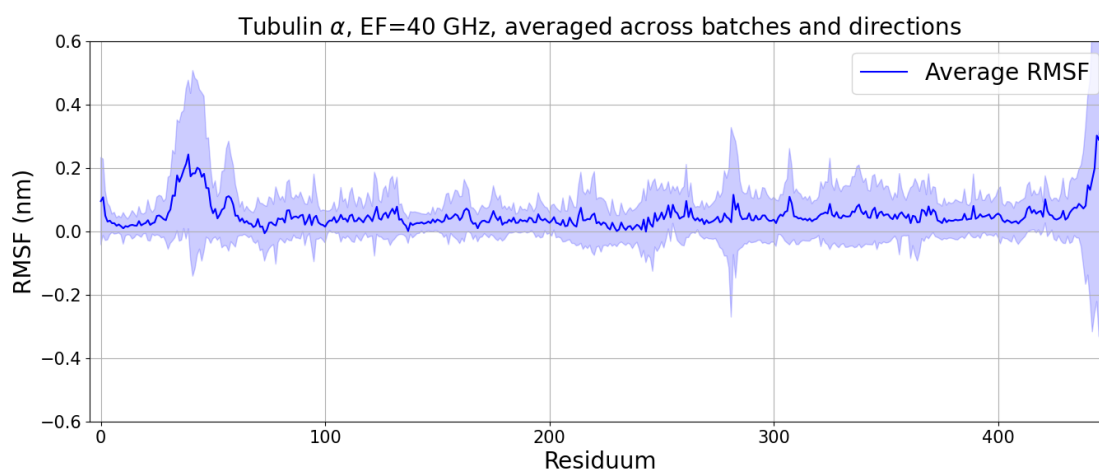


Figure 10.184: Average of $\text{RMSF}_{\text{diff}}$ of the residues of the α tubulin subjected to the electric field of frequency 40 GHz

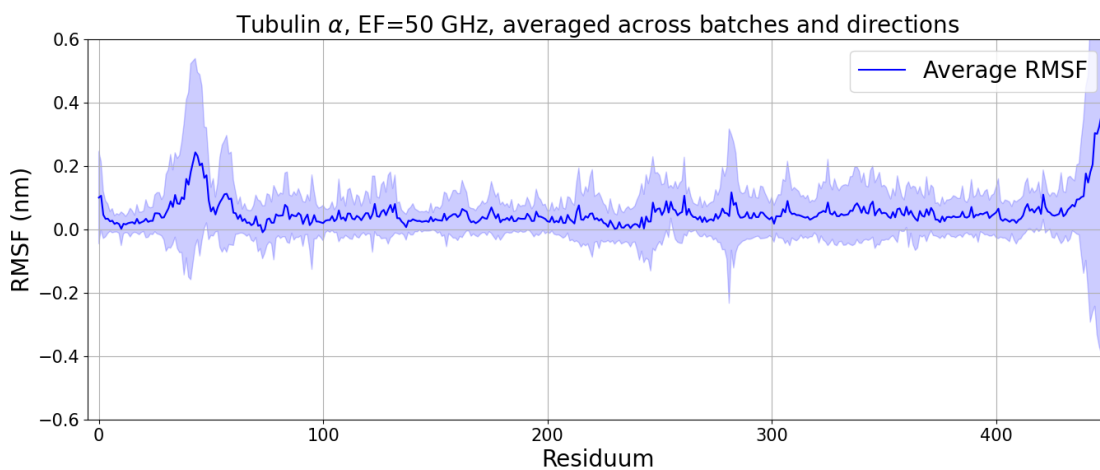


Figure 10.185: Average of $\text{RMSF}_{\text{diff}}$ of the residues of the α tubulin subjected to the electric field of frequency 50 GHz

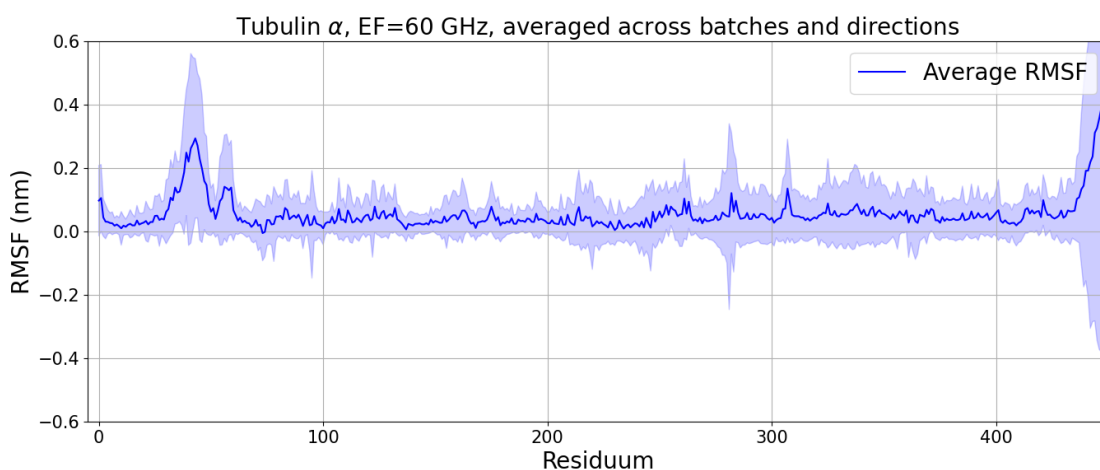


Figure 10.186: Average of $\text{RMSF}_{\text{diff}}$ of the residues of the α tubulin subjected to the electric field of frequency 60 GHz

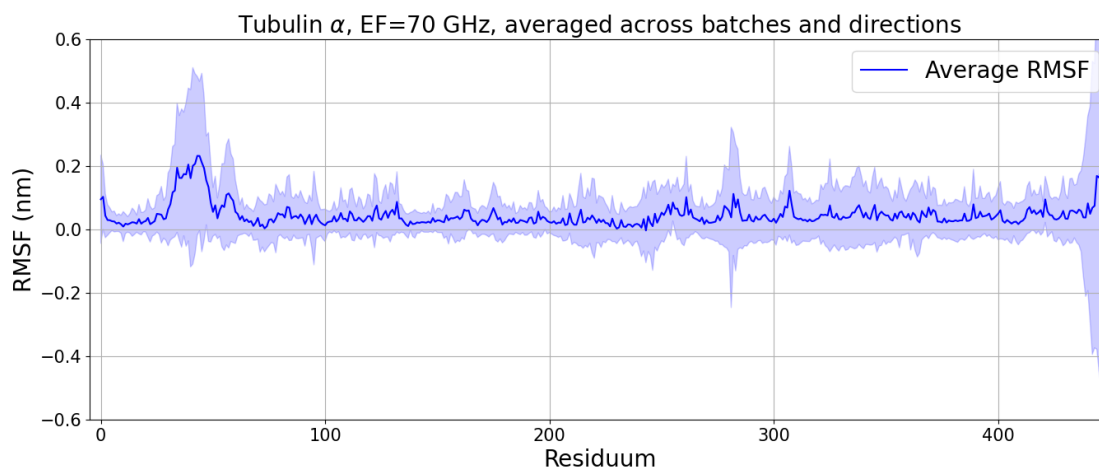


Figure 10.187: Average of $\text{RMSF}_{\text{diff}}$ of the residues of the α tubulin subjected to the electric field of frequency 70 GHz

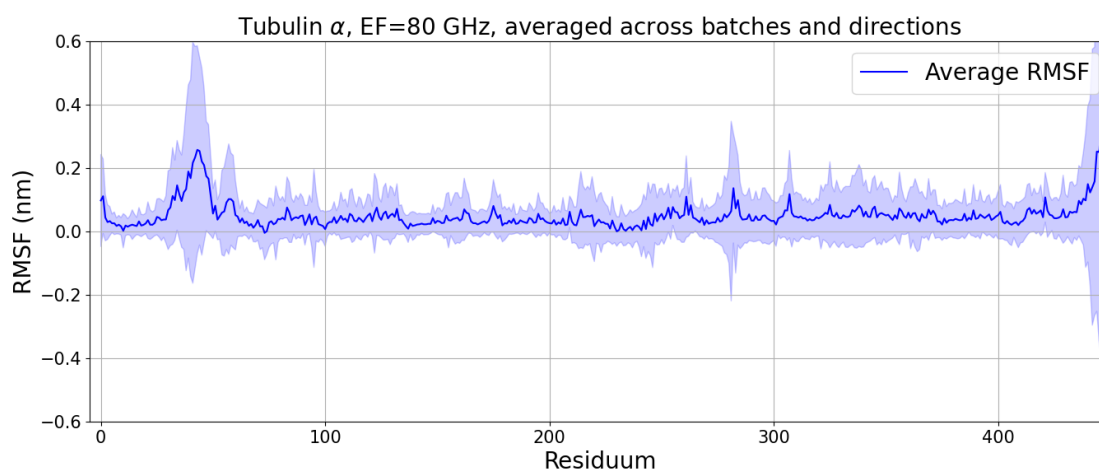


Figure 10.188: Average of $\text{RMSF}_{\text{diff}}$ of the residues of the α tubulin subjected to the electric field of frequency 80 GHz

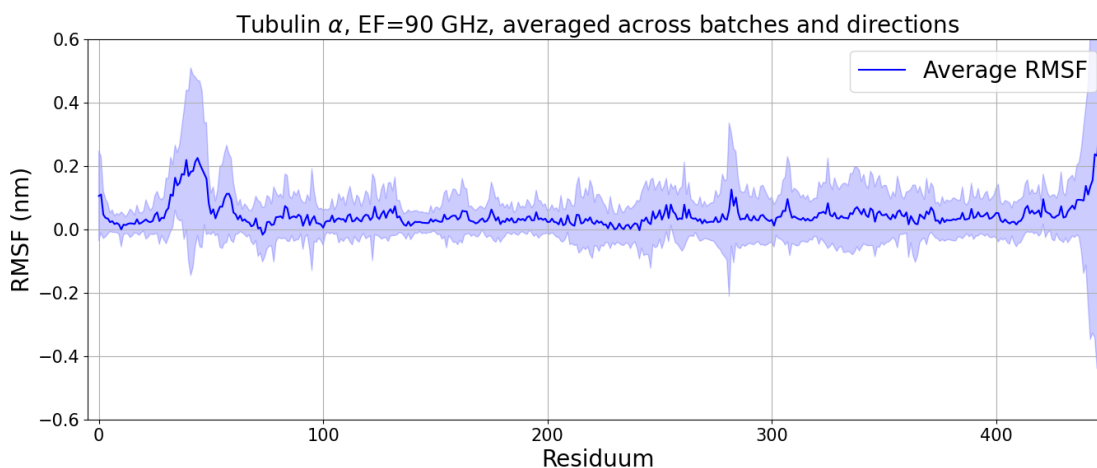


Figure 10.189: Average of $\text{RMSF}_{\text{diff}}$ of the residues of the α tubulin subjected to the electric field of frequency 90 GHz

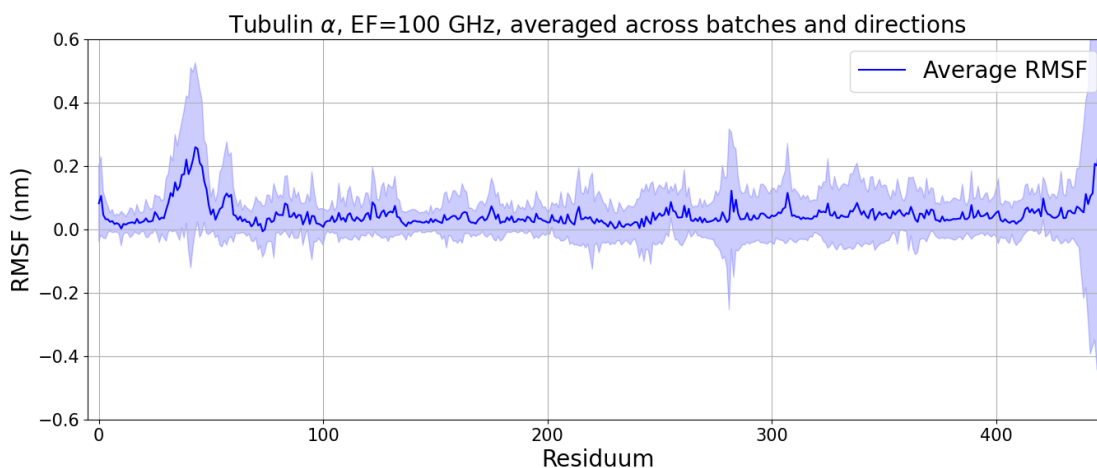


Figure 10.190: Average of $\text{RMSF}_{\text{diff}}$ of the residues of the α tubulin subjected to the electric field of frequency 100 GHz

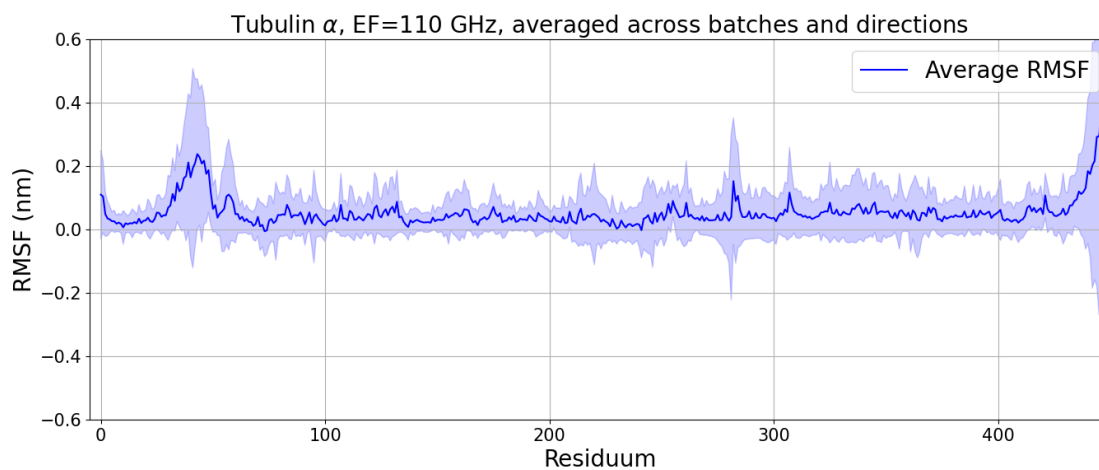


Figure 10.191: Average of $\text{RMSF}_{\text{diff}}$ of the residues of the α tubulin subjected to the electric field of frequency 110 GHz

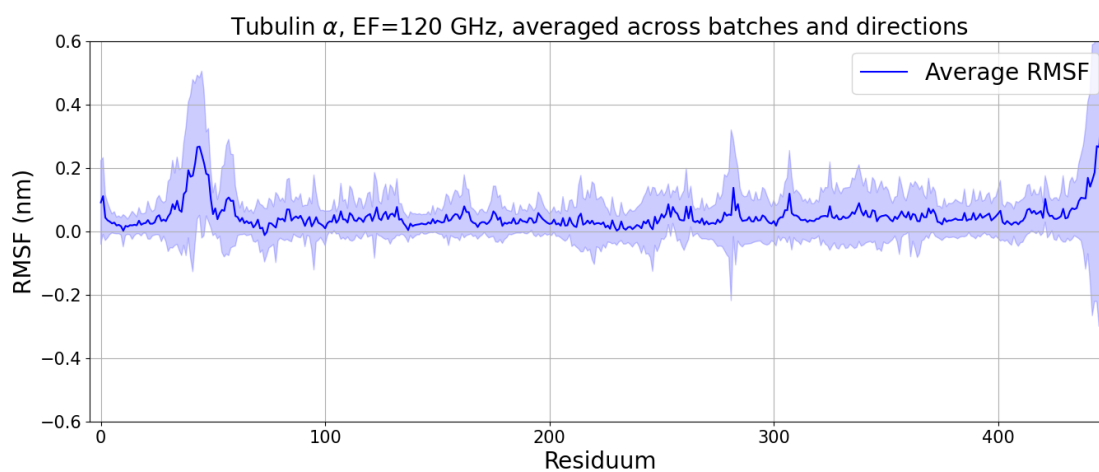


Figure 10.192: Average of $\text{RMSF}_{\text{diff}}$ of the residues of the α tubulin subjected to the electric field of frequency 120 GHz

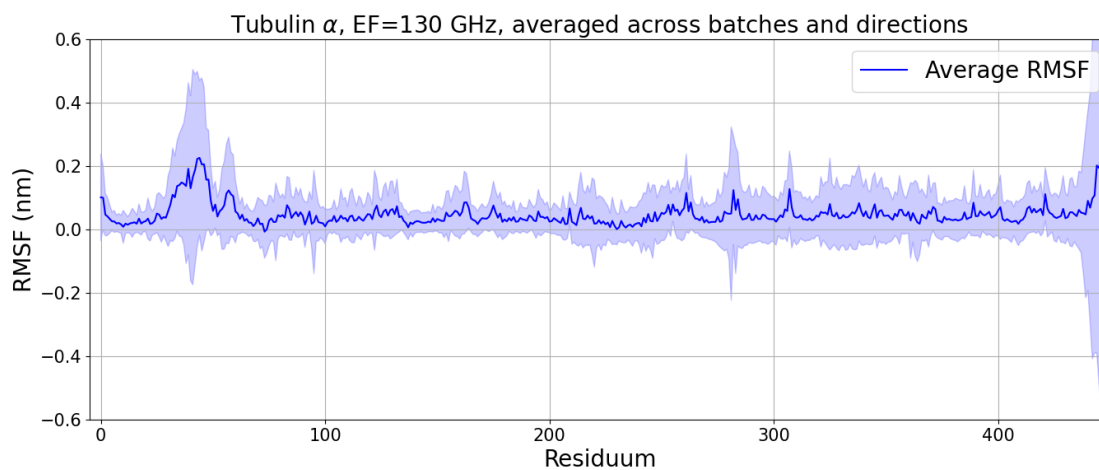


Figure 10.193: Average of $\text{RMSF}_{\text{diff}}$ of the residues of the α tubulin subjected to the electric field of frequency 130 GHz

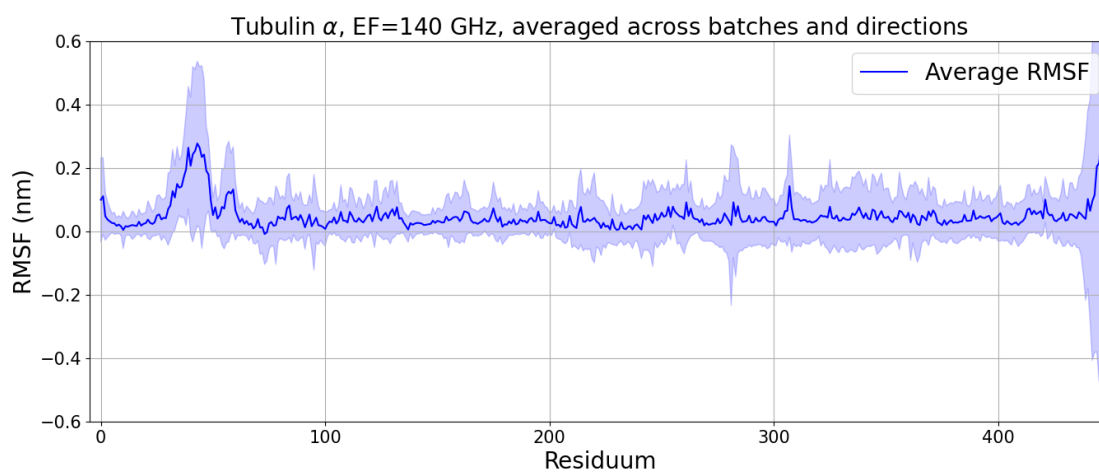


Figure 10.194: Average of $\text{RMSF}_{\text{diff}}$ of the residues of the α tubulin subjected to the electric field of frequency 140 GHz

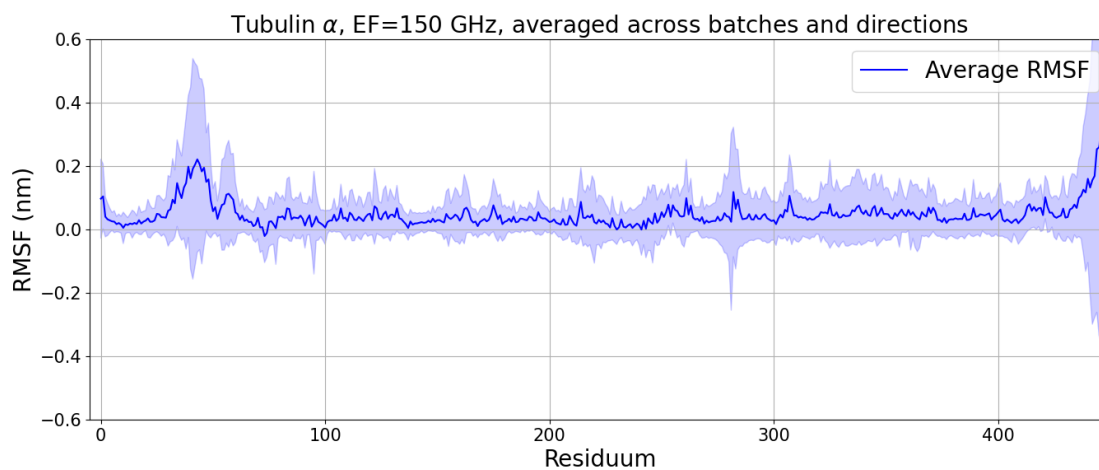


Figure 10.195: Average of $\text{RMSF}_{\text{diff}}$ of the residues of the α tubulin subjected to the electric field of frequency 150 GHz

10.10.2 Tubulin β

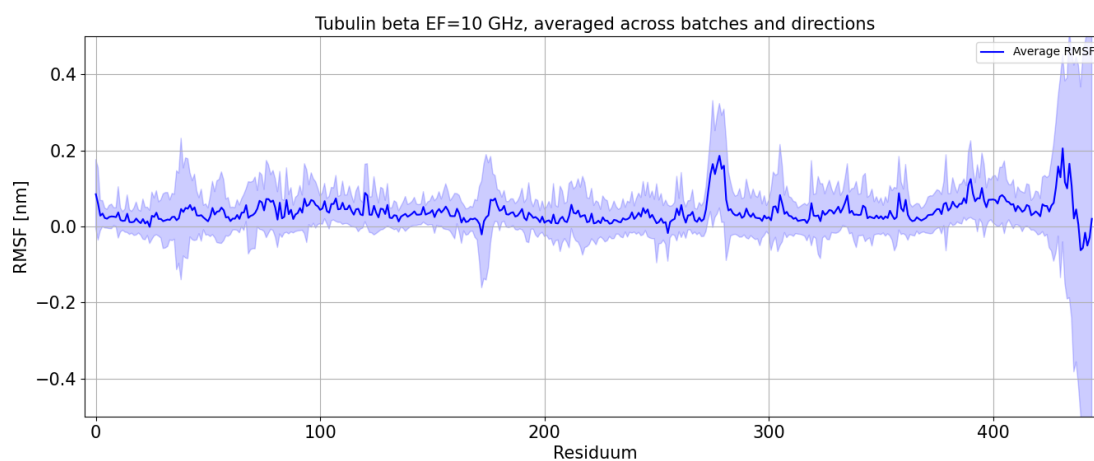


Figure 10.196: Average of $\text{RMSF}_{\text{diff}}$ of the residues of the β tubulin subjected to the electric field of frequency 10 GHz

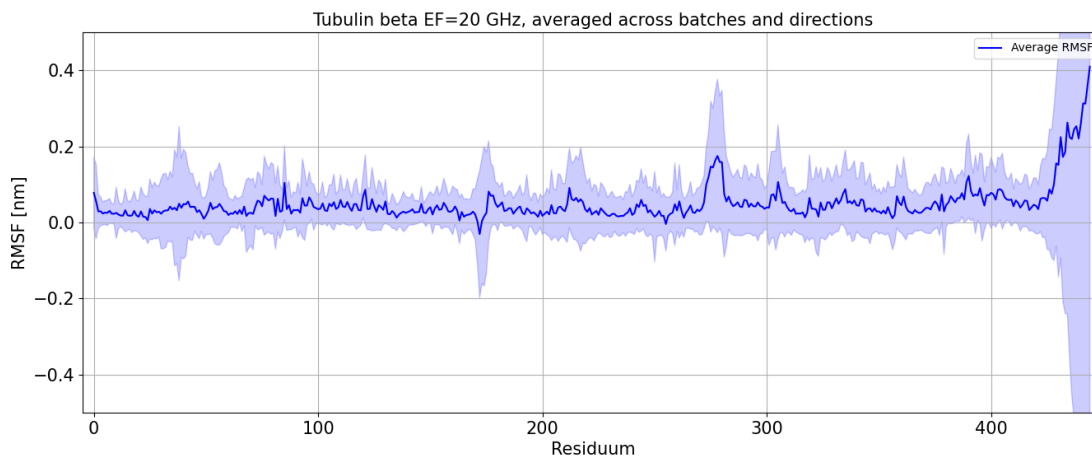


Figure 10.197: Average of $\text{RMSF}_{\text{diff}}$ of the residues of the β tubulin subjected to the electric field of frequency 20 GHz

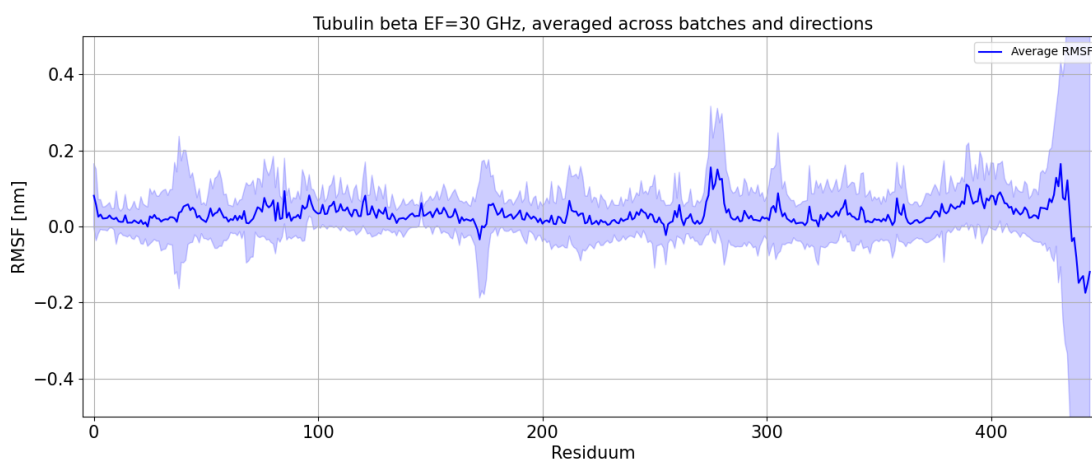


Figure 10.198: Average of $\text{RMSF}_{\text{diff}}$ of the residues of the β tubulin subjected to the electric field of frequency 30 GHz

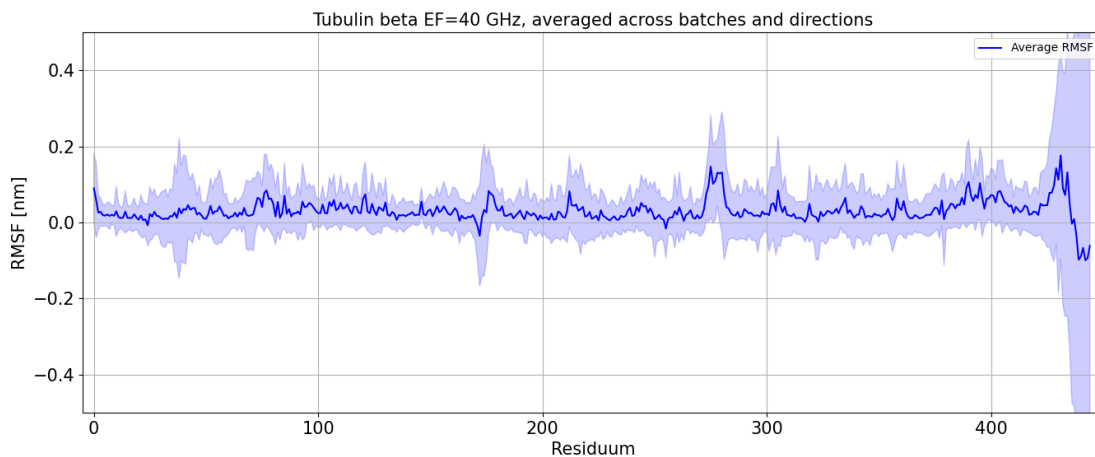


Figure 10.199: Average of $\text{RMSF}_{\text{diff}}$ of the residues of the β tubulin subjected to the electric field of frequency 40 GHz

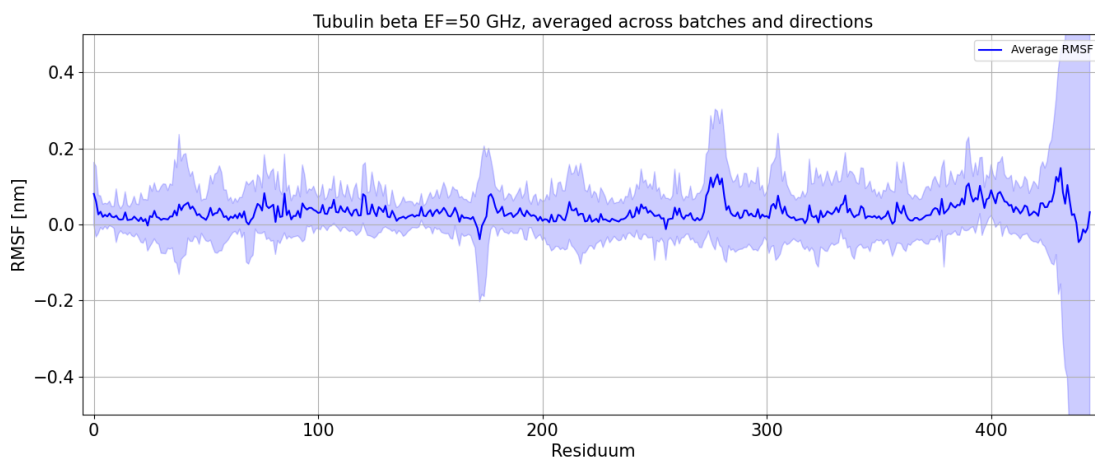


Figure 10.200: Average of $\text{RMSF}_{\text{diff}}$ of the residues of the β tubulin subjected to the electric field of frequency 50 GHz

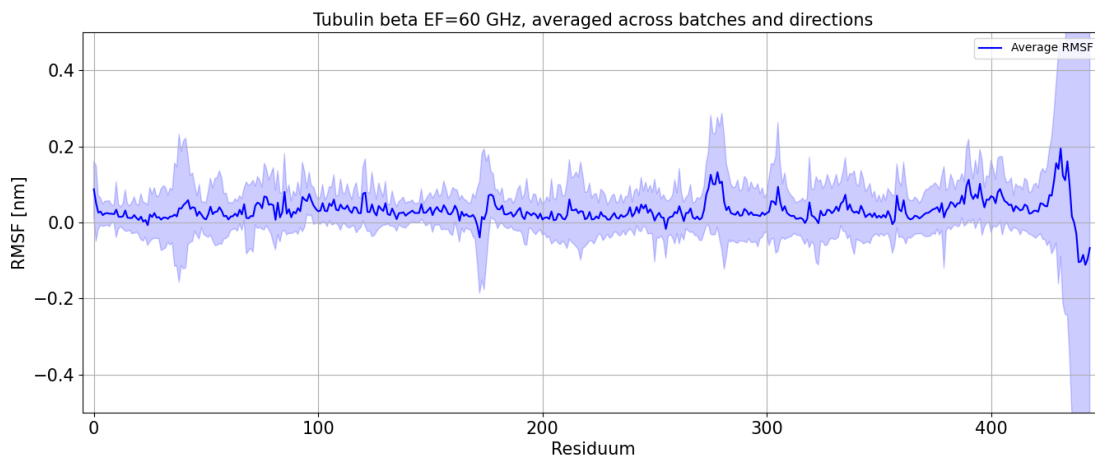


Figure 10.201: Average of $\text{RMSF}_{\text{diff}}$ of the residues of the β tubulin subjected to the electric field of frequency 60 GHz

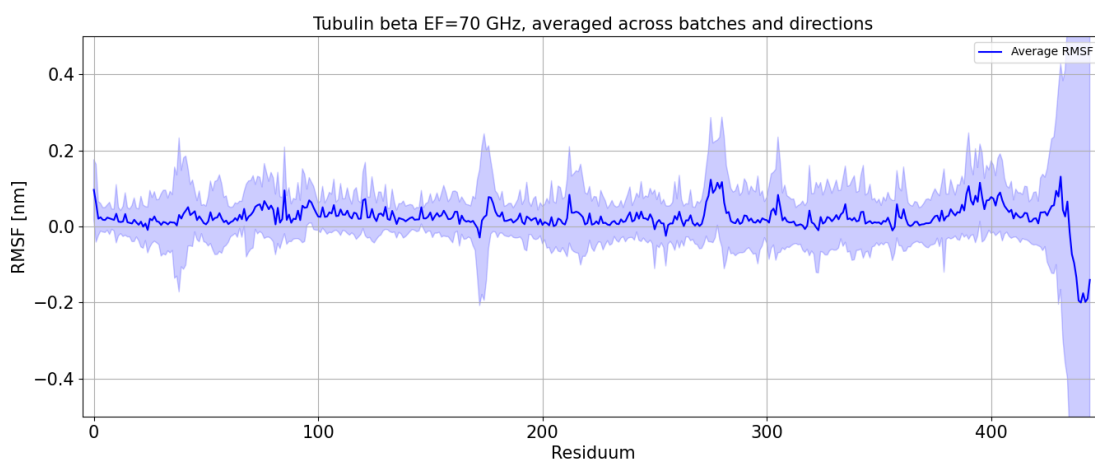


Figure 10.202: Average of $\text{RMSF}_{\text{diff}}$ of the residues of the β tubulin subjected to the electric field of frequency 70 GHz

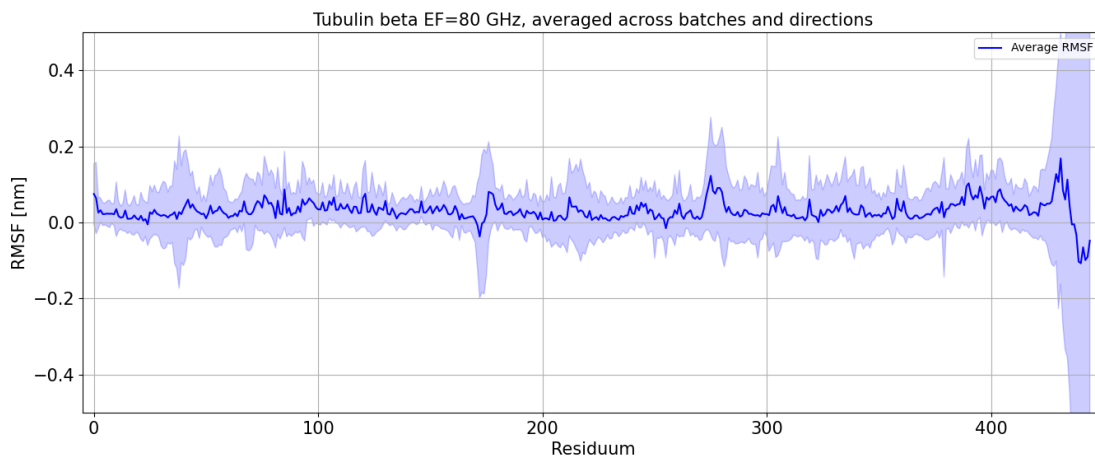


Figure 10.203: Average of $\text{RMSF}_{\text{diff}}$ of the residues of the β tubulin subjected to the electric field of frequency 80 GHz

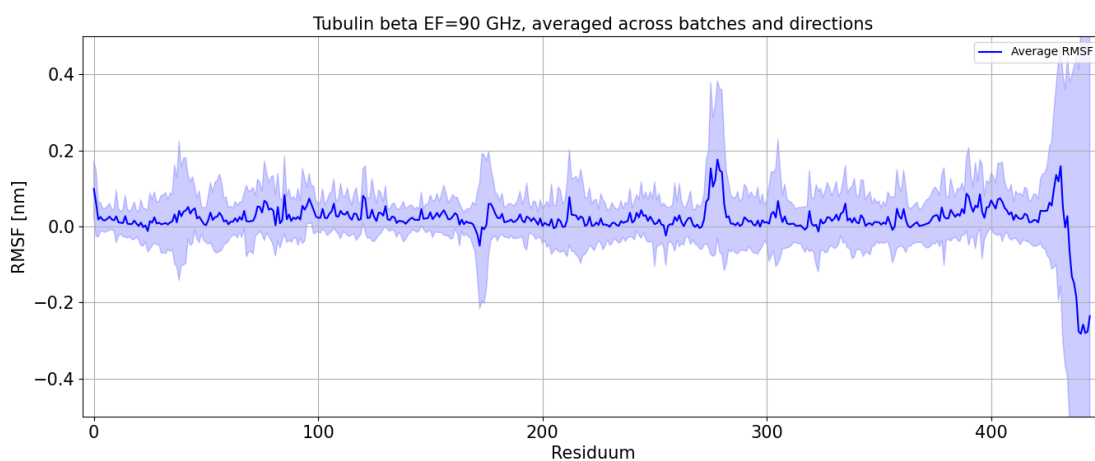


Figure 10.204: Average of $\text{RMSF}_{\text{diff}}$ of the residues of the β tubulin subjected to the electric field of frequency 90 GHz

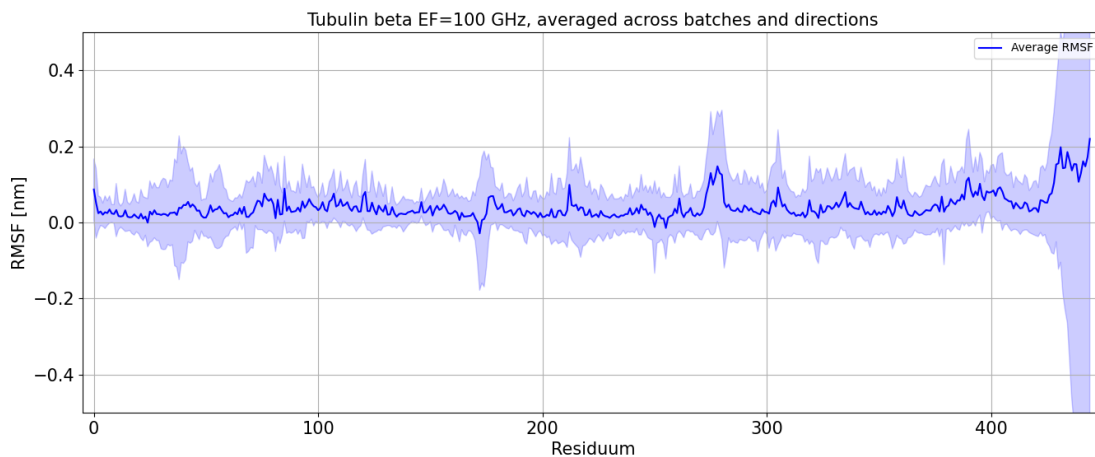


Figure 10.205: Average of $\text{RMSF}_{\text{diff}}$ of the residues of the β tubulin subjected to the electric field of frequency 100 GHz

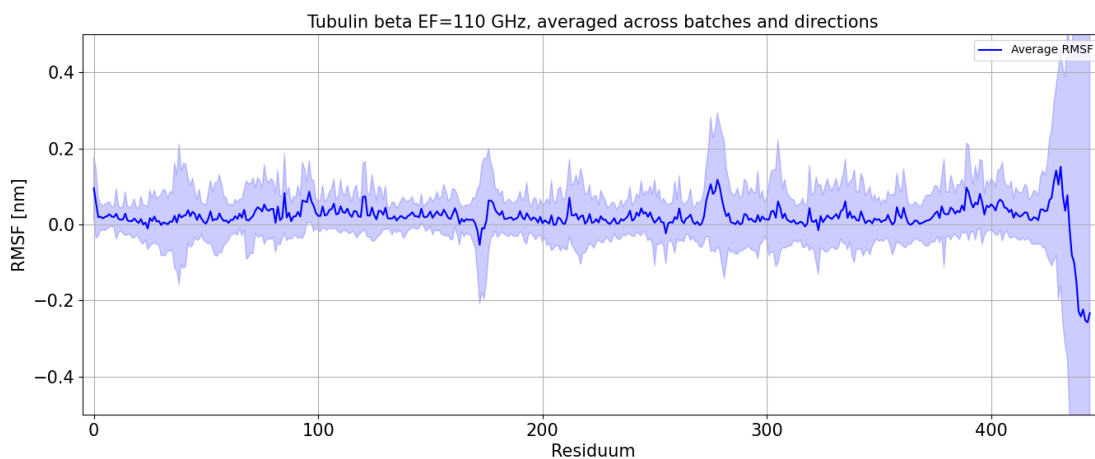


Figure 10.206: Average of $\text{RMSF}_{\text{diff}}$ of the residues of the β tubulin subjected to the electric field of frequency 110 GHz

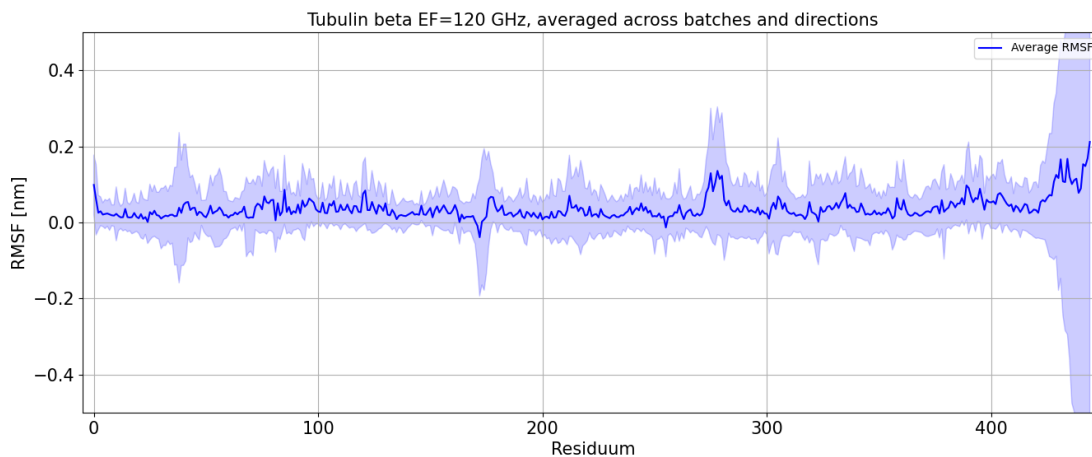


Figure 10.207: Average of $\text{RMSF}_{\text{diff}}$ of the residues of the β tubulin subjected to the electric field of frequency 120 GHz

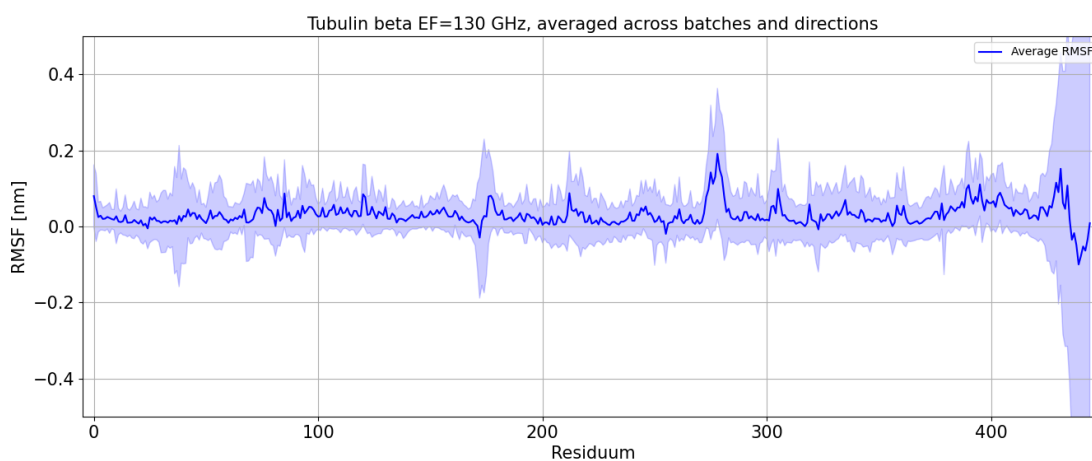


Figure 10.208: Average of $\text{RMSF}_{\text{diff}}$ of the residues of the β tubulin subjected to the electric field of frequency 130 GHz



Figure 10.209: Average of $\text{RMSF}_{\text{diff}}$ of the residues of the β tubulin subjected to the electric field of frequency 140 GHz

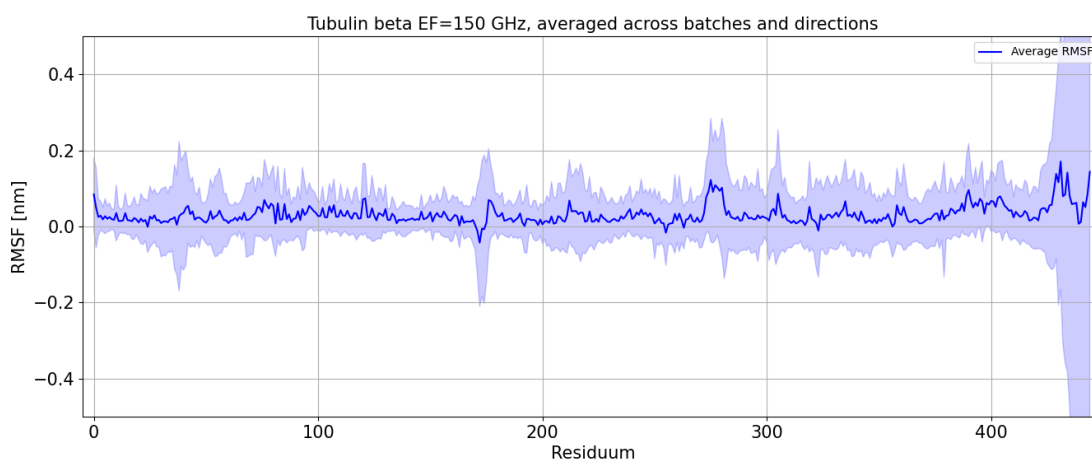


Figure 10.210: Average of $\text{RMSF}_{\text{diff}}$ of the residues of the β tubulin subjected to the electric field of frequency 150 GHz

10.11 RMSF of residues - averaged only over initial conditions

10.11.1 Tubulin α

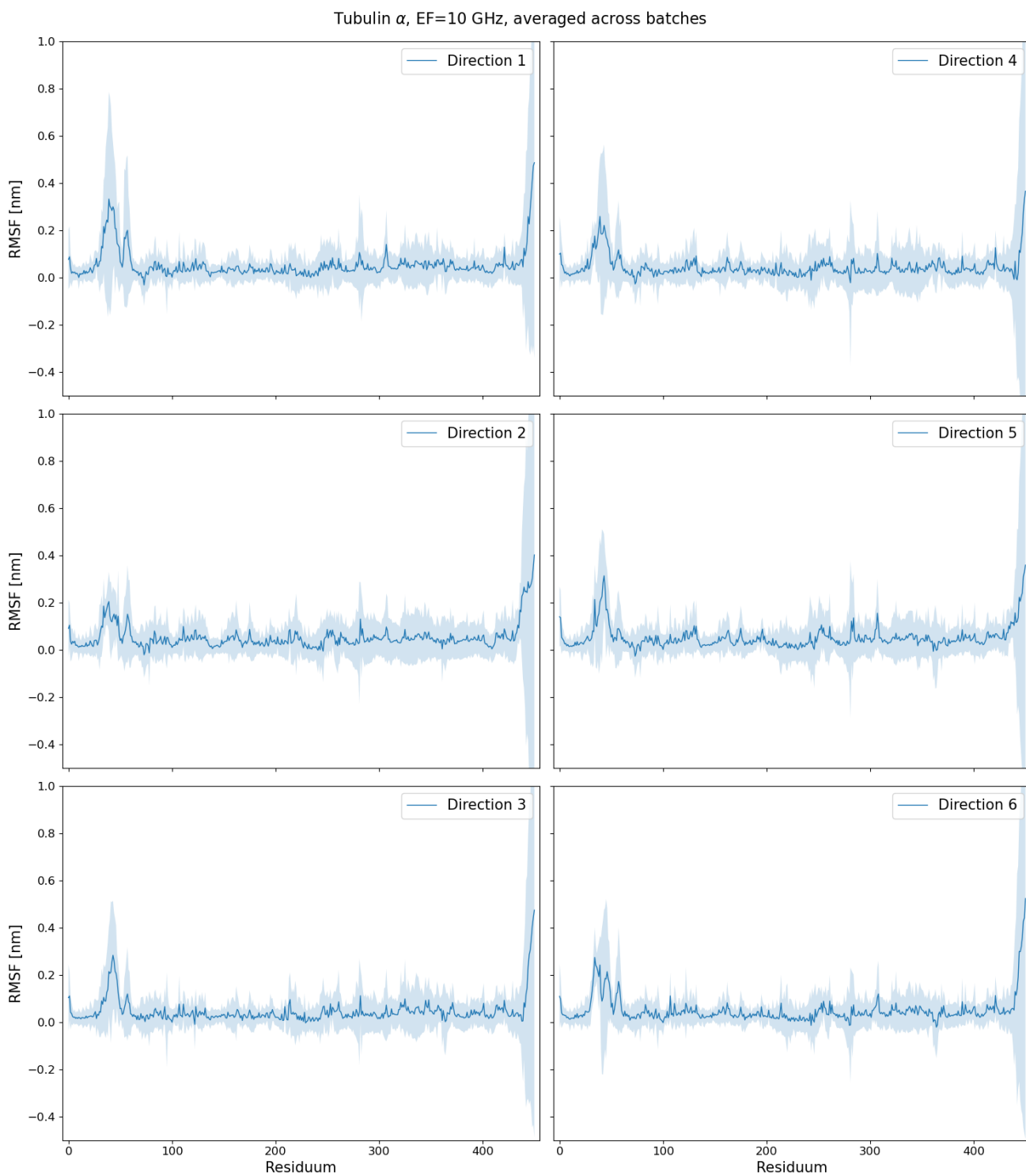


Figure 10.211: $\text{RMSF}_{\text{diff}}$ difference graphs of tubulin α with 10 GHz EF - averaged over batches

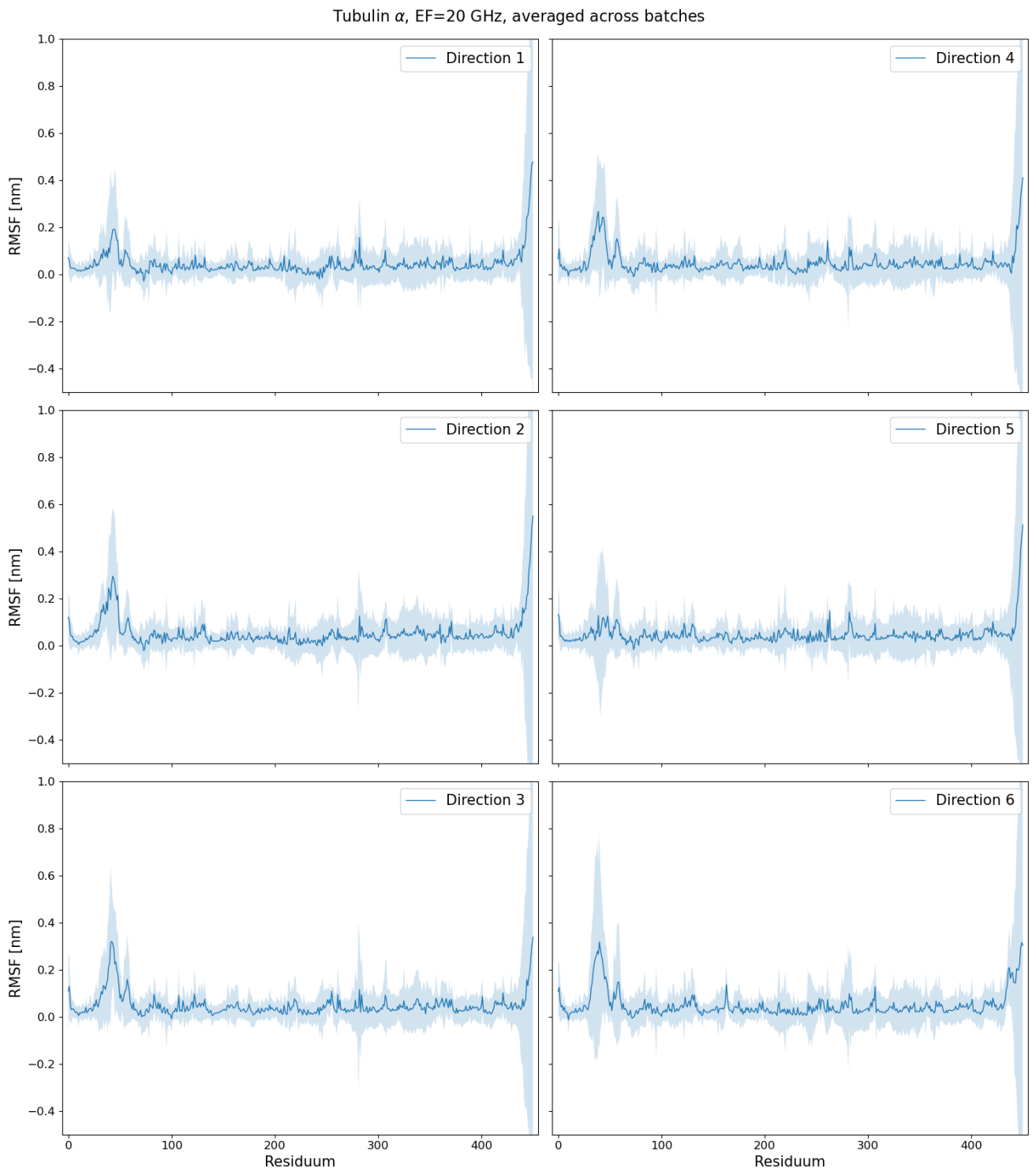


Figure 10.212: $\text{RMSF}_{\text{diff}}$ difference graphs of tubulin α with 20 GHz EF - averaged over batches

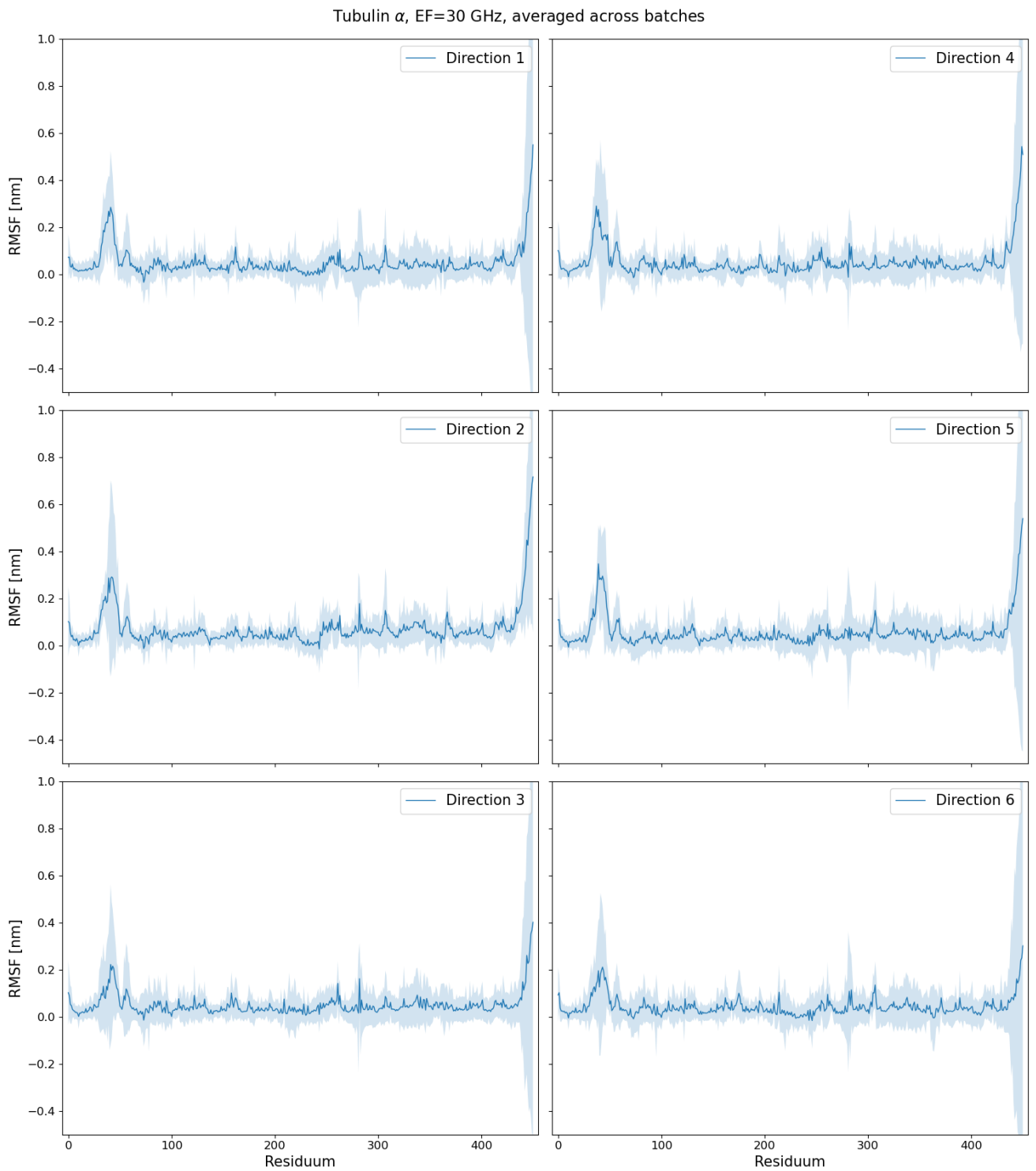


Figure 10.213: $\text{RMSF}_{\text{diff}}$ difference graphs of tubulin α with 30 GHz EF - averaged over batches

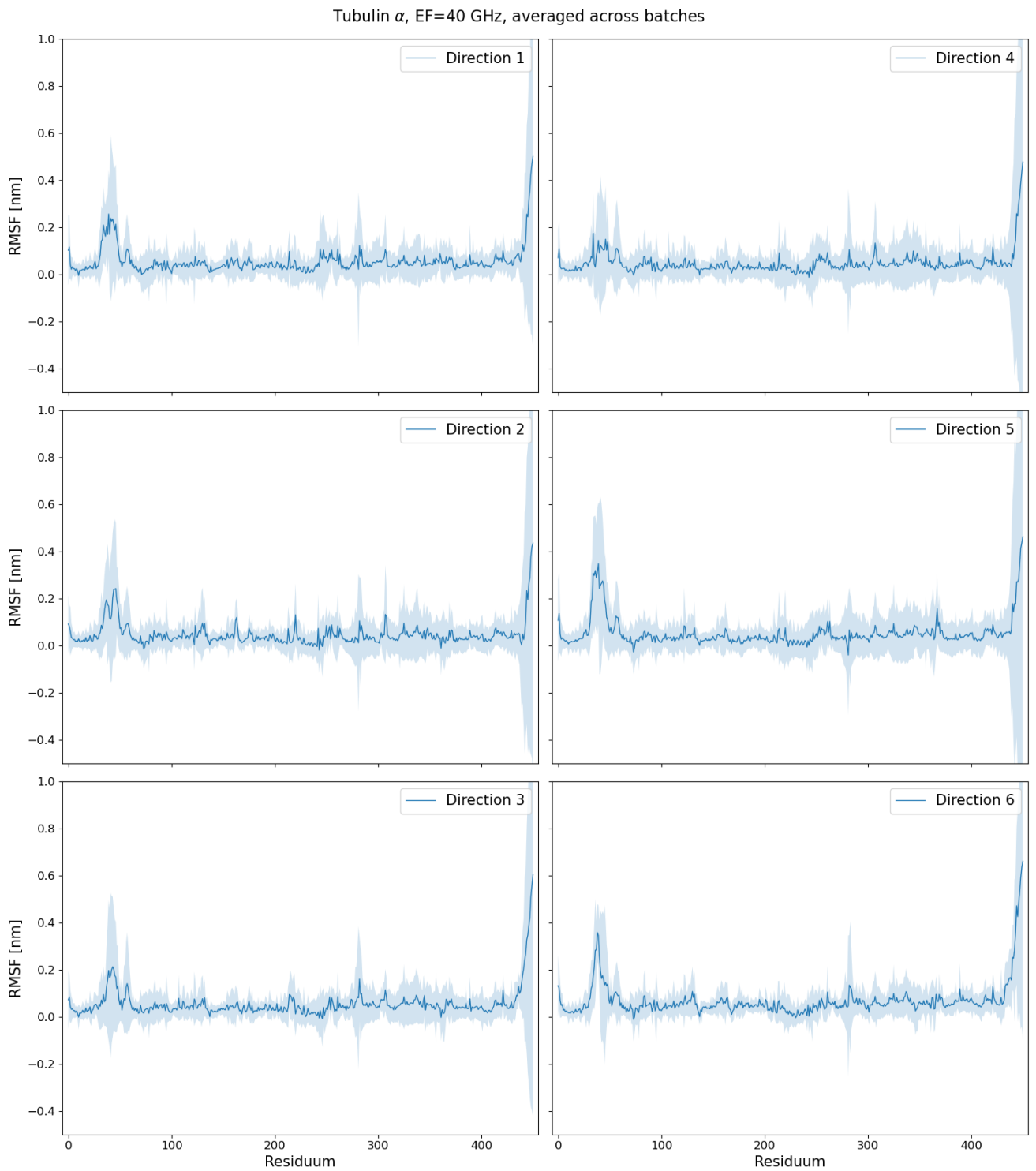


Figure 10.214: $\text{RMSF}_{\text{diff}}$ difference graphs of tubulin α with 40 GHz EF - averaged over batches

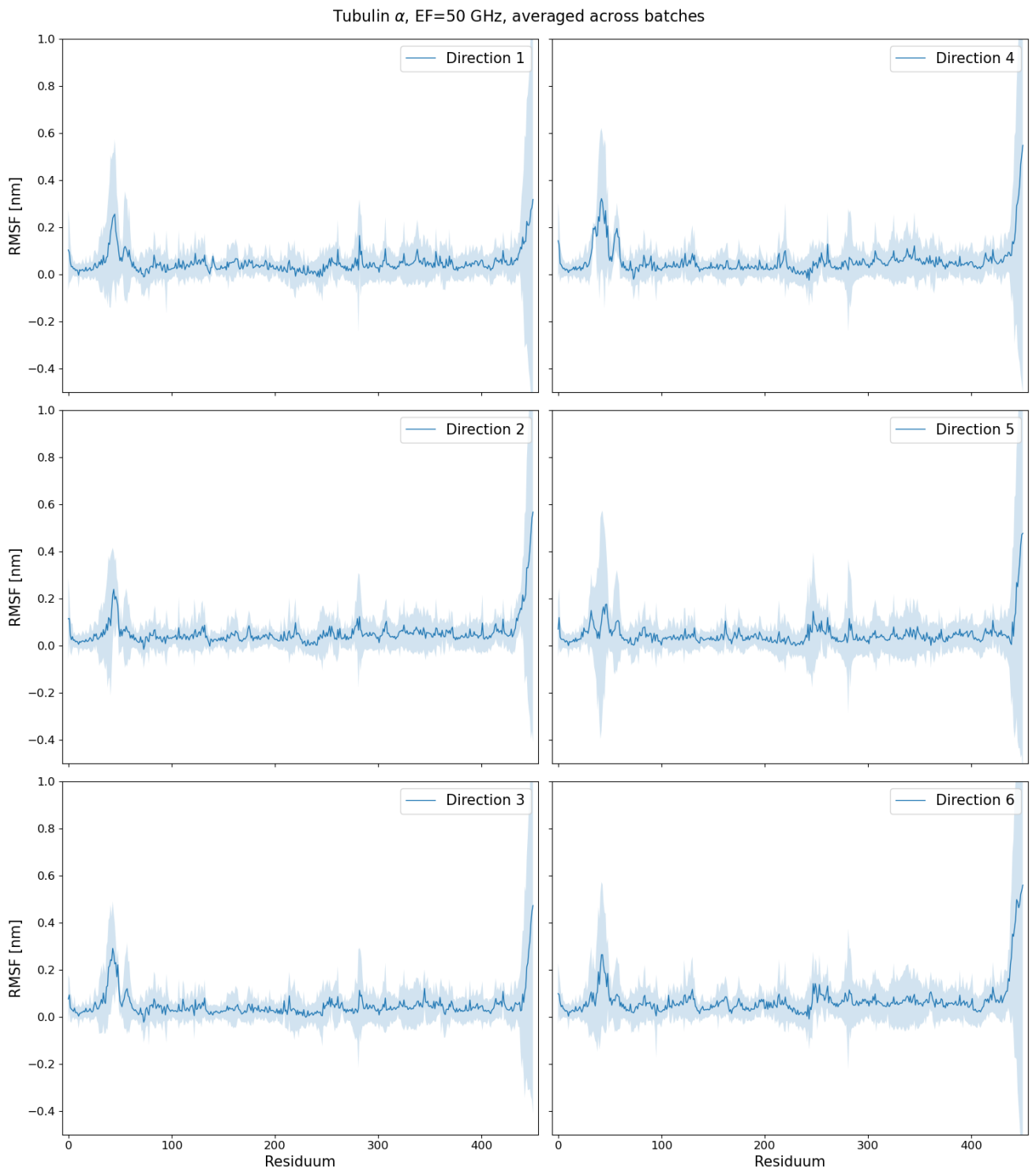


Figure 10.215: $\text{RMSF}_{\text{diff}}$ difference graphs of tubulin α with 50 GHz EF - averaged over batches

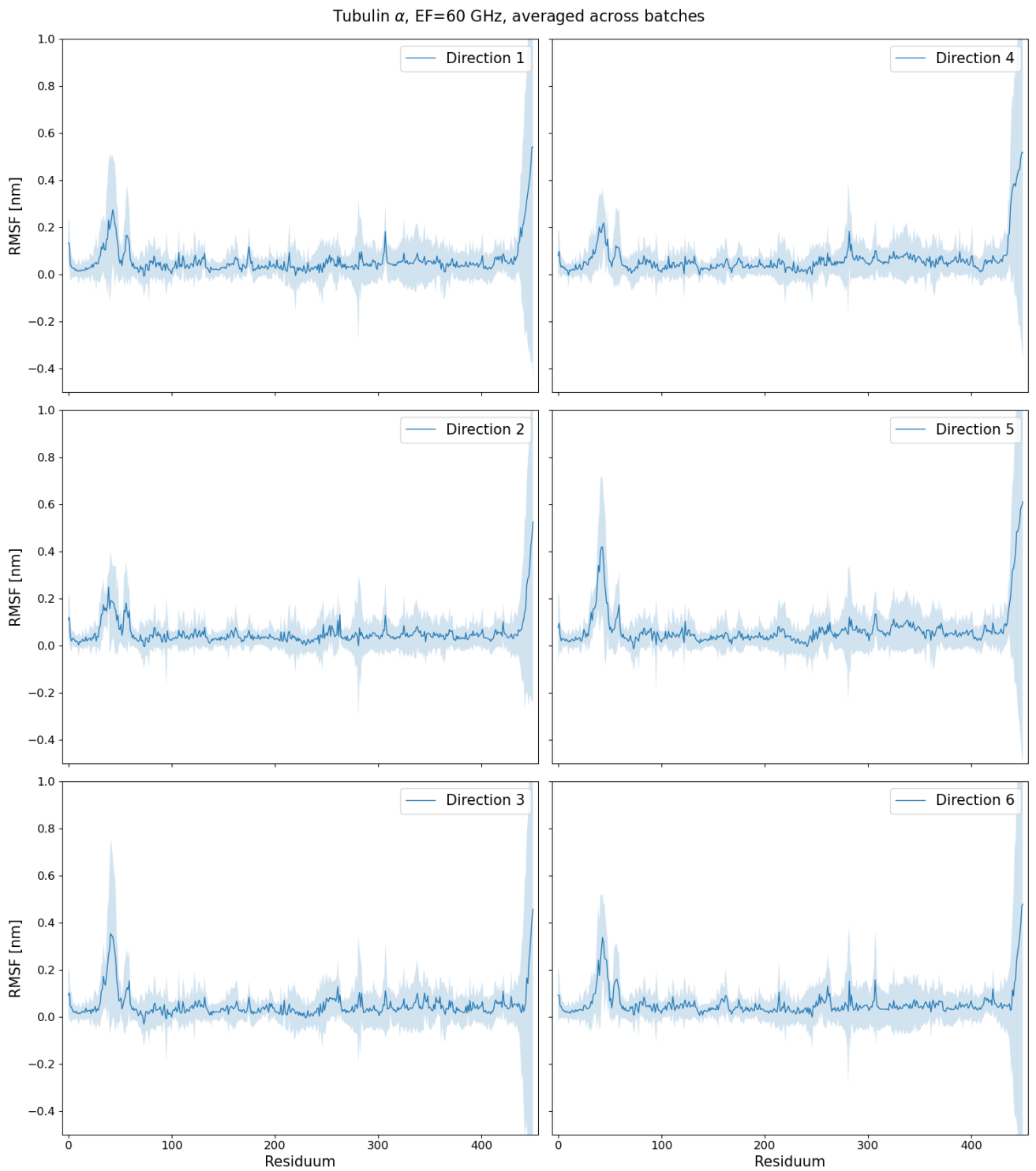


Figure 10.216: $\text{RMSF}_{\text{diff}}$ difference graphs of tubulin α with 60 GHz EF - averaged over batches

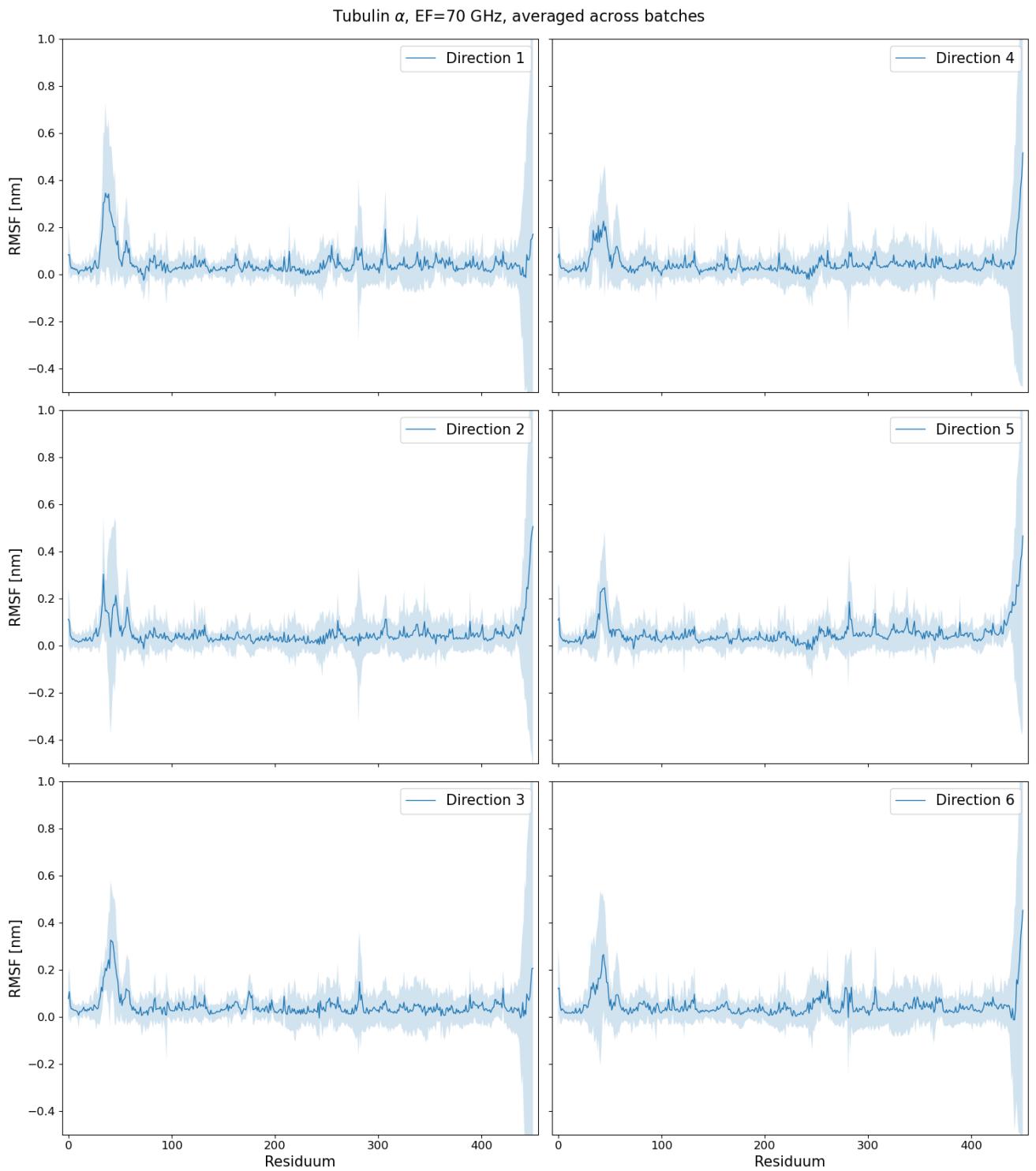


Figure 10.217: $\text{RMSF}_{\text{diff}}$ difference graphs of tubulin α with 70 GHz EF - averaged over batches

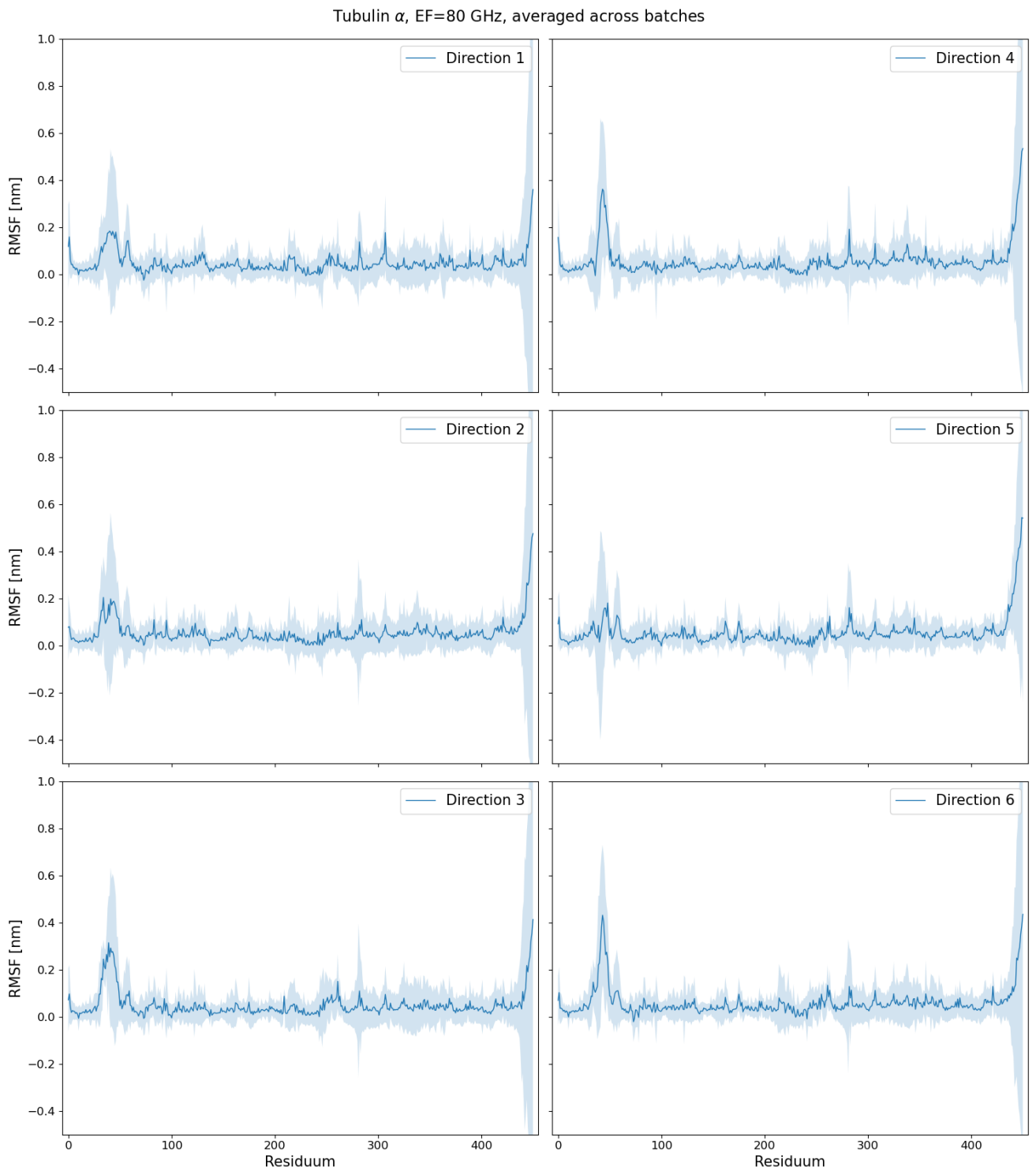


Figure 10.218: $\text{RMSF}_{\text{diff}}$ difference graphs of tubulin α with 80 GHz EF - averaged over batches

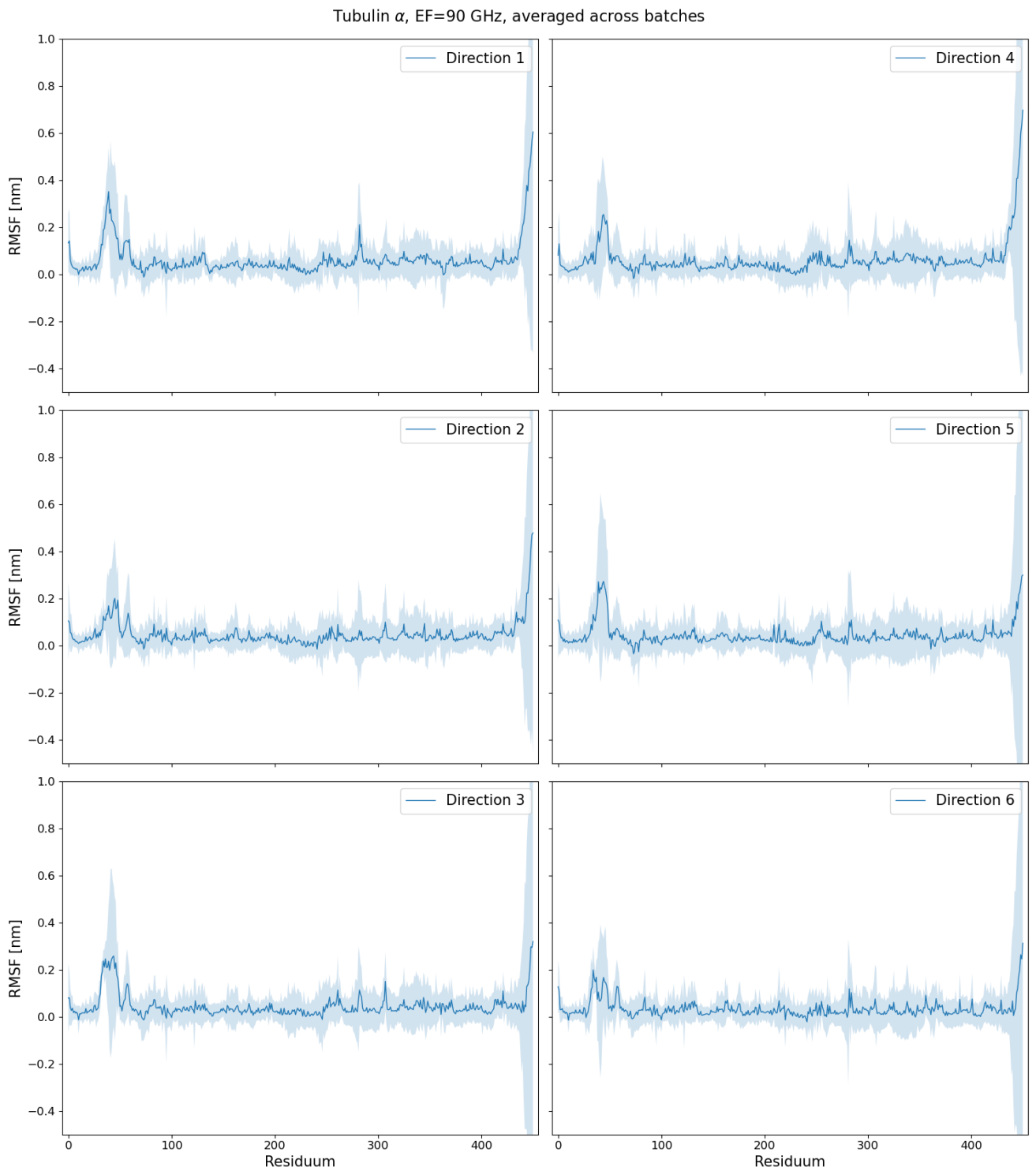


Figure 10.219: $\text{RMSF}_{\text{diff}}$ difference graphs of tubulin α with 90 GHz EF - averaged over batches

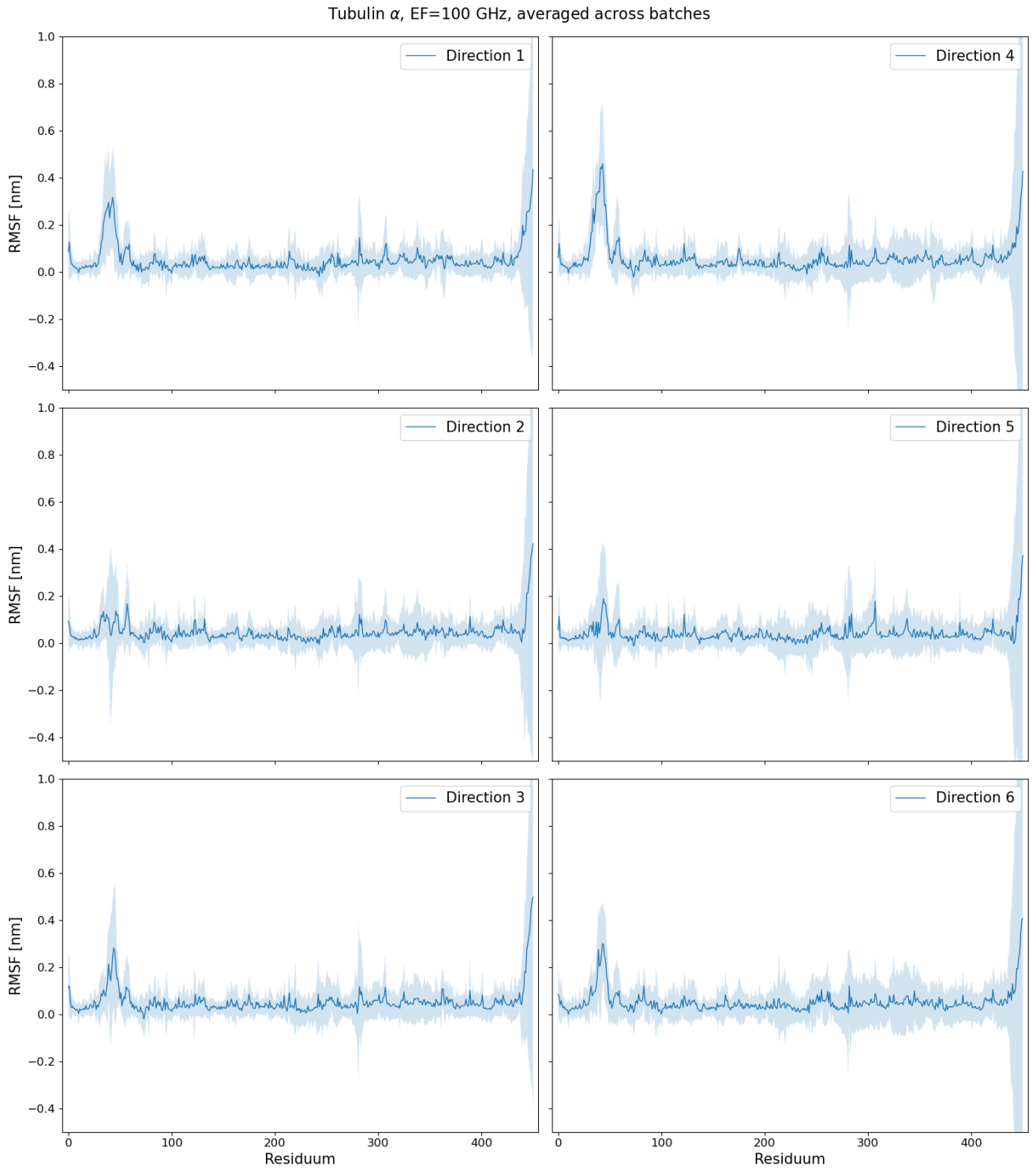


Figure 10.220: $\text{RMSF}_{\text{diff}}$ difference graphs of tubulin α with 100 GHz EF - averaged over batches

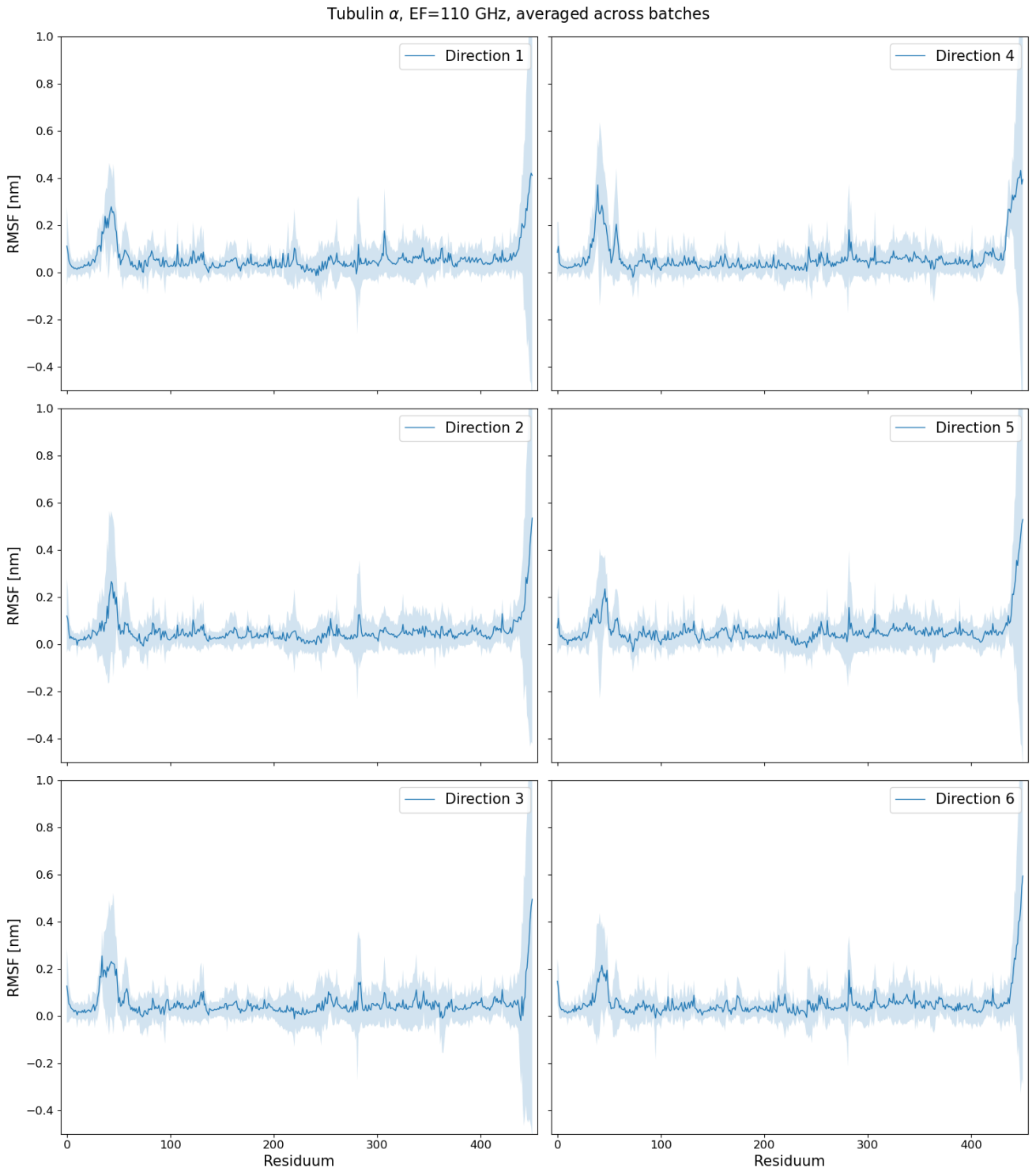


Figure 10.221: $\text{RMSF}_{\text{diff}}$ difference graphs of tubulin α with 110 GHz EF - averaged over batches

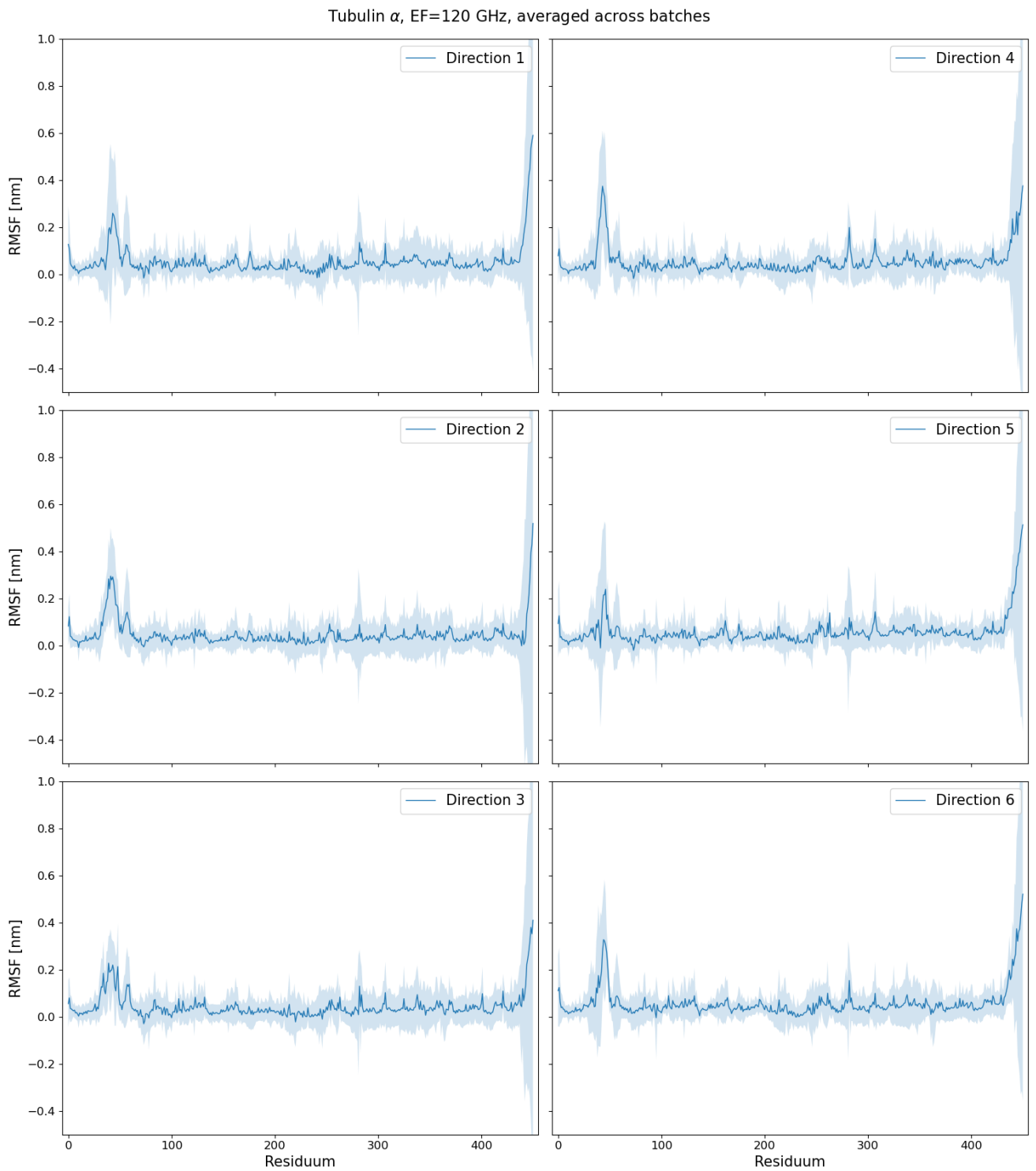


Figure 10.222: RMSF_{diff} difference graphs of tubulin α with 120 GHz EF - averaged over batches

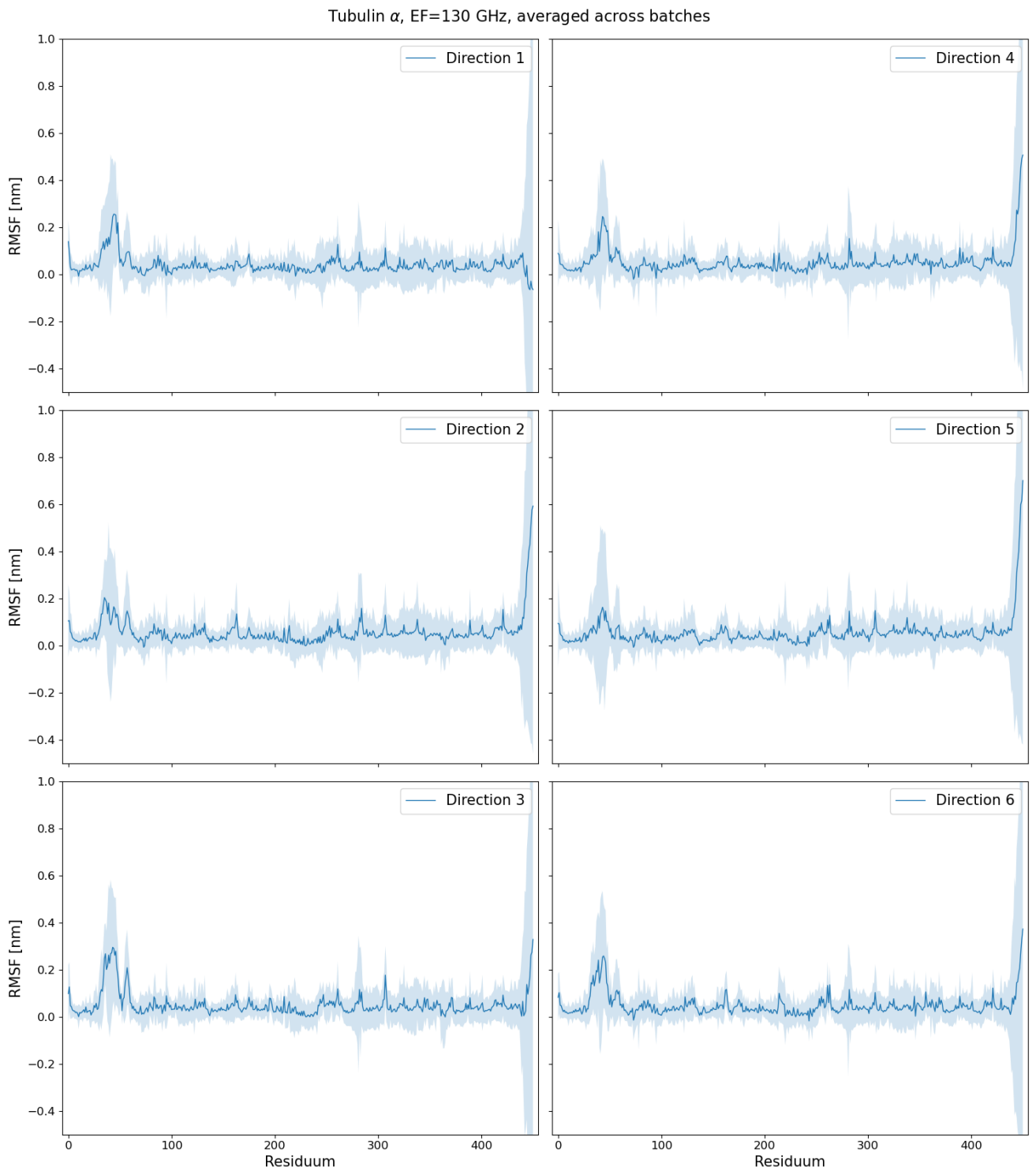


Figure 10.223: $\text{RMSF}_{\text{diff}}$ difference graphs of tubulin α with 130 GHz EF - averaged over batches

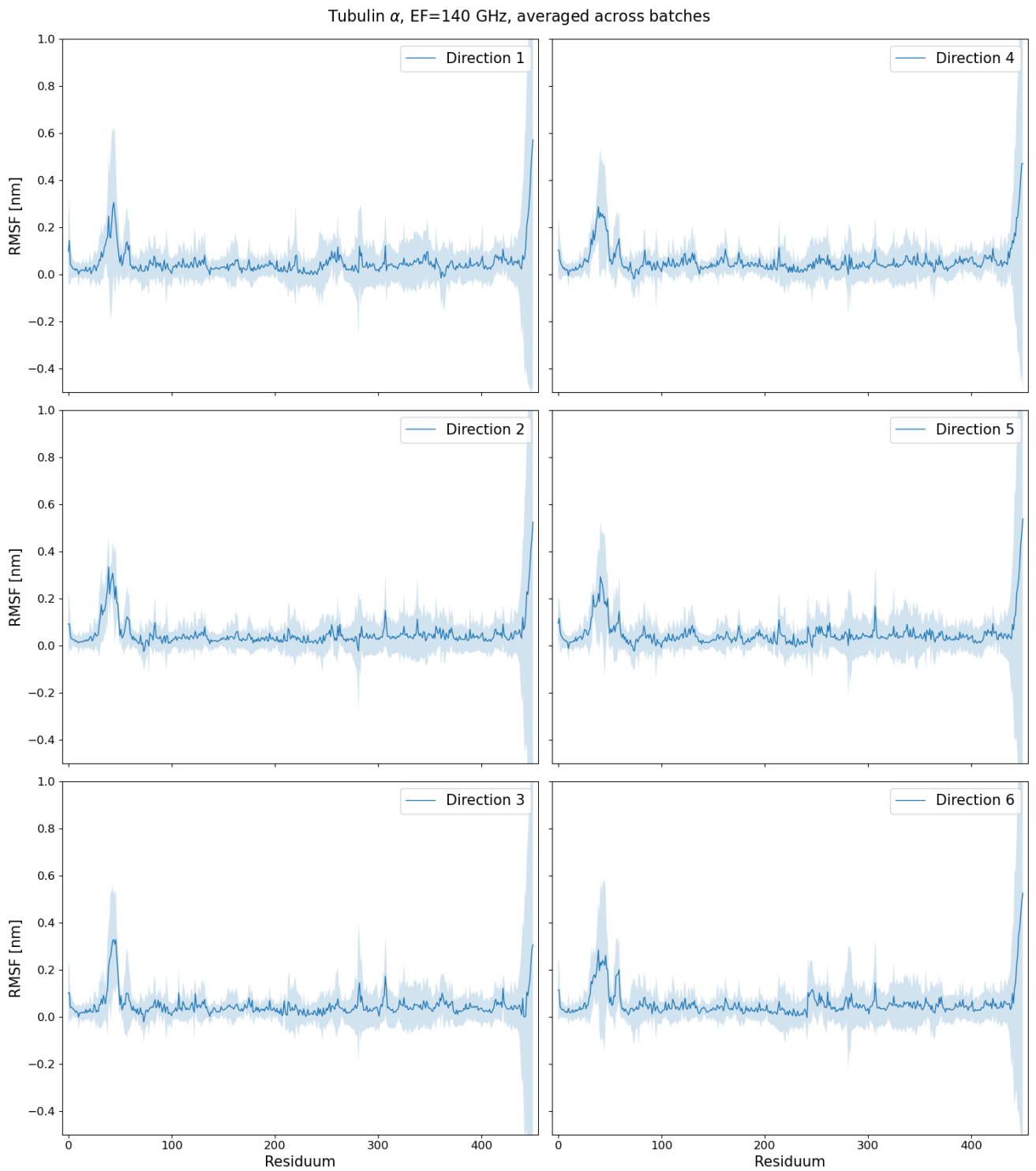


Figure 10.224: $\text{RMSF}_{\text{diff}}$ difference graphs of tubulin α with 140 GHz EF - averaged over batches

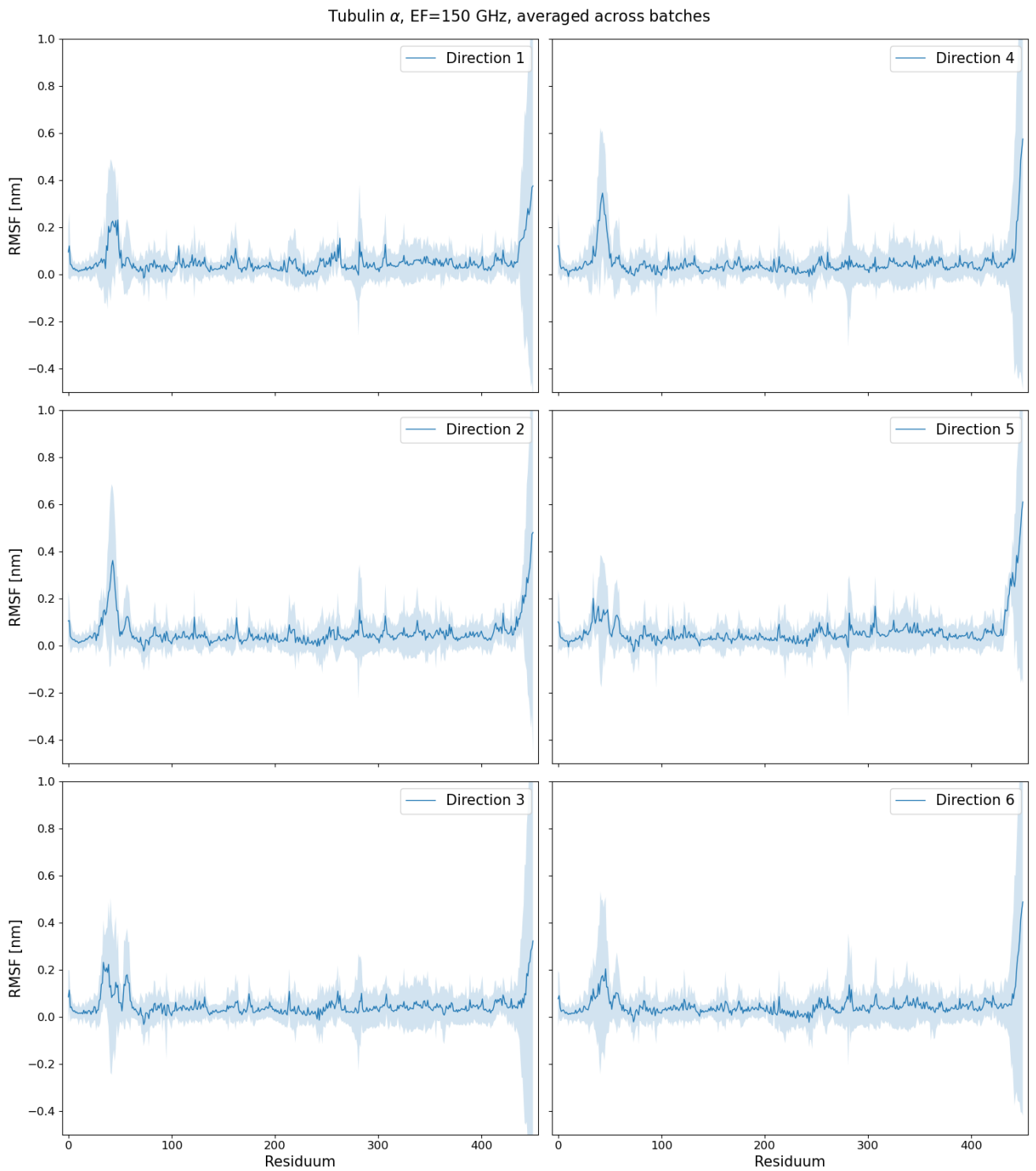


Figure 10.225: $\text{RMSF}_{\text{diff}}$ difference graphs of tubulin α with 150 GHz EF - averaged over batches

10.11.2 Tubulin β

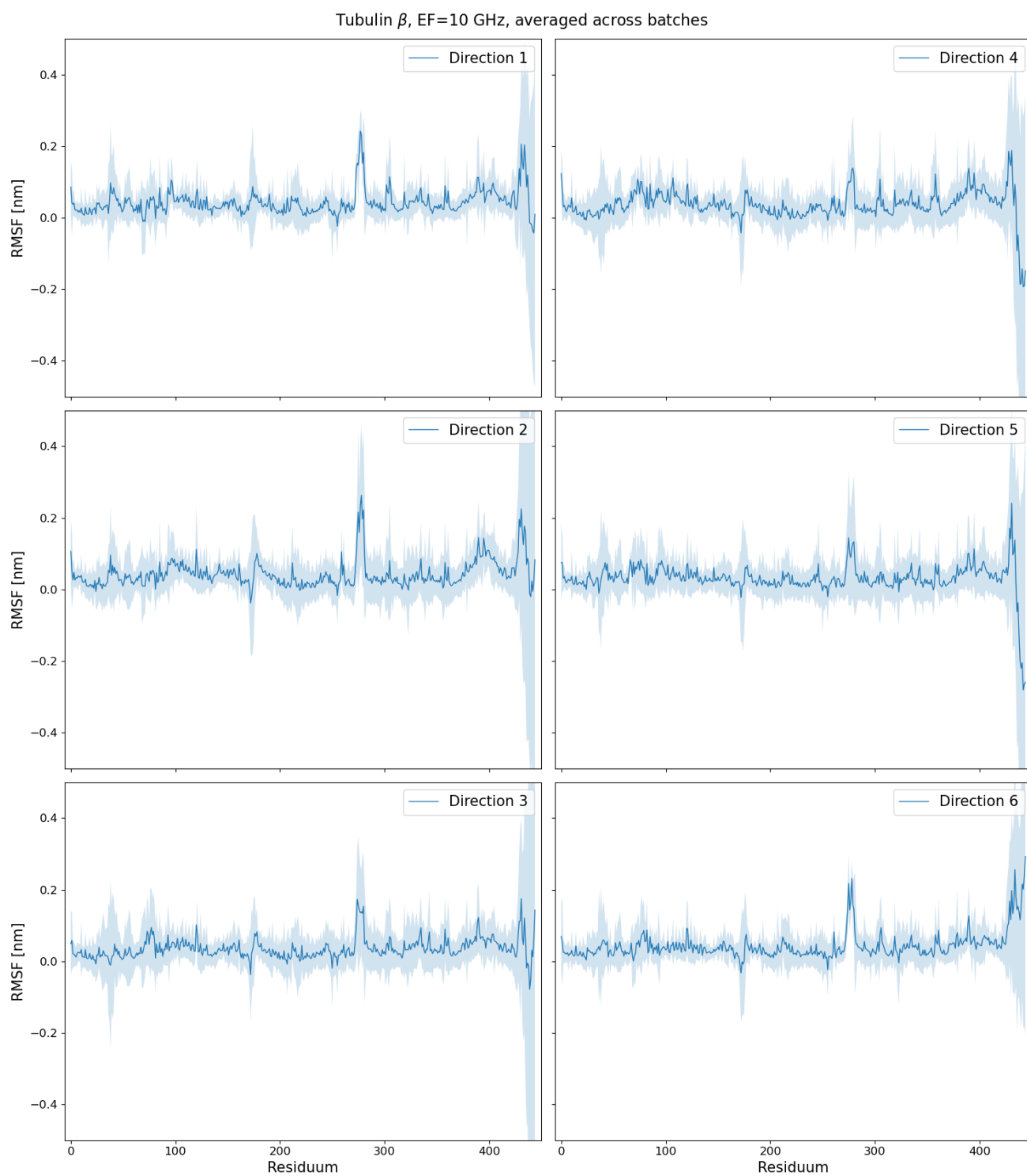


Figure 10.226: $\text{RMSF}_{\text{diff}}$ difference graphs of tubulin β with 10 GHz EF - averaged over batches

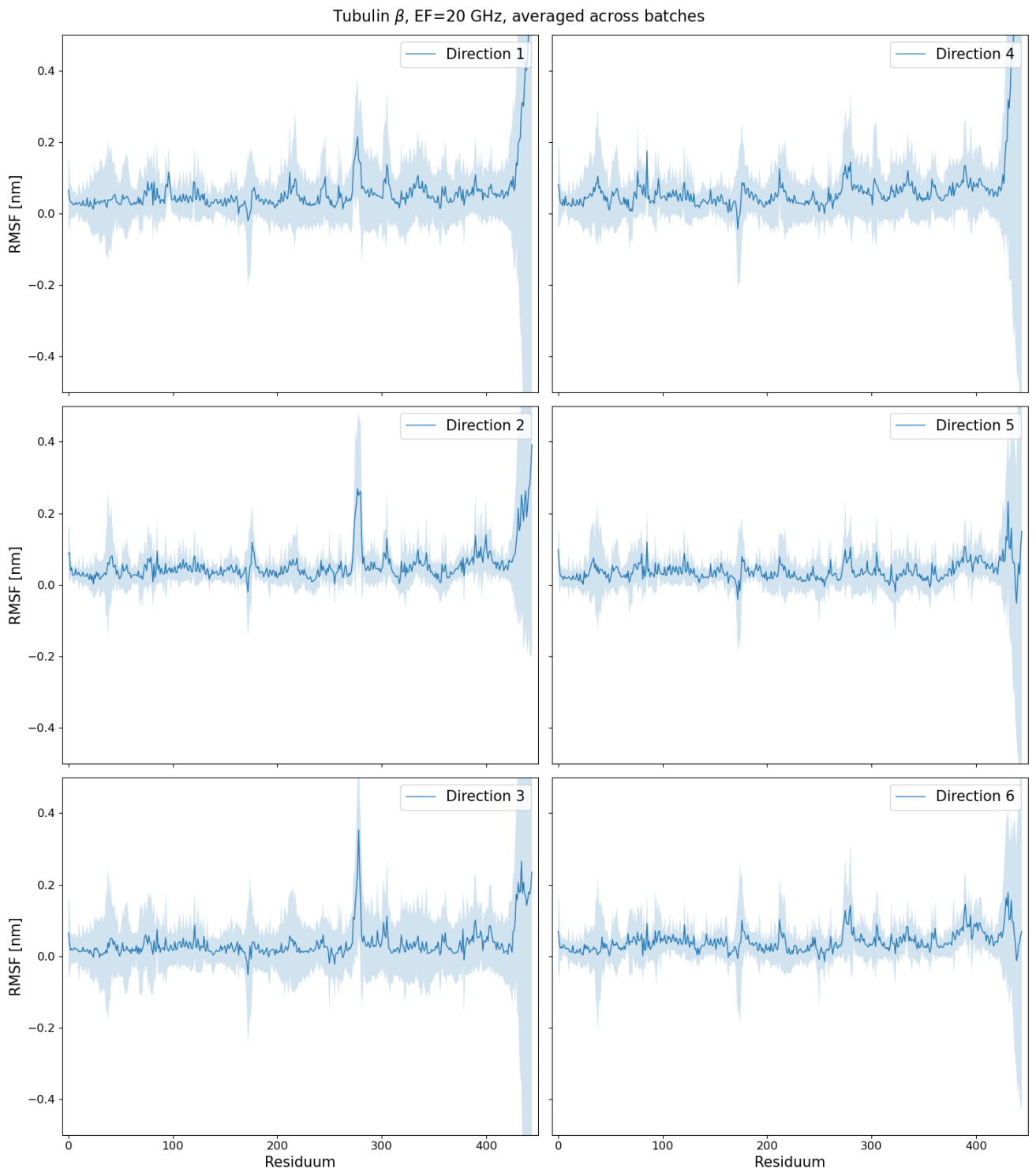


Figure 10.227: $\text{RMSF}_{\text{diff}}$ difference graphs of tubulin β with 20 GHz EF - averaged over batches

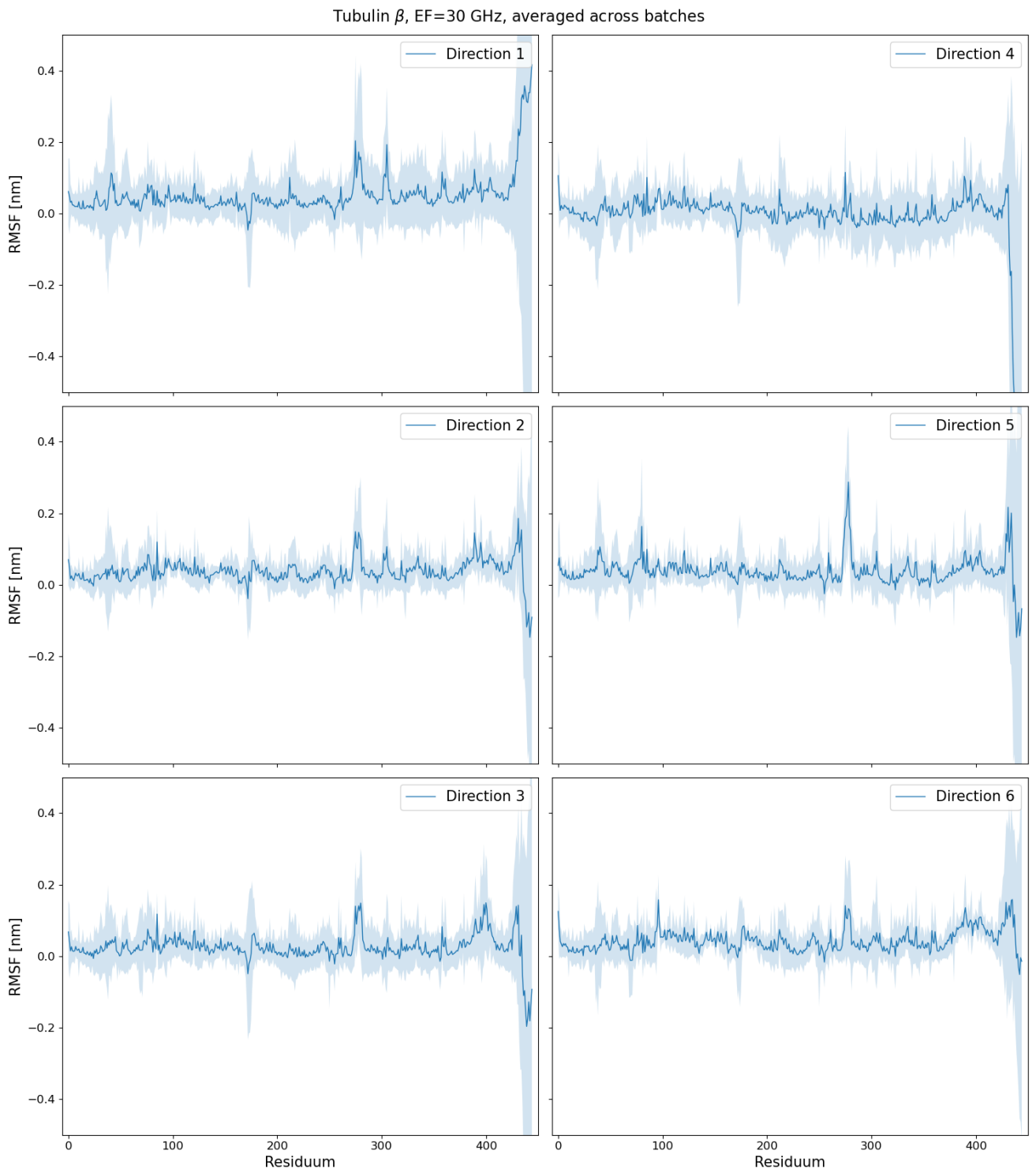


Figure 10.228: $\text{RMSF}_{\text{diff}}$ difference graphs of tubulin β with 30 GHz EF - averaged over batches

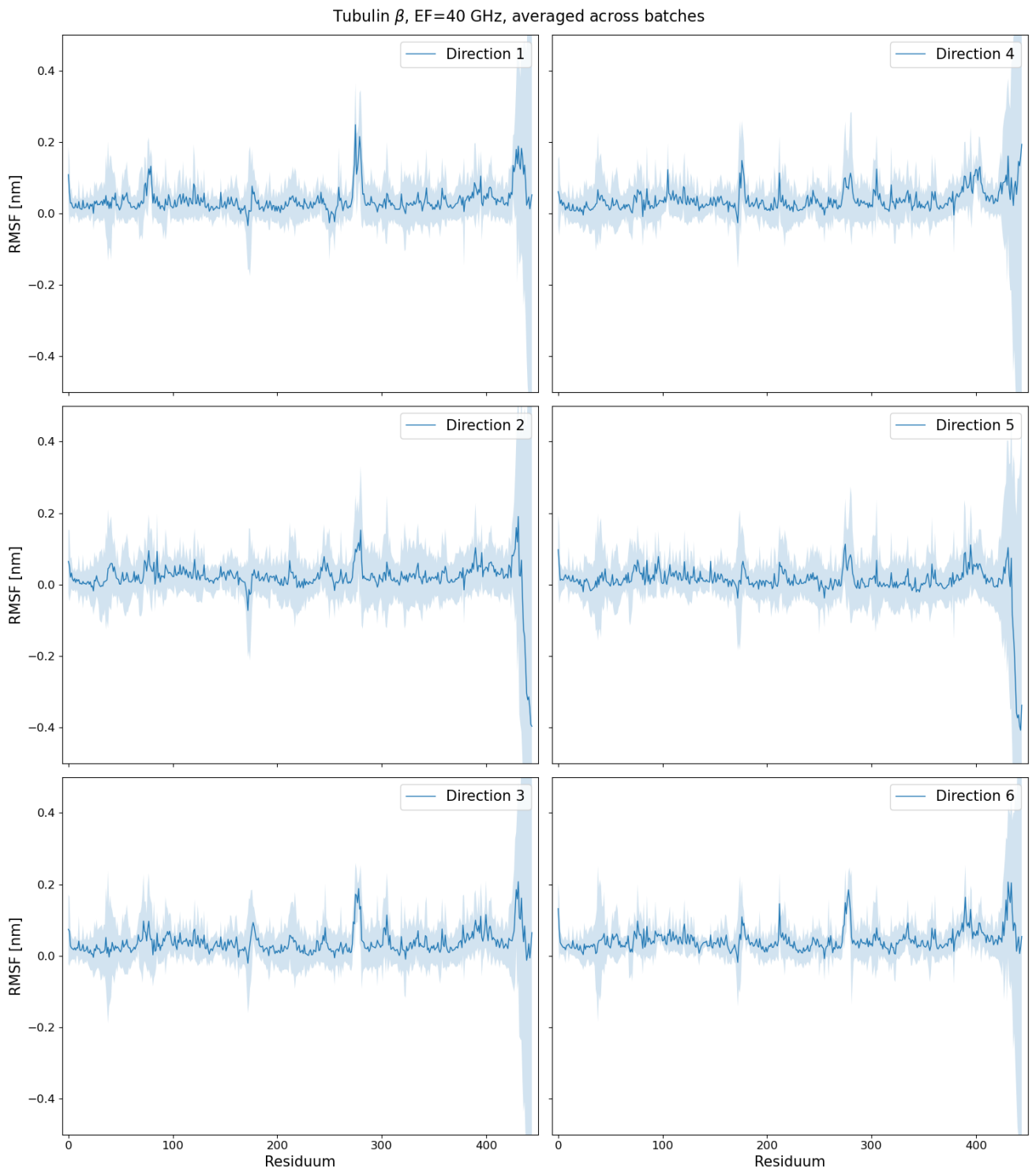


Figure 10.229: $\text{RMSF}_{\text{diff}}$ difference graphs of tubulin β with 40 GHz EF - averaged over batches

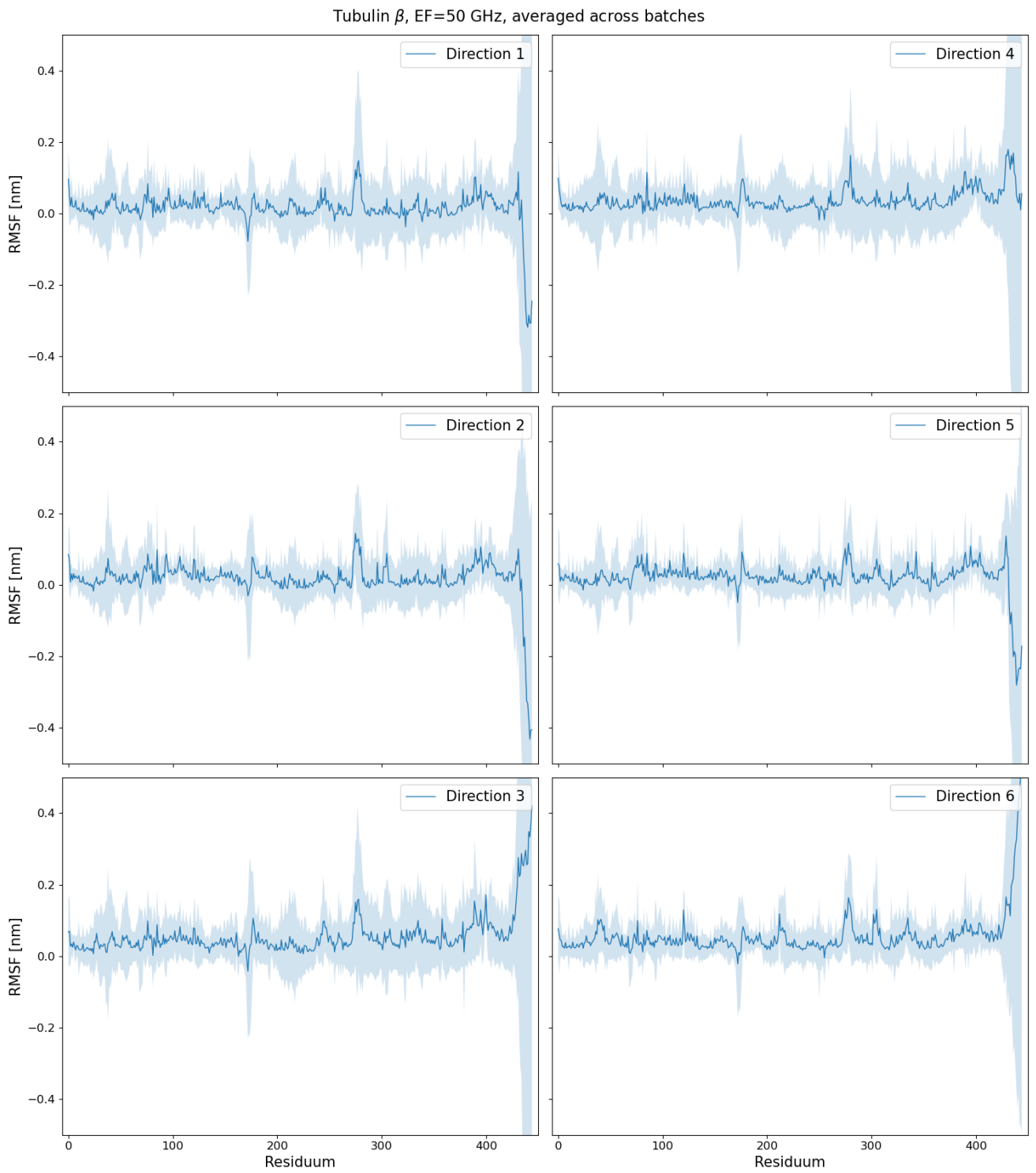


Figure 10.230: $\text{RMSF}_{\text{diff}}$ difference graphs of tubulin β with 50 GHz EF - averaged over batches

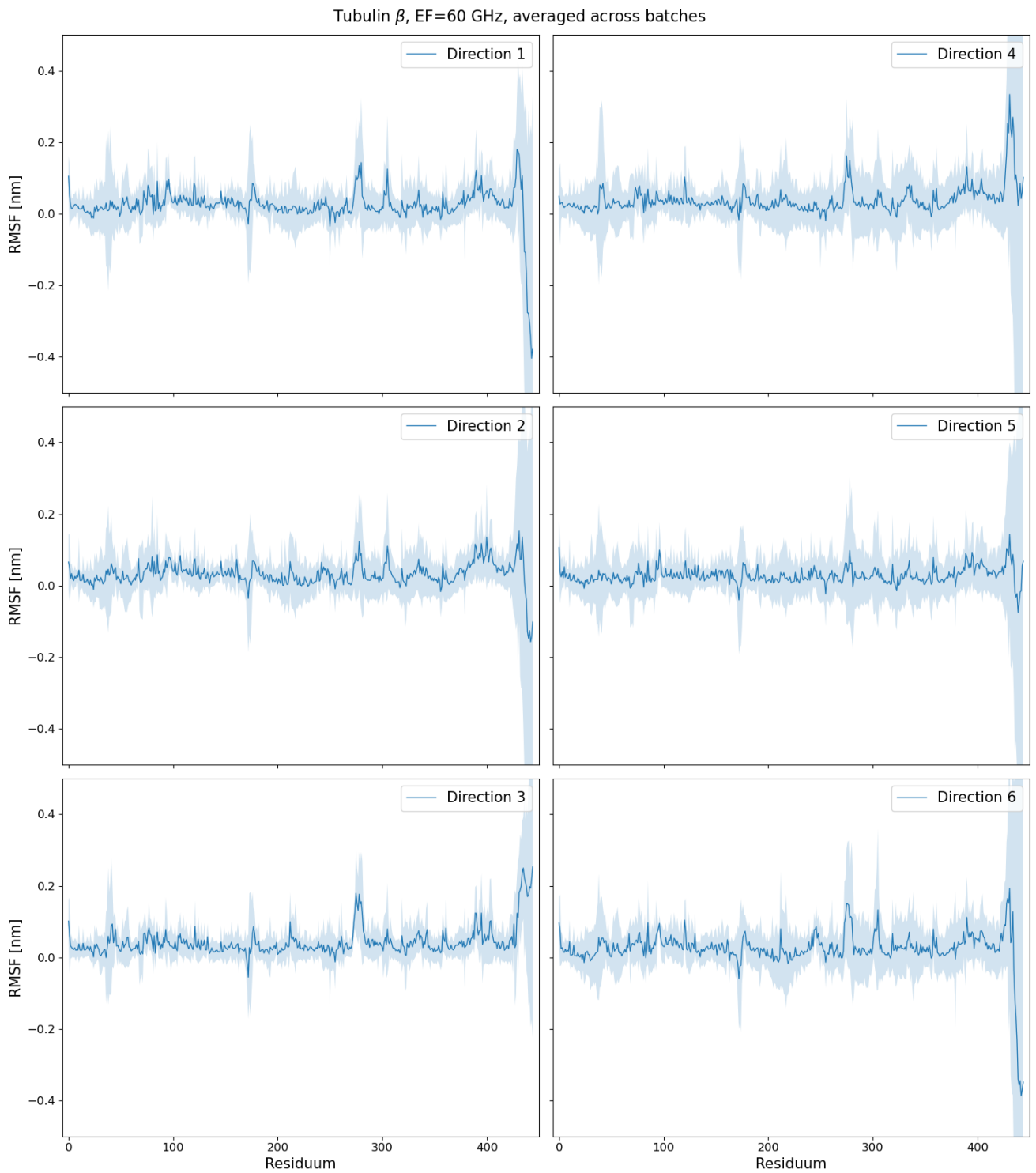


Figure 10.231: $\text{RMSF}_{\text{diff}}$ difference graphs of tubulin β with 60 GHz EF - averaged over batches

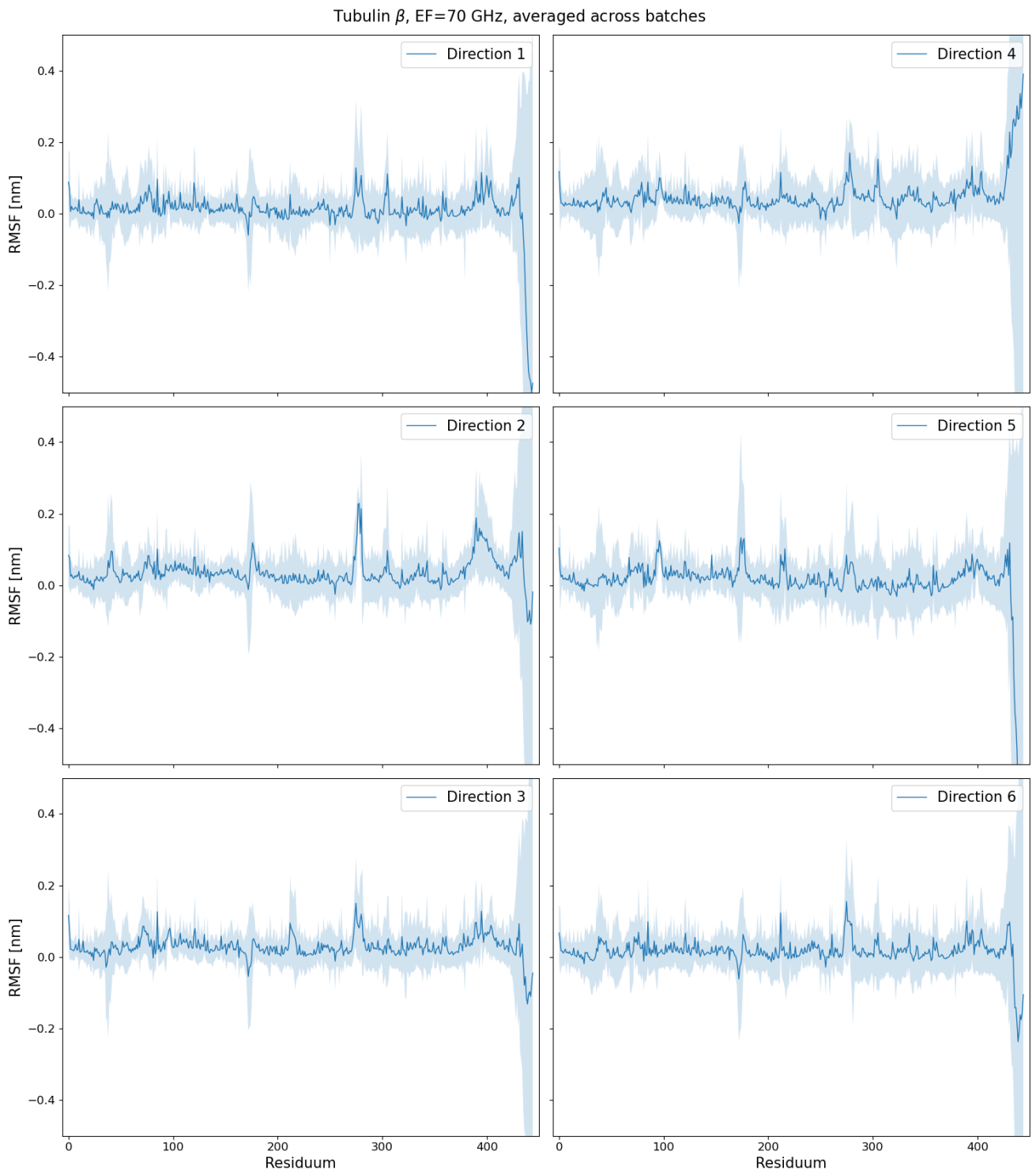


Figure 10.232: $\text{RMSF}_{\text{diff}}$ difference graphs of tubulin β with 70 GHz EF - averaged over batches

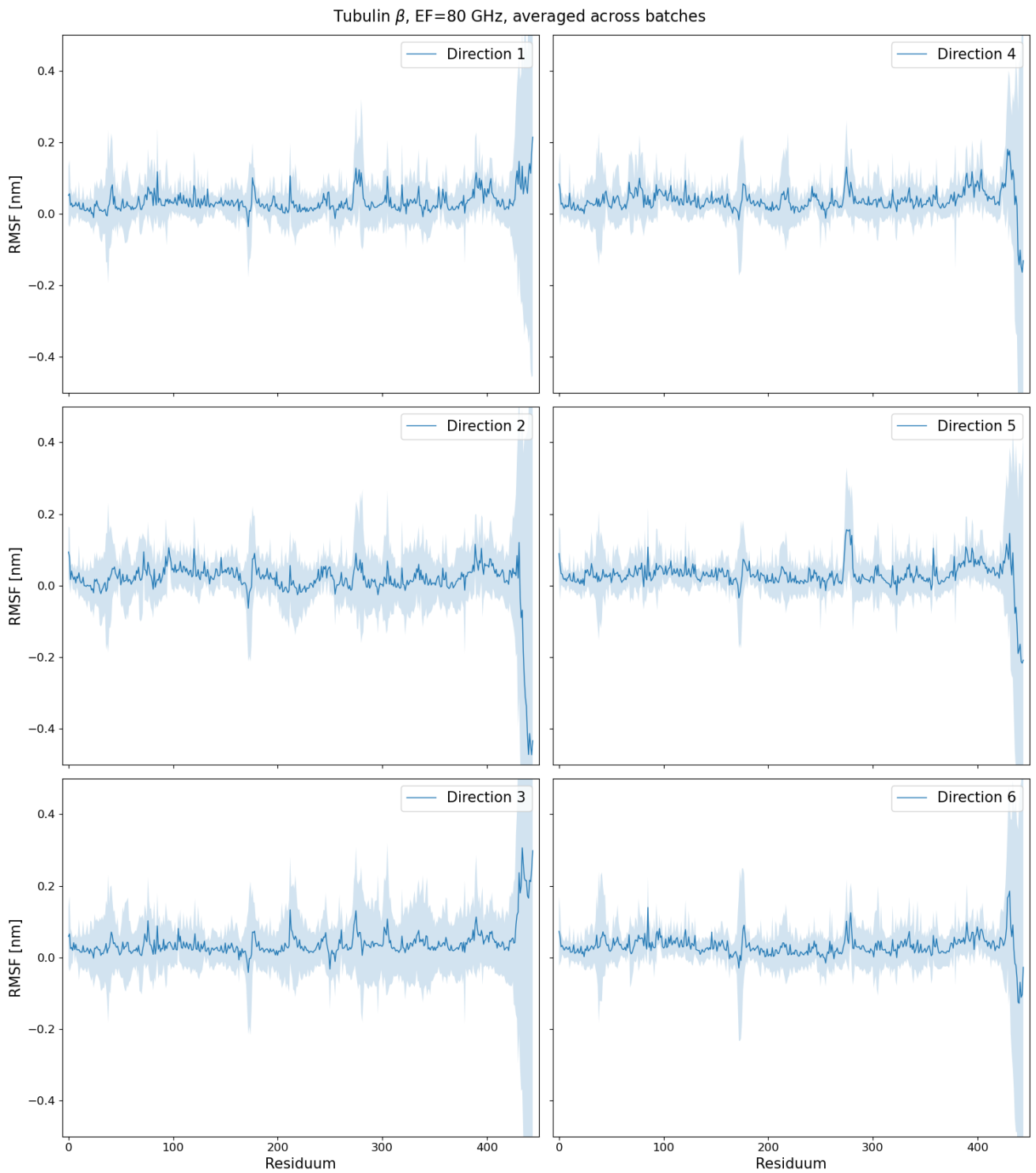


Figure 10.233: $\text{RMSF}_{\text{diff}}$ difference graphs of tubulin β with 80 GHz EF - averaged over batches

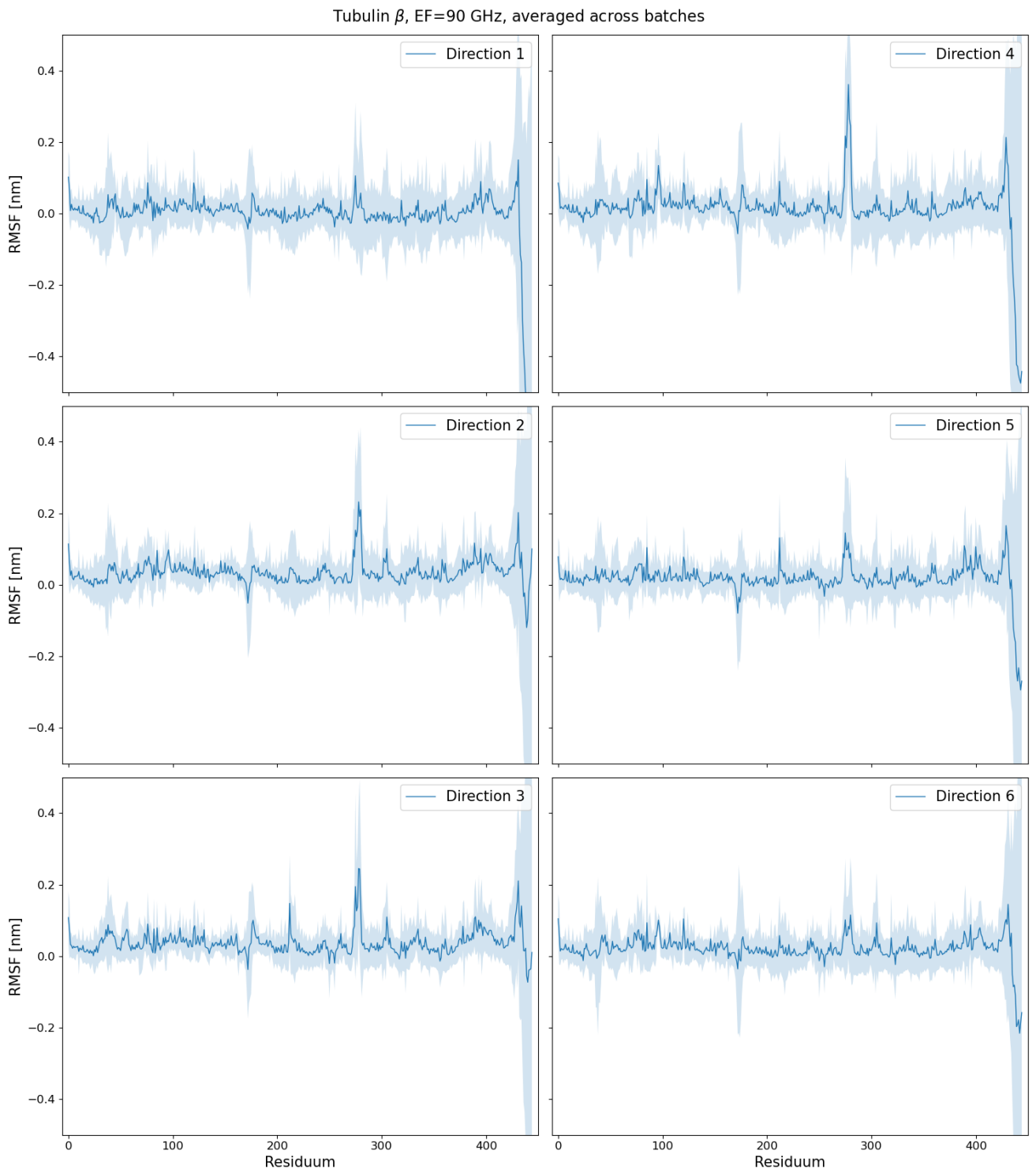


Figure 10.234: $\text{RMSF}_{\text{diff}}$ difference graphs of tubulin β with 90 GHz EF - averaged over batches

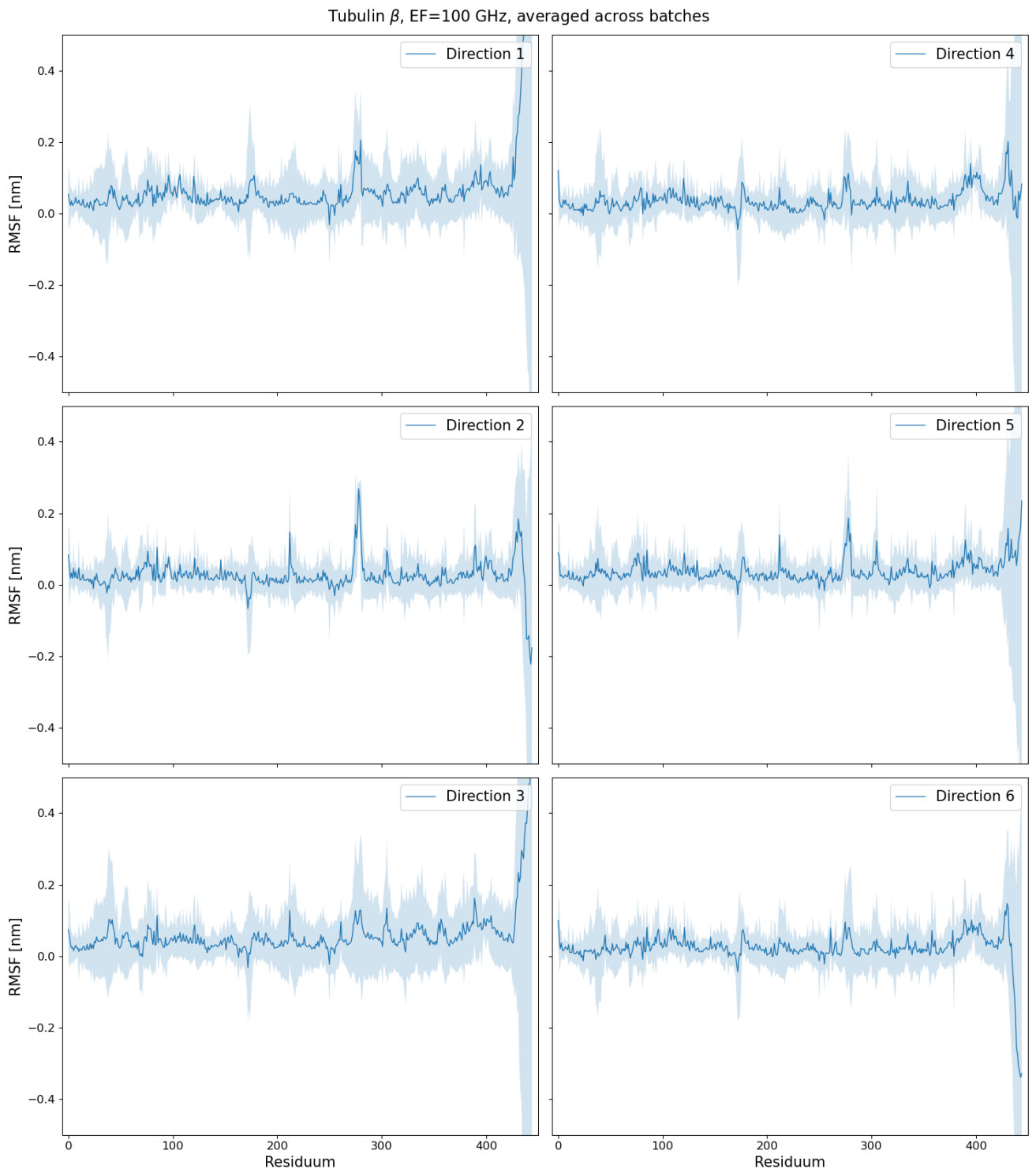


Figure 10.235: $\text{RMSF}_{\text{diff}}$ difference graphs of tubulin β with 100 GHz EF - averaged over batches

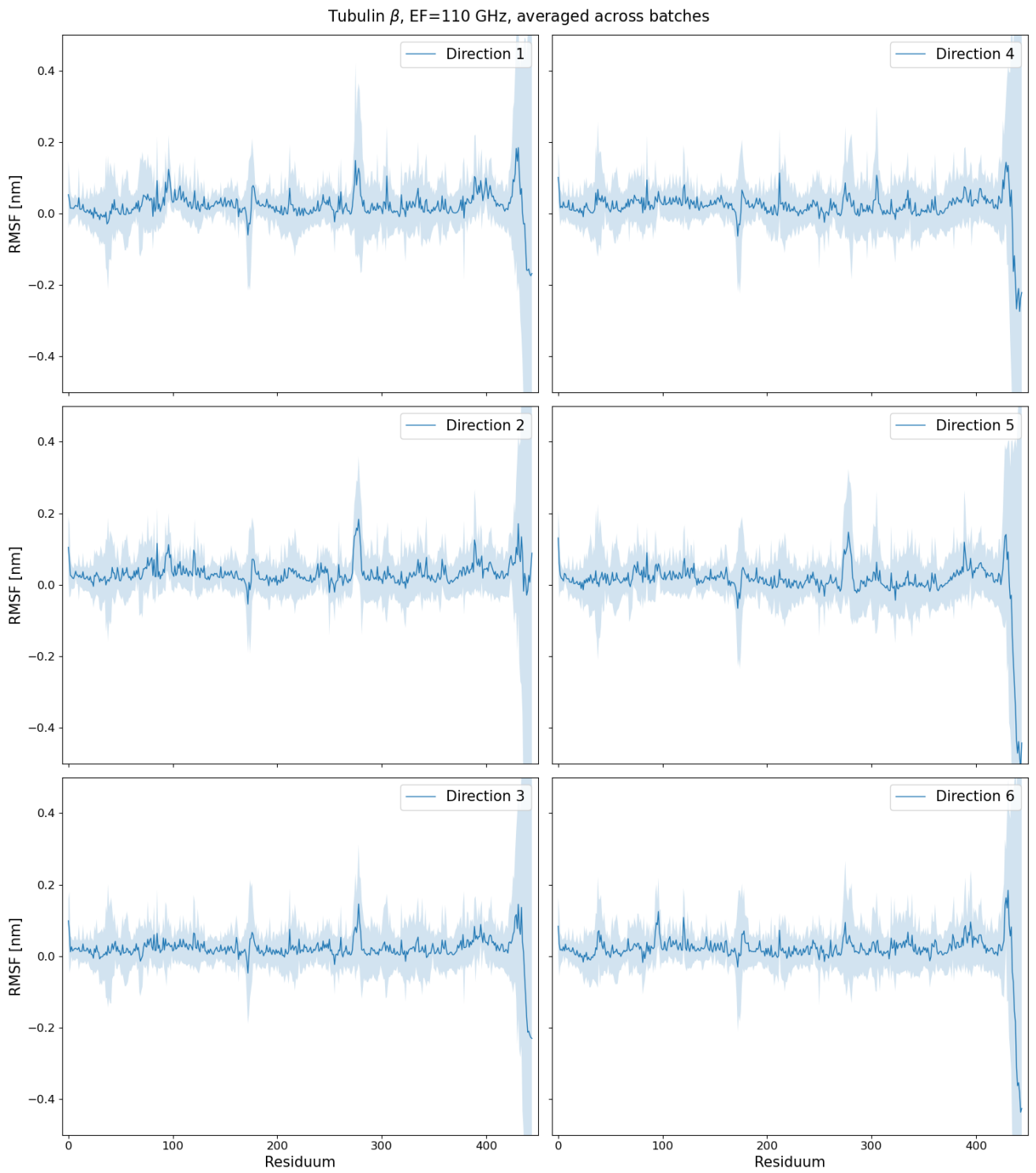


Figure 10.236: $\text{RMSF}_{\text{diff}}$ difference graphs of tubulin β with 110 GHz EF - averaged over batches

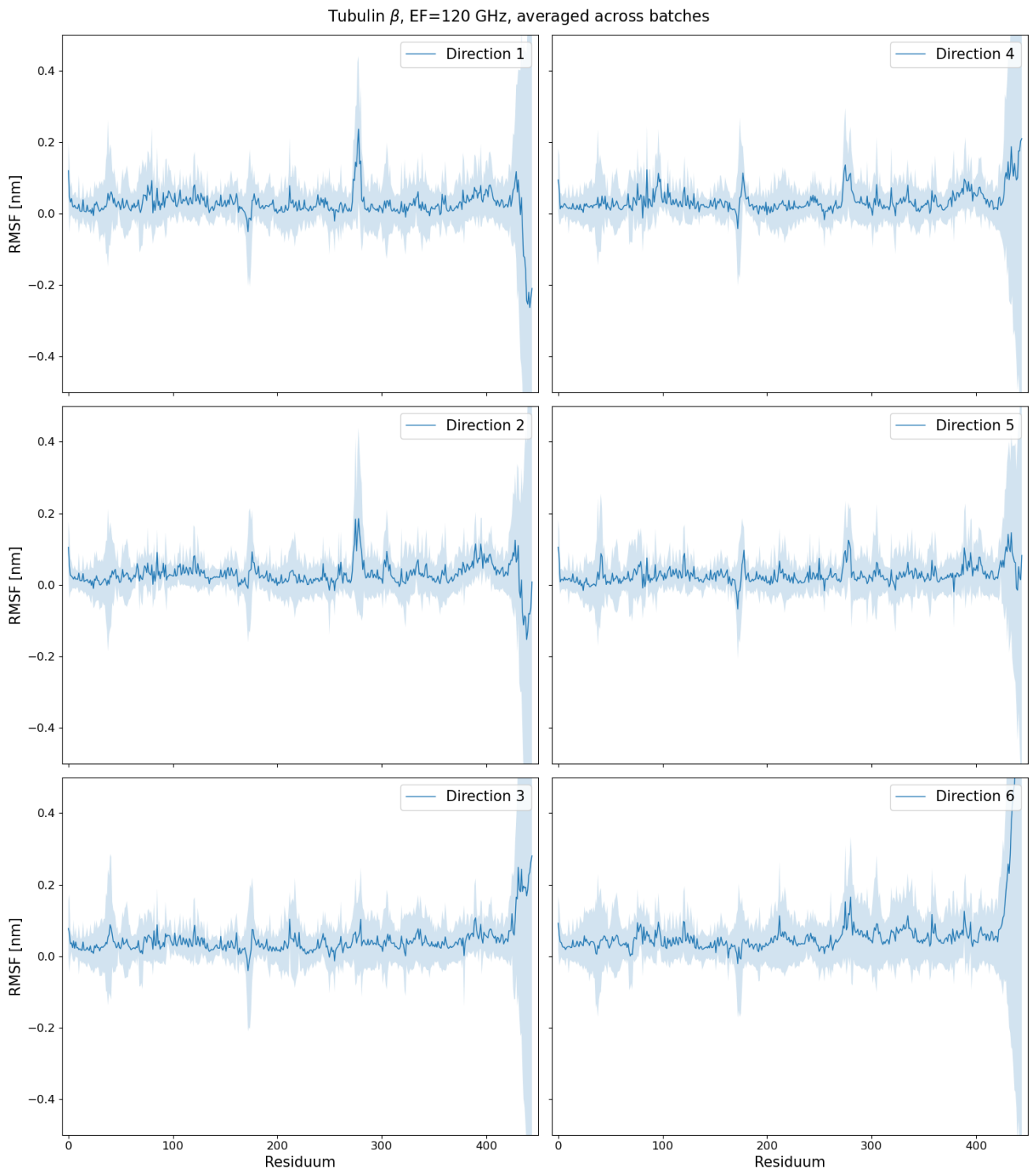


Figure 10.237: RMSF_{diff} difference graphs of tubulin β with 120 GHz EF - averaged over batches

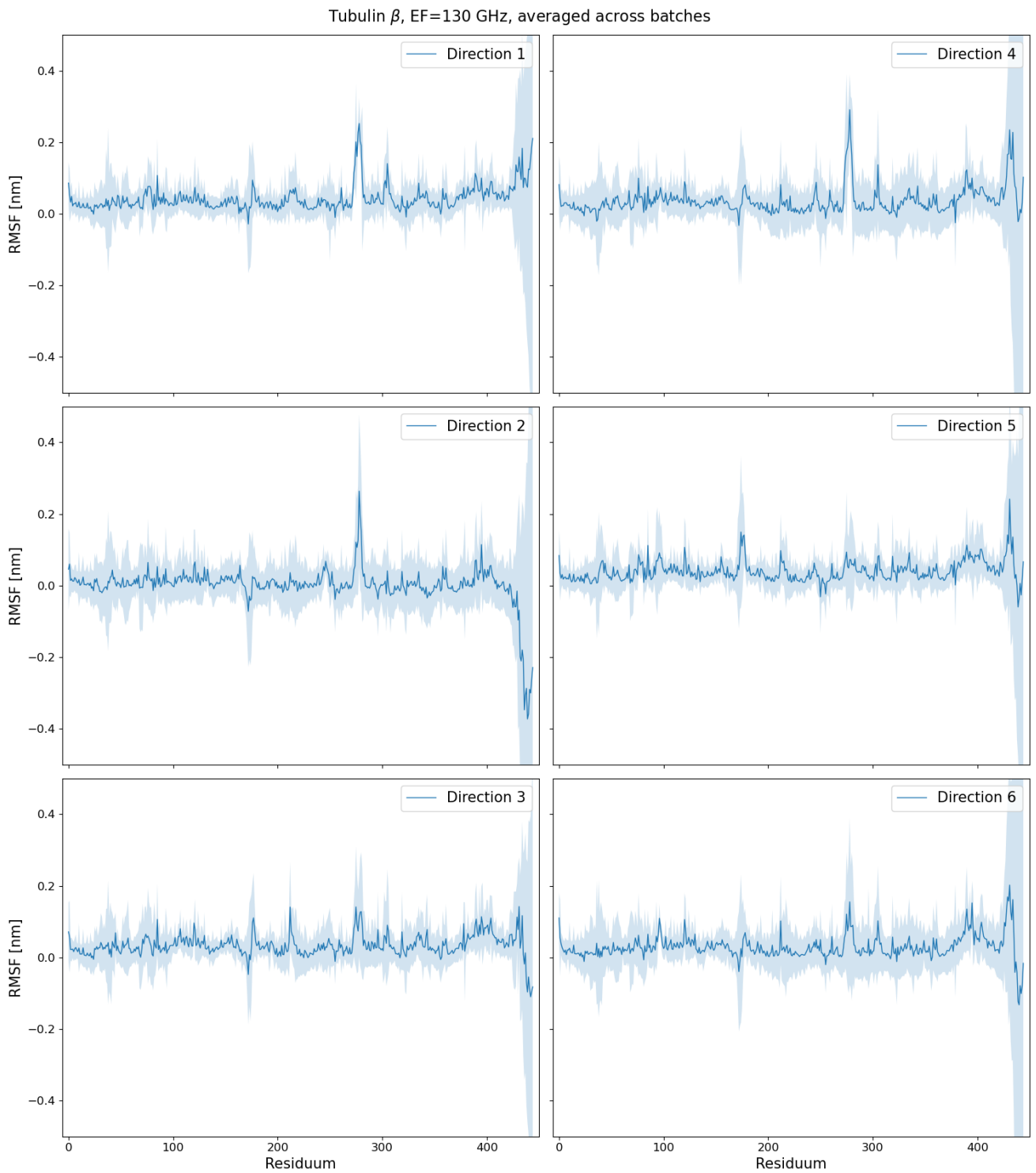


Figure 10.238: $\text{RMSF}_{\text{diff}}$ difference graphs of tubulin β with 130 GHz EF - averaged over batches

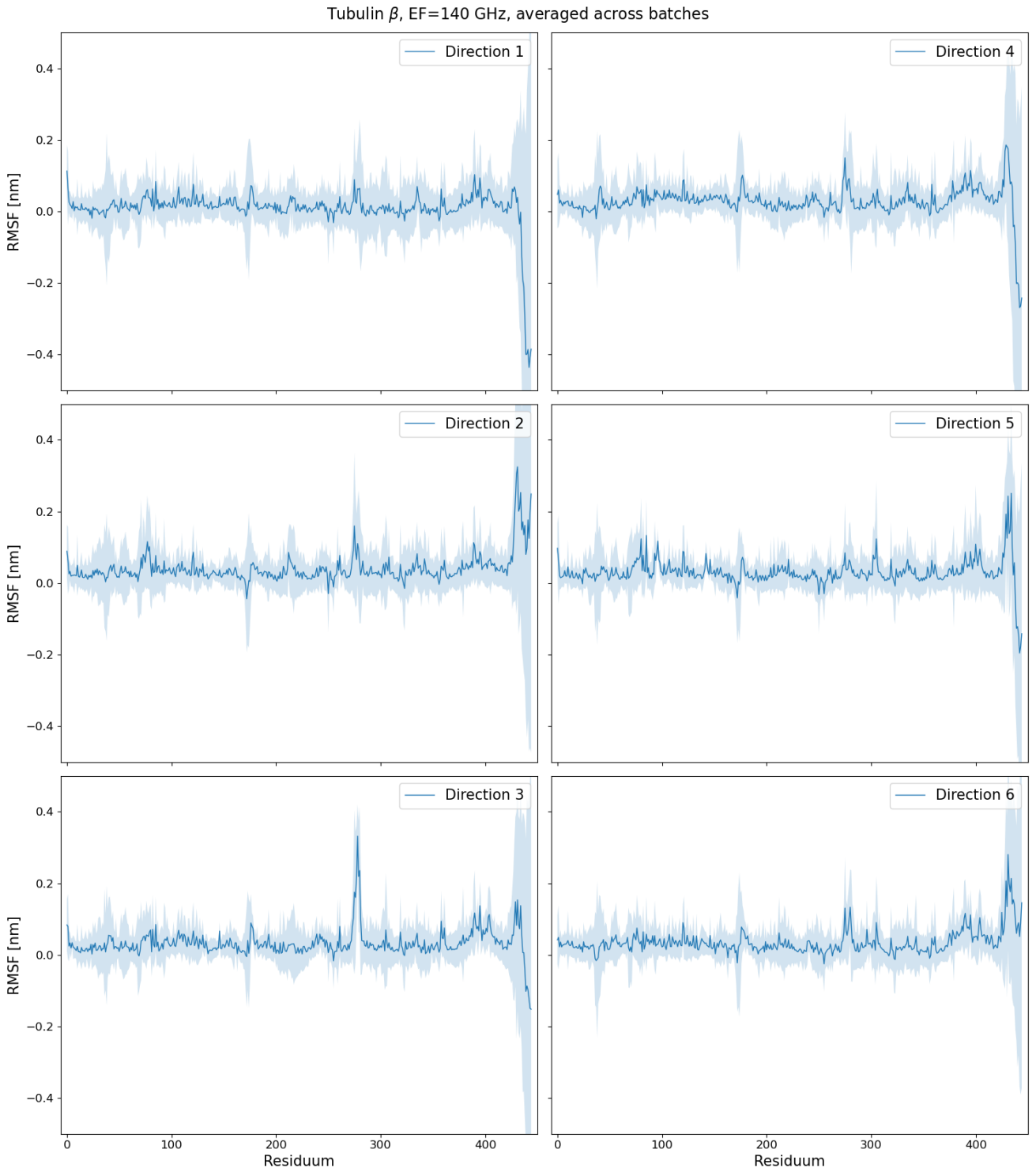


Figure 10.239: RMSF_{diff} difference graphs of tubulin β with 140 GHz EF - averaged over batches

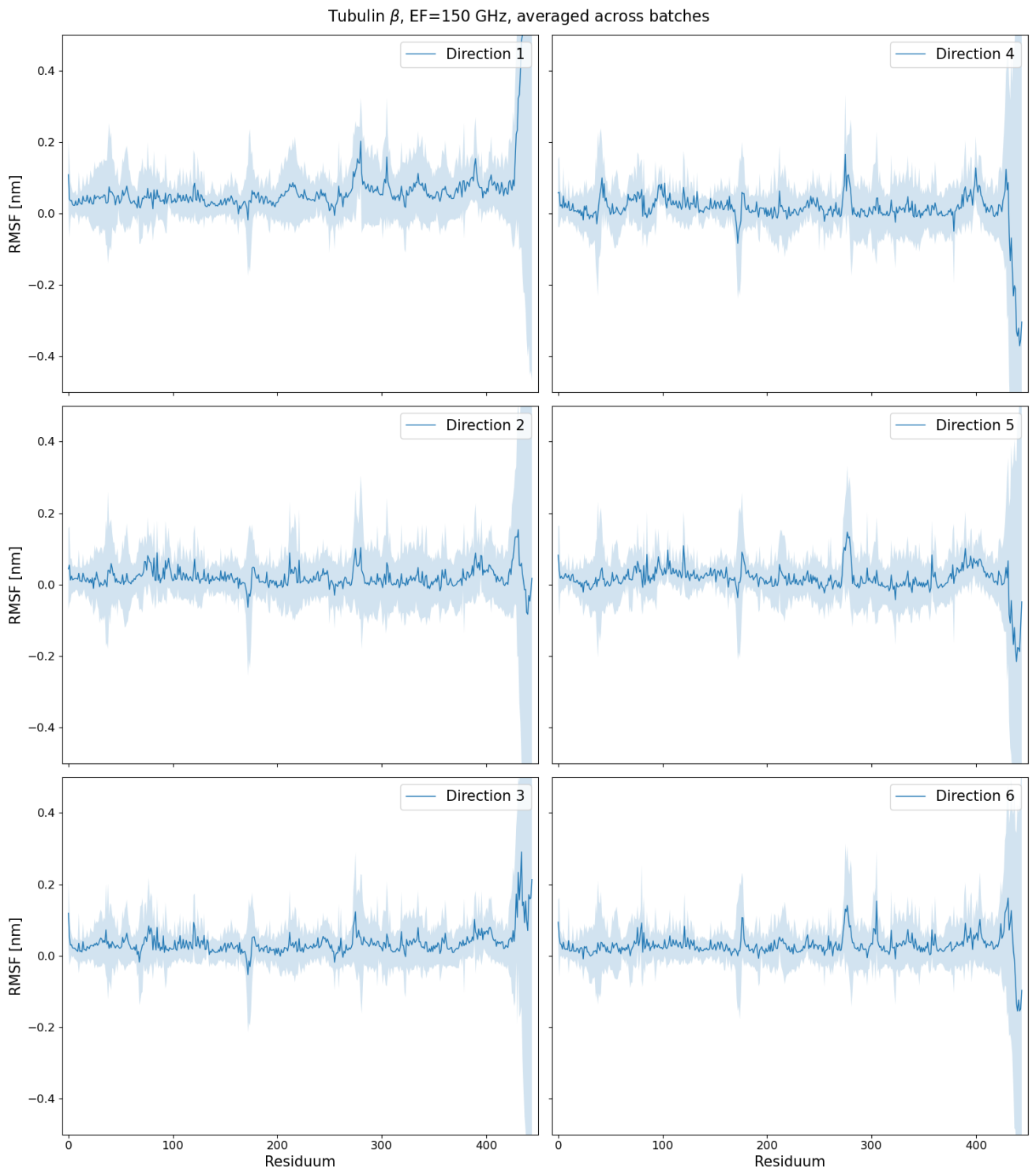


Figure 10.240: RMSF_{diff} difference graphs of tubulin β with 150 GHz EF - averaged over batches

10.12 RMSF - Binding sites of vinca alkaloids

Here we present the rest of the graphs depicting RMSF of residues that mediates the interaction between vinca alkaloids and tubulin. To go back to results, click: [8.5](#).

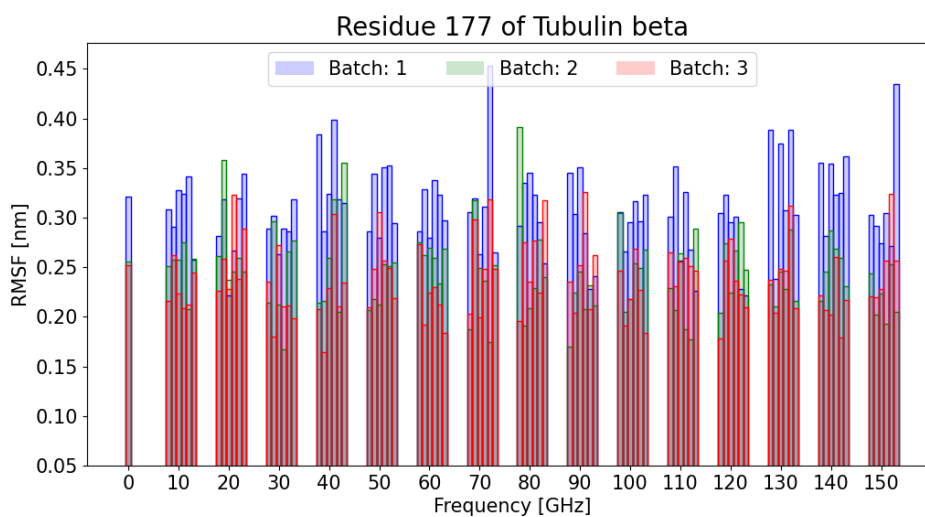


Figure 10.241: RMSF of residue 177 of tubulin beta - different directions and batches; the bars for 0 GHz mean that no EF is applied

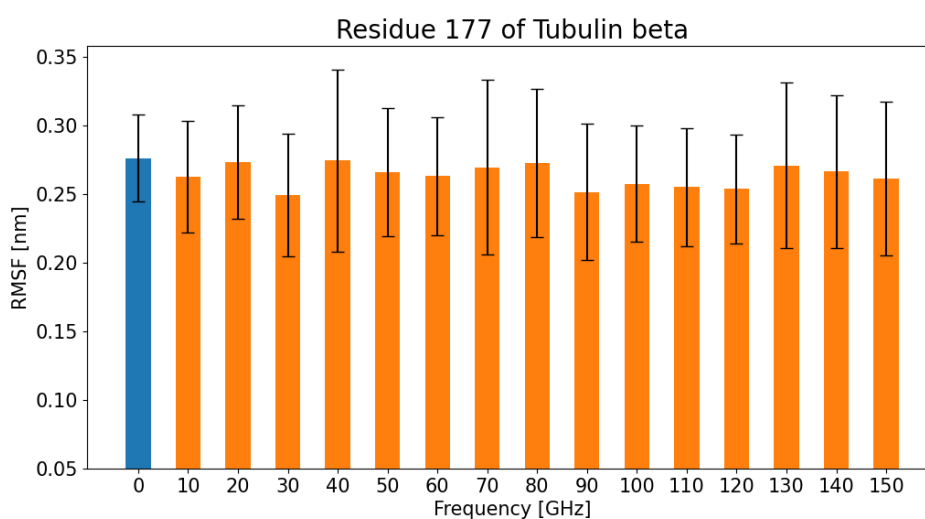


Figure 10.242: RMSF of residue 177 of tubulin beta - averaged over directions and batches; the bars for 0 GHz mean that no EF is applied

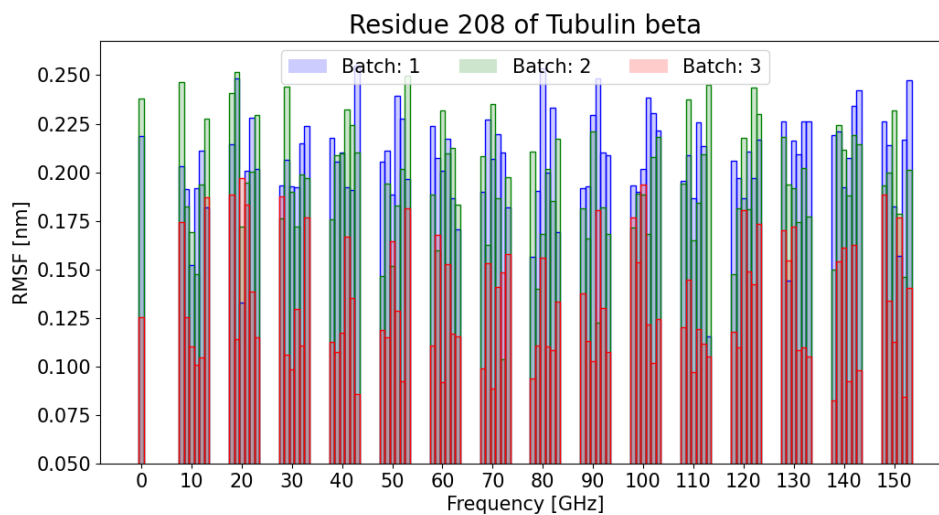


Figure 10.243: RMSF of residue 208 of tubulin beta - different directions and batches; the bars for 0 GHz mean that no EF is applied

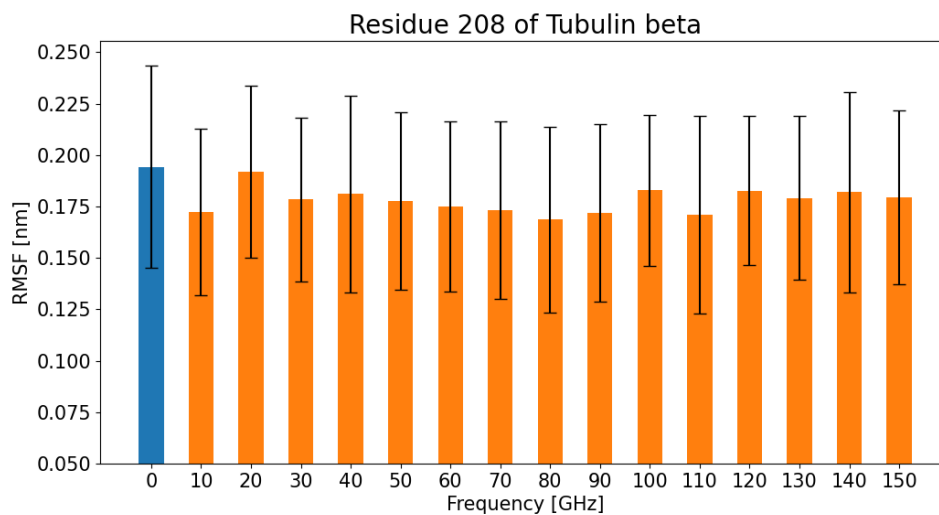


Figure 10.244: RMSF of residue 208 of tubulin beta - averaged over directions and batches; the bars for 0 GHz mean that no EF is applied

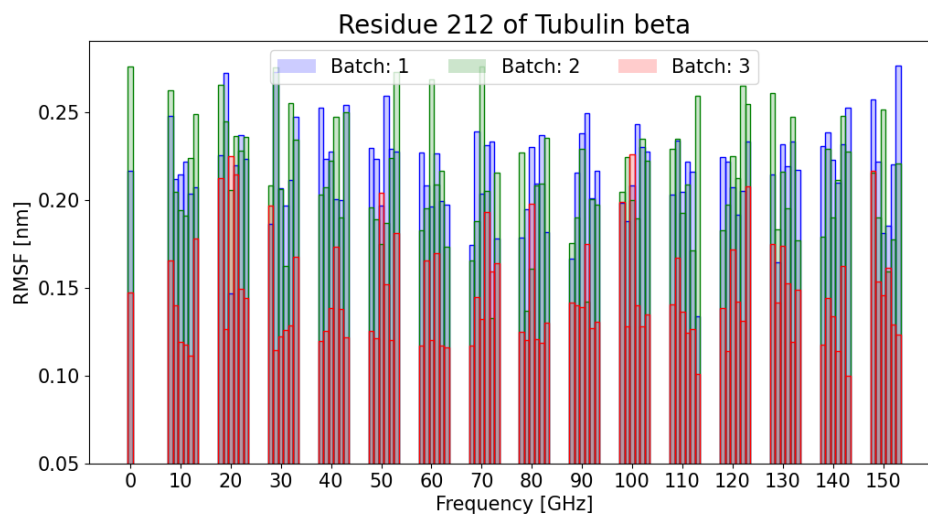


Figure 10.245: RMSF of residue 212 of tubulin beta - different directions and batches; the bars for 0 GHz mean that no EF is applied

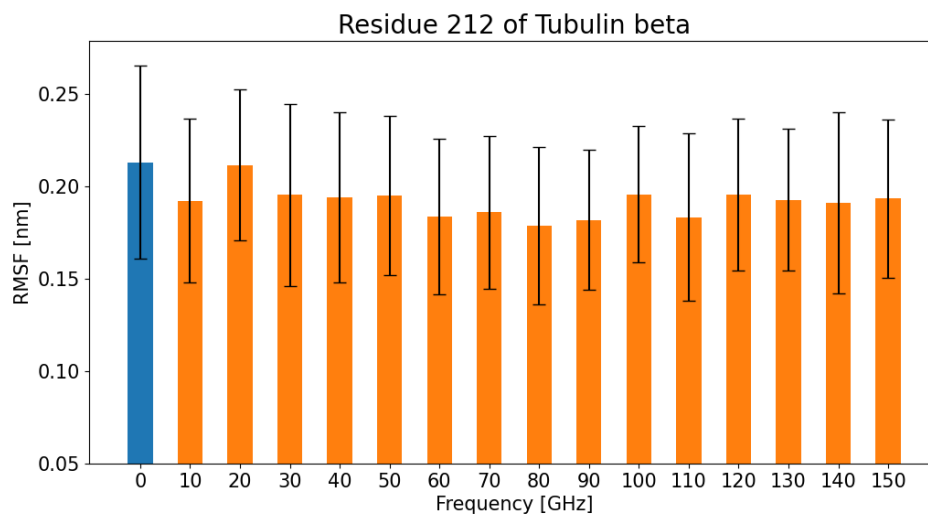


Figure 10.246: RMSF of residue 212 of tubulin beta - averaged over directions and batches; the bars for 0 GHz mean that no EF is applied

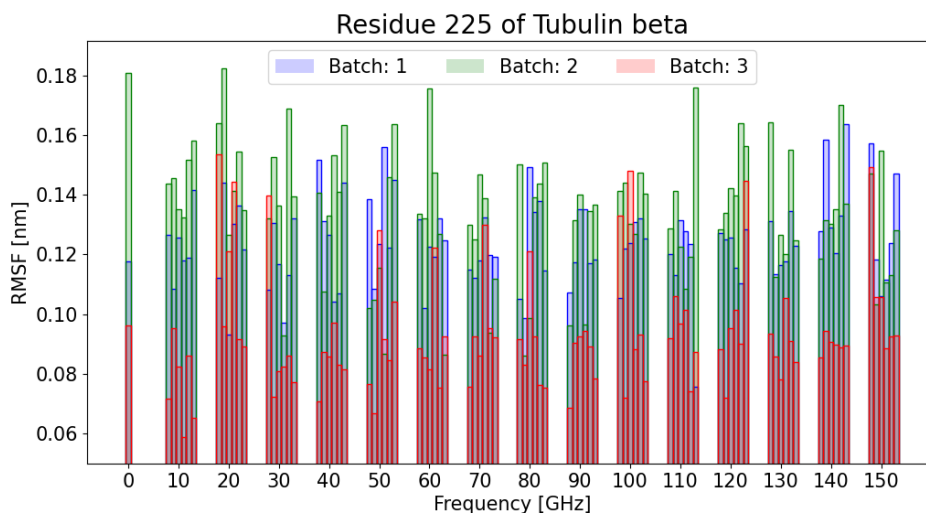


Figure 10.247: RMSF of residue 225 of tubulin beta - different directions and batches; the bars for 0 GHz mean that no EF is applied

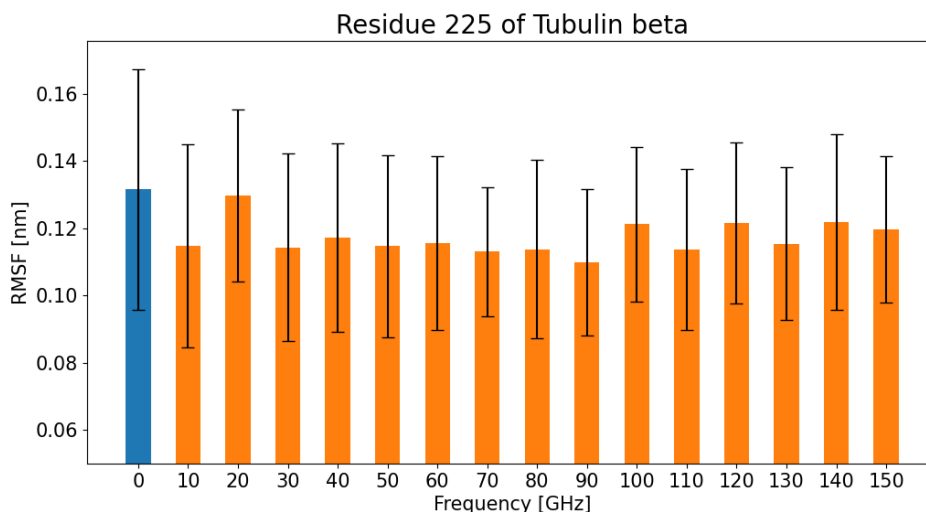


Figure 10.248: RMSF of residue 225 of tubulin beta - averaged over directions and batches; the bars for 0 GHz mean that no EF is applied

10.13 RMSF - Binding sites of colchicine

Here we present the rest of the graphs depicting RMSF of residues that mediates the interaction between colchicine and tubulin. To go back to results, click: [8.5.1](#)

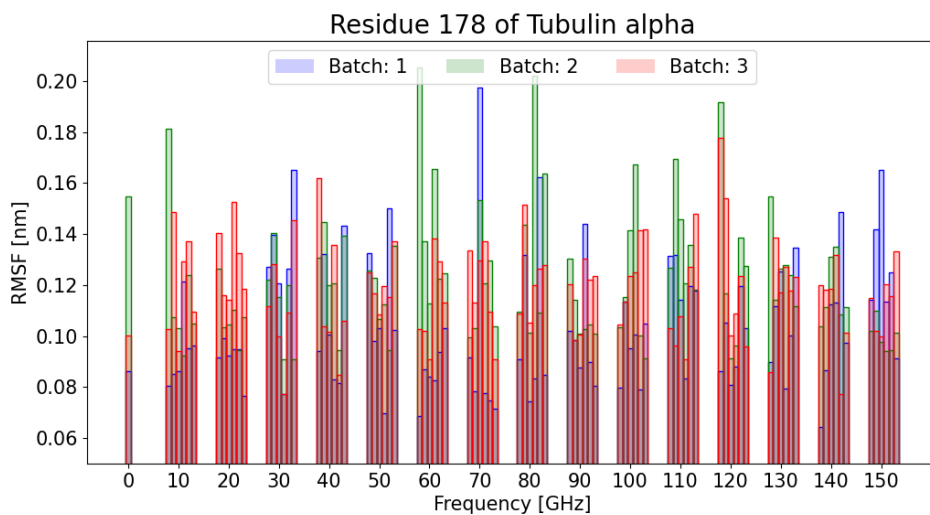


Figure 10.249: RMSF of residue 178 of tubulin alpha - different directions and batches; the bars for 0 GHz mean that no EF is applied

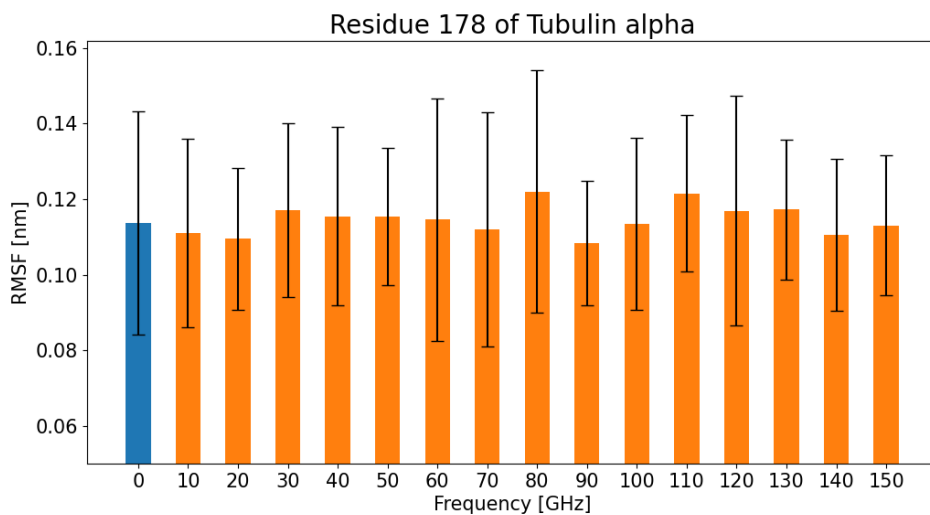


Figure 10.250: RMSF of residue 178 of tubulin alpha - averaged over directions and batches; the bars for 0 GHz mean that no EF is applied

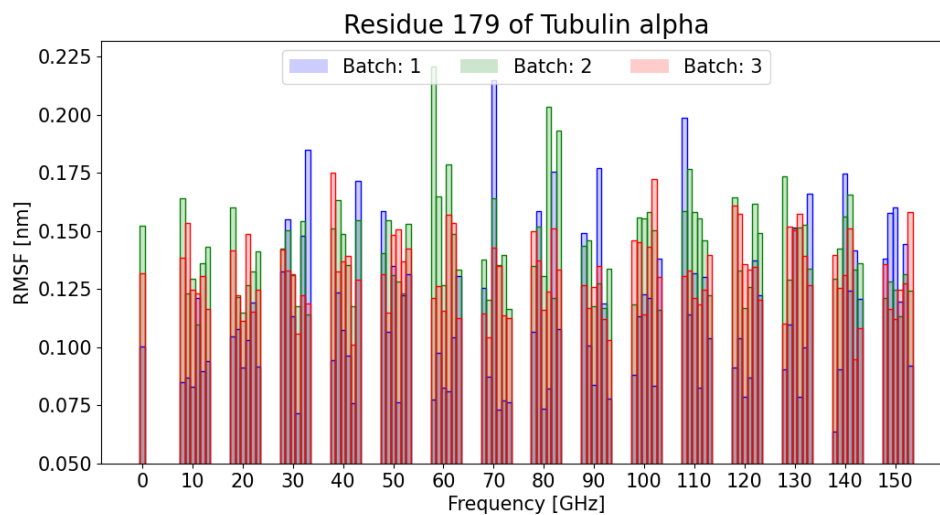


Figure 10.251: RMSF of residue 179 of tubulin alpha - different directions and batches; the bars for 0 GHz mean that no EF is applied

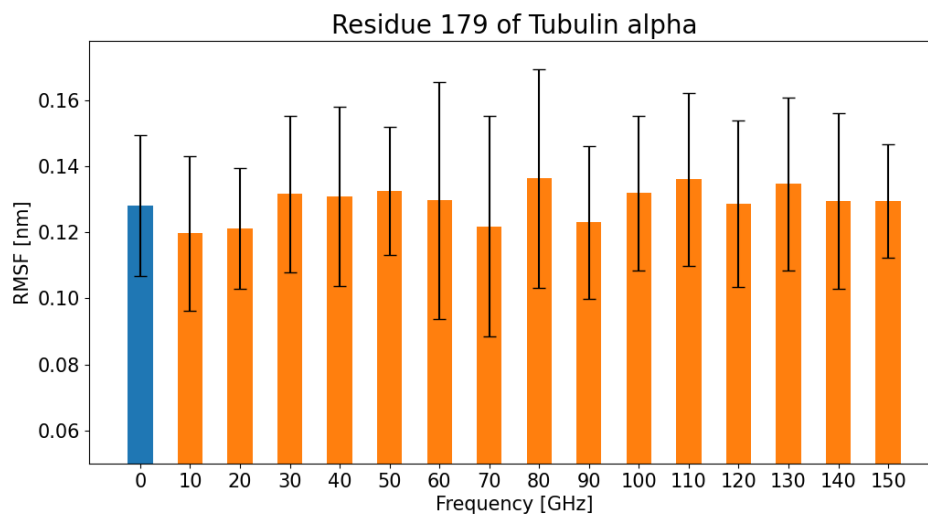


Figure 10.252: RMSF of residue 179 of tubulin alpha - averaged over directions and batches; the bars for 0 GHz mean that no EF is applied

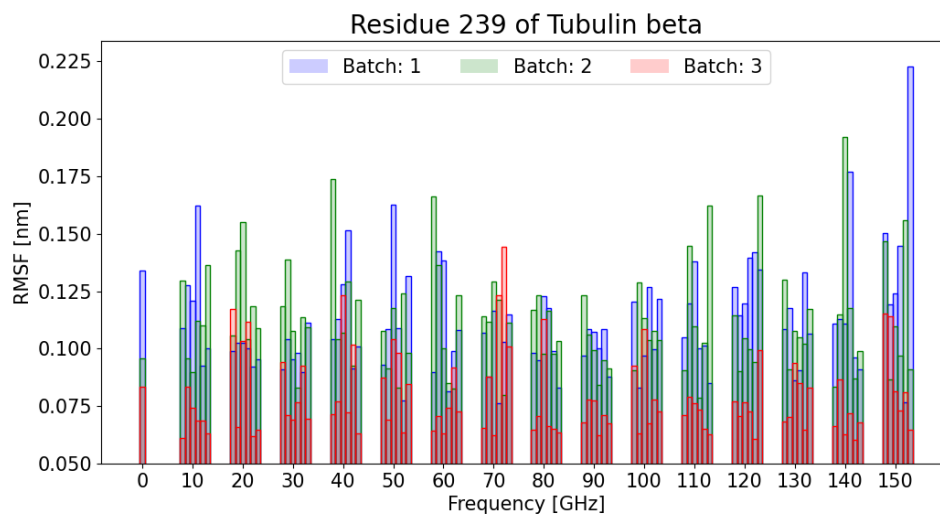


Figure 10.253: RMSF of residue 239 of tubulin beta - different directions and batches; the bars for 0 GHz mean that no EF is applied

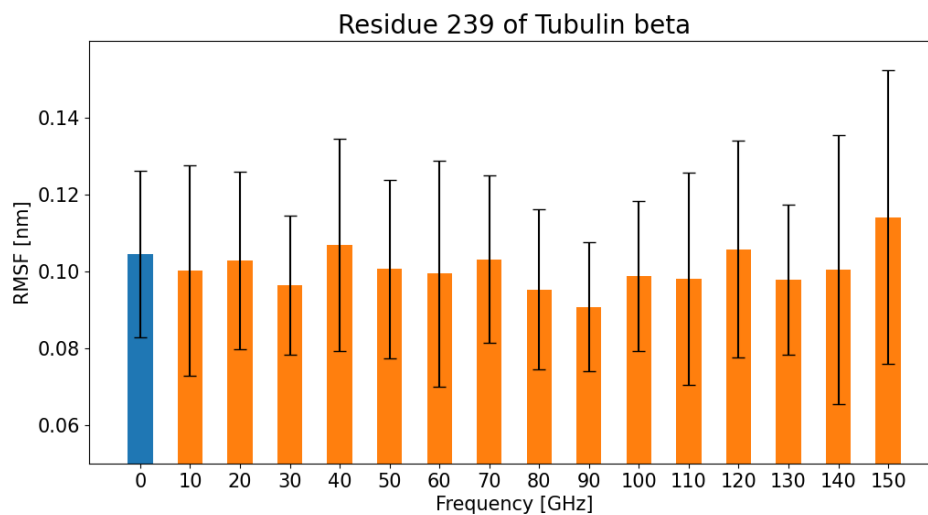


Figure 10.254: RMSF of residue 239 of tubulin beta - averaged over directions and batches; the bars for 0 GHz mean that no EF is applied

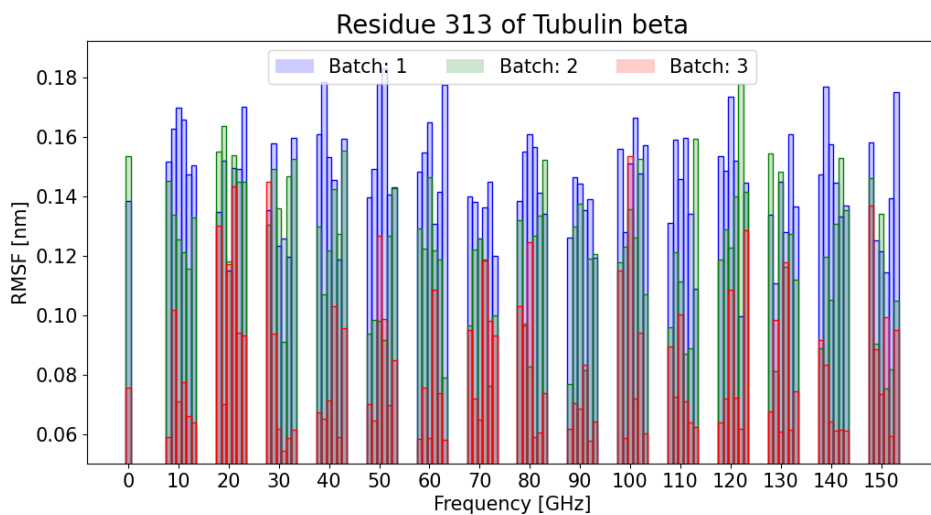


Figure 10.255: RMSF of residue 313 of tubulin beta - different directions and batches; the bars for 0 GHz mean that no EF is applied

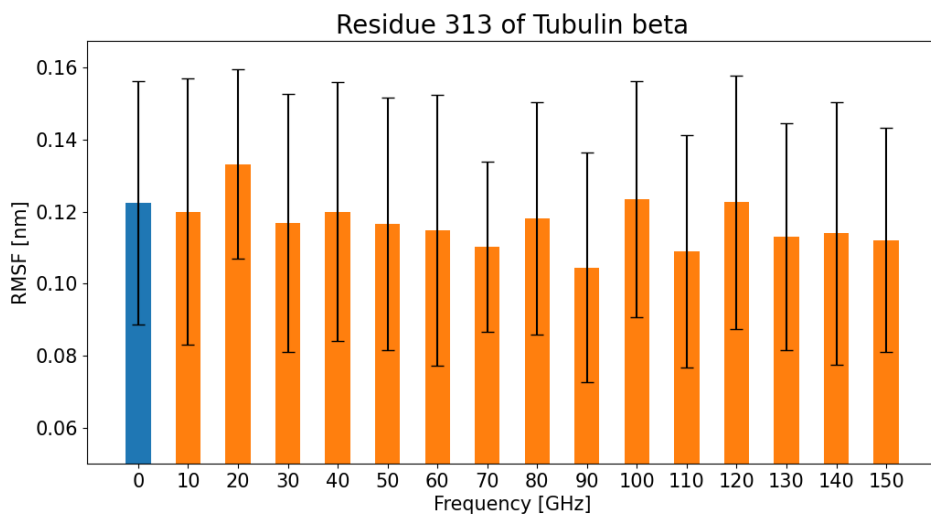


Figure 10.256: RMSF of residue 313 of tubulin beta - averaged over directions and batches; the bars for 0 GHz mean that no EF is applied

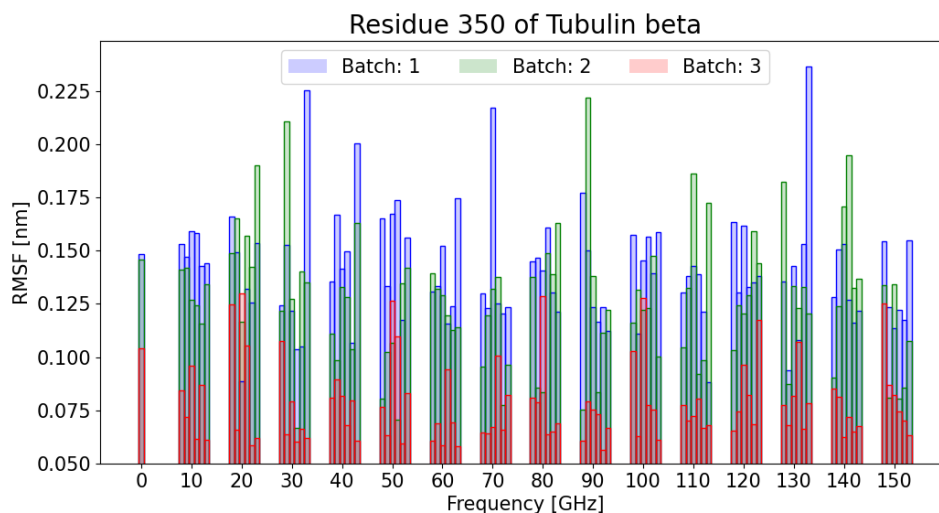


Figure 10.257: RMSF of residue 350 of tubulin beta - different directions and batches; the bars for 0 GHz mean that no EF is applied

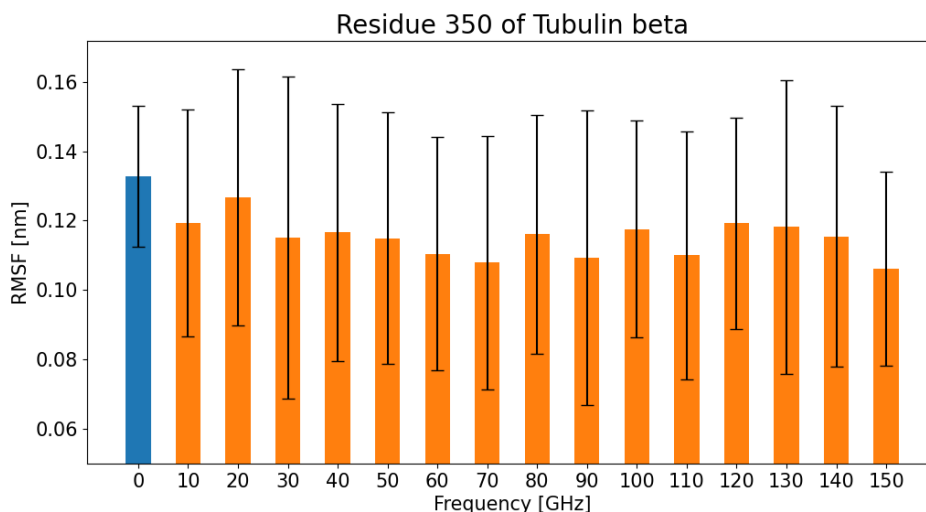


Figure 10.258: RMSF of residue 350 of tubulin beta - averaged over directions and batches; the bars for 0 GHz mean that no EF is applied

10.14 RMSF - Binding sites of paclitaxel

Here we present the rest of the graphs depicting RMSF of residues that mediates the interaction between paclitaxel and tubulin. To go back to results, click: [8.5.2](#)

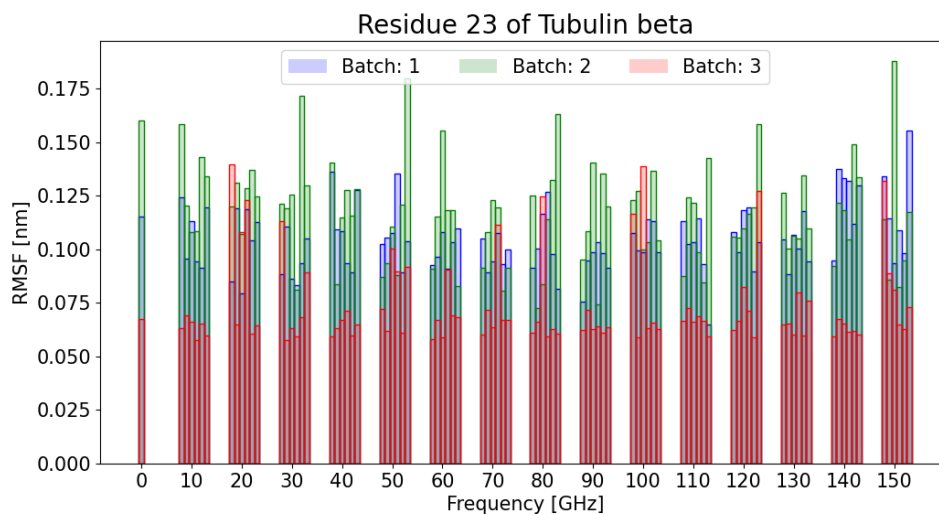


Figure 10.259: RMSF of residue 23 of tubulin beta - different directions and batches; the bars for 0 GHz mean that no EF is applied

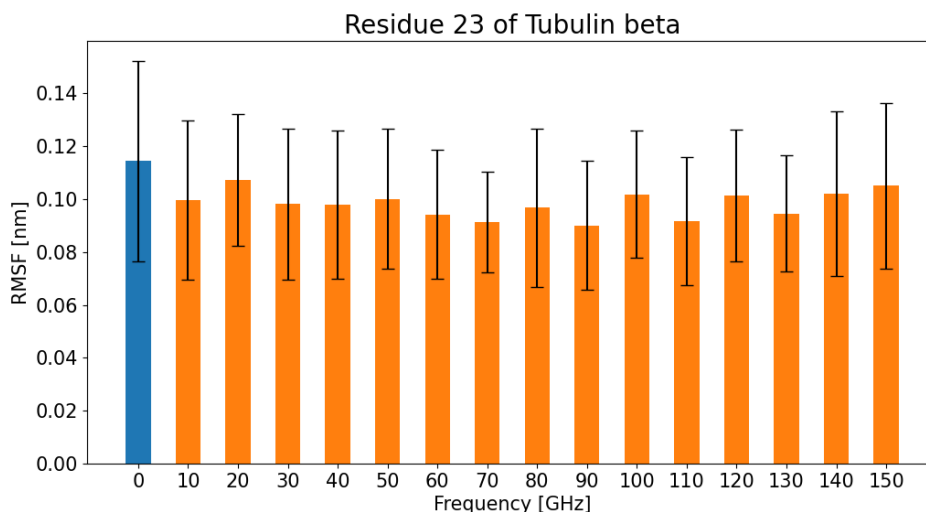


Figure 10.260: RMSF of residue 23 of tubulin beta - averaged over directions and batches; the bars for 0 GHz mean that no EF is applied

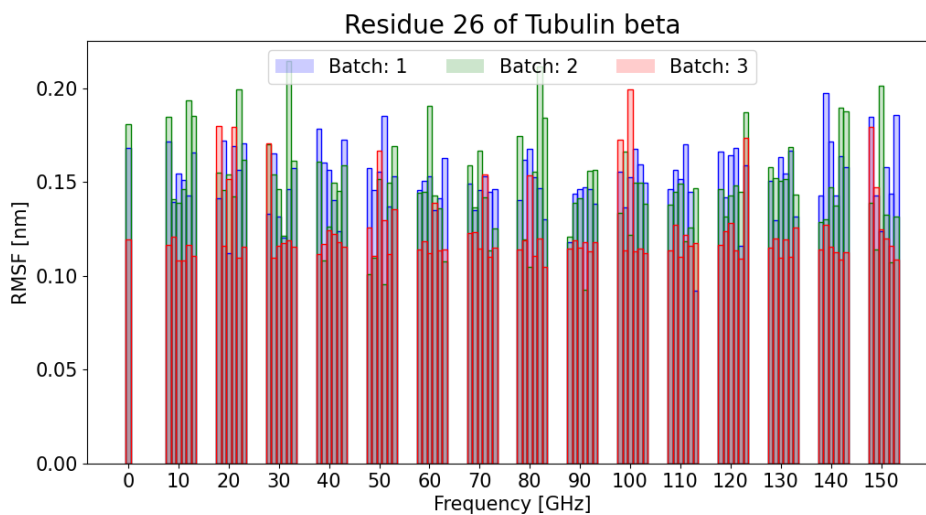


Figure 10.261: RMSF of residue 26 of tubulin beta - different directions and batches; the bars for 0 GHz mean that no EF is applied

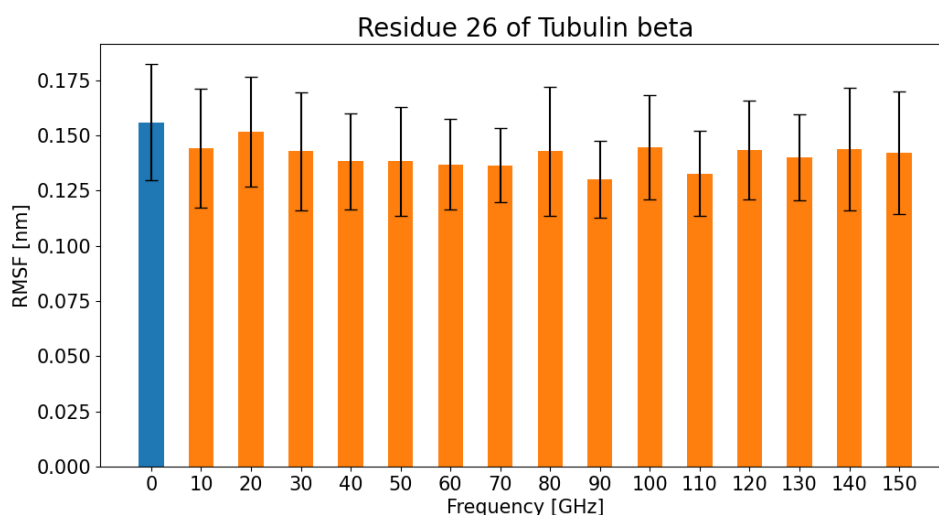


Figure 10.262: RMSF of residue 26 of tubulin beta - averaged over directions and batches; the bars for 0 GHz mean that no EF is applied

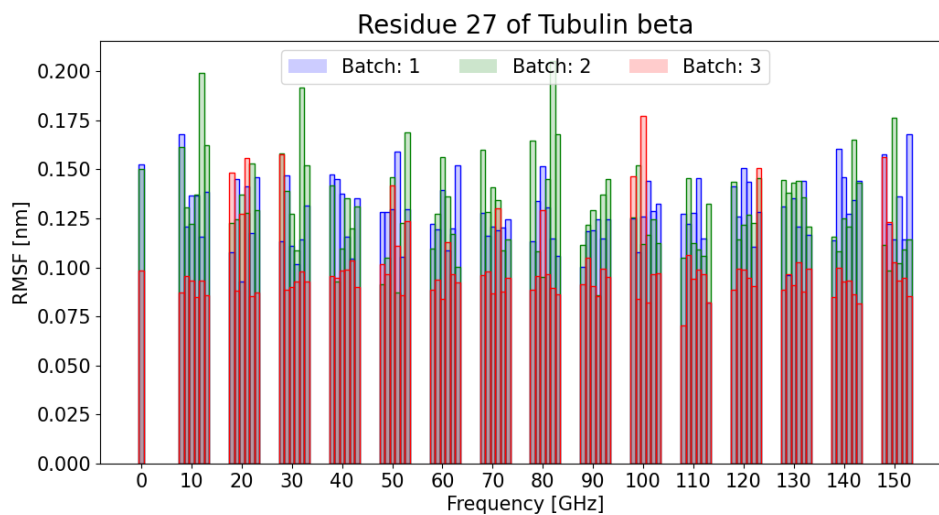


Figure 10.263: RMSF of residue 27 of tubulin beta - different directions and batches; the bars for 0 GHz mean that no EF is applied

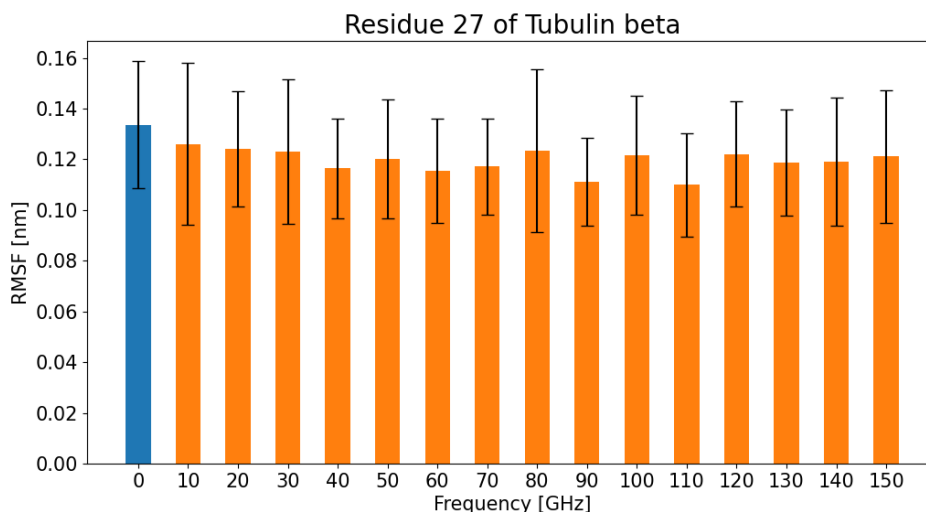


Figure 10.264: RMSF of residue 27 of tubulin beta - averaged over directions and batches; the bars for 0 GHz mean that no EF is applied

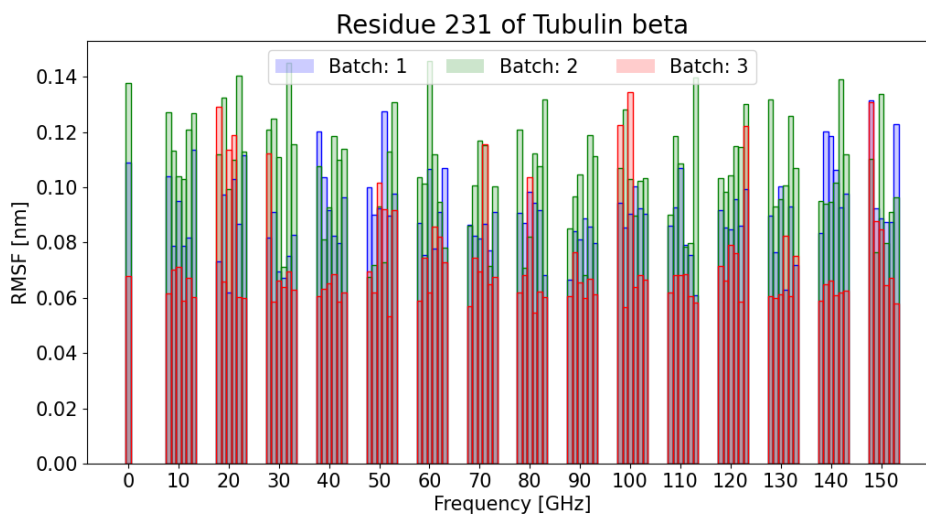


Figure 10.265: RMSF of residue 231 of tubulin beta - different directions and batches; the bars for 0 GHz mean that no EF is applied

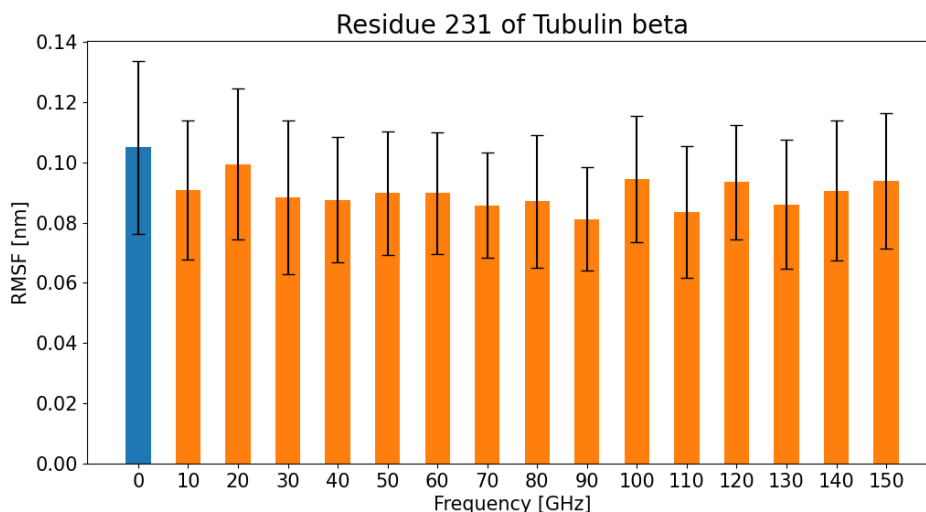


Figure 10.266: RMSF of residue 231 of tubulin beta - averaged over directions and batches; the bars for 0 GHz mean that no EF is applied

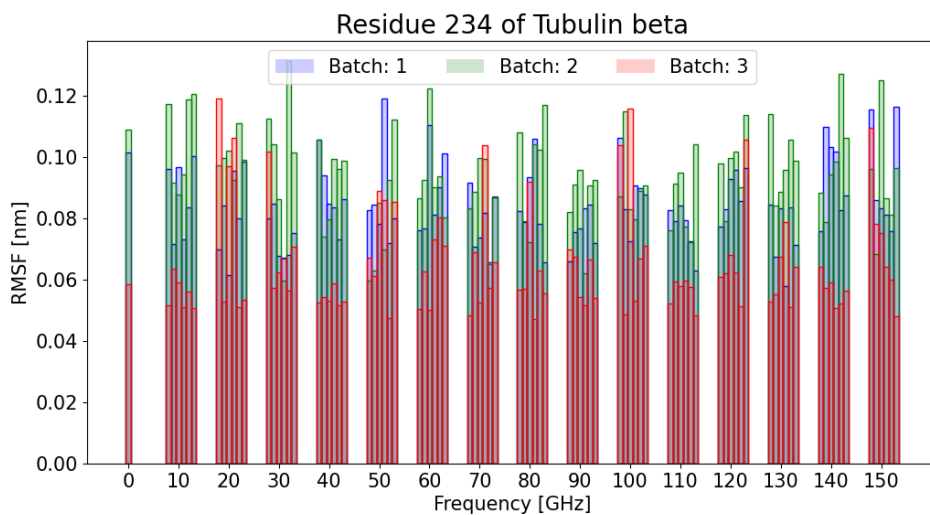


Figure 10.267: RMSF of residue 234 of tubulin beta - different directions and batches; the bars for 0 GHz mean that no EF is applied

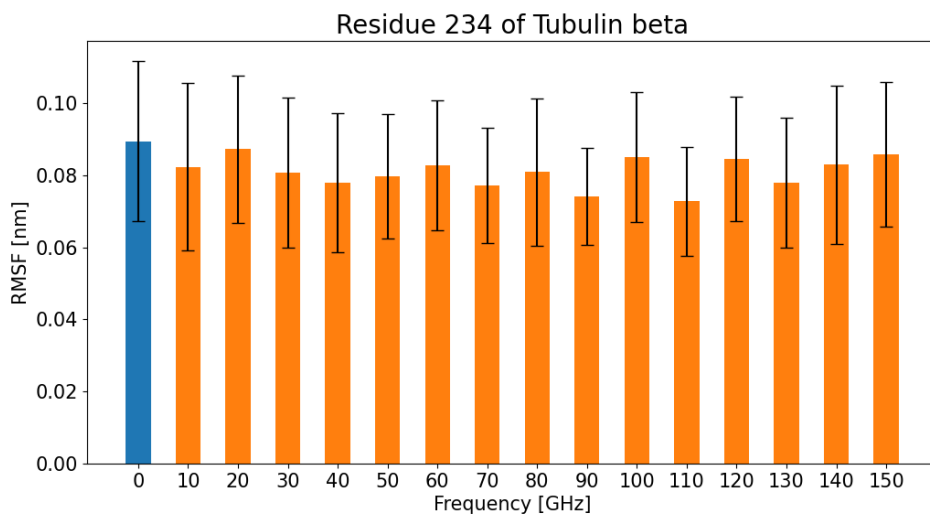


Figure 10.268: RMSF of residue 234 of tubulin beta - averaged over directions and batches; the bars for 0 GHz mean that no EF is applied

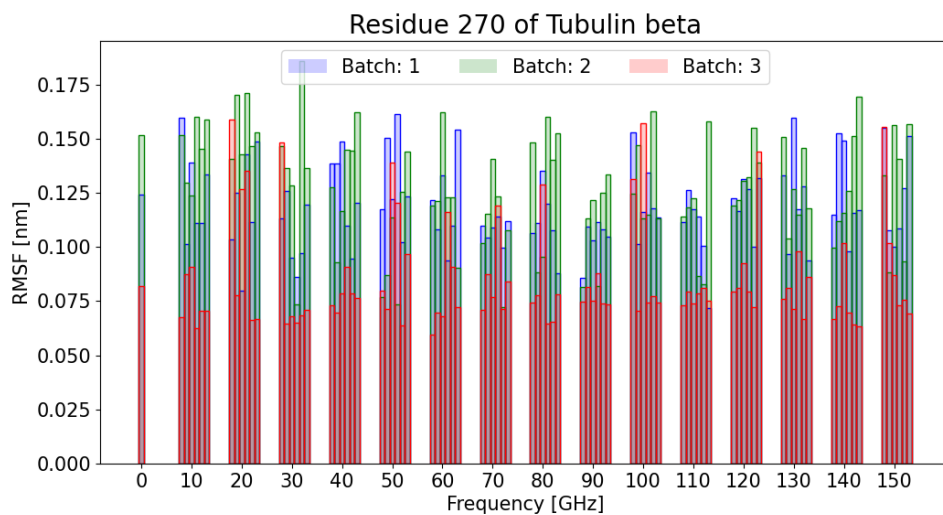


Figure 10.269: RMSF of residue 270 of tubulin beta - different directions and batches; the bars for 0 GHz mean that no EF is applied

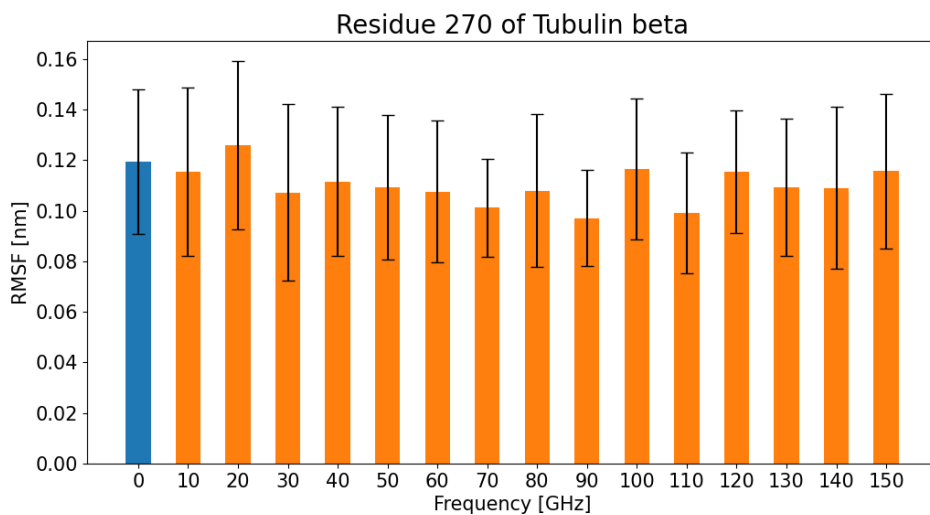


Figure 10.270: RMSF of residue 270 of tubulin beta - averaged over directions and batches; the bars for 0 GHz mean that no EF is applied

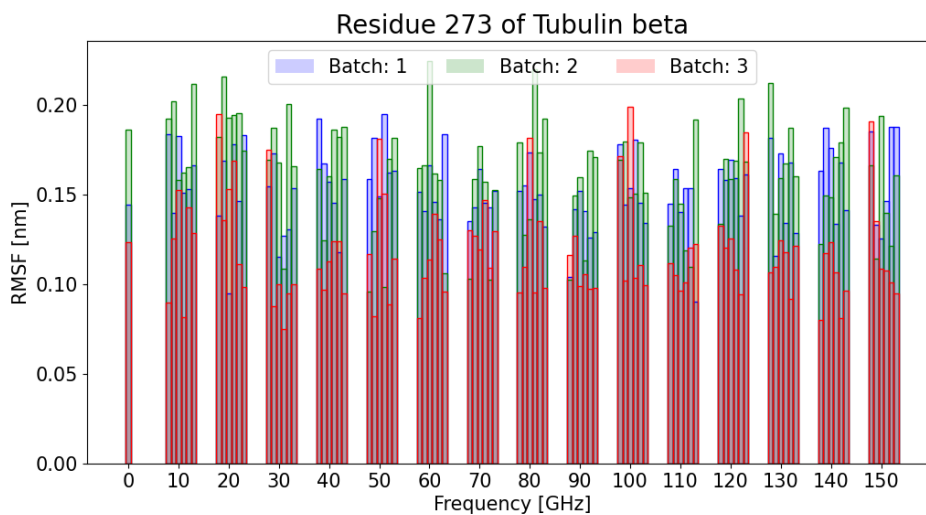


Figure 10.271: RMSF of residue 273 of tubulin beta - different directions and batches; the bars for 0 GHz mean that no EF is applied

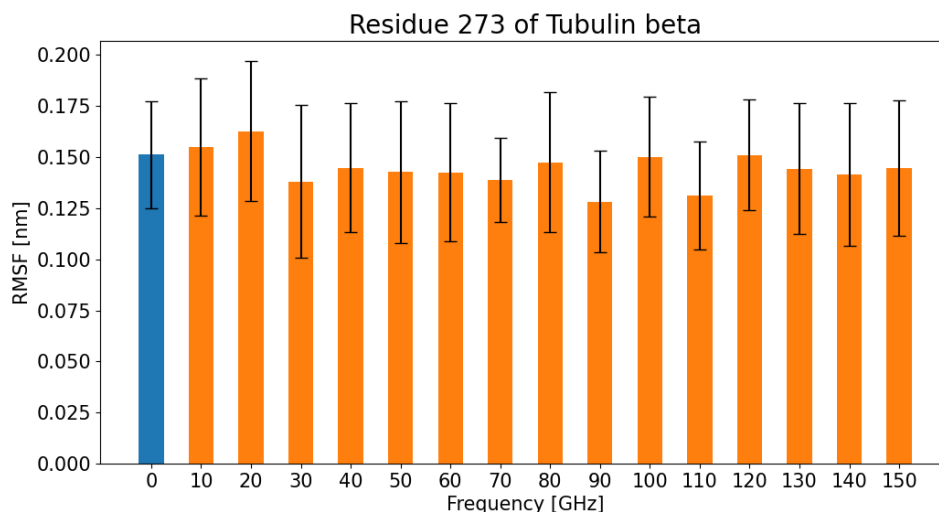


Figure 10.272: RMSF of residue 273 of tubulin beta - averaged over directions and batches; the bars for 0 GHz mean that no EF is applied

10.15 Rotational dynamics

Time spent oriented - Batch 2

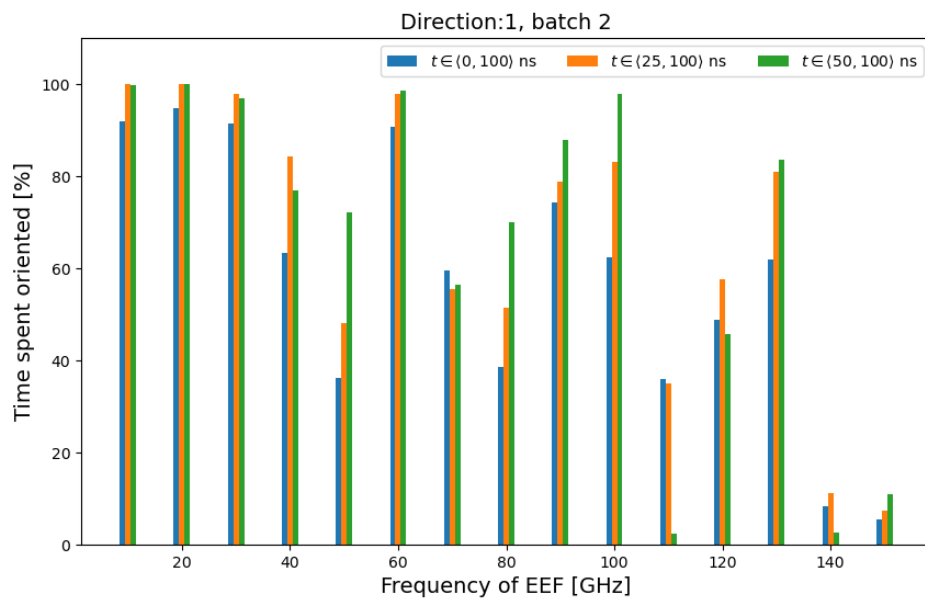


Figure 10.273: Time spent approximately parallel to the electric field direction of oscillation - batch 2, direction 1

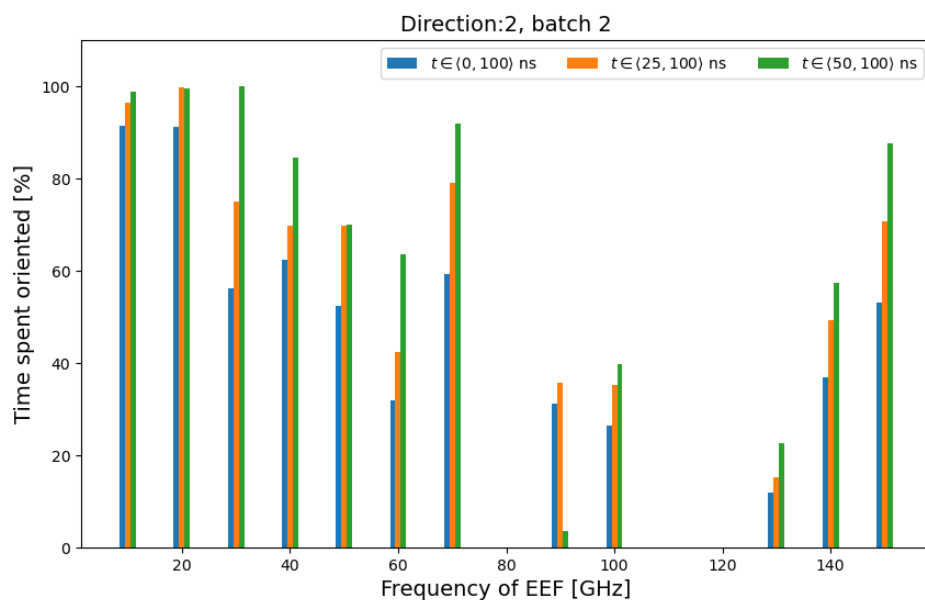


Figure 10.274: Time spent approximately parallel to the electric field direction of oscillation - batch 2, direction 2

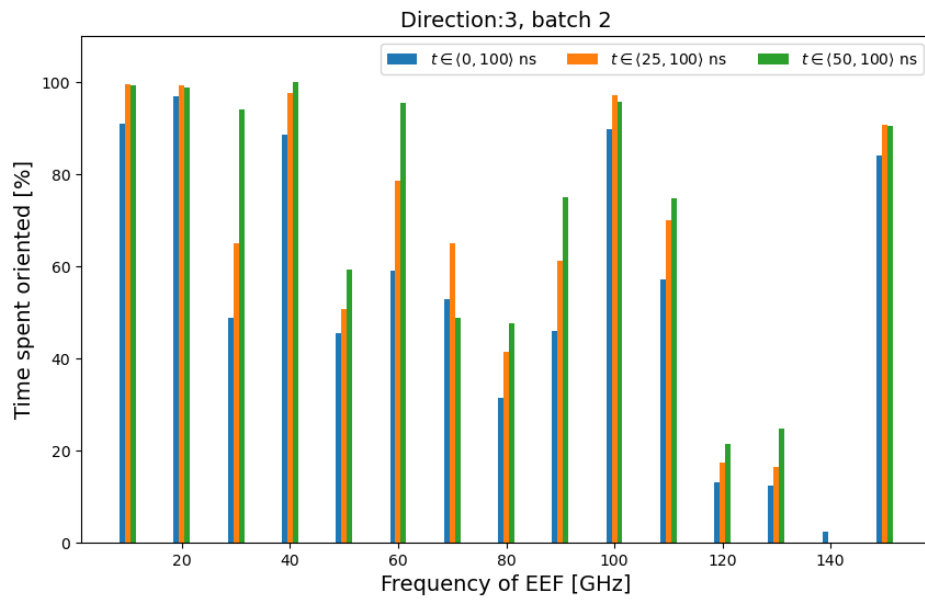


Figure 10.275: Time spent approximately parallel to the electric field direction of oscillation - batch 2, direction 3

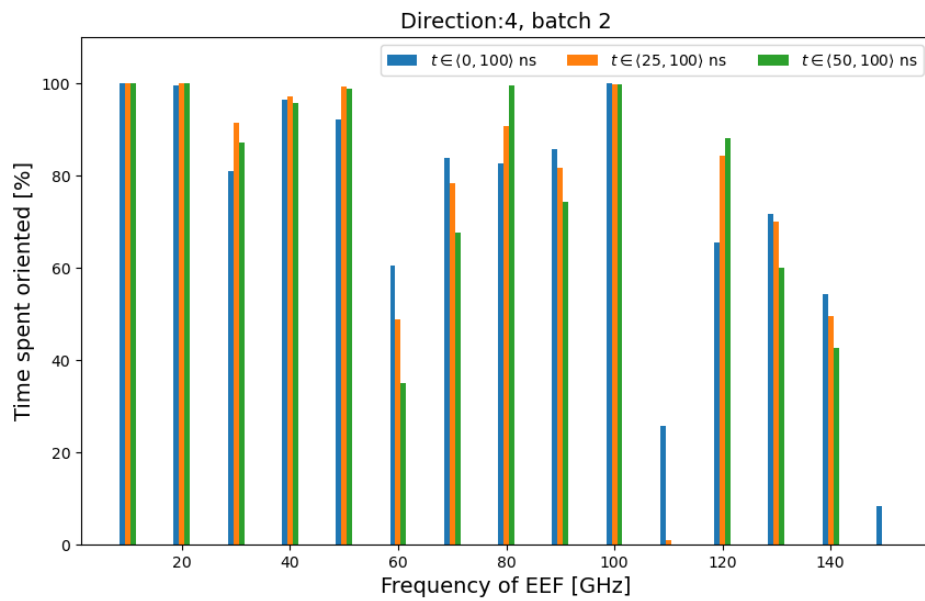


Figure 10.276: Time spent approximately parallel to the electric field direction of oscillation - batch 2, direction 4

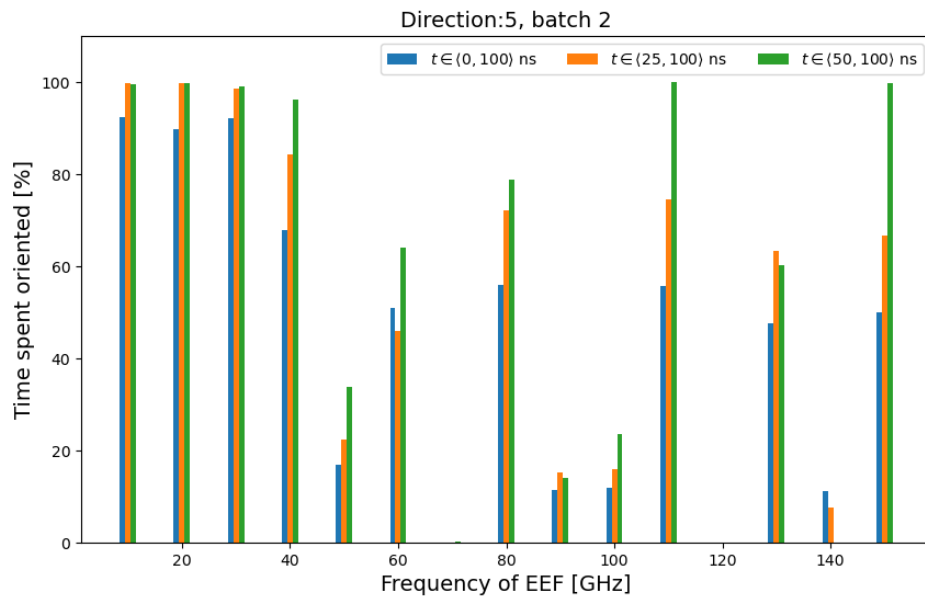


Figure 10.277: Time spent approximately parallel to the electric field direction of oscillation - batch 2, direction 5

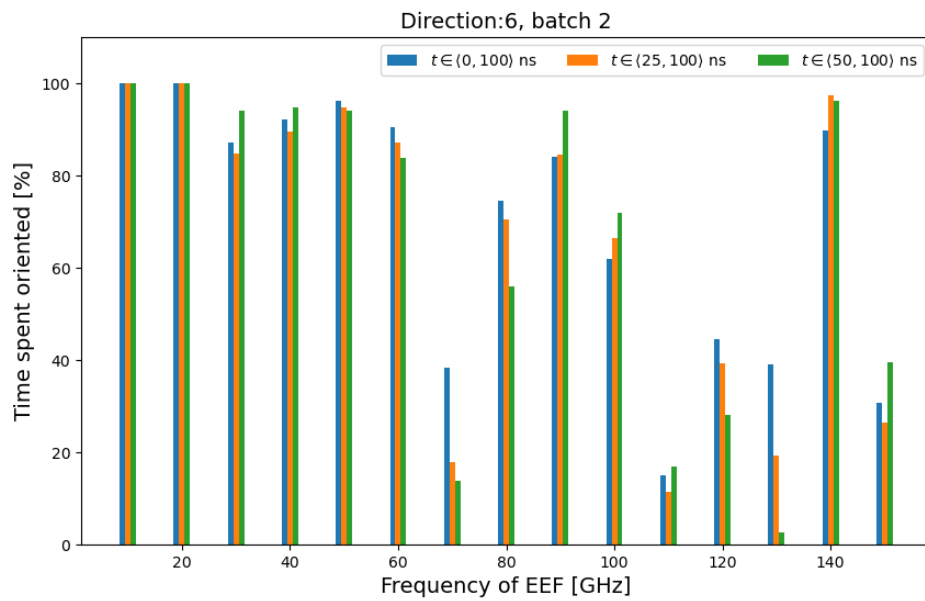


Figure 10.278: Time spent approximately parallel to the electric field direction of oscillation - batch 2, direction 6

Time spent oriented - Batch 3

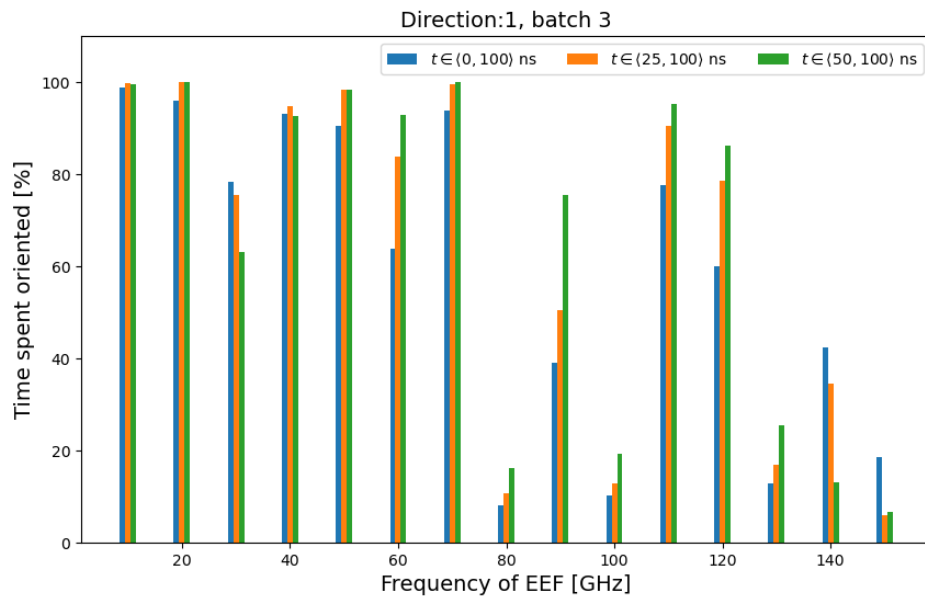


Figure 10.279: Time spent approximately parallel to the electric field direction of oscillation - batch 3, direction 1

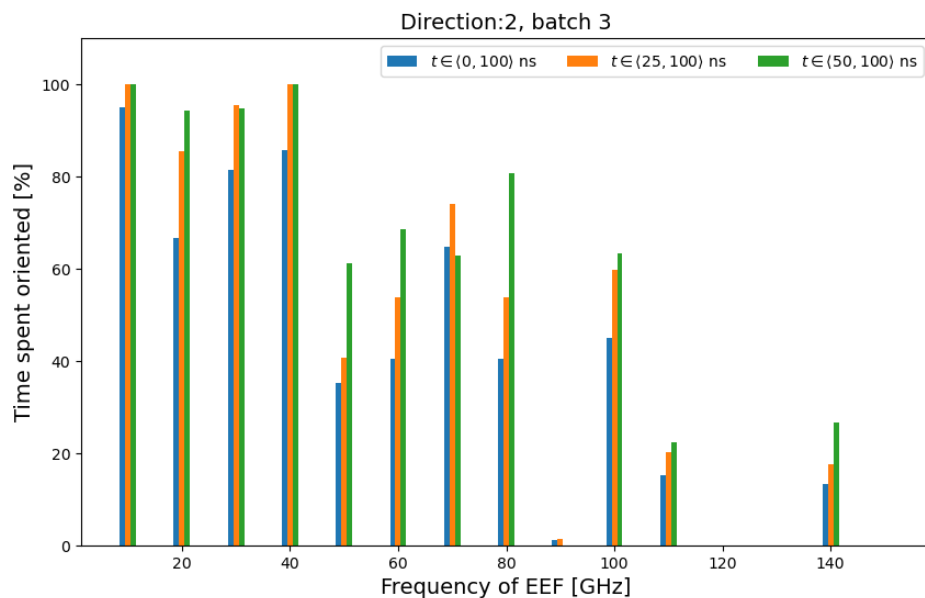


Figure 10.280: Time spent approximately parallel to the electric field direction of oscillation - batch 3, direction 2

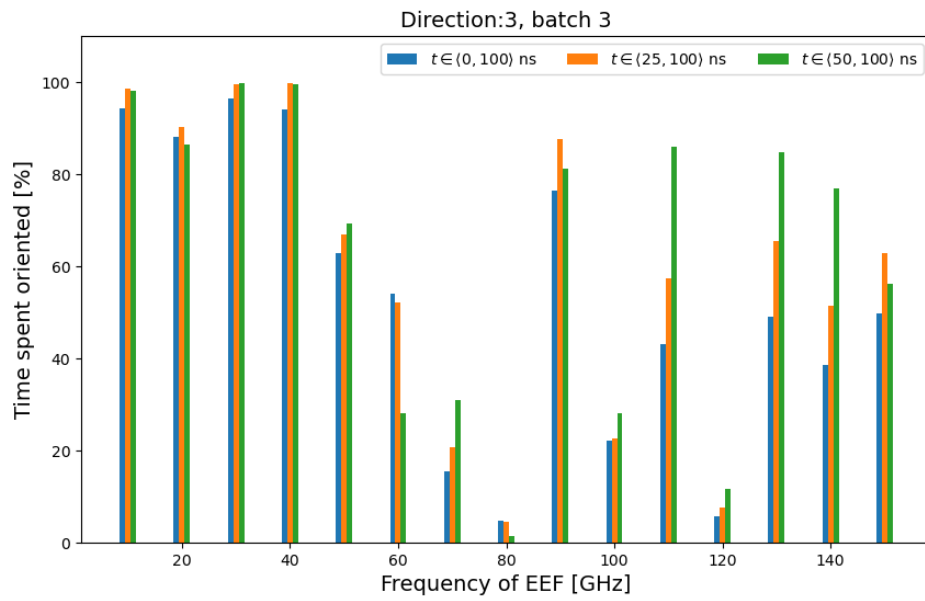


Figure 10.281: Time spent approximately parallel to the electric field direction of oscillation - batch 3, direction 3

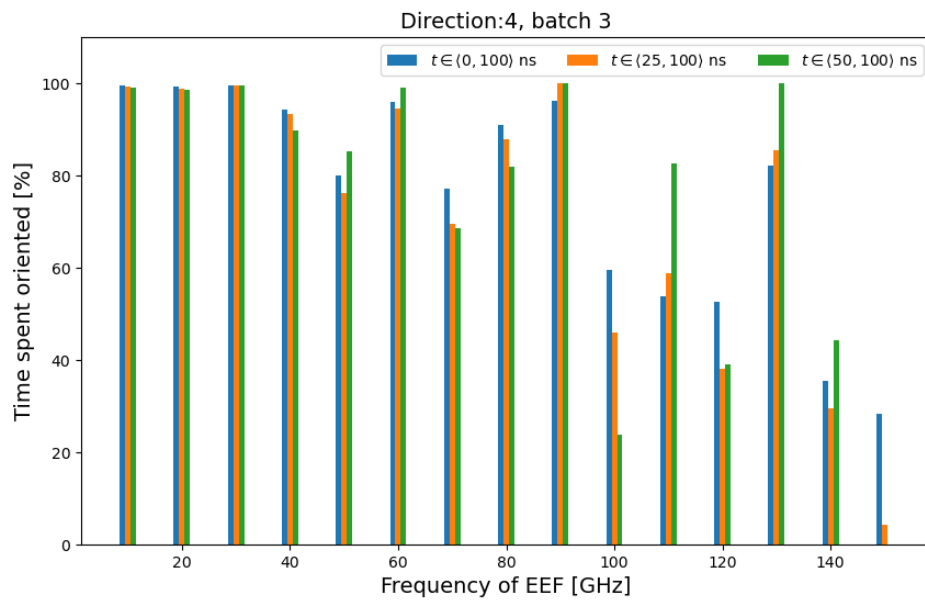


Figure 10.282: Time spent approximately parallel to the electric field direction of oscillation - batch 3, direction 4

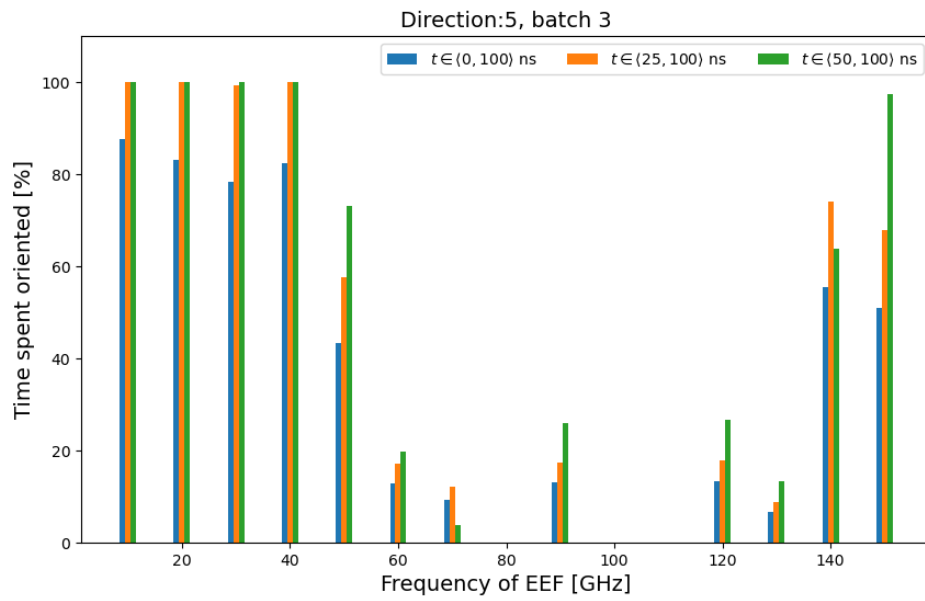


Figure 10.283: Time spent approximately parallel to the electric field direction of oscillation - batch 3, direction 5

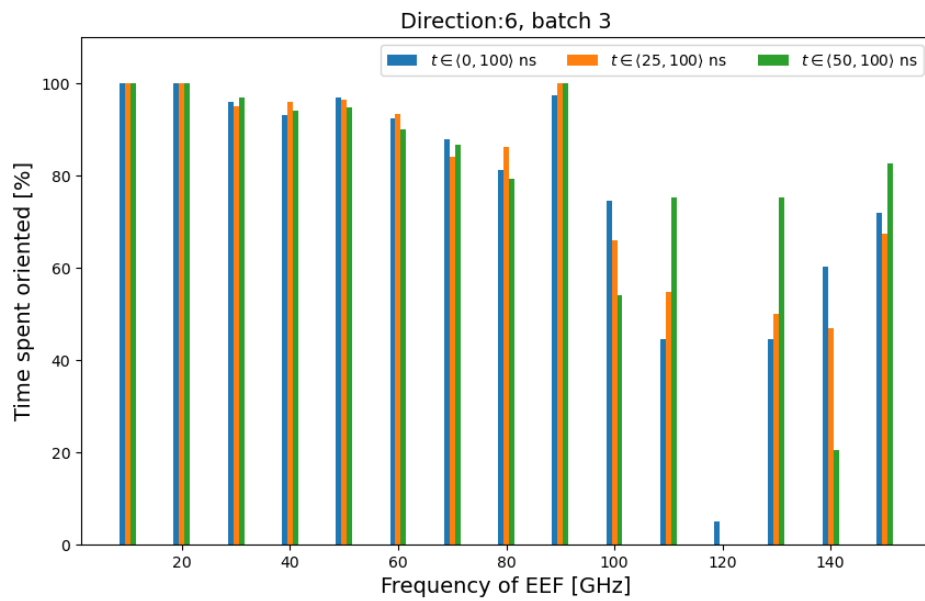


Figure 10.284: Time spent approximately parallel to the electric field direction of oscillation - batch 3, direction 6

10.16 Dipole moment graphs

Time series and distributions of the magnitude of the dipole moment of tubulin dimer - Batch 2

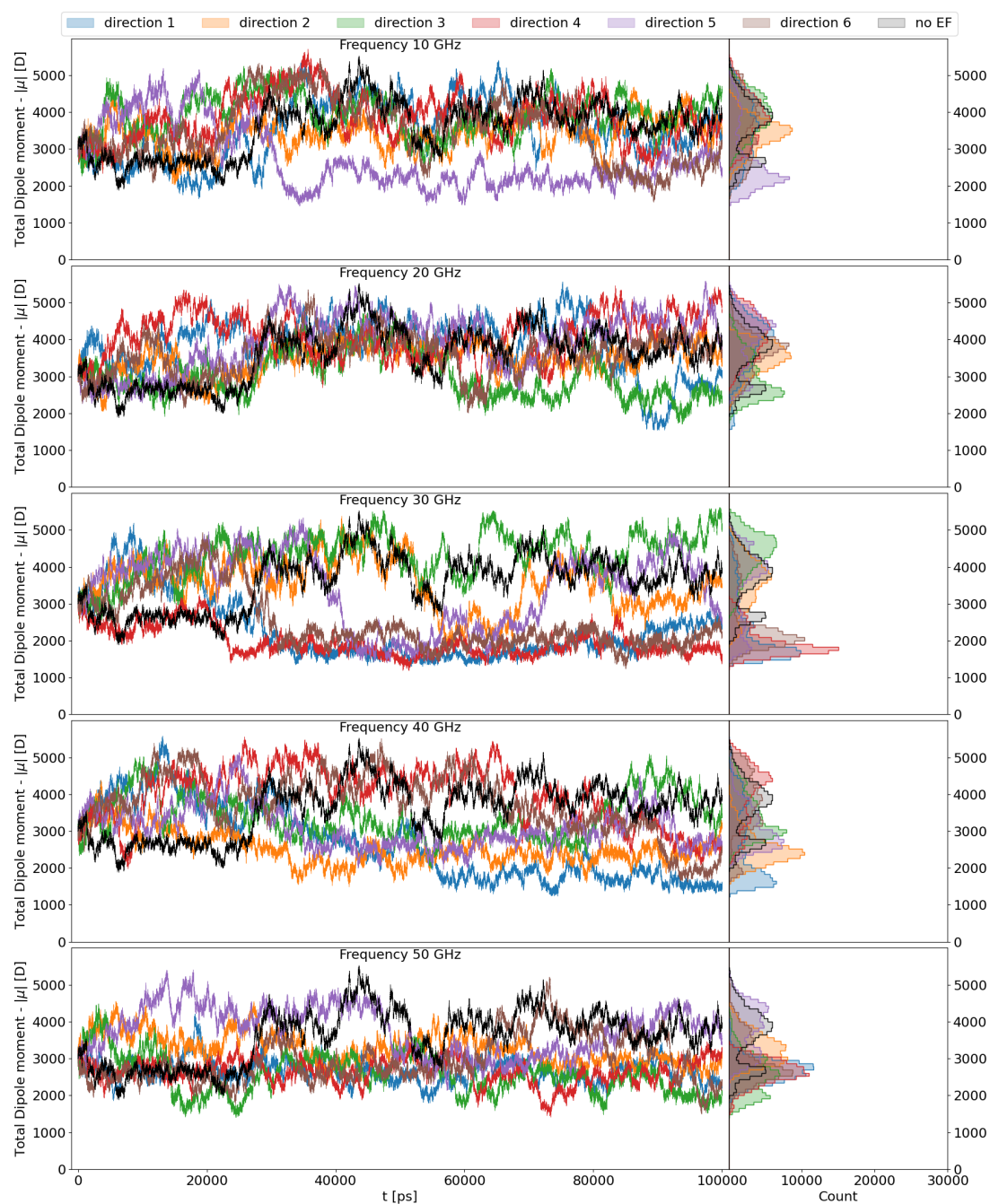


Figure 10.285: Magnitude of the dipole moment of tubulin heterodimer - time series and distributions - batch 2, Frequencies 10-50 GHz

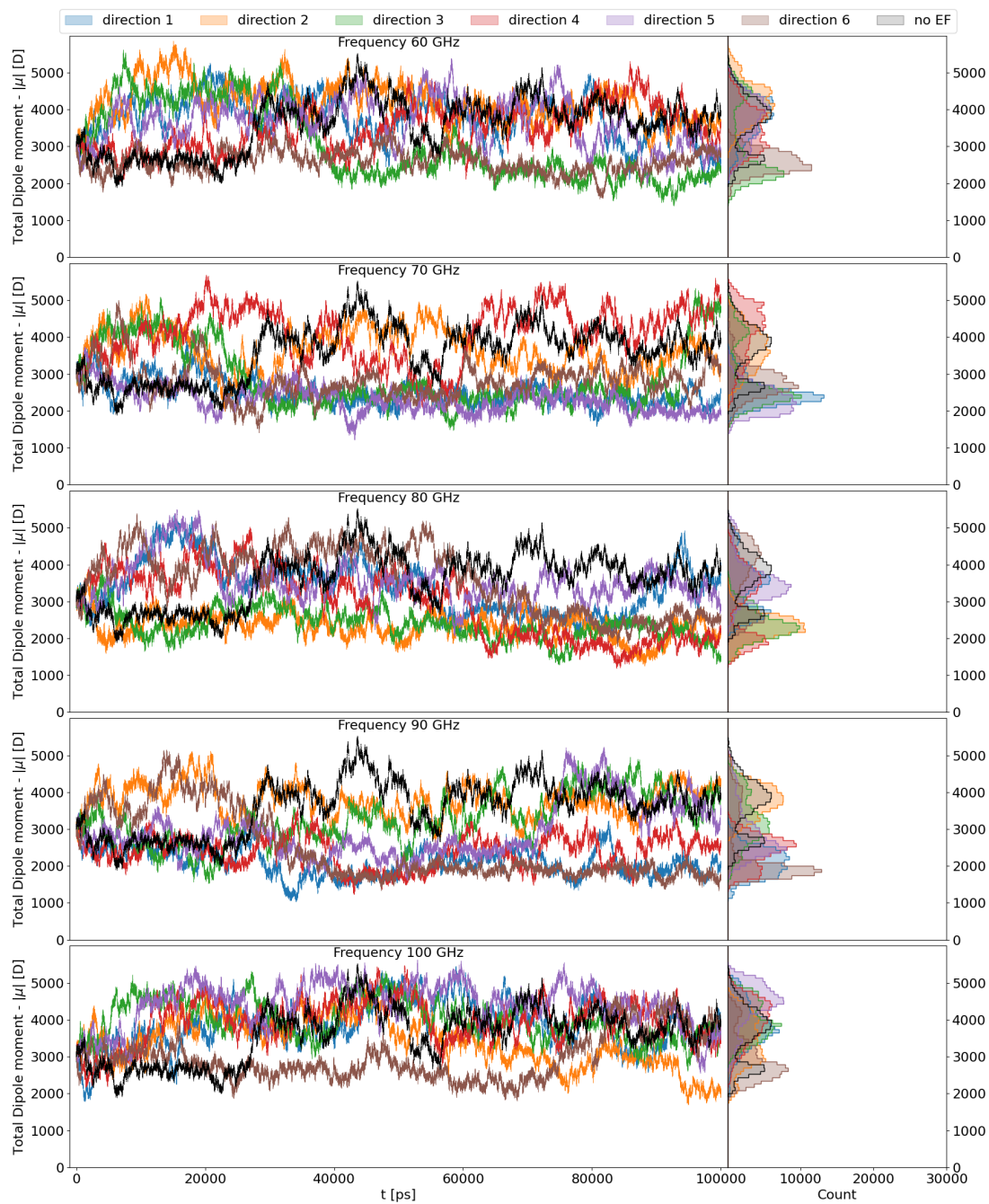


Figure 10.286: Magnitude of the dipole moment of tubulin heterodimer - time series and distributions - batch 2, Frequencies 60-100 GHz



Figure 10.287: Magnitude of the dipole moment of tubulin heterodimer - time series and distributions - batch 2, Frequencies 110-150 GHz

Time series and distributions of the magnitude of the dipole moment of tubulin dimer - Batch 3

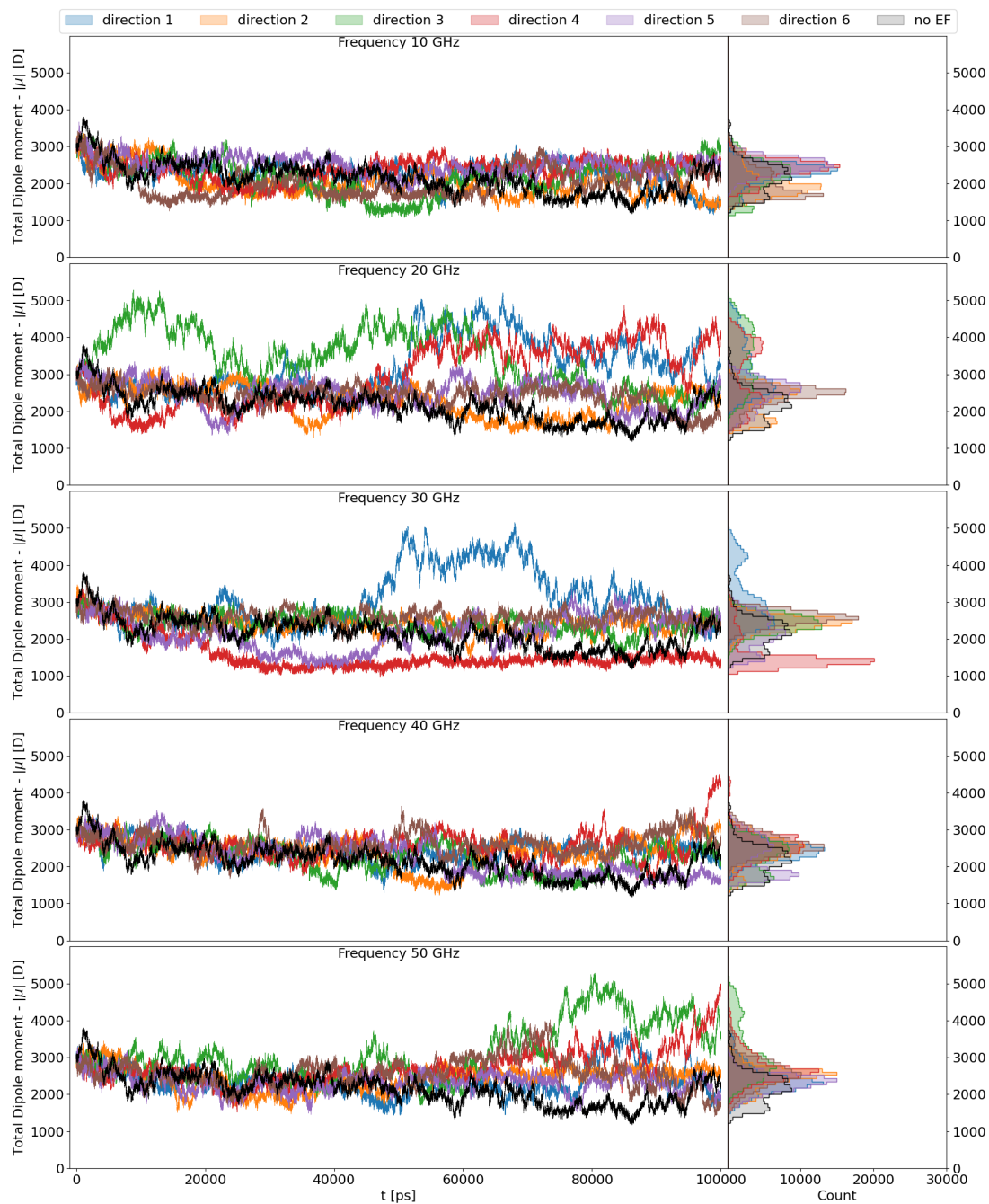


Figure 10.288: Magnitude of the dipole moment of tubulin heterodimer - time series and distributions - batch 3, Frequencies 10-50 GHz

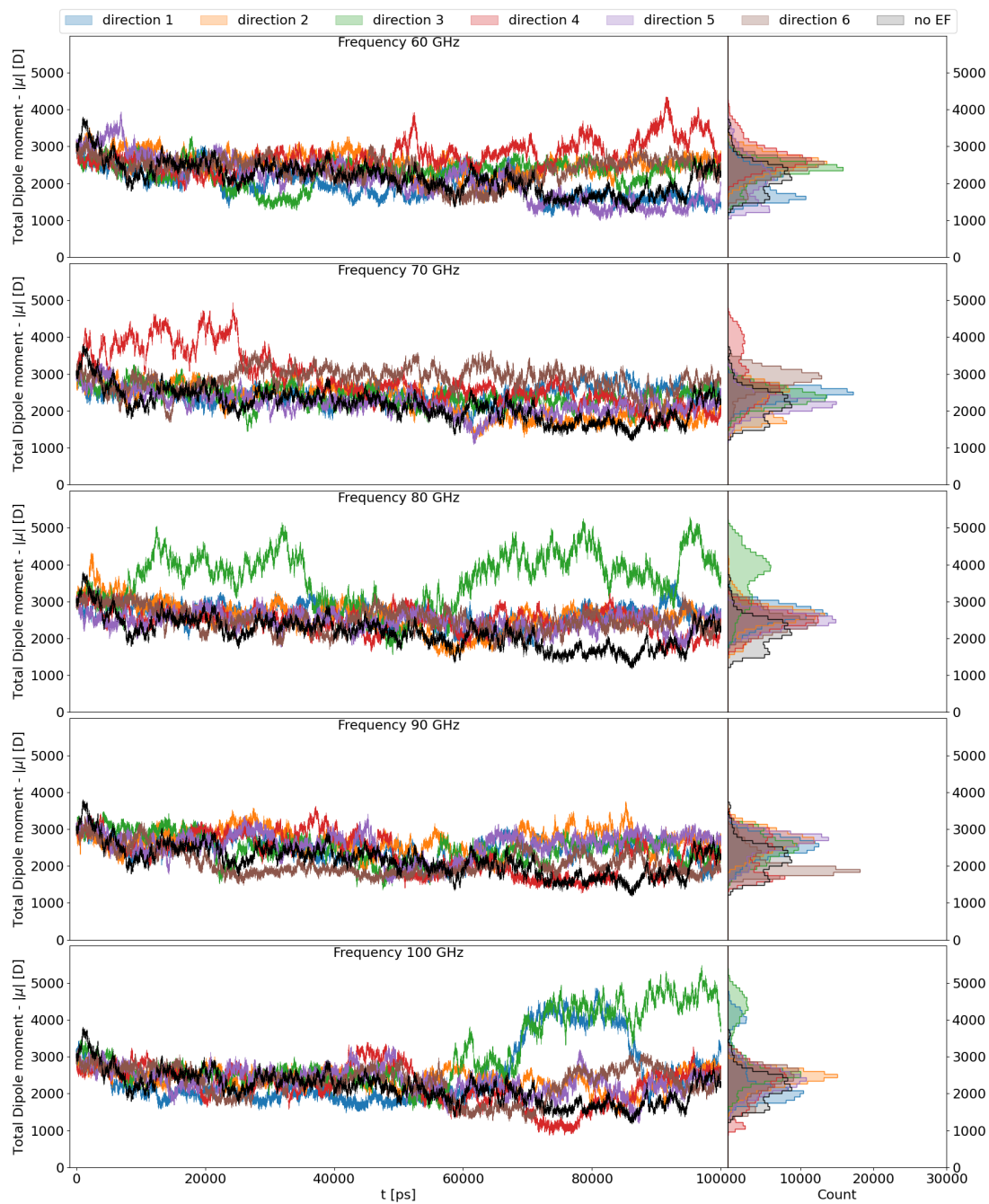


Figure 10.289: Magnitude of the dipole moment of tubulin heterodimer - time series and distributions - batch 3, Frequencies 60-100 GHz

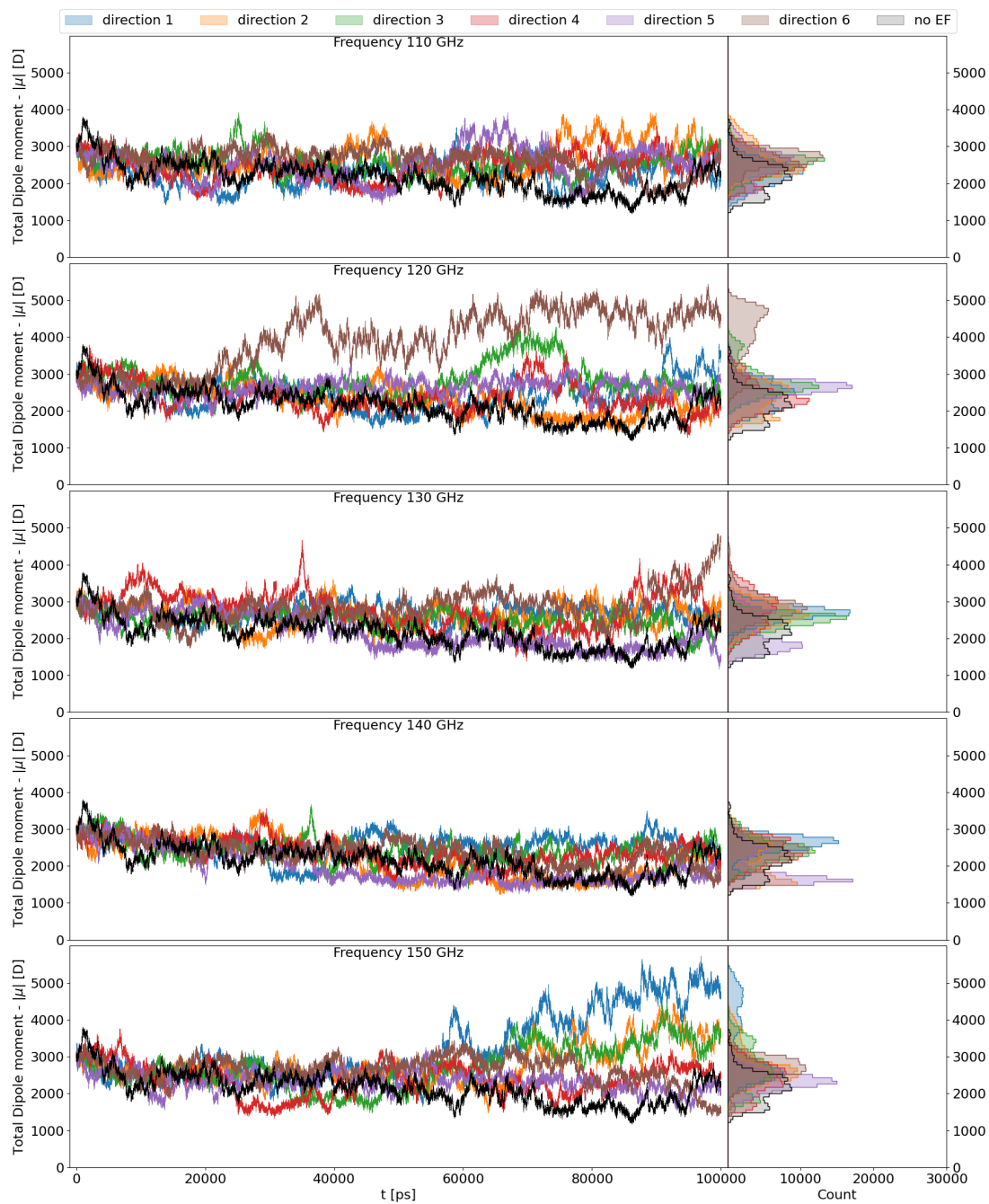


Figure 10.290: Magnitude of the dipole moment of tubulin heterodimer - time series and distributions - batch 3, Frequencies 110-150 GHz

Time series and distributions of the projection of the dipole moment - Batch 2

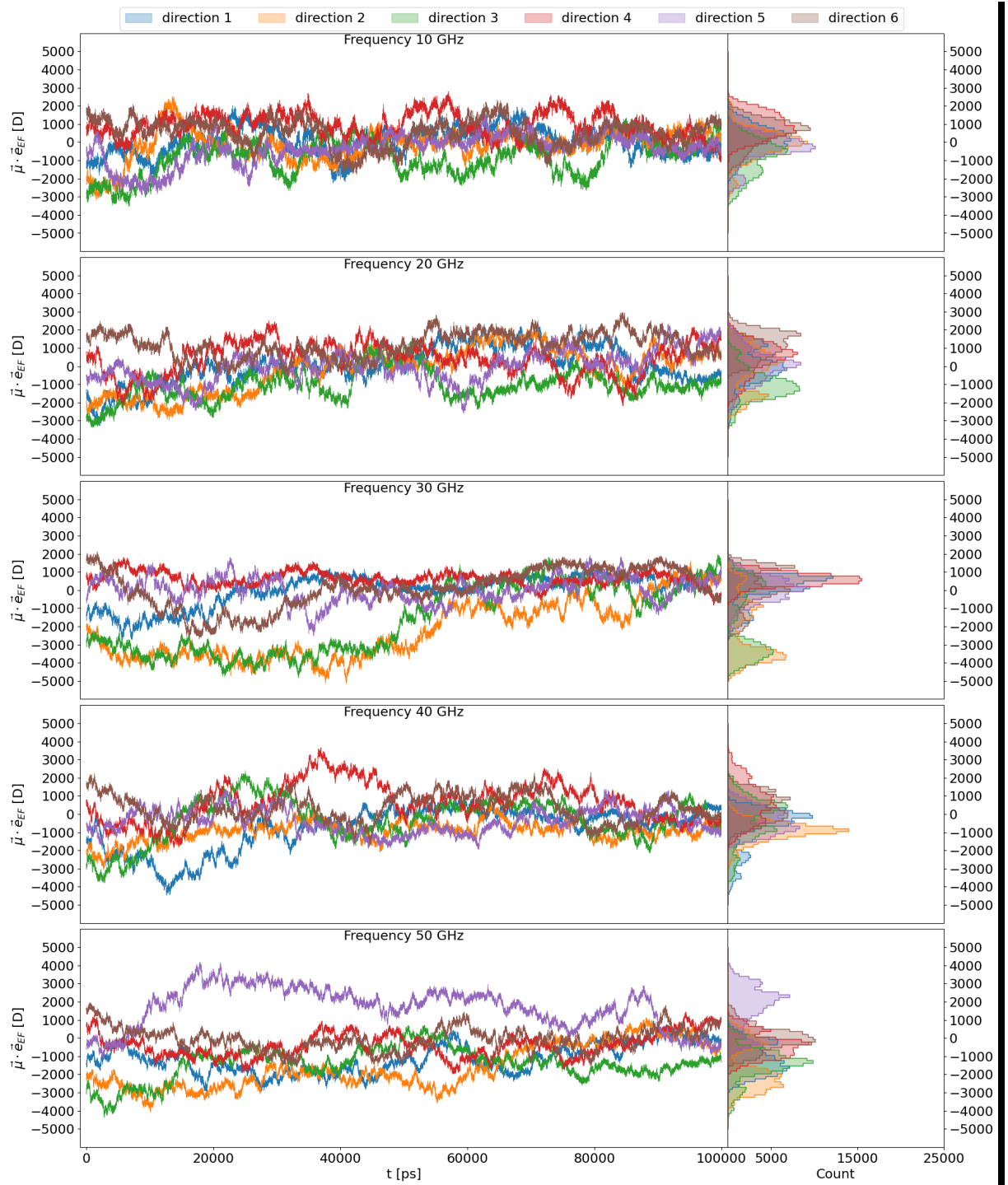


Figure 10.291: Time series and distributions of the projection of dipole moment of tubulin dimer onto the axis of electric field oscillations - batch 2, Frequencies 10-50 GHz

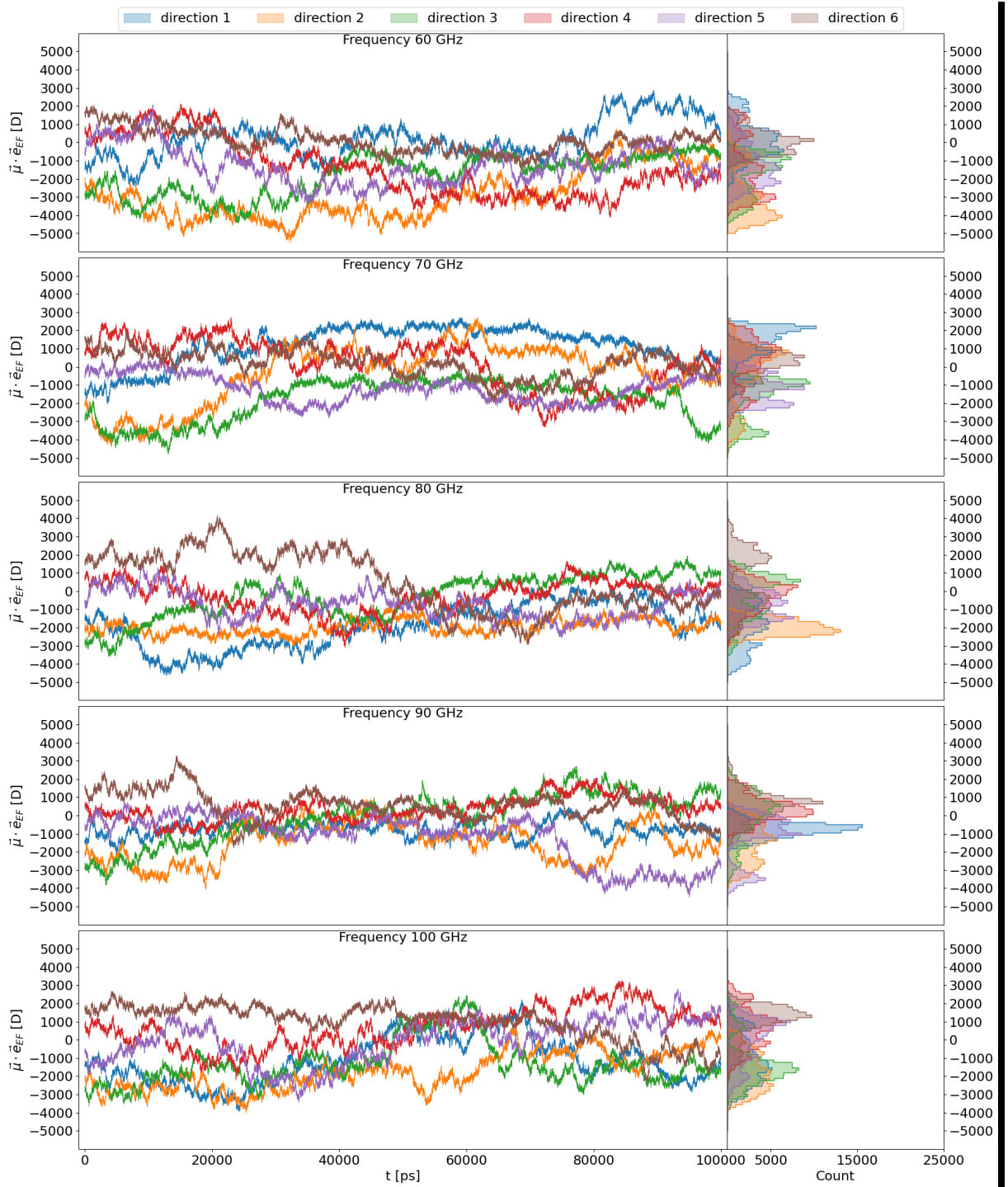


Figure 10.292: Time series and distributions of the projection of dipole moment of tubulin dimer onto the axis of electric field oscillations - batch 2, Frequencies 60-100 GHz

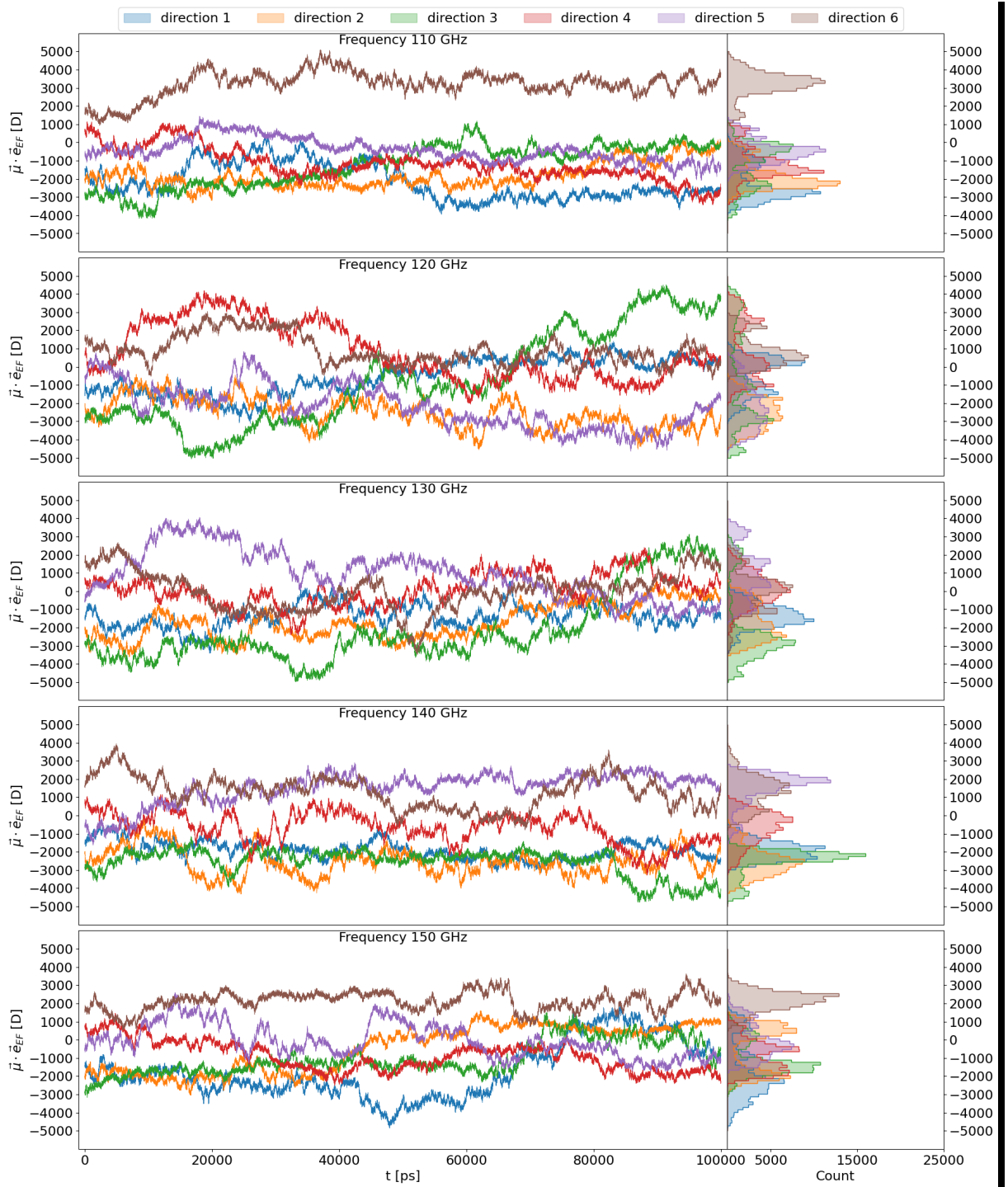


Figure 10.293: Time series and distributions of the projection of dipole moment of tubulin dimer onto the axis of electric field oscillations - batch 2, Frequencies 110-150 GHz

Time series and distributions of the projection of the dipole moment - Batch 3

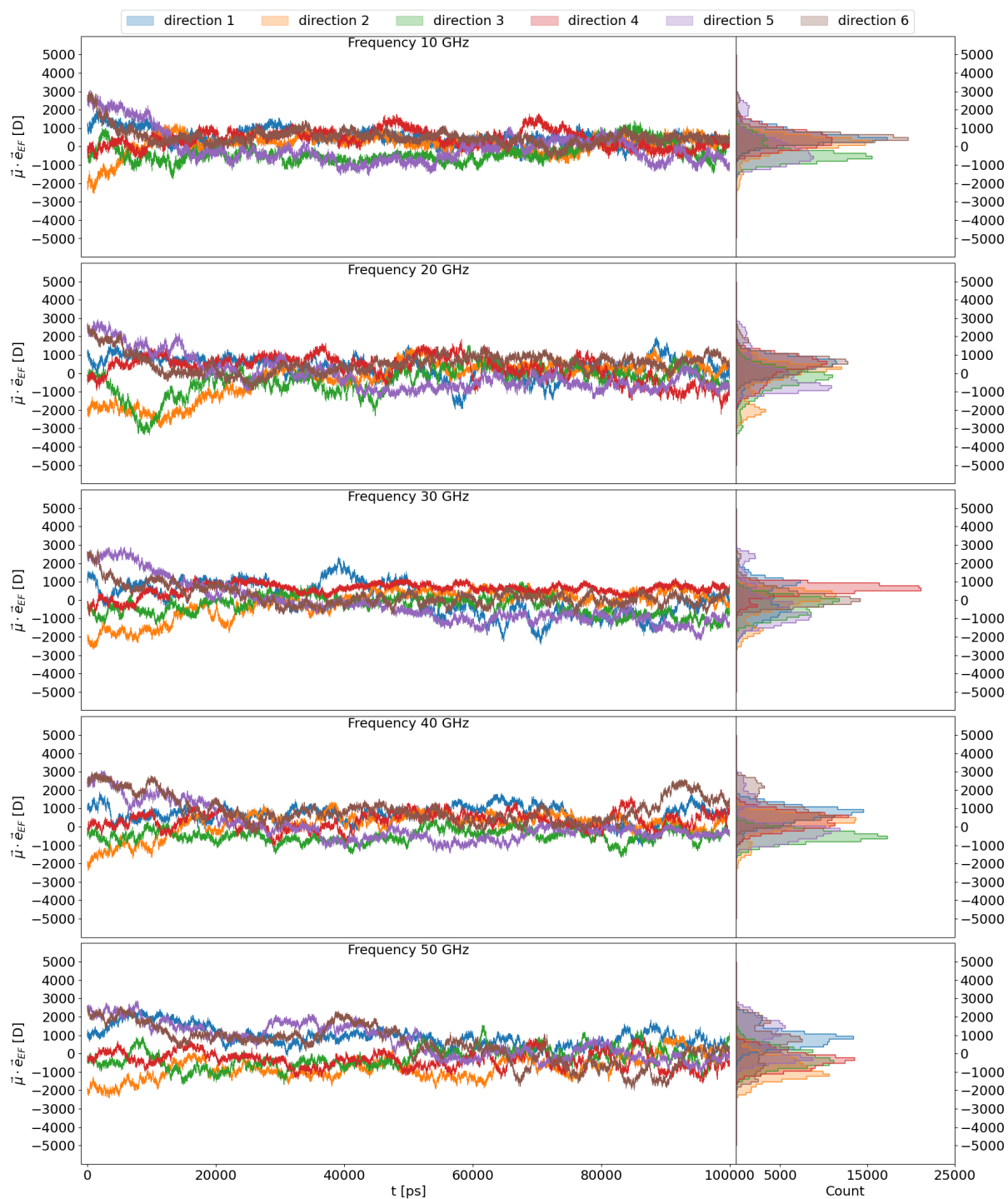


Figure 10.294: Time series and distributions of the projection of dipole moment of tubulin dimer onto the axis of electric field oscillations - batch 3, Frequencies 10-50 GHz

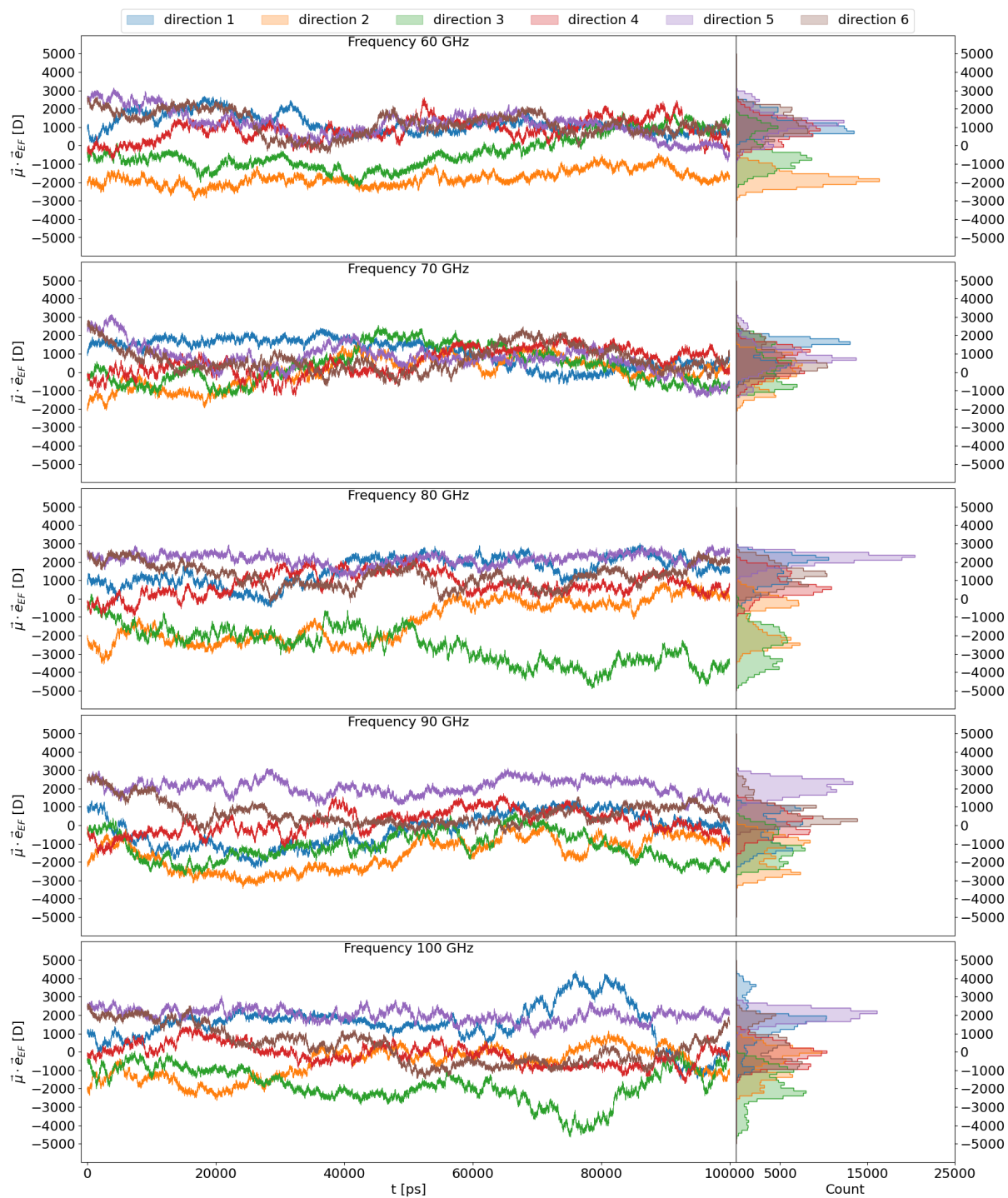


Figure 10.295: Time series and distributions of the projection of dipole moment of tubulin dimer onto the axis of electric field oscillations - batch 3, Frequencies 60-100 GHz

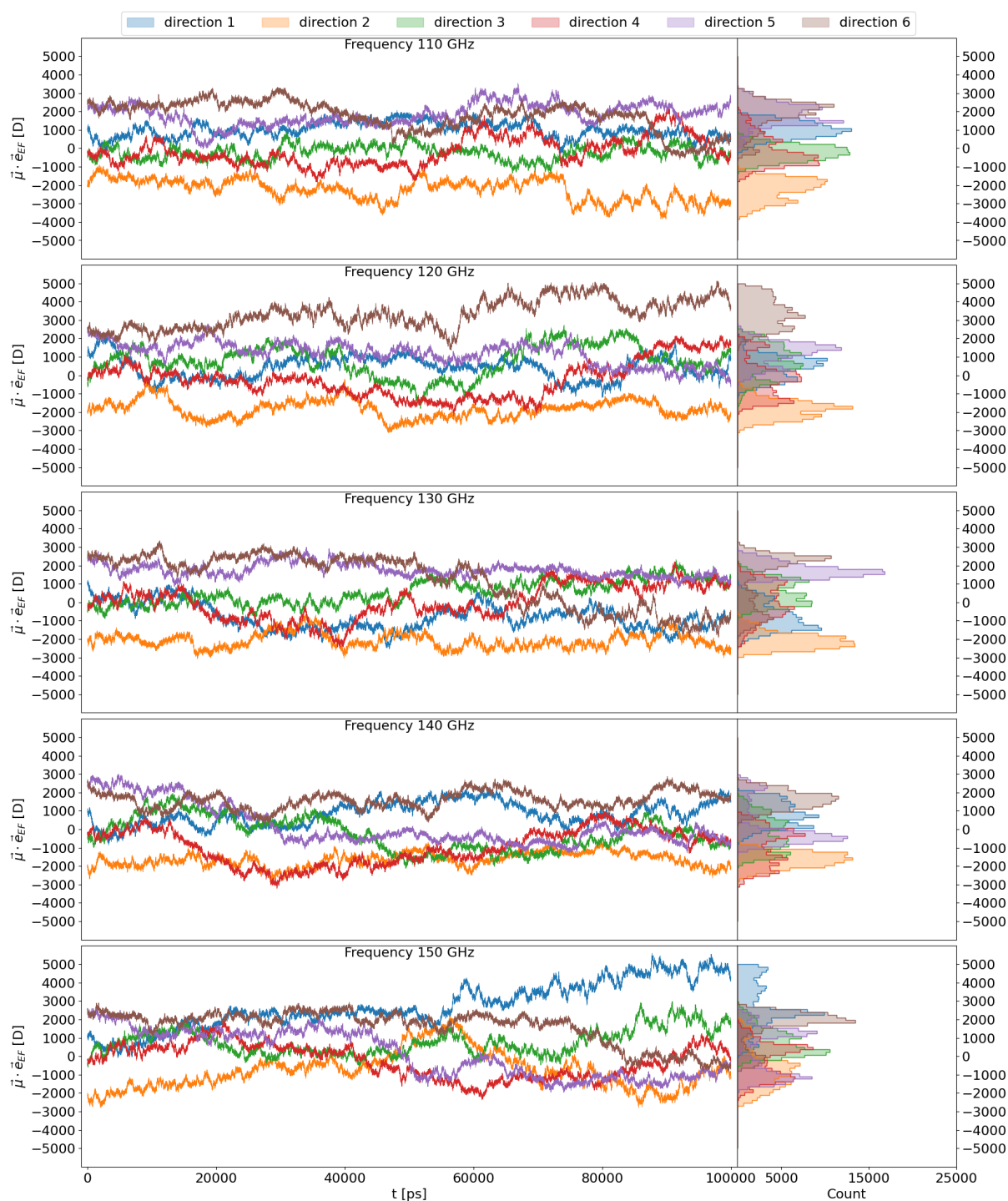


Figure 10.296: Time series and distributions of the projection of dipole moment of tubulin dimer onto the axis of electric field oscillations - batch 3, Frequencies 110-150 GHz

10.17 What did not make it into the thesis

Preliminary findings also showed that there is an oscillatory effect in the bending angle between subunits that depends on the frequency of EF. This suggests that the EF of specific frequencies is coupling to this bending mode of tubulin dimer,

thus, potentially influencing a microtubule's rigidity. However, due to a non-rigid structure, a more robust definition of the angle needs to be used to confirm these findings.

We have also calculated another batch - batch 4, where we also saved the water molecules. Unfortunately, there was not a time to fully analyze them, therefore they are not a part of this thesis.